PACIFIC EARTHQUAKE ENGINEERING RESEARCH CENTER

Technical Background Report for Structural Analysis and Performance Assessment

A Report for the "Quantifying the Performance of Retrofit of Cripple Walls and Sill Anchorage in Single-Family Wood-Frame Buildings" Project

David P. Welch

Gregory G. Deierlein

John A. Blume Earthquake Engineering Center
Department of Civil and Environmental Engineering
Stanford University

PEER Report 2020/22
Pacific Earthquake Engineering Research Center
Headquarters, University of California at Berkeley

November 2020

Technical Background Report for Structural Analysis and Performance Assessment

A Report for the “Quantifying the Performance of Retrofit of Cripple Walls and Sill Anchorage in Single-Family Wood-Frame Buildings” Project

David P. Welch

Gregory G. Deierlein

John A. Blume Earthquake Engineering Center
Department of Civil and Environmental Engineering
Stanford University

PEER Report 2020/22
Pacific Earthquake Engineering Research Center
Headquarters at the University of California, Berkeley

November 2020

ABSTRACT

This report outlines the development of earthquake damage functions and comparative loss metrics for single-family wood-frame buildings with and without seismic retrofit of vulnerable cripple wall and stem wall conditions. The underlying goal of the study is to quantify the benefits of the seismic retrofit in terms of reduced earthquake damage and repair or reconstruction costs. The earthquake damage and economic losses are evaluated based on the *FEMA P-58* methodology, which incorporates detailed building information and analyses to characterize the seismic hazard, structural response, earthquake damage, and repair/reconstruction costs. The analyses are informed by and include information from other working groups of the Project to: (1) summarize past research on performance of wood-frame houses; (2) identify construction features to characterize alternative variants of wood-frame houses; (3) characterize earthquake hazard and ground motions in California; (4) conduct laboratory tests of cripple wall panels, wood-frame wall subassemblies and sill anchorages; and (5) validate the component loss models with data from insurance claims adjustors. Damage functions are developed for a set of wood-frame building variants that are distinguished by the number of stories (one- versus two-story), era (age) of construction, interior wall and ceiling materials, exterior cladding material, and height of the cripple walls. The variant houses are evaluated using seismic hazard information and ground motions for several California locations, which were chosen to represent the range seismicity conditions and retrofit design classifications outlined in the *FEMA P-1100* guidelines for seismic retrofit.

The resulting loss models for the Index Building variants are expressed in terms of three outputs: *Mean Loss Curves* (damage functions), relating expected loss (repair cost) to ground-motion shaking intensity, *Expected Annual Loss*, describing the expected (mean) loss at a specific building location due to the risk of earthquake damage, calculated on an annualized basis, and *Expected RC250 Loss*, which is the cost of repairing damage due to earthquake ground shaking with a return period of 250 years (20% chance of exceedance in 50 years). The loss curves demonstrate the effect of seismic retrofit by comparing losses in the existing (unretrofitted) and retrofitted condition across a range of seismic intensities.

The general findings and observations demonstrate: (1) cripple walls in houses with exterior wood siding are more vulnerable than ones with stucco siding to collapse and damage; (2) older pre-1945 houses with plaster on wood lath interior walls are more susceptible to damage and losses than more recent houses with gypsum wallboard interiors; (3) two-story houses are more vulnerable than one-story houses; (4) taller (e.g., 6-ft-tall) cripple walls are generally less vulnerable to damage and collapse than shorter (e.g., 2-ft-tall) cripple walls; (5) houses with deficient stem wall connections are generally observed to be less vulnerable to earthquake damage than equivalent unretrofitted cripple walls with the same superstructure; and (6) the overall risk of losses and the benefits of cripple wall retrofit are larger for sites with higher seismicity. As summarized in the report, seismic retrofit of unbraced cripple walls can significantly reduce the risk of earthquake damage and repair costs, with reductions in Expected RC250 Loss risk of up to 50% of the house replacement value for an older house with wood-frame siding at locations of high seismicity. In addition to the reduction in repair cost risk, the seismic retrofit has an important additional benefit to reduce the risk of major damage that can displace residents from their house for many months.

EXECUTIVE SUMMARY

This report is one of a series of reports documenting the methods and findings of a multi-year, multi-disciplinary project coordinated by the Pacific Earthquake Engineering Research Center (PEER) and funded by the California Earthquake Authority (CEA). The overall project is titled "*Quantifying the Performance of Retrofit of Cripple Walls and Sill Anchorage in Single-Family Wood-Frame Buildings*," henceforth referred to as the "PEER–CEA Project."

The overall objective of the PEER–CEA Project is to provide scientifically based information (e.g., testing, analysis, and loss models) to assess the effectiveness of seismic retrofit to reduce the risk of damage and associated losses (repair costs) of wood-frame houses with cripple wall and sill anchorage deficiencies as well as retrofitted conditions that address those deficiencies. This report is a product of Working Group 5 (WG) of the PEER–CEA Project, whose scope of work is to develop models and perform detailed structural analyses and performance-assessment analyses to create earthquake damage functions and loss metrics for sets of representative house configurations. Comparative analyses of houses with and without seismic retrofit are performed to quantify the benefits of the retrofit. The analyses described in this report are informed by and include information from other working groups to: (1) collect and summarize existing information and past research on performance of wood-frame houses; (2) identify construction features to characterize alternative variants of wood-frame houses; (3) characterize earthquake hazard and ground motions at representative sites in California; (4) develop cyclic loading protocols and conduct laboratory tests of cripple wall panels, wood-frame wall subassemblies, and sill anchorages to measure and document their response (strength and stiffness) under cyclic loading; and (5) the development of loss models as informed by a workshop with claims adjustors.

The earthquake damage and losses are evaluated based on the *FEMA P-58* methodology, which represents the state-of-the-art in building-specific seismic performance assessment. The framework is termed building-specific as it incorporates detailed information for a given house in a multi-staged framework that includes building definition, seismic hazard analysis, structural response analysis, damage assessment, and finally consequence (loss) assessment to quantify specific decision variables. The performance assessment framework is illustrated in Figure I, where information on the building variants and earthquake ground motions are used to develop and analyze detailed structural analysis models, data from which are used to estimate damage to building components and the associated economic losses (cost of repairs or building replacement). Structural response is quantified by distributions of engineering demand parameters (EDPs) such as story drift ratio (SDR) and peak floor acceleration (PFA). Damage assessment is conducted using component fragility functions that relate the EDP demands to the probability of a given component in a given Damage State (DS). Economic consequences (losses) are estimated by consequence (repair cost) functions for different building components in a specific damage state, in combination with consequences associated with the probability of structural collapse that is quantified by the collapse fragility function for the building.

Using information developed by the PEER–CEA Project WG2, variants of house configurations for the performance analyses considered available information within the literature regarding the inventory of residential houses and construction trends in California, as well as typical considerations made by risk modelers. The initial collection of variants focused on identifying building characteristics that are likely to (1) have a significant impact on seismic damage and losses, (2) exhibit differential benefits, in terms of reduced seismic losses, due to cripple wall and anchorage retrofitting, and (3) have significant representation of California wood-framed residential buildings. Risk modelers typically distinguish these construction characteristics between primary and secondary modifiers to evaluate the risk of earthquake damage and losses. Primary variants include easily accessible and documented information for residential homes, such as the number of stories and year of construction. Secondary variants typically include features that are observable, such as whether a cripple wall is present and the exterior cladding material of the house, but secondary variants may also include unobservable features, such as the presence of horizontal or diagonal wood sheathing beneath the exterior cladding. The building variant list developed by WG2 both informed the set of house variants used in the analysis and loss studies summarized in this report, as well as the scope of the laboratory testing of house components, conducted by WG4.

As illustrated in Figure II, the primary building variants considered in this study include number of stories, era (age) of construction, interior wall and ceiling materials, exterior cladding material, and height of the cripple walls. The main distinction between the eras of construction is the interior wall and ceiling finish materials, where the pre-1945 houses generally have wood lath and plaster interiors, the 1956–1970 houses have gypsum wallboard interiors, and the 1945–1956 houses represent a transition period where both materials were commonly used. The three types of exterior cladding materials are horizontal wood siding, cementitious stucco siding, and T1-11 panel siding. Wood and stucco cladding are common in all construction eras, whereas the T1-11 is limited to the 1956–1970 era. The three cripple wall heights encompass the expected 2-ft- and 6-ft-height range of unbraced cripple walls, along with the "zero-height" condition that applies to houses with perimeter stem walls that may have vulnerable anchorage between the first-floor framing and the foundation stem wall.

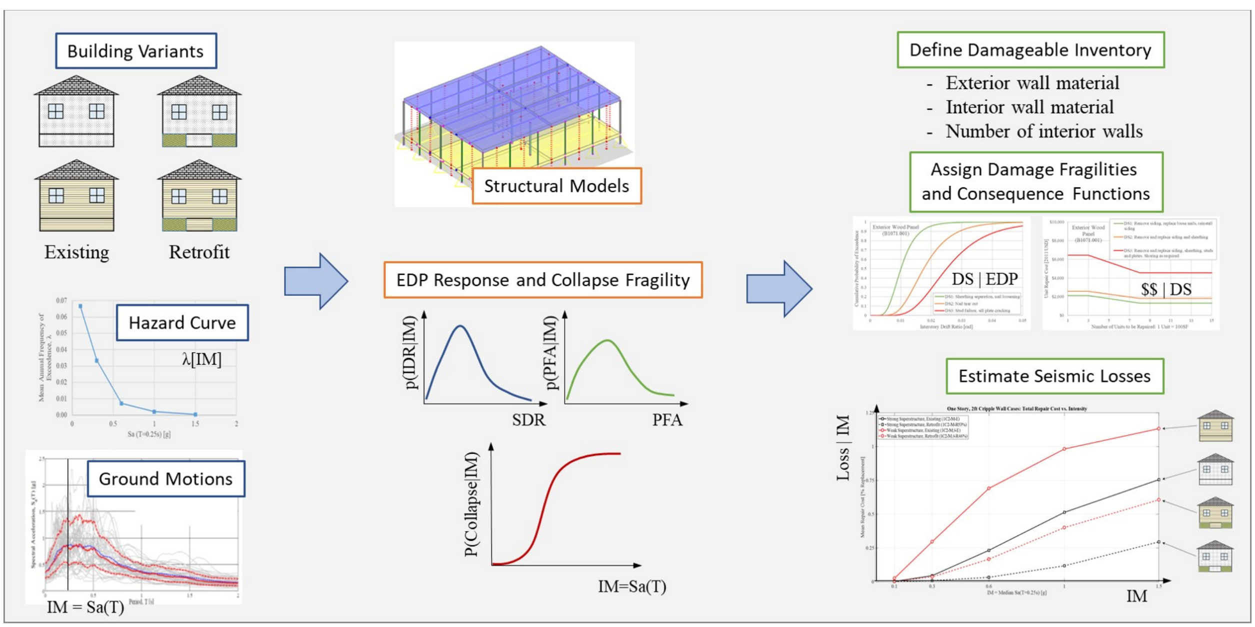

Figure I **Illustration of the building-specific seismic performance assessment process.**

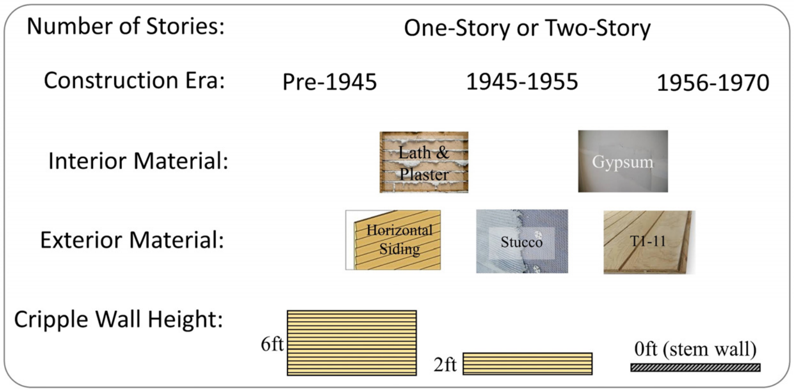

Figure II Illustration of the principal building variants investigated.

In collaboration with WG3, the seismic hazard was investigated for ten sites in California to characterize the range of earthquake ground shaking throughout the state. Through preliminary structural analyses, these ten sites were narrowed down to four sites for the detailed seismic retrofit and analysis studies. The four sites (Bakersfield, San Francisco, Northridge, and San Bernardino) are chosen to represent the range seismicity conditions and retrofit design classifications outlined in the *FEMA P-1100* guidelines, which are based on short-period design spectral accelerations (S_{DS}) ranging from 1.0g to 1.5g. The earthquake hazard is represented by conditional spectra with a conditioning period of 0.25 sec. For each of the four sites, ten intensities of conditional spectra using spectral acceleration at 0.25 sec as an intensity measure are established, with return periods ranging from 15 to 2500 years to represent ground shaking intensities from the onset of damage up through structural collapse. Forty-five pairs of ground motions are selected and scaled to the ten conditional spectra for each of the four sites (1800 ground motions in total) to use in the nonlinear dynamic analyses of the index house models.

Nonlinear structural analysis models were developed and run for each of the Index Building variants. The analysis model parameters were developed based an extensive review of existing information and data from tests conducted by WG4. As shown in Figure III, the three-dimensional models employ a macro-element approach using the *OpenSees* v2.5.2 analysis program, where nonlinear shear spring elements are used to model the perimeter superstructure, cripple walls, and the interior walls. The wall springs use the *Pinching4* material in *OpenSees*, where two springs are combined in parallel to capture the cyclic behavior from small displacements (onset of damage) up through large displacements (collapse). The shear springs are calibrated to represent the stiffness and strength of the walls, considering the sheathing materials, effective wall lengths and connection details. The floor and roof levels are represented by rigid diaphragms, which are supported by elastic co-rotational truss elements that carry vertical gravity loads to capture second-order (P-delta) effects. Modeling of stem wall houses uses the same approach for modeling of the superstructure with the unretrofitted stem wall connection (i.e., floor joist-sill connections) modeled using a combination of nonlinear springs and friction elements to capture the strength and stiffness of toe-nail connections and sliding resistance provided by the weight of the structure, respectively.

Nonlinear dynamic structural analyses are run using ground motions for each of the earthquake intensities to calculate story drift ratios and peak floor accelerations for each building variant, statistics from which are used to estimate structural and nonstructural damage. Structural collapse is assumed to occur when loss of structural resistance leads to excessive lateral drifts in the superstructure, cripple wall, or sill plate. An illustration of how collapse and non-collapse analysis realizations are calculated is shown in Figure IV(a), where a drift ratio of 0.2 (20%) is assumed as the collapse threshold for the superstructure and cripple walls. Collapse fragilities are calculated by fitting a lognormal distribution using the maximum likelihood approach to collapse data at multiple intensities of ground motions. The record-to-record variability (dispersion) in the collapse fragilities and Engineering Demand Parameters (EDPs) conditioned on non-collapse (β_{RTR} ranging from 0.2 to 0.6) is modified to include additional variability to account for modeling uncertainty (β_{mod} equal to 0.35), consistent with *FEMA P-58* guidelines, using a square root of the sum of squares (SRSS) approach. This approach for combining record-to-record and modeling uncertainty in the collapse fragility is illustrated in Figure IV(b).

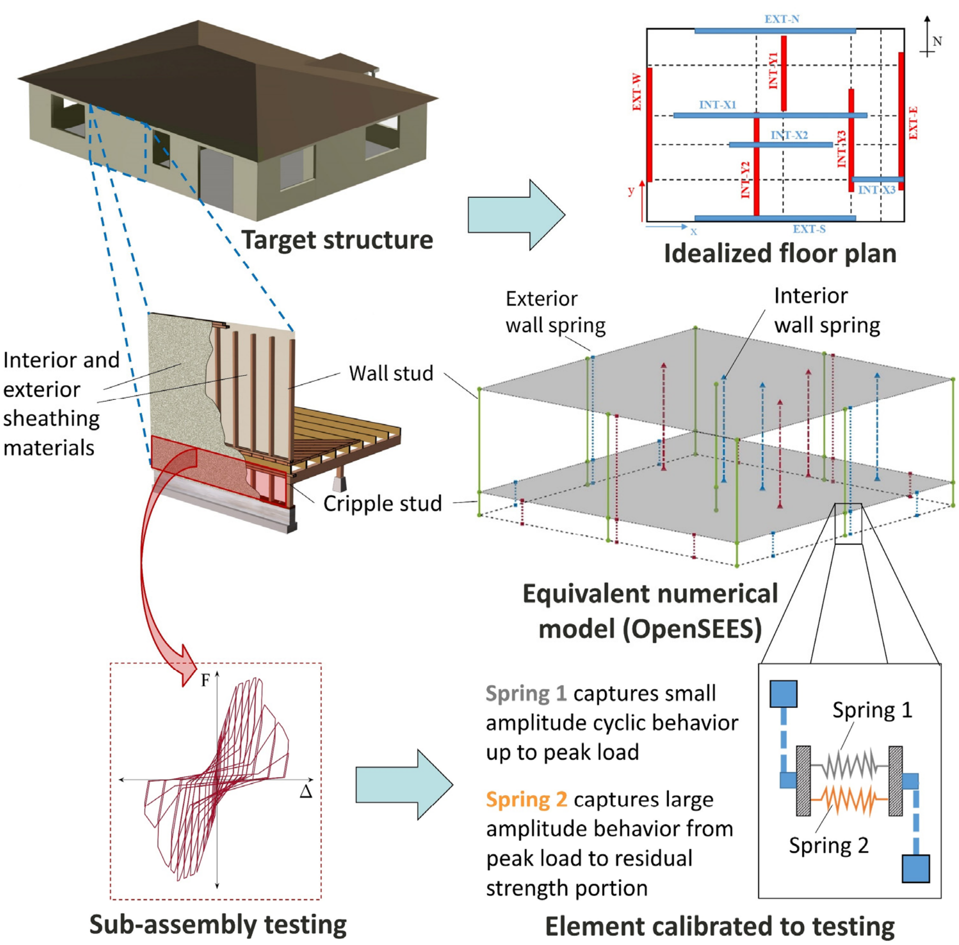

Figure III **Illustration of the three-dimensional modeling concept used to simulate the wood-frame house response to earthquakes.**

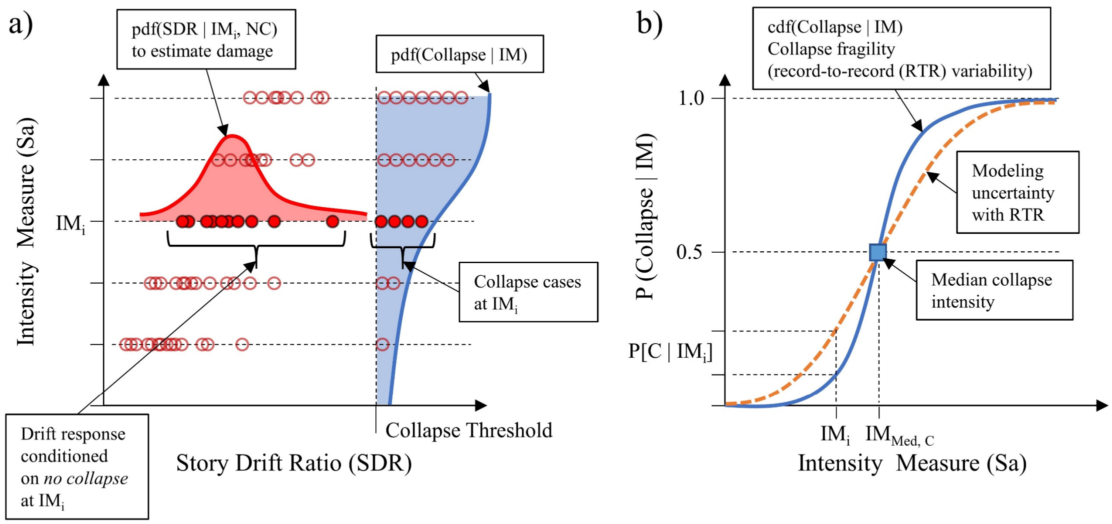

Figure IV **Data processing from nonlinear dynamic structural analysis: (a) Separation of response statistics for non-collapse and collapse cases; and (b) generation of collapse fragility considering record-to-record variability (solid line) and including modeling uncertainty (dashed line).**

Damage and loss models for individual components (termed component fragility and consequence functions, respectively) of residential houses, which are available in the *FEMA P-58* database, were reviewed and modified for this project to: (1) account for cripple wall and sill plate conditions; (2) incorporate new information from component tests conducted by WG4; and (3) incorporate adjustments based on a workshop with claims adjustors organized by WG6. Two of the more significant adjustments made to damage functions are illustrated in Figure V. One adjustment is to apply a height-dependent relationship to relate damage state fragility functions of full-height stucco walls to those of shorter cripple walls, where recent test data supported an approximately 2.5 times increase in damage state drift capacity when comparing 2-ft to 8-ft damage-state thresholds; see Figure V(a). Another is to adapt an existing damage fragility function for gypsum wallboard to plaster on wood lath interior wall finishes; see Figure V(b). Each of the damage states in these and other fragility functions have associated loss functions, based on necessary repair measures and costs. The assumed loss functions are based on those from *FEMA P-58*, including some adjustments to conditions in the wood-frame houses.

The repair-cost consequence functions of *FEMA P-58* were reviewed, modified, and then vetted in comparison with data from a workshop with claims adjustors with experience in assessing earthquake damage costs, which was organized by WG6. Damage description packages were developed for three case study houses, including photographs, drawings and textual descriptions of different materials, and sub-assemblies at various damage states within a home. Case study buildings were purposefully devised to provide comparisons to available *FEMA P-58* materials (e.g., exterior stucco, gypsum wallboard) as well as gain much needed information on the repair costs for sheathing materials that are not included in the *FEMA P-58* fragility database (e.g., plaster on wood lath). The results of the damage workshop allowed for cross comparison with existing *FEMA P-58* repair-cost consequence functions as well as expanding the range of consequence functions for repair costs of older wood-frame dwellings. Further, data from the workshop supported use of the assumed building replacement cost of \$200/ft^2.

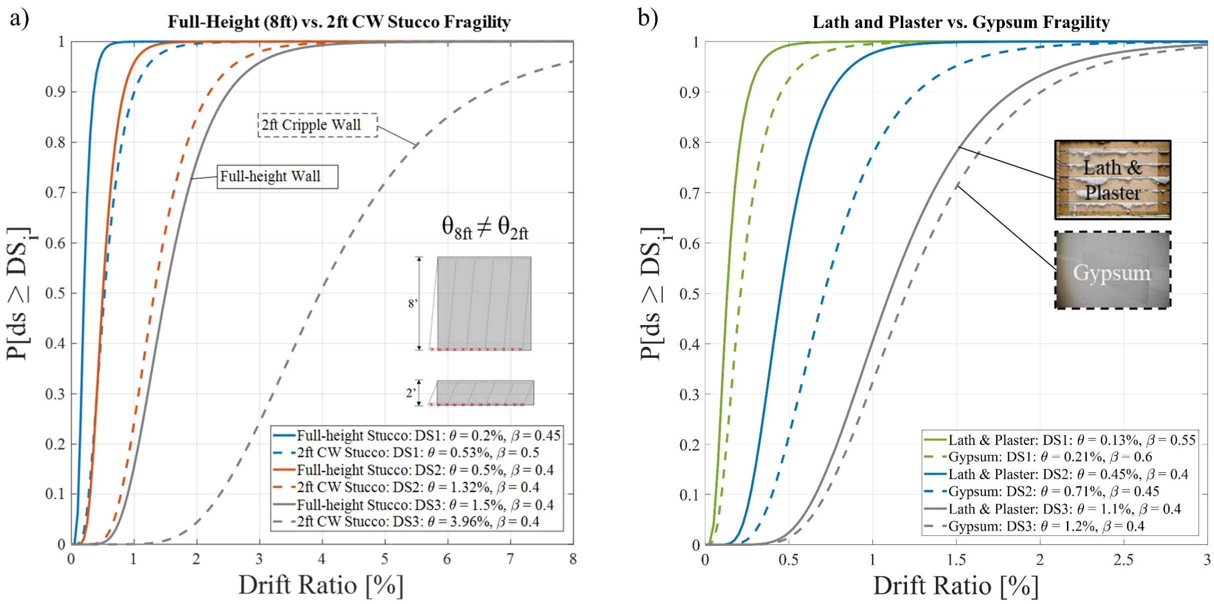

Figure V Damage fragility adjustments: (a) height-dependent relationship to capture damageability of shorter stucco walls; and (b) revised lath and plaster fragilities compared to gypsum wallboard.

An important consideration for the assessment of cripple wall dwellings is the consequences and cost of repair associated by failure (collapse) of the cripple wall. Supported by reconnaissance reports following earthquakes, the economic consequences of cripple wall failure can vary widely. In the best-case scenario, the cripple wall fails without significantly damaging the flooring or occupied stories such that the house can be lifted back to position, the cripple wall rebuilt, and the utilities reconnected. At the other extreme, the failing cripple wall may cause significant racking damage to flooring and interior walls, resulting in a total loss. Based on previous studies, practitioner surveys, and reconnaissance review, the cost of repairing a failed cripple wall is estimated to range from approximately 33% to 100% (total loss) of building replacement cost. Based on input from the Project Advisory Team, in calculating the loss (damage) functions, the cripple wall failure is assumed to incur a cost equal to 67% of house replacement value. The ability to vary this assumption and investigate the sensitivity to other loss ratios is maintained within project documentation.

The resulting loss models for the Index Building variants are expressed in terms of three outputs:

- *Mean Loss* (Damage) *Curves* – The average (mean) loss, expressed in percent of house replacement cost, as a function of ground-motion shaking intensity, described in terms of spectral acceleration at 0.25 sec. This relationship is often referred to as a “damage function” by catastrophe risk modelers.
- *Expected Annual Loss* (EAL) – The expected (mean) loss, due to the risk of earthquake damage, calculated on an annualized basis. This value is obtained through integration of the mean loss versus intensity curve with the site hazard curve that relates ground-motion shaking intensity to an annual rate of exceedance.

- *Expected RC250 Loss* – The mean repair cost for earthquake shaking with a return period of 250 years (RC250). This is an intensity-based metric that represents the average loss for earthquake ground shaking with a specified return period. The 250-year return period was selected as a representative point of comparison based on discussion with catastrophe risk modelers.

Note that the expected annual loss and expected RC250 loss values depend on the site where they are calculated since their calculation involves the site-specific seismic hazard curve. While the mean loss curves were calculated using ground motions that were selected and scaled for specific sites, the curves are less site-specific since they are expressed as a function of ground-shaking intensity. Comparisons between curves computed for the unretrofitted Index Buildings at the four sites are similar, especially between the three highly seismic sites (San Francisco, Los Angeles, and San Bernardino). However, since the cripple wall retrofit design (e.g., nail spacing, wood structural panel brace length, etc.) is based on the site-specific hazard, mean loss curves for the retrofitted cases differ between the four sites.

An illustration of the loss metrics to demonstrate the impact of seismic cripple wall retrofitting are shown in Figure VI. The figure shows two existing (unretrofitted) and retrofitted pairs of one-story houses with 2-ft-tall cripple walls with wood siding and stucco exteriors. The structures represent the later 1956–1970 construction era with gypsum wallboard interior walls, and the ground motions and retrofit design are for the San Francisco site. The loss curves in Figure V(a) show the effect of seismic retrofitting of the cripple wall by comparing the solid (unretrofitted) and dashed (retrofitted) lines across a range of seismic intensities. The influence of the different exterior materials (stucco versus wood siding) is shown through comparison of the different line colors (orange for wood siding; green for stucco). The expected annual loss and expected RC250 loss metrics are shown as bar charts in Figure VI(b) and Figure VI(c), respectively.

The unretrofitted and retrofitted values are overlaid such that the difference between the solid bars and hatched bars illustrate the reduced losses achieved by the retrofitting. For example, in the wood siding house, retrofitting the cripple wall reduces the expected annual loss by about 0.6% replacement value (from 0.67% to 0.10%), and the expected RC250 loss by about 40% (from 45% to 5%). Based on the house replacement value of $240,000, the 40% reduction corresponds to about a $96,000 reduction in loss. The large reduction in loss is primarily associated with the reduced risk of cripple wall failure with the seismic retrofit. There is a significant reduction in losses with the retrofit for both cases, although the benefit is higher for the house with wood siding (orange) compared to stucco (green) since the cripple wall with wood siding is much weaker than with stucco.

Losses for the primary set of eight Index Building variants are compared in terms of expected annual loss and expected RC250 loss in Figures VII and VIII, respectively. The figures present wood siding and exterior stucco of one- and two-story variants grouped by construction era. The two bounding eras are represented (i.e., pre-1945 and 1956–1970), where the small cut away in the icons for the pre-1945 era signifies that these variants have plaster on wood lath interior wall material, whereas the more modern 1956–1970 era have gypsum wallboard interiors. The different exterior cladding and interior wall materials affect the weight (seismic mass), strength, stiffness, damageability, and associated repair costs. The color-coded column bars represent the four index sites of Bakersfield, San Francisco, Northridge, and San Bernardino, presented in order of increasing seismicity. Note that the Bakersfield site has significantly lower seismicity as compared to the other three.

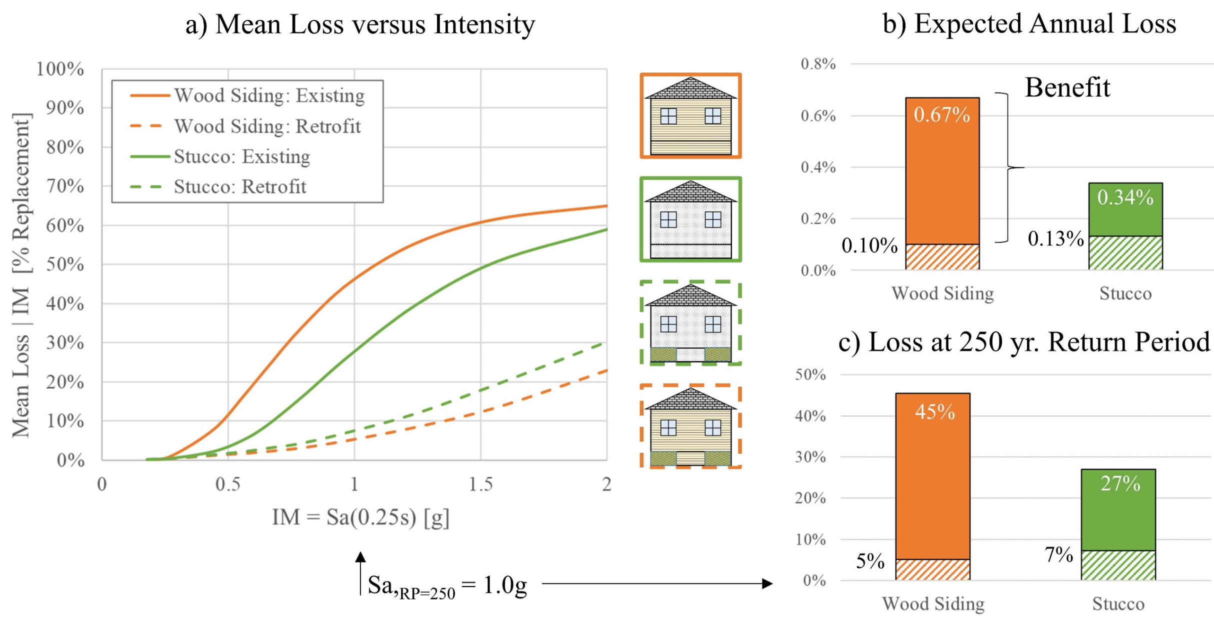

Figure VI **Example of primary performance outputs for 1956–1970 era one-story houses with 2-ft-tall cripple walls located in San Francisco showing the effect of seismic retrofit: (a) mean loss (damage) curve; and (b) expected annual loss; and (c) expected RC 250 loss.**

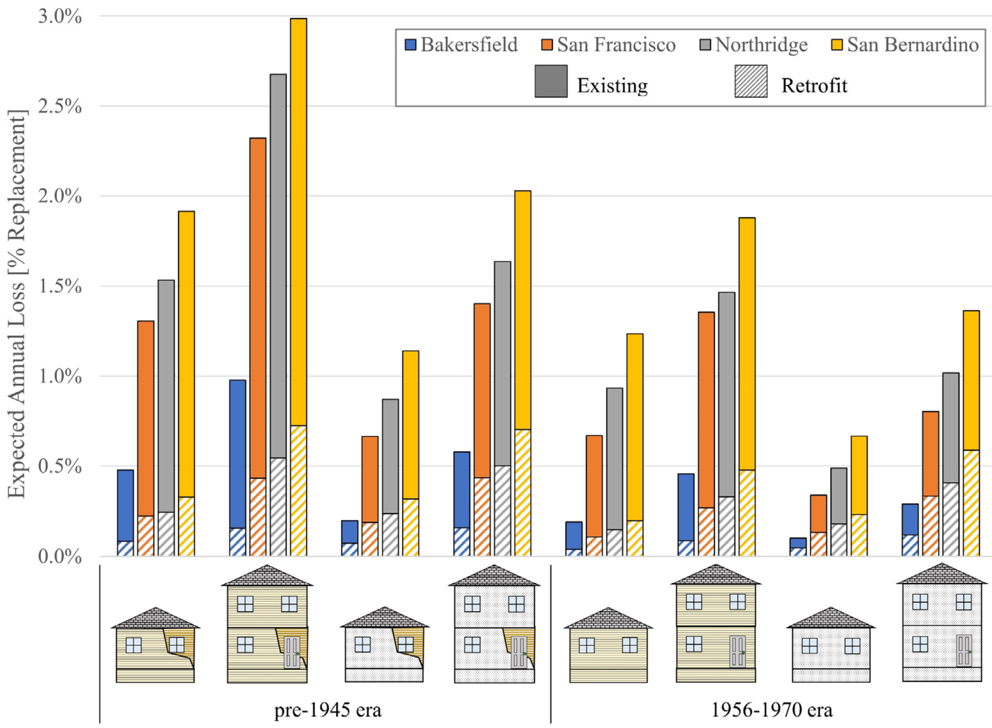

Figure VII Expected annual loss results for houses with cripple walls.

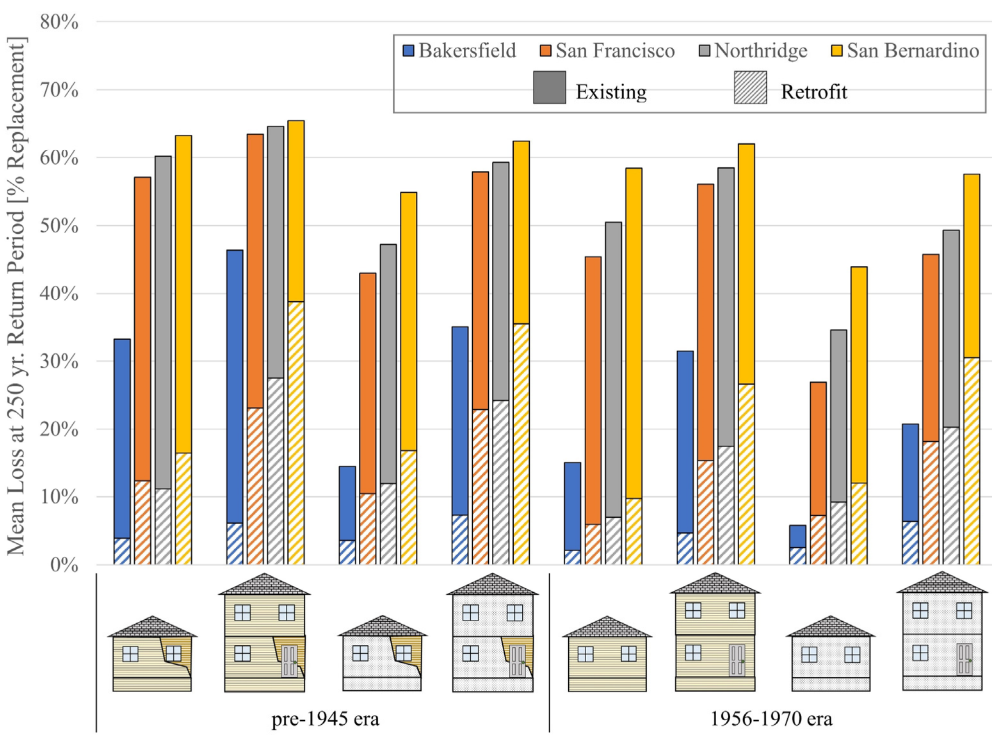

Figure VIII Expected RC250 loss for houses with cripple walls.

The general findings and observations for cripple wall dwellings can be summarized as the following:

- *Influence of Exterior Material* –Wood siding cripple wall dwellings without retrofit are more susceptible to damage and losses compared to equivalent stucco exterior cases. For example, under design level (250-year return period) shaking in regions of high seismicity, the collapse probabilities and expected losses for houses with wood siding range from 10% to 100% higher than for houses with stucco exteriors. This due to the lower strength of the wood siding cripple walls. Accordingly, houses with wood siding generally benefit the most from retrofitting the cripple walls. For houses with retrofitted cripple walls, the damage and losses are comparable for wood siding and stucco houses, since their superstructure strengths do not differ as much between wood and stucco exteriors, due the presence of common interior wall types. In fact, in some cases the retrofitted stucco houses experience slightly higher losses due to the lower drift damage threshold and higher repair costs for stucco, as compared to wood siding. However, these slight differences are much less than the overall reduction in losses achieved by retrofitting the vulnerable cripple walls.

- *One-Story versus Two-Story Houses* – As expected, the performance of two-story houses is worse compared to one-story houses, primarily because the weight (mass) of the second story effectively doubles the imposed earthquake forces on the cripple walls and first-story walls. For the existing (unretrofitted) cases, the two-story houses begin to experience cripple wall damage, collapse, and associated losses at much lower seismic intensities (i.e., accelerations) as compared to equivalent one-story houses. For example, under design level (250-year return period) shaking in regions of high seismicity, the collapse probabilities for existing two-story houses range from 10% to 30% higher than for one-story houses, and the expected losses (normalized by replacement value) range from 10% to 70% higher for the two-story houses. The two-story houses with retrofitted cripple walls also experience higher losses as compared to one-story cases, although the differences between the two vary more depending on the exterior and interior wall materials and level of seismicity. Since the retrofitted cripple wall design accounts for the differences in building weight, the retrofitted cripple walls are much stronger for the two-story as compared to one-story configurations. This stronger retrofit allows higher forces to be developed in the first occupied story of the superstructure, with the net effect being that displacements and damage in the retrofit cases shift from the cripple wall into the first story of the superstructure. However, it is important to note that the damage in the first story of the retrofitted houses initiates at much higher seismic intensity as compared to damage and collapse in the cripple walls of non-retrofitted houses.

- *Influence of Interior Wall Material* – Older pre-1945 variants with plaster on wood lath interior walls generally experience more damage and losses than the 1956–1970 era houses with gypsum drywall interiors. For example, under design level (250-year return period) shaking in regions of high seismicity, the collapse probabilities are about 10% to 30% higher for pre-1945 era compared to 1957–1970 era houses, and the expected losses (normalized by replacement value) range from 10% to 60% higher for the pre-1945 era houses. While plaster on wood lath interior is generally stronger and stiffer than gypsum wallboard, it is significantly heavier, more easily damaged, and more expensive to repair than gypsum wallboard. The increased mass of houses with plaster and wood lath leads to larger seismic forces in the cripple walls. Similar to the situation with two-story houses, the larger seismic inertial forces lead to cripple wall damage and collapse at lower ground-motion intensities for non-retrofitted cripple walls. The differences are less for retrofitted houses since the retrofit design of the cripple walls accounts for the seismic forces associated with the heavier plaster interior walls. Thus, the increase in damage and losses for wood lath and plaster compared to gypsum wallboard is more significant for unretrofitted cripple wall cases as compared to the retrofitted cases.

- *Site Seismicity* – As expected, the overall risk of losses and the benefits of cripple wall retrofit are larger for sites with higher seismicity, i.e., for the San Francisco, Northridge, and San Bernardino sites, as compared to the Bakersfield site. But, even in Bakersfield, the benefits of the cripple wall retrofit are significant. The smallest benefit occurs in the one-story 1956–1970 stucco house, where the overall losses are low and the reduction in the Expected RC250 Loss from the seismic retrofit is about 3% of the house replacement value (about $7500).

In addition to the parameters considered in the comparisons in Figures VII and VIII, the study also evaluated the effect of the following factors on the performance of houses with vulnerable cripple walls: roof weight, cripple wall height, T1-11 siding, and variability in the expected strength and stiffness of structural response. In general, the structural response and resulting damageability of the houses were not surprising. For example, the presence of heavy tile roofs or lower strength/stiffness compared to the expected values increased susceptibility to damage. Comparisons of houses with different height cripple walls indicate that taller cripple walls (e.g., 6 ft-tall) are less susceptible to damage and collapse than shorter (e.g., 2-ft-tall) walls, which is attributed to larger displacement capacity, less susceptibility to P-delta collapse, and longer elastic fundamental periods. Houses clad with T-11 siding, which is observed in houses constructed in the 1956–1970 era, had performance between that of comparable houses with wood siding or stucco cladding.

This study also investigated the benefits of anchorage retrofit to older houses with stem wall foundations. These houses have a crawlspace below the first-floor framing, which is created by a concrete or masonry "stem" wall, where there is a potential vulnerability at the connection between the first-floor framing (i.e., floor joists) to the wooden sill plate and its attachment to the stem wall (i.e., foundation). Retrofitting of sill plate connections can eliminate this vulnerability by installing framing-to-sill clips and foundation anchor bolts (or other anchorage devices). The main observations for seismic damage and losses related to retrofit of stem wall connections are summarized as follows:

- *Stem Wall versus Cripple Wall* – Houses with deficient stem wall connections are generally observed to be less vulnerable to earthquake damage than equivalent unretrofitted cripple walls with the same superstructure. This reflects the fact that typical stem wall connections (i.e., toe-nails and friction between the floor joists and sill plate) are inherently more resistant to failure than unbraced cripple walls. Further, the consequence of damage to the stem wall connections is generally less than that associated with failure of cripple walls. In many of the cases that were studied, damage to the stem wall connection was limited to small to moderate sliding displacements, repairs of which are less extensive as compared to cripple wall damage and collapse. Even in the most extreme cases where the house slides off the stem walls, the damage and required repairs are assumed to cost less than the 67% replacement cost assumed for cripple wall collapses.

- *One-Story versus Two-Story Stem Wall* – Owing to the lower vulnerability in unretrofitted stem walls as compared to cripple walls, the expected benefits for retrofitting of stem walls are less than for retrofitting equivalent houses with cripple walls but still significant relative to the cost of the retrofit. The one-story houses with stem walls are observed to show benefits due to retrofitting that range from almost no benefit for the Bakersfield site with relatively low seismicity to slight benefits for the higher seismicity sites. For example, at the San Francisco site, retrofitting of the stem wall connection reduced the mean repair cost for the 250-year return period hazard from about 8–14% (of house replacement value) for the non-retrofitted case to 4–6% with the retrofit (savings on the order of $14,000 for a one-story house). Results for two-story houses with stem wall show mixed results, where in some cases the stem wall connection retrofit slightly increases the losses compared to unretrofitted stem wall cases. For example, at the San Francisco site, the losses for the two-story houses range at the 250-year return period hazard change from about 15–16% for the non-retrofitted cases to 15–23% for the retrofit cases. This is explained by the fact that the damage and losses calculated for the two-story stem wall houses typically occur in the first story. In some cases, the unretrofitted cases experience connection failure and sliding, which results in a base isolation effect for the superstructure, such that the repair costs for the stem wall connection failure are offset by reduced repairs in the superstructure. It should be noted, however, that the net differences in these cases is small and subject to assumptions made in the analysis models. Should the actual stem wall connections be weaker than assumed, leading to larger sliding displacements of the unretrofitted cases, or should the superstructure be stronger than assumed, then the retrofitting would reduce the losses and provide a net benefit.

As summarized in this report, seismic retrofitting of unbraced cripple walls can significantly reduce the risk of earthquake damage and repair costs to one- and two-story residential houses. An important additional benefit is the reduced risk of major damage that can displace residents from their house. Seismic retrofit of sill plate connections for stem-wall foundations can also reduce losses, though not to the same extent as the seismic retrofit of cripple walls.

While the structural and loss analyses employ the latest technologies, data, and methods for performance-based engineering, there are significant uncertainties in each step of the analysis—from characterization of the seismic hazard, through structural analysis and estimation of damage and repair costs. Most of the analyses are based on mean values of the expected damage or loss for typical conditions, which are primarily intended for estimates of overall losses over large inventories of houses. Owing to the inherent diversity of housing and uncertainties in response and damage estimates, the actual damage and losses for individual houses are likely to vary considerably, on the order of plus/minus 50% from the expected values. For example, whereas the expected loss for cripple wall failure is assumed to be 67%, data suggest that the actual loss could range from 30% to 100% of the house replacement value. Nevertheless, the comparative estimates of expected losses provide robust and compelling evidence of the cost-effectiveness of seismic retrofit of houses with unbraced cripple walls and/or vulnerable sill-plate connections.

ACKNOWLEDGMENT AND DISCLAIMER

ACKNOWLEDGMENT

This research project benefited from the interaction of many researchers and practitioners. The authors would like to thank the following project team members for their input and feedback Yousef Bozorgnia, Jack Baker, Henry Burton, Kelly Cobeen, Seb Ficcadenti, Bret Lizundia, Curt Haselton, Tara Hutchinson, Grace Kang, Charlie Kircher, Thor Matteson, Frank McKenna, Vahid Mahdavifar, Silvia Mazzoni, Gilberto Mosqueda, Sharyl Rabinovici, Evan Reis, Brandon Schiller, Chia-Ming Uang, John van de Lindt, and Farzin Zareian. The assistance and feedback of the Project Review Panel consisting of Colin Blaney, Doug Hohbach, John Hooper, and Charles Scawthorn is greatly appreciated. Support from the CEA team members Shawna Ackerman, Janiele Maffei, Badie Rowshandel, Erin Rogers and their Advisory Team Members Tom Heaton, Brian McDonald, John Osteraas, and Keith Porter is gratefully acknowledged. The authors also acknowledge the assistance of Joseph Harijanto and Zhengxiang Yi during the various stages of the Project. Finally, the assistance and feedback with performance assessment programs from Katie Wade and Ed Almeter at HBRisk as well as Adam Zsarnoczay at Stanford University is also gratefully appreciated.

DISCLAIMER

This research study was funded by the California Earthquake Authority (CEA). The support of CEA is gratefully acknowledged.

The opinions, findings, conclusions, or recommendations expressed in this publication are those of the authors and do not necessarily reflect the views of the CEA, Pacific Earthquake Engineering Research Center (PEER), members of the Project Team, or the Regents of the University of California.

CONTENTS

LIST OF TABLES

LIST OF FIGURES

1 Introduction

1.1 PROJECT OVERVIEW

This report is one of a series of reports documenting the methods and findings of a multi-year, multi-disciplinary project coordinated by the Pacific Earthquake Engineering Research Center (PEER) and funded by the California Earthquake Authority (CEA). The overall project is titled "*Quantifying the Performance of Retrofit of Cripple Walls and Sill Anchorage in Single-Family Wood-Frame Buildings*," henceforth referred to as the "PEER-CEA Project."

The overall objective of the PEER–CEA Project is to provide scientifically based information (e.g., testing, analysis, and resulting loss models) that measure and assess the effectiveness of seismic retrofit to reduce the risk of damage and associated losses (repair costs) of wood-frame houses with cripple wall and sill anchorage deficiencies as well as retrofitted conditions that address those deficiencies. Tasks that support and inform the loss-modeling effort are: (1) collecting and summarizing existing information and results of previous research on the performance of wood-frame houses; (2) identifying construction features to characterize alternative variants of wood-frame houses; (3) characterizing earthquake hazard and ground motions at representative sites in California; (4) developing cyclic loading protocols and conducting laboratory tests of cripple wall panels, wood-frame wall subassemblies, and sill anchorages to measure and document their response (strength and stiffness) under cyclic loading; and (5) the computer modeling, simulations, and the development of loss models as informed by a workshop with claims adjustors.

Within the PEER–CEA Project, detailed work was conducted by seven Working Groups, each addressing a particular area of study and expertise, and collaborating with the other Working Groups. The seven Working Groups are the following:

Working Group 1: Literature Review

Working Group 2: Index Buildings

Working Group 3: Ground Motions and Loading Protocol

Working Group 4: Experimental Testing

Working Group 5: Structural Analysis and Loss Modeling

Working Group 6: Interaction with Claims Adjustors and Catastrophe Modelers

Working Group 7: Reporting

This report is a product of Working Group 5 (WG5): *Structural Analysis and Loss Modeling*. This working group handled: (1) the development, calibration, and analysis of structural models of building variants; (2) development earthquake damage and loss model parameters for component-based damage fragilities and repair cost functions for components of the building variants; and (3) calculation and compilation of resulting damage (loss) functions and scalar loss metrics for the building variants. This report summarizes background information for the modeling techniques, analysis assumptions, and assumptions made for developing loss models for different building variants. Finally, results of the structural and loss analyses are presented and discussed.

The WG5 report presented herein represents a collaborative effort between all working groups involved on the project. The working group interaction is shown in Figure 1.1. The solid arrows represent the nominal ordering of working groups, which separates the project tasks into a logical linear progression beginning from literature review and ending with seismic loss estimation considerations for building variants, including interaction with catastrophe modelers working within the insurance industry. Importantly, the dashed lines in Figure 1.1 represent the numerous interactions between working groups that were critical in achieving the Project's goals.

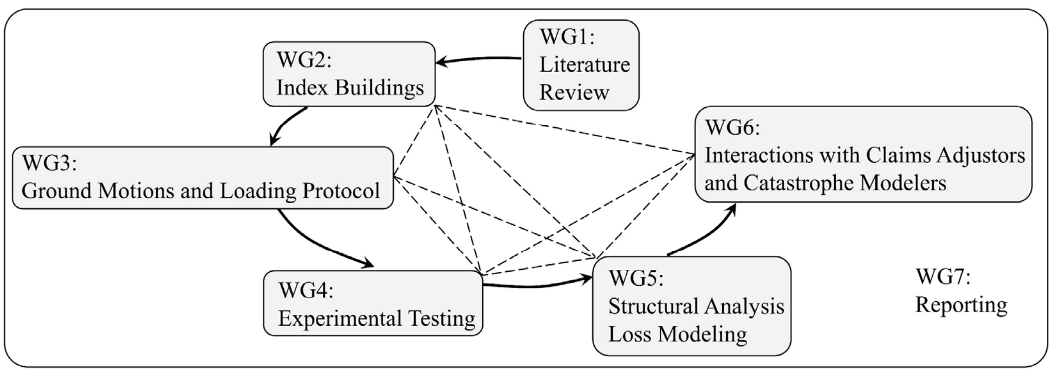

Figure 1.1 Illustration of the linear flow of information within working group structure (arrows) and the numerous interactions between working groups throughout the project (dashed lines).

1.2 BACKGROUND

This report discusses the structural analysis and seismic damage and loss assessment of existing (unretrofitted) and retrofit crawlspace dwellings. With the intent of estimating the possible benefits of seismic retrofit of a specific classification of residential structure, some key background information is provided in order to give the reader a better sense of the previous work upon which this research is founded. The *FEMA P-1100* guidelines [FEMA 2018]—used to define the level of seismic retrofitting—are first introduced followed by a brief discussion of the *FEMA P-58* [FEMA 2012] framework that serves as the basis for estimating seismic losses. Finally, a brief overview of HAZUS [NIBS 1997] is provided to illustrate the current trends and treatment of seismic loss assessment on a regional scale.

1.2.1 *FEMA P-1100* Prestandard

The *FEMA P-1100 Vulnerability-Based Seismic Assessment and Retrofit of One- and Two-Family Dwellings* [FEMA 2018] represents the guidelines by which retrofit of crawlspace dwellings is followed within the PEER–CEA Project. *FEMA P-1100* is the result of the ATC-110 project that targeted a number of known seismic vulnerabilities in residential dwellings including: crawlspace dwellings, living-space-over-garage dwellings, hillside dwellings, and masonry chimneys.

The main purpose of the *FEMA P-1100* document is to provide guidance on performing assessments for each type of vulnerability (to identify whether retrofit is required) and also to provide guidelines on how the retrofit can be detailed and implemented. Depending on the vulnerability, the assessment approach can be simplified, detailed, or engineered. Similarly, the retrofit design can be prescriptive or engineered. For example, crawlspace and living-space-over-garage dwellings provide plan sets for prescriptive retrofit design that can be implemented when eligibility criteria are met; otherwise, a simplified engineering retrofit design must be performed. In contrast to the other conditions, hillside dwellings do not have prescriptive design plan sets, and the retrofit design must be performed using simplified engineering analysis.

The PEER–CEA Project focuses on crawlspace dwellings that are defined within *FEMA P-1100* as a dwelling in which:

1. the space below the lowest framed floor is predominantly unoccupied, including area enclosed by crawlspace walls, open areas, or a combination of the two;
2. the tallest crawlspace cripple wall clear height does not exceed 7 ft-0 in.; and
3. when averaged across the full length or width of the dwelling the grade slope does not exceed 1 vertical in 5 horizontal.

Crawlspace dwellings may use the prescriptive plan set [FEMA 2019(a)] provided that all eligibility criteria are met. The current project will be dealing with archetype buildings that are assumed to be eligible for prescriptive retrofit according to *FEMA P-1100* [2018] for details. The crawlspace dwelling plan set varies the design according to four basic parameters, namely: site seismicity, number of stories, building weight class, and cripple wall height. Note that the *FEMA P-1100* requirements also address the retrofit of sill plate connections, where the first-floor framing is supported directly on the foundation stem wall.

The site seismicity is determined according to the Seismic Design Category (SDC) as defined by ASCE/SEI 7 Chapter 11, *International Residential Code* (IRC) Section R301.2.2.1 [ICC 2018]. For prescriptive retrofit designs, dwellings falling into SDC B through E are eligible for using the prestandard. The plan set uses three distinct values of short-period design spectral acceleration (S_{DS}). These values are 1.0g, 1.2g, and 1.5g, and are referred to within the plan set as "Seismic", "High Seismic," and "Very High Seismic", respectively. Dwellings in SDC B through D_1 are classified as "Seismic" and have an S_{DS} = 1.0g. Dwellings in SDC D_2 are classified as "High Seismic" and have an S_{DS} = 1.2g. Dwellings in SDC E are classified as "Very High Seismic" and have an S_{DS} = 1.5g. Alternatively, the S_{DS} may be obtained according to ASCE/SEI 7, provided that the next highest plan set value be used for intermediate cases. For S_{DS} values greater than 1.5g, plan set schedules for S_{DS} = 1.5g are permitted for use.

The crawlspace dwelling plan set schedules are separated by seismicity and number of stories, where only one- and two-story dwellings are considered eligible for prescriptive retrofit (a total of 6 sheets are provided [FEMA 2019(a)]). To navigate the retrofit schedule sheets, the dwellings weight classification must be determined. The weight classification flow chart from *FEMA P-1100* is reproduced here as Figure 1.2. The flow chart begins by identifying the exterior finish of the dwelling, distinguishing between stucco (or plaster) and wood siding (or shingle) exterior. Then the roofing material must be classified as either concrete tile or asphalt shingle (or composition) roofing. The final step in determining the weight classification is the interior wall material, where the two nominal choices are plaster or gypsum wallboard interior. Based on these three steps, the dwelling can be classified as either "Heavy", "Medium," or "Light". These choices represent the most common configurations of materials and further discussion of estimating weight classification is provided in *FEMA P-1100* [2018].

To obtain the appropriate design detail, the plan set retrofit schedules require some of the geometric details of the dwelling. The floor area of the house, in combination with weight classification allows for the appropriate row of the plan set sheet to be determined; see Figure 1.4. Further, the design details vary for the two different types of crawlspace dwellings, which are cripple wall and stem wall. For cripple wall dwellings, the plan set specifies the required amount of wood structural panel (WSP) sheathing to be applied in each corner of the cripple wall as well as the number of anchor bolts and floor-to-cripple wall connectors (see left of Figure 1.3). The required length of WSP is a function of cripple wall height and whether the design will include tie-down devices. For stem wall dwellings, the plan set specifies the required number of joist-to-sill connectors and sill-to-foundation anchors; see right of Figure 1.3.

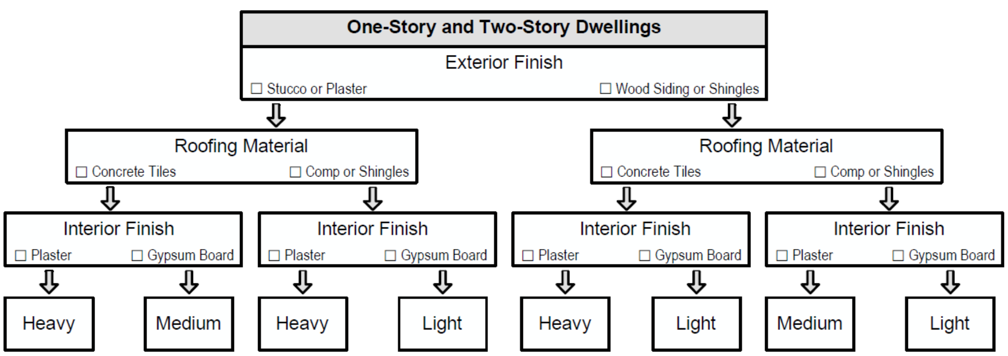

Figure 1.2 **Weight classifications for using *FEMA P-1100* prescriptive retrofit plan sets for crawlspace dwellings (image adapted from FEMA [2019(b)].**

An example plan set retrofit schedule table is shown in Figure 1.4 for one-story dwellings with S_{DS} = 1.2*g* (i.e., high seismic) governing the design details. The figure shows that the plan set covers a range of floor plan sizes (<800 to 3000 ft^2 for one-story) and cripple wall heights (0 to 7 ft). Further, a range of connector types for force transfer elements are considered to cover availability of materials and adapt to various conditions found in the field. The plan sets also provide numerous detailing options (e.g., blocking, plate splices, and framing-to-foundation) to accommodate a variety of situations expected when performing a seismic retrofit on an existing (unretrofitted) crawlspace dwelling.

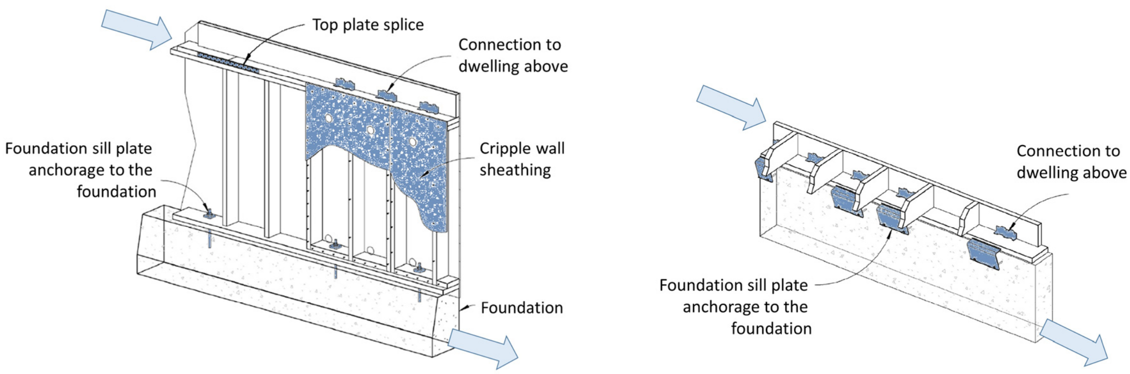

Figure 1.3 **Different force-resisting elements of a crawlspace dwelling retrofit: cripple wall (left) and stem wall (right). Images adapted from FEMA [2018].**

EARTHQUAKE RETROFIT SCHEDULE (S_{DS}= 1.2 High Seismic) ONE-STORY

① Weight Category	② Total Area in Square Feet	③ ☒ Mark row that applies	⑤ Length Each of Two Braced Wall Sections Required Along Each Perimeter Wall Line — Wood Structural Panels — ④ Cripple Wall Height: up to 1' Without Tie-downs	1'-1" to 2' Without Tie-downs	2'-1" to 4'-0" Without Tie-downs	2'-1" to 4'-0" With Tie-downs	4'-1" to 6'-0" Without Tie-downs	4'-1" to 6'-0" With Tie-downs	6'-1" to 7'-0" Without Tie-downs	6'-1" to 7'-0" With Tie-downs	Panel Edge Nailing	Number of Foundation Connectors or Anchors at Each Perimeter Wall Line, Assume Distributed Along Length — ⑥ Foundation Sill Anchors: Type "A"	Type "B"	Type "C"	1/2"ø Bolt	5/8"ø Bolt	⑦ Floor to Cripple Wall or Floor to Foundation Sill: Type "D"	Type "E" or "F"	Type "G"
1-Story Light Construction	up to 800		6.7'	6.7'	8.0'	6.7'	10.7'	6.7'	10.7'	8.0'	4"	5	8	8	8	6	13	12	16
	801 to 1000		6.7'	8.0'	9.3'	6.7'	12.0'	8.0'	12.0'	8.0'	4"	6	9	10	10	7	15	15	19
	1001 to 1200		8.0'	8.0'	10.7'	8.0'	13.3'	9.3'	13.3'	9.3'	4"	7	11	12	12	8	18	17	22
	1201 to 1500		9.3'	9.3'	12.0'	9.3'	14.7'	10.7'	16.0'	10.7'	4"	8	13	14	14	10	21	20	27
	1501 to 2000		12.0'	12.0'	14.7'	12.0'	17.3'	12.0'	18.7'	13.3'	4"	10	16	18	18	12	27	26	34
	2001 to 2500		14.7'	14.7'	17.3'	14.7'	20.0'	14.7'	21.3'	16.0'	4"	12	19	21	21	15	33	31	41
	2501 to 3000		17.3'	17.3'	18.7'	17.3'	21.3'	17.3'	22.7'	17.3'	4"	14	23	25	25	17	38	37	48
1-Story Medium Construction	up to 800		5.3'	6.7'	9.3'	6.7'	10.7'	8.0'	12.0'	8.0'	3"	6	9	10	10	7	15	15	19
	801 to 1000		6.7'	8.0'	10.7'	6.7'	12.0'	8.0'	13.3'	9.3'	3"	7	11	12	12	8	18	17	23
	1001 to 1200		8.0'	8.0'	10.7'	8.0'	13.3'	9.3'	14.7'	10.7'	3"	8	12	13	13	9	21	20	26
	1201 to 1500		9.3'	9.3'	12.0'	9.3'	14.7'	10.7'	16.0'	12.0'	3"	9	15	16	16	11	24	23	31
	1501 to 2000		10.7'	12.0'	14.7'	10.7'	17.3'	13.3'	18.7'	14.7'	3"	12	18	20	20	14	30	29	39
	2001 to 2500		13.3'	13.3'	17.3'	13.3'	20.0'	14.7'	21.3'	16.0'	3"	14	22	24	24	16	36	35	46
	2501 to 3000		14.7'	14.7'	18.7'	14.7'	21.3'	17.3'	22.7'	18.7'	3"	16	25	27	27	19	42	40	53
1-Story Heavy Construction	up to 800		6.7'	8.0'	9.3'	6.7'	12.0'	8.0'	12.0'	9.3'	2"	7	10	11	11	8	17	17	22
	801 to 1000		6.7'	8.0'	10.7'	8.0'	13.3'	9.3'	14.7'	10.7'	2"	8	12	14	13	9	21	20	26
	1001 to 1200		8.0'	9.3'	12.0'	9.3'	14.7'	10.7'	16.0'	12.0'	2"	9	14	16	15	11	24	23	30
	1201 to 1500		9.3'	10.7'	13.3'	10.7'	16.0'	12.0'	17.3'	13.3'	2"	11	17	18	18	13	28	27	36
	1501 to 2000		10.7'	13.3'	16.0'	12.0'	18.7'	14.7'	20.0'	16.0'	2"	13	21	23	23	16	36	34	45
	2001 to 2500		13.3'	14.7'	18.7'	13.3'	21.3'	16.0'	22.7'	17.3'	2"	16	25	28	28	19	43	41	54
	2501 to 3000		14.7'	16.0'	20.0'	16.0'	22.7'	18.7'	25.3'	20.0'	2"	19	29	32	32	22	50	48	63

Figure 1.4 **Example retrofit plan set schedule sheet for crawlspace dwellings within *FEMA P-1100* [2019(a)]. Current table is for one-story dwellings with S_{DS} = 1.2*g*.**

1.2.2 *FEMA P-58* Methodology for Building-Specific Performance Assessment

The *FEMA P-58 Seismic Performance Assessment of Buildings* [2012] is a multi-volume document representing the state-of-the-art methodology for building-specific seismic loss estimation and performance assessment. The multi-staged building-specific performance assessment framework outlined by the *FEMA P-58* guidelines [2012] is based on prior research by PEER [Porter 2003, 2006; Moehle and Deierlein 2004] and earlier research on assembly-based vulnerability assessment [Porter and Kiremidjian 2001]. A key aspect of the *FEMA P-58* methodology is that damage and losses are determined for individual components of a building based on earthquake demands estimated using structural analysis. A key feature of the framework is that every stage of the seismic performance assessment (i.e., from site hazard to repair costs) treats the variables as probabilistic distributions, allowing for the uncertainties in each stage to be preserved and carried through the assessment.

The basic staging of information in the *FEMA P-58* assessment process is illustrated in Figure 1.5. The process begins with facility definition, where the building is defined in terms of materials, design criteria, and local site conditions. This is followed by the four primary analysis stages. Beginning with hazard analysis, the site location and soil conditions are used to define the seismicity of the site, typically using probabilistic seismic hazard analysis (PSHA), which relates the likelihood of seismic demands in terms of an intensity measure (*IM*) that is appropriate for the building or facility. An intermediate step between hazard analysis and structural analysis is the selection of appropriate ground motions to represent the site hazard and analyze structural models. The structural analysis stage involves the development of numerical models in order to capture the seismic response of the structure, resulting in probabilistic distributions of engineering demand parameters (*EDP*) such as story drift ratio (*SDR*) or peak floor accelerations (*PFA*) that can be related to damage and collapse potential. The distributions of EDP response are then used for the damage analysis stage, where the damageable assemblies are attributed damage fragilities that relate the appropriate damage measure (*DM*) of different assemblies to the EDP response of the structure. Finally, the loss analysis stage allows for the estimates of damage and collapse potential to be translated into meaningful decision variables (*DV*) that quantify the seismic performance in terms of metrics useful for making decisions about the current structure or design. Three common decision metrics are direct reconstruction and repair costs, restoration time (time to make repairs), and casualties.

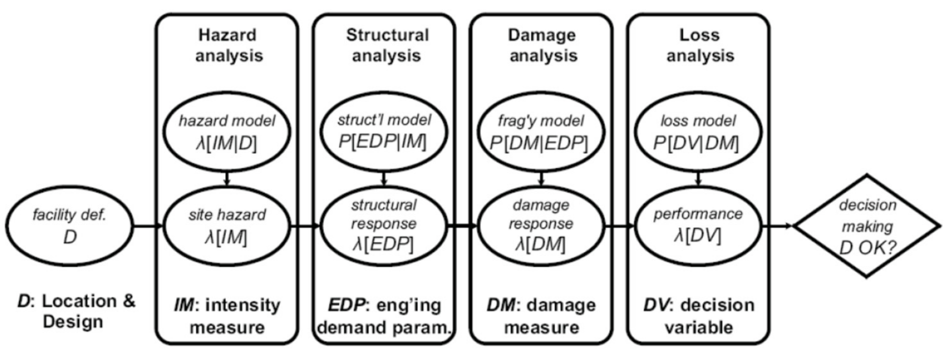

Figure 1.5 **Flow chart of the four analysis stages for seismic performance assessment according to *FEMA P-58* (figure after Porter [2003]).**

The general probabilistic approach for the framework can be illustrated mathematically as shown in Equation (1.1) for the annual probability of exceeding a given *DV* for an assumed site and structure using the total probability theorem:

$$\lambda[DV|D]=\iiint p[DV \mid DM]\cdot p[DM \mid EDP]\cdot p[EDP \mid IM]\cdot\lambda[\mathrm{IM}]\cdot dIM\cdot dEDP\cdot dDM \qquad (1.1)$$

where $p[X|Y]$ represents the probability density of X conditioned on Y, and $\lambda[X]$ is the mean annual exceedance frequency of X. As pointed out by Moehle and Deierlein [2004], the expression of the framework in the triple integral format is a rather concise way of illustrating a very complex problem. However, the transfer of information through the various analysis stages shown in Figure 1.5 reflects the multi-disciplinary nature of the framework. Although requiring that each analysis stage treat variables in a probabilistic manner, the framework is of a very open nature, allowing for each stage to be tailored to the specific structural type or performance metrics of interest, while incorporating new developments from each stage in order to improve the accuracy and reliability of assessments.

1.2.3 HAZUS and Regional Assessment

In contrast to the *FEMA P-58* methodology that is primarily geared to detailed performance evaluation of individual buildings, HAZUS [NIBS 1997; Whitman et al. 1997] is geared to catastrophe risk modeling of large building inventories and regional analyses. HAZUS regional assessments are based on building damage (loss) functions that have been developed based on a combination of loss data from past earthquakes, simplified structural and loss analysis, and judgment [Kircher et al. 1997]. For single-family residential houses, HAZUS has one category of damage functions (W1), which applies to one- and two-story houses, distinguished between four categories (High-Code, Moderate-Code, Low-Code, and pre-Code) based on the building code requirements and practices to which the buildings are assumed to have been designed [HAZUS 2013]. In high seismic regions of coastal California, the W1 category is distinguished into three sub-categories corresponding to date of construction (Post-1975, 1941–1975, and pre-1941). The HAZUS W1 damage functions have been calibrated through comparison to observed performance and losses to residential houses from the 1994 Northridge earthquake [Kircher et al. 1997].

While the HAZUS W1 damage functions offer an obvious point of comparison to this Project, they have several important limitations and shortcomings. First and foremost, while the W1 functions provide some distinction based on assumed lateral strength and stiffness (e.g., High- versus pre-Code), they do not explicitly address the vulnerability due to unbraced cripple walls or weak foundation anchorages. They also do not explicitly distinguish between the different types of exterior and interior wall finish materials, i.e., stucco versus wood siding exteriors or gypsum board versus wood lath and plaster interior walls. Finally, the W1 category does not distinguish between number of stories (i.e., one- and two-story houses are lumped into a single category), which are known to significantly affect their seismic response and damage [Heresi and Miranda 2019]. In contrast to the standard HAZUS damage curves, the HAZUS Advanced Engineering Building Module (HAZUS-AEBM) [Kircher et al. 2006], allows for the HAZUS damage functions to be modified and customized for specific building types and detailing. However, implementation of the HAZUS-AEBM approach to address cripple wall and stem wall vulnerabilities of wood houses is not straightforward, and its underlying static pushover analysis basis would likely not capture the cyclic degradation and other effects that are more directly simulated using the nonlinear response history analyses and *FEMA P-58* damage and loss models employed in this study.

1.3 OBJECTIVES AND SCOPE

1.3.1 Objectives

The overall objective of this study is to develop damage (loss) functions of residential houses to quantify the reduction in risk to damage and economic losses that can be achieved by seismically retrofitting deficient cripple wall and foundation sill plate conditions. This overall objective encompasses the following tasks:

- Design and investigate a set of building variants, which generally represent the one- and two-story residential housing stock in California that can benefit from retrofit of deficient cripple wall and foundation sill plate connections. Essentially, this involves translating the Index Building characteristics summarized in the report by WG2 [Reis 2020(a)] into specific house designs (without and with seismic retrofits) to be modeled and evaluated in this study;
- Develop seismic hazard data and ground motions used to design the seismic retrofits and simulate the structural response of the building variants to earthquakes. This task requires close coordination with WG3 to: (1) identify appropriate locations in California, based on their seismic hazard characteristics and relationship to the seismic retrofit categories of the *FEMA P-1100* plan sets; and (2) the approach to characterizing the seismic hazard and selecting ground motions for use in nonlinear dynamic structural analyses of the building variants;
- Develop idealized mathematical models and perform nonlinear dynamic structural analyses of the one- and two-story house variants. This task involves a detailed review of existing literature to develop modeling strategies and criteria to simulate the response of one- and two-story houses, considering the types and configurations of structural materials in the foundation connections, cripple walls, and superstructure. The task involves coordination with WG4 to identify important gaps where laboratory tests are needed and to incorporate data from tests conducted by WG4 on unretrofitted and retrofitted cripple walls, connections, and superstructure components;
- Synthesize, review, develop and apply building component damage and repair cost functions to translate structural response into damage and loss estimates for the one- and two-story house variants. This task involves a critical review of the existing *FEMA P-58* damage and loss functions, and extensions of the functions to address the specific issues arising in houses with vulnerable cripple wall and sill plate foundation connections. The review includes coordination with WG6 on a workshop with claims adjustors to validate the *FEMA P-58* loss functions; and
- Execute the nonlinear structural analyses, damage, and loss calculations for the building variants to obtain pairs of building damage (loss) functions and loss statistics, comparing the response and losses in the original and seismically retrofitted condition. The loss functions were integrated with site hazard curves to calculate annualized scalar loss metrics (e.g., expected annual loss) and also

used to report discrete intensity-based metrics (e.g., expected RC250 loss) for evaluating the economic benefits of risk reduction by seismic retrofitting.

Overall, about thirty pairs (with and without retrofit) of building variants were investigated in this study. The calculations involved several hundred thousand nonlinear dynamic structural analyses of the building variants, results of which are input into probabilistic Monte Carlo damage and loss assessment calculations. The structural analyses are performed using the *OpenSees* software [McKenna et al. 2000], and the loss calculations are performed using the NHERI SimCenter's *pelicun* software implementation [Zsarnoczay 2019] of the *FEMA P-58* methodology. The *pelicun* implementation of the *FEMA P-58* calculations was verified against independent calculations using the *SP3* software [HBrisk 2020]. The computations were conducted by running computational workflows on the Sherlock High Performance Computing cluster at Stanford University [Sherlock, 2020].

1.3.2 Building Variants for Analysis

The development of the building variant scope for numerical analysis considered available information within the literature regarding residential inventory and construction trends in California, as well as typical considerations within the insurance industry. The initial collection of possible variants focused on having a significant impact on seismic damage and, more importantly, having the differential in seismic losses due to retrofitting be affected by the presence of the variant. Preliminary variants included both primary and secondary modifiers applicable to the insurance industry. Primary variants include easily accessible and documented information for residential homes such as the number of stories and era of construction. Secondary variants can be observable, such as the exterior material of the home, or unobservable, such as the presence of horizontal or diagonal wood sheathing beneath the exterior finish. Initial development of the building variant list also drove the scope for experimental testing, with subsequent test data and accompanying numerical studies informing decisions on important variants to maintain throughout the course of the project. More detailed information on the development of the initial building variant list for numerical analysis can be found within the WG2 report [Reis 2020(a)].

The project considers three eras of construction ranging from pre-1945 to 1956–1970. The main distinction for construction era is the interior material, with the earliest era assuming lath and plaster interior and the later assuming gypsum wallboard. The intermediate era represents the transition period where both materials were commonly used, and this era of construction was not analyzed explicitly. Exterior materials consist of exterior stucco, horizontal wood siding, and T1-11 (panelized plywood) siding. Notably, building variants with T1-11 exterior are only considered applicable to the 1956–1970 era and assume a gypsum wallboard interior. The different cripple wall heights range from 2-ft- and 6-ft-tall cripple walls to a "zero-height" or stem wall condition, including cases with vulnerable anchorage between the superstructure and a perimeter stem wall. An illustration of the main building variants considered within the numerical analysis scope are shown in Figure 1.6.

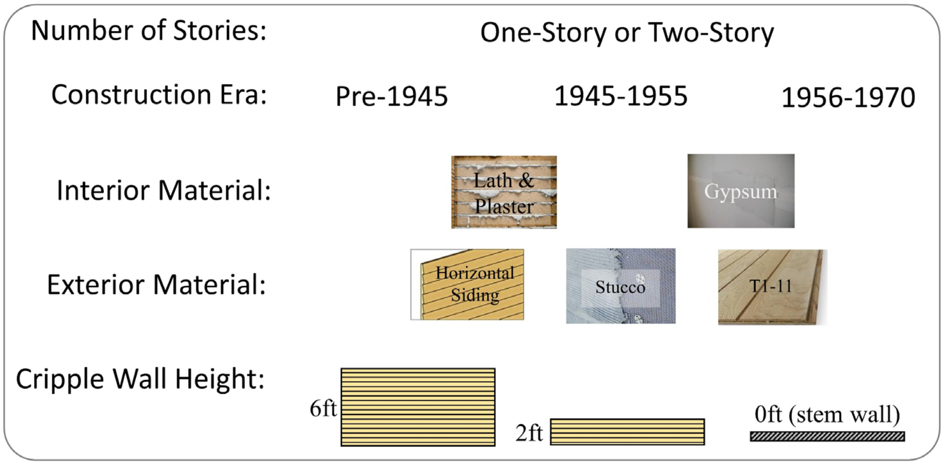

Figure 1.6 Illustration of the principal building variants investigated within the numerical analysis scope.

Each of the building variant combinations in Figure 1.6 have an existing and retrofitted pair, representing the unretrofitted and retrofitted crawlspace. All retrofitting details were implemented according to the recent *FEMA P-1100* prestandard [2018] developed from the ATC-110 project; see Section 1.2.1.

In addition to assumed materials and crawlspace details, the configuration and layout of the archetype dwellings was a key component to the building-specific loss assessment of crawlspace dwellings. The role the configuration of the dwelling played in the performance assessment process is illustrated graphically in Figure 1.7. Consider a single building variant combination from those shown in Figure 1.6 (e.g., single-story pre-1945 era, light roof construction, 2-ft-tall cripple walls, stucco exterior, and lath and plaster interior). These will determine the structural weights (i.e., seismic mass) and material properties required for interior and exterior sheathing (i.e., strength and stiffness). Further, when combined with an assumed site hazard, the total building weight and cripple wall geometry will be combined with seismic design loads to develop the appropriate retrofitting scheme. These properties can then be combined into the analytical models where the mass, strength, and stiffness will be in proportion to the variant properties assumed. This proportioning is critical since it will affect both structural response (i.e., EDP response) as well as loss model development. The types of interior and exterior sheathing materials will drive component fragility selection while the amount of interior and exterior walls (governed by the assumed configuration) will determine the damageable quantities to be combined with component consequence (i.e., repair cost) functions.

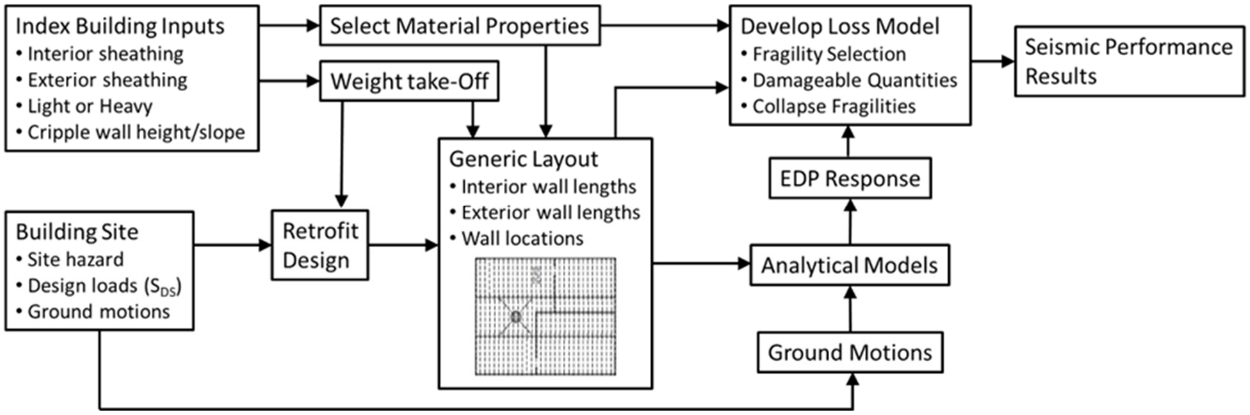

Figure 1.7 Flow chart highlighting the importance of the dwelling layout to the various stages of seismic performance assessment for crawlspace dwellings.

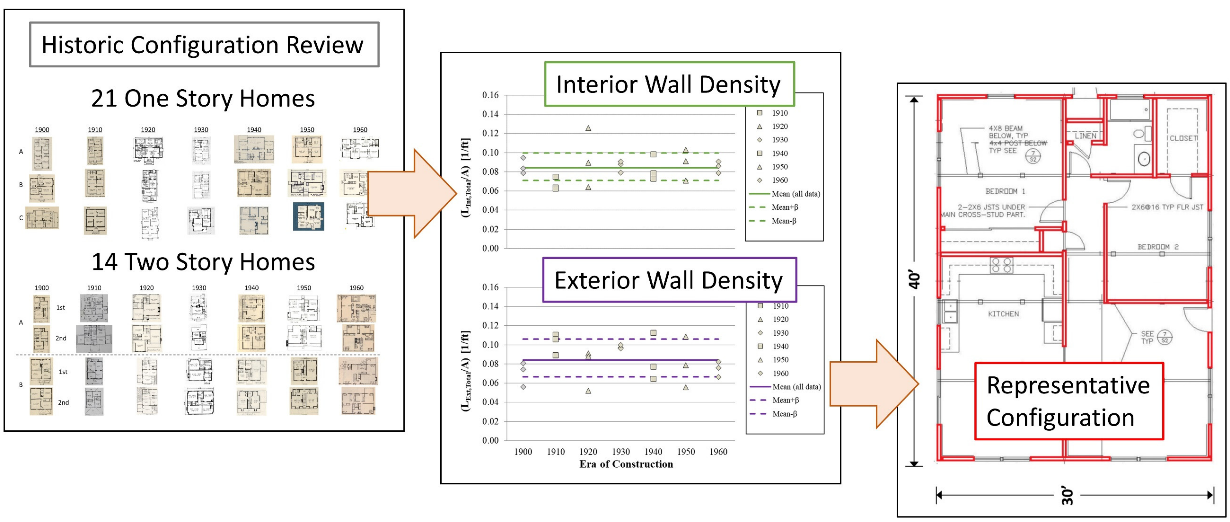

Figure 1.8 Summary illustration of the development and verification of representative superstructure configurations based on actual plan configurations from historic homes.

Consistent with the ATC-110 project, the current project targeted a small-to-moderate-sized plan area of 1200 ft^2 with an aspect ratio of 0.75 (i.e., 40 ft × 30 ft). Geometrical data from the ATC-110 project was collected for a number of one- and two-story homes from archived housing catalogs ranging in construction era from 1900 to 1969. This data was used in to maintain realistic interior and exterior wall densities as well as relative wall densities from first to second stories of two-story dwellings. Baseline configurations were selected and developed using this information, with a mean configuration targeted. The floor plan of one-story variants and the first story of two-story variants were based on the "CUREE Small House" that was designed, modeled, and analyzed during the CUREE-Caltech Woodframe Project [Isoda et al. 2002; Porter et al. 2002; Reitherman and Cobeen 2003]. The second story of two-story variants has a symmetrical layout in terms of assumed exterior openings and locations of interior walls. The percentage of openings in the second story is assumed to be 15% less than the first story based on findings from the configuration data. A summary illustration of the development of superstructure configurations based on historic data is shown in Figure 1.8. In interests of brevity, the entire configuration study is not developed and discussed within the main report. An in-depth discussion of the configuration study is presented in Appendix A. Details of the assumed configuration and implementation within numerical models are provided in Chapter 2.

1.3.3 Site Hazard and Ground Motions

The assumed building sites used for analysis of building variant models consist of a sub-set of the ten sites provided by WG3 [Mazzoni et al. 2020]. The selected building sites are Bakersfield, San Francisco, Northridge, and San Bernardino, and are all assumed to be located on Soil D with a target upper 30-m shear-wave velocity (V_{S30}) of 270 m/sec. These sites were selected to cover the range of seismicity levels within the *FEMA P-1100* crawlspace dwelling plan sets [2019(a)], i.e., with short period seismic design base shears, S_{DS}, equal to 1.0, 1.2, and 1.5*g*. A full description of site hazard description and probabilistic seismic hazard analysis assumptions for the sites can be found within the WG3 report [Mazzoni et al. 2020].

Each of the selected sites has a suite of 45 ground-motion pairs (two horizontal components each) for ten intensity levels with return periods of 15, 25, 50, 75, 100, 150, 250, 500, 1000, and 2500 years, respectively. The target criteria for ground-motion selection assumes conditional spectra consisting of a conditional mean spectrum and conditional spectra variability at spectral periods away from the conditioning period (T^*). A constant short-period conditioning period of 0.25 sec is used for all sites and intensity levels. Further discussion of the ground-motion selection process is described within the WG3 report [Mazzoni et al. 2020]. Discussion of the selected building sites and ground-motion selection targets are provided in Chapter 4 of this report.

1.4 ORGANIZATION OF REPORT

The report is organized into seven chapters that provide details on each stage of the multi-step *FEMA P-58* implementation to assess the seismic performance of existing (unretrofitted) and retrofitted crawlspace dwellings. Chapter 2 covers the numerical modeling assumptions for nonlinear structural analyses to estimate the seismic response of building variants. Chapter 3 provides background on the development of material properties for the range of materials considered within the project scope; including the incorporation of new experimental data obtained from WG4, the experimental working group [Cobeen et al. 2020; Schiller and Hutchinson 2020]. Chapter 4 describes characterization of ground-motion hazard and record selection assumptions based on interactions with WG3, the ground-motion working group [Mazzoni et al. 2020]. Chapter 5 presents the damage fragility assumptions and models that were used to relate structural response to damage. Chapter 6 provides background information on repair costs and other economic considerations for developing loss models, as well as an overview of the performance assessment process. Chapter 7 summarizes the final results of the structural, damage, and loss analyses, and the resulting damage functions for the building variants considered in this study. Finally, Chapter 8 wraps up the report with a short summary of the key findings, concluding remarks, and discussion of future work.

2 Numerical Modeling and Structural Analysis of Archetype Buildings

2.1 OVERVIEW

The damage and loss analyses are based on numerical simulations to estimate the seismic response of the one- and two-story house variants and understand the effectiveness of seismic retrofit. The structural analysis approach balances the available knowledge about the behavior of the wood-frame house systems and materials with state-of-the-art methods in nonlinear dynamic structural analyses. This chapter covers the various aspects of the structural modeling, including individual components of the numerical models, analysis assumptions and related considerations.

2.2 GENERAL NUMERICAL MODELING STRATEGY

The basic modeling approach employs three-dimensional macro-element or phenomenological elements [Jayamon et al. 2018], where the idealized model can be calibrated to force-displacement data from tests of structural wall panels and cripple wall sub-assembly tests. This type of approach has been widely used for the nonlinear dynamic response estimation of wood-frame structures with various objectives, including: quantification of collapse safety for seismic design [Rosowsky 2002; Christovasilis et al. 2009(a); Goda and Atkinson 2010], validation against shake table testing [Folz and Filiatrault 2004(b) (c); van de Lindt et al. 2010], quantification of modeling and design uncertainties [Yin and Li 2010; Pang and Shirazi 2012], and seismic loss assessment [Porter et al. 2002; Porter 2006; Pei and van de Lindt 2009; and Black et al. 2010]. This type of modeling is widely used for the nonlinear dynamic analysis of wood-frame structures since it reduces the order of complexity of the models to allow for feasible computational demands, while maintaining sufficient accuracy and resolution to represent the nonlinear response of structural components, systems, and force transfer mechanisms. This approach to creating nonlinear models for analysis of wood-frame buildings is used as an example within the recent publication by the National Institute of Standards and Technology *Guidelines for Nonlinear Structural Analysis and Design of Buildings* [NIST 2017].

The *OpenSees* software platform [McKenna et al. 2000] is used to model and carry out structural analysis of building variant models. The basic modeling concept is illustrated in Figure 2.1 for a one-story model with 2-ft-tall cripple walls. The figure shows that the layout and geometry of the structure is idealized in terms of the spatial distribution and lengths of walls, as well as the story height and plan dimensions. The model incorporates a series of nonlinear spring elements that represent the location and length of each wall. Material properties are based on calibrations to data from experimental tests of structural sub-assemblies and components. Details of the idealized *OpenSees* model implementation are described in the following sections.

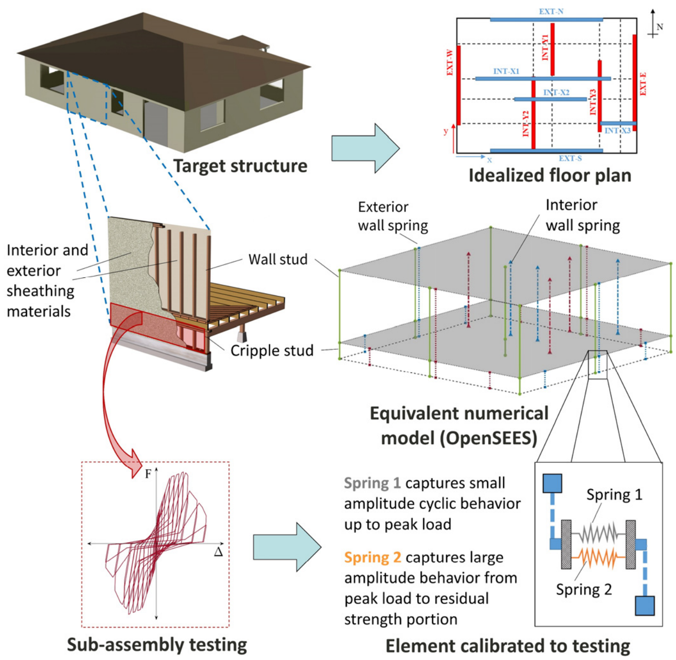

Figure 2.1 **Illustration of the three-dimensional macro-element modeling concept used for modeling and analysis of building variants.**

2.2.1 Modeling of Superstructure

The building variants are all based on a 40-ft (*X*-direction, east–west) by 30-ft (*Y*-direction, north–south) rectangular plan (A_{plan} = 1200 ft^2). The interior and exterior wall layouts (i.e., openings in exterior, locations of full-height partitions on interior) are the same for all variants. The superstructure story heights are assumed to be 9 ft, and the roof weight considered an 18-in. eave overhang and a hip roof with a 6:12 pitch.

Referring to Figure 2.2, the general node naming scheme is based on the grid locations created by intersecting *elasticbeamColumn* elements that create the rigid floor or roof diaphragm at each level. This grid is spaced in 5-ft increments and has grid locations 1 through 9 in the *X*-direction (east–west direction) and locations 1 through 7 in the *Y*-direction (north–south direction). This grid represents the locations for structural nodes for defining connectivity between the walls and floor or roof diaphragms. The "PlanID" for a given structural node is the *x*-grid number times ten plus the *y*-grid number. An illustration of PlanID for a node near the north–east corner of the plan is shown in Figure 2.2. To completely define a structural node in three dimensions, the elevation of the node is defined using "ElevID" that corresponds to the elevation level within the structure. The right portion of Figure 2.2 shows an example of the nodal definitions corresponding to PlanID of "86," i.e., 4086 for a node located at the roof level of a two-story variant, 3086 for the roof level of a one-story variant, etc. The ElevID values for top of a foundation and the underside of first floor framing are 1000 and 2000, respectively. Note that variants assumed to be on a rigid base only have nodes with the ElevIDs corresponding to diaphragm locations. In other words, a one-story on rigid base variant has the nodes with ElevID = 2000 connected directly to the ground and ElevID = 3000 still corresponds to the roof level. This is similar for the two-story variants on a rigid base. The use of a PlanID and ElevID to determine location of nodes is used for all building variant models. Notably, all models use the first translational degree of freedom (DOF) as the *x*-direction and the third translational DOF as the *y*-direction. The vertical direction is modeled as the second translational DOF in *OpenSees*.

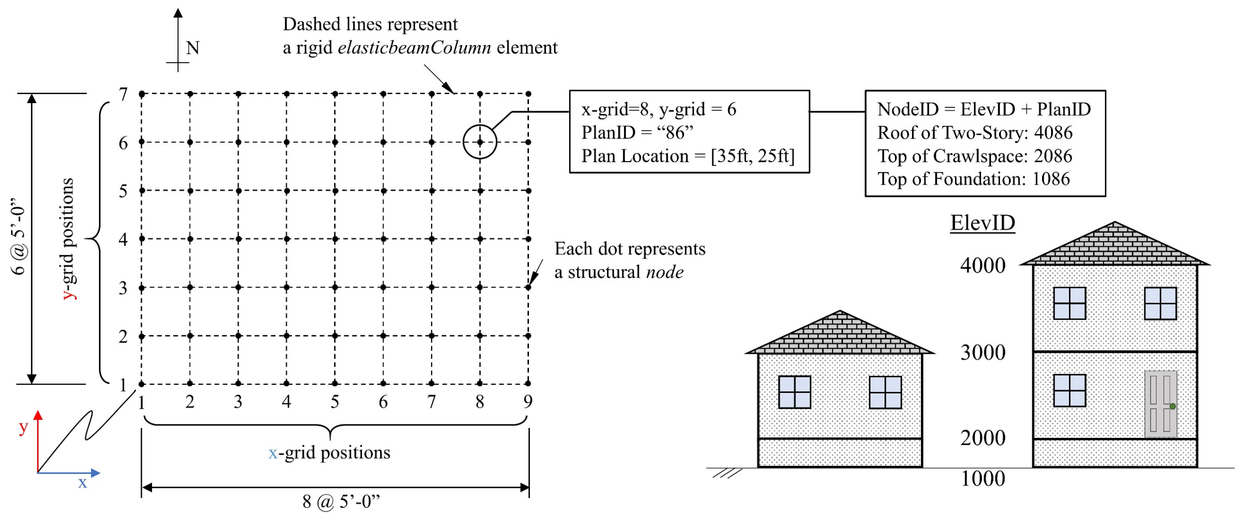

Figure 2.2 **Layout of a typical beam-column grid to represent floor and roof diaphragms that provides rigid-diaphragm behavior and locations for structural nodes (left); and illustration of node naming scheme (right).**

The assumed interior and exterior wall density of the first (or only) occupied story of the archetype superstructure models is presented in Figure 2.3(a). The figure separates interior and exterior walls and uses color to distinguish between the *x*- and *y*-directions. Each section of wall is modeled as a single material element with properties (defined in Chapter 3) that represent the effective wall length. The locations of the wall elements for the first occupied story are shown in Figure 2.3(b). Typically, exterior wall elements have base element identification numbers of 300000 and interior wall elements use 400000 for the occupied stories of the superstructure. Variants with horizontal wood siding exterior and gypsum wallboard interior assume superimposed materials, whereas all other exterior materials are based on testing of wall panels with combined materials (or assumed to be representative as such). Variant models with this material combination have an additional exterior wall element base identification of 305000. These elements represent the gypsum wallboard on the inside face of the exterior walls.

The second-story wall elements assume a symmetrical wall layout, assuming a larger wall density of exterior walls than the first story based on review of typical house designs. The wall layout for the second-story walls is shown in Figure 2.4(a). Similar to the first-story wall element identification, the second-story walls use the same base identification numbers yet continue the element numbering from the first-story walls. The wall element identification numbers are shown for the second-story superstructure walls in Figure 2.4(b). Summary tables illustrating the node connectivity of each wall element, plan location and assumed effective wall length are shown in Table 2.1 and Table 2.2 for exterior and interior superstructure walls, respectively.

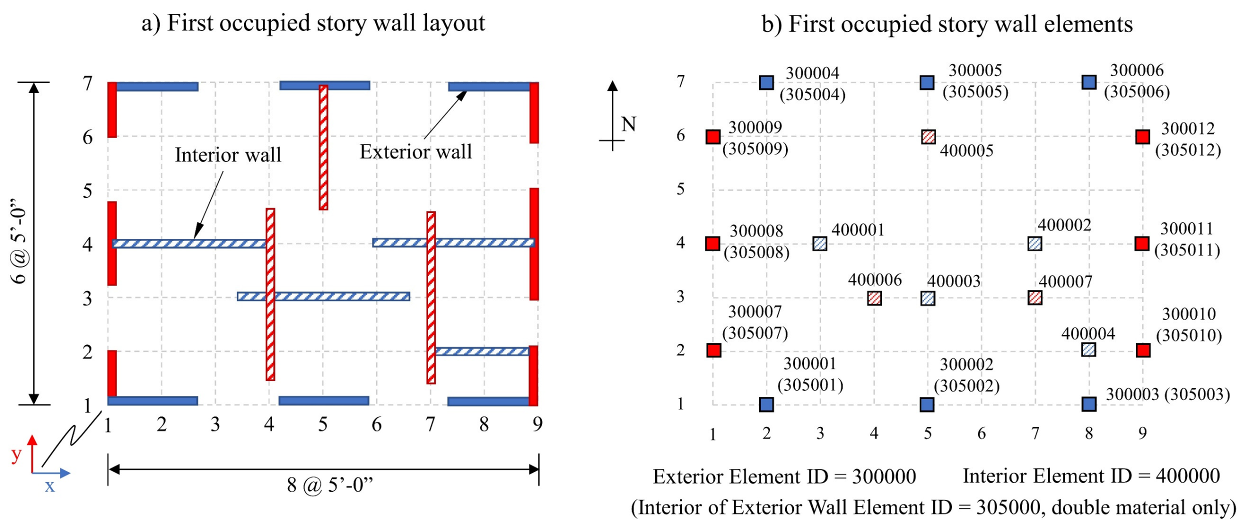

Figure 2.3 **Locations of walls assumed in the first occupied story of building archetype models: (a) general layout and length of walls: and (b) wall element positions and identification numbers used in *OpenSees*.**

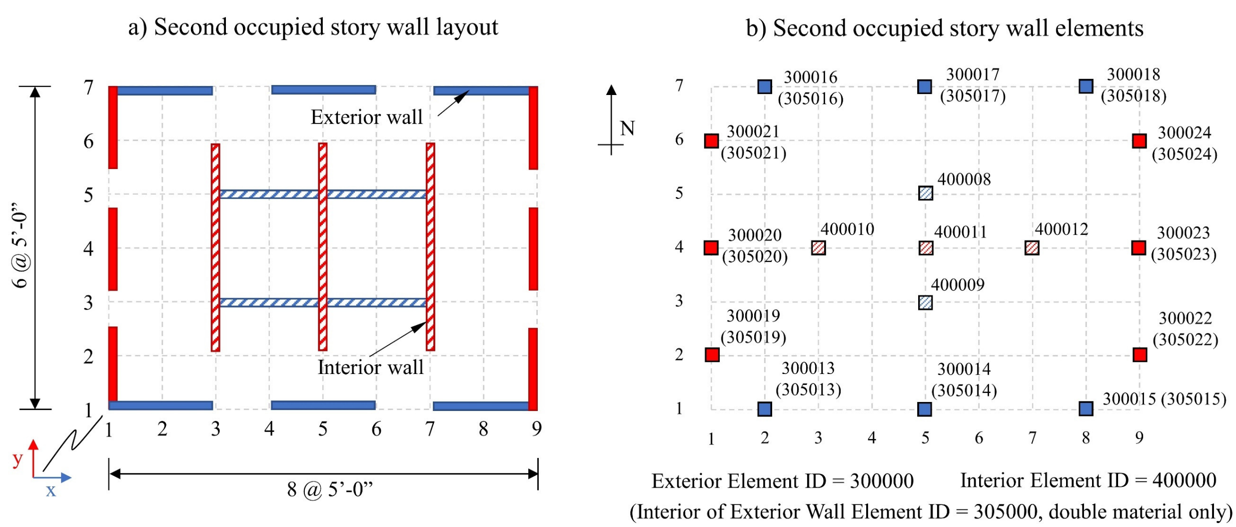

Figure 2.4 **Locations of walls assumed in the second occupied story of building archetype models (two-story archetypes only): (a) general layout and length of walls; and (b) wall element positions and identification numbers used in *OpenSees*.**

Table 2.1 Summary of exterior wall elements for modeling of the superstructure.

Wall type	Story	Direction	Element ID[1]	Node *i* [2]	Node *j* [2]	*x* (ft) [3]	y (ft) [3]	L_{wall} (ft) [4]
Exterior	1st	*X*	300001	2021	3021	5	0	8.33
Exterior	1st	*X*	300002	2051	3051	20	0	8.33
Exterior	1st	*X*	300003	2081	3081	35	0	8.33
Exterior	1st	*X*	300004	2027	3027	5	30	8.33
Exterior	1st	*X*	300005	2057	3057	20	30	8.33
Exterior	1st	*X*	300006	2087	3087	35	30	8.33
Exterior	1st	*Y*	300007	2012	3012	0	5	5.00
Exterior	1st	*Y*	300008	2014	3014	0	15	7.67
Exterior	1st	*Y*	300009	2016	3016	0	25	5.00
Exterior	1st	*Y*	300010	2092	3092	40	5	5.50
Exterior	1st	*Y*	300011	2094	3094	40	15	10.33
Exterior	1st	*Y*	300012	2096	3096	40	25	5.50
Exterior	2nd	*X*	300013	3021	4021	5	0	9.58
Exterior	2nd	*X*	300014	3051	4051	20	0	9.58
Exterior	2nd	*X*	300015	3081	4081	35	0	9.58
Exterior	2nd	*X*	300016	3027	4027	5	30	9.58
Exterior	2nd	*X*	300017	3057	4057	20	30	9.58
Exterior	2nd	*X*	300018	3087	4087	35	30	9.58
Exterior	2nd	*Y*	300019	3012	4012	0	5	7.50
Exterior	2nd	*Y*	300020	3014	4014	0	15	7.50
Exterior	2nd	*Y*	300021	3016	4016	0	25	7.50
Exterior	2nd	*Y*	300022	3092	4092	40	5	7.50
Exterior	2nd	*Y*	300023	3094	4094	40	15	7.50
Exterior	2nd	*Y*	300024	3096	4096	40	25	7.50

[1] Exterior wall elements can be combined with an additional interior material element assuming superimposed wall materials. These elements have the same locations as exterior wall elements but with a base ID of 305000 (not provided in table).
[2] Node numbers for connectivity of the bottom (*i*) and top (*j*) of the wall element.
[3] Locations of the element in plan with respect to the origin taken as the Southwest corner of the plan layout.
[4] Total length of wall assumed for contribution to strength and stiffness, noting that the entire perimeter is considered for contribution to lateral mass and gravity load.

Table 2.2 Summary of interior wall elements for modeling of the superstructure.

Wall type	Story	Direction	Element ID[1]	Node i [2]	Node j [2]	x (ft) [3]	y (ft) [3]	L_{wall} (ft) [4]
Interior	1st	X	400001	2034	3034	10	15	15.00
Interior	1st	X	400002	2074	3074	30	15	15.00
Interior	1st	X	400003	2053	3053	20	10	16.00
Interior	1st	X	400004	2082	3082	35	5	8.00
Interior	1st	Y	400005	2056	3056	20	25	11.50
Interior	1st	Y	400006	2043	3043	15	10	16.00
Interior	1st	Y	400007	2073	3073	30	10	16.00
Interior	2nd	X	400008	3055	4055	20	20	20.00
Interior	2nd	X	400009	3053	4053	20	10	20.00
Interior	2nd	Y	400010	3034	4034	10	15	19.17
Interior	2nd	Y	400011	3054	4054	20	15	19.17
Interior	2nd	Y	400012	3074	4074	30	15	19.17

[1] Node numbers for connectivity of the bottom (*i*) and top (*j*) of the wall element.
[2] Locations of the element in plan with respect to the origin taken as the southwest corner of the plan layout.
[3] Total length of wall assumed for contribution to lateral mass and gravity load. Interior partition walls will use twice this length for strength and stiffness using materials developed based on single-sided properties.

2.2.2 Modeling of Existing and Retrofit Cripple Walls

The cripple walls are idealized by three evenly distributed wall panel elements along each side of the archetype building; see Figure 2.5(a). The wall element base identification for existing (unretrofitted) cripple wall elements is 100000. The plan location and element IDs for an existing cripple wall model with constant height is shown in Figure 2.5(b). A summary of node connectivity of wall elements, plan location, and effective wall length for the existing (unretrofitted) cripple walls is provided in Table 2.3.

Retrofit cripple wall variants have an additional element base identification of 105000 for the retrofit materials. The lengths of different cripple wall elements are controlled by the required amount of wood structural panel braced length (l_{WSP}) for the particular retrofit design, noting that this length varies according to the requirements of *FEMA P-1100*; see Section 1.2.1. This is illustrated in Figure 2.6(a) where the end elements in each corner represent the retrofit material and the center element of each side represents the difference of the total dimension and the required retrofit length. The element IDs used for cripple wall elements are shown in Figure 2.6(b). Table 2.4 presents the node connectivity and plan locations for cripple wall elements for the retrofitted case.

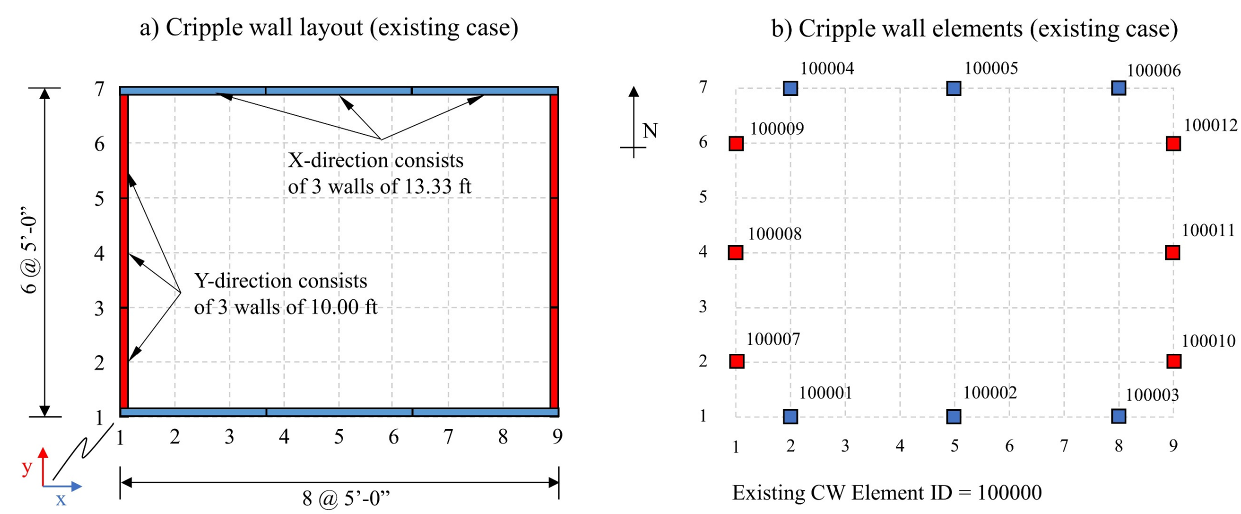

Figure 2.5 Locations of walls assumed for the existing (unretrofitted) cripple walls in archetype models: (a) general layout and length of walls; and (b) wall element positions and identification numbers used in *OpenSees*.

Table 2.3 Summary of cripple wall elements for modeling of the existing (unretrofitted) cripple wall variants.

Wall type	Story	Direction	Element ID[1]	Node i [2]	Node j [2]	x (ft) [3]	y (ft) [3]	L_{wall} (ft) [4]
CW-E [4]	Crawlspace	X	100001	1021	2021	5	0	13.33
CW-E	Crawlspace	X	100002	1051	2051	20	0	13.33
CW-E	Crawlspace	X	100003	1081	2081	35	0	13.33
CW-E	Crawlspace	X	100004	1027	2027	5	30	13.33
CW-E	Crawlspace	X	100005	1057	2057	20	30	13.33
CW-E	Crawlspace	X	100006	1087	2087	35	30	13.33
CW-E	Crawlspace	Y	100007	1012	2012	0	5	10.00
CW-E	Crawlspace	Y	100008	1014	2014	0	15	10.00
CW-E	Crawlspace	Y	100009	1016	2016	0	25	10.00
CW-E	Crawlspace	Y	100010	1092	2092	40	5	10.00
CW-E	Crawlspace	Y	100011	1094	2094	40	15	10.00
CW-E	Crawlspace	Y	100012	1096	2096	40	25	10.00

[1] Node numbers for connectivity of the bottom (i) and top (j) of the wall element.
[2] Locations of the element in plan with respect to the origin taken as the southwest corner of the plan layout.
[3] Total length of wall assumed for contribution to lateral mass, gravity load, strength, and stiffness.
[4] CW-E represents an existing (unretrofitted) cripple wall element.

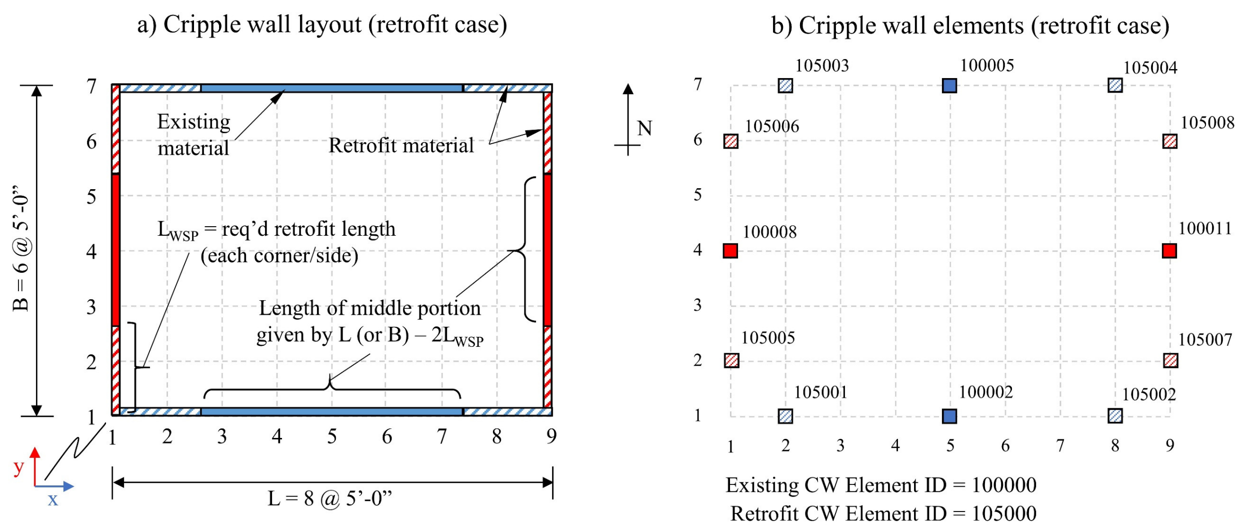

Figure 2.6 **Locations of walls assumed for the retrofit cripple walls in archetype models: (a) general layout and length of walls; and (b) wall element positions and identification numbers used in *OpenSees*.**

Table 2.4 **Summary of cripple wall elements for the retrofit cripple wall variants. Example case shown for a required retrofit panel length of 8 ft in each corner and side of the crawlspace.**

Wall type	Story	Direction	Element ID[1]	Node i [2]	Node j [2]	x (ft) [3]	y (ft) [3]	L_{wall} (ft) [4]
CW-R [4]	Crawlspace	*X*	105001	1021	2021	5	0	L_{WSP}=8.00
CW-E	Crawlspace	*X*	100002	1051	2051	20	0	24.00
CW-R	Crawlspace	*X*	105002	1081	2081	35	0	8.00
CW-R	Crawlspace	*X*	105003	1027	2027	5	30	8.00
CW-E	Crawlspace	*X*	100005	1057	2057	20	30	24.00
CW-R	Crawlspace	*X*	105004	1087	2087	35	30	8.00
CW-R	Crawlspace	*Y*	105005	1012	2012	0	5	8.00
CW-E	Crawlspace	*Y*	100008	1014	2014	0	15	14.00
CW-R	Crawlspace	*Y*	105006	1016	2016	0	25	8.00
CW-R	Crawlspace	*Y*	105007	1092	2092	40	5	8.00
CW-E	Crawlspace	*Y*	100011	1094	2094	40	15	14.00
CW-R	Crawlspace	*Y*	105008	1096	2096	40	25	8.00

[1] Node numbers for connectivity of the bottom (i) and top (j) of the wall element.
[2] Locations of the element in plan with respect to the origin taken as the southwest corner of the plan layout.
[3] Total length of wall assumed for contribution to lateral mass, gravity load, strength, and stiffness. These lengths are based on an *exemplary* required retrofit length (L_{WSP}) of 8 ft and lengths of existing portions are based on the plan dimensions of L = 40 ft and B = 30 ft in the x- and y-directions, respectively.
[4] CW-E represents an existing (unretrofitted) cripple wall element, and CW-R represents a retrofit cripple wall element.

2.2.3 Considerations for Modeling Stem Wall Anchorage

The modeling of stem wall dwellings—those dwellings with a raised perimeter foundation wall with the first-floor framing resting directly on the mudsill—requires a number of upfront assumptions. The first main assumption is that the vulnerability is concentrated at the interface of the first-floor framing (i.e., floor joists) to the mudsill on top of the perimeter foundation beams. This assumption is borne out by tests and calculations that show this connection to typically be more vulnerable than the mudsill-to-foundation connection, in addition to observed stem wall failures following seismic events. The current study assumes that the floor framing consists of 2 × 10 (nominal) floor joists spaced at 16 in. on center with joists running along the shorter 30-ft (y-direction) of the plan layout supported by two intermediate sub-floor beams. This assumes that joist end connections are along the 40-ft dimension of the perimeter foundation wall with blocking or end joists. Rim joists are assumed along the foundation in the shorter 30-ft dimension.

Joist connections are assumed to be three 8-penny (i.e., 3-8d) toe-nail connections for each joist end bearing on the sill plate. Rim joists are assumed to have single 8-penny toe-nail connections spaced at 24 in. on center along the end joist. The toe-nail connections are included in the model in terms of the number of full capacity toe-nail connections that contribute to the element location around the perimeter. Rim joist connections (i.e., single 8d toe-nails) are assumed to act in-plane only with respect to the direction of the perimeter foundation. Joist end connections (i.e., 3-8d toe-nails) are assumed to act in both orthogonal directions. The toe-nail connection elements are coupled with constant friction elements at each pair of structural nodes. More detailed discussion of the selection of material properties and additional assumptions is provided in Chapter 3. The remainder of this sub-section provides details on the structural modeling of stem wall variants.

The modeling assumptions for stem wall dwellings initially vary from cripple wall cases in the treatment of the first-floor diaphragm. Although still constructed as an array of rigid *elasticBeamColumn* elements, the node locations are coincidental in elevation with structural nodes representing the same locations on the sill plate around the perimeter foundation (modeled as fixed nodes within *OpenSees*). The first-floor diaphragm nodes are constrained from displacing in the vertical direction, where only relative horizontal movement is permitted between the first floor and foundation nodes. The horizontal DOF are connected through *zeroLength* elements, properties of which are selected to represent the strength and stiffness of the toe-nail connections and friction resistance.

The location of the different joist-to-sill toe-nail connections are illustrated in Figure 2.7(a). The figure shows the assumed location of joist bearing connections (3-8d toe-nails per joist) and rim joist connections (single 8d toe-nail spaced at 24 in. on center). Toe-nail elements have a base element identification of 500000. Toe-nail elements represent groups of toe-nails at different locations around the perimeter foundation. Material properties are attributed to these groups using properties normalized per toe-nail connection. The element IDs for toe-nail groups are shown in Figure 2.7(b). The current study assumed that only half of the toe-nail capacity could be relied on when comparing to laboratory testing for most cases considered; see Chapter 3. The number of toe-nails assumed in each element are provided in Table 2.5 and labeled $n_{TN,100\%}$ and $n_{TN,50\%}$ for full and half capacity assumptions, respectively. Similar to other model elements, Table 2.5 also provides node connectivity, plan location, and the assumed direction (or directions) the toe-nail resistance acts within the model.

The use of friction elements assumes that the entire perimeter contributes to a simplified constant friction force based on an assumed distributed dead load (i.e., normal force) and coefficient of friction; see Chapter 3 for input information. The perimeter is broken up into tributary lengths that correspond to the assumed locations of toe-nails groups as discussed previously. The tributary lengths and individual element IDs are shown for the friction elements in Figure 2.8, noting that the element base identification is 600000 for friction elements. The node connectivity, plan location, and assumed tributary length (L_{frict}) is summarized for all friction elements in Table 2.6.

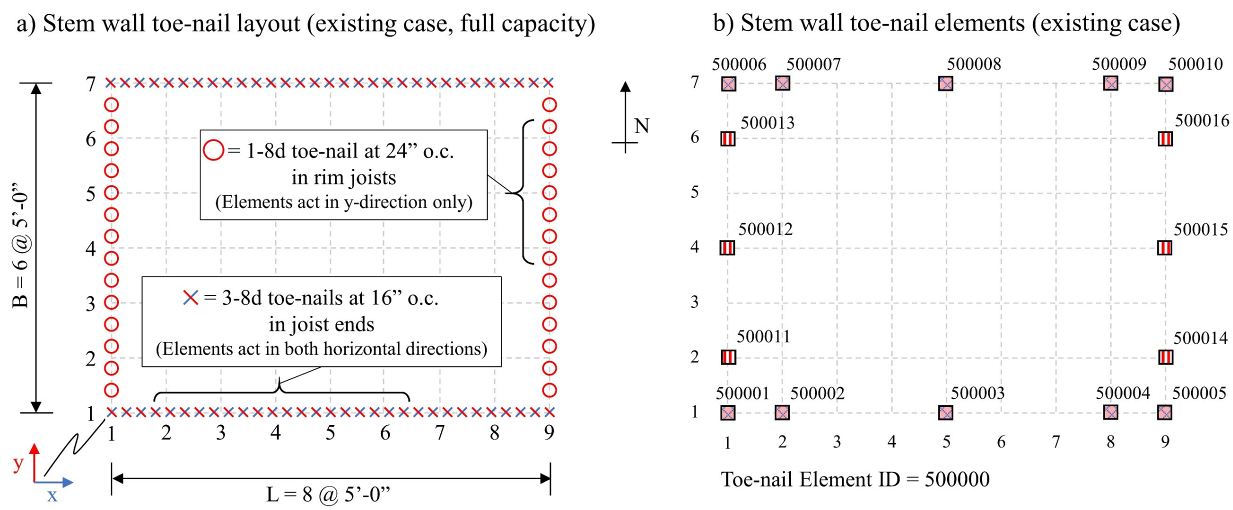

Figure 2.7 Locations of joist-to-sill toe-nail connections assumed for the existing (unretrofitted) stem walls in archetype models: (a) general layout and type of connection; and (b) lumped element positions and identification numbers used in *OpenSees*.

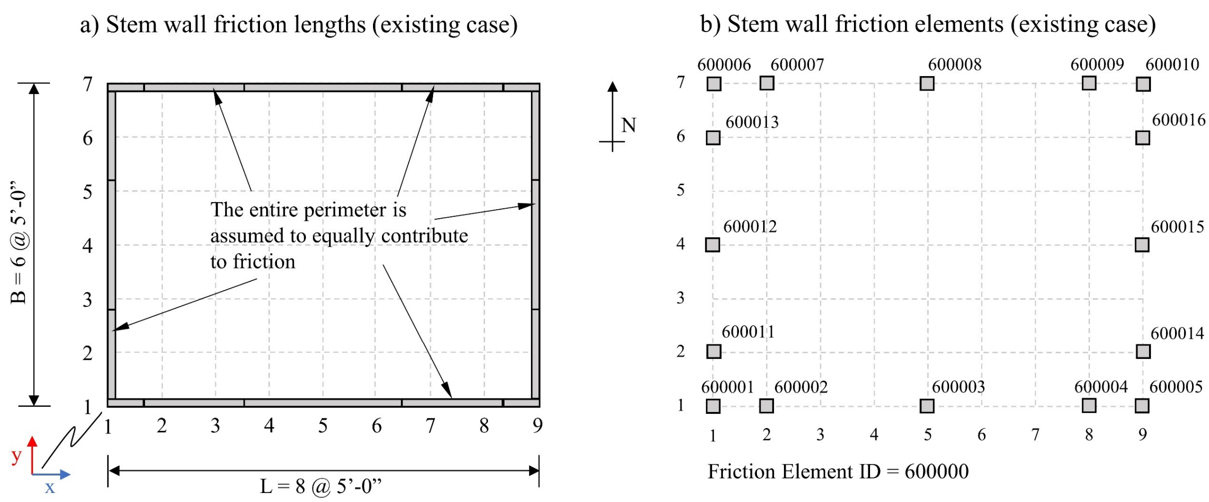

Figure 2.8 Locations of joist-to-sill friction elements assumed for the existing (unretrofitted) stem walls in archetype models: (a) general perimeter contribution; and (b) lumped element positions and identification numbers used in *OpenSees*.

Table 2.5 **Summary of toe-nail joist-to-sill connection elements for the existing (unretrofitted) stem wall variants. Number of toe-nails contributing to each element are presented for full- and half-capacity assumptions.**

Toe-nail type	Story	Direction	Element ID	Node i [1]	Node j [1]	x (ft) [2]	y (ft) [2]	$n_{TN,100\%}$ [3]	$n_{TN,50\%}$ [3]
End [4]	Crawlspace	X and Y	500001	1011	2011	0	0	9	4.5
End	Crawlspace	X and Y	500002	1021	2021	5	0	21	10.5
End	Crawlspace	X and Y	500003	1051	2051	20	0	33	16.5
End	Crawlspace	X and Y	500004	1081	2081	35	0	21	10.5
End	Crawlspace	X and Y	500005	1091	2091	40	0	9	4.5
End	Crawlspace	X and Y	500006	1017	2017	0	30	9	4.5
End	Crawlspace	X and Y	500007	1027	2027	5	30	21	10.5
End	Crawlspace	X and Y	500008	1057	2057	20	30	33	16.5
End	Crawlspace	X and Y	500009	1087	2087	35	30	21	10.5
End	Crawlspace	X and Y	500010	1097	2097	40	30	9	4.5
Rim	Crawlspace	Y	500011	1012	2012	0	5	4	2.0
Rim	Crawlspace	Y	500012	1014	2014	0	15	6	3.0
Rim	Crawlspace	Y	500013	1016	2016	0	25	4	2.0
Rim	Crawlspace	Y	500014	1092	2092	40	5	4	2.0
Rim	Crawlspace	Y	500015	1094	2094	40	15	6	3.0
Rim	Crawlspace	Y	500016	1096	2096	40	25	4	2.0

[1] Node numbers for connectivity of the bottom (i) and top (j) of the toe-nail element.
[2] Locations of the element in plan with respect to the origin taken as the southwest corner of the plan layout.
[3] Total number of toe-nails considered acting at element location to be included using material normalized for single connection. 50% considers half of the assumed toe-nails contributing to that particular element.
[4] 'End' represents joist end bearing connections with 3-8d toe-nails assumed at every joist and acting in both horizontal directions, 'Rim' represents rim joist locations with one 8d toe-nail spaced at 24 in. on center and assumed to act in the *y*-direction only.

Table 2.6 **Summary of friction elements for the existing (unretrofitted) stem wall variants. Total length of friction element reflects how much of the perimeter is considered at that element.**

Element type	Story	Direction	Elem-ent ID	Node *i* [1]	Node *j* [1]	*x* (ft) [2]	*y* (ft) [2]	L_{frict} (ft) [3]
Friction	Crawlspace	X and Y	600001	1011	2011	0	0	3.33
Friction	Crawlspace	X and Y	600002	1021	2021	5	0	9.33
Friction	Crawlspace	X and Y	600003	1051	2051	20	0	14.67
Friction	Crawlspace	X and Y	600004	1081	2081	35	0	9.33
Friction	Crawlspace	X and Y	600005	1091	2091	40	0	3.33
Friction	Crawlspace	X and Y	600006	1017	2017	0	30	3.33
Friction	Crawlspace	X and Y	600007	1027	2027	5	30	9.33
Friction	Crawlspace	X and Y	600008	1057	2057	20	30	14.67
Friction	Crawlspace	X and Y	600009	1087	2087	35	30	9.33
Friction	Crawlspace	X and Y	600010	1097	2097	40	30	3.33
Friction	Crawlspace	X and Y	600011	1012	2012	0	5	4
Friction	Crawlspace	X and Y	600012	1014	2014	0	15	6
Friction	Crawlspace	X and Y	600013	1016	2016	0	25	4
Friction	Crawlspace	X and Y	600014	1092	2092	40	5	4
Friction	Crawlspace	X and Y	600015	1094	2094	40	15	6
Friction	Crawlspace	X and Y	600016	1096	2096	40	25	4

[1] Node numbers for connectivity of the bottom (*i*) and top (*j*) of the friction element.
[2] Locations of the element in plan with respect to the origin taken as the southwest corner of the plan layout.
[3] Total tributary length for friction element that includes a constant friction force along the perimeter of the foundation based on assumed gravity loading and coefficient of friction.

2.3 SELECTION OF HYSTERETIC MODELS

All nonlinear behavior is concentrated in hysteretic shear spring elements. The hysteretic models used to simulate the force-displacement behavior of wall materials use a two spring in parallel approach with hysteretic properties governed by the *Pinching4* material model in *OpenSees* [Lowes et al. 2004]. Toe-nail connections for stem wall dwellings are modeled with the *SAWS* [Folz and Filiatrault, 2004a] material model in *OpenSees*. Detailed discussion of the assumptions and procedures for hysteretic modeling of different materials used for the analysis of building variants can be found in Chapter 3.

2.4 OTHER MODELING CONSIDERATIONS

2.4.1 Weight Take-Offs

The assumed weight take-offs for modeling of building variants is largely based on values reported within the ATC-110 project for development of the *FEMA P-1100* prestandard [2018]. Some modifications were made to the ATC-110 values based on the building variant properties. The floor (flat) loads assumed for floor diaphragms are presented in Table 2.7. The same loads were assumed for the first-floor diaphragms of all variants since there is no era-specific material assumed beneath the first floor (i.e., within the crawlspace). The second-floor diaphragms are separated between construction eras to reflect when plaster on wood lath (pre-1945) or gypsum wallboard (post-1955) is assumed as the ceiling material on the underside of the floor diaphragm.

The assumed roof weights are presented in Table 2.8. The roof loads are separated into "Light" and "Heavy" classifications. The light classification assumes asphalt or composition shingle, while the heavy classification assumes concrete tile roofing. The roof weights consider the weight of the ceiling finish material on the underside of the roof diaphragm level, allowing for distinction based on the assumed era of construction. The two sets of values provided in Table 2.8 correspond to the assumed roof load (w) and the converted projected plan area load considering the horizontal projection of a 6:12 roof pitch ($w_{6:12}$) with the latter being applied to all building variant models. When calculating roof loads, all variant models include an 18-in. eave overhang, resulting in a total roof area of 1410 ft^2.

The exterior wall loads for the superstructure (occupied stories) are presented in Table 2.9. Exterior wall loads are applied considering the entire perimeter. Reductions of exterior loads to account for openings was not considered since these are assumed to offset the weight of windows and doors. The assumed weights for interior partition walls are presented in Table 2.10. These loads assume the partition material is on both sides of the wall. Only the full-height wall lengths of interior partitions are considered for weight calculations. Weight contribution of headers and interior doors were ignored.

The assumed weights for cripple wall materials are presented in Table 2.11. These loads assume there is no finish material on the interior of the cripple wall (i.e., within the crawlspace). Variants with wood siding cripple walls for the pre-1945 era increase the cripple wall weight by 2 psf to include the weight of horizontal sheathing.

Table 2.7 Summary of floor load weight take-offs for floor diaphragms.

Load type	Description	*w* (psf) [1]
1st Floor	First-floor diaphragm, used for all variants, no finish on underside.	12.0
2nd Floor, pre-1945, Light[2]	Second-floor diaphragm, lath and plaster on ceiling below, used when shingle or composition roof assumed (light flooring).	17.5
2nd Floor, pre-1945, Heavy[2]	Second-floor diaphragm, lath and plaster on ceiling below, used when concrete tile roof assumed (hardwood flooring).	21.0
2nd Floor, post-1955, Light[2]	Second-floor diaphragm, gypsum wallboard on ceiling below, used when shingle or composition roof assumed (light flooring).	12.0
2nd Floor, post-1955, Heavy[2]	Second-floor diaphragm, gypsum wallboard on ceiling below, used when concrete tile roof assumed (hardwood flooring).	15.5

[1] Pounds per square foot.
[2] Light weight take-off is assumed as standard, heavy cases include heavier flooring in combination with assumed concrete roof tile. Second-floor diaphragm weights are only applicable to two-story variants.

Table 2.8 Summary of roof weight take-offs.

Roof type	Description	*w* (psf) [1]	$w_{6:12}$ (psf) [2]
pre-1945, Light	Asphalt or composition shingle roofing, lath and plaster on ceiling below	18.5	20.7
pre-1945, Heavy	Concrete tile roofing, lath and plaster on ceiling below	26.0	29.0
post-1955, Light	Asphalt or composition shingle roofing, gypsum wallboard on ceiling below	13.0	14.5
post-1955, Heavy	Concrete tile roofing, gypsum wallboard on ceiling below	20.5	22.9

[1] Roof load in pounds per square foot.
[2] Roof flat load considering horizontal projection of an 6:12 roof pitch (assumed pitch for all variants).

Table 2.9 Summary of exterior wall load weight take-offs for superstructure walls.

Material type	Description	*w* (psf) [1]
Stucco, pre-1945	Stucco exterior, lath and plaster interior	23.0
Stucco, post-1955	Stucco exterior, gypsum wallboard interior	17.0
Wood siding, pre-1945	Horizontal wood siding exterior, lath and plaster interior	15.0
Wood siding, post-1955	Horizontal wood siding exterior, gypsum wallboard interior	7.0
T1-11 siding, post-1955	T1-11 panelized plywood siding exterior, gypsum wallboard interior	7.0

[1] Pounds per square foot.

Table 2.10 Summary of interior partition wall load weight take-offs for superstructure walls.

Material Type	Description	*w* (psf)
Plaster on woodlath, pre-1945	Two sides of finish material	18.0
Gypsum wallboard, post-1955	Two sides of finish material	7.0

Table 2.11 Summary of cripple wall load weight take-offs for superstructure walls.

Material type	Description	*w* (psf) [1]
Stucco	Stucco exterior, includes weight of wood sheathing	14.0
Wood siding/ T1-11 siding	Horizontal wood siding or plywood siding exterior	4.0 (6.0)[2]

[1] Pounds per square foot.
[2] Add 2 psf to include 1-in. nominal wood sheathing behind siding for pre-1945 wood siding cases.

2.4.2 Mass Discretization

The placement of mass within the *OpenSees* models considers the tributary mass distributed between each of the rigid diaphragm nodes at each floor or roof level; see Figure 2.2. The masses apply the floor or roof diaphragm loads according to tributary area (A_{trib}). Mass contribution from interior and exterior walls are applied to the nodes based on the length of wall tributary to that node. Wall lengths are multiplied by one half of the story height to obtain the wall area. These wall areas are then scaled by the appropriate unit weight (see Section 2.4.1) before converting to mass. For cripple wall dwellings, the wall masses for the first-floor diaphragm consider one half of the wall height of the occupied story above the diaphragm and one half of the cripple wall height below the diaphragm. Existing (unretrofitted) stem wall dwellings assume that a 1-ft-tall wall of exterior cripple wall material is tributary to the first-floor diaphragm, including the weight of the exterior material over the floor joists and sill plate. Rigid base models do not include the weight of the first-floor diaphragm as this is assumed to be fixed to the foundation. One half of first-story wall weights are attributed to the roof diaphragm (one-story models) or second-floor diaphragm (two-story models) depending on the number of stories. The areas and wall lengths used for mass distribution at the first-floor diaphragm are provided in Table 2.12, with similar values for the roof diaphragm of one-story variant models provided in Table 2.13.

The corresponding values for the roof diaphragm of two-story variant models are provided in Table 2.14. The interior walls of the second occupied story are distributed evenly as an equivalent flat load (distributed over the floor plan area) based on tributary area due to the symmetrical wall layout assumed. This is reflected in zeros being provided in the interior wall length column (L_{INT}) in Table 2.14. The equivalent flat load for second-story interior walls assumes the interior wall unit weight multiplied by an area defined by a total length of 97.5 ft of interior wall and half the story height distributed evenly over the 1200 ft^2 plan area of the floor. Weight and mass calculations for the second-floor diaphragm of two-story variants must consider the interior wall layout below the floor (Table 2.12) and the evenly distributed interior wall loads in the second occupied story. A similar approach is used for determining gravity loads applied to P-Delta columns, which is discussed in the following sub-section.

Table 2.12 First floor diaphragm lateral mass contributions expressed as tributary areas and wall lengths to diaphragm nodes.

Node PlanID [1]	A_{trib} (ft^2) [2]	L_{INT} (ft) [3]	L_{EXT} (ft) [4]		Node PlanID [1]	A_{trib} (ft^2) [2]	L_{INT} (ft) [3]	L_{EXT} (ft) [4]
11	6.25	0	5.0		64	25.0	2.5	0
21	12.5	0	5.0		74	25.0	10.0	0
31	12.5	0	5.0		84	25.0	5.0	0
41	12.5	2.5	5.0		94	12.5	2.5	5.0
51	12.5	0	5.0		15	12.5	0	5.0
61	12.5	0	5.0		25	25.0	0	0
71	12.5	0	5.0		35	25.0	0	0
81	12.5	0	5.0		45	25.0	0	0
91	6.25	0	5.0		55	25.0	4.0	0
12	12.5	0	5.0		65	25.0	0	0
22	25.0	0	0		75	25.0	2.5	0
32	25.0	0	0		85	25.0	0	0
42	25.0	5.0	0		95	12.5	0	5.0
52	25.0	0	0		16	12.5	0	5.0
62	25.0	0	0		26	25.0	0	0
72	25.0	5	0		36	25.0	0	0
82	25.0	5	0		46	25.0	0	0
92	12.5	1.5	5.0		56	25.0	5.0	0
13	12.5	0	5.0		66	25.0	0	0
23	25.0	0	0		76	25.0	0	0
33	25.0	0.5	0		86	25.0	0	0
43	25.0	10.0	0		96	12.5	0	5.0
53	25.0	5.0	0		17	6.25	0	5.0
63	25.0	5.0	0		27	12.5	0	5.0
73	25.0	5.5	0		37	12.5	0	5.0
83	25.0	0	0		47	12.5	0	5.0
93	12.5	0	5.0		57	12.5	2.5	5.0
14	12.5	2.5	5.0		67	12.5	0	5.0
24	25.0	5.0	0		77	12.5	0	5.0
34	25.0	5.0	0		87	12.5	0	5.0
44	25.0	6.0	0		97	6.25	0	5.0
54	25.0	0	0					

[1] See Figure 2.2 for grid layout.
[2] Tributary area for floor and roof loads.
[3] Length of interior wall.
[4] Length of exterior wall.

Table 2.13 One-story roof diaphragm lateral mass contributions expressed as tributary areas and wall lengths to diaphragm nodes.

Node PlanID [1]	A_{trib} (ft^2) [2]	L_{INT} (ft) [3]	L_{EXT} (ft) [4]		Node PlanID [1]	A_{trib} (ft^2) [2]	L_{INT} (ft) [3]	L_{EXT} (ft) [4]
11	13.75	0	5.0		64	25.0	0	0
21	20.0	0	5.0		74	25.0	0	0
31	20.0	0	5.0		84	25.0	0	0
41	20.0	2.5	5.0		94	20.0	0	5.0
51	20.0	0	5.0		15	20.0	0	5.0
61	20.0	0	5.0		25	25.0	0	0
71	20.0	0	5.0		35	25.0	0	0
81	20.0	0	5.0		45	25.0	0	0
91	13.75	0	5.0		55	25.0	0	0
12	20.0	0	5.0		65	25.0	0	0
22	25.0	0	0		75	25.0	0	0
32	25.0	0	0		85	25.0	0	0
42	25.0	5.0	0		95	20.0	0	5.0
52	25.0	0	0		16	20.0	0	5.0
62	25.0	0	0		26	25.0	0	0
72	25.0	5.0	0		36	25.0	0	0
82	25.0	5.0	0		46	25.0	0	0
92	20.0	1.5	5.0		56	25.0	0	0
13	20.0	0	5.0		66	25.0	0	0
23	25.0	0	0		76	25.0	0	0
33	25.0	0.5	0		86	25.0	0	0
43	25.0	10.0	0		96	20.0	0	5.0
53	25.0	5.0	0		17	13.75	0	5.0
63	25.0	5.0	0		27	20.0	0	5.0
73	25.0	5.5	0		37	20.0	0	5.0
83	25.0	0	0		47	20.0	0	5.0
93	20.0	0	5.0		57	20.0	0	5.0
14	20.0	2.5	5.0		67	20.0	0	5.0
24	25.0	5.0	0		77	20.0	0	5.0
34	25.0	5.0	0		87	20.0	0	5.0
44	25.0	6.0	0		97	13.75	0	5.0
54	25.0	0	0					

[1] See Figure 2.2 for grid layout.
[2] Tributary area for floor and roof loads.
[3] Length of interior wall.
[4] Length of exterior wall.

Table 2.14 Two-story roof diaphragm lateral mass contributions expressed as tributary areas and wall lengths to diaphragm nodes.

Node PlanID [1]	A_{trib} (ft^2) [2]	L_{INT} (ft) [3]	L_{EXT} (ft) [4]		Node PlanID [1]	A_{trib} (ft^2) [2]	L_{INT} (ft) [3]	L_{EXT} (ft) [4]
11	13.75	0	5.0		64	25.0	0	0
21	20.0	0	5.0		74	25.0	0	0
31	20.0	0	5.0		84	25.0	0	0
41	20.0	0	5.0		94	20.0	0	5.0
51	20.0	0	5.0		15	20.0	0	5.0
61	20.0	0	5.0		25	25.0	0	0
71	20.0	0	5.0		35	25.0	0	0
81	20.0	0	5.0		45	25.0	0	0
91	13.75	0	5.0		55	25.0	0	0
12	20.0	0	5.0		65	25.0	0	0
22	25.0	0	0		75	25.0	0	0
32	25.0	0	0		85	25.0	0	0
42	25.0	0	0		95	20.0	0	5.0
52	25.0	0	0		16	20.0	0	5.0
62	25.0	0	0		26	25.0	0	0
72	25.0	0	0		36	25.0	0	0
82	25.0	0	0		46	25.0	0	0
92	20.0	0	5.0		56	25.0	0	0
13	20.0	0	5.0		66	25.0	0	0
23	25.0	0	0		76	25.0	0	0
33	25.0	0	0		86	25.0	0	0
43	25.0	0	0		96	20.0	0	5.0
53	25.0	0	0		17	13.75	0	5.0
63	25.0	0	0		27	20.0	0	5.0
73	25.0	0	0		37	20.0	0	5.0
83	25.0	0	0		47	20.0	0	5.0
93	20.0	0	5.0		57	20.0	0	5.0
14	20.0	0	5.0		67	20.0	0	5.0
24	25.0	0	0		77	20.0	0	5.0
34	25.0	0	0		87	20.0	0	5.0
44	25.0	0	0		97	13.75	0	5.0
54	25.0	0	0					

[1] See Figure 2.2 for grid layout.
[2] Tributary area for floor and roof loads.
[3] Length of interior wall.
[4] Length of exterior wall.

2.4.3 Vertical Supports and Inclusion of P-Delta Effects

The horizontal diaphragms are connected by a series of elastic co-rotational truss elements (*corotTruss* in *OpenSees*), which support vertical gravity loads and allow modeling of second-order (P-delta) effects. These are modeled as axially rigid by specifying a large cross-sectional area and a high modulus of elasticity.

At each story or cripple wall level, the vertical truss elements are defined at nine locations in plan as shown in Figure 2.9(a). For the first-floor diaphragm of cripple wall dwellings and the second-floor diaphragm of two-story dwellings, the tributary areas (A_{trib}) considered for each vertical P-Delta column are as shown in Figure 2.9(a). Roof diaphragms considered an additional 18 in. of eave overhang for contribution of roof loads [not pictured in Figure 2.9(a)]. The base element identification number for P-Delta columns is 800000. Cripple wall vertical elements are numbered 1 through 9, the elements in the first occupied story of the superstructure are numbered 10 through 18, and 19 through 27, representing the elements in the second occupied story (if applicable). An example of the element numbering for the ground-to-cripple wall vertical elements is shown in Figure 2.9(b). Note that the existing (unretrofitted) stem wall and rigid base variants do not have the first level of vertical P-Delta column elements.

The node locations of the P-Delta column elements are provided with the corresponding tributary areas and wall lengths assumed for the gravity load calculations in Table 2.15 (first floor), Table 2.16 (one-story roof), and Table 2.17 (two-story roof). The same assumptions discussed previously in Section 2.4.2 apply, yet with larger areas contributing to each of the nine P-Delta columns.

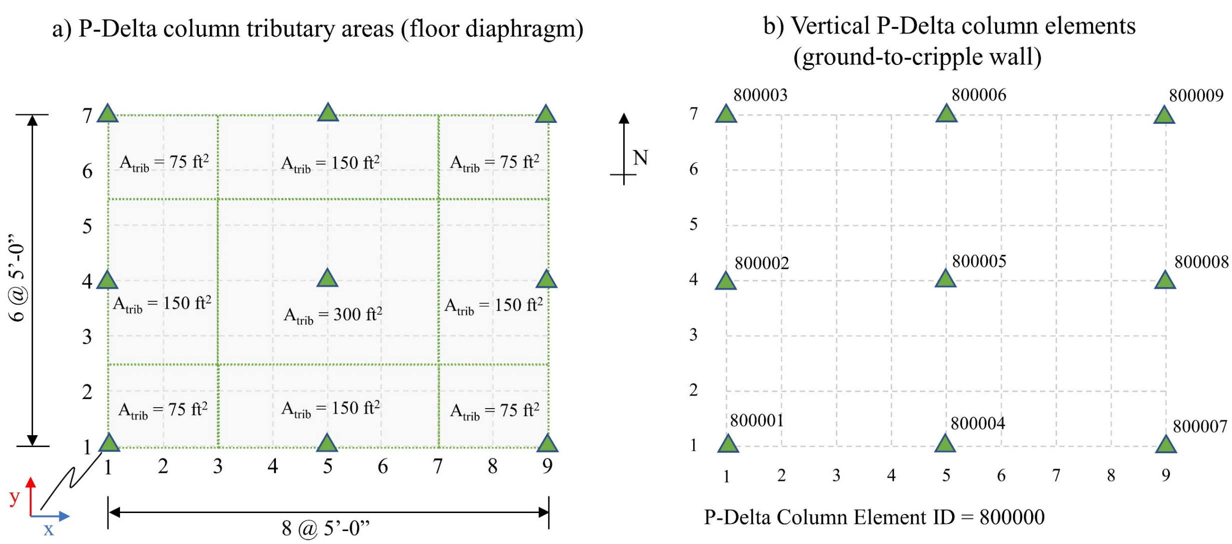

Figure 2.9 Locations of vertical co-rotational truss elements to provide vertical support between diaphragm levels and include second-order effects: (a) example of tributary areas for a typical floor diaphragm (roof level includes 18-in. eave around perimeter); and (b) example of element naming scheme for vertical co-rotational truss elements (ground-to-cripple wall case shown).

Table 2.15 First floor diaphragm load contributions for P-Delta column elements expressed as tributary areas and wall lengths to diaphragm nodes.

Node PlanID [1]	A_{trib} (ft^2)[2]	L_{INT} (ft) [3]	L_{EXT} (ft) [4]
11	75.0	0	17.5
14	150.0	5.0	15.0
17	75.0	0	17.5
51	150.0	6.9	20.0
54	300.0	40.1	0
57	150.0	7.0	20.0
91	75.0	12.5	17.5
94	150.0	26.0	15.0
97	75.0	0	17.5

[1] See Figure 2.2 for grid layout.
[2] Tributary area for floor and roof loads.
[3] Length of interior wall.
[4] Length of exterior wall.

Table 2.16 One-story roof diaphragm load contributions for P-Delta column elements expressed as tributary areas and wall lengths to diaphragm nodes.

Node PlanID [1]	A_{trib} (ft^2)[2]	L_{INT} (ft) [3]	L_{EXT} (ft) [4]
11	101.25	0	17.5
14	172.50	5.0	15.0
17	101.25	0	17.5
51	180.00	6.9	20.0
54	300.00	40.1	0
57	180.00	7.0	20.0
91	101.25	12.5	17.5
94	172.50	26.0	15.0
97	101.25	0	17.5

[1] See Figure 2.2 for grid layout.
[2] Tributary area for floor and roof loads.
[3] Length of interior wall.
[4] Length of exterior wall.

Table 2.17 Two-story roof diaphragm load contributions for P-Delta column elements expressed as tributary areas and wall lengths to diaphragm nodes.

Node PlanID [1]	A_{trib} (ft^2)[2]	L_{INT} (ft) [3]	L_{EXT} (ft) [4]
11	101.25	0	17.5
14	172.50	0	15.0
17	101.25	0	17.5
51	180.00	0	20.0
54	300.00	0	0
57	180.00	0	20.0
91	101.25	0	17.5
94	172.50	0	15.0
97	101.25	0	17.5

[1] See Figure 2.2 for grid layout.
[2] Tributary area for floor and roof loads.
[3] Length of interior wall.
[4] Length of exterior wall.

2.4.4 Treatment of Damping

The treatment of damping for nonlinear dynamic analysis is not straightforward. In a traditional earthquake engineering sense, the use of equivalent viscous damping was commonly attributed to linear models to represent the energy dissipation of the system based on the expected level of nonlinear demand [Newmark and Hall, 1969]. For nonlinear (inelastic) models, where most of the energy dissipation is considered to be captured through hysteretic response, equivalent viscous damping (also termed inherent damping in this sense) is assumed to account for the energy dissipated: (i) by the structural system in the linear response range of the model (e.g., cracking or friction) (ii) through the foundation level, including radiation damping: (iii) by nonstructural components, and (iv) by structural components that are either not represented in the model or modeled elastically [Priestley et al. 2007]. For the nonlinear modeling of older (e.g., pre-1970) wood-frame dwellings considered in the PEER–CEA Project, most of the walls and wall finish materials are explicitly modeled such that viscous damping is included only to represent the unmodeled energy dissipation in the house and its and foundation. Explicit influence of soil–structure-interaction is not included in the Project scope, with contemporary work on the subject for wood light-frame structures within the ATC-116 project [Kircher et al. 2016] suggesting that it is not a critical issue for estimating the seismic response of these structures.

A recent state-of-the-art review assembled by Jayamon et al. [2018] provides explicit details on the previous study of damping in wood-frame structures in the past fifty years. This sub-section provides discussion with respect to damping measurements of actual structures, damping assumptions used in previous numerical studies for wood-frame buildings, and finally, the inherent damping assumptions used for the analysis of this study.

2.4.4.1 Damping Measurements for Wood-Frame Structures

The quantification of damping in structures can be done with a number of methods and procedures. For laboratory shake table tests or instrumented buildings, damping ratios can be measured using ambient vibrations (half-power bandwidth) or impulse testing (logarithmic decrement) at very small excitation amplitudes. Alternatively, dynamic responses of test specimens can be measured using forced vibration testing using a shaking device or monitor actual dynamic responses using system identification methods [Camelo et al. 2002; Camelo 2003].

To illustrate the difference in damping measurements using different techniques and at different response amplitudes, Figure 2.10 compares the damping ratio estimates for the shake table testing of a two-story house conducted by Fischer et al. [2001] and analyzed by Camelo et al. [2002]. The bar charts represent different seismic intensity scenarios for two different construction phases. The numbered intensities range from an assumed frequent low-intensity (99% in 50-years, Level 1) to infrequent high-intensity (2% in 50-years exceedance probability, Level 5) ground motion. Construction Phase 9 has only structural sheathing and framing connections [Figure 2.10(a)], while Phase 10 represents the most realistic case with exterior stucco, interior drywall finishes, windows and a pedestrian door installed; see Figure 2.10(b). The different color and texture of bars illustrate the damping estimates using the entire dynamic time-history response using system identification techniques [Camelo et al. 2002] (solid bars) and the small amplitude impulse loading tests conducted after each test [Fischer et al. 2001] (hatched bars).

The main observation to glean from Figure 2.10 is that the measured damping for the full dynamic response can be on the order of two to five times the estimate using forced vibration analysis following the test. This is likely due to the dynamic response estimate including all sources of energy dissipation, including the hysteretic response of the structure. This is best shown by comparing the Phase 10 results in Figure 2.10(b), where the first two lower levels behaved elastically in terms of global base shear and roof displacement [Fischer et al. 2001], with the higher intensities producing more pronounced hysteretic energy dissipation when referring to global hysteresis loops. The difference between the two damping estimates is minimal for the first two intensities, where a clear deviation can be observed moving to intensity three to five. Notably, forced vibration using small amplitude impulse loading from all seismic tests by Fischer et al. [2001] resulted in an average damping ratio of 7.2% with values ranging from 3.3% to 12.9% with a standard deviation of 2.3%. These values are all conducted using a small amplitude pulse at the measured fundamental frequency following each dynamic shake table test and measured with the logarithmic decrement method. These values correspond to a total of 43 measurements representing a wide range of building construction phases and seismic intensities for the shake table testing. The damping estimates for the Phase 9 and Phase 10 structures before dynamic ground-motion testing were 4.2% and 3.3%, respectively. Note that a majority of the sheathing and framing in the structure had been tested with numerous phases of construction prior to Phase 9.

Damping measurements of *in situ* wood-frame structures conducted by Camelo [2003] consist of actual ground-motion recordings of instrumented buildings and forced vibration tests of wood-frame buildings using a shaking device. Notably, the ground-motion instrumentation recordings are for small magnitude events at close distance (e.g., **M**4 at 1 km) or moderate magnitude at a far distance (e.g., **M**6 at 60 km). As such, the estimated roof drifts for these structures are on the order of 0.008% to 0.021%, representing small amplitude shaking demands

[Camelo 2003]. Forced vibration tests using a shaking machine at various eccentricity levels also caused low amplitude displacements with peak story drift ratios on the order of 0.005% to 0.04%.

A key difference in these two sets of damping estimates is the method in which the damping ratio is estimated. The results from ground-motion recordings use a system identification software that optimizes the system parameters (i.e., frequency and damping ratio) within the time domain. The forced vibration tests using a shaking machine to estimate damping ratios uses a curve-fitting regression technique in the frequency domain. The comparative summary of the two sets of results is provided in Table 2.18, noting that the analyzed buildings are similar, yet not identical between the studies. The damping estimates show that average values are approximately 12% and 5% for the time-domain method (ground-motion excitation) and the frequency-based curve fitting method (forced vibration), respectively. Although the number and exact distribution of structures varies between the two methods used, the fact that the minimum value from the ground-motion excitation (i.e., 6.3%) is larger than the mean value from forced vibration testing (i.e., 5.3%) suggests that the two methods can produce significantly different damping estimates, recalling that all structural responses are responding in the small amplitude range. When combining the two datasets, the average damping ratio is approximately 7% of critical as shown in Table 2.18.

The damping measurements using forced vibration testing provided by Camelo [2003] included two older houses that are most applicable to the current project scope; see Figure 2.11. Both of these structures are two-story houses with a plan area of roughly 2000 ft^2, wood exteriors, and lath and plaster interiors. The first structure was built around 1940 and is reportedly on short cripple walls, with damping ratios of 2.7% and 4.1% for the fundamental frequencies in each orthogonal direction at 20% shaker eccentricity; see Figure 2.11(a). This structure represents the lower bound of damping estimates for forced vibration tests shown in Table 2.18.

The second structure was built around 1920. Camelo [2003] does not report this structure being on cripple walls, yet the photo shows steps leading up to the front door suggesting that some kind of crawlspace is present considering the vintage of the home; see Figure 2.11(b). Whether the crawlspace is created by cripple walls or perimeter stem walls is unknown. This structure has reported damping ratios of 4.7% and 4.0% for the fundamental frequencies in each orthogonal direction at 20% shaker eccentricity. The values at 20% eccentricity were selected since this was the highest eccentricity level tested that is common to both structures. For a sense of shaking amplitude, the reported peak drift displacements at this eccentricity were 0.006 in (0.14 mm) and 0.01 in (0.25 mm) for the first [Figure 2.11(a]) and second [Figure 2.11(b)] structure, respectively.

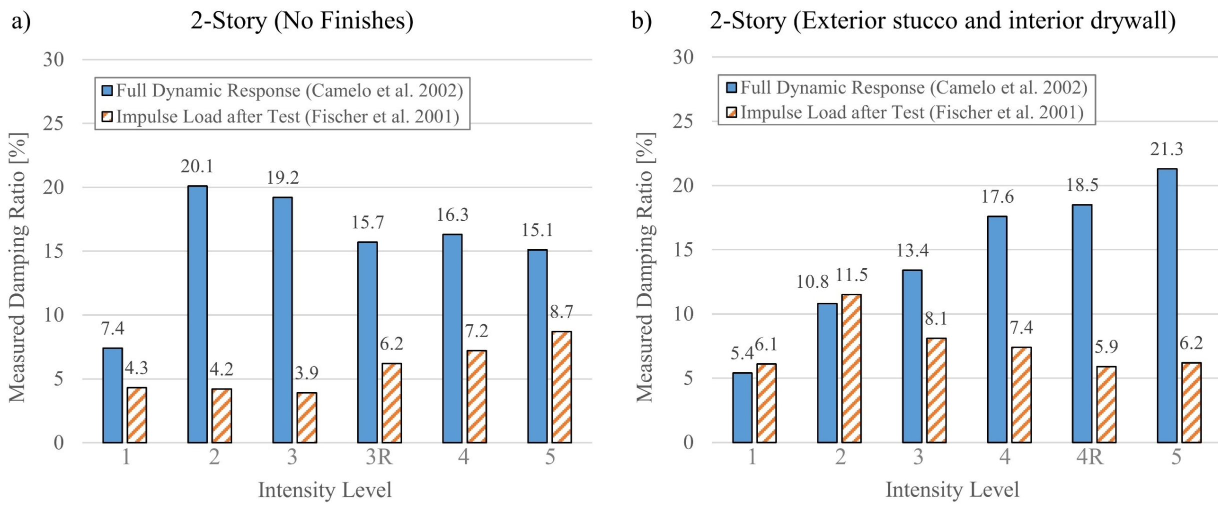

Figure 2.10 **Comparing damping ratio estimates using system identification of entire response (solid bars) and forced vibration following test (hatched bars) for the two-story shake table results of Fischer et al. [2001]: (a) Phase 9 – only structural sheathing and framing; and (b) Phase 10 – including exterior stucco and interior drywall finish. Figures adapted from Camelo et al. [2002].**

Table 2.18 **Summary of damping measurements of instrumented wood-frame buildings from Camelo [2003].**

Study	Groud-motion excitation of instrumented buildings[1]	Forced vibration tests[2]	All data points (both studies)
No. of buildings	5	5	10
No. of measurements	16	55	71
ξ_{Avg} [%][3]	**11.8**	**5.3**	**6.8**
σ_{ξ} [%]	3.6	1.4	3.4
ξ_{Min} [%]	6.3	2.6	2.6
ξ_{Max} [%]	17.3	8.8	17.3

[1] Estimates are calculated using a system identification software using time-domain analysis.
[2] Forced vibration tests are conducted using a shaking device at various levels of eccentricity (amplitude) and damping is estimated using curve-fitting in the frequency domain.
[3] Data rows provide mean, standard deviation, minimum and maximum values of measure damping ratio expressed as a percentage of critical damping.

a) 2-Story House built around 1940

Camelo [2003]

- Roughly 2000 ft^2 in plan
- Exterior is wood shingle
- Interior is lath and plaster
- Reportedly on short cripple walls
- System properties at 20% eccentricity:

Mode 1	Mode 2
f_1 = 4.9 Hz	f_2 = 4.9 Hz
T_1 = 0.20 s	T_2 = 0.19 s
ξ_1 = 2.7%	**ξ_2 = 4.1%**

b) 2-Story House built around 1920

Camelo [2003]

- Roughly 2000 ft^2 in plan
- Exterior is horizontal wood siding
- Interior is lath and plaster
- Steps indicate presence of crawlspace
- System properties at 20% eccentricity:

Mode 1	Mode 2
f_1 = 4.7 Hz	f_2 = 5.1 Hz
T_1 = 0.21 s	T_2 = 0.20 s
ξ_1 = 4.7%	**ξ_2 = 4.0%**

Figure 2.11 System properties from forced vibration tests of two older crawlspace dwellings conducted by Camelo [2003]: (a) two-story house built around 1940; and (b) two-story house built around 1920. Note: 20% eccentricity selected for comparison between the two structures.

A final set of damping measurements are discussed for the three-story asymmetric structure (e.g., first-story garage) tested via shake table by Mosalam et al. [2002]. Camelo [2003] implemented similar forced vibration techniques using a shaker machine and frequency-based curve fitting that was discussed previously when comparing to dynamic system identification techniques using the time-domain; see Table 2.18. The forced vibration testing was conducted both before and after the dynamic shake table tests consisting of numerous intensity levels. This was done for two phases of construction, with Phase I having no finish materials (e.g., structural paneling and framing) and Phase III with added exterior stucco, interior drywall, and windows. Prior to demolition of the test structure, numerous high-intensity ground-motion shake table tests were conducted. Damping evaluation was also conducted following these repeated tests. Damping estimates were obtained for the first modes in the two orthogonal directions based on two different shaking directions and various levels of shaking eccentricity. All measurements are assumed to be reflecting small global displacements in the structure, similar to results presented in Table 2.18. The measured damping ratios for the Mosalam et al. [2002] tests are presented in Table 2.19.

The Phase I testing produced damage to sheathing to framing connections in the bottom story of the structure. The damping estimates before and after testing of this phase show a significant increase in the average damping from 3% to 5%, indicating that nonlinear response of individual connections (e.g., cracking and opening of fastener holes) and that localized damage allowed for more energy to be dissipated at small displacements. This trend is similar for the addition of stucco and drywall in Phase III, where the pre-test damping ratios are shown to reduce slightly due to the addition of the finish materials. Notably, the localized damage to sheathing and framing was repaired prior to adding finishes, yet the framing and sheathing was not completely replaced. The post-test damping ratios show a similar increase in average damping estimates for Phase III as found for Phase I (e.g., on the order of 1.5–2%). These results show that increased nonlinear demands in the structure can cause increases in the energy dissipation measured at small displacements. This is explained by the opening of fastener embedments and cracking of finishes. However, this behavior is not always observed; the measurements for the finished (e.g., stucco) building tested and measured by Fischer et al. [2001] showed damping measurements initially increasing then decreasing following tests of higher intensity; see Figure 2.10(b).

The damping measurement summaries for all tests discussed in this sub-section are collected and provided in Table 2.20. The table shows that by treating all sources of damping measurements (i.e., measurement method, structure type) equal, the average small amplitude damping ratio is approximately 6.0%. The significant variation in the measurements is reflected in the large standard deviation (i.e., coefficient of variation of 0.44) with average plus and minus one standard deviation bounds of 3.5% to 9.1%. Further, the range of values included spans 2.3% at the lower bound and 17.3% at the upper bound.

Table 2.19 Summary of small amplitude damping measurements reported in Camelo [2003] at various stages of shake table testing conducted by Mosalam et al. [2002].

Stage	Before Phase I (no finishes)[1]	After Phase I (no finishes)	Before Phase III (with finishes)	After Phase III (with finishes)	After repeated strong shaking (with finishes)	All data points
No. of data points	9	19	9	20	19	76
ξ_{Avg} (%)[2]	**3.0**	**5.0**	**4.3**	**5.6**	**6.3**	**5.1**
σ_ξ (%)	0.5	1.3	1.3	1.2	1.6	1.6
ξ_{Min} (%)	2.3	2.9	2.5	3.9	1.6	2.3
ξ_{Max} (%)	4.0	6.8	6.4	8.1	3.1	8.8

[1] Forced vibration tests are conducted using a shaking device at various levels of eccentricity (amplitude) and damping is estimated using curve-fitting in the frequency domain before and after shake table testing (not during).
[2] Data rows provide mean, standard deviation, minimum and maximum values of measure damping ratio expressed as a percentage.

Table 2.20 Summary of small amplitude damping ratio measurements of wood-frame structures reported from various studies.

Study	Ground-motion response identification (*in situ*)[1, 3]	Shaker tests on *in situ* structures[1, 4]	Impulse loading on 2-story shake table specimen [2, 5]	Shaker tests on 3-story shake table specimen [1, 4]	All data points
No. of data points	16	55	43	76	190
ξ_{Avg} (%) [6]	**11.8**	**5.3**	**7.6**	**5.1**	**6.3**
σ_ξ (%)	3.6	1.4	2.3	1.6	2.8
ξ_{Min} (%)	6.3	2.6	3.3	2.3	2.3
ξ_{Max} (%)	17.3	8.8	12.9	8.8	17.3

[1] See Camelo [2003].
[2] See Fischer et al. [2001].
[3] Estimates are calculated using a system identification software using time-domain analysis on instrumented structures.
[4] Forced vibration tests are conducted using a shaking device at various levels of eccentricity (amplitude) and damping is estimated using curve-fitting in the frequency domain.
[5] Study uses small amplitude sinusoidal pulse at measured fundamental frequency with damping quantified using logarithmic decrement.
[6] Data rows provide mean, standard deviation, minimum and maximum values of measure damping ratio expressed as a percentage.

2.4.4.2 Previous Treatment of Inherent Damping for Numerical Modeling

The use of inherent damping in the numerical modeling of wood-frame structures is briefly reviewed in this section. An abridged list of publications illustrating inherent damping assumptions for numerical studies on wood-frame structures is provided in Table 2.21. The table shows a brief description of the study as well as any references cited for the assumptions regarding inherent damping. The main observation is that a low damping ratio on the order of 0% to 5% of critical is typically applied as the inherent damping ratio in numerical models. The main conceptual justification is that nonlinear models for wood-frame structures undergoing earthquake excitation provide a majority of the energy dissipation through hysteretic damping. Interestingly, many studies that provide references can be traced back to the work of Foliente [1995], which suggests the inherent damping of wood-frame structures can be in the range of 0% to 5% of critical, citing early material tests of wood connections [Yeh et al. 1971; Chui and Smith, 1989].

Table 2.21 Various inherent damping assumptions from past numerical studies.

Study	Description	Damping model	Damping ratio (%)	Cited references
Yeh et al. [1971]	Damping components of wood-frame connections. Includes wood material damping, connection slip and adhesives. Small amplitude tests	Proposed material damping is 0.35%. Conventional construction is 1:6:2 for material, slip and adhesive, respectively	Material damping of wood: 0.35% Conventional (no adhesive): 2.5% Conventional (adhesive): 3.2%	N/A
Foliente [1995]	Behavior of woodframe joints and dynamic analysis of shear walls	SDOF (constant)	1% to 5%	Yeh et al. [1971]; Chui and Smith [1989]
Folz and Filiatrault [2001]	Nonlinear dynamic validation of SDOF produced from CASHEW	SDOF (constant)	1%	Foliente [1995]
Isoda et al. [2002]	Development of analytical MDOF models for the CUREE-Caltech Woodframe Project	Initial stiffness proportional Rayleigh damping	1%	N/A
Porter et al. [2002]	Performed loss assessment of the index buildings developed by Isoda et al. [2002]	Initial stiffness proportional Rayleigh damping	Mean: 10% St. Dev.: 4%	Camelo et al. [2002]
Rosowsky [2002]	Reliability study of wood shearwall performance	SDOF (constant)	2%	Foliente [1995]
Filiatrault et al. [2003]	Numerical study using shake table results from Fischer et al. [2001] for validation. Study focuses on quantifying hysteretic damping.	Initial stiffness proportional Rayleigh damping	0.1% (for shake table validation high intensity) 2% (general small displacement inherent damping)	Foliente [1995]
Folz and Filiatrault [2004b]	Numerical study replicating shake table testing of 2-story house tested by Fischer et al. [2001]	Initial stiffness proportional Rayleigh damping	1%	Foliente [1995]; Folz and Filiatrault [2001]
Ayoub [2007]	Developed an equivalent SDOF model approach and validated with shake table testing by Fischer et al. [2001]	SDOF (constant)	1%	Foliente [1995]
Pang et al. [2009]	Performed fragility analysis considering various limit states and failure modes for conventional one- and two-story homes	Initial stiffness proportional Rayleigh damping	1%	Folz and Filiatrault [2004b]
Pei and van de Lindt [2009]	Development of a probabilistic loss framework using two wood-frame building configurations	Constant damping	1%	N/A
van de Lindt et al. [2010]	Numerical study replicating shake table testing of 2-story house tested for the NEESWood Project	Initial stiffness proportional Rayleigh damping	1%	N/A
Yin and Li [2010]	Evaluation of seismic collapse risk of wood-frame construction including uncertainties. Damping was not a variable.	Damping model not specified	1%	Foliente [1995]; Folz and Filiatrault [2001]; Rosowsky [2002]
Pang and Shirazi [2012]	Peformed stochastic analysis on an archetype wood-frame model	Initial stiffness proprtional Rayleigh damping	2%	N/A
Jayamon et al. [2015]	*FEMA P-695* collapse assessment of modern wood shear wall structures from 1 to 5 stories	Initial stiffness proprtional Rayleigh damping	1%	*FEMA P-695* Woodframe example [FEMA 2009]

Study	Description	Damping model	Damping ratio (%)	Cited references
Koliou et al. [2018]	Numerical modeling of a 5-story apartment building comparing new materials with ASCE 41 [ASCE, 2013]	Rayleigh damping (treatment of stiffness term not specified)	3%	N/A
Acevedo [2018]	Numerical models for conventional and unibody construction (use of adhesive and enhanced fasteners).	Tangent-stiffness damping (test calibration and collapse study) Modal damping (archetype analysis/ loss assessment)	2.5% (test calibration) 5.0% (archetype analysis)	N/A
Heresi and Miranda [2019]	Used nonlinear lumped mass models to quantify the difference in seismic losses between 1- and 2-story houses	Damping model not specified	10% for one-story 8% for two-story	Camelo [2003]

Yeh et al. [1971] proposed an average material damping of wood of 0.35% and found that the contributions to conventional construction connection damping was in the proportion of 1:6:2 for material, sliding, and adhesive damping, respectively. This results in damping estimates for conventional construction connections of 3.2% and 2.5% for connections with and without adhesive, respectively. These values only represent small amplitude testing of wood-frame connections yet have seemingly been the basis for the treatment of inherent damping in nonlinear numerical models for numerous studies in recent decades. However, a few studies [Porter et al. 2002; Heresi and Miranda 2019] assume larger damping ratios on the order of 10% of critical based on the damping measurements conducted by Camelo et al. [2002] and Camelo [2003]. Both of these previous studies involved loss estimation of wood-frame structures. It is a logical assumption that damping measurements of real structures would be applicable to loss estimation studies targeting the most realistic response possible. Recalling that the damping measurements by Camelo represent the damping at small amplitude displacements, there is no clear evidence that these damping ratios can be applied to nonlinear structural models at large displacements that dissipate hysteretic energy through nonlinear elements.

An important consideration for the treatment of damping in the nonlinear modeling of wood-frame structures is the separation between hysteretic and inherent damping. Hysteretic damping is the energy dissipated by the nonlinear (e.g., wall) elements within a structural model, while inherent damping is applied (typically as viscous damping) to account for additional sources of energy dissipation in the system. One of the most applicable studies to the quantification of hysteretic damping for wood-frame structures was conducted by Filiatrault et al. [2003]. The study measured the hysteretic damping in terms of equivalent viscous damping by measuring the dissipated energy of a structural model through stable cycles at various peak displacements. This dissipated energy is related to the system in terms of an equivalent viscous damping ratio at the effective period (i.e., secant stiffness period). Filiatrault et al. [2003] analyzed a total of 12 different building variants including four archetype configurations and three levels of construction quality (e.g., strength and stiffness) that were developed as index buildings within the CUREE-Caltech Woodframe Project [Isoda et al. 2002]. Equivalent viscous damping ratios were estimated at seven peak displacement levels corresponding to primary cycles of the CUREE-Caltech loading protocol [Krawinkler et al. 2000] for each building variant and orthogonal direction. A total of 24 equivalent viscous damping ratio versus roof drift curves were produced as shown in Figure 2.12.

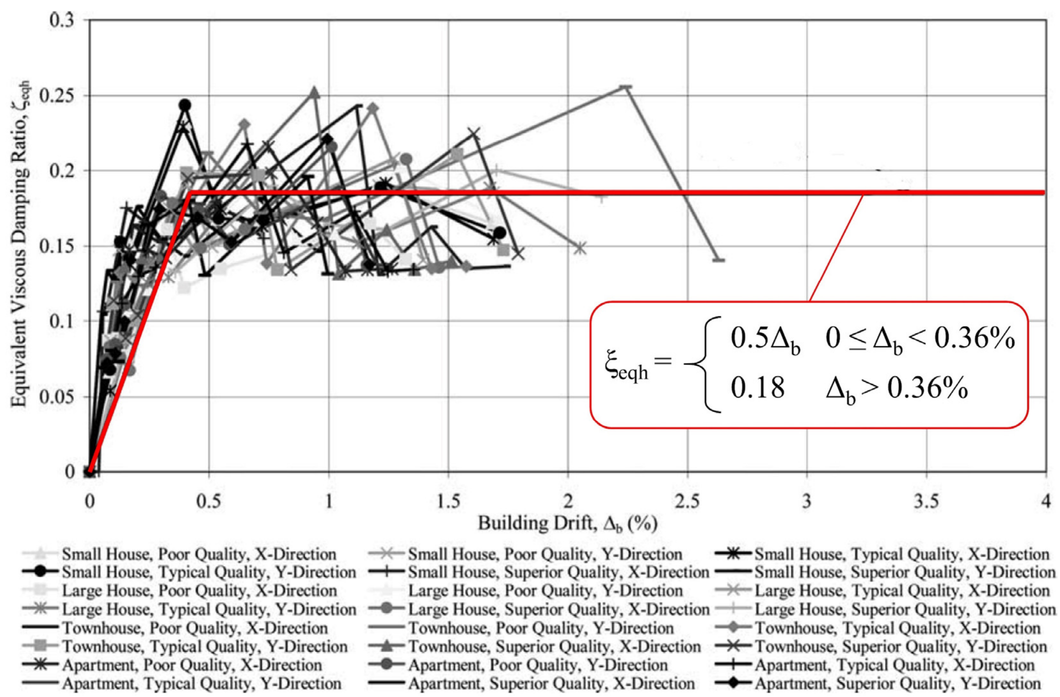

Figure 2.12 Equivalent viscous damping ratio from hysteretic energy dissipation versus building roof drift for CUREE-Caltech building variant models estimated by Filiatrault et al. [2003] with proposed relationship for design procedures (figure adapted from Filiatrault et al. [2003]).

The figure shows the proposed relationship of equivalent viscous damping from hysteretic energy dissipation as a function of building roof drift for implementation in direct displacement-based design procedures. The relationship represents the general trends of all building variants considered and shows the hysteretic energy dissipation increasing linearly until a roof drift ratio of approximately 0.4%, with a constant damping ratio of 18% for larger displacement demands. Important to the current discussion, the individual building variants (and directions) show a wide range of peak damping ratios depending on the variant, with a range of 13% to 25% for roof drift values greater than 0.5%. Similarly, the values in the small displacement range on the order of 0.1% roof drift show a range of damping values between 5% and 15% depending on the building properties. This range is similar to the range of damping values observed from damping measurements of actual wood-frame structures tested at (very) small amplitudes discussed in Section 2.4.4.1; see Table 2.20. This comparison supports the typical numerical assumptions in previous studies to use a reduced damping ratio to be applied as inherent viscous damping when the majority of hysteretic energy dissipation is captured by the nonlinear model.

Another important consideration for applying inherent damping as viscous damping within nonlinear analysis models is the type of damping model assumed. A common damping formulation used for analysis of multi-degree of freedom (MDOF) systems is some form of Rayleigh damping. For linear MDOF systems, the Rayleigh damping model consists of a stiffness-proportional and mass-proportional term, with the stiffness-proportional term constant for linear systems (i.e., initial elastic stiffness). For nonlinear MDOF systems, there are differing opinions as to whether the stiffness proportional terms should be based on a constant elastic stiffness or a tangent stiffness, where the resulting damping effects would reduce with reducing tangent stiffness. Opinions also differ as to the merits of modal versus Rayleigh damping (e.g., see Hall [2006]; Charney [2008]; Hardyniec and Charney [2015]; Chopra and McKenna [2016]; Hall [2016]; and Hall [2017]).

2.4.4.3 Inherent Damping Assumptions for Analysis of Building Variants

Following the review of literature related to damping measurements, treatment of damping in previous studies and modeling approaches for applying inherent viscous damping in nonlinear models, the damping assumptions applied in this study include:

- *Damping Ratio* - A damping ratio of 2.5% of critical is assumed. This is based on the lower bound of damping measurements using low amplitude excitation conducted by Camelo [2003], representing a value measured from an actual cripple wall dwelling. Similarly, this lower damping ratio is similar to measurements of undamaged experimental specimens [Fischer et al. 2001; Mosalam et al. 2002]. Targeting this damping ratio acknowledges that low amplitude displacements should have some amount of inherent damping to provide a realistic onset of damage and estimation of seismic losses at low intensity levels. Further, at large displacement demands, which is important for estimating collapse and large drift demands, the use of 2.5% damping is assumed to be a reasonable value to include some level of energy dissipation, while not overestimating or double counting energy dissipated through the hysteretic behavior of wall elements.
- *Damping Formulation* - The damping formulation assumes tangent stiffness proportional Rayleigh damping with the 2.5% damping assigned to the first and third fundamental modes. The use of tangent stiffness proportional damping is justified due to the large stiffness changes expected in wood-frame buildings, where constant damping based on initial stiffness could lead to unrealistically high damping forces when the structure moves into the nonlinear range. Tangent stiffness proportional damping will naturally reduce the damping forces as the hysteretic wall elements lose stiffness. Although using tangent stiffness proportional Rayleigh damping still has some conceptual and technical issues, many studies have shown this to be a much better formulation than using initial stiffness proportional Rayleigh damping in terms of limiting damping forces during significant nonlinear response [Chopra and McKenna, 2016].
- *Application of Damping Model* - Only hysteretic wall spring elements are assigned the stiffness proportional damping. Similarly, only diaphragm mass nodes are applied the mass proportional damping. This is to avoid spurious damping forces as recommended by previous researchers [Hall 2006; Charney 2008; and Chopra and McKenna 2016]. Further, when modeling existing (unretrofitted) stem wall dwellings with a combination of anchorage and friction elements, no stiffness proportional damping is applied at the stem wall slip interface.

These assumptions are based on a review of current literature dealing with various aspects of treatment of damping for the nonlinear analysis of wood-frame structures. They reflect the current understanding of damping in wood-frame structures and currently accepted methods for including inherent damping within nonlinear models.

2.5 STRUCTURAL RESPONSE

For performance-based interpretation using *FEMA P-58* [2012], the structural analysis outputs are grouped in two categories: (i) engineering demand parameters (EDP) conditioned on no-collapse; and (ii) recorded number of collapse cases for collapse fragility estimation. An illustration of this grouping of response under increasing ground motion intensity is shown in Figure 2.13; the drift response at various ground motion intensity (stripe) levels is shown in Figure 2.13(a). Based on the assumed collapse threshold, the instances of collapse are separated out and used to determine the collapse fragility (cumulative distribution function) in Figure 2.13(b).

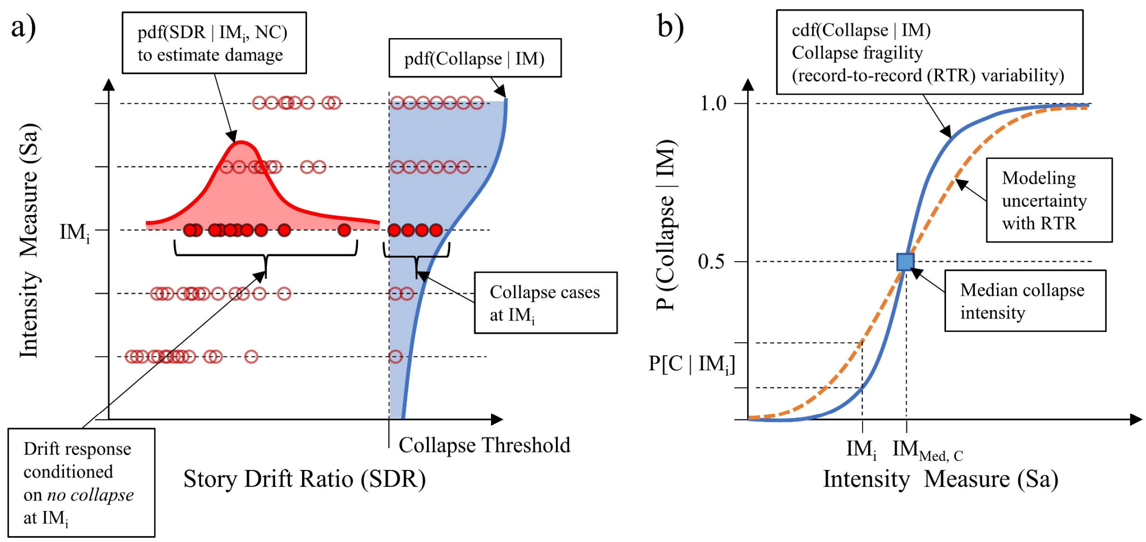

Figure 2.13 **Important concepts for treating structural analysis data: (a) separation of non-collapse and collapse responses for statistics for damage and collapse assessment; and (b) collapse fragility considering record-to-record variability (solid line) and additional modeling uncertainty (dashed line).**

2.5.1 Estimation of Collapse Fragility

Structural analysis within the PEER–CEA Project is based on a multiple stripe analysis (MSA) approach [Jalayer, 2003] where each building site has representative ground motions selected for each return period (RP) based on the causal parameters for that specific site and intensity level. Ground-motion suites of 45 recordings of two horizontal components were used for each site with return periods of 15, 25, 50, 75, 100, 150, 250, 500, 1000, and 2500 years. Ground-motion intensities were measured in term of the average RotD50 5% damped spectral acceleration at a period of 0.25 sec, which is the conditioning period used for record selection based on conditional spectra (refer to WG3 ground-motion report, [Mazzoni et al. 2020]).

In this study, collapse is evaluated using a threshold story drift ratio (SDR) demand, beyond which the structural analysis model has insufficient remaining strength to resist excessive (runaway) drifts under gravity P-Delta effects. The collapse SDR threshold is defined as the exceedance of 20% drift anywhere in the structure. This was implemented as a constraint in the *OpenSees* analysis scripts to streamline the computations and avoid scaling ground motions and running analyses beyond this threshold. Alternative thresholds (e.g., other SDR values) were checked to verify that this assumption was valid for all building variants. Results for individual building variants tracked the location of the collapse cases (i.e., in an occupied story or at the cripple wall), which is important for attributing collapse consequences; see Chapter 6.

Collapse fragilities are modeled as cumulative lognormal distributions, which is a standard assumption according to *FEMA P-58* [2012]. The collapse fragility is defined by a median collapse IM, defined here as $Sa_{\mathrm{Med,C}}$ and lognormal standard deviation or dispersion β. The median collapse intensity is estimated using the maximum likelihood approach for multiple stripe analysis proposed by Baker [2015]. Where necessary, additional ground-motion intensities beyond the 2500-year return period were run by scaling up the 2500-year return period ground motions to up to six additional intensities (scale factors of 1.2, 1.5, 1.8, 2.0, 2.2, and 2.5) with a maximum multiplier of 2.5 times. Since the ground-motion sets scaled to extreme intensities are no longer consistent with hazard assumptions, a truncated IM approach is used whereby these additional intensities are only investigated when the median collapse intensity would otherwise be poorly defined. This approach controls for the estimation of median collapse intensity of building variants without severe vulnerabilities.

This approach is discussed in *FEMA P-58* for the treatment of collapse results using limited ground-motion suites for time-based assessments. For cases that do not produce counted collapse probabilities (i.e., number of collapses divided by number of ground motions) of at least 0.45 for the 2500-year return period, additional intensities are included in the fitting. These two scenarios are depicted in Figure 2.14. Figure 2.14(a) shows a weaker structure, where the median collapse case is well defined within the primary ten intensities, in which case additional intensities are not considered (circles) in fitting the collapse fragility curve. Figure 2.14(b) shows a stronger house, where the first collapse instances only occur at the 2500-year return period. Figure 2.14(b) shows that two additional intensities are included in the collapse fragility fitting, up to the median collapse intensity. The remaining additional intensities are not included in the fitting.

The maximum likelihood fitting provides the estimate of the median collapse intensity and the record-to-record dispersion (β_{RTR}). Additional modeling uncertainty is assumed for the collapse fragility of building variants. According to *FEMA P-58* [2012], the modeling uncertainty (β_{Mod}) for collapse fragility development should consider the uncertainty in building definition and quality assurance as well as the uncertainty in the quality and completeness of the structural model. For the current study, the average recommended values of 0.25 were assumed for each, resulting in a SRSS value of approximately 0.35. The total collapse fragility dispersion (β_{c}) is taken as the SRSS of the record-to-record dispersion from maximum likelihood fitting (β_{RTR}) and the assumed modeling dispersion ($\beta_{\mathrm{Mod}} = 0.35$) as shown in Equation (2.1).

$$\beta_{\mathrm{c}} = \sqrt{\beta_{\mathrm{RTR}}^{2} + \beta_{\mathrm{Mod}}^{2}} \tag{2.1}$$

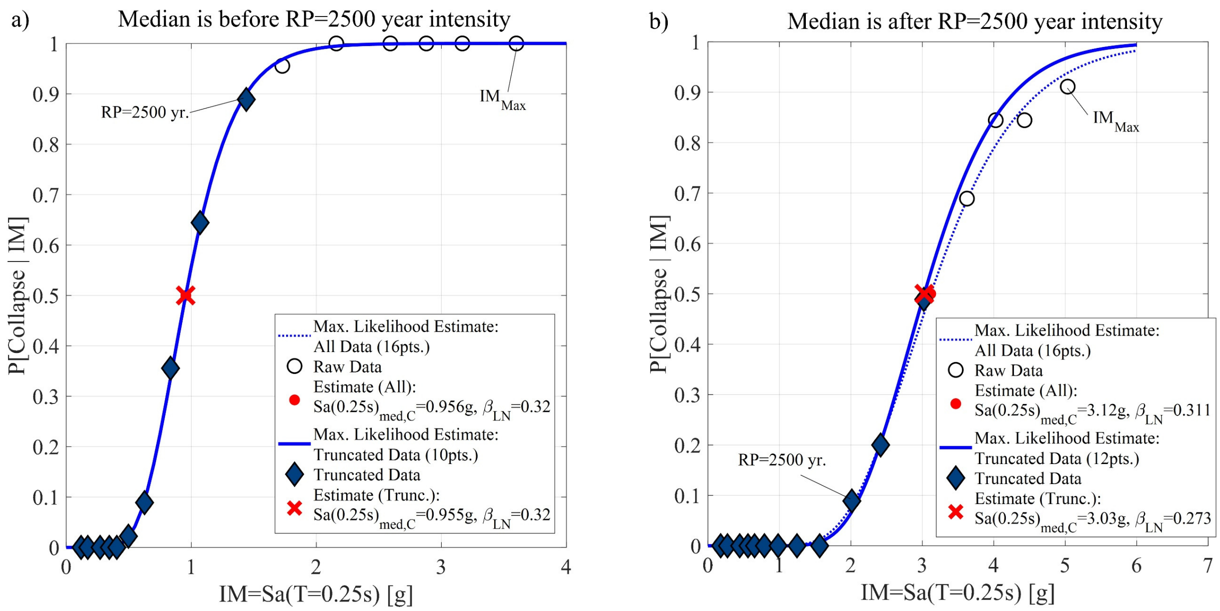

Figure 2.14 Illustration of truncated IM concept used for estimating median collapse intensity and record-to-record variability building variants with median collapse intensity: (a) weak structure using all ten primary intensities; and (b) strong structure using the minimum additional intensities to define the median.

2.5.2 Engineering Demand Parameters Conditioned on No Collapse

The EDPs conditioned on no collapse are used to create probabilistic distributions and correlation matrices for the *FEMA P-58* performance assessment. These response results are only output for the ten primary return period intensities (i.e., from 15-year to 2500-year return periods) for each site. The EDPs recorded from *OpenSees* for each building variant include the SDR, PFA, and residual drift ratio (RDR).

The SDRs are recorded for each story level and direction. The primary performance assessment results use the SDRs corresponding to the average peak value of each corner of the dwelling model. This is assumed to be the most representative for applying a single vector of drift demands for each story level and direction (format required in typical performance calculation tools). The SDRs corresponding to the center of diaphragm (COD) and the maximum anywhere in the story (Max) for a single direction are also recorded and available within the electronic documentation.

The PFA are recorded at the COD of each level of the dwelling for each orthogonal direction. The RDRs are taken as the maximum occurring anywhere in the story for each orthogonal direction. Each time history run duration is padded by 10 sec to allow for free vibration before sampling for the residual drift output.

3 Material Properties for the Assessment of Crawlspace Dwellings

3.1 SCOPE OF MATERIALS FOR THE PEER–CEA PROJECT

The range of material properties considered is limited to older construction eras between 1900 and 1970. With the exception of the materials used to retrofit the cripple walls, the material scope targets dwellings that do not use wood structural paneling (WSP) such as plywood or oriented strand board (OSB) as a sheathing material were not considered in this Project. The materials targeted for structural analysis have already been defined in Chapter 1, with a summary illustration provided in Figure 1.6. The material scope consisted of two primary exterior materials, stucco and horizontal wood siding. Additionally, T1-11 panelized (non-shear wall detailed) wood siding was considered for the later construction era of 1956–1970. Interior materials considered included plaster on wood lath for the pre-1945 construction era and gypsum wallboard for the 1956–1970 era. As mentioned in Section 1.3.2, the intermediate era of 1945–1955 is assumed to represent the transition era where both interior materials were prevalent.

Each combination of interior and exterior materials for the occupied stories was accompanied by representative materials for cripple walls below the first occupied story of the dwelling. Experimental testing conducted by WG4 produced data to support the modeling of cripple walls, either in their existing (unretrofitted) or retrofitted condition. These data are important to assess the difference in structural response between unretrofitted and retrofitted cripple wall houses. For stem wall houses, with inadequate anchorage of the first-floor framing to the foundation, the models were based on existing experimental information in combination with judgment to estimate expected capacities for the superstructure to foundation connection.

The chapter summarizes the data and procedures used for characterizing the force-displacement response of the various wall sheathing materials and calibration of the analysis models. Section 3.2 discusses different aspects of material quality and the scope of its treatment within the project. The calibration approach for modeling the different materials is discussed in Section 3.3. Individual material types are discussed in Section 3.4 to 3.7, and the input material properties used for the project are summarized in Section 3.8.

3.2 TREATMENT OF MATERIAL QUALITY

The PEER–CEA Project considered several sheathing and anchorage materials to represent the expected variations in housing variants. Notwithstanding the breadth of different materials to be considered, many of them with limited testing information, there are additional challenges in characterizing the *in situ* strength and stiffness properties of the materials in the large variety of existing houses. In targeting older homes (i.e., those constructed between 1900 and 1970), the variation in material properties can be affected by improper or sub-optimal installation performed when the structure was originally built as well as the effects of deterioration due to weathering, insect/fungus damage, and even previous seismic events over the life of the structure. Conversely, superior detailing and construction quality could improve the strength and stiffness properties. For the intent of this study, the treatment of quality aims to include the best understanding of the behavior of different materials based on reconnaissance observations, experimental testing, and judgment. A few different perspectives are discussed followed by the underlying assumptions and limitations of the estimation of material properties for the Project.

From an engineering design standpoint, previous seismic events have shown that there are numerous deficiencies that exist for older single-family wood-frame housing, leading to modern design code and construction practices that, when adhered to, have shown to provide adequate seismic performance. This includes elimination of the unbraced cripple walls and deficient sill anchorage, addressed in this Project, as well as torsional or discontinuous load paths associated with highly irregular shaped plans, houses over garages, and split-level configurations. Additionally, past earthquakes have shown that damage and failure of single-family dwellings is often attributed to improper installation of finishes, especially for older dwellings where finish materials provide much of the lateral resistance. Following the 1971 San Fernando, California, earthquake, numerous sources of significant and severe damage to homes was attributed to poor connections of finish materials (e.g., exterior stucco and interior plaster or gypsum wallboard) to the sill plates, which did not allow for finish resistance to be developed beyond the capacity of framing to resist uplift forces [McClure 1971; ATC-HUD 1974]. An example of this behavior is shown in Figure 3.1(b). Additionally, severe stucco damage due to improper detailing was observed following the 1994 Northridge, California, earthquake, where the lack of wire lath embedment was the cause of complete delamination of stucco sections; see Figure 3.1(a) [Hall et al. 1996]. Significant damage was also observed due to fastener failure (e.g., staples or furring nails) or even lack of fastener embedment into framing [Schierle 2001].

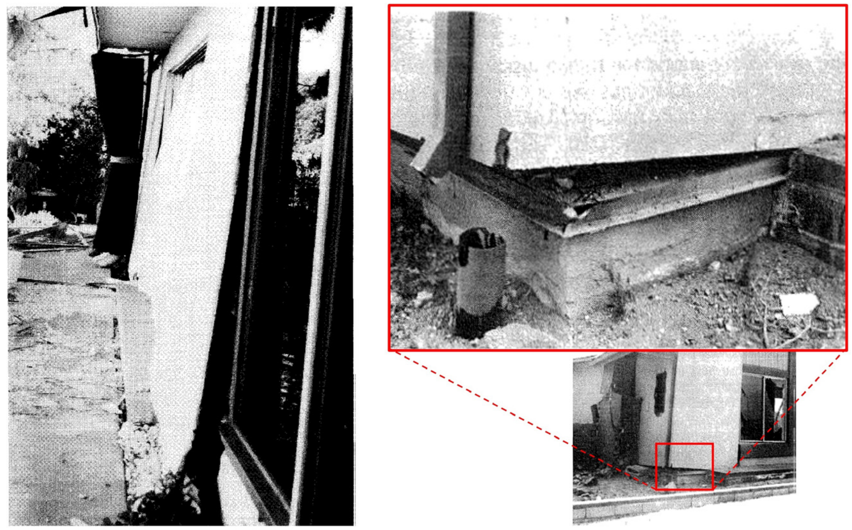

a) b)

Figure 3.1 Examples of improper detailing severely reducing seismic performance of exterior stucco walls: (a) lack of wire lath embedment causing panel delamination [Hall et al. 1996]; and (b) lack of connection to bottom sill plate [ATC-HUD 1974].

In summarizing damage to wood-frame houses following the 1994 Northridge event, both Hall et al. [1996] and Schierle [2001] acknowledge that while severe damage to interior and exterior finishes can be due to design flaws, in many cases the lack of quality control and disregard of building codes and requirements was the major cause for extremely poor performance of wood-frame dwellings that otherwise would have performed better. With the primary goal to ensure life safety, reconnaissance observations such as those presented in Figure 3.1, among a myriad of others, has led to a general progression of building codes to increase seismic design restrictions for residential wood-frame buildings. This is reflected in the historical progression of Los Angeles City Code requirements for wood-frame buildings shown in Table 3.1. The table shows that from 1952–1994 (post-Northridge), the required seismic design coefficients have increased, while the allowable loads for finish materials (e.g., stucco and drywall) have drastically been reduced. Hall et al. [1996] pointed out that the recommended code changes following the 1994 Northridge earthquake [LATF 1992] acknowledged that current design capacities for finish materials were not realistic for current construction practices combined with cyclic loading. These observations and changes prompted the City of Los Angeles to sponsor wall testing at the University of California, Irvine [COLA 2001]. Experimental testing serves as an important means of gaining a better understanding of older wood-frame structures, information that is critical for attempting to assess their seismic performance.

Table 3.1 History of code changes in the Los Angeles City Code from 1956–1994 following the 1994 Northridge earthquake (after Hall et al. [1996]).

Year of code	Seismic design coefficient[1]	Allowable shear loads (lb/ft)		
		Plywood[2]	Stucco[3]	Drywall[4]
1956	0.092	355	200	-
1962	0.133	355	200	125
1966	0.133	355	200	125
1970	0.133	360	200	125
1972	0.133	360	200	125
1976	0.186	360	180	125
1980	0.186	360	180	125
1985	0.140[7] /0.186[8]	360[5]	180	125
1991	0.138[7] /0.183[8]	360[5]	180	62.5
1994[6]	0.138[7] /0.183[8]	200	90	30

[1] Seismic design coefficient (base shear/building weight) for a two-story wood building.
[2] One-in. top grade Douglas Fir, 8d nails at 4 in. blocked, 2 framing.
[3] One-inch Portland cement plaster with metal lath.
[4] One-in. gypsum wallboard, blocked with nails at 7 in. or unblocked with nails at 4 in.
[5] 432 lb/ft if face grain laid across studs and stud spacing not exceeding 16 in.
[6] Post-Northridge earthquake.
[7] Seismic design coefficient for a two-story plywood building.
[8] Seismic design coefficient for other type of two-story building.

To convey some of the challenges associated with older wood-frame construction, a few comparisons from the CUREE-Caltech Woodframe Project are highlighted. The structural modeling used for the CUREE-Caltech project was conducted by Isoda et al. [2002] with loss analysis performed by Porter et al. [2002]. When defining structural material properties for the one-story CUREE Small House (the basis for the house configurations analyzed in this project), the exterior stucco and interior gypsum properties were based on testing conducted as part of the COLA-UCI testing campaign [COLA 2001], which represented the highest quality data for these materials to date. Acknowledging the importance of quality of the materials, the data based on COLA testing were attributed as having "Superior" quality. "Typical" quality materials, which are considered more representative of actual houses, are assumed to have 90% and 85% of the stiffness and strength of the "high-quality" tests (i.e., the COLA tests) for stucco and gypsum, respectively. Similarly, "Poor" quality materials are assumed to have 70% and 75% of the stiffness and strength of "high-quality" tests for stucco and gypsum, respectively. Notably, the basis of the quality reductions is based on judgment. The normalized backbone curves for combined stucco and gypsum materials used for structural analysis by Isoda et al. [2002] are shown in Figure 3.2(a). The figure shows a range of strengths ranging from approximately 550 plf for "Superior" quality to 400 plf for "Poor" quality materials.

Experimental testing conducted within the CUREE projects [Pardoen et al. 2003; Arnold et al. 2003(b)] included a range of stucco exterior wall specimens with interior gypsum wallboard (without structural sheathing). A key difference from the previous COLA testing was the inclusion of window and door openings as well as varying boundary conditions for the finish materials.

These tests resulted in tremendous increases in peak capacity of these materials compared to previous COLA tests. Further, stiffness and displacement capacity were also shown to vary widely depending on the boundary conditions of the test. Figure 3.2(b) compares a sub-set of CUREE test backbones with the previous material ranges considered by Isoda et al. [2002]. Note that an excellent explanation and interpretation of the different tests shown in Figure 3.2(b) is provided in *FEMA P-1100*, Vol. 3 [2019(b)]. Clearly, this comparison suggests that the definition of "high quality" test data to anchor a "Superior" quality starting point could vary significantly with the addition of new information. Further, using the range of available test data to represent how actual wall materials could vary is highly dependent on how variations in experimental results reflect reality. While the difference between "Superior" and "Poor" can be considerable based on laboratory testing, the actual range within the building stock would likely be just as broad.

A key point of this discussion is that the work of Isoda et al. [2002] used the best available data and sound judgment to estimate material properties. Increased breadth of available testing illustrates that the understanding of existing wood-frame structures is an evolving process. Within the current project material scope, some materials have a good source of experimental data, either from previous testing or testing included within the project scope. Conversely, other materials have very little data from which to develop appropriate material properties, leading to a similar scenario faced by Isoda et al. [2002] in the early stages of the CUREE-Caltech Woodframe project.

This project used the term "best estimate" to describe material properties for the analysis of building variants, which reflects that every source of information for a given material is considered to estimate the strength and stiffness properties. The available information varies widely, including experimental data, knowledge of behavior and detailing of actual buildings, and observations from past earthquakes. The initial Project scope entailed the definition of three condition bounds of "Good," "Average," and "Poor" for comparison of results with catastrophe loss modeler groups. However, the PEER–CEA team decided against using these distinctions based on discussions with the catastrophe loss modelers and the Project Review Panel (PRP) on the grounds that attempting to include material condition would only be compounding judgment-based decisions not backed by actual data to differentiate the quality of construction. Moreover, the catastrophe loss modeler groups revealed that the treatment of material conditions ranging from "Poor" to "Good" quality, as considered in their models, did not produce significant changes in loss metrics. This reflects the difficulty in assessing the condition of a home from typical visual inspections by claims adjustors. More discussion of the "best estimate" treatment of material quality and condition can be found in the WG6 report [Reis 2020(b)].

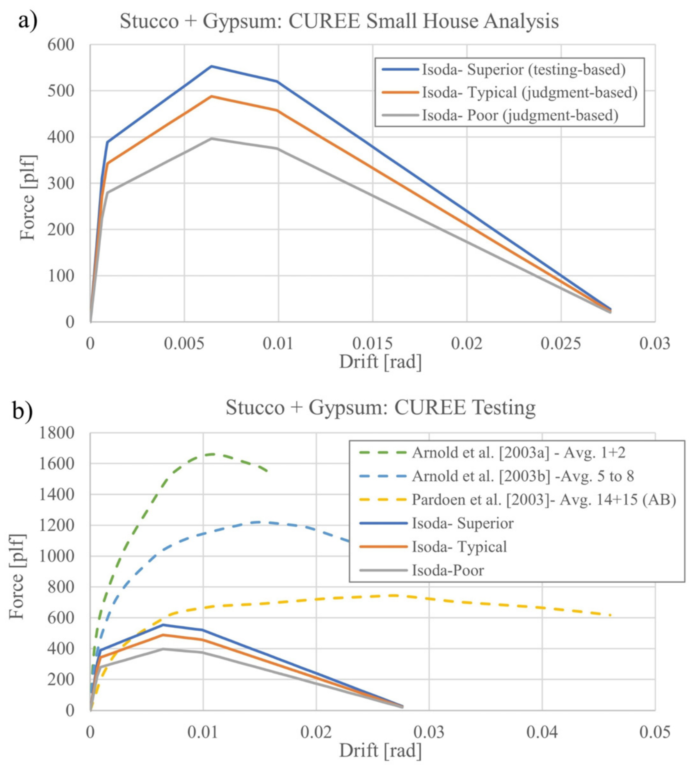

Figure 3.2 **Evolution of knowledge of stucco exterior walls with gypsum wallboard interior within the CUREE Woodframe Project: (a) numerical material backbones based on current data with judgment-based reductions for quality [Isoda et al. 2002]; and (b) comparing numerical materials used with backbone curves obtained through CUREE testing.**

3.3 MATERIAL CALIBRATION APPROACH

The calibration of material properties for structural analysis consists of three main steps. Initially, all relevant experimental data for the material under question is reviewed to define the basis for the force-displacement backbone of the material. The backbone (envelope) curve of the force-displacement response of the hysteretic model is then fit to the applicable experimental data. Finally, cyclic properties of the hysteretic model are fit to applicable test data or estimated based on the most relevant information that is available.

3.3.1 Effective Length for Normalized Material Properties

The material backbone properties for wall materials are expressed in normalized units. Displacements are expressed in terms of drift ratio (e.g., displacement divided by wall height), and shear capacity is expressed in pounds per linear foot of wall (plf; lb/ft). Openings in the walls are based on assumed effective lengths (L_{eff}), equal to the sum of the full height portion of the walls (i.e., full-height piers) as originally proposed by Patton-Mallory [1985].

While the existing technical literature has many alternatives for treatment of openings of *plywood shear walls* [Yasamura and Sugiyama, 1984; Sugiyama and Matsumoto, 1994; Johnson, 1997; and FEMA 2012], the full-height effective length assumption was the most convenient to maintain consistency when considering numerous material types and configurations considered in this Project. The necessity of this assumption reflects, in part, the lack of available information for existing finish materials that encompass the scope of the project, where relationships for wall perforations within the existing literature deal almost exclusively with wood structural panels (e.g., plywood or OSB) shear walls. The approach of basing the effective wall length on the full-height portion of the walls was also used when measuring plan configurations to estimate average wall density parameters (see Appendix A) and the selection of Index Building configurations.

The full-height effective length assumption was carried through from the collection and interpretation of material backbone experimental data to the applied material properties within numerical models. In other words, if a set of wall tests contains openings, the material properties (e.g., strength in pounds per linear foot) are based on the effective full-height wall length before combining with other tests that may not have openings. In this way, the general effect of the openings is built into the numerical studies from configuration development to consistent definition of material properties.

To cross check the full-height assumption for wall openings, a sub-set of the available perforation factor relationships within the literature are considered, as defined in Figure 3.3. Notably, all relationships besides the "full-pier height" effective length assumption proposed by Patton-Mallory et al. [1985] require the calculation of a sheathing area ratio (r) (see Figure 3.3). These different perforation factors were applied to the original CUREE Small House [Isoda et al. 2002], where the different exterior wall lines are presented with the necessary inputs to determine the sheathing area ratios (r) in Figure 3.4. The values range from 0.81 for the east wall to 0.73 for the north wall.

To illustrate the expected variability due to the treatment of openings, the perforation factor relationships defined in Figure 3.3 were applied to the exterior walls of the original CUREE Small House [Isoda et al. 2002] used for numerical analysis within the CUREE-Caltech Woodframe Project; see Figure 3.4. The corresponding perforation factors (α) using the relationships in Figure 3.3 are compared to the full-pier height effective length assumption in Table 3.2. Although the estimates can vary as much as 23% when compared to the effective length assumption, the differences are within 15% for a majority of the comparisons. Notably, the relationship proposed in Equation 4-3 of *FEMA P-807* [2012(d)] was found to give similar results as those obtained using the simpler full wall pier height assumption. This is important since the *FEMA P-807* guidelines are intended to assess the existing (unretrofitted) condition of older soft-story structures with a variety of materials similar to the PEER–CEA numerical studies.

Sheathing Area Ratio (r) (Sugiyama and Matsumoto, 1994)

- Accounts for ratio of sheathed to unsheathed areas in a wall

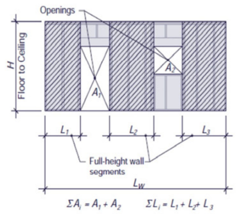

$$r = \frac{1}{1 + \frac{\sum A_i}{H \sum L_j}}$$

ΣL_j = "effective length" used in ATC-110

Perforation Factors

- Factors to adjust full wall without openings for same length L_W

α_K = stiffness factor α_F = strength factor

	α_K	α_F	Suggested Drift (θ)
Patton-Mallory et al. (1985)	$\alpha_{K,F} = \frac{\sum L_j}{L_W}$		Not specified
Johnson (1997)	$\alpha_K = e^{2.37r-2.37}$	$\alpha_F = e^{2.24r-2.24}$	Not specified
Yasamura and Sugiyama (1984)	$\alpha_{K,F} = \frac{r}{3-2r}$		θ = 1/100 rad
Sugiyama and Matsumoto (1994)	$\alpha_{K,F} = \frac{3r}{8-5r}$ (1)		θ = 1/300 rad
	$\alpha_{K,F} = \frac{r}{2-r}$ (2)		θ = 1/100 to 1/60 rad
FEMA P-807 (2012)		$\alpha_F = 0.92r - 0.72r^2 + 0.8r^3$	

Figure 3.3 Definition of different perforation factors for adjustment of strength and stiffness of exterior wall lines. Note: these relationships were developed based on testing of wood structural panel shear walls.

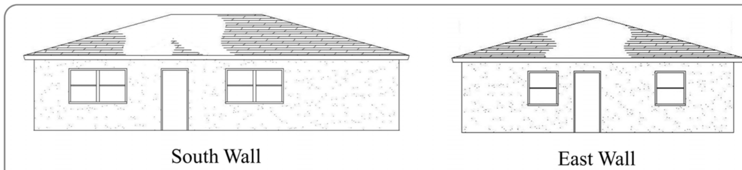

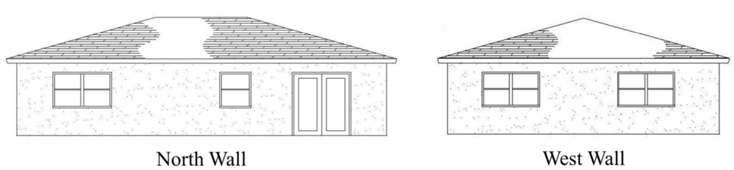

	L_W [ft]	H [ft]	ΣA_i [ft^2]	ΣL_i [ft]	r
South Wall	40.0	8.0	60.79	24.84	0.766
North Wall	40.0	8.0	72.5	25.0	0.734
East Wall	30.0	8.0	39.79	21.33	0.811
West Wall	30.0	8.0	42.0	18.0	0.774

$$r = \frac{1}{1 + \frac{\sum A_i}{H \sum L_j}}$$

Figure 3.4 Calculation of sheathing area ratios for the CUREE Small House.

Table 3.2 **Comparing different perforation factor relationships for the exterior wall lines of the CUREE Small House.**

Reference[1]	Factor	Wall Line of CUREE Small House[3]			
		South	North	East	West
Patton-Mallory et al. [1985] [2]	L_{eff}/L_W	0.62	0.63	0.71	0.60
FEMA P-807 Eq. 4-3	α_F	0.64 (+3%)	0.60 (-3%)	0.70 (-2%)	0.65 (+9%)
Johnson [1997]	α_F	0.59 (-5%)	0.55 (-12%)	0.66 (-8%)	0.60 (0%)
Johnson [1997]	α_K	0.57 (-8%)	0.53 (-15%)	0.64 (-10%)	0.59 (-2%)
Yasamura & Sugiyama [1984]	$\alpha_{F,K}$	0.52 (-16%)	0.48 (-23%)	0.59 (-17%)	0.53 (-11%)
Sugiyama & Masumoto [1994] (1)	$\alpha_{F,K}$	0.55 (-11%)	0.51 (-19%)	0.62 (-13%)	0.56 (-6%)
Sugiyama & Masumoto [1994] (2)	$\alpha_{F,K}$	0.62 (0%)	0.58 (-7%)	0.68 (-4%)	0.63 (+5%)

1 Refer to Figure 3.3 for details.
2 The full-height effective length assumption is adopted for PEER–CEA numerical studies.
3 See Figure 3.4 for wall line details, percentages indicate relative change from full-height effective length assumption.

3.3.2 Hysteretic Modeling of Materials

The modeling of wall materials considered the available hysteretic material models that are commonly used for the nonlinear analysis of wood-frame structures. One commonly used material model is the *SAWS* model, developed as part of the CUREE Caltech Woodframe Project [Folz and Filiatrault 2001; Folz and Filiatrault 2004(a)]. An illustration of the *SAWS* hysteretic model is provided in Figure 3.5. The *SAWS* model combines earlier hysteretic modeling features including a smooth exponential backbone from initial stiffness to peak capacity [Foschi 1974; Foschi 1977] and pinching and reloading behavior similar to the model proposed by Stewart [1987]. The *SAWS* model is defined by ten different parameters that are illustrated in Figure 3.5 and defined in Table 3.3. The *SAWS* model is widely used for the analysis of modern wood-frame structures with wood structural panel shear walls. The model offers the additional versatility of converting individual fastener behavior calibrated with the *SAWS* material to global shear-wall behavior using specialized software such as *CASHEW* [Folz and Filiatrault, 2000] or *SAPWood - NailPattern* [Pei and van de Lindt 2010].

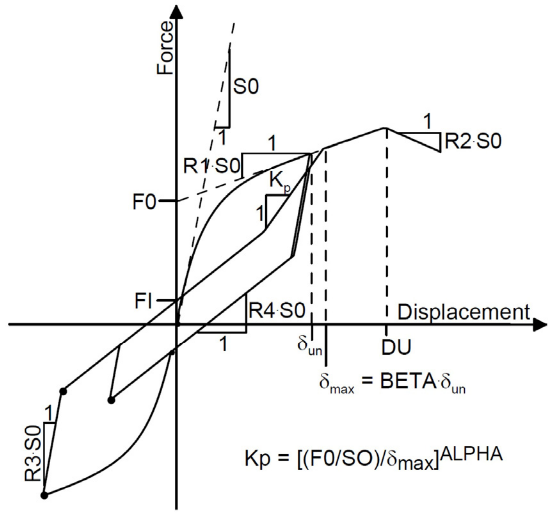

Figure 3.5 **Illustration of the SAWS hysteretic model and parameter definitions (figure adapted from Christovasilis and Filiatrault [2009(b)]).**

Table 3.3 **Definition of the ten parameters used to define a material using the SAWS model.**

SAWS Parameter	Description
S0	Initial stiffness
F0	Force intercept of the asymptotic stiffness at ultimate strength
FI	Zero-displacement load intercept for cyclic reloading
DU	Displacement at peak load
R1	Asymptotic pre-peak stiffness ratio under monotonic loading
R2	Post-peak stiffness ratio on monotonic backbone
R3	Unloading stiffness ratio
R4	Reloading pinched stiffness ratio
α	Hysteretic parameter defining the reloading stiffness to backbone
β	Hysteretic parameter defining the reloading stiffness to backbone

* See Figure 3.5 for an illustration of parameters.

The *SAWS* material model is relatively straightforward to implement, although it has some shortcomings in capturing the behavior of wood shear-wall assemblies. Limitations of the *SAWS* model include use of a constant reloading intercept and stiffness (FI, R4) at all displacement levels and a constant unloading stiffness (R3), along with the lack of the ability to apply a residual strength portion of the backbone curve. The work of Pang et al. [2007] developed the Evolutionary Parameter Hysteretic Model (*EPHM*), which aims to further the hysteretic modeling capabilities beyond the *SAWS* model; the *EPHM* model is only available in the *Timber3D* [Pang et al. 2012] and *SAPWood* [Pei and van de Lindt 2010] software packages.

The PEER–CEA study uses the *Pinching4* material model in *OpenSees* [McKenna et al. 2000] to capture the hysteretic behavior of wall materials. Originally developed by Lowes et al. [2004] for the modeling of reinforced concrete beam-column joints, the material backbone curve of *Pinching4* is characterized by four discrete points in each direction, creating a multi-linear backbone with two pre-peak stiffnesses, a post-peak stiffness, and a residual strength portion. An illustration of the *Pinching4* backbone is provided in Figure 3.6. *Pinching4* allows for the pinching behavior (e.g., force intercept and reloading stiffness) to vary based on the previous maximum displacement excursion during cyclic loading. This is controlled by three parameters for each direction, *rForce*, *rDisp*, and *uForce* as shown in Figure 3.6. Notably, *uForce* always scales the maximum (minimum) backbone strength [defined by point $eP(N)f_3$] to define the force at which reloading along the pinched stiffness slope begins.

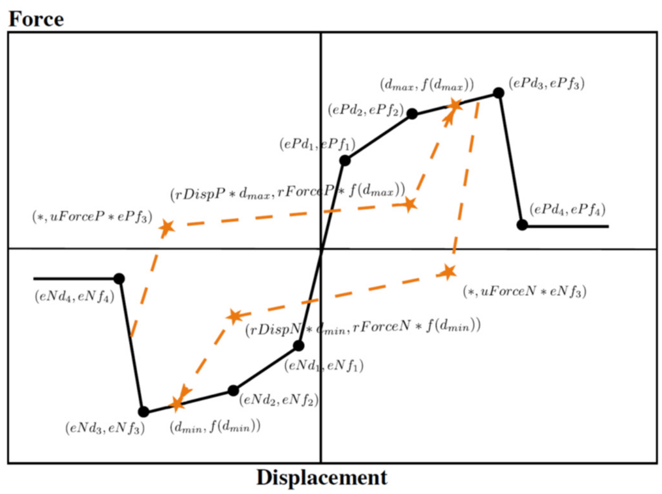

Figure 3.6 ***Pinching4* material backbone and cyclic loading definitions (figure from Acevedo [2018]).**

Pinching4 allows for the following three different types of degradation to be incorporated: reloading stiffness degradation, unloading stiffness degradation, and force (strength) degradation. Each type of degradation (if included) can be controlled by a series of four parameters that allow for degradation based on previous displacement history, dissipated energy, or both. The relationship for including degradation is based on the damage index proposed by Park and Ang [1985] for reinforced concrete members. The general form of the degradation model is shown in Equation (3.1):

$$\boldsymbol{\delta_i = g_1 (d_{max})^{g3} + g_2 \left(\frac{E_i}{E_{mono}}\right)^{g4} < g_{lim}} \tag{3.1}$$

where δ_i is the damage index (0 to 1), d_{max} is the maximum displacement excursion, E_i is the hysteretic energy dissipated in increment *i*, and E_{mono} is the total energy under the monotonic backbone curve. The terms g_1 through g_4 are the leading coefficients and exponents that control the rate of degradation, and g_{lim} is the user-defined limit on the degradation. The damage indices are related to unloading stiffness degradation according to Equation (3.2):

$$\boldsymbol{k_i = k_0 (1 - \delta d_i)} \tag{3.2}$$

where k_i is the current unloading stiffness, k_0 is the initial unloading stiffness, and δd_i is the current unloading stiffness damage index. Similarly, force degradation is defined according to Equation (3.3):

$$\boldsymbol{f_{max,i} = f_{max,0} (1 - \delta f_i)} \tag{3.3}$$

where $f_{max,i}$ is the current envelope (backbone) strength, $f_{\max,0}$ is the envelope strength without degradation, and δf_i is the current value of the strength damage index. The reloading stiffness degradation changes the target displacement when reloading from the pinched stiffness to the current backbone curve, as shown by the segment leading up to the point "[d_{max}, $f(d_{max})$]" in Figure 3.6. The reloading stiffness degradation is governed by Equation (3.4):

$$\boldsymbol{d_{max,i}}=\boldsymbol{d_{max,0}}(\mathbf{1}+\boldsymbol{\delta d_i}) \tag{3.4}$$

where $d_{max,i}$ is the current deformation that defines the end of the reloading cycle for increasing deformation demand (i.e., further deformation follows current backbone curve), $d_{\max,0}$ is the maximum historic deformation demand, and δd_i is the current value of the reloading stiffness damage index.

The *Pinching4* material is extremely versatile, with a large number of features that can be included (or excluded) to define the hysteretic behavior. Previous studies using *Pinching4* have used it to model the response of steel connections [Elkady and Lignos 2015], fire sprinkler systems [Soroushian et al. 2015], hybrid steel-timber systems [Tesfamariam et al. 2014], and novel wood-frame systems [Fragiacomo et al. 2012; Acevedo 2018].

Acevedo [2018] used *Pinching4* to model the experimental response of wood light-frame unibody construction. Unibody construction consists of relying only on finish materials (e.g., stucco and gypsum) but with enhanced connection strength using adhesives and improved connection details. The target behavior of unibody construction produces extremely stiff and strong wall assemblies that are capable of withstanding large acceleration demands with little damage. To capture the widely ranging cyclic behavior between the small displacement (near elastic) response and the post-peak behavior (highly nonlinear) at large displacements, Acevedo [2018] proposed using two *Pinching4* springs in parallel to define individual wall assemblies. Considering the range of different materials considered in the current project, the two spring in parallel approach was also adopted in the PEER–CEA study.

The two spring in parallel *Pinching4* approach is illustrated in Figure 3.7 for a sample experimental backbone. The figure shows that the "combined backbone" represents the total response that targets the experimental backbone of interest. "Spring 1" captures the cyclic behavior at small displacements and "Spring 2" captures the cyclic behavior for displacements near peak capacity and in the post-peak range. The two springs are combined using the parallel *uniaxialMaterial* feature in *OpenSees*. Defining Spring 1, the four-point backbone in each direction (see Figure 3.6) are scaled by weighting factors *a*, *b*, *c*, and *d*. Conversely, the Spring 2 backbone forces are scaled by (1-*a*), (1-*b*), (1-*c*), and (1-*d*) to obtain the total target backbone. For the current study, constant values of these weighting factors were used. Weighting factors of 0.80, 0.75, 0.30, and 0.1 are used for *a*, *b*, *c*, and *d*, respectively. The effect of the weighting factors can be observed by the different shapes of the individual spring backbones (dashed lines) in the plot within Figure 3.7.

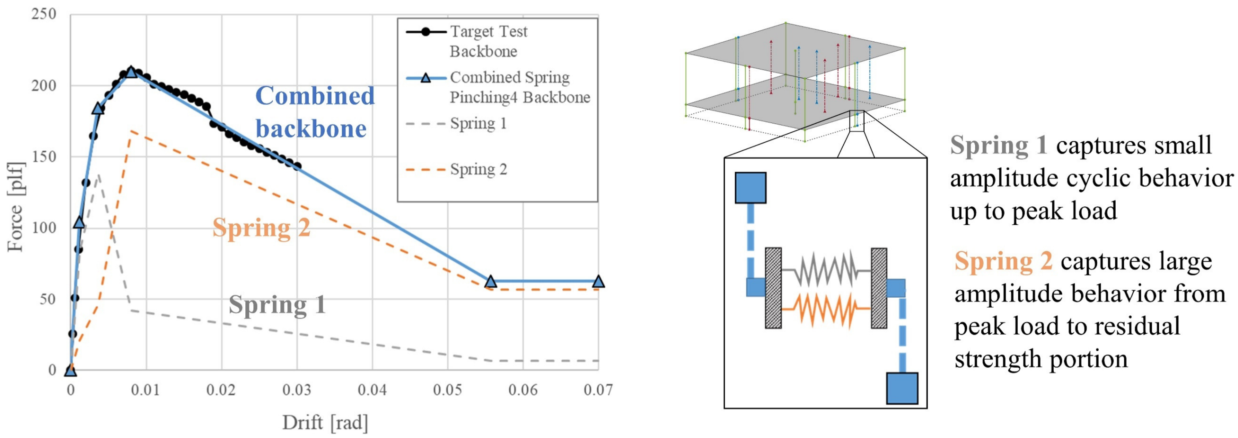

Figure 3.7 Illustration of the two spring in parallel concept used to capture small and large displacement cyclic behavior for wall materials.

The current study employs both unloading and reloading stiffness degradation features of the *Pinching4* material. Cyclic strength degradation is not considered in the wall materials. The available information for each material varies significantly, with some material types having very little experimental data. Further, materials with numerous experimental tests often do not have sufficient pairs of monotonic and cyclic tests (with the same boundary conditions) to reliably calibrate strength reduction from the monotonic backbone curve. The unloading and reloading stiffness degradation is included only as a function of displacement excursions and does not include degradation based on hysteretic energy. Further, only the scalar degradation coefficients (e.g., g_1) and the degradation limits (g_{lim}) are used for each type of degradation [see Equation (3.1)]. This results in a total of 22 distinct parameters used to define each wall material, noting that all materials are assumed symmetrical in each loading direction, i.e., parameters are not defined in terms of “P” (positive) and “N” (negative) as in *OpenSees* documentation. The 22 parameters are defined in Table 3.4.

Material calibration is conducted by fitting the target test backbone to the four-point material backbone. The initial point (*ed1*, *ef1*) defines the initial stiffness and is selected to represent the initial stiffness of the representative tests, with target displacements of similar magnitude to the corresponding initial damage states of the material; see Chapter 5. This is important for wall finish materials in the superstructure to accurately capture the accumulation of damage at low drift levels. This is in contrast to analyses focused on collapse or life safety assessment, where the choice of initial stiffness has relatively little effect on the outcome (e.g., models based on a secant stiffness to an arbitrary drift or displacement, such as the 0.5% drift secant stiffness used in *FEMA P-807* [2012(d)]). The peak point (*ed3*, *ef3*) is typically matched directly to the representative experimental backbone. The second point of the backbone (*ed2*, *ef2*) defining the intermediate or “cracked” stiffness, and the final point (*ed4*, *ef4*) defining the post-peak stiffness and the residual strength portion, are fit to the available test data using a least squares regression approach. When test data does not indicate a residual strength portion (due to lack of experimental loading into this region), point (*ed4*, *ef4*) is attributed a residual strength of 30% of peak load (i.e., *ef4*/*ef3* = 0.3) based on preliminary findings within the ATC-116 Project. When *ef4* is set to a fixed value, the regression is used to adjust *ed4* to represent the post-peak stiffness observed from the test data.

Table 3.4 Definition of the 22-parameters used to define wall materials using two *Pinching4* springs in parallel.

***Pinching4* parameter**		**Description [1]**
Backbone [2]	(*ed*1, *ed*1)	Deformation (d) and force (f) defining initial stiffness of backbone curve
	(*ed*2, *ef*2)	Deformation (d) and force (f) defining "cracked" portion of backbone curve
	(*ed*3, *ef*3)	Deformation (d) and force (f) defining ultimate strength point on backbone curve
	(*ed*4, *ef*4)	Deformation (d) and force (f) defining the residual strength portion of backbone curve
Spring 1	rDisp1	Ratio of deformation at which reloading occurs to the maximum historic deformation demand
	rForce1	Ratio of force at which reloading occurs to the force corresponding to the maximum historic deformation demand
	uForce1	Ratio of strength developed upon reversal of loading to the peak strength developed
	gD11	Reloading stiffness degradation coefficient
	gDLim1	Reloading stiffness degradation limit
	gK11	Unloading stiffness degradation coefficient
	gKLim1	Unloading stiffness degradation limit
Spring 2	rDisp2	Ratio of deformation at which reloading occurs to the maximum historic deformation demand
	rForce2	Ratio of force at which reloading occurs to the force corresponding to the maximum historic deformation demand
	uForce2	Ratio of strength developed upon reversal of loading to the peak strength developed
	gD12	Reloading stiffness degradation coefficient
	gDLim2	Reloading stiffness degradation limit
	gK12	Unloading stiffness degradation coefficient

[1] See Figure 3.6 for an illustration of parameters.
[2] Backbone parameters are defined for the total target backbone, Spring 1 is scaled by a to d = [0.8 0.75 0.3 0.1], and Spring 2 is scaled by (1-a) to (1-d) = [0.2 0.25 0.7 0.9].

Cyclic calibration is conducted through visual iterations of parameters targeting representative response in terms of changes in stiffness and overall force-displacement behavior. Absorbed hysteretic energy is targeted to match representative experimental tests, yet the calibration effort is weighted more heavily toward matching local stiffness changes between small displacements and displacements in the range of approximately 50% strength loss.

The treatment of existing (unretrofitted) stem wall joist-to-sill plate connections uses the *SAWS* material, where development of the input parameters is discussed later in Section 3.7.

3.4 EXTERIOR SUPERSTRUCTURE WALL MATERIALS

The exterior wall materials in the superstructure acknowledge that occupiable stories of the house generally have exterior walls composed of two materials, that for the exterior and that for the interior. As pointed out in *FEMA P-1100* Vol. 3 [2019(b)], the experimental basis for exterior walls should ideally test both interior and exterior materials together, since they generally reach their peak loads at different drifts and gain/lose strength at different rates. This was a driving factor for the selection of the tests conducted by WG4 [Cobeen et al. 2020], which targeted material combinations for which existing test data is lacking.

3.4.1 Horizontal Wood Siding and Sheathing

3.4.1.1 Available Experimental Data on Horizontal Wood Siding and Sheathing

The available test data for horizontal wood siding or horizontal wood sheathing includes early Forest Products Laboratory (FPL) testing [Trayer 1956; Anderson 1965], and more recent tests conducted by Carroll [2006], Ni and Karacabeyli [2007], and Bahmani and van de Lindt [2016].

The FPL testing defines the "baseline curve" for comparing the effects of various details (among other FPL tests) using the average of four test specimens with 1- × 8-in. horizontal wood sheathing loaded monotonically (e.g., Trayer [1956] and Anderson [1965]). The test specimens are solid (no openings) panels of either 14-ft-long × 9-ft-tall or 12-ft-long × 7.33-ft-tall specimens (two of each). Each board has two 8d nails installed per stud location, and studs are spaced at 16 in. on center. The four tests correspond to panels 1 through 4 reported by Trayer [1956]. Other FPL tests of the era report the difference in peak load from this baseline curve at a displacement of approximately 0.5 in. as a measure of relative stiffness and report the peak force as a multiple (or fraction) of the peak load of the baseline curve as an indication strength. The baseline curve is estimated to have a normalized strength of 200 plf and a drift capacity of approximately 3.3%. These tests typically had stiff overturning restraints at the wall ends.

Carroll [2006] tested lumber sheathed walls extracted from dwellings scheduled for demolition. Houses 1, 3, and 5 were constructed in 1948, 1945, and 1950, respectively. Walls with a length of 4 ft and a height just under 8 ft were extracted for testing in the lab. The horizontal sheathing was attached with nails similar to 8d nails. The walls were tested monotonically. The only dead load resisting uplift was provided by the self-weight of the loading beam. Supplemental uplift anchorage does not appear to have been provided. The short 4-ft length of the wall specimens may account for the capacity being lower than tests by FPL, which used walls approximately 12 to 14 ft in length.

Ni and Karacabeyli [2007] tested three horizontal (transverse) lumber sheathed shear walls approximately 8 ft tall × 16 ft long. Walls 12 and 13 were sheathed with 1 × 6 horizontal sheathing, and Wall 14 with 1 × 10. All walls were nailed with 8d common nails. Walls 12 and 14 were tested monotonically and Wall 13 cyclically. Wall 13 had gypsum wallboard attached to the opposite side of the specimen from the sheathing while Walls 12 and 14 had horizontal sheathing only. Tie-downs were provided on end studs for all tests, and no dead load was superimposed. Bahmani and van de Lindt [2016] tested two 8-ft × 8-ft horizontal wood siding specimens using cyclic loading based on the CUREE protocol. Siding was 1 × 8 nominal attached with 8d common nails with (presumably) two nails per stud location. Tie-downs were installed at boundary studs to prevent premature uplift.

3.4.1.2 Numerical Material Properties for Horizontal Wood Siding Walls

A collection of horizontal wood siding and sheathing backbone curves is presented in Figure 3.8. The best estimate backbone for horizontal wood siding (W2) assumes the same backbone used in the ATC-110 project for numerical studies [FEMA 2019(b)]. Note that the best estimate strengths for superstructure materials, previously reviewed within ATC-110, are included in the building variant scope by WG2 [Reis 2020(a)]. The W2 curve, shown as the solid green curve in Figure 3.8, was originally based on the *SAWS* material. The figure shows that the best estimate W2 curve is below the FPL baseline curve yet above the collection of horizontal siding and sheathing tests from other studies (gray curves). The use of this curve acknowledges the uncertainty of actual boundary conditions when attempting to compare older tests to more recent tests that do not include realistic opening boundaries (windows and door frames). To give a sense of strength attributed to the exterior wood siding, the two PEER–CEA test specimens with horizontal wood siding are shown for comparison. Test A-7 is a 2-ft-tall × 12-ft-long cripple wall with horizontal wood siding. Test A-13 is a 6-ft-tall × 12-ft-long cripple wall with horizontal siding [Schiller et al. 2020(b)]. The best estimate wood siding material assumes a peak strength of 190 plf at a drift ratio of 4.0%. A comparison of the *Pinching4* backbone to the target backbone curve for horizontal wood siding is shown in Figure 3.9.

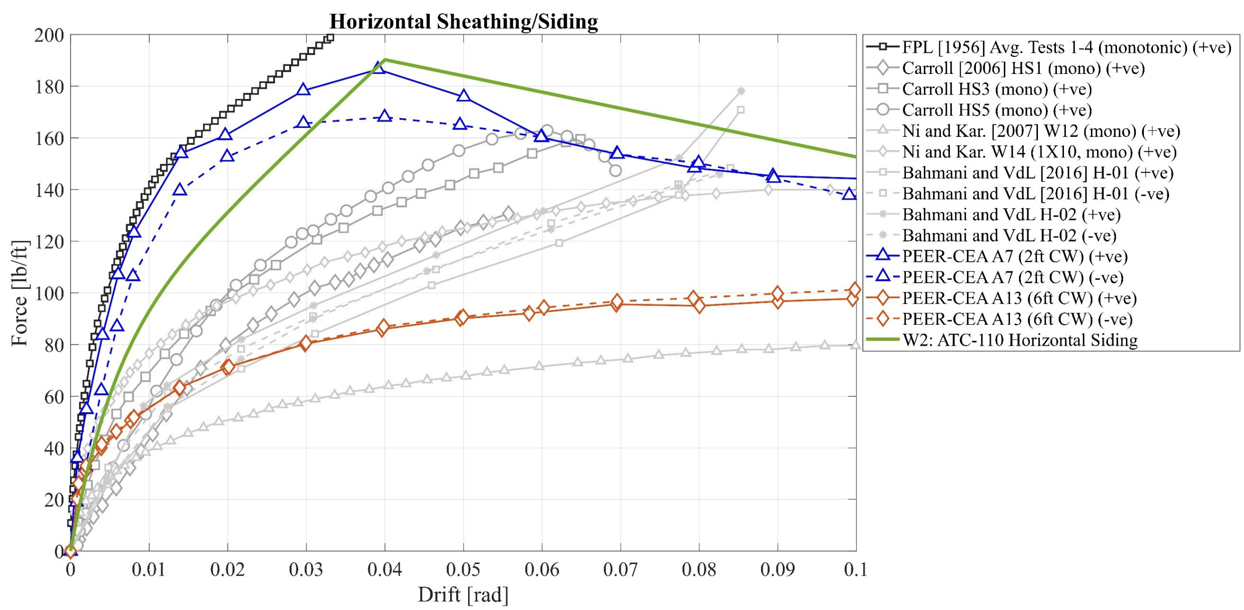

Figure 3.8 **Horizontal wood sheathing and wood siding backbone curves from collected test data with basis for best estimate (W2) from the ATC-110 Project.**

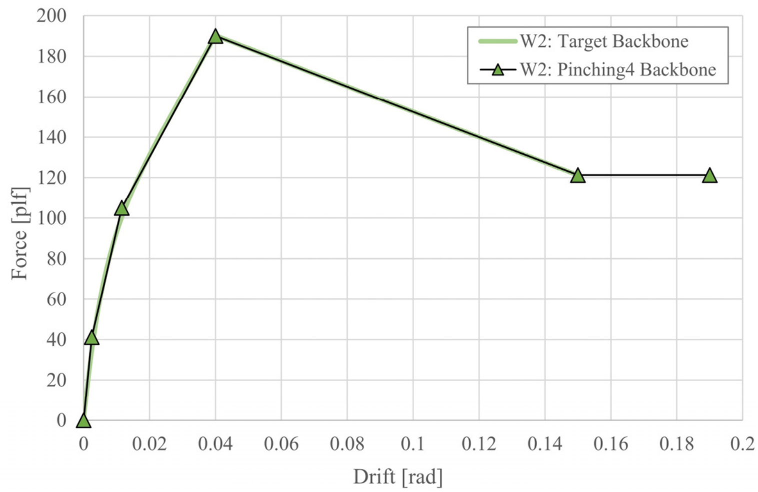

Figure 3.9 **Four-point *Pinching4* backbone compared to target test data: best estimate horizontal wood siding (W2).**

Cyclic properties are calibrated to PEER–CEA Test A-13 (6-ft-tall cripple wall with horizontal wood siding; see Schiller et al. [2020(b)]). The cyclic fit of the *Pinching4* material, using the two spring in parallel approach, is compared with PEER–CEA Test A-13 in Figure 3.10, showing global hysteresis loops and cumulative hysteretic energy. Figure 3.11 shows the best estimate horizontal wood siding material (W2) in normalized units and loaded using the PEER–CEA loading protocol [Zareian and Lanning 2020]. A summary of the *Pinching4* material parameters for horizontal wood siding is provided in Table 3.5.

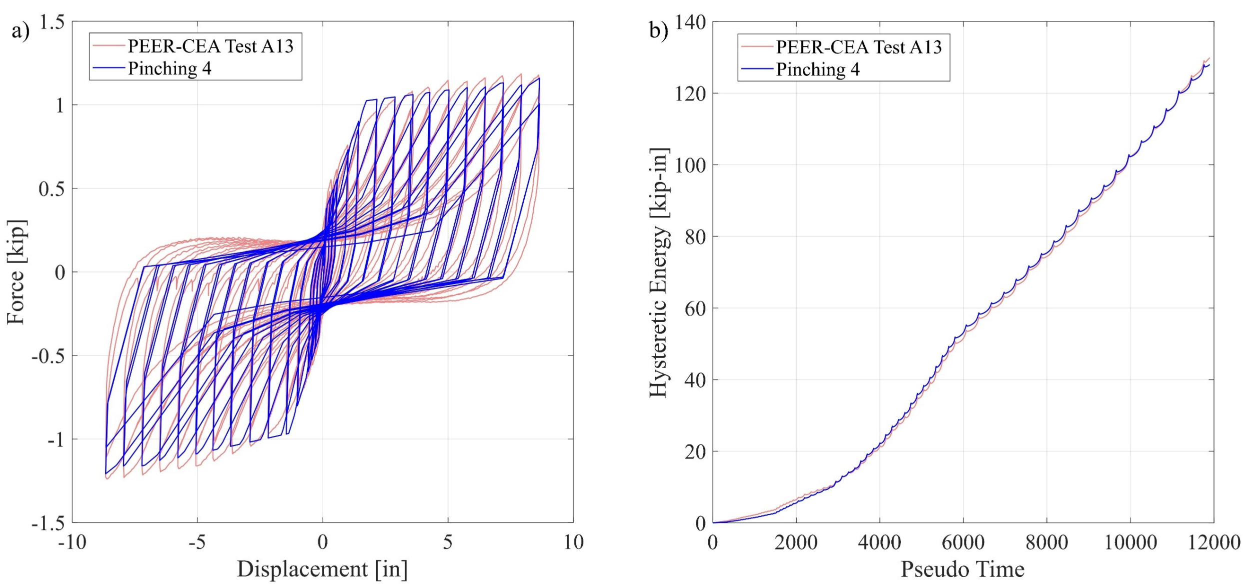

Figure 3.10 **Comparing the *Pinching4* material calibrated to PEER–CEA test A-13 by Schiller et al. [2020]: (a) hysteretic response; and (b) hysteretic energy.**

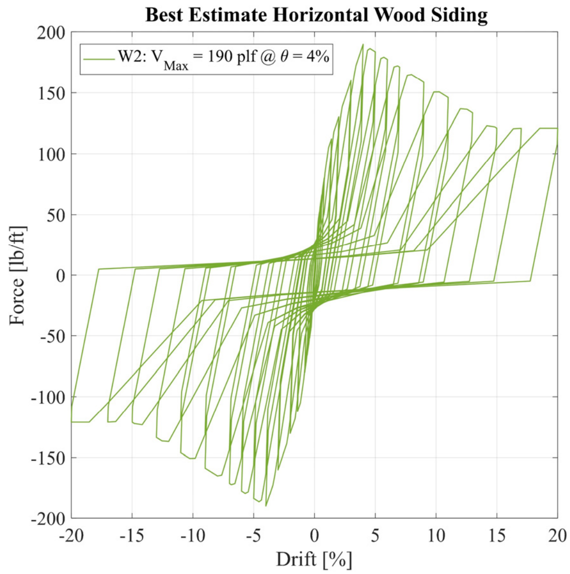

Figure 3.11 **Best estimate horizontal wood siding (W2) material shown in normalized units and loaded with the PEER–CEA loading protocol.**

Table 3.5 **Summary of *Pinching4* material parameters for exterior horizontal wood siding for the superstructure.**

Material	**Backbone deformation points (% drift)**				**Backbone force points (plf)**			
	*ed*1	*ed*2	*ed*3	*ed*4	*ef*1	*ef*2	*ef*3	*ef*4
W2 (best estimate)	0.24	1.16	4.00	15.00	41	105	190	121
Cyclic properties	Spring 1	rDisp1	rForce1	uForce1	gK11	gKLim1	gD11	gDLim1
		0.18	0.35	-0.08	-0.10	-1.00	0.14	0.50
	Spring 2	rDisp2	rForce2	uForce2	gK12	gKLim2	gD12	gDLim2
		0.50	0.12	-0.05	0	0	0.09	0.20

*Definition of material model parameters is provided in Table 3.4; this material is developed as a single-sided material.

3.4.1.3 Combining Horizontal Wood Siding and Gypsum Wallboard

Exterior walls, representing the 1956–1970 era of construction with exterior wood siding and interior gypsum wallboard, assume that the material is combined by superimposing the interior and exterior materials as separate *Pinching4* materials. This is the only exterior wall material considered for building variant analysis that uses this assumption. Definition of the gypsum wallboard material properties is discussed in Section 3.5.1.

The superposition of various wall materials is addressed within the FEMA P-807 [FEMA 2012(d)] guidelines and was investigated experimentally by Bahmani and van de Lindt [2016]. *FEMA P-807* proposes that 100% of the strongest material be combined with 50% of any additional sheathing materials. Bahmani and van de Lindt [2016] found that the *FEMA P-807* combinations were found to be conservative when comparing to combined tests with all sheathing materials on the specimen, but they consider that the conservatism is within an acceptable range.

This study was primarily focused on issues related to combining wood structural panels (e.g., plywood) with other finish materials (e.g., stucco).

Two sources of experimental testing results were found to assess the appropriateness of full superposition of gypsum wallboard and horizontal wood siding materials. The first is from Bahmani and van de Lindt [2016], who performed cyclic testing on horizontal siding (e.g., H-02) and gypsum wallboard separately (e.g., G-02), and also examined the combined variant (e.g., HG-02). The average backbone response of these materials is shown in Figure 3.12(a), illustrating that the superimposed sheathing materials are in good agreement with the combined test until the post-peak region. The other comparison is from cyclic testing conducted by Ni and Karacabeyli [2007], where the isolated sheathing materials (e.g., W12 and W17) were compared with the combined material specimen (e.g., W13). The cyclic backbone envelopes of the superimposed and combined materials are shown in Figure 3.12(b), demonstrating that the curves are in good agreement from initial loading until the post-peak region. The positive loading direction in Figure 3.12(b) shows similar results to the Bahmani and van de Lindt [2016] example, with the superimposed test overestimating the combined test at large displacements. However, the negative direction shows much better agreement. This example is important to illustrate that the implications of the superposition assumption for this material combination was considered in the PEER–CEA Project.

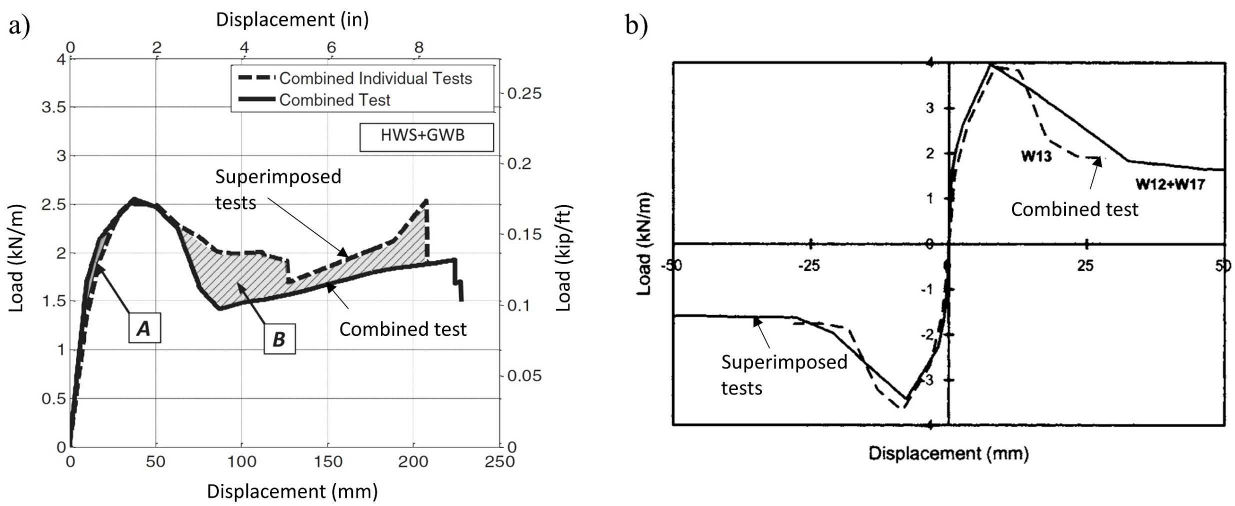

Figure 3.12 Comparison of superimposed gypsum wallboard and wood siding tests with tests including both materials: (a) Bahmani and van de Lindt [2016]; and (b) Ni and Karacabeyli [2007].

3.4.1.4 Bracing in Horizontal Wood Siding Walls

Throughout the project, there was significant discussion among the PEER–CEA researchers and project reviewers regarding the effects of incidental bracing in the wall framing, especially regarding the strength of horizontal wood siding walls.

The different types of bracing that can be found within the framing of older wood-frame construction can vary considerably. A sample of the influence of different bracing configurations for horizontal wood siding and sheathing walls uses FPL testing conducted by Trayer [1956] and other testing summarized by Anderson [1965]. Figure 3.13 compares the best estimate backbone curve (W2) used to represent exterior horizontal wood siding and sheathing with the FPL backbone curve. Additionally, approximate backbones of different bracing and sheathing types were estimated from relative stiffness and ultimate strength factors reported by Anderson [1956]. These factors are expressed relative to the FPL baseline curve where the relative stiffness factor reportedly corresponds to the force at 0.5 in. and the strength factor is with respect to the ultimate strength of the baseline curve (200 plf in normalized units). The ultimate displacement capacities are approximated for illustration, but the increase in strength is adjusted directly from the baseline curve. Note that FPL testing is conducted with monotonic loading.

The curve corresponding to bevel siding has the lowest strength of approximately 100 plf at a drift of 3%, strengths very similar to the recent testing on pure horizontal wood siding and sheathing; see gray plots in Figure 3.8. Conversely, the strongest curve in Figure 3.13 represents the addition of 1- × 4-in. let-in bracing behind the bevel siding, producing an increase in peak strength of over six-fold (660 plf versus 100 plf). Herringbone bracing is shown to give marginal increase in strength and stiffness. This type of bracing has previously been identified to give negligible resistance under earthquake loading [McClure 1973]. Cut-in bracing (individual blocks between studs) is shown to provide a significant increase in strength and stiffness compared to the backbone curve. However, this increase was not reproduced under dynamic cyclic loading conducted by Elkhorabi and Mosalam [2007] when testing a similar bracing configuration for two parallel 8-ft-tall × 19.5-ft-long wall specimens with chevron cut-in bracing and 1 × 10 shiplap siding. The positive backbone envelope from this test is shown as the dashed line in Figure 3.13; note that the curve is from a second loading sequence, following a series of small amplitude loading (less than 0.3% drift). Further, the increase to peak strength for this test was attributed to the engagement of the 1 × 10 siding fasteners, and the cut-in braces had reportedly failed before this force increase. This could be viewed as a lower bound result for this type of bracing yet highlights that cyclic loading can drastically change the capacity of framing braces.

The effect of seismic loading on let-in braces is expected to vary significantly based on a number of factors. Let-in braces are, in concept, designed as compression members that will act in combination with finish materials (e.g., stucco and gypsum wallboard) to provide lateral resistance. As pointed out by McClure [1973], during earthquake loading, let-in braces are typically not activated until the finish materials (e.g., stucco and gypsum wallboard) are severely cracked, which causes the load to be transferred (not shared) to the brace. Further, tension loading of let-in bracing typically results in failure at the top and bottom plate connections, and it occurs at loads on the order of half of unconfined let-in braces loaded in compression [NAHB 2008]. This suggests highly variable results depending on the loading history, where a brace failing in tension could unseat (or fracture) the brace and make it ineffective upon load reversal. Examples of different types of let-in brace failures from previous seismic events are shown in Figure 3.14.

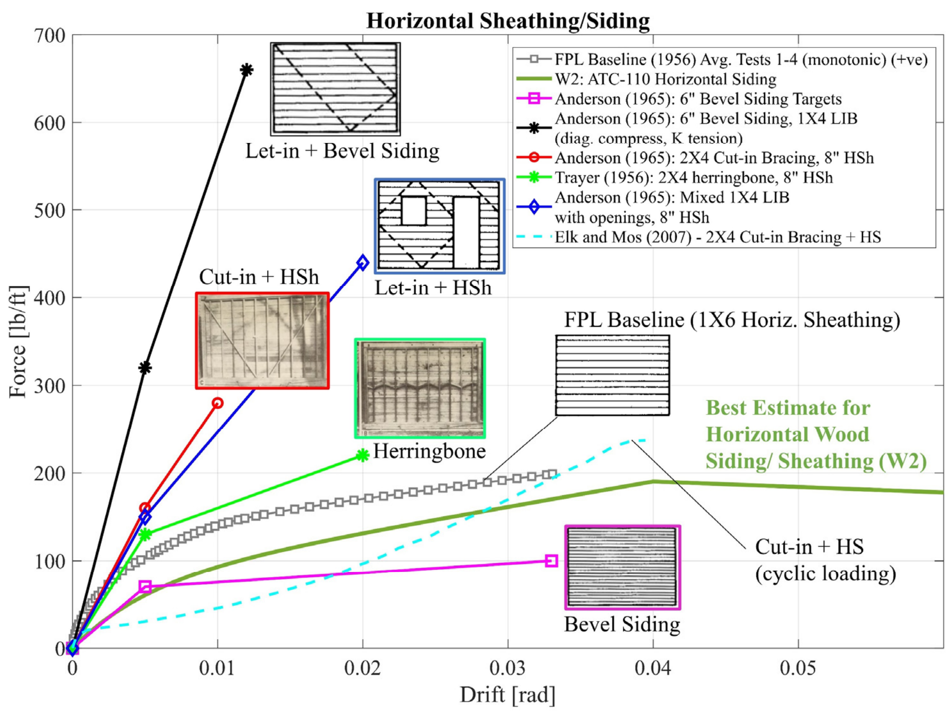

Figure 3.13 Comparing the best estimate horizontal wood sheathing curve with approximate backbones based on early FPL testing with a variety of bracing conditions and details; images from Trayer [1956] and Anderson [1965].

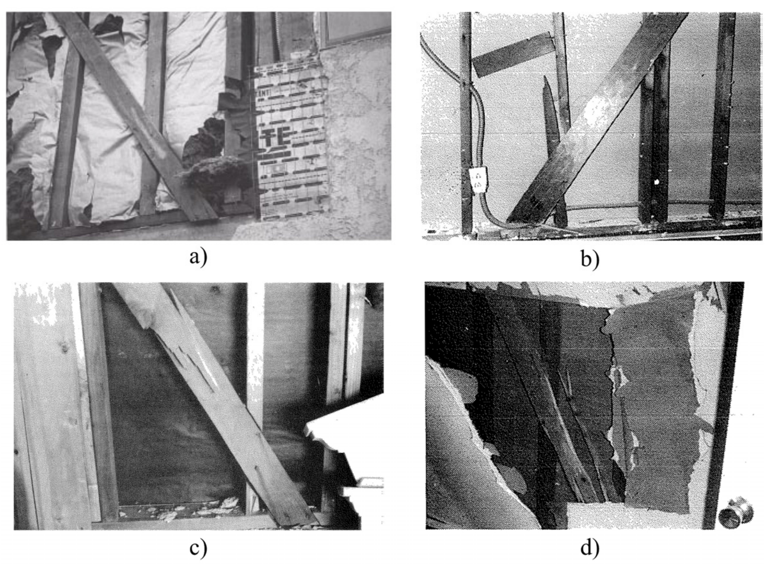

Figure 3.14 Examples of let-in bracing failures from previous seismic events: (a) failure of bottom sill connection in tension [NAHB-HUD 1994]; (b) tension failure of sill connection and stud damage [ATC-HUD 1974]; (c) compression failure of let-in brace [McClure 1973]; and (d) tension failure of let-in brace [ATC-HUD 1974].

The effect of confinement on let-in bracing is an additional factor that could drastically change its influence on wall response. Figure 3.15 compares the effect of unconfined let-in braces loaded in compression with another test where horizontal wood sheathing is applied over the let-in brace, providing confinement. The unconfined curves are an average of configuration 1 testing conducted by NAHB [2008] and a single specimen reported by FPL/Anderson [1965]. The confined example is reported by Anderson [1965]. The displacement capacity for the FPL tests is assumed to be 1% drift based on the average of the NAHB tests for comparison. The figure shows that there is reasonable agreement between the unconfined strengths between the two testing campaigns. Covering the let-in brace with horizontal wood sheathing results in a significant increase in peak strength; note that the strengths of the sheathing and bracing do not combine directly since they are reached at different drift levels.

The review of existing data for braced framing indicates that there could be significant variability in its effectiveness due to numerous factors. Based on this review, the contribution of bracing was not considered in determining the best estimate materials of exterior superstructure walls. The review of results suggests that including bracing effects could be important for defining the range of strengths expected in existing wood-frame dwellings, yet future research is required to incorporate the effects.

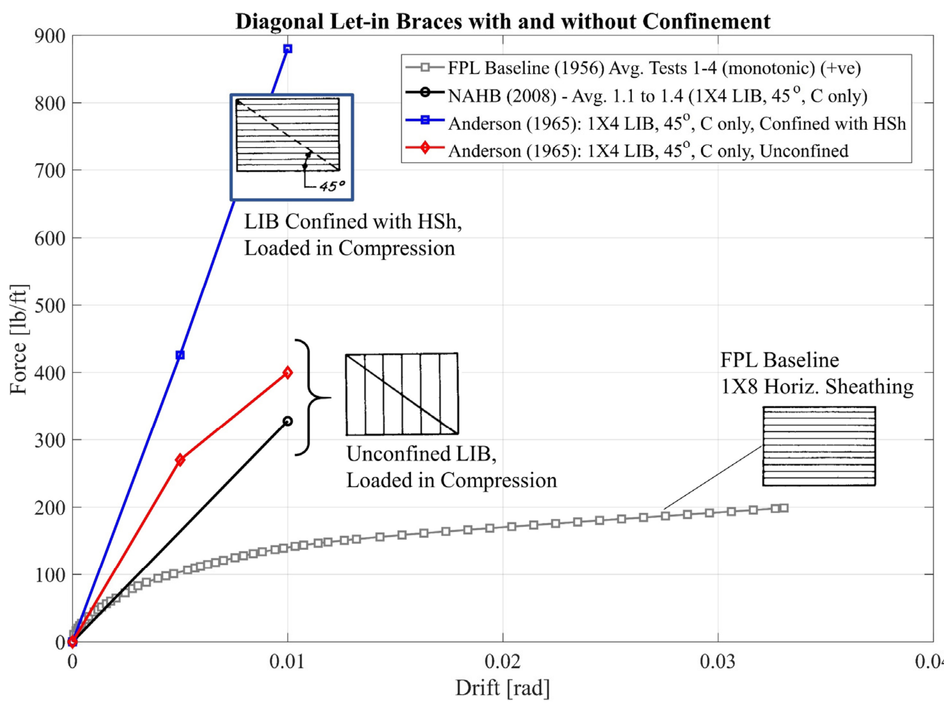

Figure 3.15 **Comparing let-in braces loaded in compression without confinement to a similar brace confined with horizontal wood sheathing; images from Trayer [1956] and Anderson [1965].**

3.4.2 Horizontal Wood Siding with Plater on Wood Lath Interior

The best estimate material properties for combined exterior horizontal wood siding with lath and plaster interior are based on PEER–CEA Test C-1 [Cobeen et al. 2020]. Additional information of testing of lath and plaster is included in the discussion of interior partition materials in Section 3.5.2 and in the WG4 large-component testing report [Cobeen et al. 2020]. Specimen C-1 is 8 ft tall × 20 ft long with dual walls tested in parallel with continuous end return walls. Each principal wall has one door and one window, with 11 ft of full-height wall per side (L_{eff} = 22 ft). Figure 3.16 includes a photograph of the specimen and the resulting hysteretic response from cyclic loading according to the PEER–CEA loading protocol [Zareian and Jennings 2020].

Figure 3.17 shows the cyclic backbone envelopes (positive and negative loading directions and mean value) for Test C-1 in comparison with the assumed *Pinching4* backbone curve. The best estimate backbone curve is based on the average initial stiffness of both backbone envelopes of Test C-1. The peak strength of the expected response for the *Pinching4* backbone curve is based on the positive direction. The positive peak value, as opposed to the average peak value, is used considering that Test C-1 was not found to be an upper bound test when compared to other tests in the literature (refer to Section 3.5.2 and Cobeen et al. [2020]). The residual strength portion of the *Pinching4* backbone was decreased to 200 plf from the 300 plf observed from the test. This was done to be consistent with the current peak strength assumptions used for exterior wood siding for other building variants.

The cyclic calibration of Test C-1 required that the raw data from WG4 be corrected for the baseline displacement, i.e., shifting the data so that loading begins at zero displacement. Further, a small amount of smoothing was applied to the data. This was done using a first pass with a Savitsky-Golay filter (*sgolayfilt* in Matlab) using third-order smoothing with a 25-point window. A second pass using moving average with a 5-point window was also applied (*movemean* in Matlab) to remove data noise. The raw and smoothed test hysteresis loops are compared in Figure 3.18.

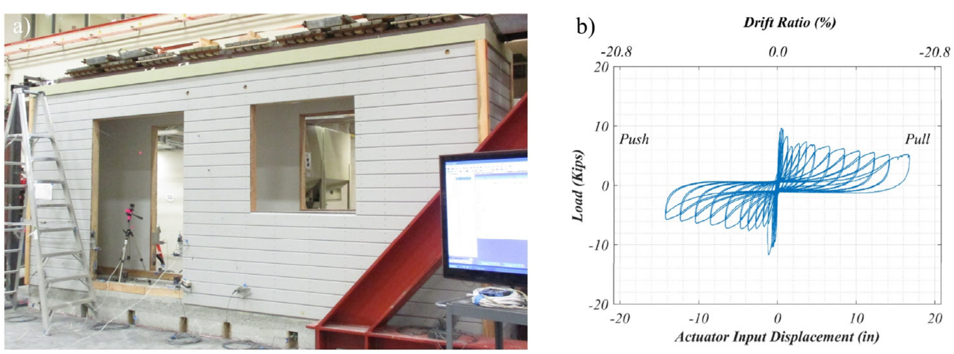

Figure 3.16 PEER–CEA large-component test C-1 [Cobeen et al. 2020] used for modeling exterior horizontal wood siding with interior plaster on wood lath: (a) photograph of specimen; and (b) hysteretic response.

The cyclic fitting using the *Pinching4* material is compared to the target test for force-displacement response and hysteretic energy in Figure 3.19. This test had a large displacement range owing to the residual strength provided by the horizontal wood siding. Reference points are annotated on the figure to understand where on the energy plot different points of loading are. A closer zoomed in view is provided in Figure 3.20 to illustrate the smaller amplitude displacement response. The *Pinching4* material parameters for best estimate horizontal wood siding with interior plaster on wood lath (Material C1) are provided in Table 3.6. A summary hysteretic response in normalized units is shown in Figure 3.21.

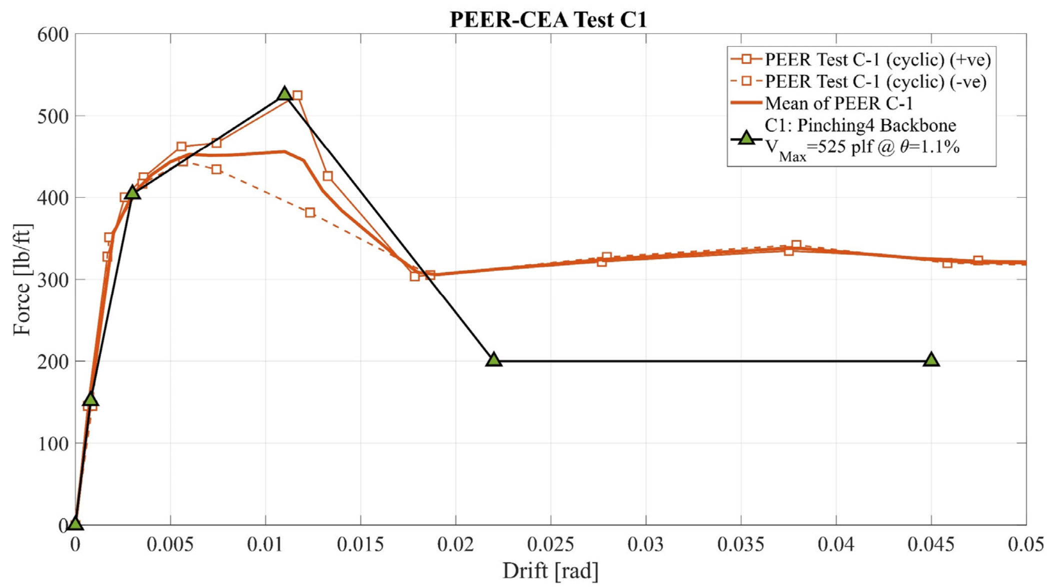

Figure 3.17 Backbone curves for PEER–CEA large-component test C-1 [Cobeen et al. 2020] and best estimate *Pinching4* backbone for exterior horizontal wood siding with interior plaster on wood lath.

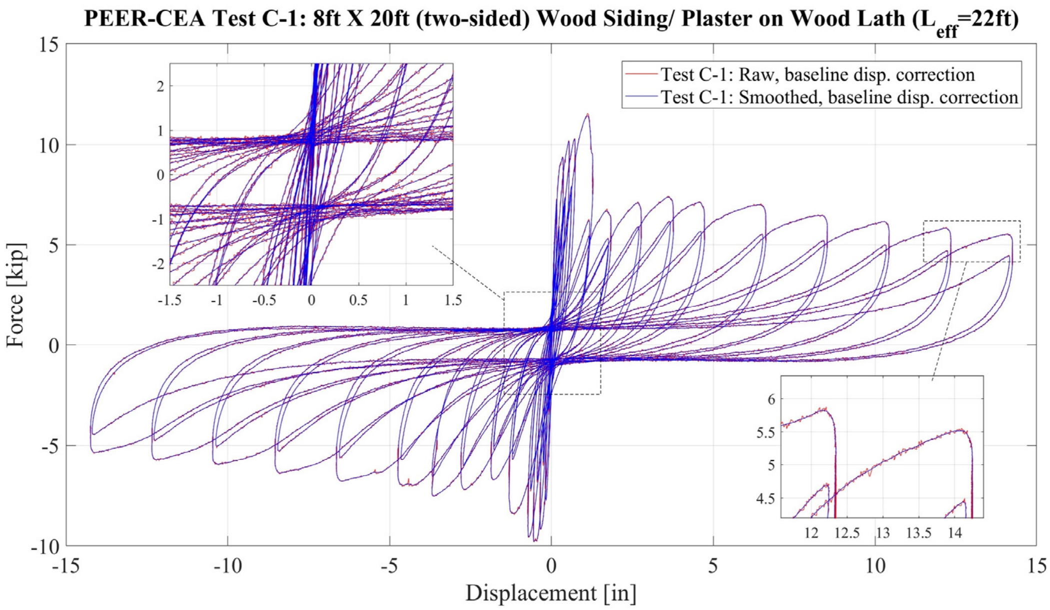

Figure 3.18 Illustrating the baseline displacement correction and small amount of smoothing applied to test C-1 prior to cyclic calibration.

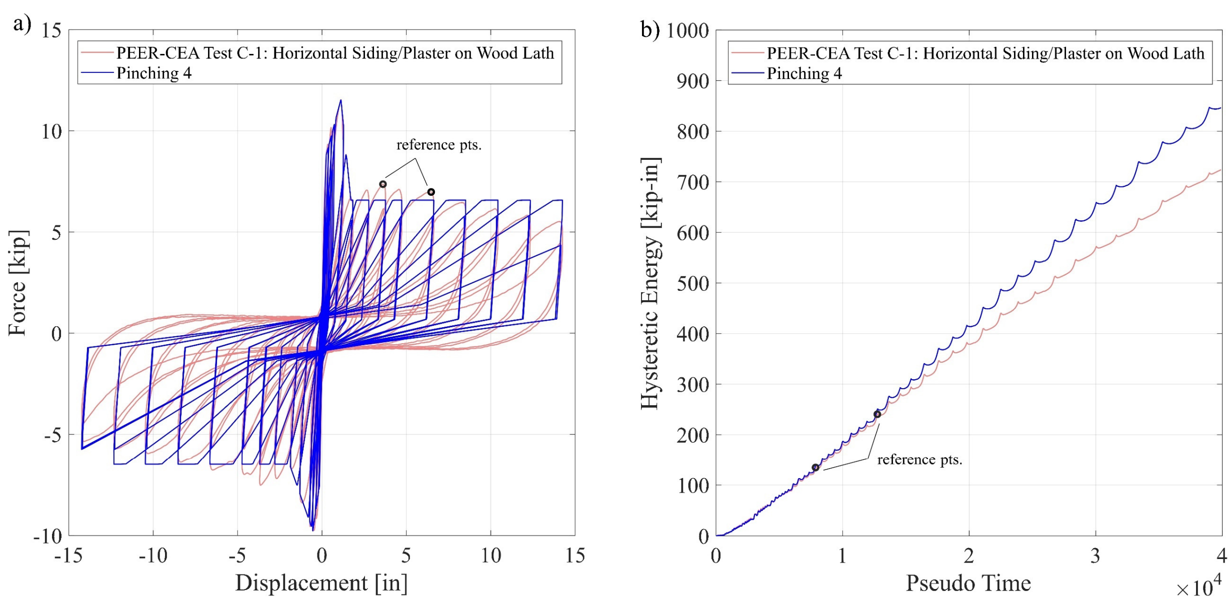

Figure 3.19 Comparing the *Pinching4* material calibrated to horizontal wood siding with plaster on wood lath test C-1 [Cobeen et al. 2020]: (a) hysteretic response; and (b) hysteretic energy.

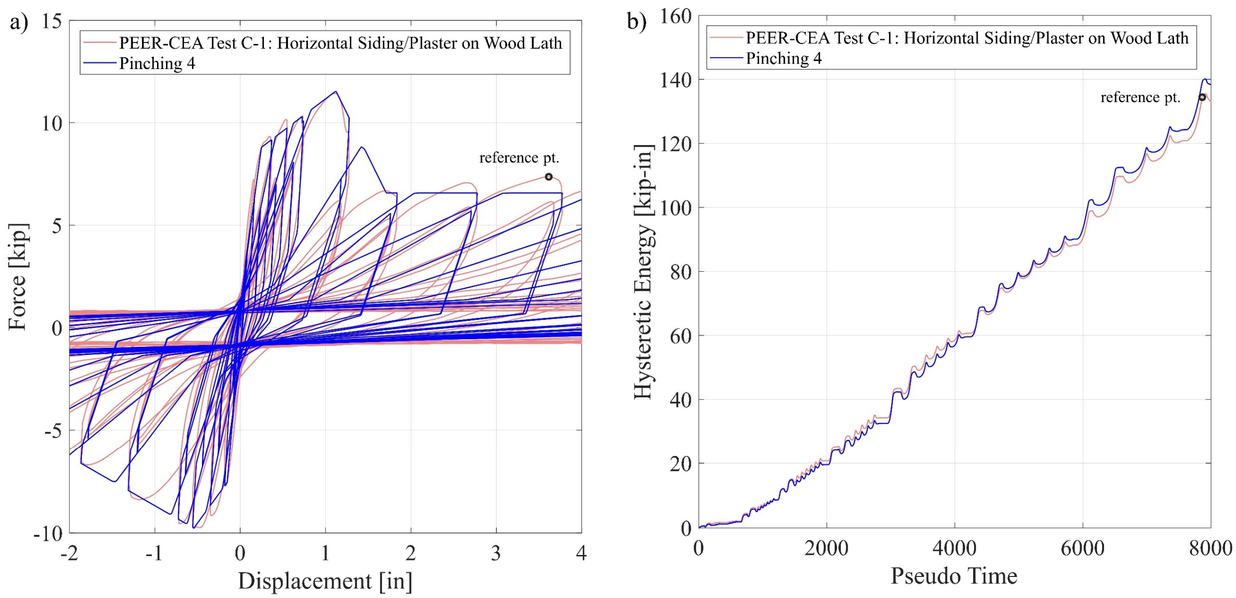

Figure 3.20 Zoomed view comparing the *Pinching4* material calibrated to horizontal wood siding with plaster on wood lath test C-1 [Cobeen et al. 2020]: (a) hysteretic response; and (b) hysteretic energy.

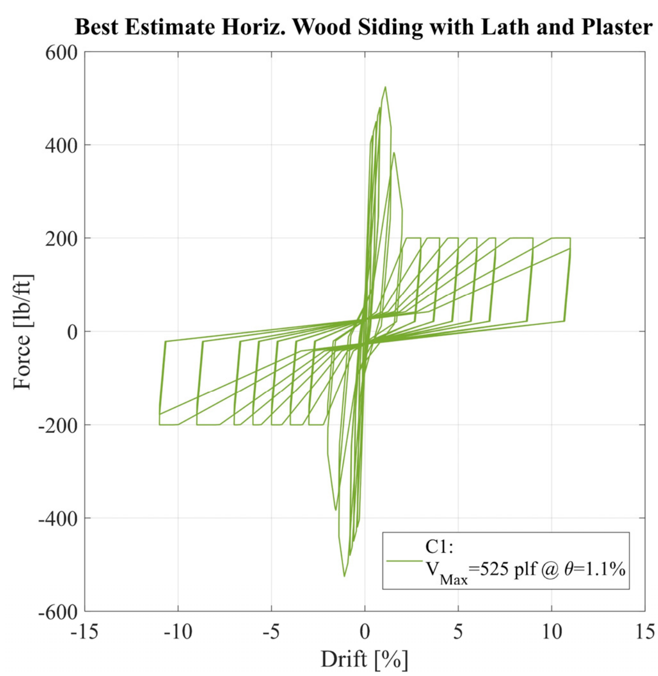

Figure 3.21 Best estimate horizontal wood siding with interior plaster on wood lath (C1) material shown in normalized units and loaded with the PEER–CEA loading protocol.

Table 3.6 Summary of *Pinching4* material parameters for exterior horizontal wood siding with plaster on wood lath interior.

Material		Backbone deformation points (%drift)				Backbone force points (plf)			
		*ed*1	*ed*2	*ed*3	*ed*4	*ef*1	*ef*2	*ef*3	*ef*4
C1 (best estimate)		0.08	0.30	1.10	2.20	152	404	525	200
Cyclic properties	Spring 1	rDisp1	rForce1	uForce1	gK11	gKLim1	gD11	gDLim1	
		0.06	0.31	0.14	-0.07	-0.50	0.14	0.30	
	Spring 2	rDisp2	rForce2	uForce2	gK12	gKLim2	gD12	gDLim2	
		0.28	0.18	-0.11	-0.05	-0.20	0.11	0.30	

*Definition of material model parameters is provided in Table 3.4; this material is developed as a double-sided material including both exterior and interior finish.

3.4.3 Exterior Stucco with Gypsum Wallboard

3.4.3.1 Experimental Data for Stucco combined with Gypsum Wallboard

Available experimental testing on stucco exterior walls with gypsum wallboard interior comes exclusively from CUREE testing as part of either the CUREE-Caltech Woodframe Project or the CUREE Earthquake Damage Assessment and Repair Project (CUREE-EDA). This includes testing conducted by Pardoen et al. [2003] during the CUREE Woodframe Project and tests conducted as part of a two-phase series by Arnold et al. [2003(a); 2003(b)]. Notably, these tests are discussed in detail within the *FEMA P-1100* background documentation [2019(b)].

Testing conducted by Pardoen et al. [2003] includes four tests with combined stucco and gypsum wallboard, tests 14A, 14B, 15A, and 15B. The stucco material is applied in three coats (7/8-in. finish thickness) to line wire and hex mesh and fastened with 7/16-in. leg staples spaced at 7 in. on center. Stucco stops were provided at all boundaries, but the stucco was free to slide past the framing. Gypsum wallboard was applied horizontally (4-ft × 8-ft sheets) attached with 1-1/4-in. coarse threaded drywall screws spaced at 7 in. on center. The test setup used 8-ft-high × 16-ft-long walls. Test group 14 included a garage door opening (two 3-ft-0-in. wide piers for a total of 6 ft of full height bracing wall), and Test group 15 included a standard door opening (two 6-ft-6-in.-wide piers for a total of 13 ft of full-height wall). An illustration of the specimen geometry for Pardoen et al. [2003] tests is shown in Figure 3.22. Testing used the CUREE protocol [Krawinkler et al. 2000]. As mentioned in *FEMA P-1100*, Vol. 3 [2019b], significant slip between stucco and framing occurred, resulting in retained strength at drift levels much higher than seen in other stucco testing and not thought to be representative of the behavior of real houses. The strength levels, however, are thought to reasonably represent a mid-level capacity of stucco in good condition.

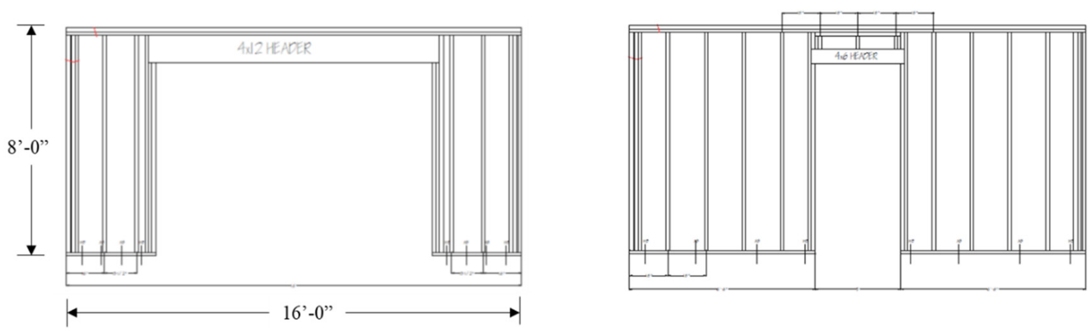

Figure 3.22 Different wall openings for stucco plus gypsum wallboard specimens tested by Pardoen et al. [2003]: Group 14 with garage door (left, L_{eff} = 6 ft); Group 15 with pedestrian door (right, L_{eff} = 13 ft).

Relevant tests conducted by Arnold et al. [2003(a); 2003(b)] included tests 1 and 2 and tests 5 through 8. All tests used three-coat 7/8-in. stucco embedded in 17-gauge hex lath and fastened with furring nails spaced at 6 in. on center. Tests 1, 2, 5, and 6 had 1/2-in. chop strand fibers included in the stucco base coats. Gypsum wallboard was applied horizontally (4-ft × 8-ft sheets) with either staggered and non-staggered (tests 6 and 8) joints attached with 6d cooler nails spaced at 7 in. on center. The test setup used 8-ft-high × 16-ft-long walls, one configuration with two window openings and the other configuration with one window and one door; see Figure 3.23. The wall with two window openings had a total of 8 ft of full-height wall, while the wall with the window plus door had 9 ft-4 in. of full-height wall. Actual windows and doors were placed in the openings to make the specimens more realistic. The interior gypsum boundary conditions included returns to confine the gypsum at wall ends and at the top of the wall, representing the ceiling, but there was no confinement at the wall base due to the practice of holding the bottom up from the unfinished floor during installation. The stucco boundary conditions included wrapping the stucco around the posts at either end. No stucco confinement was provided at the wall top or bottom. In addition to typical anchor bolts, overturning restraint was provided by a series of steel rods that introduced concentrated vertical loads (intended to represent gravity dead loads) at three or four points along the wall, where the applied forces were maintained constant through the testing. No specific additional tie-down devices were provided.

Walls 1 and 2 [Arnold et al. 2003(a)] were intended to represent the bottom story of a two-story residence. The gravity dead load applied during this testing was equivalent to 450 plf applied in three concentrated loads. The loading was distributed to the wall with a W10 loading beam. CUREE-CEA Walls 5 through 8 [Arnold et al. 2003(b)] were intended to represent the top story of a two-story or a single-story dwelling. A gravity dead load of 250 plf was applied in four concentrated loads, and the loading beam was replaced with a 3/8-in. steel strap. *FEMA P-1100*, Vol. 3 [2019(b)] considered these tests to be the upper bound of capacity from available testing. This is attributed to the effect of the boundary conditions on the finish material and the observed ability for the entire stucco face to mobilize all fasteners when reaching peak strength, after which the specimen began to degrade and break into isolated sections (of stucco) that rotated independently with increasing displacement. Figure 3.24 provides a comparison of the stucco end boundary conditions between the two sources of information for the stucco/gypsum wallboard tests.

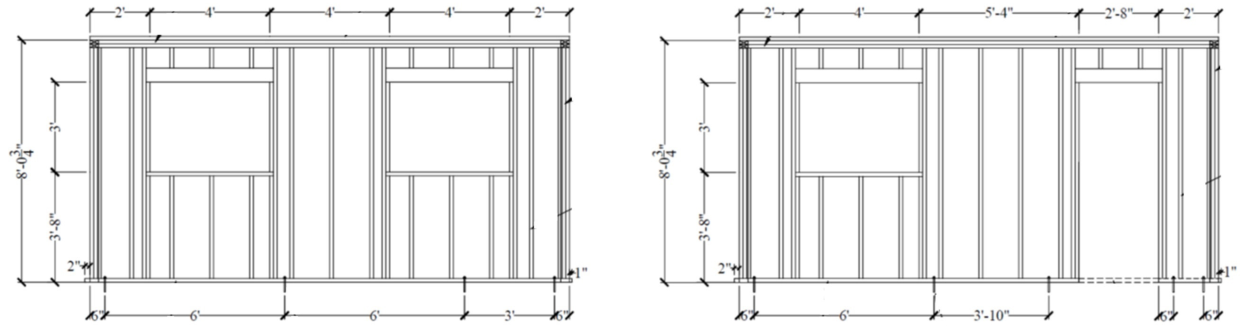

a) b)

Figure 3.23 Different wall openings for stucco plus gypsum wallboard specimens tested by Arnold et al. [2003]: (a) odd-numbered tests (L_{eff} = 8 ft); and (b) even-numbered tests (L_{eff} = 9.33 ft).

a) b)

Figure 3.24 Different stucco end boundary conditions: (a) Arnold et al. [2003(b)]; and (b) Pardoen et al. [2003].

3.4.3.2 Numerical Material Properties for Exterior Stucco plus Gypsum Walls

The interpretation of available testing for combined exterior stucco and gypsum wallboard was conducted as part of the ATC-110 project [FEMA 2019(b)]. As per recommendations of the WG2 building variant report [Reis 2020(a)], the treatment of superstructure strength would be according to the findings of ATC-110, especially for material combinations that were not explicitly addressed through further testing by WG4. As such, the best estimate strength for stucco plus gypsum wallboard assumes an 800 plf peak strength based on previous review and interpretation of test data in ATC-110. As part of this Project, the existing experimental data was reviewed further to estimate a realistic backbone shape appropriate for seismic loss assessment. Notably, the stucco plus gypsum properties were developed earlier in the Project when a range of material properties was expected to be included, as opposed to only using best estimate properties.

Figure 3.25 shows a collection of experimental backbone curves and basis curves and strengths used for a range of material bound assumptions. The upper bound backbone curve (S4, solid red line) is based on the average of CUREE-EDA Walls 5 through 8 [Arnold et al. 2003(b)]. The phase one tests (Walls 1 and 2) were not included in the upper bound, but the positive and negative backbone curves for CUREE-EDA Wall 1 [Arnold et al. 2003(a)] are shown in black for comparison. The purple curve in Figure 3.25 represents the average of representative tests (CUREE-EDA Walls 5 through 8 and Pardoen tests), denoted S3. The green flat line represents the ATC-110 best estimate strength of 800 plf. The gray flat line represents the strength associated with a lower bound (S1) proposed by ATC-110. The lowest test backbone is the 8-ft × 8-ft stucco-only cyclic test 20C conducted by COLA [2001], included in Figure 3.25 for comparison.

The four-point *Pinching4* material backbones for each of the material strength levels are shown in Figure 3.26. The peak point of the best estimate curve (S2) was based on the best estimate strength from ATC-110 and a drift of 1.5%, which is assumed to be the same as the peak point of the average (S3) curve. The other pre-peak points on the S2 curve were chosen to give 80% of the stiffness of the S3 curve. The post-peak stiffness of S2 was based on the same descending stiffness as the S3 curve, with the last point defined based on a residual strength equal to 30% of the peak strength. The lower bound curve (S1) is assumed to have two-thirds of the initial stiffness of the S3 curve, with its intermediate force point (*ef2*) reached at a force equal to half that of the best estimate curve (S2), which also has twice the assumed peak capacity. This lower bound material was developed for possible sensitivity studies.

The cyclic properties were estimated using CUREE-EDA Walls 5 through 8 [Arnold et al. 2003(b)]. These were the only available tests with reliable cyclic data. Initially, all four walls were used to determine the range of cyclic behavior, and data for Wall 5 was eventually used for fine tuning of properties since this specimen had the cleanest data. The general cyclic trends did not vary considerably between tests. Figure 3.27 provides a comparison of the *Pinching4* material compared to CUREE-EDA Wall 5 [Arnold et al. 2003(b)] in terms of hysteresis loops and hysteretic energy. Figure 3.28 shows a zoomed view to show the cyclic properties in the small displacement range. Figure 3.29 shows the best estimate stucco plus gypsum wallboard *Pinching4* material (S2) in normalized units and loaded using the PEER–CEA loading protocol [Zareian and Lanning 2020]. The *Pinching4* material parameters for stucco plus gypsum wallboard are provided in Table 3.7.

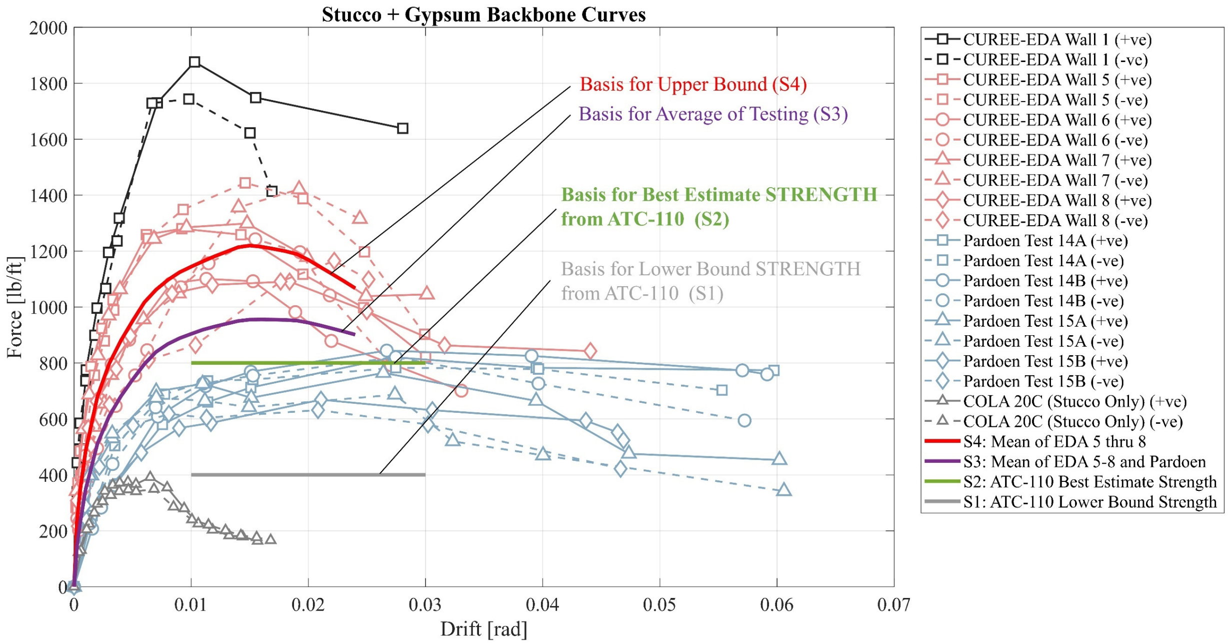

Figure 3.25 **Backbone curves considered for stucco plus gypsum wallboard properties with assumed average backbones of tests or ATC-110 strengths corresponding to upper bound (S3), relevant test average (S3), best estimate (S2), and lower bound materials (S1).**

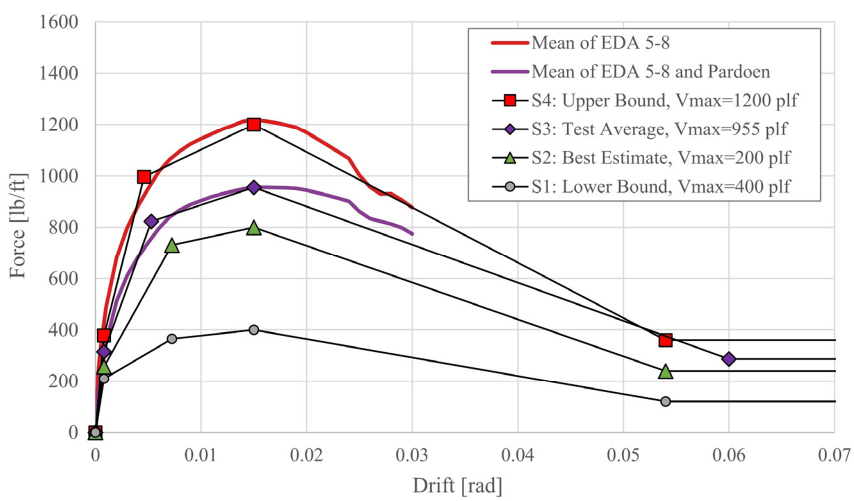

Figure 3.26 **Four-point *Pinching4* backbone compared to target test data: various strength levels of stucco plus gypsum wallboard; best estimate is material S2.**

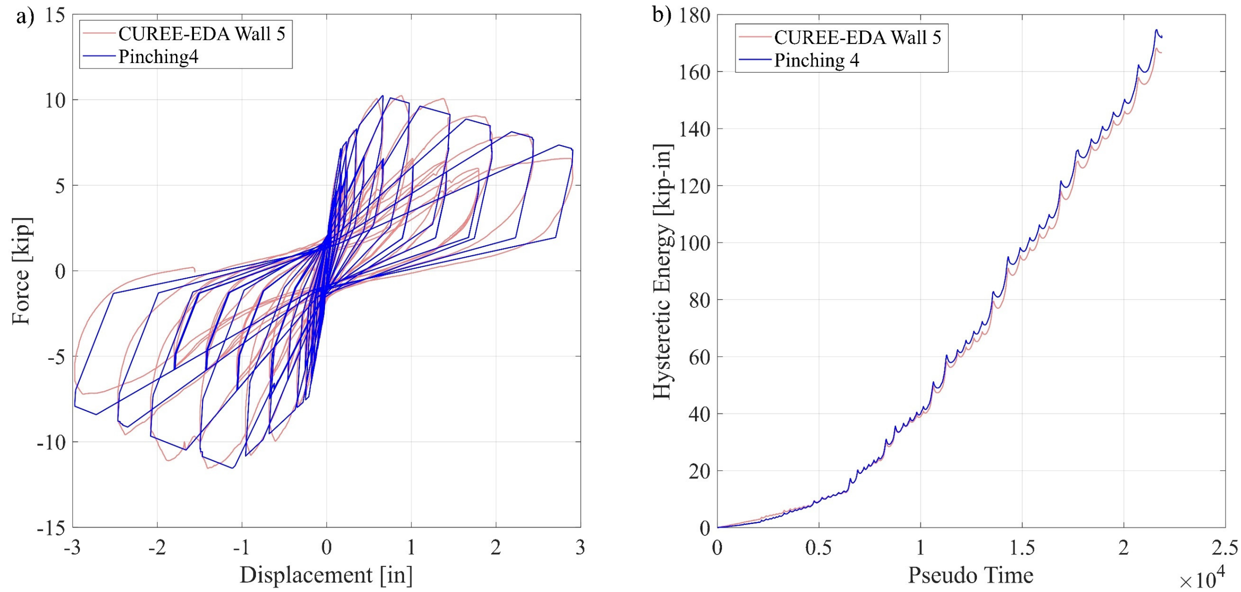

Figure 3.27 **Comparing the *Pinching4* material calibrated to stucco plus gypsum wallboard Test 5 by Arnold et al. [2003(b)]: (a) hysteretic response; and (b) hysteretic energy.**

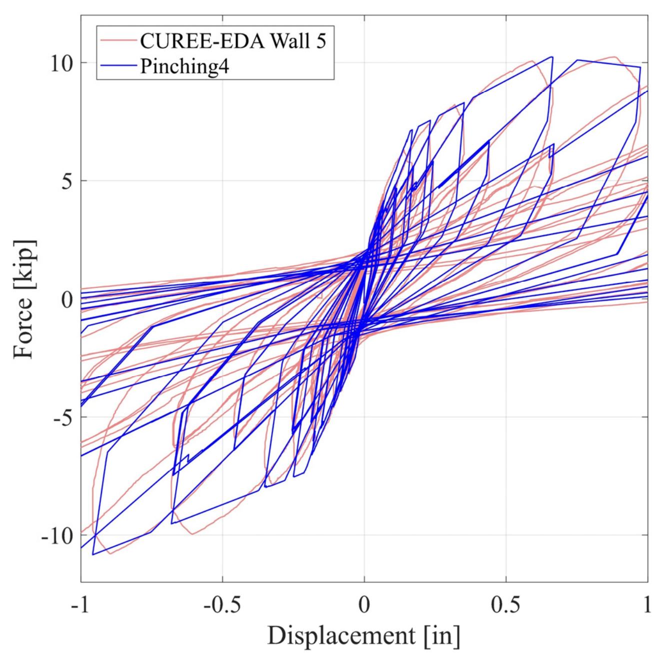

Figure 3.28 **Comparing the *Pinching4* material calibrated to stucco plus gypsum wallboard Test 5 by Arnold et al. [2003(b)]: zoomed view of hysteretic response.**

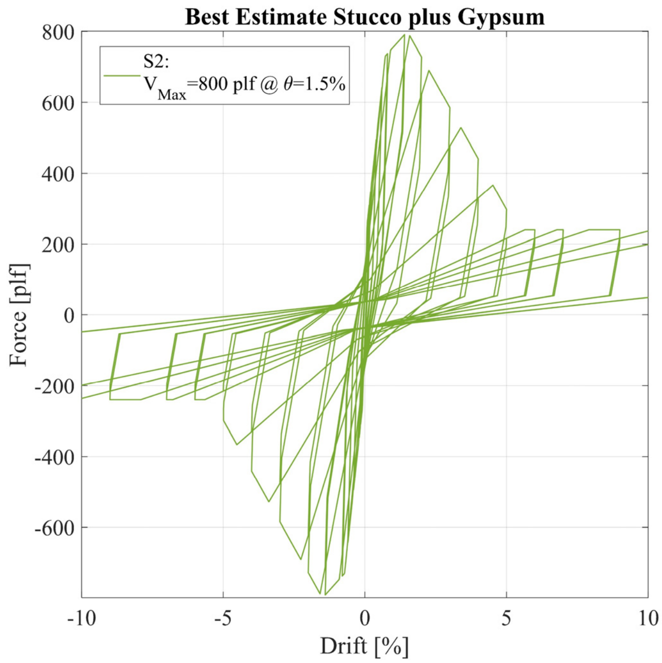

Figure 3.29 **Best estimate stucco plus gypsum wallboard (S2) material shown in normalized units and loaded with the PEER–CEA loading protocol.**

Table 3.7 **Summary of *Pinching4* material parameters for stucco plus gypsum wallboard.**

Material	Backbone deformation points (%drift)				Backbone force points (plf)			
	*ed*1	*ed*2	*ed*3	*ed*4	*ef*1	*ef*2	*ef*3	*ef*4
S1 (lower bound)	0.08	0.72	1.50	5.40	210	366	400	120
S2 (best estimate)	**0.08**	**0.72**	**1.50**	**5.40**	**257**	**731**	**800**	**240**
S3 (test average)	0.08	0.53	1.50	6.00	315	823	955	287
S4 (upper bound)	0.08	0.46	1.50	5.40	378	996	1200	360
Cyclic properties	Spring 1	rDisp1	rForce1	uForce1	gK11	gKLim1	gD11	gDLim1
		0.06	0.26	-0.20	0	0	0.13	2.0
	Spring 2	rDisp2	rForce2	uForce2	gK12	gKLim2	gD12	gDLim2
		0.06	0.17	-0.23	0.30	2.0	0.13	2.0

*Definition of material model parameters is provided in Table 3.4; this material is developed as a double-sided material including both exterior and interior finish.

3.4.4 Exterior Stucco with Lath Plaster

No experimental data on combined exterior stucco with interior lath and plaster was found in the published literature. Absent test data, the proposed modeling parameters for this combination is based on the best available information from published tests of similar materials and the PEER–CEA testing conducted by WG4. The available information is combined with judgment to develop material properties that reflect the best estimate of the behavior of these two finish materials.

The contribution of exterior stucco to the wall response of the combined materials considers tests 17A and 17B conducted by Pardoen et al. [2003]. These tests have the same stucco construction details discussed in Section 3.4.3 and have the geometry shown in the right portion of Figure 3.22 with a single standard door. Additionally, PEER–CEA Test A-25 [Schiller et al. 2020(c)] was considered for stucco contribution to the exterior face of the combined material. As described in more detail in Section 3.6.2, Test A-25 is a 6-ft-tall × 12-ft-long stucco cripple wall specimen. This combination of tests was selected to include stucco data of larger sub-assemblies with openings (Pardoen 17A and 17B) and walls with confined end boundaries (Test A-25). Figure 3.30 shows the individual and average backbone curves for the stucco only material considered for combination with interior plaster on wood lath.

The participation of plaster on wood lath assumes the same best estimate backbone curve used for interior partitions. The basis of this material backbone is developed and discussed in Section 3.5.2. Figure 3.31 illustrates the relative contribution of stucco and plaster on wood lath, as well the best estimate for the combined material (SLP2). The proposed *Pinching4* material backbone for upper bound stucco plus gypsum wallboard is included in the figure for reference, confirming that the peak capacity and initial stiffness of the proposed SLP2 curve is roughly in line with the upper bound stucco plus gypsum testing. This curve is based on the average of CUREE-EDA Walls 5 through 8 [Arnold et al. 2003(b)]; see Section 3.4.3. The combined SLP2 curve has a peak strength of approximately 1050 plf. This is 250 plf larger than that assumed for best estimate stucco and gypsum material S2; see Figure 3.29. The best estimate gypsum wallboard material (G2) has an assumed peak strength of 210 plf, while the best estimate lath and plaster material (LP2) has a strength of 445 plf. Despite the lack of experimental data, the assumed peak strength for best estimate stucco with lath and plaster (SLP2) is reasonably consistent with other materials assumed in the study. Shown in Figure 3.32 are the results of fitting the four-point *Pinching4* backbone to the best estimate stucco with plaster on wood lath (SLP2).

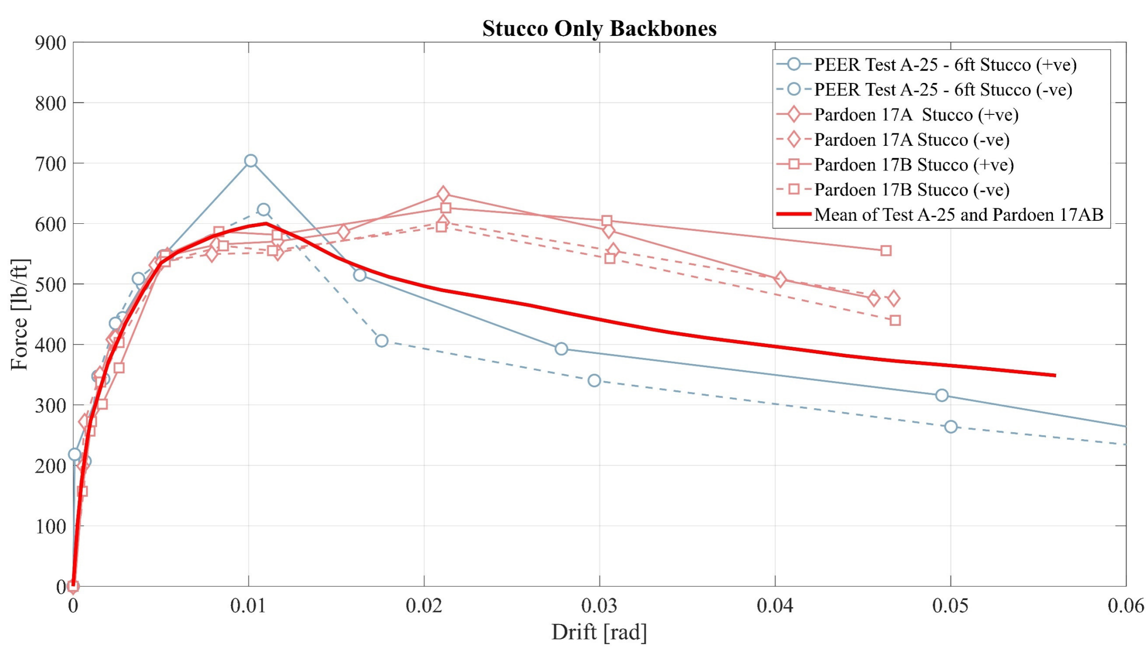

Figure 3.30 Stucco only test backbones and mean (bold line) assumed for combination with interior plaster on wood lath.

The participation of plaster on wood lath assumes the same best estimate backbone curve used for interior partitions. The basis of this material backbone is developed and discussed in Section 3.5.2. Figure 3.31 illustrates the relative contribution of stucco and plaster on wood lath, as well the best estimate for the combined material (SLP2). The proposed *Pinching4* material backbone for upper bound stucco plus gypsum wallboard is included in the figure for reference, confirming that the peak capacity and initial stiffness of the proposed SLP2 curve is roughly in line with the upper bound stucco plus gypsum testing. This curve is based on the average of CUREE-EDA Walls 5 through 8 [Arnold et al. 2003(b)]; see Section 3.4.3. The combined SLP2 curve has a peak strength of approximately 1050 plf. This is 250 plf larger than that assumed for best estimate stucco and gypsum material S2; see Figure 3.29. The best estimate gypsum wallboard material (G2) has an assumed peak strength of 210 plf, while the best estimate lath and plaster material (LP2) has a strength of 445 plf. Despite the lack of experimental data, the assumed peak strength for best estimate stucco with lath and plaster (SLP2) is reasonably consistent with other materials assumed in the study. Shown in Figure 3.32 are the results of fitting the four-point *Pinching4* backbone to the best estimate stucco with plaster on wood lath (SLP2).

Cyclic properties for combined stucco and plaster on wood lath assume the same properties attributed to stucco plus gypsum walls. This assumption was made out of necessity since no better information is currently available. The development of these cyclic properties is discussed in Section 3.4.3. Figure 3.33 shows the hysteretic response of the best estimate stucco plus plaster on wood lath *Pinching4* material (SLP2) in normalized units, where loading is based on the PEER–CEA loading protocol [Zareian and Lanning 2020]. The *Pinching4* material parameters for best estimate stucco plus plaster on wood lath (SLP2) are provided in Table 3.8.

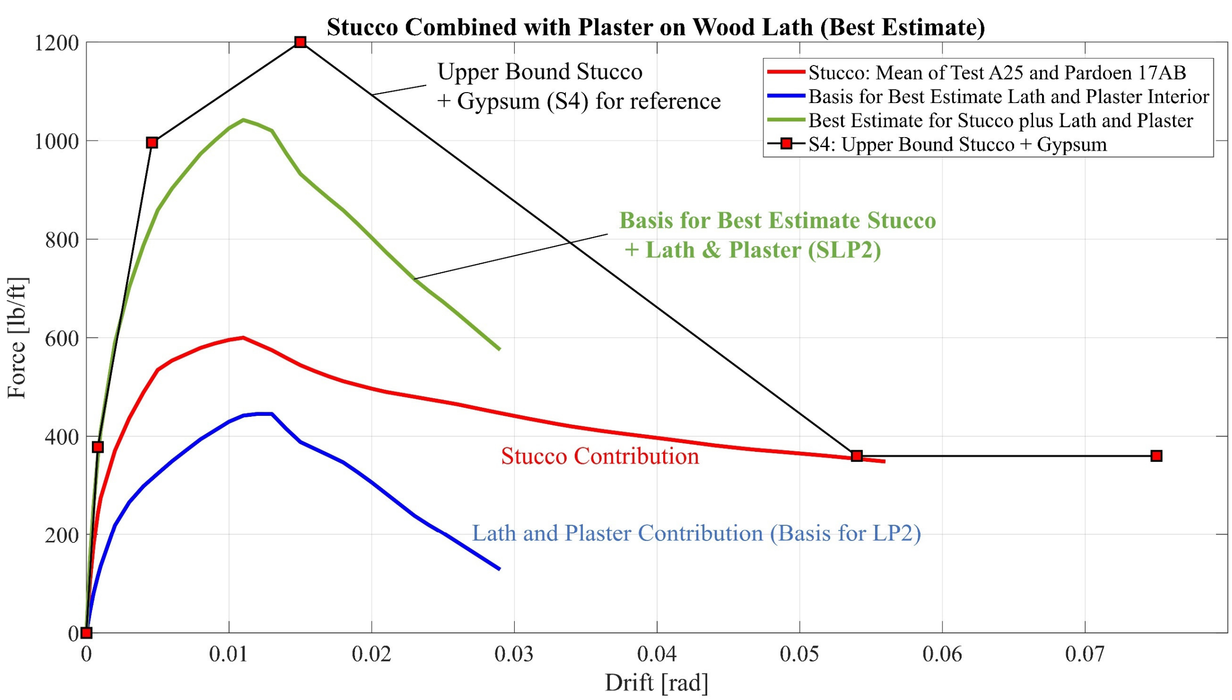

Figure 3.31 **Basis for best estimate stucco with lath and plaster material backbones showing the assumed contribution of stucco and lath and plaster.**

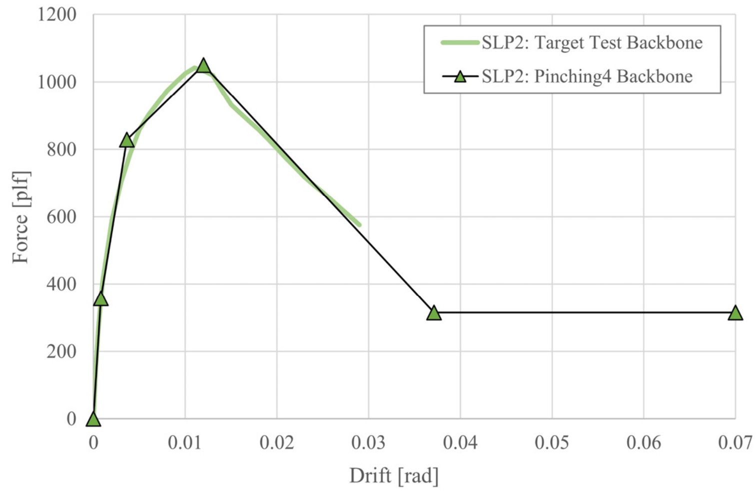

Figure 3.32 Best estimate *Pinching4* backbone for combined exterior stucco and interior plaster on wood lath compared with target test backbone.

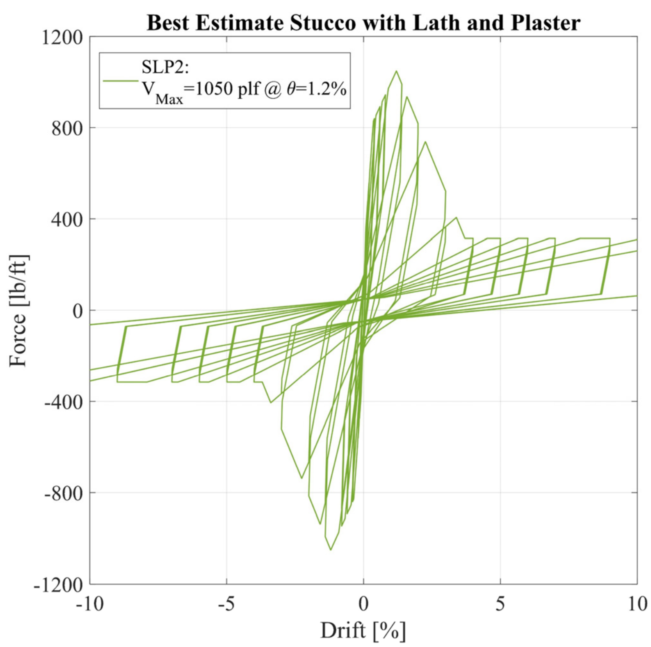

Figure 3.33 Best estimate stucco plus plaster on wood lath (SLP2) material shown in normalized units and loaded with the PEER–CEA loading protocol.

Table 3.8 Summary of *Pinching4* material parameters for exterior stucco with plaster on wood lath interior.

Material		Backbone deformation points (%drift)				Backbone force points (plf)			
		*ed*1	*ed*2	*ed*3	*ed*4	*ef*1	*ef*2	*ef*3	*ef*4
SLP2 (best estimate)		0.08	0.36	1.20	3.70	357	829	1050	315
Cyclic properties	Spring 1	rDisp1	rForce1	uForce1	gK11	gKLim1	gD11	gDLim1	
		0.06	0.26	-0.20	0	0	0.13	2.0	
	Spring 2	rDisp2	rForce2	uForce2	gK12	gKLim2	gD12	gDLim2	
		0.06	0.17	-0.23	0.3	2.0	0.13	2.0	

*Definition of material model parameters is provided in Table 3.4; this material is developed as a double-sided material including both exterior and interior finish.

3.4.5 Panelized Plywood Siding (T1-11) with Gypsum Wallboard

Existing information on T1-11 siding is extremely limited, with two monotonic backbones from APA testing [APA 1993] provided in the material backbone development in *FEMA P-807* [2012(d)]. The average of the two curves has a capacity of 565 plf at a drift of 2%. As information on combined T1-11 and gypsum wallboard was not available, this combination was selected for testing by PEER–CEA WG4.

The best estimate material properties for combined T1-11 (panelized wood) siding with gypsum wallboard interior are based on PEER–CEA Test C-2 [Cobeen et al. 2020]. Specimen C-2 is 8 ft tall × 20 ft long with dual walls tested in parallel with continuous end return walls between the two principal walls. Each wall has one door and one window, with 11 ft of full-height wall per side (L_{eff} = 22 ft). Figure 3.34 provides a photograph of the specimen and the resulting hysteretic response from cyclic loading according to the PEER–CEA loading protocol [Zareian and Jennings 2020].

Figure 3.35 shows the cyclic backbone envelopes (positive, negative, and mean) for Test C-2 in comparison with the fitted *Pinching4* backbone curve with material designation “T1.” The best estimate backbone curve is based on the average of both loading directions of test C-2, where the estimated peak strength is 852 plf. In contrast, the *FEMA P-807* strength of 565 plf combined with the best estimate gypsum strength of 210 plf (see Section 3.5.1) would give a strength of 775 plf with full superposition or 670 plf using the *FEMA P-807* combination rule [2012(d)].

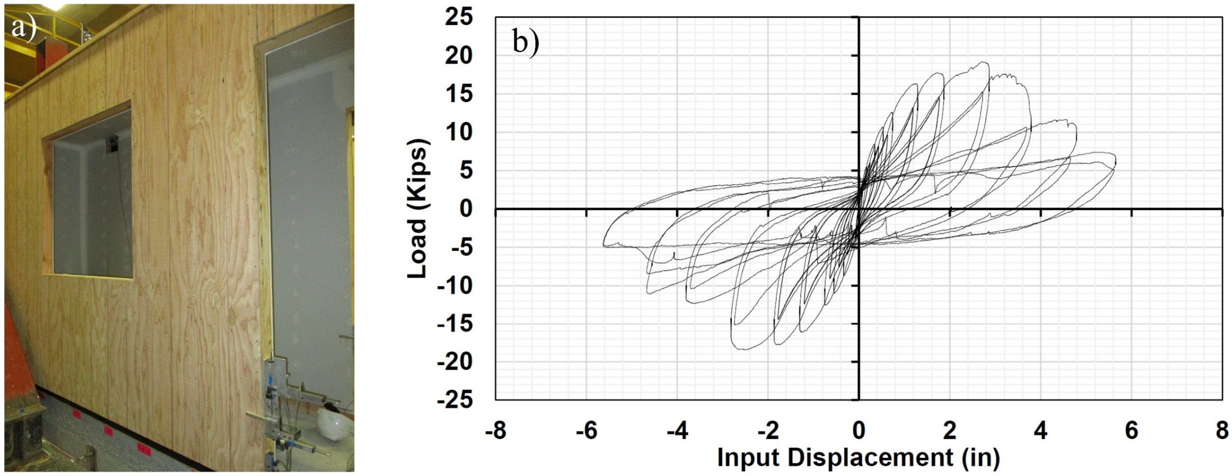

Figure 3.34 **PEER–CEA large-component test C-2 [Cobeen et al. 2020] used for modeling exterior T1-11 siding with interior gypsum wallboard: (a) photograph of specimen; and (b) hysteretic response.**

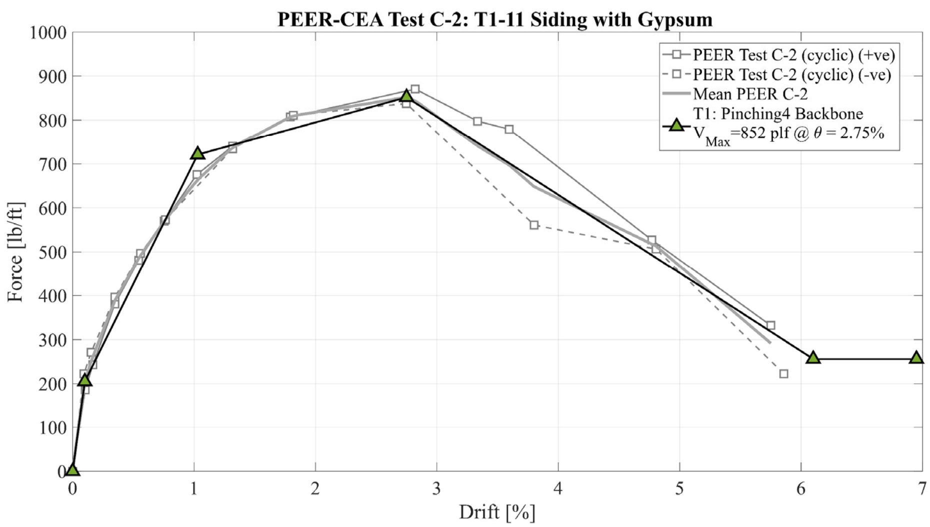

Figure 3.35 **Backbone curves for PEER–CEA large-component test C-2 [Cobeen et al. 2020] and best estimate *Pinching4* backbone (material T1) for exterior T1-11 siding with interior gypsum wallboard.**

The cyclic calibration of Test C-2 required that the raw data from WG4 be corrected for the baseline displacement, i.e., shifting the data so that loading begins at zero displacement. Further, a small amount of smoothing was applied to the data. This was done using a similar process as Test C-1, as described in Section 3.4.2 and illustrated in Figure 3.18. The cyclic fitting using the *Pinching4* material is compared to the target test for force-displacement response and hysteretic energy in Figure 3.36. The figure shows very good agreement with the experimental results except for the largest displacement cycles. Figure 3.37 shows the best estimate T1-11 siding and gypsum wallboard *Pinching4* material (T1) in normalized units and loaded using the PEER–CEA loading protocol [Zareian and Lanning 2020]. The *Pinching4* material parameters for best estimate T1-11 siding with interior gypsum wallboard (Material T1) are provided in Table 3.9.

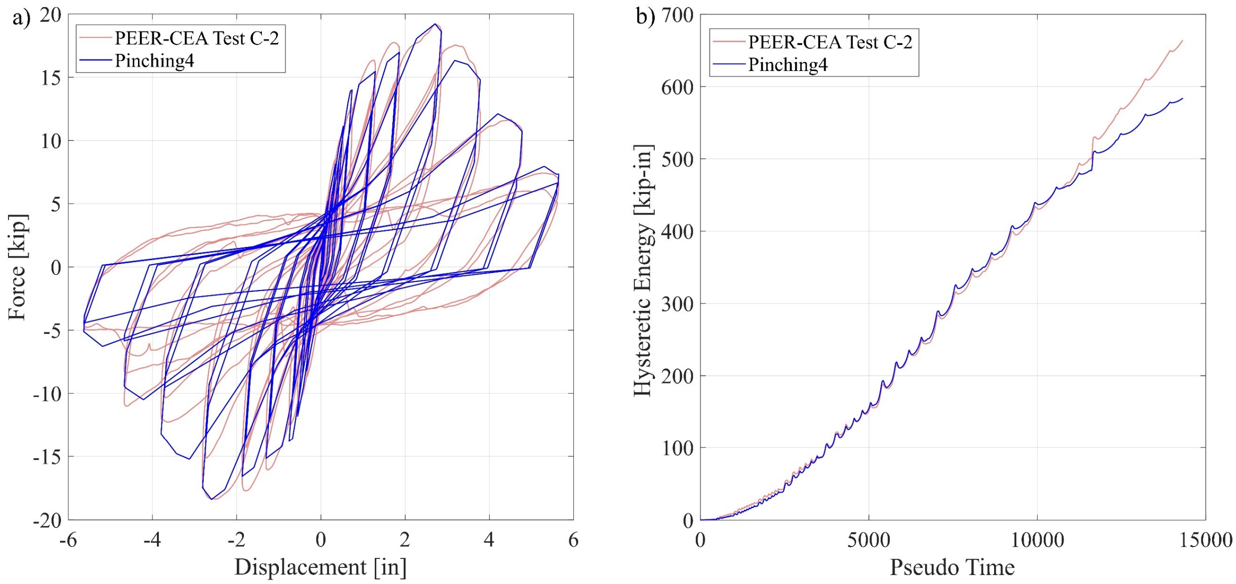

Figure 3.36 **Comparing the *Pinching4* material calibrated to T1-11 siding with gypsum wallboard test C-2 [Cobeen et al. 2020]: (a) hysteretic response; and (b) hysteretic energy.**

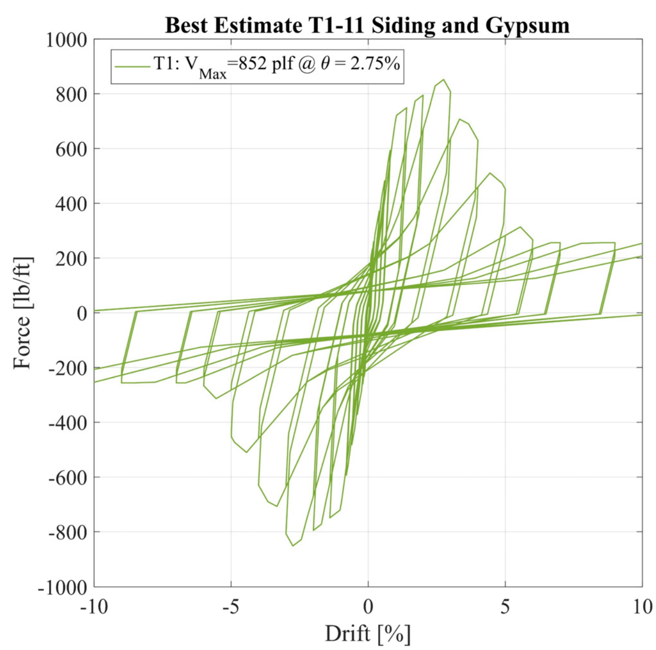

Figure 3.37 **Best estimate T1-11 siding with interior gypsum wallboard (T1) material shown in normalized units and loaded with the PEER–CEA loading protocol.**

Table 3.9 Summary of *Pinching4* material parameters for T1-11 siding with gypsum wallboard interior.

Material	Backbone deformation points (%drift)				Backbone force points (plf)			
	*ed*1	*ed*2	*ed*3	*ed*4	*ef*1	*ef*2	*ef*3	*ef*4
T1 (best estimate)	0.10	1.03	2.75	6.10	205	721	852	256
Cyclic properties	Spring 1	rDisp1	rForce1	uForce1	gK11	gKLim1	gD11	gDLim1
		0.30	0.25	-0.01	0	0	0.22	2.0
	Spring 2	rDisp2	rForce2	uForce2	gK12	gKLim2	gD12	gDLim2
		0.50	0.50	0.02	0	0	0.11	3.0

*Definition of material model parameters is provided in Table 3.4; this material is developed as a double-sided material including both exterior and interior finish.

3.5 INTERIOR SUPERSTRUCTURE MATERIALS

3.5.1 Gypsum Wallboard

Gypsum wallboard is a typical interior material for houses constructed after the mid-1950s [HUD 2001] and is used for the recent eras considered within the PEER–CEA Project. This section reviews the available experimental information on gypsum wallboard, followed by the selection of different test specimen combinations to develop strength and stiffness bounds based on the observed range of material behavior. The section then describes the monotonic and cyclic calibration of numerical models and the proposed set of hysteretic modeling parameters.

3.5.1.1 Available Experimental Data on Gypsum Wallboard

A large number of experimental tests exist within the literature for gypsum wallboard. The majority of the most reliable tests in terms of boundary conditions and loading protocol come from the various testing campaigns conducted as part of the CUREE-Caltech Woodframe Project [Gatto and Uang 2002; McMullin and Merrick 2002; and Pardoen et al. 2003]. More recently, gypsum wallboard tests were also conducted by Bahmani and van de Lindt [2016]. Notably, all of the considered test results used monotonic loading or cyclic loading based on the CUREE-Caltech loading protocol [Krawinkler et al. 2000].

Gatto and Uang [2002] tested a large number of 8-ft × 8-ft wall specimens investigating the effects of various loading protocols on the force-deformation response of wood-frame shear walls with different sheathing and finish combinations. While most of their tests included sheathing combinations with wood structural panel (WSP) shear walls, Gatto and Uang [2002] tested two gypsum wallboard-only specimens under monotonic loading. Test specimen 12 (east and west) consisted of an 8-ft × 8-ft wall with 1/2-in.-thick gypsum applied with two gypsum panels placed horizontally with 1-1/4-in.-long drywall screws placed at 16 in. on center. The specimens did not have any wall openings, and the edges of the wallboard panels were unrestrained. Although unclear, it is assumed that vertical loading was not applied to the test specimens.

McMullin and Merrick [2002] tested 17 wall specimens with double-sided gypsum wallboard. Specimens were 8 ft tall × 16 ft long and considered of range of openings, fastener types, boundary nailing at the top plate, and loading protocol (i.e., monotonic and cyclic). Importantly, the tests considered realistic confinement of the gypsum wallboard along the end boundaries and along the top course of wallboard. An illustration of the typical gypsum boundary conditions tested by McMullin and Merrick [2002] are shown in Figure 3.38. The two different opening configurations considered a single door or a combined door and window as shown in Figure 3.39. Note that effective lengths (L_{eff}) considered that gypsum was applied on both sides of the wall framing.

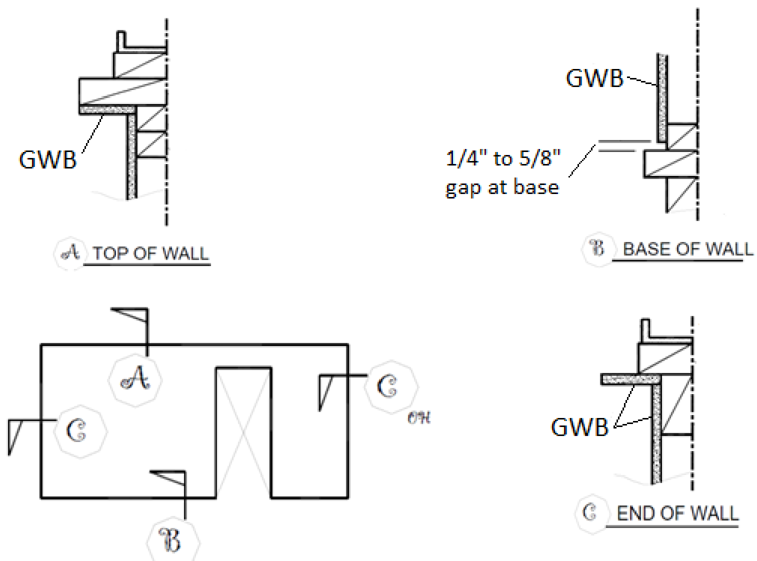

Figure 3.38 Illustration of gypsum boundary conditions constructed for specimens tested by McMullin and Merrick [2002] (figure adapted from McMullin and Merrick [2002]).

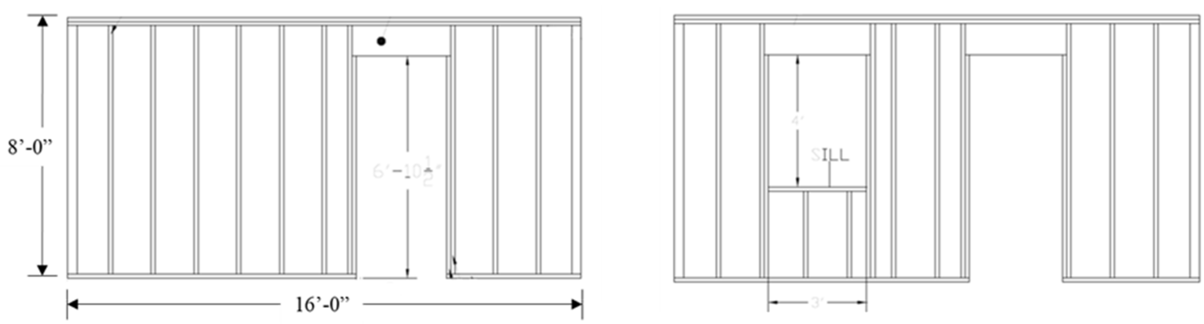

Figure 3.39 Different wall openings for double-sided gypsum wallboard specimens tested by McMullin and Merrick [2002]: single door (left, L_{eff} = 26 ft); door and window (right, L_{eff} = 20 ft).

McMullin and Merrick [2002] considered two variants of vertical loading with both a free- and fixed-top. The free top had vertical loads simulated via steel rods at the wall ends only to simulate an upper story or single-story condition. The fixed top condition had an additional pair of steel rods near the center of the wall to simulate bottom story (of a two-story structure) conditions. The gravity loading roughly corresponds to 250 lb/ft and 500 lb/ft for the free- and fixed-top conditions, respectively.

Testing conducted by Pardoen et al. [2003] included single sided-gypsum specimens on 8 ft-wall × 16-ft-long walls. The tests were conducted in pairs for each detail group (A and B); with groups 18 and 19 representing the tests conducted with gypsum wallboard only. Group 18 had a large garage door opening (10-ft wide) with gypsum wallboard attached with #6 drywall screws at 7 in. on center. Group 19 had a smaller 3-ft-wide pedestrian door with #6 screws placed at 7 in. on center. The gypsum edge boundaries were not confined. It is unclear as to the amount of gravity loading (if any) applied to these test specimens. An illustration of the different wall openings considered is shown in Figure 3.40.

Finally, testing by Bahmani and van de Lindt [2016] considered two similar gypsum wallboard specimens as part of an investigation into the combination of sheathing materials for wood-frame structures, namely specimens G-01 and G-02. The specimens were 8-ft × 8-ft walls, without any openings, constructed with 1/2-in.-thick gypsum wallboard placed vertically. The panels were attached with #6 drywall screws spaced at 16 in. on center at the edge and in the field. These panels had free boundary conditions and hold-downs were installed at each end to prevent uplift.

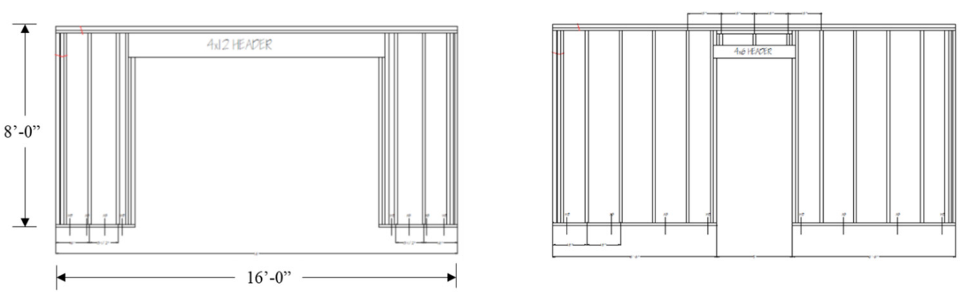

Figure 3.40 Different wall openings for gypsum wallboard specimens tested by Pardoen et al. [2003]: Group 18 with garage door (left, L_{eff} = 6 ft); Group 19 with pedestrian door (right, L_{eff} =13 ft).

3.5.1.2 Numerical Material Properties for Gypsum Wallboard

The backbone response curves from the gypsum wallboard tests are shown in Figure 3.41, which illustrates the large range of backbone behavior across all tests considered. The selection of representative tests for best estimate properties used previous work conducted in the ATC-110 project (see FEMA [2019(b)]) as a starting point for interpreting the different tests. The best estimate backbone curve is assumed to be the average envelope of McMullin and Merrick [2002] tests 1, 6, 7, and 11. These were deemed representative of realistic boundary conditions and combine the behavior of drywall nails and screws. Further, different opening configurations are included. Notably, the best estimate gypsum wallboard is denoted “G2” as a material tag. For future research purposes, lower bound (G1) and upper bound (G3) gypsum wallboard backbone properties were estimated. At the lower bound, Gatto and Uang [2002] test 12 (east and west), Pardoen et al. [2003] tests 18A, 18B, 19A, and 19B, and Bahmani and van de Lindt [2016] tests G-01 and G-02 were considered for backbone properties. The upper bound considers McMullin and Merrick [2002] tests 5, 8, and 17. An illustration of the assumed backbone curves for the basis of material fitting are shown with the corresponding test data in Figure 3.41. The four-point *Pinching4* backbone fitting is shown for the best estimate gypsum material (G2) in Figure 3.42. Properties for all three gypsum wallboard materials are summarized in Table 3.10.

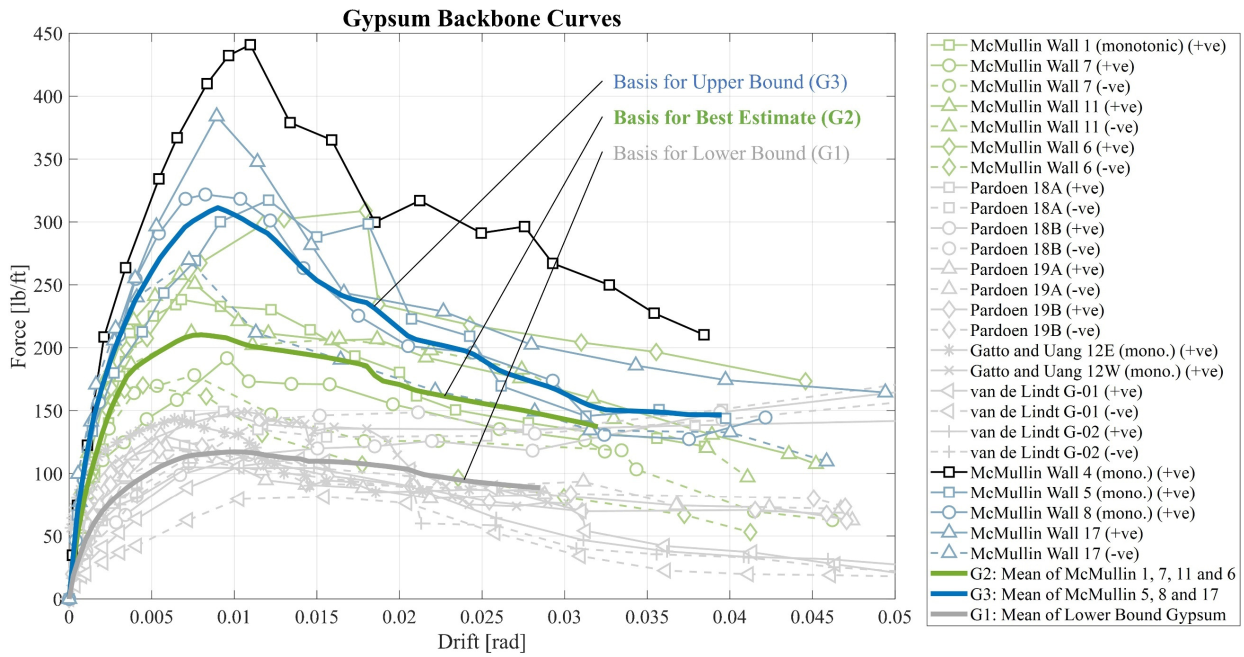

Figure 3.41 Backbone curves considered for gypsum wallboard properties with assumed average backbones of tests corresponding to upper bound (G3), best estimate (G2), and lower bound materials (G1).

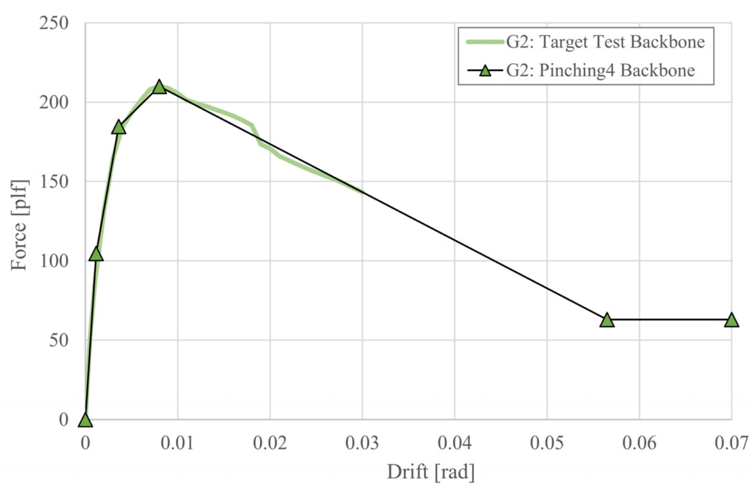

Figure 3.42 Four-point *Pinching4* backbone compared to target test data: best estimate gypsum wallboard (G2).

Figure 3.41 shows a single test with a black line, representing McMullin and Merrick [2002] test 4. This is a monotonic test with a closer drywall screw spacing (8 in.), as compared to the other tests with drywall screws (16 in.). This test was not included for calculating the upper bound properties for analysis, yet it helps demonstrate the range of gypsum wallboard strengths from available experimental data. The strongest test included in the upper bound calculation is the positive loading envelope for McMullin and Merrick [2002] test 17. Interestingly, this is a cyclic test with a door jamb, door trim, and baseboard trim included in the specimen. This specimen has identical cyclic (test 6) and monotonic (test 5) test specimens that did not include trim. A comparison of the effect of including trim on gypsum wallboard specimens is summarized in Figure 3.43. The figure illustrates that by adding door trim, baseboard, and door jambs, the peak strength increases by nearly 25% to 60% depending on the direction of loading, yet the displacement at peak load decreased by 50% in the positive direction and increased by more than 60% in the negative direction. This highlights how sensitive wood-frame sub-assembly testing can be to small changes in boundary conditions. For completeness, Figure 3.43 shows that the monotonic and cyclic backbones without trim were very similar, which gives a sense of the repeatability of response for similarly constructed specimens.

The cyclic properties for gypsum wallboard are based on fitting to a subset of tests conducted by McMullin and Merrick [2002]. Tests 7 and 11 were deemed most appropriate for capturing cyclic loading behavior. The cyclic fit of the *Pinching4* material using the two-spring in parallel approach is compared with McMullin and Merrick Test 11 in Figure 3.44, showing global hysteresis loops and cumulative hysteretic energy. A closer look in the small displacement range is presented in Figure 3.45, illustrating that the small displacement spring is capturing the small cycles quite well. Figure 3.46 shows the best estimate gypsum wallboard material (G2) in normalized units and loaded using the PEER–CEA loading protocol [Zareian and Lanning 2020]. A summary of the *Pinching4* material parameters for gypsum wallboard is provided in Table 3.10.

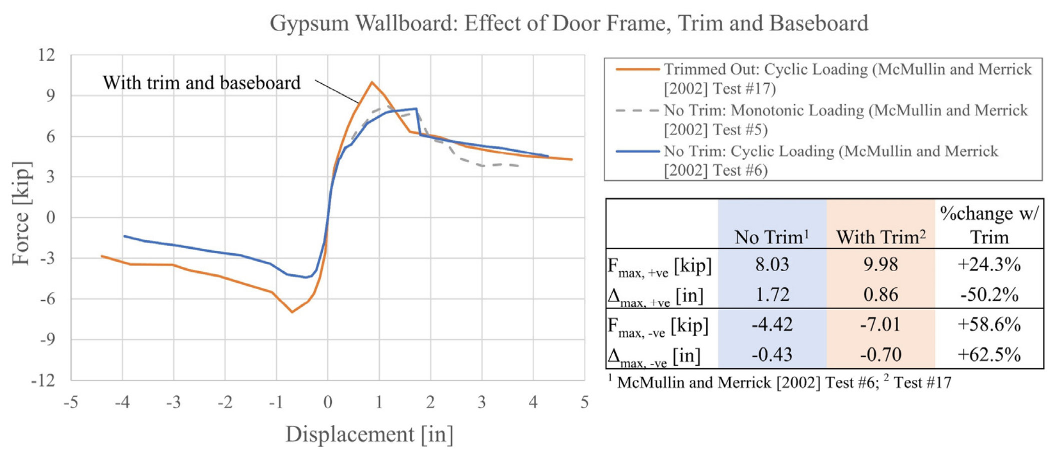

	No Trim[1]	With Trim[2]	%change w/ Trim
$F_{max, +ve}$ [kip]	8.03	9.98	+24.3%
$\Delta_{max, +ve}$ [in]	1.72	0.86	-50.2%
$F_{max, -ve}$ [kip]	-4.42	-7.01	+58.6%
$\Delta_{max, -ve}$ [in]	-0.43	-0.70	+62.5%

[1] McMullin and Merrick [2002] Test #6; [2] Test #17

Figure 3.43 Influence of including trim and baseboard on the envelope backbone response of gypsum wallboard tests conducted by McMullin and Merrick [2002].

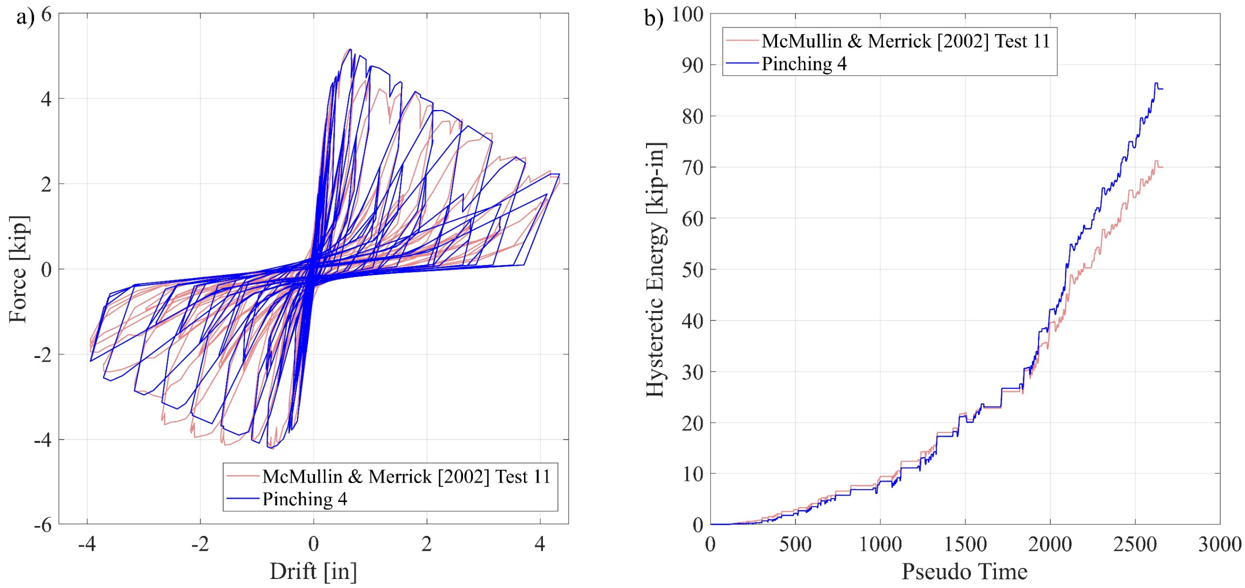

Figure 3.44 **Comparing the *Pinching4* material calibrated to gypsum wallboard Test 11 by McMullin and Merrick [2002]: (a) hysteretic response; and (b) hysteretic energy.**

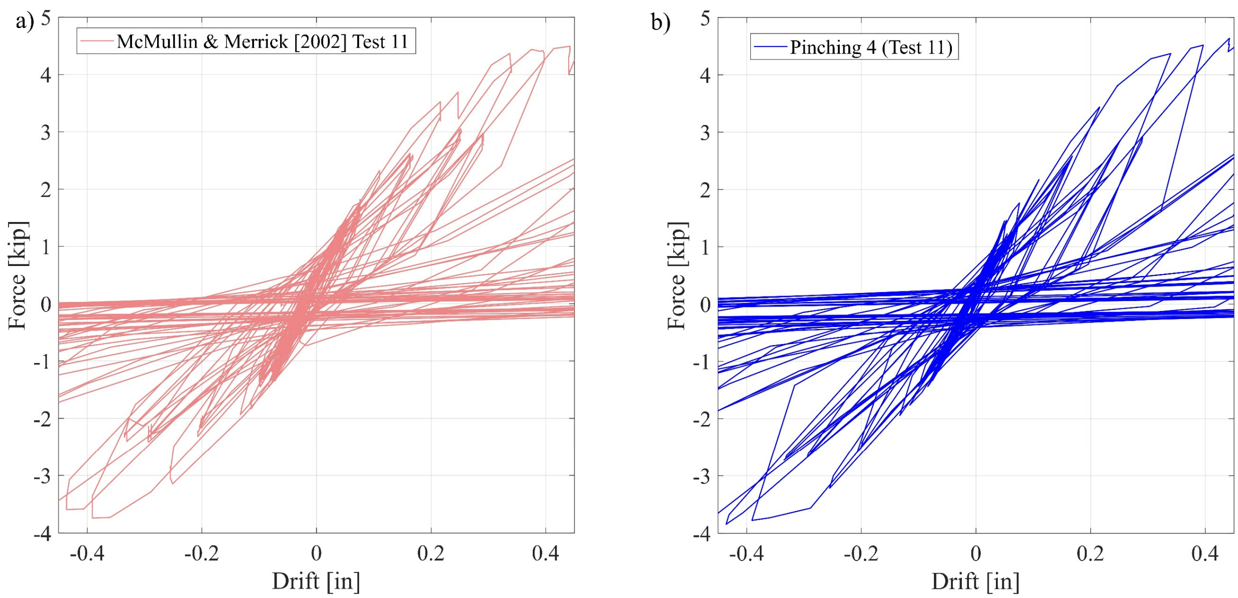

Figure 3.45 **Zoomed view comparing the *Pinching4* material calibrated to gypsum wallboard Test 11 by McMullin and Merrick [2002]: (a) experiment; and (b) numerical material.**

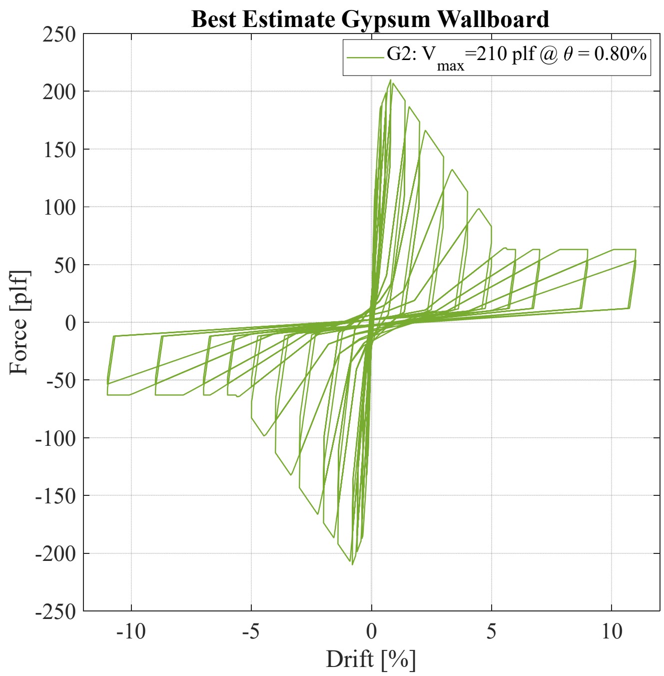

Figure 3.46 **Best estimate gypsum wallboard (G2) material shown in normalized units and loaded with the PEER–CEA loading protocol.**

Table 3.10 **Summary of *Pinching4* material parameters for gypsum wallboard.**

Material	**Backbone deformation points (%drift)**				**Backbone force points (plf)**			
	*ed*1	*ed*2	*ed*3	*ed*4	*ef*1	*ef*2	*ef*3	*ef*4
G1	0.08	0.48	1.00	6.42	51	106	117	35
G2 (best estimate)	**0.12**	**0.36**	**0.80**	**5.65**	**105**	**185**	**210**	**63**
G3	0.08	0.43	0.90	3.73	116	256	311	93
Cyclic properties	Spring 1	rDisp1	rForce1	uForce1	gK11	gKLim1	gD11	gDLim1
		0.15	0.22	-0.21	-0.30	-1.00	0.1	2.00
	Spring 2	rDisp2	rForce2	uForce2	gK12	gKLim2	gD12	gDLim2
		0.40	0.12	-0.19	0.20	2.00	0.12	2.00

*Definition of material model parameters is provided in Table 3.4; this material is developed as a single-sided material.

3.5.2 Plaster on Wood Lath

Plaster on wood lath is an important material for the PEER–CEA Project. This material represents the most common interior finish for older homes and is the assumed interior for the pre-1945 era.

Plaster on wood lath, or lath and plaster, consists of a series of lath boards placed on structural framing that serve as an application surface for layers of plaster finish. Lath boards are typically four feet long with a cross section of approximately 1-3/4 in. × 1/4 in. Boards are spaced approximately 1/4 in. and attached to structural framing with single nails (e.g., 3d common) at every stud location. The gaps in the lath courses allow for the plaster to form "keys" that anchor the first coat of plaster to the lath boards. A second coat of plaster is typically applied over the initial coat to a finish thickness of 7/8 in. to 1 in. [Trayer 1956; Carroll 2006]. An illustration of the interior of typical plaster on wood lath walls is shown in Figure 3.47.

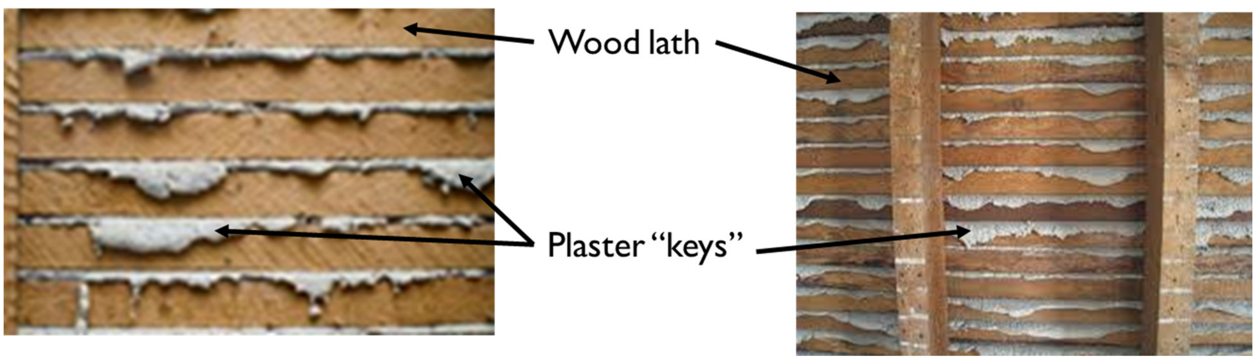

Figure 3.47 Illustration of wood lath and plaster from the interior of the wall.

3.5.2.1 Available Experimental Data on Plaster on Wood Lath

Experimental data for plaster on wood lath interior is significantly limited when compared to data for modern gypsum wallboard. Early tests include those by the FPL, which reported results of monotonic loading with reference to a baseline horizontal wood sheathing curve [Trayer 1956; Anderson 1965]. Schmid [1984] tested two *in situ* 8-ft × 8-ft specimens with limited cyclic loading. These earlier tests are illustrated in Figure 3.48.

Carroll [2006] tested a series of 19 wall specimens extracted from houses scheduled for demolition, obtaining original framing and either horizontal wood or plywood exterior sheathing. Nine of the horizontal sheathing specimens were applied lath and plaster (in the laboratory) and tested with either cyclic (using CUREE protocol) or monotonic loading. The specimens ranged in height from 6 ft to 8 ft, and wall lengths were typically two or three stud bays with lengths of 4 ft and 5.33 ft. An example of the test set up and laboratory constructed lath and plaster is shown in Figure 3.49. More discussion of previous testing on lath and plaster walls can be found in the WG4 large-component testing report [Cobeen et al. 2020].

The most recent data obtained for plaster on wood lath interior came directly from PEER–CEA testing conducted by WG4 [Cobeen et al. 2020]. PEER–CEA test C-1 is a double-walled specimen with 8-ft-tall × 20-ft-long walls with window and door openings on each side (the full-height wall length is 11 ft on each side). The exterior material is horizontal wood shiplap siding, and the interior material is plaster on wood lath as shown in Figure 3.50.

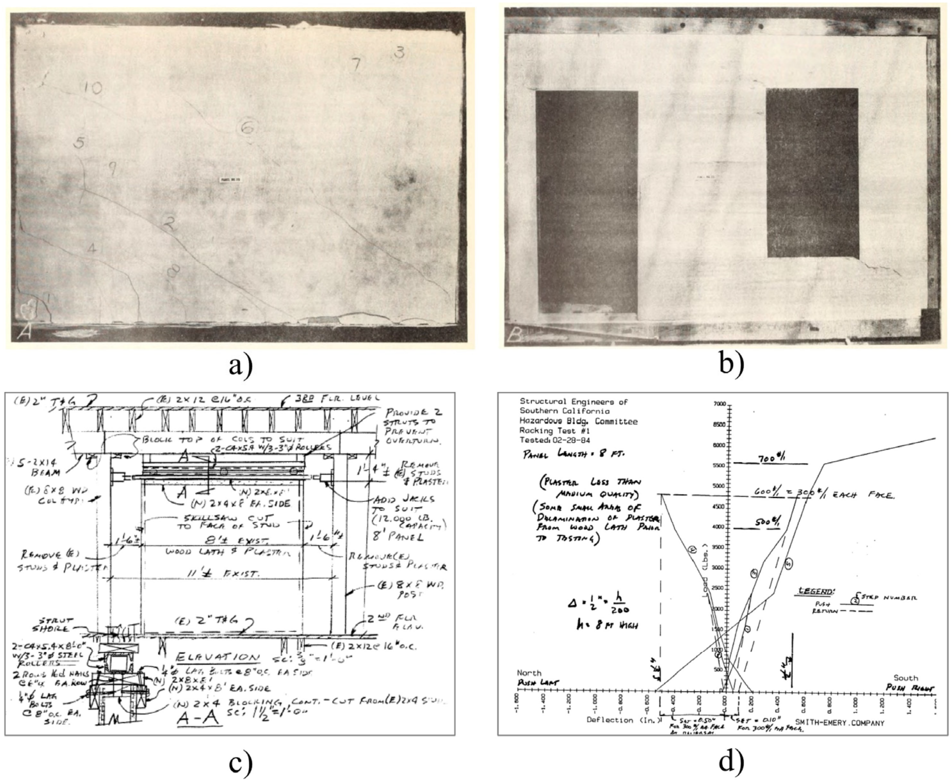

Figure 3.48 **Examples of earlier testing on plaster on wood lath: (a) solid panel tested by Trayer [1956] (presumably Panel 11); (b) Panel 23 with openings tested by Trayer [1956]; (c) *in situ* test setup used by Schmid [1984]; and (d) load deflection results for Wall 1 tested by Schmid [1984].**

Figure 3.49 **Photographs of testing conducted by Carroll [2006]: (a) experimental setup; and (b) lath and plaster specimens constructed in the laboratory.**

Figure 3.50 PEER–CEA large-component Test C-1 [Cobeen et al. 2020].

3.5.2.2 Numerical Material Properties for Plaster on Wood Lath

The backbone data used to develop model parameters for plaster on wood lath considered all of the available information. To better understand the range of force-displacement backbone shapes for plaster on wood lath, the three cyclic tests conducted by Carroll [2006] (Test 1, 3 and 17) are shown in Figure 3.51. These tests considered 4-ft-long wall lengths with no openings and horizontal sheathing on the opposite side of the wall that was already tested to failure prior to applying the lath and plaster [Carroll 2006]. Figure 3.51 shows that there were three distinct force-displacement behaviors.

Test 3 produced the largest positive direction strength and shows an abrupt loss of strength once the peak load was reached in both directions. This type of behavior was also reported by Trayer [1956], with specimens without openings having the largest strength and smallest displacement capacity. This can be interpreted as the lack of openings allowing forces in the plaster keys to be developed throughout the specimen until their capacity is reached simultaneously.

Among the three cases considered, Test 1 had an intermediate positive direction strength. The force-displacement backbones show a sustained peak load to the maximum displacements in both loading directions. This behavior is explained by the plaster keys loading incrementally; when local key failures occurred, there were others that resisted the redistributed loads.

Finally, Test 17 returned the lowest positive direction peak strength of the three tests. Comparing the positive loading backbones of the three tests (solid lines in Figure 3.51), Test 17 showed signs of early plaster key failure. This suggests that there were never enough plaster keys resisting loads simultaneously to develop similar strengths to Test 1. The degrading post-peak behavior also shows a lack of plaster keys working in unison. This comparison of tests shows the high variability associated with lath and plaster; recall that these three specimens were constructed using the same techniques and tested with a similar loading protocol.

Figure 3.52 shows the force-displacement backbone curves for all of the collected plaster on wood lath testing. The figure shows three bold and annotated plots corresponding to the average backbones of PEER–CEA Test C-1, Carroll [2006] test 17, and the common points of all tests considered.

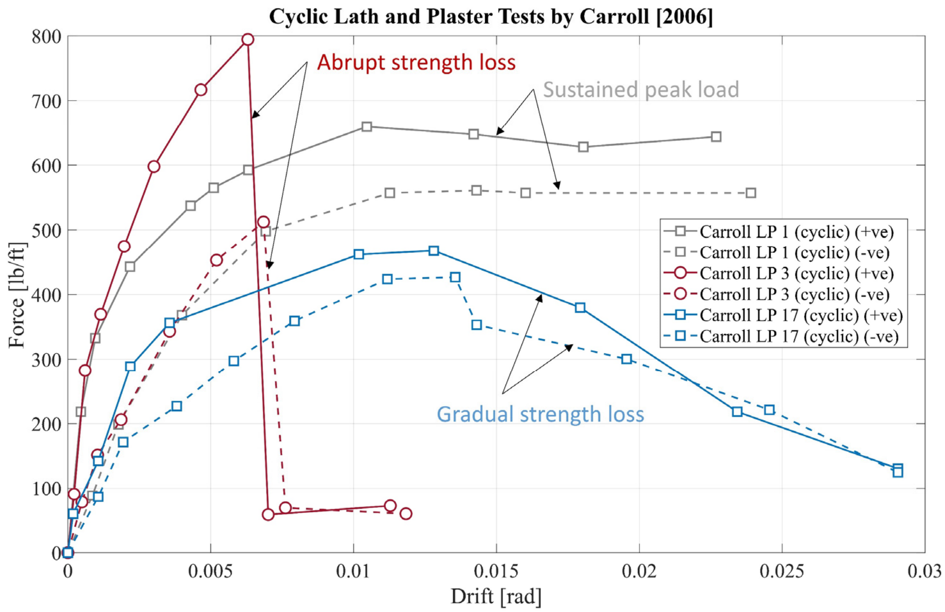

Figure 3.51 Backbones of three plaster on wood lath specimens tested cyclically by Carroll [2006] illustrating widely varying backbone shapes.

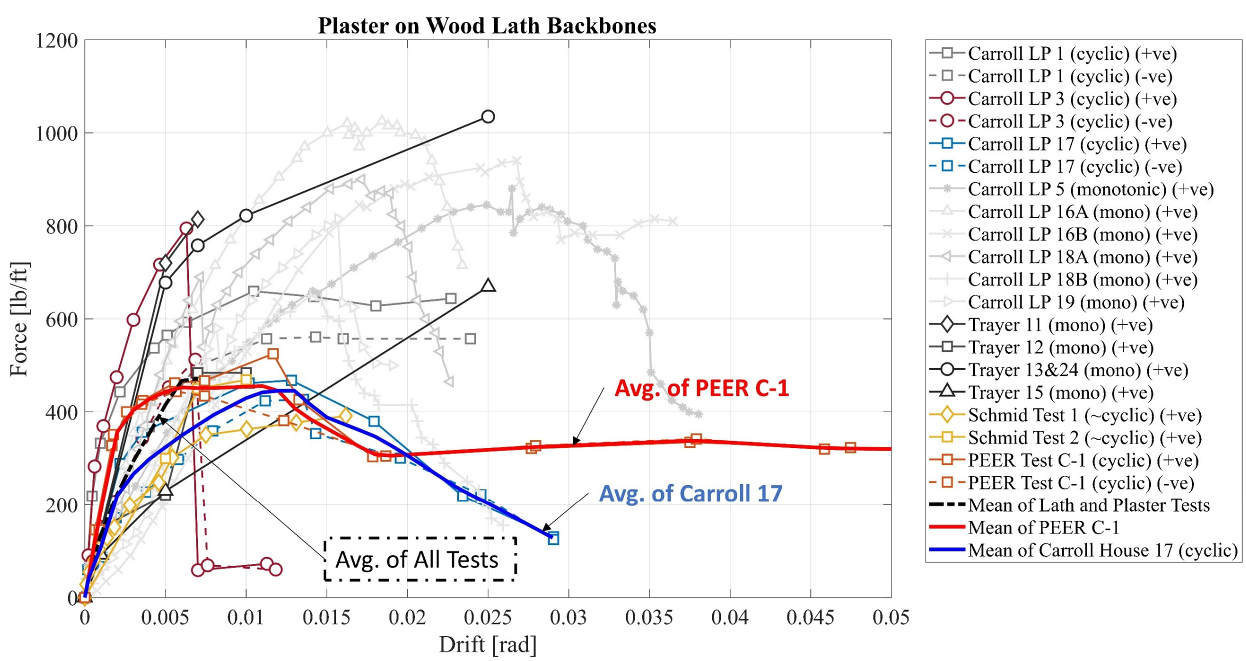

Figure 3.52 Lath and plaster backbones from collected test specimens.

The best estimate backbone curve for interior partitions with plaster on wood lath is based on the average backbone envelope of Carroll [2006] test 17 with a peak strength of 445 plf at a drift of 1.2%. This assumption is based on the following observations:

- The peak strength of 445 plf is in agreement with other tests from different sources. Importantly, PEER–CEA test C-1 has an average peak strength of 456 plf at a drift of 1.1%. Additionally, Trayer [1956] test 12, a lath and plaster (no other sheathing or bracing) specimen with openings, has a peak strength of 484 plf. Further, the 445 plf strength value is bounded by the range of limited in-situ testing conducted by Schmid [1984] with strengths of 391 plf and 469 plf for walls 1 and 2, respectively.
- The initial stiffness of the proposed target backbone is in good agreement with average of all collected test data.
- The post-peak stiffness of the proposed backbone curve is in very good agreement with that observed for PEER–CEA test C-1.
- The lower intermediate stiffness leading up to peak load is assumed reasonable considering that the material will be applied on either side of interior walls and this stiffness acknowledges the possibility of plaster keys not resisting load equally on either side of the partition wall.

The *Pinching4* material backbone fit to the target test backbone for plaster on wood lath (LP2) is shown in Figure 3.53. Note that the peak-strength assumed for plaster on wood lath is more than twice that assumed for gypsum wallboard. Cyclic properties for this material were taken directly from the calibration of PEER–CEA Test C-1. Details of these cyclic properties can be found in Section 3.4.2. The summary of the *Pinching4* material properties for best estimate plaster on wood lath for interior partitions is provided in Table 3.11.

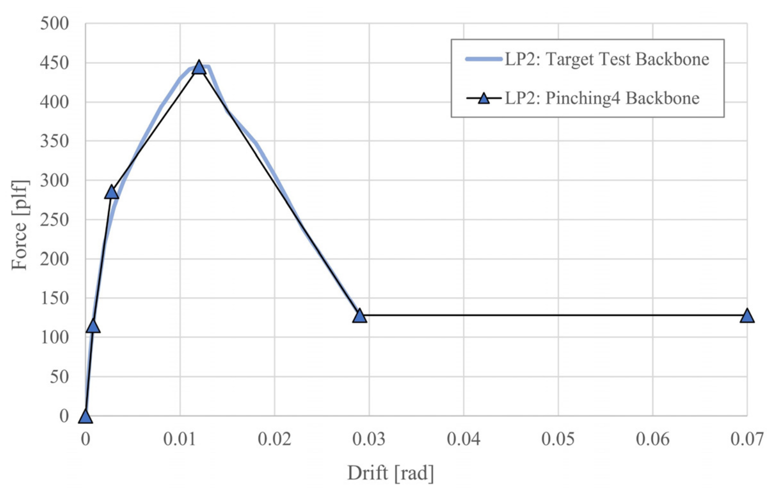

Figure 3.53 Four-point *Pinching4* backbone compared to target test data: best estimate plaster on wood lath (LP2).

Table 3.11 **Summary of *Pinching4* material parameters for plaster on wood lath interior partitions.**

<table>
<tr><th rowspan="2">Material</th><th colspan="4">Backbone deformation points (%drift)</th><th colspan="4">Backbone force points (plf)</th></tr>
<tr><th>ed1</th><th>ed2</th><th>ed3</th><th>ed4</th><th>ef1</th><th>ef2</th><th>ef3</th><th>ef4</th></tr>
<tr><td colspan="2">LP2 (best estimate)</td><td>0.08</td><td>0.28</td><td>1.20</td><td>2.90</td><td>115</td><td>286</td><td>445</td><td>128</td></tr>
<tr><td rowspan="4">Cyclic properties</td><td rowspan="2">Spring 1</td><td>rDisp1</td><td>rForce1</td><td>uForce1</td><td>gK11</td><td>gKLim1</td><td>gD11</td><td>gDLim1</td></tr>
<tr><td>0.06</td><td>0.31</td><td>-0.10</td><td>-0.07</td><td>-0.50</td><td>0.14</td><td>0.30</td></tr>
<tr><td rowspan="2">Spring 2</td><td>rDisp2</td><td>rForce2</td><td>uForce2</td><td>gK12</td><td>gKLim2</td><td>gD12</td><td>gDLim2</td></tr>
<tr><td>0.28</td><td>0.18</td><td>-0.11</td><td>-0.05</td><td>-0.20</td><td>0.11</td><td>0.30</td></tr>
</table>

*Definition of material model parameters is provided in Table 3.4; this material is developed as a single-sided material.

3.6 CRIPPLE WALL MATERIALS

3.6.1 PEER–CEA Test Campaign on Cripple Wall Sub-Assemblies

The experimental testing of cripple wall sub-assemblies conducted by WG4 greatly enhanced the available knowledge for the analyses of unretrofitted and retrofitted cripple wall variants. All components are loaded cyclically according to the PEER–CEA loading protocol developed by WG3 [Zareian and Jennings 2020].

Small-component cripple wall tests conducted at the University of California, San Diego, (UCSD) examined a total of 28 cripple wall sub-assemblies that were 12 ft in length with various cripple wall heights. The UCSD testing was conducted in four phases: Phase I wet specimens (stucco finish), Phase II and IV dry specimens (non-stucco finish), and Phase III wet specimens (stucco finish) [Schiller et al. 2020(a); 2020(b); 2020(c)]. Phase I testing included Specimens A-1 through A-6, which considered 2-ft-tall stucco over horizontal wood sheathing cripple walls with a range of boundary conditions [Schiller et al. 2020(a)]. Phase II testing included Specimens A-7 through A-14, which addressed unretrofitted (existing) and retrofitted pairs with various wood finishes including horizontal wood siding, T1-11 panelized siding and horizontal wood siding over diagonal sheathing [Schiller et al. 2020(b)]. Phase III testing included Specimens A-15 through A-22, which were unretrofitted (existing) and retrofitted pairs of stucco cripple walls with no sheathing, horizontal wood sheathing and diagonal wood sheathing [Schiller et al. 2020(c)]. Phase IV testing included Specimens A-25 and A-26, 6-ft-tall stucco specimens with unretrofitted (existing) and retrofitted conditions, and Specimen A-27, a 2-ft-tall stucco over horizontal sheathing specimen tested with monotonic loading [Schiller et al. 2020(c)]. Specimens A-23 and A-24 were unretrofitted and retrofitted pairs of 6-ft-tall T1-11 siding sub-assemblies, and Specimen A-28 was a 2-ft-tall unretrofitted horizontal wood siding over diagonal sheathing specimen with lighter gravity loading of 250 plf [Schiller et al. 2020(b)]. All other small-component cripple wall tests assumed 450 plf for gravity loading.

Large-component cripple wall tests, conducted at the University of California, Berkeley (UCB), consisted of specimens with two parallel walls 20 ft in length with continuous transverse return walls at each end [Cobeen et al. 2020]. Test AL-1 and AL-2 have unretrofitted and retrofitted 2-ft-tall cripple walls with a continuous stucco finish applied from the base of the cripple wall to an 8-ft-tall superstructure configuration above the first-floor diaphragm. Test B-1 investigated the effectiveness of load path connections for a 2-ft-tall × 20-ft-long retrofit cripple wall with horizontal wood siding as the exterior finish material [Cobeen et al. 2020]. Test B-1 focused on the cripple wall alone and did not include the superstructure above the first-floor diaphragm.

3.6.2 Stucco Cripple Walls

Stucco cripple wall material models address four different best estimate classifications for building variant analysis: (1) unretrofitted 2-ft tall cripple walls; (2) retrofitted 2-ft-tall cripple walls; (3) unretrofitted 6-ft-tall cripple walls; and (4) retrofitted 6-ft-tall cripple walls.

3.6.2.1 Unretrofitted Case

Two-ft-tall stucco cripple wall specimens considered a range of different boundary conditions in small-component Phase I and III testing as well as large-component Specimen AL-1. Descriptions of the various unretrofitted 2-ft-tall stucco cripple wall tests, along with peak strengths and associated drifts, are summarized in Table 3.12. One 6-ft-tall specimen (Specimen A-25) was tested, which had an average peak strength of 656 plf at a drift ratio of 1%. The backbone curves considered for unretrofitted stucco cripple walls are presented in Figure 3.54. The best estimate material for 2-ft-tall cripple walls (CW2-S2) is based on test Specimens A-17, A-20, A-21, and A-22. These specimens had the most realistic detailing as discussed among the PEER–CEA Project Team Members. Notably, although all of these specimens had stucco extended down the side of the footing, the stucco in these tests did not exhibit a strong bond as was observed for large-component test AL-1. Although this bond could be a significant source of initial strength, the inability for two different testing campaigns to produce the same results indicates the large amount of variability that could be expected in the field.

The average backbone of tests A-2 and A-3 were assembled as a "test-average" material (CW2-S3); note that these two specimens had horizontal wood sheathing behind the stucco that bore on the foundation. A lower bound material (CW2-S1) assumed COLA test 20C as the basis for strength [COLA 2001] and the average of PEER–CEA tests A-1 and A-20 for a lower bound initial stiffness. The assumed four-point *Pinching4* material backbones for the different unretrofitted cripple wall stucco materials are shown in Figure 3.55.

Table 3.12 Summary of the unretrofitted 2-ft-tall stucco cripple walls with and without horizontal wood sheathing tested by WG4.

Index	Description[4]	Loading direction	Peak strength (plf)	Drift at peak strength (%)
A-1[1]	2 ft × 12 ft, Stucco+HSh, free end boundaries, stucco outboard, HSh bearing	+ve	502	3.00
		-ve	427	2.96
A-2	2 ft × 12 ft, Stucco+HSh, small returns, stucco outboard, HSh bearing	+ve	770	4.30
		-ve	714	2.27
A-3	2 ft × 12 ft, Stucco+HSh, large 2ft returns, stucco outboard, HSh bearing	+ve	745	1.94
		-ve	701	1.95
A-4	2 ft × 12 ft, Stucco+HSh, small returns, wall centered on footing, Stucco and HSh bearing on foundation	+ve	1032	3.93
		-ve	898	3.56
A-6	2 ft × 12 ft, Stucco+HSh, small returns, wet-set sill condition, Stucco and HSh bearing on foundation	+ve	813	2.99
		-ve	825	3.97
A-17[2]	2 ft × 12 ft, Stucco+None, small returns, stucco extended to footing, poor stucco bond	+ve	568	1.71
		-ve	578	1.21
A-20	2 ft × 12 ft, Stucco+HSh, small returns, stucco extended to footing, poor stucco bond, HSh outboard of footing	+ve	617	2.03
		-ve	556	2.71
A-21	2 ft × 12 ft, Stucco+HSh, small returns, wet-set sill condition, stucco extended to side of footing, poor stucco bond, HSh likely bearing on footing	+ve	644	2.97
		-ve	611	2.01
A-22	2 ft × 12 ft, Stucco+None, small returns, no stucco extension, stucco outboard of footing	+ve	553	1.14
		-ve	582	1.28
A-27	2 ft × 12 ft, Monotonic loading, Stucco+HSh, small returns, stucco extended to footing, poor bond, stucco and HSh outboard of footing	Monotonic	737	5.35
AL-1[3]	2 ft × 20 ft, Large-component (double-sided, L_{eff} = 40 ft), stucco+HSh, full returns, good stucco bond on foundation, HSh bearing on foundation	+ve	1259	2.59
		-ve	1351	2.94
Mean	Average of all tests		737	2.71

[1] Tests A-1 through A-6 are reported in Schiller et al. [2020(a)].
[2] Tests A-17 through A-27 are reported in Schiller et al. [2020(b)].
[3] Test AL-1 is reported in Cobeen et al. [2020], [4] HSh = horizontal wood sheathing.

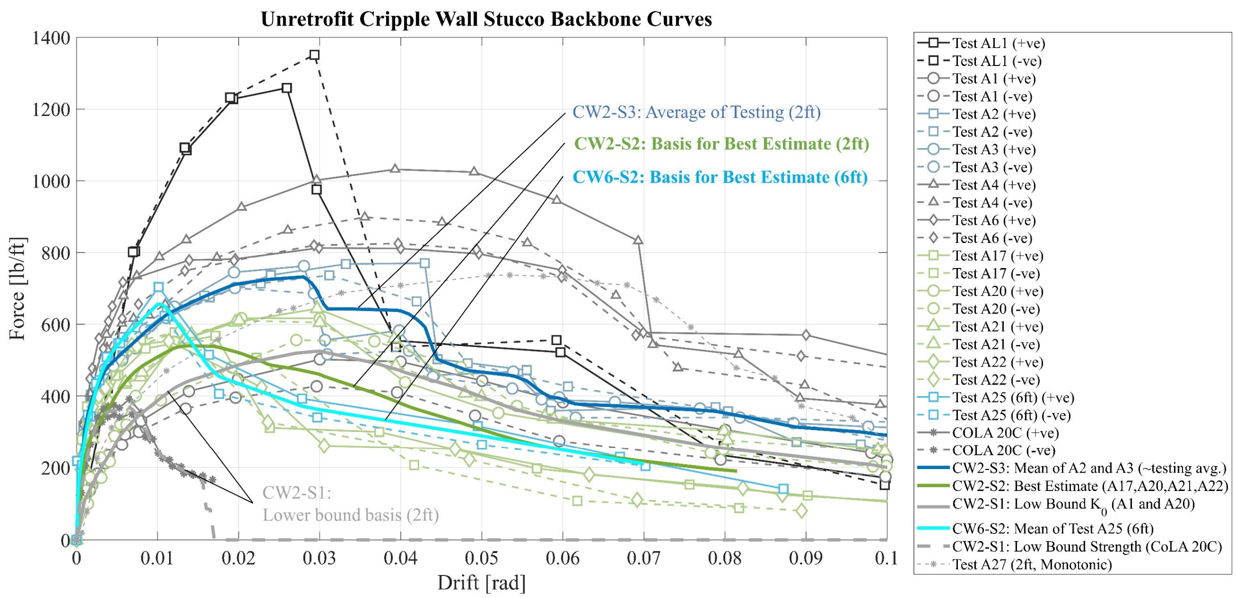

Figure 3.54 Backbone curves considered for unretrofitted stucco cripple wall properties: relevant test average for 2 ft (CW2-S3), best estimate 2 ft (CW2-S2), best estimate 6 ft (CW6-S2), and lower bound 2 ft (CW2-S1).

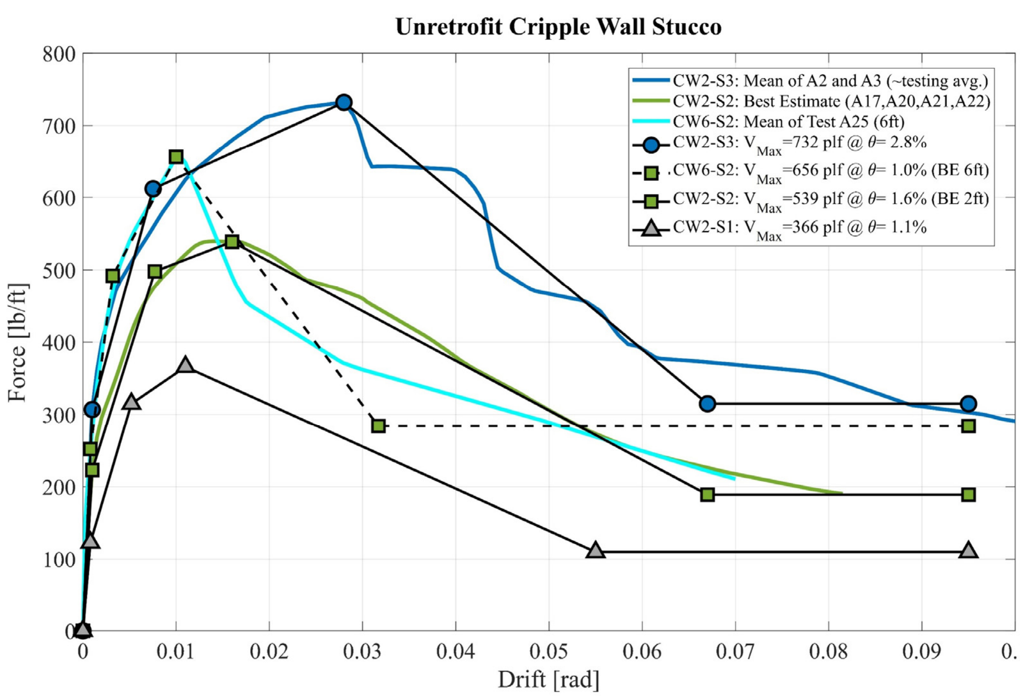

Figure 3.55 ***Pinching4*** **material backbones assumed for best estimate 2-ft-tall and 6-ft-tall stucco cripple walls (squares), and two additional variations of 2-ft-tall stucco properties representing the average of testing (circles) and an assumed lower bound (triangles).**

Cyclic properties for unretrofitted stucco cripple walls came from different tests, depending on the cripple wall height and material bound assumed. The stronger 2-ft-tall wall material (CW2-S3) represents the testing average based on cyclic properties from Tests A-2 and A-3 [Schiller et al. 2020(a)]. An example of the cyclic *Pinching4* fitting to Test A-2 is shown in Figure 3.56. The best estimate 2-ft-tall stucco cripple wall (CW2-S2) and approximate lower bound 2-ft-tall stucco cripple wall (CW2-S1) have cyclic properties based on Test A-17 [Schiller et al. 2020(c)]. The cyclic fitting to Test A-17 using the *Pinching4* material is shown in Figure 3.57. The 6-ft best estimate stucco material (CW6-S2) has cyclic properties based on Test A-25 [Schiller et al. 2020(c)]. An example of the cyclic *Pinching4* fitting to Test A-25 is shown in Figure 3.86. The *Pinching4* parameters to define the unretrofitted stucco cripple wall materials are shown for 2-ft-tall and 6-ft-tall cripple walls in Table 3.13 and Table 3.14, respectively.

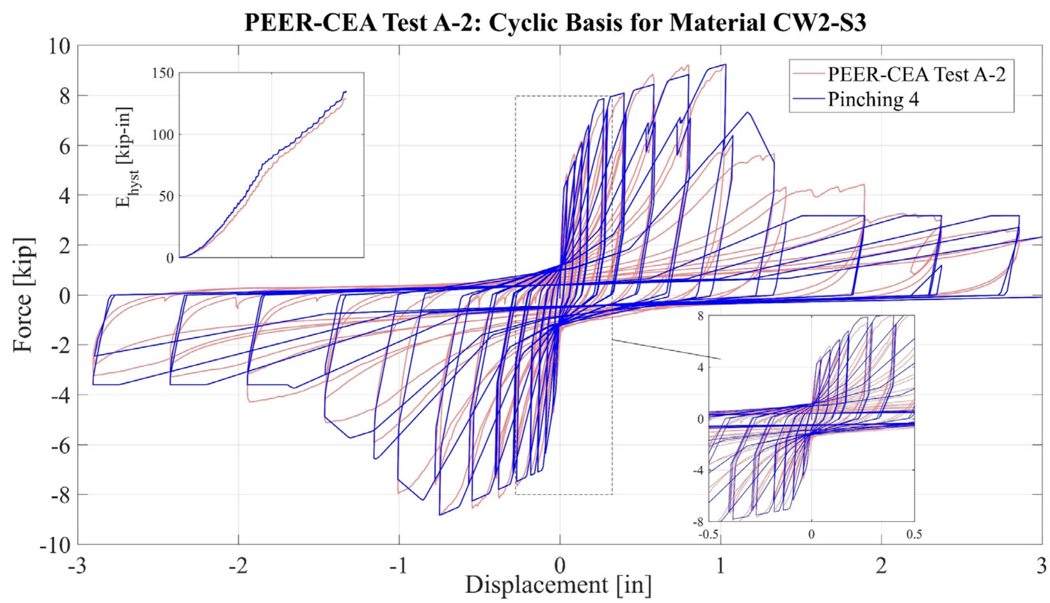

Figure 3.56 Comparing the ***Pinching4*** material calibrated to 2-ft-tall stucco cripple wall test A-2 by Schiller et al. [2020(a)]: (a) hysteretic response; and (b) hysteretic energy.

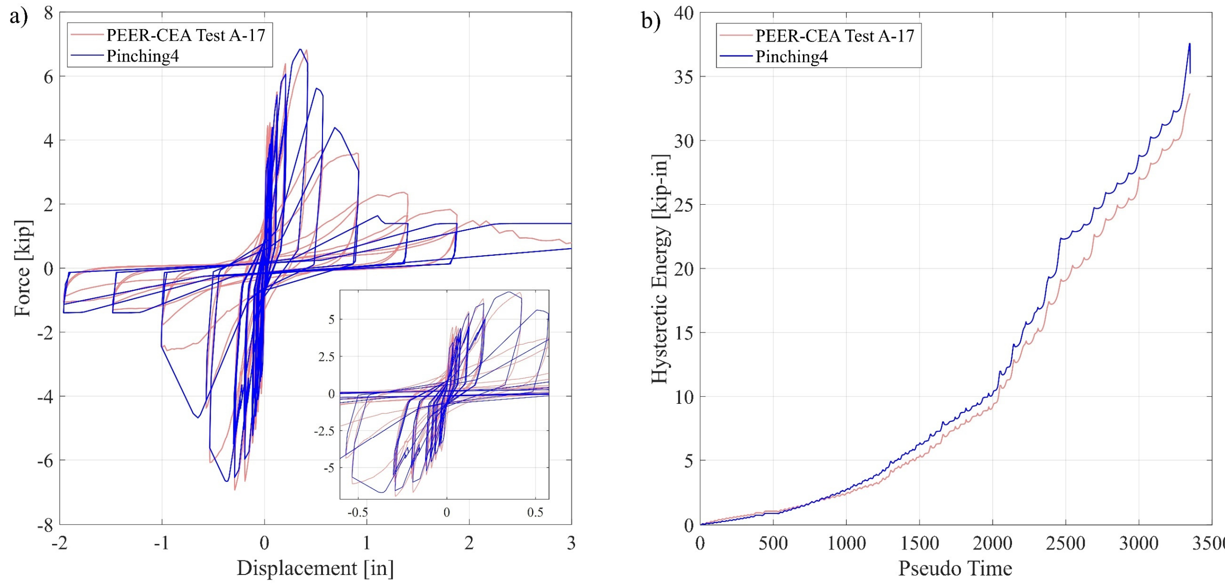

Figure 3.57 **Comparing the *Pinching4* material calibrated to 2-ft-tall stucco cripple wall test A-17 by Schiller et al. [2020(c)]: (a) hysteretic response; and (b) hysteretic energy.**

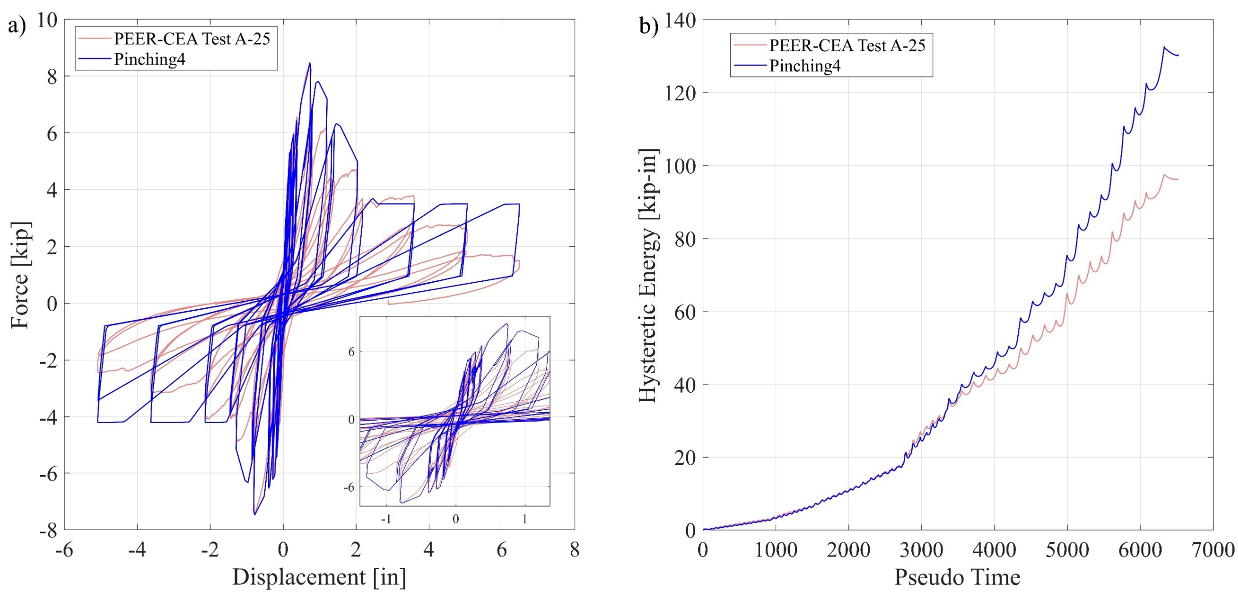

Figure 3.58 **Comparing the *Pinching4* material calibrated to 6-ft-tall stucco cripple wall test A-25 by Schiller et al. [2020(c)]: (a) hysteretic response; and (b) hysteretic energy.**

Table 3.13 Summary of *Pinching4* material parameters for the unretrofitted 2-ft-tall stucco cripple walls.

Material		Backbone deformation points (%drift)				Backbone force points (plf)			
		*ed*1	*ed*2	*ed*3	*ed*4	*ef*1	*ef*2	*ef*3	*ef*4
CW2-S1		0.08	0.52	1.10	5.50	123	315	366	110
CW2-S2 (best estimate 2 ft)		**0.10**	**0.77**	**1.60**	**6.70**	**223**	**498**	**539**	**189**
CW2-S3		0.08	0.75	2.80	6.70	307	612	732	315
Cyclic properties (**CW2-S2**, CW2-S1)	Spring 1	rDisp1	rForce1	uForce1	gK11	gKLim1	gD11	gDLim1	
		0.05	0.20	-0.10	0	0	0.30	3.0	
	Spring 2	rDisp2	rForce2	uForce2	gK12	gKLim2	gD12	gDLim2	
		0.25	0.16	-0.10	0	0	0.20	2.0	
Cyclic properties (CW2-S3)	Spring 1	rDisp1	rForce1	uForce1	gK11	gKLim1	gD11	gDLim1	
		0.06	0.18	-0.07	-0.25	-1.0	0.15	2.0	
	Spring 2	rDisp2	rForce2	uForce2	gK12	gKLim2	gD12	gDLim2	
		0.37	0.20	0.08	0.12	0.50	0.12	0.40	

*Definition of material model parameters is provided in Table 3.4; this material is developed as a single-sided material.

Table 3.14 Summary of *Pinching4* material parameters for the unretrofitted 6-ft-tall stucco cripple walls.

Material		Backbone deformation points (%drift)				Backbone force points (plf)			
		*ed*1	*ed*2	*ed*3	*ed*4	*ef*1	*ef*2	*ef*3	*ef*4
CW6-S2 (best estimate 6 ft)		0.08	0.32	1.00	3.17	252	492	656	284
Cyclic properties	Spring 1	rDisp1	rForce1	uForce1	gK11	gKLim1	gD11	gDLim1	
		0.04	0.31	-0.05	-0.12	-0.75	0.30	3.0	
	Spring 2	rDisp2	rForce2	uForce2	gK12	gKLim2	gD12	gDLim2	
		0.25	0.16	-0.25	-0.09	-0.30	0.20	2.0	

*Definition of material model parameters is provided in Table 3.4; this material is developed as a single-sided material.

3.6.2.2 Retrofitted Case

The 2-ft-tall stucco cripple walls with wood structural panel (WSP) seismic retrofit were considered in numerous tests conducted by WG4. Phase I small-component testing included Specimen A-5, which is a 2-ft-tall stucco cripple wall with WSP and edge nailing of 8d at 4 in. on center [Schiller et al. 2020(a)]. Phase III small-component testing included 2-ft-tall cripple walls, Specimens A-18 and A-19, which were retrofitted with WSP and edge nailing of 8d at 3 in. on center [Schiller et al. 2020(c)]. Similarly, large-component test AL-2 had a 2-ft-tall cripple wall retrofitted with WSP and edge nailing of 8d at 3 in. on center [Cobeen et al. 2020].

An important assumption carried through the numerical analyses is that the WSP nailing is targeted to have 8d at 3 in. on center as the best estimate, at least for cripple walls with stucco or horizontal wood siding finish materials. This assumption was based on testing specimens selecting 3-in. nail spacing as representative of *FEMA P-1100* [2018] retrofits, which is the middle spacing of 4, 3, and 2 in. specified in *FEMA P-1100* plan sets for "Light," "Medium," and "Heavy" weight classifications. Further, for the current archetype geometry (i.e., 1200 ft^2 plan area), the required WSP retrofit braced length is the same, whether 3-in. or 4-in. nail spacing is specified in the plan set calculations. This is due to the length of WSP required typically being governed by overturning assumptions rather than shear strength of the WSP [McCormick 2018].

The experimental backbone curves used as a basis for the best estimate 2-ft-tall stucco plus WSP cripple wall material (CW2-S-R2) are based on a combined average of Tests A-19, A-18, and AL-2, as shown in Figure 3.59. Figure 3.59 also shows Test A-5 [Schiller et al. 2020(a)] and Specimen 2 from Chai et al. [2002] (CUREE). Both these additional tests were 2 ft-tall × 12-ft-long specimens with stucco finish and fully sheathed with WSP and 8d at 4-in. nail spacing. Test A-5 had closed return walls and was reportedly influenced by interaction of the WSP with the small return wall framing during testing. Chai Specimen 2 had free edge boundary conditions and did not include the same detailing as the PEER–CEA tests, which followed *FEMA P-1100* detailing. The figure shows a large difference in the force-displacement behavior of the two tests; note that the framing interaction was not prevalent in further testing of WSP specimens by WG4.

To investigate the influence of a reduced retrofit material capacity, the best estimate backbone for 8d at 3-in. spacing was scaled by 0.78 (12% reduction) to reflect the difference in nominal shear-wall capacities within Table 4.3A of the *NDS-Special Design Provisions for Wind and Seismic* [AWC 2015] for 8d nailing at 4 in. versus 3 in. This reduced peak force is shown as horizontal dashed line in Figure 3.59. This reduced strength material has an index of "CW2-S-R1." The *Pinching4* material backbones for the unretrofitted 2-ft stucco cripple wall materials are shown in Figure 3.60.

Retrofitted stucco cripple walls with a 6 ft in height are based on PEER–CEA small-component Specimen A-26 [Schiller et al. 2020(c)]. This was the only 6-ft-tall test that combined the retrofit with a stucco finish. The test included tie-down devices, which is consistent with the retrofit requirements for 6-ft stucco cripple walls "with tie-downs" in the *FEMA P-1100* plan sets. Figure 3.61 shows the average backbone for Test A-26 compared with the four-point *Pinching4* backbone curve for best estimate retrofitted 6-ft-tall stucco cripple walls (CW6-S-R2).

Cyclic properties for 2-ft-tall cripple walls with WSP retrofit were estimated from PEER–CEA small-component Specimen A-18 [Schiller et al. 2020(c)]. The cyclic fitting to Test A-18 using the *Pinching4* material is shown in Figure 3.62. The *Pinching4* material parameters for the retrofitted 2-ft-tall stucco cripple walls are provided in Table 3.15.

The 6-ft-tall cripple walls with stucco and WSP retrofit have cyclic properties based on PEER–CEA Specimen A-26 [Schiller et al. 2020(c)]. The cyclic fitting to Test A-26 using the *Pinching4* material is shown in Figure 3.63. The *Pinching4* material parameters for retrofitted 6-ft-tall stucco cripple walls are provided in Table 3.16.

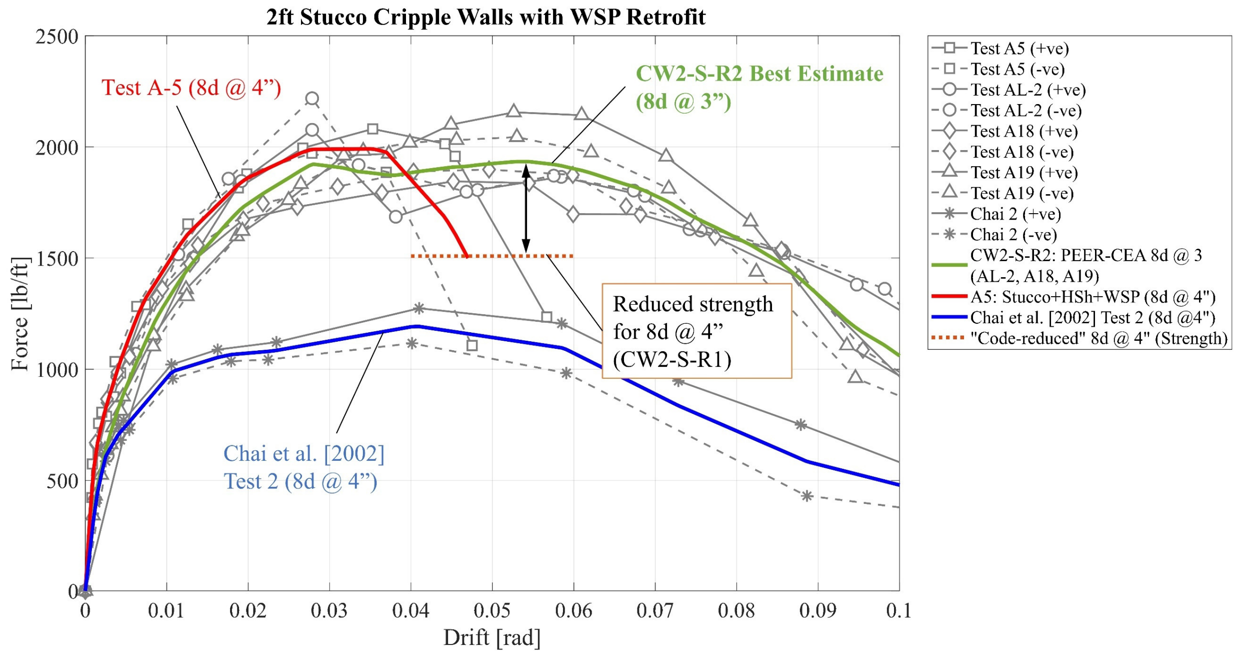

Figure 3.59 **Backbone curves considered for retrofitted stucco cripple wall properties: best estimate 2 ft (CW2-S-R2) with 8d @ 3 in. nailing, test A-5 with 8d @ 4 in. nailing, Chai et al. [2002] test 2 with 8d @ 4 in. nailing, and strength basis (dashed line) for reducing best estimate to reflect 8d @ 4 in. capacity from code tables.**

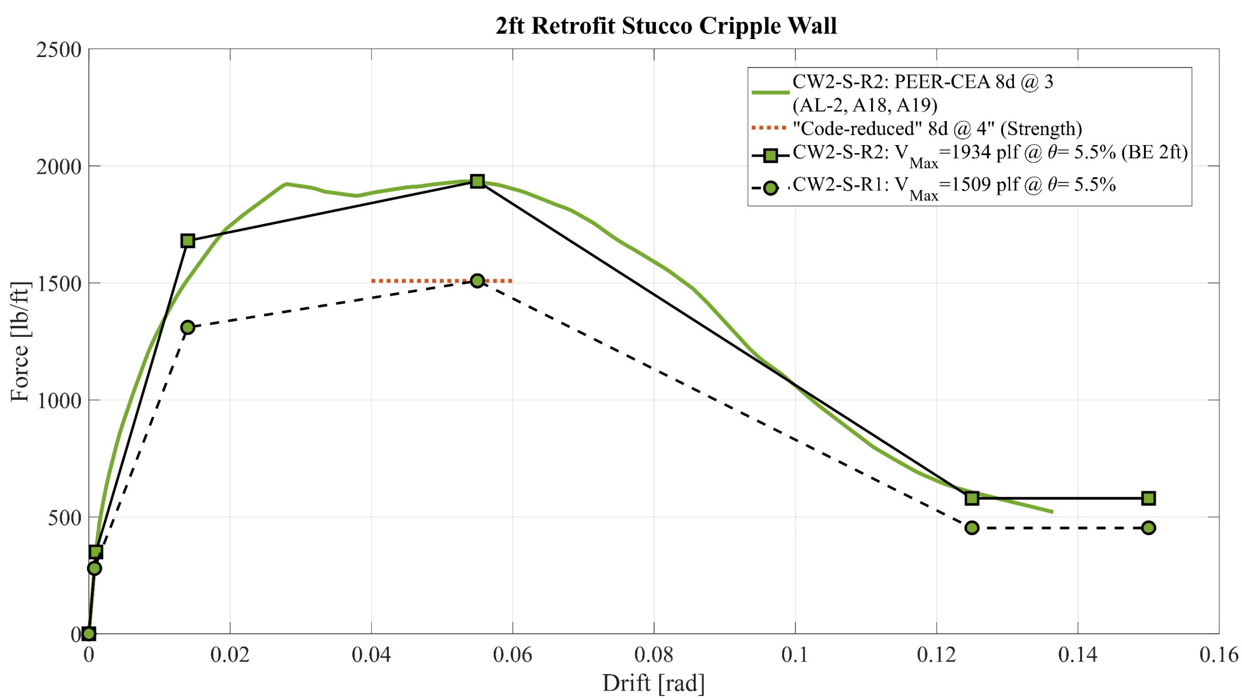

Figure 3.60 ***Pinching4*** **material backbones assumed for best estimate retrofitted 2-ft-tall stucco cripple walls with 8d @ 3 in nailing (squares) and a reduced material capacity to reflect 8d @ 4 in. nailing (circles).**

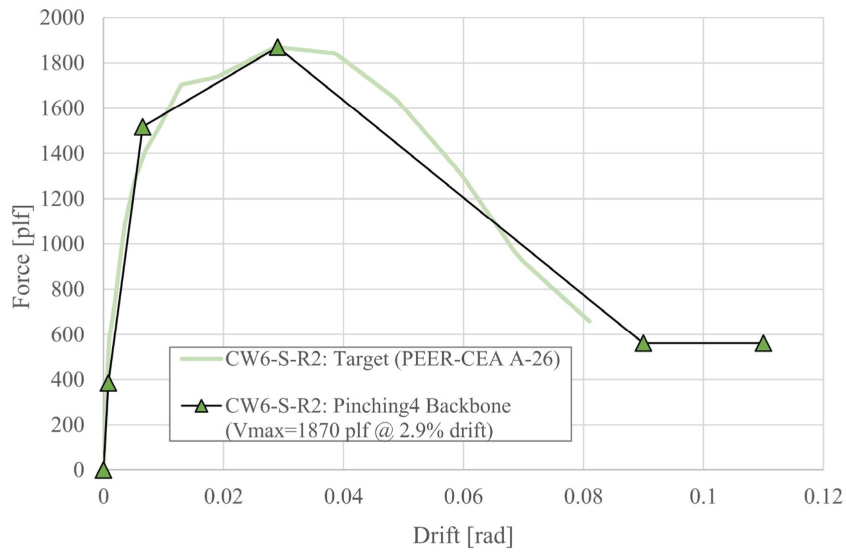

Figure 3.61 ***Pinching4*** **material backbone assumed for best estimate retrofitted 6-ft-tall stucco cripple walls with 8d @ 3 in. nailing (triangles) compared with the average backbone of PEER–CEA test A-26 [Schiller et al. 2020(c)].**

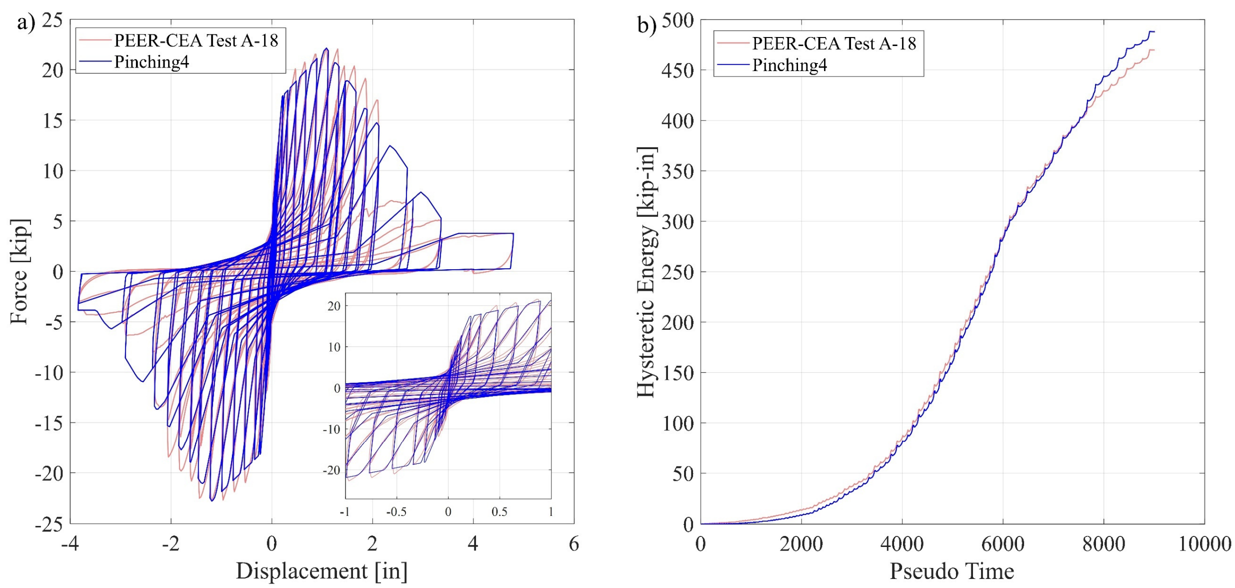

Figure 3.62 **Comparing the** ***Pinching4*** **material calibrated to the retrofitted 2-ft-tall stucco cripple wall test A-18 by Schiller et al. [2020(c)]: (a) hysteretic response; and (b) hysteretic energy.**

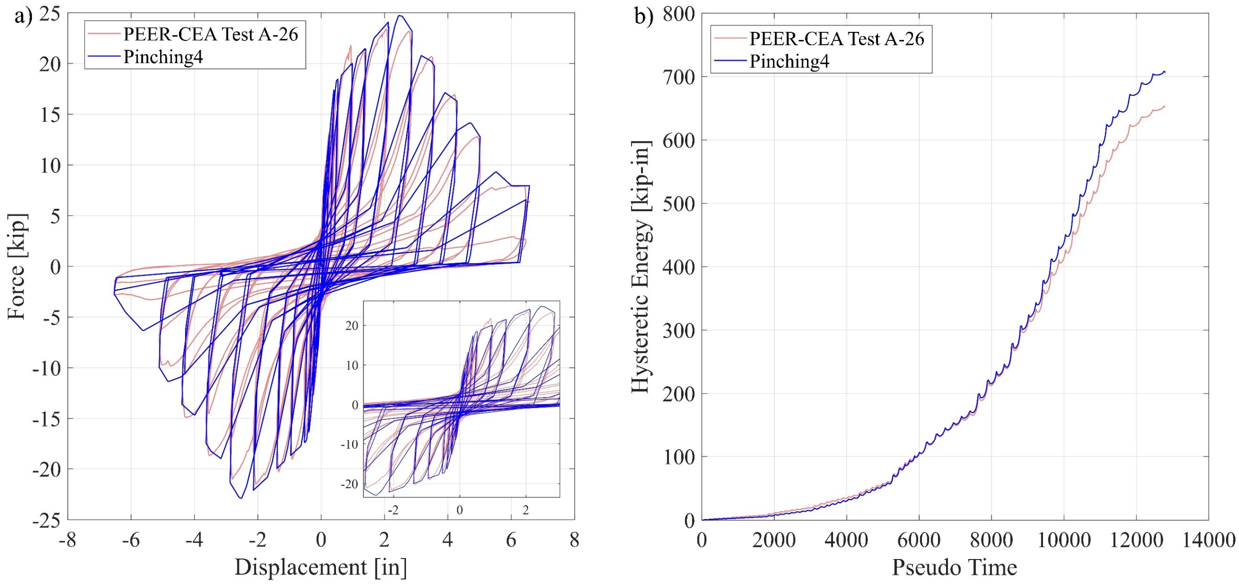

Figure 3.63 **Comparing the *Pinching4* material calibrated to the retrofitted 6-ft-tall stucco cripple wall test A-26 by Schiller et al. [2020(c)]: (a) hysteretic response; and (b) hysteretic energy.**

Table 3.15 **Summary of *Pinching4* material parameters for the retrofitted 2-ft-tall stucco cripple walls.**

Material	**Backbone deformation points (%drift)**				**Backbone force points (plf)**			
	*ed*1	*ed*2	*ed*3	*ed*4	*ef*1	*ef*2	*ef*3	*ef*4
CW2-S-R2 (best estimate)	**0.10**	**1.40**	**5.50**	**12.5**	**349**	**1680**	**1934**	**580**
CW2-S-R1	0.08	1.40	5.50	12.5	279	1310	1509	453
Cyclic properties	Spring 1	rDisp1	rForce1	uForce1	gK11	gKLim1	gD11	gDLim1
		0.05	0.37	-0.05	0	0	0.15	2.0
	Spring 2	rDisp2	rForce2	uForce2	gK12	gKLim2	gD12	gDLim2
		0.55	0.13	-0.07	0	0	0.10	0.50

*Definition of material model parameters is provided in Table 3.4; this material is developed as a double-sided material including both exterior existing finish and retrofit material on the interior.

Table 3.16 Summary of *Pinching4* material parameters for the retrofitted 6-ft-tall stucco cripple walls.

Material		Backbone deformation points (%drift)				Backbone force points (plf)			
		*ed*1	*ed*2	*ed*3	*ed*4	*ef*1	*ef*2	*ef*3	*ef*4
CW6-S-R2 (best estimate)		0.08	0.65	2.90	9.00	385	1517	1870	561
Cyclic properties	Spring 1	rDisp1	rForce1	uForce1	gK11	gKLim1	gD11	gDLim1	
		0.09	0.31	-0.05	-0.10	-0.30	0.21	2.0	
	Spring 2	rDisp2	rForce2	uForce2	gK12	gKLim2	gD12	gDLim2	
		0.49	0.16	-0.15	0	0	0.10	1.0	

*Definition of material model parameters is provided in Table 3.4; this material is developed as a double-sided material including both exterior existing finish and retrofit material on the interior.

3.6.3 Cripple Walls with Horizontal Wood Siding

As evident in post-earthquake reconnaissance reports and borne out by laboratory tests, cripple walls with horizontal wood siding are the most vulnerable type of existing cripple wall configurations considered in this study. Examples of horizontal wood siding cripple wall failures are presented in Figure 3.64 from several earthquakes, beginning with the 1940 Imperial Valley, California, earthquake to the more recent 2014 South Napa, California, earthquake. These and other examples demonstrate that houses with wood-siding cripple walls have shown very poor performance in previous earthquakes throughout California.

Figure 3.64 Horizontal siding cripple wall failures from previous seismic events.

3.6.3.1 Unretrofitted Case

Unretrofitted horizontal wood siding tests were conducted by WG4 within Phase II of small-component testing [Schiller et al. 2020(b)]. Test A-7 and Test A-13 are 12-ft-long cripple wall sub-assemblies with heights of 2 ft and 6 ft, respectively. These specimens had 1 × 6 shiplap siding applied to studs with 2-8d nails at each stud location. Except for the vertical stud framing and the horizontal siding, these tests had no auxiliary bracing, which resulted in lower bound estimates of conditions likely to be encountered in actual houses. Therefore, for the structural and loss analyses, a key question we addressed is how to combine the data from tests A-7 and A-13 with other available evidence to determine the "best estimate" properties of existing horizontal wood siding to use in the analyses.

The question of whether or not pure horizontal wood siding cripple walls (i.e., as represented by tests A-7 and A-13) is a lower bound to actual conditions in houses was raised by PEER–CEA Project Team members and Reviewers, who noted that some type of bracing is often present within the cripple walls. While such bracing could be equally present in cripple walls with horizontal wood siding or stucco exterior, the bracing would have proportionally much more effect on the response of the comparatively weak horizontal wood siding cripple walls. The types of possible bracing configurations include cut-in bracing (blocks placed between studs), continuous braced framing with studs cut above and below a continuous brace, and retained block bracing where cut-in braces are supported in compression by additional blocks sistered to studs and blocks placed in adjacent stud bays. As shown in Figure 3.65, examples of such bracing are evident in photographs from houses with cripple walls. The presence or absence of bracing, as well as detailing of the bracing, can vary significantly in existing houses. Aside from concerns about bracing the house to resist lateral earthquake or wind loading, the bracing is likely to be present to stabilize the house during construction. In this regard, houses with taller cripple walls or two-story houses would be even more likely to have bracing.

Structural response parameters of the baseline cripple wall wood siding condition are estimated from PEER–CEA Test A-7 for a 2-ft-tall cripple wall. Results of this test were in good agreement with the strength and stiffness attributed to exterior horizontal wood siding for the superstructure (see Section 3.4.1). The backbone curve for Test A-7 is shown in Figure 3.66 with an average peak strength of 177 plf at a drift ratio of 4%. The *Pinching4* material backbone fit the A-7 curve is denoted 'CW-HS1'. The adjusted response curve that includes the possibility of effective braces assumes twice the initial stiffness and peak strength of the CW-HS1 curve and one half of the displacement capacity. This adjusted backbone curve is taken as the best estimate for horizontal wood siding and is denoted material 'CW-HS2'. The doubling of the effective strength and halving the displacement capacity is based on the assumption that framing braces can resist a larger load initially yet will not provide significant displacement capacity. The factor of two increase in strength and decrease in displacement is based on review of data from previous tests of different bracing configurations on full-height walls (see Section 3.4.1). The two *Pinching4* material backbones are shown in Figure 3.66. These materials do not distinguish between cripple wall height. For analysis properties of retrofitted cripple walls, the participation of framing braces is neglected and the unretrofitted portion (length between wood structural panel sections for retrofit) assumes material CW-HS1.

Figure 3.65 Examples of different types of framing braces that could be present in cripple walls: (a) cut-in/block bracing (single piece); (b) cut-in/block bracing (multiple pieces) (c) continuous braced framing; and (d) retained block bracing. (photographs courtesy of the CEA).

The cyclic properties for unretrofitted cripple walls with horizontal wood siding are estimated from PEER–CEA Test A-7 [Schiller et al. 2020(b)]. The cyclic fitting to Test A-7 using the *Pinching4* material is shown in Figure 3.67. The *Pinching4* material parameters for unretrofitted horizontal wood siding cripple walls are provided in Table 3.17.

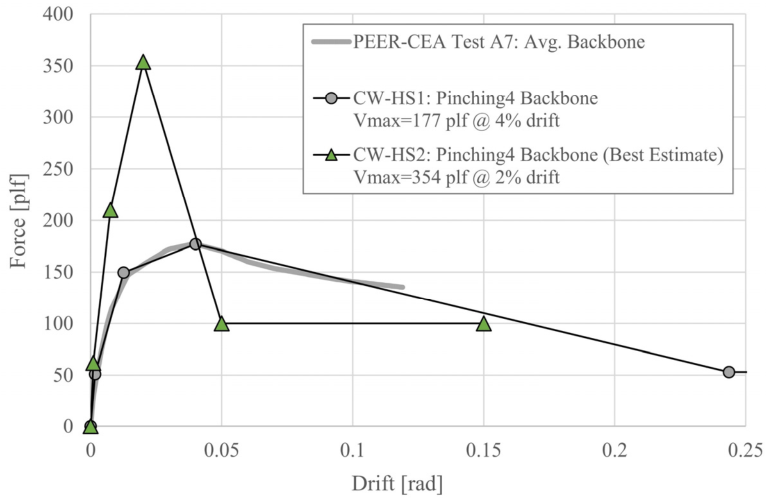

Figure 3.66 ***Pinching4*** **material backbones assumed for best estimate unretrofitted horizontal wood siding cripple walls including the possibility of framing braces (triangles) and unbraced horizontal wood siding based on PEER–CEA test A-7 [Schiller et al. 2020(b)] (circles).**

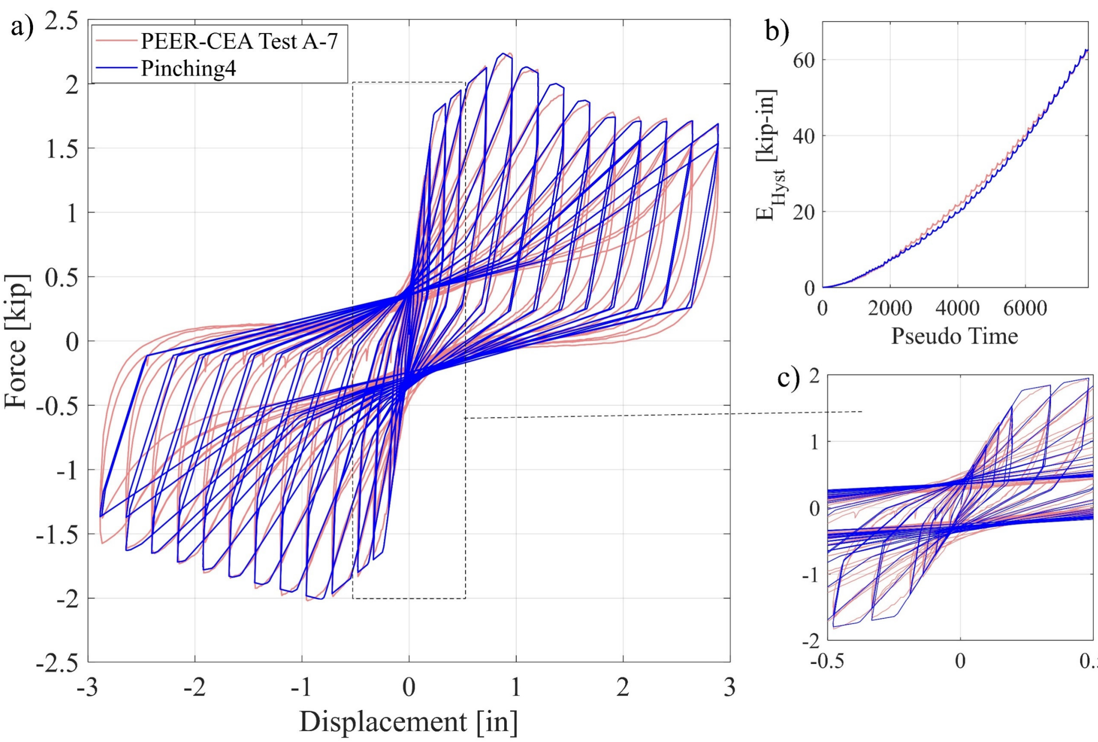

Figure 3.67 **Comparing the *Pinching4* material calibrated to 2-ft-tall unretrofitted horizontal wood siding cripple wall test A-7 by Schiller et al. [2020(b)]: (a) hysteretic response; (b) hysteretic energy; and (c) small displacement hysteretic response.**

Table 3.17 Summary of *Pinching4* material parameters for unretrofitted horizontal wood siding cripple walls.

Material		Backbone deformation points (%drift)				Backbone force points (plf)			
		*ed*1	*ed*2	*ed*3	*ed*4	*ef*1	*ef*2	*ef*3	*ef*4
CW-HS2 (best estimate)		**0.10**	**0.75**	**2.00**	**5.00**	**62**	**210**	**354**	**100**
CW-HS1		0.17	1.26	4.00	24.40	51	149	177	53
Cyclic properties	Spring 1	rDisp1	rForce1	uForce1	gK11	gKLim1	gD11	gDLim1	
		0.18	0.37	-0.10	-0.10	-1.0	0.14	0.30	
	Spring 2	rDisp2	rForce2	uForce2	gK12	gKLim2	gD12	gDLim2	
		0.40	0.34	-0.12	0	0	0.09	0.20	

*Definition of material model parameters is provided in Table 3.4; this material is developed as a single-sided material.

3.6.3.2 Retrofit Case

The best estimate material for 2-ft-tall horizontal wood siding cripple walls with WSP retrofit (CW2-HS-R2) is based on PEER–CEA small-component Specimen A-8 [Schiller et al. 2020(b)]. Similar to the discussion for 2-ft-tall stucco retrofit cripple walls in Section 3.6.2, the best estimate material assumes edge nailing of 8d at 3 in. on center. To investigate the effects of an increased nail spacing (8d at 4 in.), an additional material (CW2-HS-R1) was developed. The basis of the backbone curve for this material is the unretrofitted horizontal siding material (CW-HS1, based on PEER–CEA Test A-7) superimposed with the retrofit T1-11 material (based on PEER–CEA Test A-12 with 8d at 4-in. nailing, see Section 3.6.4). The backbone curves are shown in Figure 3.68. Note that large-component test B-2 [Cobeen et al. 2020] with 8d at 4-in. spacing (dashed line in Figure 3.68) was not completed at the time of calibrating wood siding materials, yet it supports using the reduction of 0.78 (see Section 3.6.2.2) to adjust for 8d at 4 in. based on test of 8d at 3-in. test data with similar detailing otherwise. The four-point *Pinching4* material backbones are shown in comparison to the target test backbones for materials CW2-HS-R2 (Figure 3.69), CW6-HS-R2 (Figure 3.70) and CW2-HS-R1; see Figure 3.71.

Cyclic properties for 2-ft-tall horizontal wood siding cripple walls with WSP retrofit are based on PEER–CEA test A-8 [Schiller et al. 2020(b)]. The cyclic fitting to Test A-8 using the *Pinching4* material is shown in Figure 3.72, and the associated model parameters are provided in Table 3.18. Cyclic properties for 6-ft-tall horizontal wood siding cripple walls with WSP retrofit are based on PEER–CEA test A-14 [Schiller et al. 2020(b)]. The cyclic fitting to Test A-14 using the *Pinching4* material is shown in Figure 3.73, and the associated modeling parameters are provided in Table 3.19.

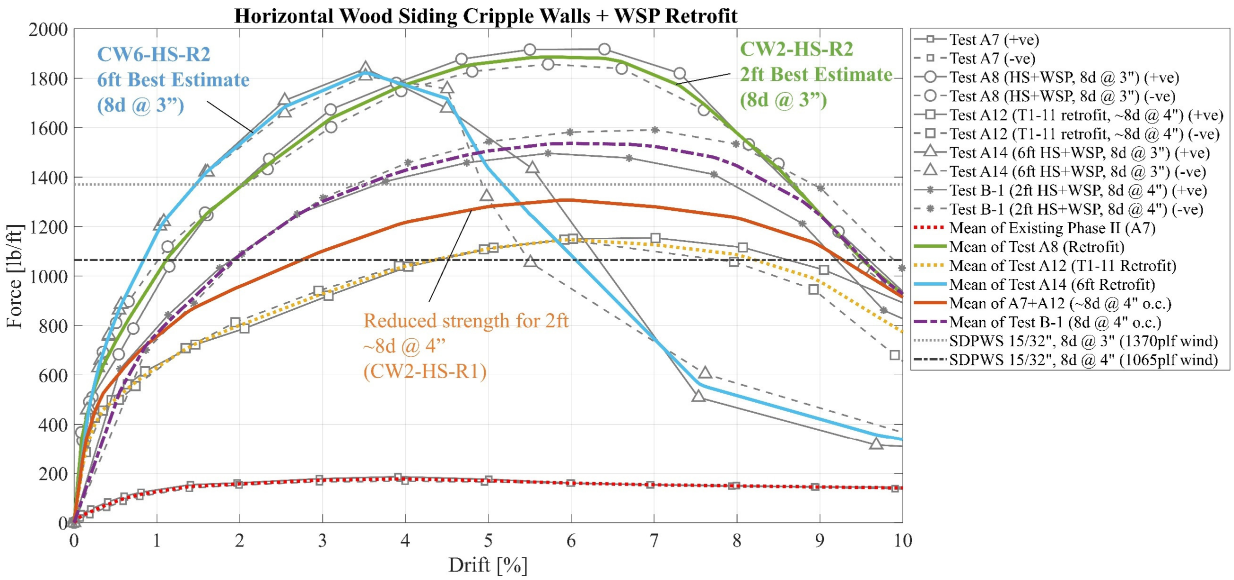

Figure 3.68 **Backbone curves considered for retrofitted horizontal wood siding cripple wall properties: best estimate 2 ft (CW2-HS-R2) with 8d @ 3 in. nailing, best estimate 6 ft (CW6-HS-R2), and reduced strength 2 ft for approximating 8d at 4 in. spacing (CW2-HS-R1).**

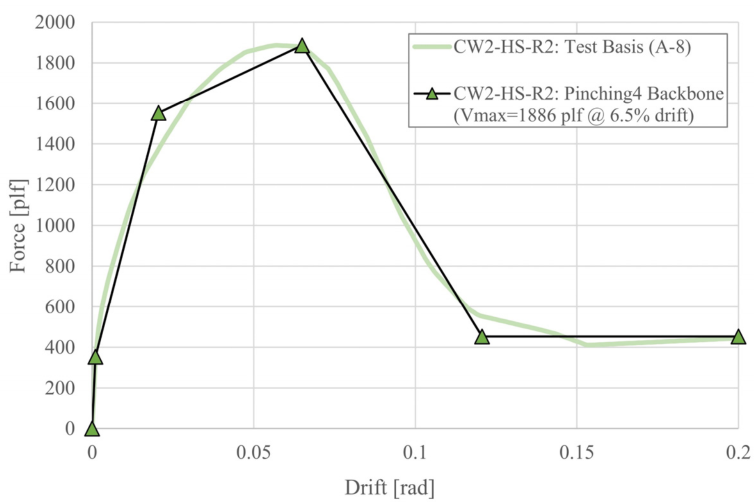

Figure 3.69 ***Pinching4* material backbone assumed for best estimate of retrofitted 2-ft-tall horizontal wood siding cripple walls with 8d @ 3 in. nailing (triangles) compared with the average backbone of PEER–CEA test A-8 [Schiller et al. 2020(b)].**

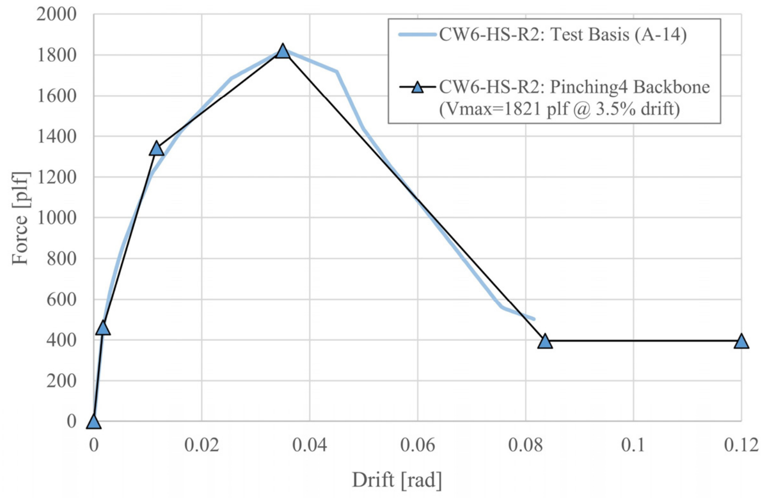

Figure 3.70 ***Pinching4*** **material backbone assumed for best estimate of retrofitted 6-ft-tall horizontal wood siding cripple walls with 8d @ 3 in. nailing (triangles) compared with the average backbone of PEER–CEA test A-14 [Schiller et al. 2020(b)].**

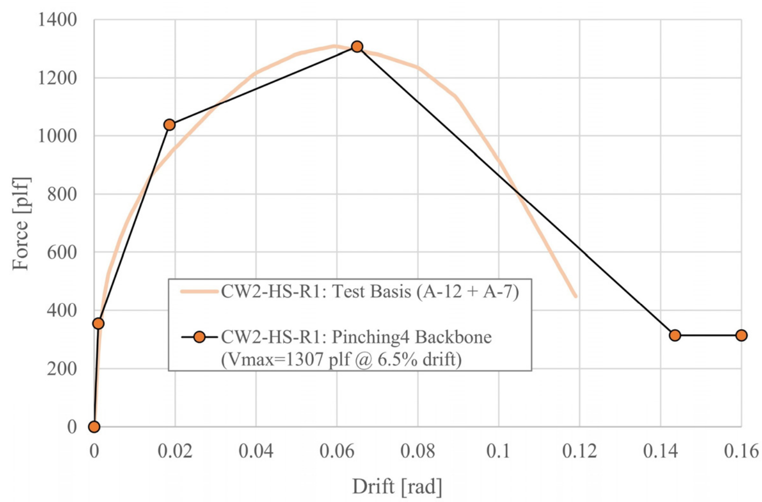

Figure 3.71 ***Pinching4*** **material backbone assumed for reduced strength of retrofitted 2-ft-tall horizontal wood siding cripple walls with 8d @ 4 in. nailing (circles) compared with the average combined backbone of PEER–CEA tests A-7 and A-12 [Schiller et al. 2020(b)].**

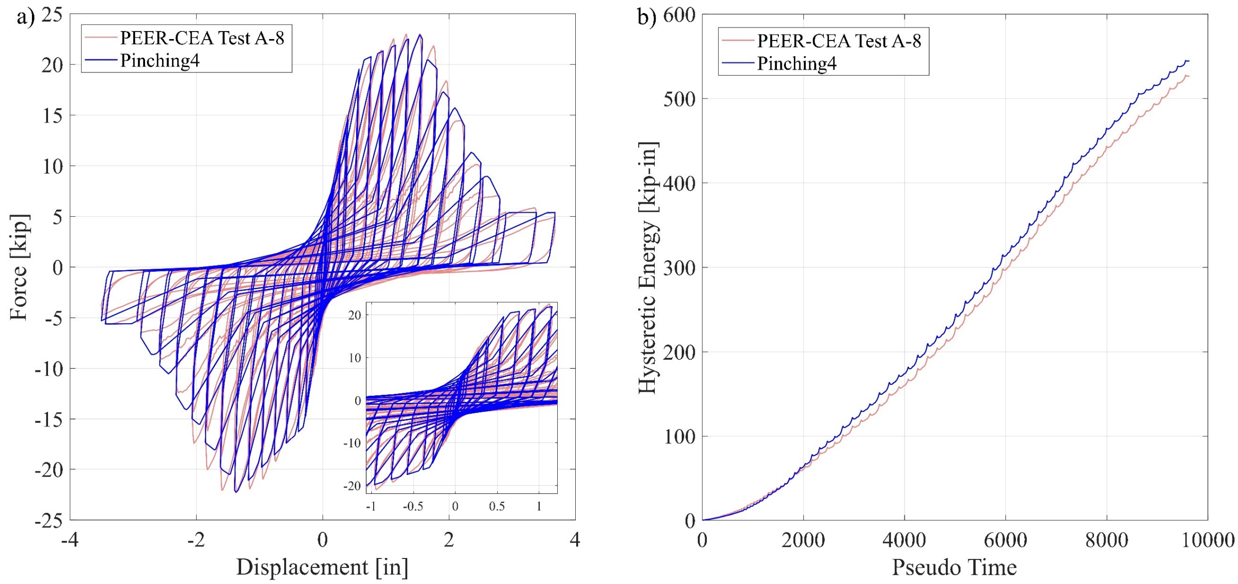

Figure 3.72 Comparing the ***Pinching4*** **material calibrated to retrofitted 2-ft-tall horizontal wood siding cripple wall test A-8 by Schiller et al. [2020(b)]: (a) hysteretic response; and (b) hysteretic energy.**

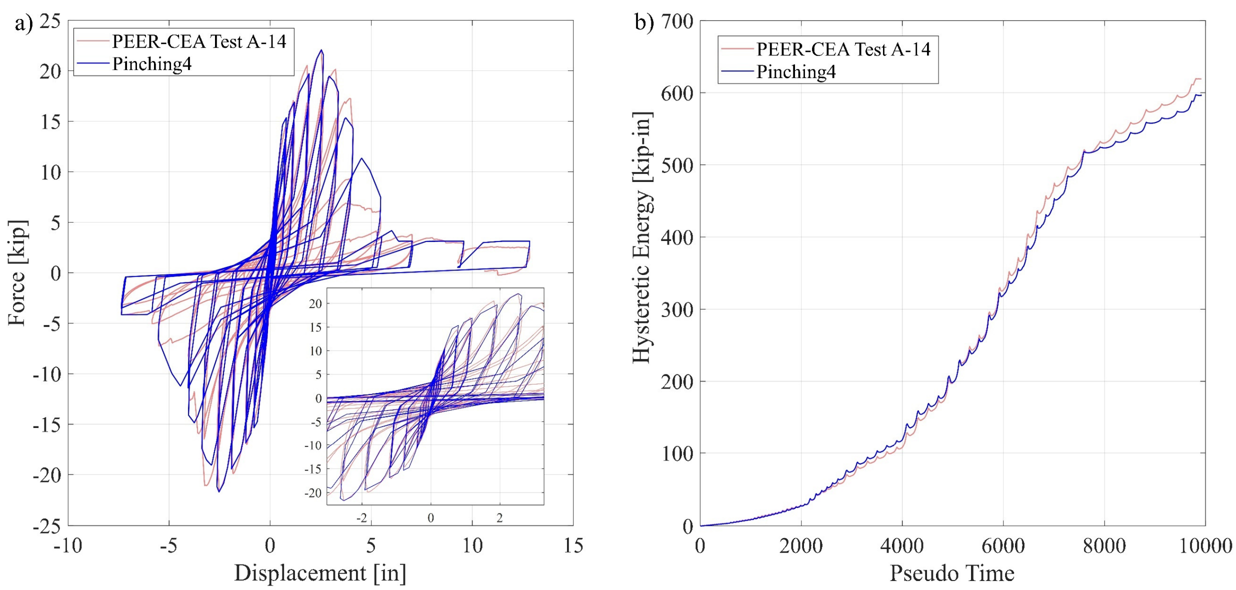

Figure 3.73 Comparing the ***Pinching4*** **material calibrated to retrofitted 6-ft-tall horizontal wood siding cripple wall test A-14 by Schiller et al. [2020(b)]: (a) hysteretic response; and (b) hysteretic energy.**

Table 3.18 Summary of *Pinching4* material parameters for retrofitted 2-ft-tall horizontal wood siding cripple walls.

Material		Backbone deformation points (%drift)				Backbone force points (plf)			
		*ed*1	*ed*2	*ed*3	*ed*4	*ef*1	*ef*2	*ef*3	*ef*4
CW2-HS-R2 (best estimate)		**0.10**	**2.06**	**6.50**	**12.1**	**354**	**1553**	**1886**	**453**
CW2-HS-R1		0.10	1.86	6.50	14.4	354	1038	1307	314
Cyclic properties	Spring 1	rDisp1	rForce1	uForce1	gK11	gKLim1	gD11	gDLim1	
		0.03	0.40	0.02	0	0	0.14	0.30	
	Spring 2	rDisp2	rForce2	uForce2	gK12	gKLim2	gD12	gDLim2	
		0.55	0.14	-0.09	0	0	0.05	1.0	

*Definition of material model parameters is provided in Table 3.4; this material is developed as a double-sided material including both exterior existing finish and retrofit material on the interior.

Table 3.19 Summary of *Pinching4* material parameters for retrofitted 6-ft-tall horizontal wood siding cripple walls.

Material		Backbone deformation points (%drift)				Backbone force points (plf)			
		*ed*1	*ed*2	*ed*3	*ed*4	*ef*1	*ef*2	*ef*3	*ef*4
CW6-S-R2 (best estimate)		0.17	1.16	3.50	8.40	462	1342	1821	396
Cyclic properties	Spring 1	rDisp1	rForce1	uForce1	gK11	gKLim1	gD11	gDLim1	
		0.06	0.38	0.02	-0.10	-1.0	0.2	0.3	
	Spring 2	rDisp2	rForce2	uForce2	gK12	gKLim2	gD12	gDLim2	
		0.55	0.20	-0.15	-0.10	-0.50	0.10	1.0	

*Definition of material model parameters is provided in Table 3.4; this material is developed as a double-sided material including both exterior existing finish and retrofit material on the interior.

3.6.4 Cripple Walls with T1-11 Siding

Material properties for panelized plywood siding or T1-11 at the cripple wall level are based on recent testing within the PEER–CEA Project conducted as part of the small-component testing [Schiller et al. 2020(b)].

Unlike other existing (unretrofitted) materials, the existing T1-11 siding provides the sheathing for seismic strengthening, where retrofitting only involves upgrading of the nailing schedule of the existing T1-11 siding. The existing (unretrofitted) case assumes 8d common nails spaced at 8 in. on center, where nailing at panel joints is limited to only the overlapping panel (i.e., leaving one vertical edge of each panel un-nailed). This detail reflects the most common situation found in the field as discussed within *FEMA P-1100* Section 8.3 [2018]. The retrofit nailing schedule requires that the perimeter of each panel be nailed using 8d common nails with a spacing of 4 in. on center. The nail spacing is governed by the *FEMA P-1100* "Light" weight classification for retrofitting. According to the retrofit requirements of *FEMA P-1100*, the entire perimeter of the house must have improved nailing (in contrast to WSP retrofitting of other cripple walls, which is installed over part of the cripple wall length). An illustration of the two nailing schedules for T1-11 siding is shown in Figure 3.74.

The UCSD small-component testing [Schiller et al. 2020(b)] looked at 2-ft- and 6-ft-tall variations of T1-11 siding specimens. Tests A-11 and A-12 (Phase II) were 2-ft-tall specimens with unretrofitted and retrofitted detailing, respectively. Tests A-23 and A-24 (Phase III) were the equivalent 6-ft-tall specimens. The average backbones of each test were used as the basis of the best estimate materials as shown in Figure 3.75. The four-point *Pinching4* material backbones are shown in comparison to the target test backbones for materials CW2-T1 (Figure 3.76), CW2-T1-R1 (Figure 3.77), CW6-T1 (Figure 3.78) and CW6-T1-R1; see Figure 3.79.

Cyclic properties for 2-ft-tall T1-11 cripple wall materials are estimated from test A-12 (retrofit case). The cyclic fitting to Test A-12 using the *Pinching4* material is shown in Figure 3.80, and the best estimate model parameters are provided in Table 3.20.

Cyclic properties for the unretrofitted 6-ft-tall T1-11 cripple wall material are based on test A-23. The cyclic fitting to Test A-23 using the *Pinching4* material is shown in Figure 3.81, and the best estimate modeling parameters (CW6-T1) are provided in Table 3.21.

Cyclic properties for the retrofitted 6-ft-tall T1-11 cripple wall material are based on test A-24. The cyclic fitting to Test A-24 using the *Pinching4* material is shown in Figure 3.82, and the best estimate modeling parameters (CW6-T1-R1) are provided in Table 3.22.

Figure 3.74 Illustration of unretrofitted (left) and retrofitted (right) nail schedules for panelized T1-11 siding. (Figure from Schiller et al. [2020(b)]).

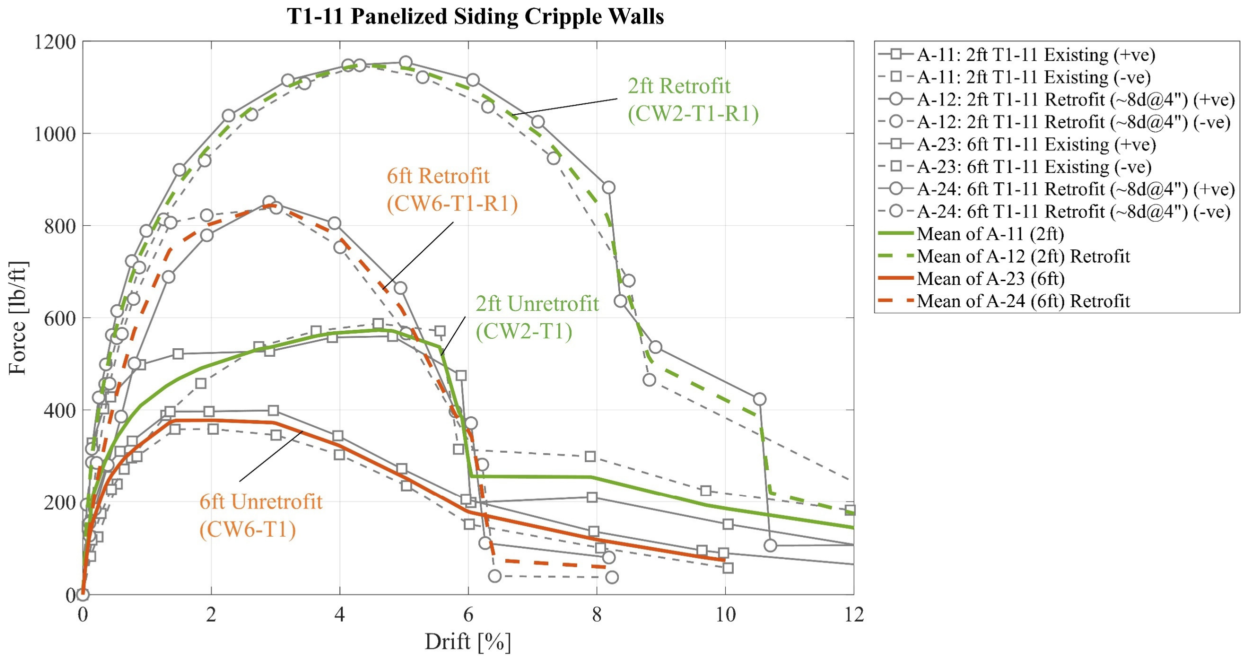

Figure 3.75 Backbone curves considered for T1-11 panelized siding cripple wall best estimate properties: unretrofitted 2-ft-tall wall (CW2-T1), unretrofitted 6-ft-tall wall (CW6-T1), retrofitted 2-ft-tall wall (CW2-T1-R1), and retrofitted 6-ft-tall wall (CW6-T1-R1).

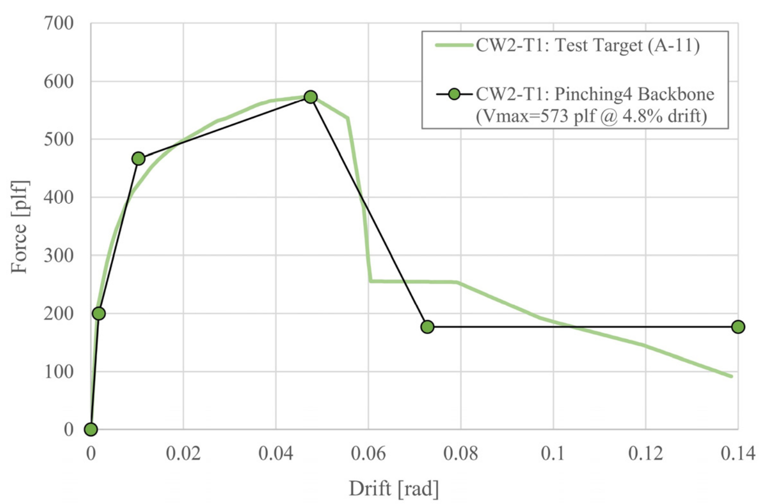

Figure 3.76 *Pinching4* material backbone for best estimate of unretrofitted 2-ft-tall T1-11 siding cripple walls (circles) compared with the average backbone of PEER–CEA test A-11 [Schiller et al. 2020(b)].

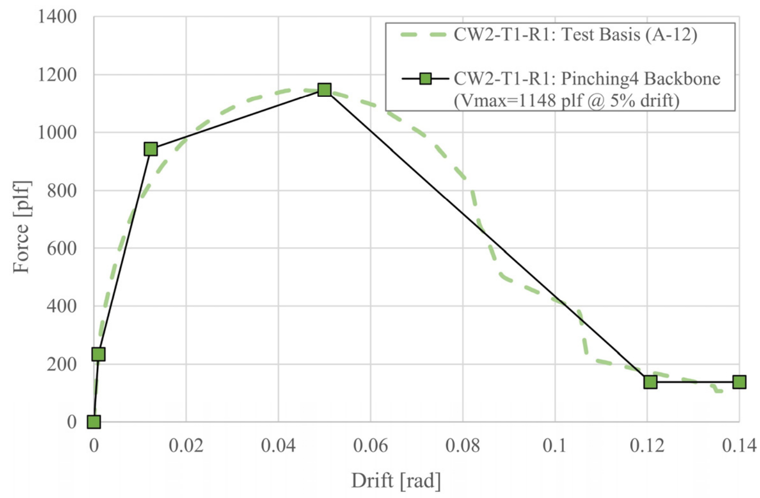

Figure 3.77 *Pinching4* **material backbone for best estimate of retrofitted 2-ft-tall T1-11 siding cripple walls (squares) compared with the average backbone of PEER–CEA test A-12 [Schiller et al. 2020(b)].**

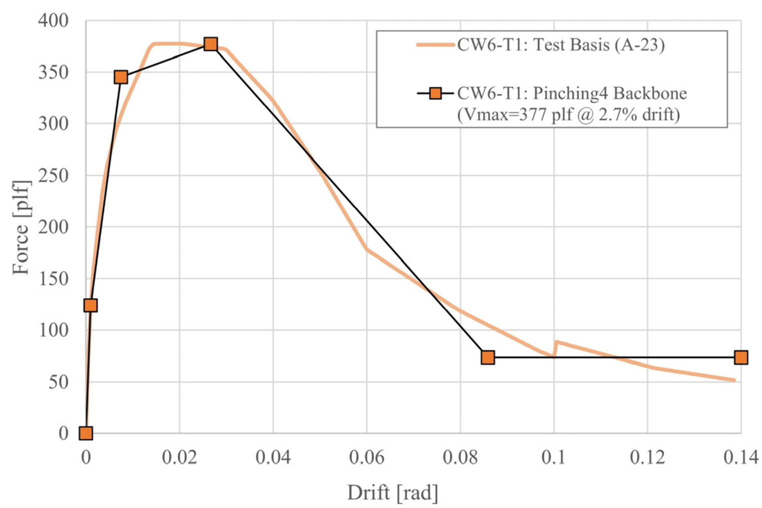

Figure 3.78 *Pinching4* **material backbone for best estimate of retrofitted 6-ft-tall T1-11 siding cripple walls (squares) compared with the average backbone of PEER–CEA test A-23 [Schiller et al. 2020(b)].**

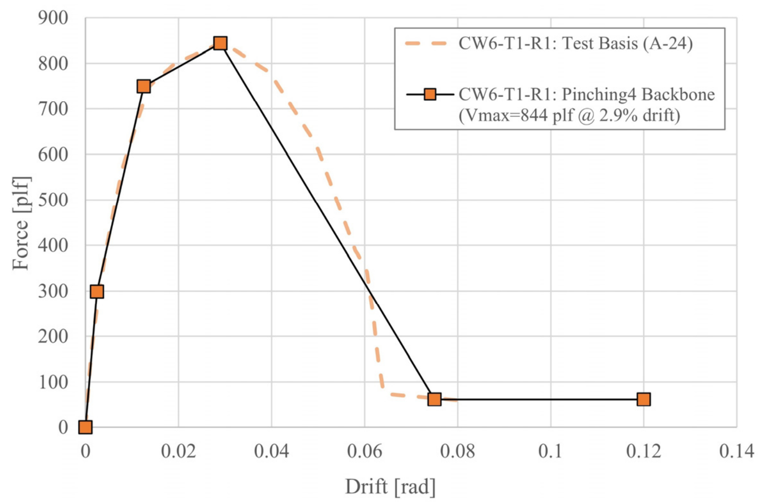

Figure 3.79 ***Pinching4*** **material backbone for best estimate of retrofitted 6-ft-tall T1-11 siding cripple walls (squares) compared with the average backbone of PEER–CEA test A-24 [Schiller et al. 2020(b)].**

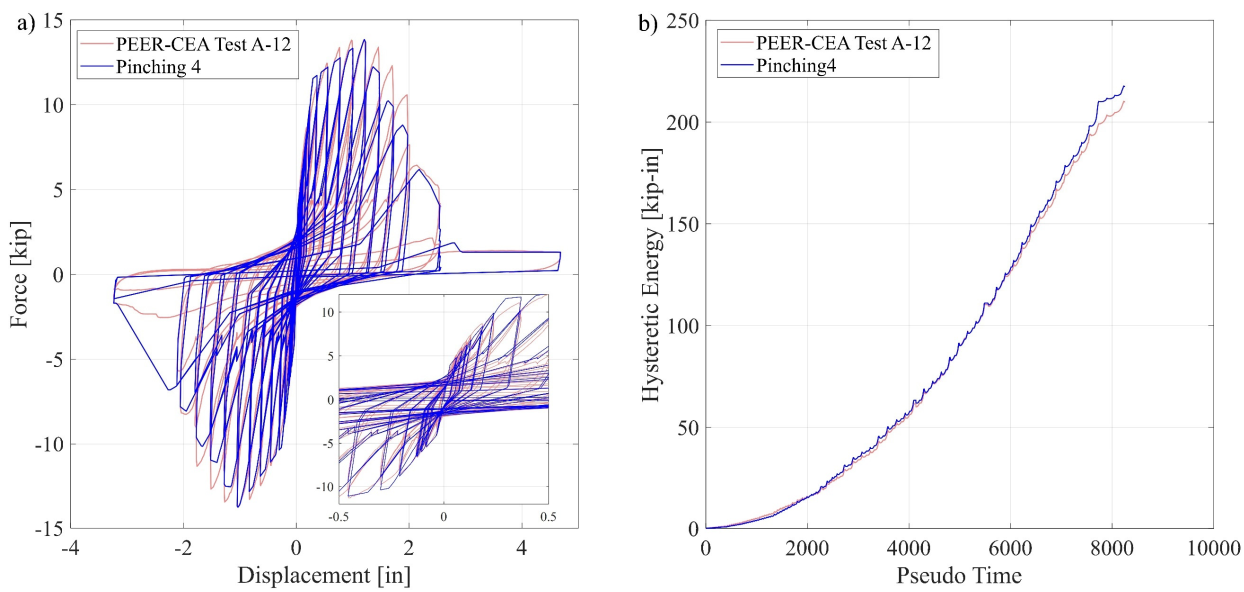

Figure 3.80 **Comparing the** ***Pinching4*** **material calibrated to the retrofitted 2-ft-tall T1-11 siding cripple wall test A-12 by Schiller et al. [2020(b)]: (a) hysteretic response; and (b) hysteretic energy.**

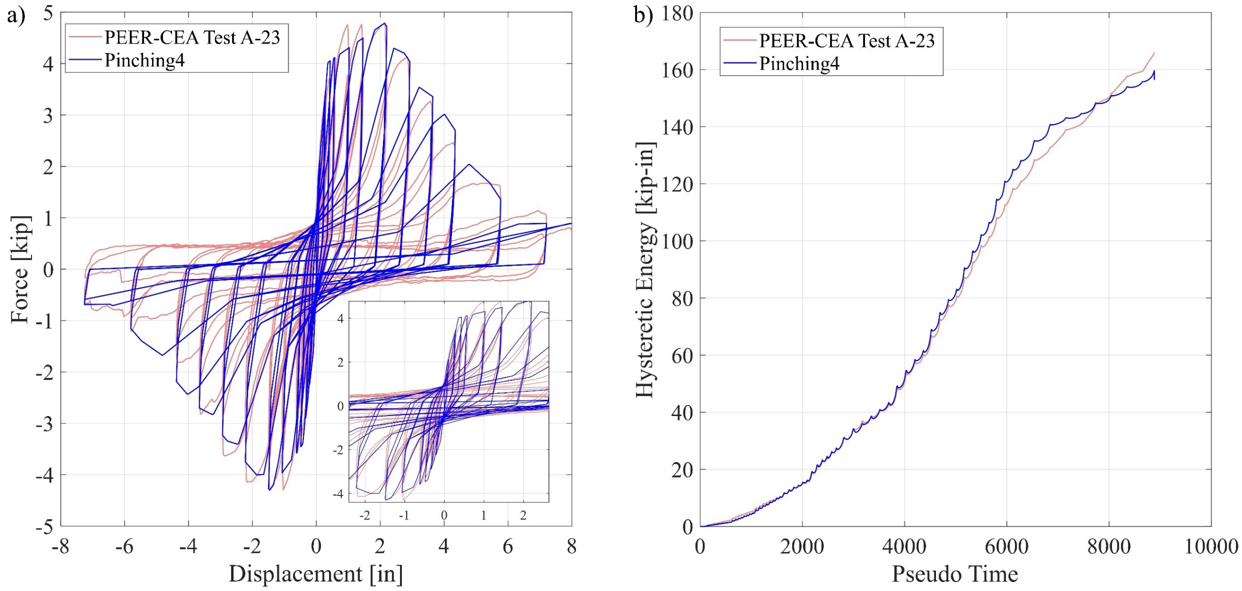

Figure 3.81 Comparing the ***Pinching4*** material calibrated to the unretrofitted 6-ft-tall T1-11 siding cripple wall test A-23 by Schiller et al. [2020(b)]: (a) hysteretic response; and (b) hysteretic energy.

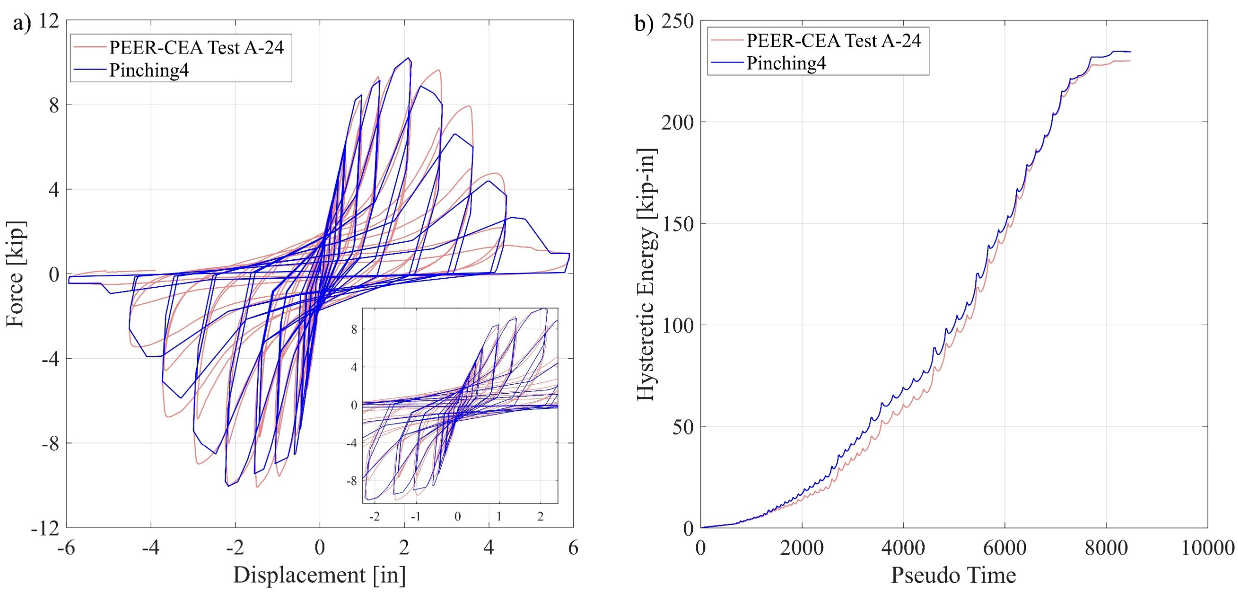

Figure 3.82 Comparing the ***Pinching4*** material calibrated to retrofitted 6-ft-tall T1-11 siding cripple wall test A-24 by Schiller et al. [2020(b)]: (a) hysteretic response; and (b) hysteretic energy.

Table 3.20 *Pinching4* material parameters for best estimate 2-ft-tall T1-11 cripple walls.

Material		Backbone deformation points (%drift)				Backbone force points (plf)			
		*ed*1	*ed*2	*ed*3	*ed*4	*ef*1	*ef*2	*ef*3	*ef*4
CW2-T1 (Unretrofit)		0.17	1.03	4.75	7.28	200	467	573	177
CW2-T1-R1 (Retrofit)		0.10	1.23	5.00	12.1	234	943	1148	139
Cyclic properties	Spring 1	rDisp1	rForce1	uForce1	gK11	gKLim1	gD11	gDLim1	
		0.06	0.30	0.01	0	0	0.2	0.3	
	Spring 2	rDisp2	rForce2	uForce2	gK12	gKLim2	gD12	gDLim2	
		0.52	0.18	-0.15	0	0	0.10	1.0	

*Definition of material model parameters is provided in Table 3.4; this material is developed as a single-sided material where retrofitting upgrades the nailing of existing siding panels.

Table 3.21 *Pinching4* material parameters for best estimate unretrofitted 6-ft-tall T1-11 siding cripple walls.

Material		Backbone deformation points (%drift)				Backbone force points (plf)			
		*ed*1	*ed*2	*ed*3	*ed*4	*ef*1	*ef*2	*ef*3	*ef*4
CW6-T1 (Unretrofit)		0.10	0.75	2.67	8.59	124	345	377	73
Cyclic properties	Spring 1	rDisp1	rForce1	uForce1	gK11	gKLim1	gD11	gDLim1	
		0.10	0.31	-0.15	0	0	0.25	1.0	
	Spring 2	rDisp2	rForce2	uForce2	gK12	gKLim2	gD12	gDLim2	
		0.54	0.29	-0.10	0	0	0.10	1.0	

*Definition of material model parameters is provided in Table 3.4, this material is developed as a single-sided material.

Table 3.22 *Pinching4* material parameters for best estimate retrofitted 6-ft-tall T1-11 siding cripple walls.

Material		Backbone deformation points (%drift)				Backbone force points (plf)			
		ed1	ed2	ed3	ed4	ef1	ef2	ef3	ef4
CW6-T1-R1 (Retrofit)		0.25	1.25	2.90	7.50	299	750	844	62
Cyclic properties	Spring 1	rDisp1	rForce1	uForce1	gK11	gKLim1	gD11	gDLim1	
		0.12	0.29	0.01	-0.05	-0.80	0.25	1.0	
	Spring 2	rDisp2	rForce2	uForce2	gK12	gKLim2	gD12	gDLim2	
		0.54	0.29	-0.15	-0.10	-0.60	0.10	1.0	

*Definition of material model parameters is provided in Table 3.4; this material is developed as a single-sided material where retrofitting upgrades the nailing of existing siding panels.

3.7 MATERIAL PROPERTIES FOR JOIST-TO-SILL CONNECTIONS FOR STEM-WALL DWELLINGS

This section covers the development of modeling parameters for the anchorage of floor framing (joists) to the sill plate connection for existing stem wall dwellings. The main observations of stem wall failures and assumptions for the controlling failure mode are discussed. The proposed material properties to model the force-displacement behavior of stem wall connections are then presented.

3.7.1 Observations and Assumptions for Stem Wall Failures

Within the PEER–CEA Project, a major assumption regarding stem-wall anchorage failure is that the weakest link is in the floor framing-to-sill plate (mudsill) connections. This is based on a critical review of reported "anchorage" failures in past earthquakes.

The term "unbolted" is seemingly used to refer to stem wall conditions that exhibit deficient resistance to lateral loads. The bolting refers to the connection of the sill plate to the perimeter stem wall foundation. When reviewing reconnaissance reports from previous earthquakes, there is little evidence that shows that the actual sill-to-foundation connection is the main culprit for stem wall failures, although there are a few exceptions. The report produced by Steinbrugge et al. [1990] following the 1983 Coalinga California, earthquake provides a classic example of a truly unbolted foundation condition. As reported by Steinbrugge et al. [1990], many houses in the town of Coalinga were transported from nearby oil fields between 1930 and 1960, and placed either directly on the ground or on perimeter foundations without any positive connection. Figure 3.83 provides an example of one of these dwellings that slid off its foundation, where the perimeter foundation was troweled smooth, reducing the frictional resistance between the wood sill plate and the top of the foundation. On the contrary, Steinbrugge et al. [1990] also point out that the lack of a visible bolt connection does not necessarily indicate this truly "unbolted" condition. They note to the previous common practice of nailing large (30-60d) spikes into the sill plate and then setting the spikes in the foundation concrete before curing. This is termed a "wet-set" sill and has shown to have considerable strength from other reconnaissance reports (e.g., Schierle [2001]). The 'wet-set' sill condition was also tested within the PEER–CEA Project (e.g., see Tests A-6 and A-21 in Schiller et al. [2020(b)]). In terms of anchor bolts, the practice of placing 1/2-in.-diameter anchor bolts at 6-ft spacing was apparently adopted within the Uniform Building Code as early as 1935 [Steinbrugge et al. 1990]. However, the date and regularity of adoption of the bolting standard is likely to vary in different regions of California.

Known issues with sill plates attached by anchor bolts are typically associated with oversized holes due to construction limitations and inadequate washer sizes [Hall et al. 1996; Mahaney and Kehoe 2002]. However, many of these observations of sill plate and framing damage are associated with more modern plywood shear walls connected directly to sill plates with a slab on grade foundation (e.g., Hall et al. [1996]). In such cases, the plywood shear walls develop much larger forces than can be developed by older construction without plywood, where the sill detail experiences both large shear forces and cross grain bending at the side of the sill plate level due to overturning. These issues were confirmed through testing conducted by Mahaney and Kehoe [2002], where anchor bolt/sill plate capacity is increased by more than a factor of four (1723 plf versus 408 plf on average) when the loading wall aspect ratio is reduced from 1 to 4 (i.e., 8 ft long × 8 ft tall versus 4 ft long × 1 ft tall). This a logical result since the effects of overturning are greatly reduced by the shorter shear wall aspect ratio. Further, testing of anchor bolts in pure shear, conducted by Fennell et al. [2009], found that 5/8-in.-diameter anchor bolts loading in direct shear had average capacities ranging from four to six times current code values. These observations highlight reasons why the anchor bolts in older houses (without plywood shear walls, and properly installed and in good condition) are unlikely to fail before other elements in the system.

The scope of the PEER–CEA Project does not include houses with plywood sheathing. Further, in older existing houses with stem walls, the first-floor framing (i.e., floor joists) typically rests directly on the sill (mudsill) plate. Because of this, numerous stem wall failures (whether bolted or using wet-set sills) are shown to occur in the connection between the floor joist and the mudsill plate. In reconnaissance reports from previous seismic events, there are many more photos of this failure mode than the actual sill-to-foundation connection. A sample of photographs of stem wall failures at the joist-to-sill connection are provided in Figure 3.84. While actual conditions could vary considerably, the current study of stem wall configurations assumes that the controlling failure mode is at the joist-to-sill connection.

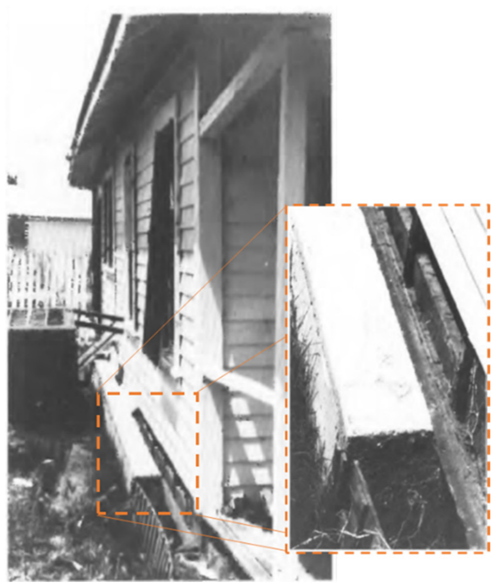

Figure 3.83 Illustration of “truly unbolted” foundation anchorage conditions observed following the 1983 Coalinga earthquake. The photo shows a relocated home placed directly on a troweled smooth perimeter foundation without anchorage (Steinbrugge et al. [1990]).

Figure 3.84 **Examples of stem wall failures at the joist-to-sill connection. (photographs courtesy of (a) CUREE [2010]; (b) Nakata et al. [1999]; and (c) FEMA [2006(b)]).**

3.7.2 Material Properties for Toe-Nail Joist-to-sill Connections

Based on discussions among the PEER–CEA project team and external experts, the typical detail for analysis of stem-wall houses is assumed to consist of first-floor joists sitting on the sill plate, where the joists are connected to the sill plate with three 8d toe-nails. Rim joists and joists running parallel to the sill plate, are assumed to have 8d toe-nails spaced at 24 in. on center.

Material properties for toe-nails were estimated based on data from tests conducted by Ryan et al. [2003] as part of the CUREE-Caltech Woodframe Project. The properties are taken by the Scenario 1 test reported by Ryan et al. [2003]. This specimen is 8 ft long where the joists are connected to the sill plate by 8d box toe-nails, with 3 nails per each perpendicular floor joist and nails spaced at 6 in. along the rim joist; see Figure 3.85(b). As shown in the figure, the specimen experienced slip displacements and failure at the toe-nailed joist to sill plate interface.

The mean backbone curve from the Scenario 1 test, shown in Figure 3.86(a), was estimated from the cyclic loading response in the positive and negative directions. The resulting backbone has a total average peak strength (i.e., 38-8d toe-nails total in two orientations) of 5850 lbs at a displacement of approximately 0.6 in. This translates to 154 lbs of peak resistance per 8d toe-nail, assuming that the mixed orientations of toe-nailing is generally representative of conditions in existing houses.

To model the force-displacement response of toe-nail connections, the SAWS [Folz and Filiatrault 2004(a); Christovasilis and Filiatrault 2009(b)] hysteretic model was selected; see Figure 3.5. Using a peak displacement (*DU*) of 0.6 in., the four other backbone parameters (*S0*, *F0*, *R1*, and *R2* in Figure 3.5) were estimated by fitting the experimental backbone using least squares regression and visual tuning of results. The *SAWS* backbone curve is shown in comparison with the Scenario 1 test conducted by Ryan et al. [2003] in Figure 3.86(b). The figure shows good agreement for the entire curve except the flat area between approximately 0.4 and 0.6 in. of displacement. This shape was difficult to achieve due to the pre-peak loading slope using the SAWS model being governed by an exponential relationship, however, this is not expected to significantly affect results. Moreover, the flat segment is more likely to be an artifact of the specific test, rather than indicative of expected behavior in practice. The cyclic intercept force (*FI*) was estimated from the experimental data with a value of 18% of peak loading in each direction on average. This was applied as an equivalent yield force (*F0*) to the fitted backbone properties.

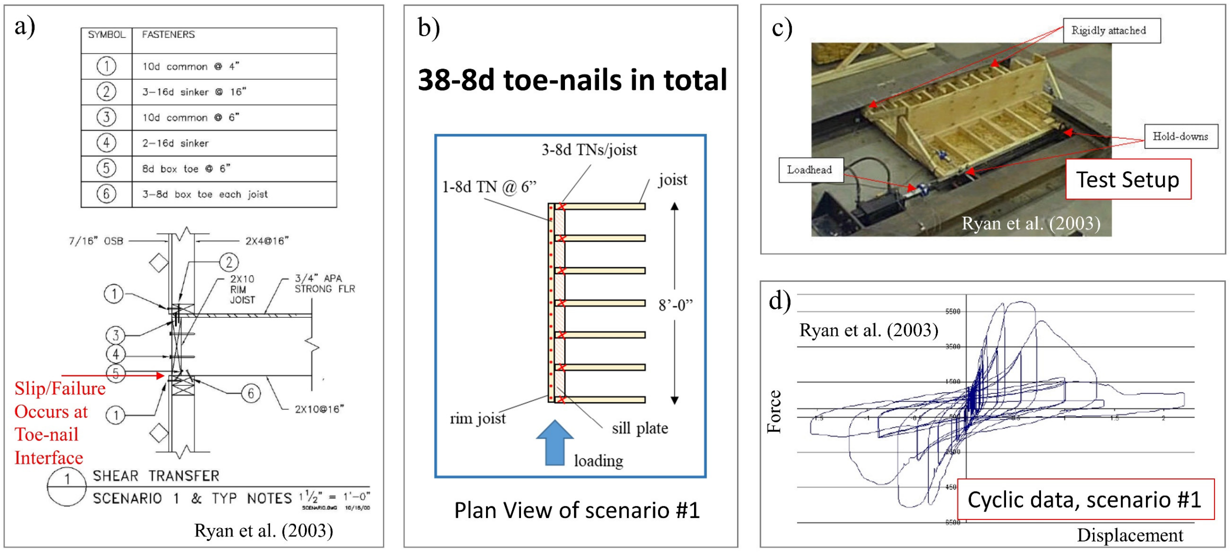

Figure 3.85 Details of testing conducted by Ryan et al. [2003] to obtain properties for 8d toe-nail joist-to-sill connections: (a) elevation drawing of force transfer test details for Scenario 1; (b) plan view sketch of Scenario 1 highlighting joist-to-sill interface (c) photograph of test setup; and (d) resulting cyclic loading data for Scenario 1.

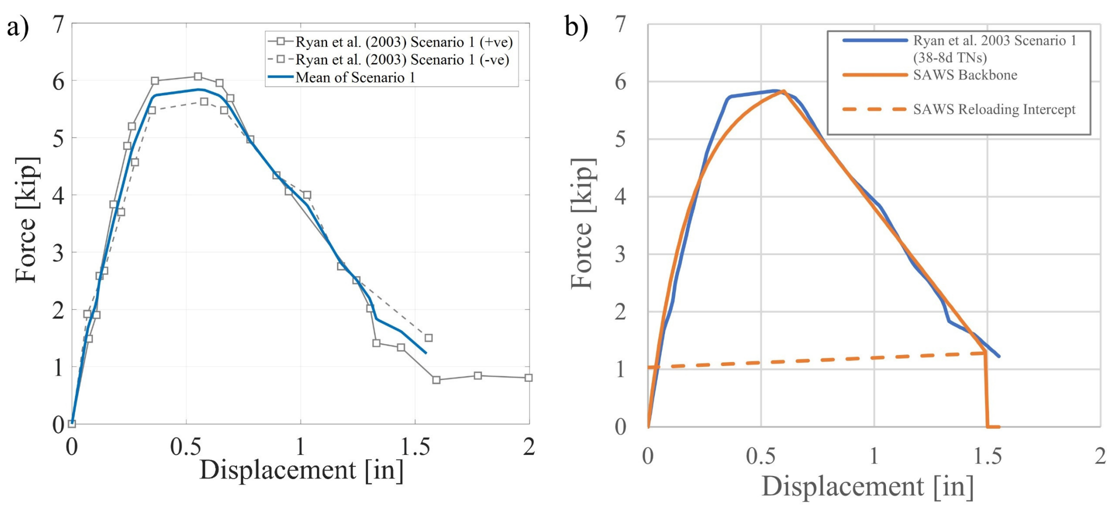

Figure 3.86 Summary of process to estimate material backbone properties of 8d toe-nail connections based on Scenario 1 tested by Ryan et al. [2003]: (a) estimating mean backbone from positive and negative cyclic envelopes; and (b) using the SAWS hysteretic model to approximate the backbone, force intercept, and failure displacement based on test data.

The SAWS model was selected for modeling the stem wall connection to take advantage of the failure displacement behavior of the model. By definition, the SAWS model incorporates an element removal effect when its failure displacement is reached, after which the element resists zero force regardless of loading direction. This failure displacement is defined by the minimum of the displacements corresponding to the following two conditions: (i) intersection of the pinched reloading slope and post-peak backbone slope; or (ii) the displacement at which the post-peak backbone reaches zero force. The former case usually controls. For the toe-nail material, the failure displacement was selected to be 1.5 in. based on experimental backbone data. The pinched reloading stiffness factor (*R4*) was adjusted with the assumed intercept force (*FI*) to obtain the target failure displacement. This is illustrated by the dashed line in Figure 3.86(b). The remaining cyclic properties of unloading stiffness factor (*R3*), reloading stiffness exponent (α) and reloading displacement factor (β) were taken directly from values assumed for toe-nails within the ATC-110 project [FEMA 2019(b)]. The properties assumed for 8d toe-nail joist-to-sill connections are provided in Table 3.23, where the properties are normalized by the number of toe-nails, based on the 38 collective toe-nails in the Scenario 1 test by Ryan et al. [2003].

Table 3.23 SAWS material properties for 8d toe-nail floor-to-joist connections based on testing conducted by Ryan et al. [2003].

S0 (kip/in.-TN)	*F0* (kip/TN)	*FI* (kip/TN)	*DU* (in.)	*R1*	*R2*	*R3*	*R4*	*α*	*β*
1.571	0.274	0.049	0.60	0.0143	-0.154	0.502	0.005	0.85	1.10

* Parameters are expressed per 8d toe-nail (TN) connection. Basis is Scenario 1 conducted by Ryan et al. [2003]

3.7.3 Considerations for Friction in Stem Wall Dwellings

Frictional sliding resistance is considered, along with the toe-nails, between the floor joist framing and the mudsill plates for stem wall foundations. The friction resistance is important for loss modeling to provide the expected level of response, as compared to a lower bound model, which excludes friction, that might be used for design. While there are many types of friction models that could be employed, for this study the friction forces are modeled assuming a constant Coulomb-type friction with the break-away (or slip friction) force (F_s) calculated as a function of the expected dead load (w_{DL}) acting at the sill plate (normal force) and an assumed coefficient of friction (μ_s). This is illustrated in Figure 3.87.

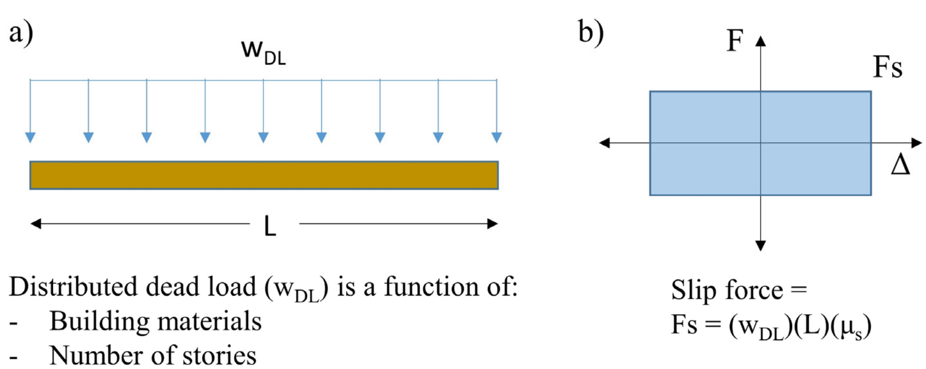

Figure 3.87 Illustration of the simplified treatment of stem wall joist-to-sill friction forces as a constant Coulomb-type friction: (a) distributed dead load along stem wall acting as normal force; and (b) friction slip force as a function of dead load and coefficient of friction.

The dead load acting along the perimeter stem wall is calculated using similar assumptions to those used within the ATC-110 project to calculate overturning resistance provided by dead load when checking uplift requirements for cripple wall retrofit design. These assumptions for estimating distributed dead loads (w_{DL}) along the perimeter include the following:

- The tributary width of roof level diaphragms is assumed to be 6 ft;
- The tributary width of floor diaphragms and interior walls is assumed to be 4 ft;
- A total of 3 interior partition walls are assumed to frame into each exterior wall.

All of the dead load weight take-offs discussed in Section 2.4.1 were used, along with these tributary areas, to calculated distributed line dead loads as input to the analysis model. The interior wall loads are converted into an equivalent distributed line load, by dividing the total assumed interior wall weights by the average of the relevant plan dimension. For example, a given interior wall load (w_{Int}) would be multiplied by the story height and the tributary width of 4 ft. This would then be multiplied by three to represent the number of partitions walls assumed to be framing into each exterior wall line. This total weight would then be divided by the average plan dimension (e.g., 35 ft for current models) to obtain an approximate distributed line load in units of pounds per linear foot (plf). A summary of the assumed perimeter dead loads is provided in Table 3.24.

The coefficient of friction (μ_s) for the stem wall connection is assumed to be 0.35. This value is intended to balance the typical static and dynamic coefficients of friction listed for wood-on-wood conditions. Published static coefficients of friction range from 0.25 to 0.50 and dynamic coefficients are typically on the order of 0.20 (*www.physlink.com; www.engineersedge.com*). The use of a middle ground value acknowledges that the initial force required to start movement may be equally or more important as the force maintained during dynamic cycles. The assumed friction slip force is provided for each of the loading combinations (i.e., building materials and number of stories) in Table 3.24.

Figure 3.88 illustrates the effect of the assumed combination of toe-nail connections and friction determined by the dead load of a given building variant. The left portion of Figure 3.88 shows the response for a one-story wood siding and gypsum wallboard (i.e., lightest) stem wall building variant, with a friction force of 616 lbs for an 8-ft section of stem wall. The right portion of Figure 3.88 shows the response for a two-story stucco with lath and plaster interior (i.e., heaviest) stem wall building variant, with a friction force of 2148 lbs for a 9-ft section of stem wall. The influence of the different levels of friction force on the hysteretic response are shown by combining the hysteretic response of Scenario 1 tested by Ryan et al. [2003] with the assumed friction (shown by the red curves) with the toe-nails (shown by the grey curves) to give the total hysteretic response (shown by green curves) in Figure 3.88.

Table 3.24 **Perimeter dead loads and friction slip forces assumed for existing (unretrofitted) stem wall variant models.**

Number of stories [1,2]	Exterior material	Interior material	w_{DL} (plf) [3]	*Fs* (plf) [4]
1	Stucco	Lath and plaster	435	152
		Gypsum wallboard	310	109
	Horizontal wood siding	Lath and plaster	345	121
		Gypsum wallboard	220	77
2	Stucco	Lath and plaster	767	268
		Gypsum wallboard	532	186
	Horizontal wood siding	Lath and plaster	587	205
		Gypsum wallboard	352	123

[1] Number of occupied stories above crawlspace.
[2] All existing (unretrofitted) stem wall models assume a light roof (asphalt/composition shingle).
[3] Assumed perimeter dead load acting on the sill plate.
[4] Friction slip force based on dead load and coefficient of friction of 0.35 (values rounded to the nearest pound per linear foot).

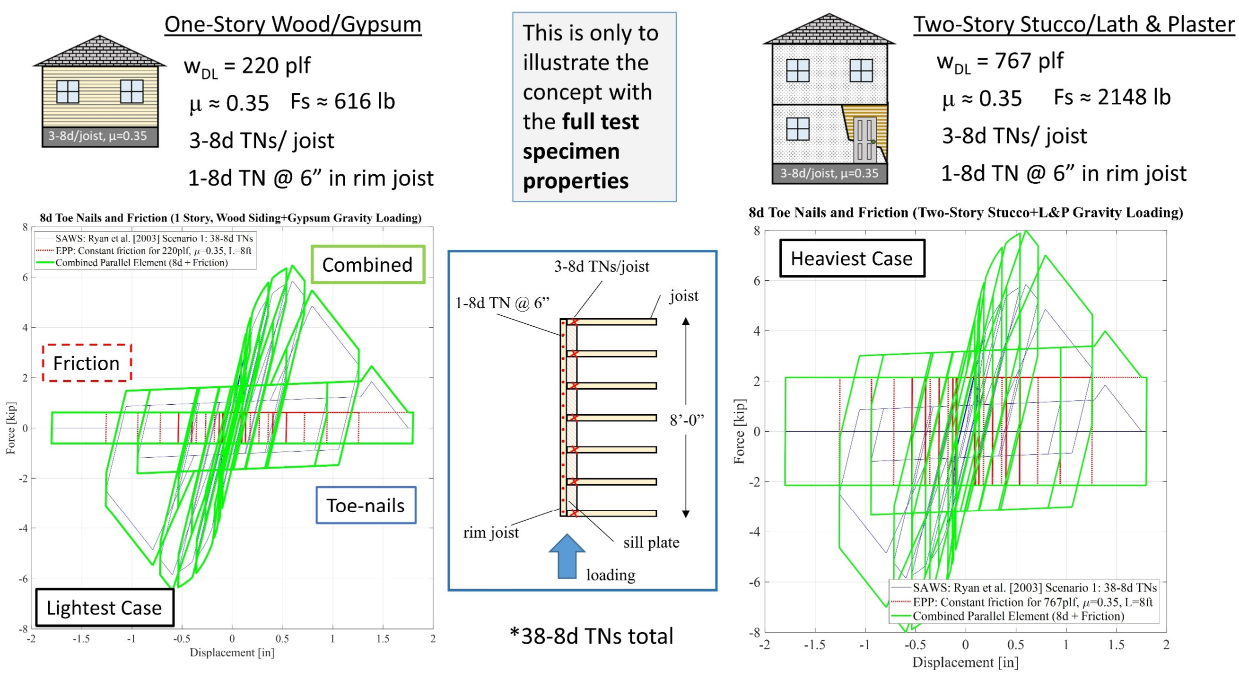

Figure 3.88 **Illustration of the effect of assumed dead load on the contribution of assumed friction properties: (left) lightest case, (right) heaviest case. Note: toe-nail properties reflect Scenario 1 tested by Ryan et al. [2003] and friction values assume an 8-ft perimeter section.**

3.8 SUMMARY OF BEST ESTIMATE MATERIAL PROPERTIES FOR STRUCTURAL ANALYSIS

This section summarizes the best estimate material properties used for structural analysis in *OpenSees*. The first set of material properties reflects the best estimate properties used for the baseline archetype models that are used for direct comparison with catastrophe modeler groups; see Reis [2020(b)]. The discussion of final performance assessment results includes additional material properties that are included in the sensitivity studies. These properties are defined previously within this chapter and referenced in the corresponding sections of Chapter 7. Existing (unretrofitted) stem wall properties are distinct from wall properties and are defined in Section 3.7. All wall properties use the *Pinching4* material model in *OpenSees* with parameter definitions and assumptions described in Section 3.3 (Figure 3.6 and Table 3.4).

A summary of best estimate exterior and interior superstructure materials is provided in Table 3.25. Material properties for 2-ft-tall cripple walls are summarized in Table 3.26. Similarly, material properties used to define 6-ft-tall cripple walls are summarized in Table 3.27.

Table 3.25 Summary of best estimate material properties for the baseline archetype set and T1-11 exterior: exterior and interior superstructure materials.

Material [1]	Wood siding [2]	Stucco + GWB	Wood siding + L&P	Stucco + L&P	T1-11 siding + GWB	Gypsum (GWB)	Lath and plaster (L&P)
Type	Exterior					Interior [3]	
Index	W2	S2	C1	SLP2	T1	G2	LP2
ed_1 [%]	0.24	0.08	0.08	0.08	0.10	0.12	0.08
ed_2 [%]	1.16	0.72	0.30	0.36	1.03	0.36	0.28
ed_3 [%]	4.00	1.50	1.10	1.20	2.75	0.80	1.20
ed_4 [%]	15.0	5.40	2.20	3.70	6.10	5.65	2.90
ef_1 [plf]	41	257	152	357	205	105	115
ef_2 [plf]	105	731	404	829	721	185	286
ef_3 [plf]	190	800	525	1050	852	210	445
ef_4 [plf]	121	240	200	315	256	63	128
rDisp1	0.18	0.06	0.06	0.06	0.30	0.15	0.06
rForce1	0.35	0.26	0.31	0.26	0.25	0.22	0.31
uForce1	-0.08	-0.20	-0.10	-0.20	-0.01	-0.21	-0.10
gD11	0.14	0.13	0.14	0.13	0.22	0.10	0.14
gDLim1	0.50	2.00	0.30	2.00	2.00	2.00	0.30
gK11	-0.10	0.00	-0.07	0.00	0.00	-0.30	-0.07
gKLim1	-1.00	0.00	-0.50	0.00	0.00	-1.00	-0.50
rDisp2	0.50	0.06	0.28	0.06	0.50	0.40	0.28
rForce2	0.12	0.17	0.18	0.17	0.50	0.12	0.18
uForce2	0.05	-0.23	-0.11	-0.23	0.02	-0.19	-0.11
gD12	0.09	0.13	0.11	0.13	0.11	0.12	0.11
gDLim2	0.20	2.00	0.30	2.00	3.00	2.00	0.30
gK12	0.00	0.30	-0.05	0.30	0.00	0.20	-0.05
gKLim2	0.00	2.00	-0.20	2.00	0.00	2.00	-0.20

[1] *Pinching4* backbone properties (ed_i, ef_i) are normalized to percent drift and pounds per linear foot. All wall materials presented use two *pinching4* springs in parallel with backbone weighting for spring one of 0.8, 0.75, 0.3, and 0.1 for the four points of the backbone, respectively.
[2] This material assumes full superposition with gypsum wallboard (G2). Models with wood siding exterior and gypsum interior have a “double exterior” modeling scheme.
[3] Interior materials are presented based on a single-sided material.

Table 3.26 Summary of best estimate material properties for the baseline archetype set and T1-11 exterior: existing (unretrofitted) and retrofitted 2-ft-tall cripple walls.

Material [1]	Horizontal wood siding		Stucco		T1-11 Siding	
Type	Existing	Retrofit	Existing	Retrofit	Existing	Retrofit
Index	CW-HS2	CW2-HS-R2	CW2-S2	CW2-S-R2	CW2-T1	CW2-T1-R1
ed_1 [%]	0.10	0.10	0.10	0.10	0.17	0.10
ed_2 [%]	0.75	2.06	0.77	1.40	1.03	1.23
ed_3 [%]	2.00	6.50	1.60	5.50	4.75	5.00
ed_4 [%]	5.00	12.10	6.70	12.50	7.28	12.07
ef_1 [plf]	62	354	223	349	200	234
ef_2 [plf]	210	1553	498	1680	467	943
ef_3 [plf]	354	1886	539	1934	573	1148
ef_4 [plf]	100	453	189	580	177	139
rDisp1	0.18	0.03	0.05	0.05	0.06	0.06
rForce1	0.37	0.40	0.20	0.37	0.30	0.30
uForce1	-0.10	0.02	-0.10	-0.05	0.01	0.01
gD11	0.14	0.14	0.30	0.15	0.20	0.20
gDLim1	0.30	0.30	3.00	2.00	0.30	0.30
gK11	-0.10	0.00	0.00	0.00	0.00	0.00
gKLim1	-1.00	0.00	0.00	0.00	0.00	0.00
rDisp2	0.40	0.55	0.25	0.55	0.52	0.52
rForce2	0.34	0.14	0.16	0.13	0.18	0.18
uForce2	-0.12	-0.09	-0.10	-0.07	-0.15	-0.15
gD12	0.09	0.05	0.20	0.10	0.10	0.10
gDLim2	0.20	1.00	2.00	0.50	1.00	1.00
gK12	0.00	0.00	0.00	0.00	0.00	0.00
gKLim2	0.00	0.00	0.00	0.00	0.00	0.00

[1] *Pinching4* backbone properties (ed_i, ef_i) are normalized to percent drift and pounds per linear foot. All wall materials presented use two *pinching4* springs in parallel with backbone weighting for spring one of 0.8, 0.75, 0.3, and 0.1 for the four points of the backbone, respectively.

Table 3.27 Summary of best estimate material properties for existing (unretrofitted) and retrofitted 6-ft-tall cripple walls.

Material [1]	Horizontal wood siding		Stucco		T1-11 Siding	
Type	Existing	Retrofit	Existing	Retrofit	Existing	Retrofit
Index	CW-HS2	CW6-HS-R2	CW6-S2	CW6-S-R2	CW6-T1	CW6-T1-R1
ed_1 [%]	0.10	0.17	0.08	0.08	0.10	0.25
ed_2 [%]	0.75	1.16	0.32	0.65	0.75	1.25
ed_3 [%]	2.00	3.50	1.00	2.90	2.67	2.90
ed_4 [%]	5.00	8.40	3.17	9.00	8.59	7.50
ef_1 [plf]	62	462	252	385	124	299
ef_2 [plf]	210	1342	492	1517	345	750
ef_3 [plf]	354	1821	656	1870	377	844
ef_4 [plf]	100	396	284	561	73	62
rDisp1	0.18	0.06	0.04	0.09	0.10	0.12
rForce1	0.37	0.38	0.31	0.31	0.31	0.29
uForce1	-0.10	0.02	-0.05	-0.05	-0.15	0.01
gD11	0.14	0.20	0.30	0.21	0.25	0.25
gDLim1	0.30	0.30	3.00	2.00	1.00	1.00
gK11	-0.10	-0.10	-0.12	-0.10	0.00	-0.05
gKLim1	-1.00	-1.00	-0.75	-0.30	0.00	-0.80
rDisp2	0.40	0.55	0.25	0.49	0.54	0.54
rForce2	0.34	0.20	0.16	0.16	0.29	0.29
uForce2	-0.12	-0.15	-0.25	-0.15	-0.10	-0.15
gD12	0.09	0.10	0.20	0.10	0.10	0.10
gDLim2	0.20	1.00	2.00	1.00	1.00	1.00
gK12	0.00	-0.10	-0.09	0.00	0.00	-0.10
gKLim2	0.00	-0.50	-0.30	0.00	0.00	-0.60

[1] *Pinching4* backbone properties (ed_i, ef_i) are normalized to percent drift and pounds per linear foot. All wall materials presented use two *pinching4* springs in parallel with backbone weighting for spring one of 0.8, 0.75, 0.3, and 0.1 for the four points of the backbone, respectively.

4 Selection of Building Sites and Treatment of Ground-Motion Hazard

4.1 BASELINE BUILDING SITES

The PEER–CEA Wood-frame Project developed a large set of ground-motion hazard information for ten building sites in Northern and Southern California [Mazzoni et al. 2020]. The information included acceleration response spectra at varying intensities, based on probabilistic seismic hazard analyses, and sets of recorded ground motion that are selected and scaled to match the target spectra. A subset of four of these ten sites is selected for building variant analysis.

The four baseline building sites are chosen in the following locations to represent a range of seismicity with large inventories of residential housing: Bakersfield, San Francisco, Northridge, and San Bernardino. All sites assume an upper 30-m shear-wave velocity (V_{S30}) of 270 m/sec, corresponding to a stiff soil site. The selection of baseline sites targeted a range of seismicity levels, with Bakersfield being the lowest and San Bernardino being the highest. Further, the four sites were selected considering the seismicity categories defined within *FEMA P-1100* prescriptive retrofit design plan sets [2018]; see Section 1.2.1. Table 4.1 provides information for each of the baseline sites including the latitude and longitude coordinates and the nominal short-period design spectral acceleration (S_{DS}) for the site. Additionally, the last column provides the short-period design spectral acceleration that is applicable when using the *FEMA P-1100* plan sets. Plan sets are only available for S_{DS} values of 1.0*g* (Seismic), 1.2*g* (High Seismic), and 1.5*g* (Very High Seismic). Lower seismicity sites default to the lowest value (1.0*g*), while other site seismicities must round up to the next applicable S_{DS} values, where the 1.5*g* value is permitted for use at the highest seismicity sites, even when the nominal S_{DS} for the site exceeds 1.5*g*. Bakersfield was selected for the lower seismicity site since it had the closest S_{DS} hazard (0.74*g*) to the minimum S_{DS} design value of 1.0*g*. San Francisco was selected as the high seismicity site since its nominal S_{DS} hazard of 1.2*g* is equivalent to that of and plan set S_{DS}. The very high seismicity sites of Northridge and San Bernardino were selected since their nominal S_{DS} hazards (1.40*g* and 1.78*g*) bracket the S_{DS} of the highest plan set value of 1.5*g*.

Table 4.1 **Basic information for the four baseline site locations selected for structural analysis of building variants.**

Location	Site index	Lat., Long. [°]	V_{S30} (m/sec)	S_{DS} (g) [1]	*FEMA P-1100* plan set S_{DS} (g)
Bakersfield	BF270	35.3736802, -119.02049	270	0.741	1.0
San Francisco	SF270	37.7792597, -122.41926	270	1.200	1.2
Northridge	NR270	34.2280556, -118.53583	270	1.398	1.5
San Bernardino	SB270	34.1045714, -117.29276	270	1.778	1.5

[1] Design short-period accelerations obtained from https:/earthquake.usgs/designmaps/beta/us for default soil D

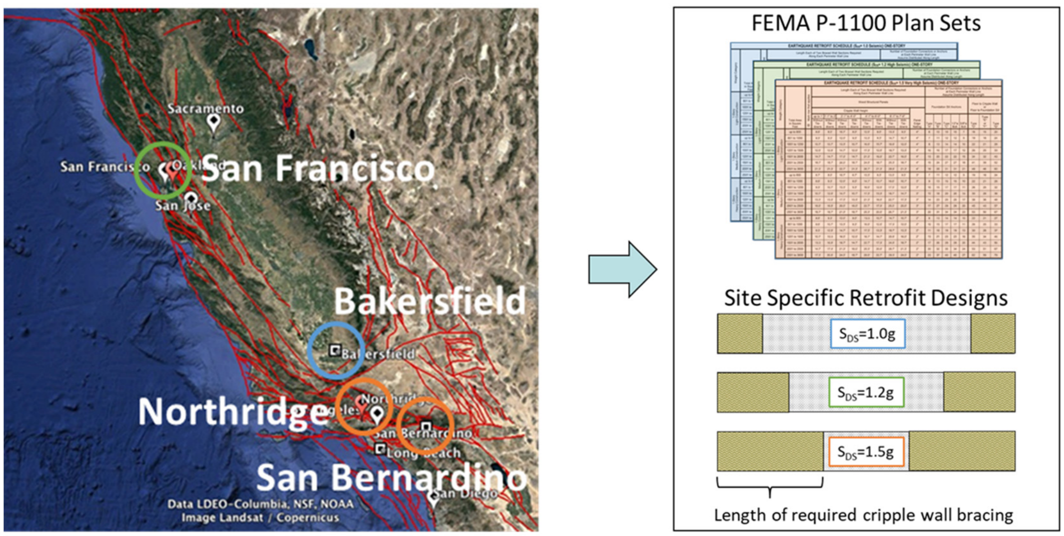

Figure 4.1 **Illustration of the relationship between selected sites and controlling seismicity level according to *FEMA P-1100* plan sets.**

Further information on the relationship of the site seismicity to detailing of the *FEMA P-1100* prescriptive retrofit is shown in Figure 4.1. Among other details, the required length of cripple wall bracing is shown to vary depending on the site seismicity with all other building conditions (e.g., plan area, number of stories, weight class, etc.) kept constant.

Each site had PSHA conducted for ten different return periods ranging from 15 years to 2500 years [Mazzoni et al. 2020]. Figure 4.2 presents the hazard curves for each of the sites for spectral acceleration at a period of 0.25 sec, *Sa*(0.25 sec). The spectral values corresponding to each of the ten return periods are provided in Table 4.2. By comparing the 500-year return period spectral values (Sa_{RP} = 500) a large range of seismicity is covered, ranging from approximately 0.6g for Bakersfield to 1.3g for San Bernardino. Complete information about site hazard can be found in the WG3 ground-motion report [Mazzoni et al. 2020].

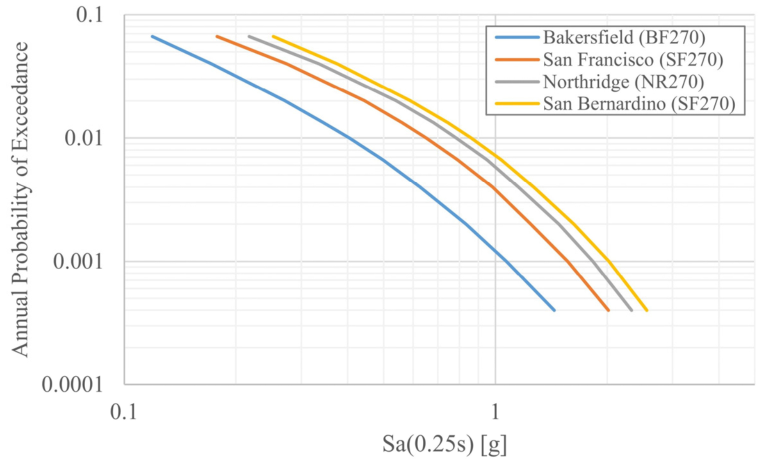

Figure 4.2 Comparison of hazard curves for the four baseline sites.

Table 4.2 Site definition and IMs for the four baseline sites.

Site	Bakersfield	San Francisco	Northridge	San Bernardino
V_{S30} (m/sec)	270	270	270	270
Abbreviation	BF270	SF270	NR270	SB270
$Sa_{RP=15}$ [g][1]	0.119	0.178	0.217	0.252
$Sa_{RP=25}$ [g]	0.172	0.274	0.335	0.375
$Sa_{RP=50}$ [g]	0.271	0.444	0.540	0.590
$Sa_{RP=75}$ [g]	0.344	0.560	0.681	0.744
$Sa_{RP=100}$ [g]	0.405	0.652	0.785	0.861
$Sa_{RP=150}$ [g]	0.497	0.790	0.948	1.036
$Sa_{RP=250}$ [g]	0.626	0.982	1.152	1.265
$Sa_{RP=500}$ [g]	0.834	1.246	1.484	1.627
$Sa_{RP=1000}$ [g]	1.071	1.564	1.829	2.021
$Sa_{RP=2500}$ [g]	1.440	2.014	2.328	2.559

[1] Mean 5% damped spectral acceleration at a period of 0.25 sec for the site and return period of RP = x years.

4.2 BASIS FOR GROUND-MOTION SELECTION AND TARGET ACCELERATION SPECTRA

Following sensitivity studies of structural analysis models to investigate the influence of spectral shape and conditioning period, the PEER–CEA Project Team agreed that using a conditional spectra hazard target with a short conditioning period (0.25 sec) would best represent the seismic hazard for the structural and loss analyses. This included comparison of results based on uniform versus conditional seismic hazard and with different conditioning periods. The short-period conditioning period is consistent with the IM used in the numerical studies behind the *FEMA P-*

1100 retrofit prestandard [2018], as well as the typical short-period spectral acceleration used by catastrophe loss modelers for residential wood-frame structures.

The ground-motion selection procedure uses Conditional Spectra (CS) with a target conditioning period of 0.25 sec. The CS, which consists of a target mean (Conditional Mean Spectrum; CMS) and variance (CS) of IM with respect to the conditioning period (T^* = 0.25), was determined to represent the state-of-the-art in characterizing seismic hazard for structural analysis and the *FEMA P-58* [2012] probabilistic loss assessment. The CS was chosen for the hazard target over the Uniform Hazard Spectra (UHS) since it is widely acknowledged to give a more realistic assessment of the seismic hazard, especially for high-intensity ground motions.

Working Group 3 prepared CS for ground-motion selection targets at each individual site and return period considered [Mazzoni et al. 2020]. At each return period, the ground-motion record set includes 45 ground motion pairs (e.g., two horizontal components). The record selection process is conducted using the RotD50 spectral acceleration [Boore 2010] of the two horizontal components and a conditioning period of 0.25 sec (i.e., T^* = 0.25 sec). Ground-motion selection is performed using a modified version of the selection tool developed by Baker and Lee [2018], which combines previous research on the development of CS and ground-motion selection procedures [Baker and Cornell 2006; Baker and Jayaram 2008; Jayaram and Baker 2008; and Jayaram et al. 2011]. Complete details of the record selection process and ground-motion sets can be found in the WG3 ground-motion report [Mazzoni et al. 2020]. All ground motions used for structural analysis of building variants are provided within the WG5 electronic documentation [PEER 2020].

The remainder of this chapter illustrates some of the considerations and discussion used to arrive at the final record selection and hazard targets adopted for structural analysis in collaboration with WG3.

4.3 CONDITIONAL SPECTRA

By definition, the UHS represents the central tendency target for ground-motion selection such that each structural period has the spectral acceleration corresponding to the same exceedance rate as the target exceedance rate for the entire spectrum. This assumes that even very rare (i.e., low exceedance probability) events produce the same level of spectral demands across the entire range of periods. As pointed out by Baker and Cornell [2006], this assumption does not reflect the reality of individual (particularly the higher intensity and less frequent) earthquake events. While UHS is a reasonable and conservative basis for design verification and code spectrum development, it results in a conservative bias that is problematic for damage and loss analysis [FEMA 2012].

Conversely, CMS represent the mean target of a given set of causal parameters (e.g., earthquake M, R, and ε) conditioned on a given period of vibration, T^*. The target spectral ordinate at T^* is identical to the UHS value, while spectral ordinates at periods away from T^* reflect the correlation between the epsilon values at these periods and the conditioning period for the same controlling magnitude and distance event [Baker 2011]. Mean response spectra of UHS- and CMS-based (T^* = 0.25 sec) ground-motions sets are compared with corresponding targets for the baseline San Francisco site (SF270) in Figure 4.3. Comparing the respective UHS [Figure 4.3(a)] and CMS [Figure 4.3(b)] for ten different return periods illustrates the significant differences, particularly at higher intensities (longer return periods). This example illustrates how the CMS spectra are lower than the UHS at periods away from the conditioning period (T*). This deviation increases with intensity and is more significant for periods larger than T*, illustrating a weaker correlation of epsilon at longer periods than shorter periods with respect to T*.

Differences in the concepts behind UHS and CS carry over to ground-motion record selection and the record-to-record variability in ground-motion sets. In the same way that the UHS is created, ground-motion selection for the UHS target aims to minimize the error of all ground motions with respect to the target UHS across all periods [Jayaram et al. 2011]. On the other hand, selection for the CMS target can follow one of two approaches. One approach is to select records that fit the entire period range of interest similar to the UHS fitting (i.e., minimizing the error to the CMS). The second, which is more consistent with the CMS concept, is to target the variances at periods away from T* to reflect the correlation in periods. This is done by creating and targeting the records to the CS, which incorporates information about both the mean and variance. The first option is most appropriate for obtaining reliable mean structural responses [Baker 2011] for design verification, whereas the latter is proposed for the PEER–CEA project to provide a more consistent measure of both central tendency and dispersion of structural response. An illustration of the difference in the ground-motion variability between the UHS and CMS-CS record sets is shown for the San Francisco site at the 2500-year return period in Figure 4.4. The influence of the differences between the two ground-motion selection targets on structural response are discussed in the following sub-sections.

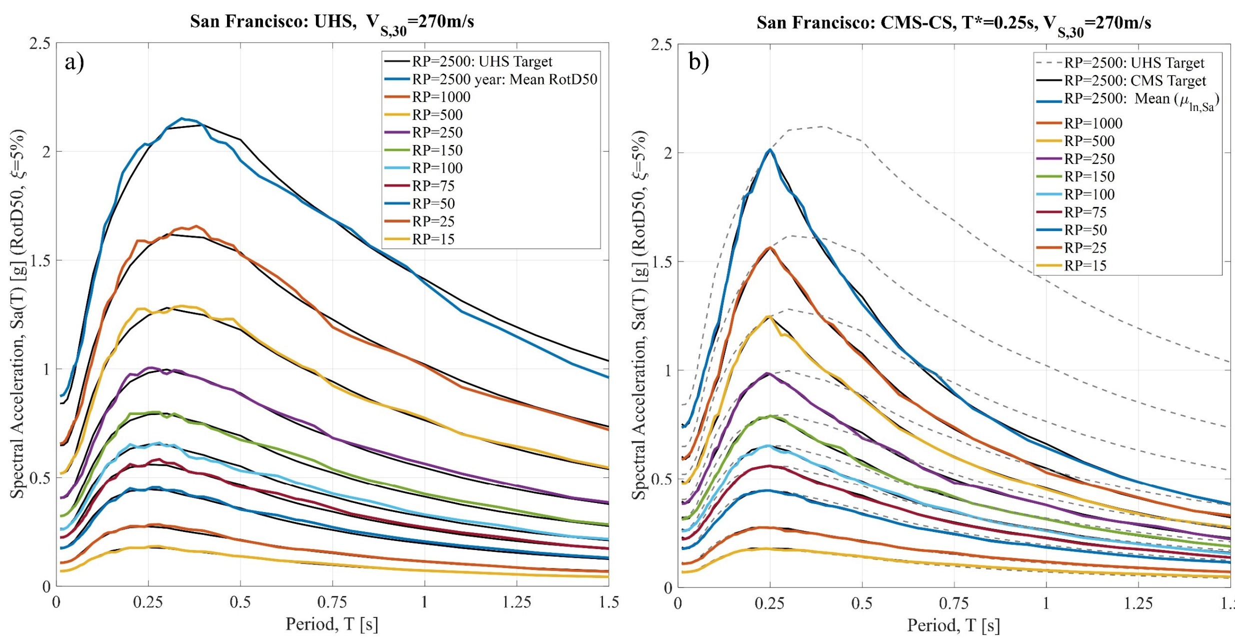

Figure 4.3 **Mean response spectra for the San Francisco V_{S30} = 270 m/sec site at ten different return periods: (a) Uniform Hazard Spectra (UHS); and (b) Conditional Mean Spectra (CMS) conditioned on a period of T* = 0.25 sec (adapted from Mazzoni et al. [2020]).**

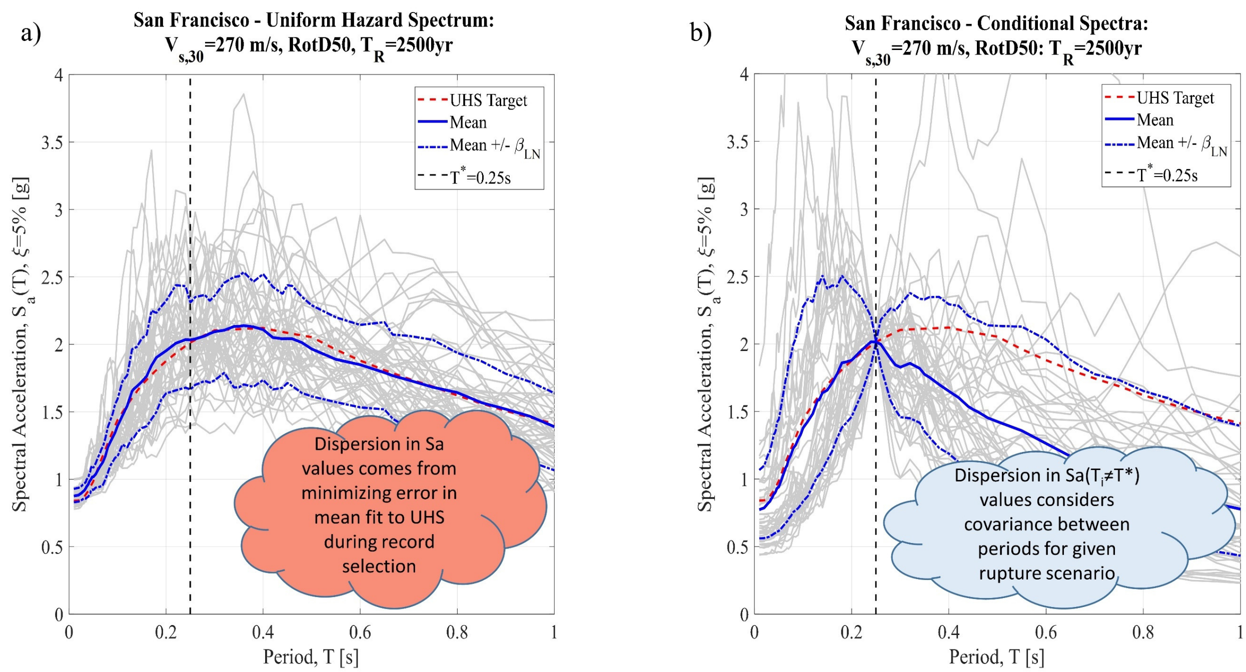

Figure 4.4 **Comparing the record-to-record variability and mean spectral shape for the San Francisco site at the 2500-year return period: (a) Uniform Hazard Spectrum; and (b) Conditional Spectrum. (adapted from Mazzoni et al. [2020])**

4.3.1 Importance of Spectral Shape

The influence of spectral shape on the seismic performance of structures estimated from dynamic analysis has been well documented in previous studies for a variety of structures; see Baker and Cornell [2005]; FEMA [2009]; Haselton et al. [2011]; and Chandramohan et al. [2013]. To illustrate the influence of spectral shape on cripple wall houses, two preliminary archetypes are considered. These archetypes represent one-story dwellings on 2-ft-tall cripple walls with exterior stucco and the interior gypsum wallboard. One archetype represents the existing (unretrofitted) cripple wall condition and the second represents the retrofitted condition. The retrofit design is controlled by the one-story S_{DS} = 1.2g plan set within *FEMA P-1100* [2018] for "Light" weight classification. Details of structural modeling are omitted for the current discussion, yet the modeling and analysis procedures are generally consistent with those defined elsewhere in this report and carried through the analyses as reported later in Chapter 7. The two archetypes are assessed for collapse performance using three different ground-motion sets:

1. SF270-UHS – Ground motions selected to fit the uniform hazard spectra corresponding to the San Francisco site with no additional ground motion variability (see Mazzoni et al. [2020] for details).
2. SF270-CS – Ground motions selected to fit the target mean and variance defined by the conditional spectra for the San Francisco site (see Mazzoni et al. [2020] for details).
3. P695FF – Ground motions from the *FEMA P-695* far-field set [2009].

The *FEMA P-695* far-field record set is included to illustrate a widely accepted method to assess collapse, including the effect of ground-motion spectral shape. Further, the protocol outlined by *FEMA P-695* was used as the basis for developing the *FEMA P-1100* prestandard that determines the retrofit detailing on which the entire PEER–CEA project is based. Figure 4.5 provides a comparison of the SF270-UHS record set at the 2500-year return period and the P695FF set scaled to match the same median *Sa*(0.25 sec) value. The figure shows that the two ground-motion sets have similar median spectral shapes in the short-period range, but significantly different record-to-record dispersion, illustrated as lognormal standard deviation bounds (dashed lines). Note that the period of 0.25 sec is the minimum allowed by *FEMA P-695* for collapse assessment procedures. The record-to-record dispersion is quantified for both site-specific ground-motion sets and the P695FF set in Figure 4.6, where the site-specific sets show four different return periods. The figure shows much lower dispersion values for the SF270-UHS set compared with the P695FF set. By definition, the variability in the SF270-CS set is zero at the conditioning period (T^* = 0.25 sec) and has increasing dispersion at periods away from the conditioning period. Finally, as shown by the superposition of return periods in Figure 4.6, the ground-motion dispersion of the two site-specific ground-motion sets (SF270-UHS and SF270-CS) are fairly constant at the various the return periods.

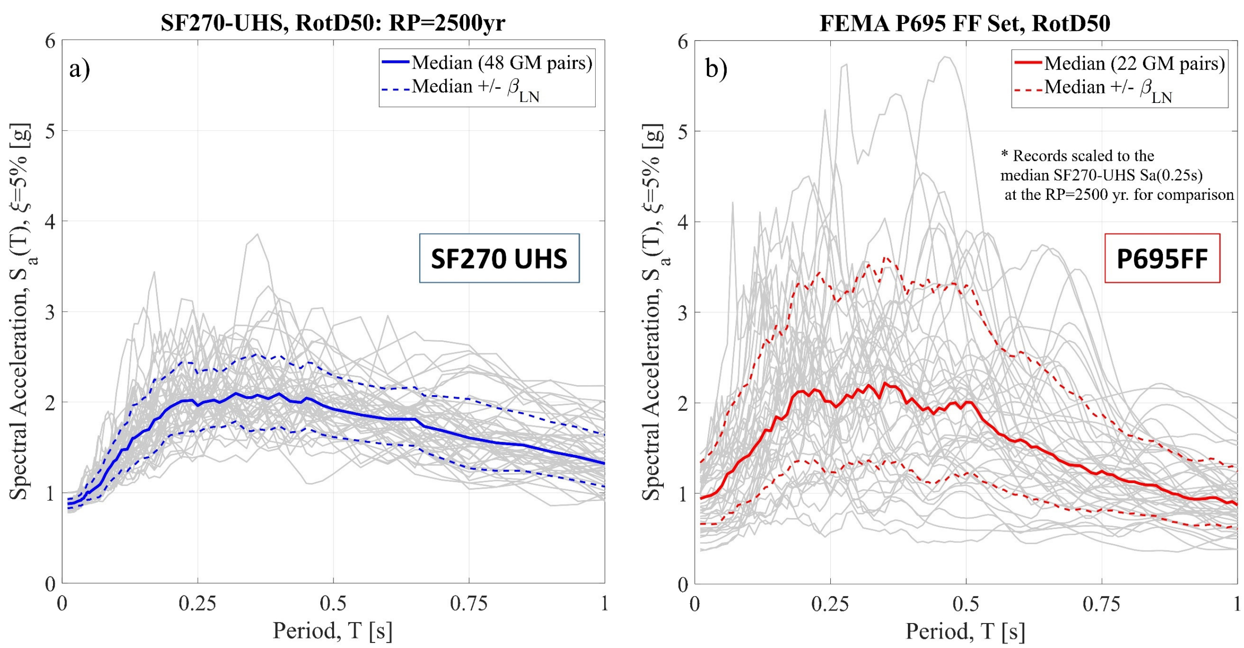

Figure 4.5 **Comparison of the (a) SF270 uniform hazard spectrum ground-motion set at the 2500-year return period with the (b) *FEMA P-695* far-field set scaled to the equivalent median *Sa*(0.25 sec). The figure illustrates very similar median spectral shapes in the short-period range.**

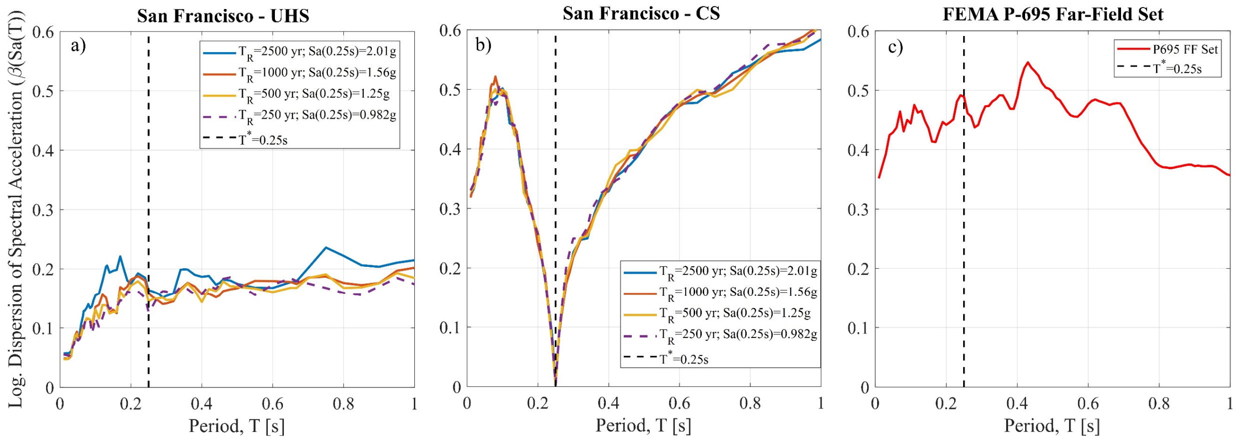

Figure 4.6 **Comparing record-to-record dispersion of different ground-motion sets: (a) San Francisco-UHS targeting minimum error fitting to the target mean; (b) San Francisco-CS including dispersion relative to conditioning period; and (c) *FEMA P-695* far-field set.**

The collapse performance for each archetype and record set is estimated by constructing a collapse fragility relating probability of collapse to a given IM, taken here as the mean spectral acceleration at a period of 0.25 sec. Unadjusted collapse fragilities are estimated as cumulative lognormal distributions using the maximum likelihood approach [Baker 2015] to calculate the median collapse intensity and record-to-record dispersion (i.e., lognormal standard deviation). For the site-specific ground-motion sets (SF270-UHS and SF270-CS), the final collapse fragility is determined by adding modeling uncertainty (β_{Mod} = 0.35) to the record-to-record dispersion (with a lower bound record-to-record variability of 0.2) using the SRSS approach discussed in Section 2.5.1 and illustrated in Figure 4.7. The collapse fragilities from the site-specific ground-motion sets do not include adjustment of median collapse intensity, since the spectral targets are intended to incorporate spectral shape effects.

The collapse fragilities calculated using the P695FF record set follow the procedures described in *FEMA P-695* [2009] to (1) adjust the median collapse intensity to adjust for spectral shape and two- versus three-dimensional modeling; and (2) assign a dispersion that accounts for record-to-record and modeling uncertainty. The two main steps are illustrated in Figure 4.8. Figure 4.8(a) illustrates that according to *FEMA P-695* a median collapse intensity adjustment is performed, including adjustment for spectral shape and three-dimensional loading effects. The adjustment for spectral shape uses a spectral shape factor (SSF) that uses ductility-based relationships from pushover analysis of structures in combination with regression relationships developed specifically for the P695FF set. An illustration of calculating the SSF for the two example variants is shown in Figure 4.9, where explicit details are omitted, and background can be found in *FEMA P-695* [2009]. The important concept is that the existing (unretrofitted) archetype has lower ductility and SSF of 1.15 (i.e., the median collapse intensity is increased by 15% to account for spectral shape). Conversely, the retrofit example archetype is more ductile and has a calculated SSF of 1.24. In addition to SSF, *FEMA P-695* suggests that a three-dimensional (3D) loading factor (F_{3D}) of 1.2 be applied when looking at structures in 3D, with the 22 ground-motion pairs analyzed in two different orientations, as was done for the current example. This results in the median collapse intensity being scaled by 1.38 and 1.49 for the existing (unretrofitted) and retrofit example archetypes, respectively. The final step is to apply the estimated collapse dispersion accounting for record-to-record variability and modeling uncertainty. For the current example, the default value of 0.6 used in *FEMA P-1100* numerical studies [2019(b)] was adopted for this comparison. Figure 4.8(b) illustrates applying the assumed collapse dispersion to the adjusted median capacity according to *FEMA P-695*.

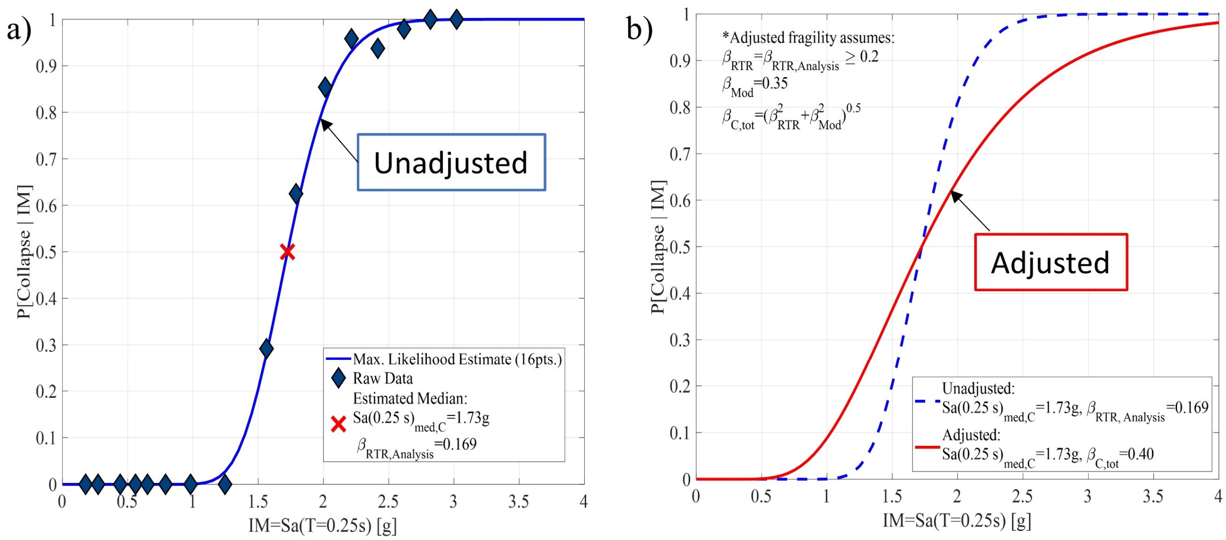

Figure 4.7 **Illustration of collapse fragility development for site-specific (San Francisco) ground-motion sets: (a) maximum likelihood estimate of median and record-to-record dispersion; and (b) adjusted collapse fragility to include modeling uncertainty.**

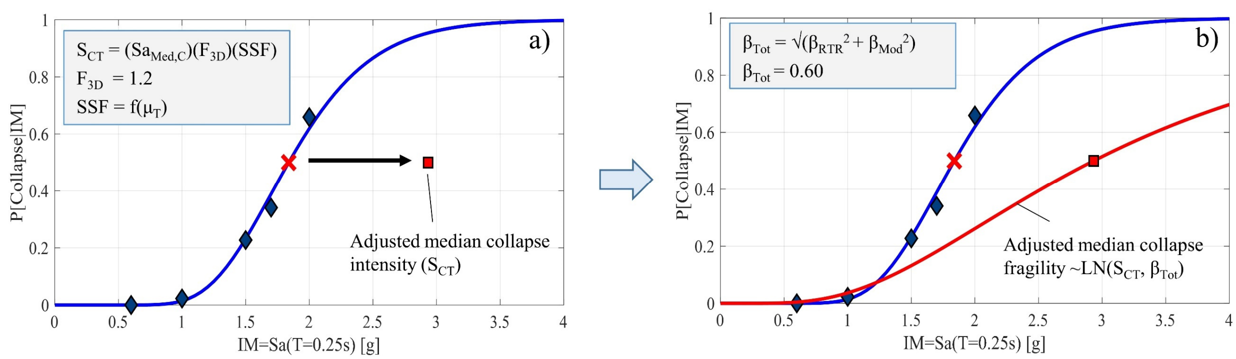

Figure 4.8 **Illustration of collapse fragility adjustments when using the *FEMA P-695* approach (P695FF record set): (a) adjustment of median collapse intensity for three-dimensional analysis and spectral shape; and (b) increased total collapse fragility dispersion to include additional modeling uncertainty.**

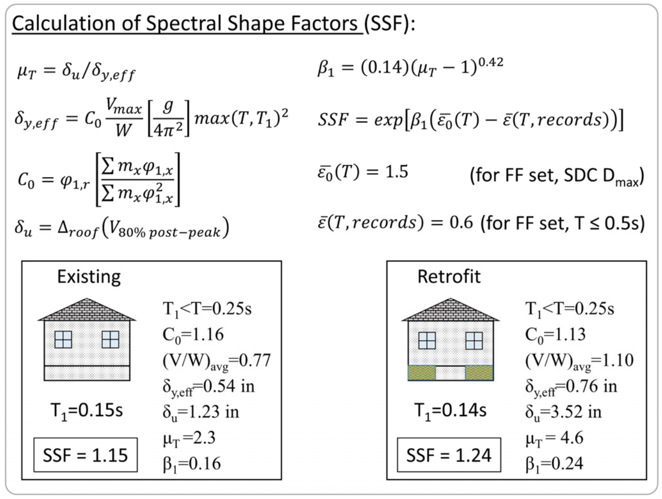

Figure 4.9 Summary of spectral shape factor calculations for two one-story archetype buildings for implementing the *FEMA P-695* [2009] collapse assessment procedure using the far-field ground-motion set.

The resulting collapse fragility curves for the two example variants are shown in Figure 4.10, where unadjusted fragilities (record-to-record variability only) are shown in light blue and the adjusted collapse fragilities (see Figure 4.7 and Figure 4.8 for assumptions) are shown in dark red. The corresponding parameters to define each collapse fragility and probabilities of collapse at the 2500-year return period are provided in Table 4.3.

The annotation in Figure 4.10 compares the adjusted probabilities of collapse at the 2500-year return period for the San Francisco site. A key observation is that the calculated probabilities are similar for the SF270-CS and P695FF record sets, in contrast to much higher values for the SF270-UHS set. The agreement between SF270-CS and P695FF approaches confirms that while they handle spectral shape effects using distinctly different methods, the end results are about the same. In contrast, without consideration of peaked spectral shape at high intensities, the SF270-UHS approach is overly conservative. By comparing the unadjusted median collapse intensities of the three methods in Table 4.3, one can see that the similarity in spectral shape between the SF270-UHS and P695FF sets is reflected in the similar unadjusted median collapse intensities for the two methods. When the spectral shape adjustment is made to the P695FF results, the adjusted median is close to that of the SF270-CS set. In concept, one could apply a spectral shape adjustment to the UHS results, in a similar manner to the P-695 approach, however, determination of the spectral shape factor would require additional assumptions and calculations. In contrast, the spectral shape is incorporated directly in the CS approach.

The influence of record-to-record variability on collapse fragility development is illustrated by comparing the dispersions of the three unadjusted record sets (SF270-UHS, SF270-CS, and P695FF) in Table 4.3. The associated fragility curves are shown by the solid, dashed, and dotted blue line collapse fragilities in Figure 4.10. The SF270-UHS results have very low record-to-record dispersion values on the order of 0.1, the SF270-CS results have intermediate values on the order of 0.2 to 0.3, and the P695FF results have the largest values on the order of 0.4. This comparison reveals that the record-to-record dispersion is not a unique value, but instead reflects the variability in the original record sets. In this regard, the record-to-record dispersion in the CS approach is more defensible since the dispersion in the CS target spectra (Figure 4.6) is based on statistics of spectral variability and correlation from the same ground-motion datasets used to develop the latest ground-motion prediction equations.

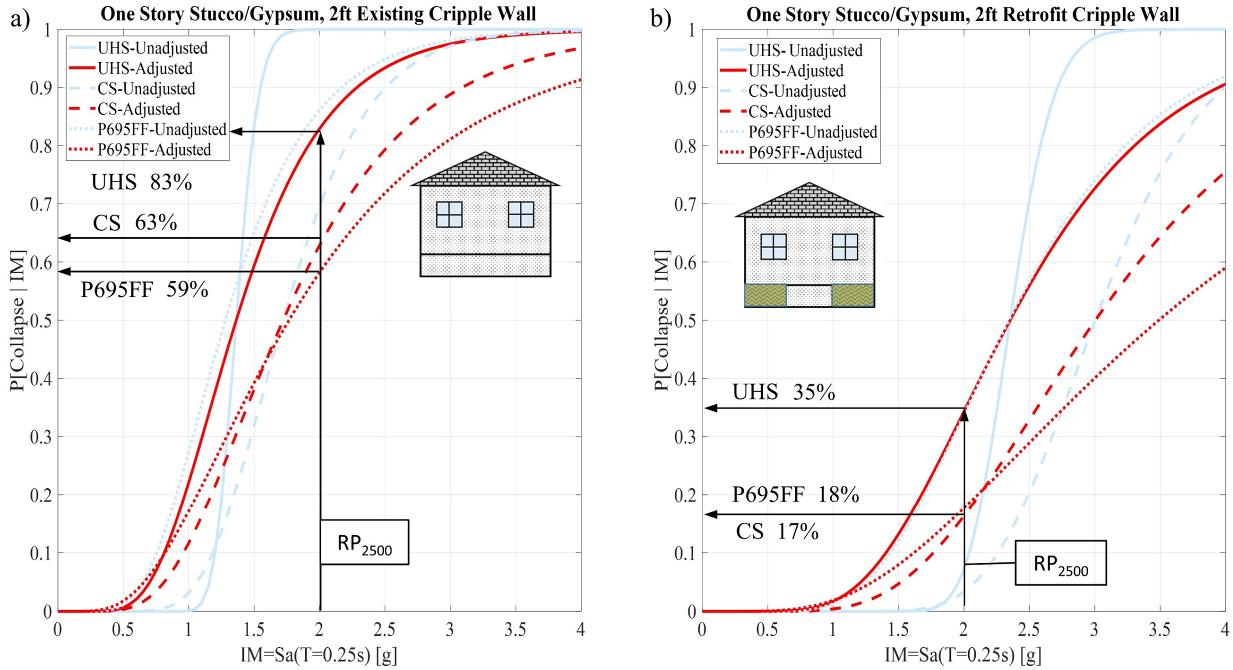

Figure 4.10 **Comparing collapse fragilities for UHS, CMS-CS, and *FEMA P-695* ground-motion sets including adjustments for modeling uncertainty (all cases) and spectral shape (*FEMA P-695* only): (a) existing (unretrofitted) cripple wall dwelling; and (b) retrofitted cripple wall dwelling. Annotated values are the probabilities of collapse at the 2500-year return period for the San Francisco site (results shown are preliminary).**

Table 4.3 **Collapse fragility summary for example existing (unretrofitted) and retrofitted archetypes analyzed with different ground-motion sets and collapse fragility adjustments (preliminary results shown).**

Archetype	Ground-motion set	Record-to-record variability only[3]			Adjusted collapse fragilities[4]		
		$Sa_{Med,C}$ (g)	β_{RTR}	P[C|Sa_{2500}]	$Sa_{Med,C}$ (g)	$\beta_{C,Tot}$	P[C|Sa_{2500}]
Existing (Unretrofitted)[1]	SF270-UHS	1.36	0.099	99.9%	1.36	0.40	83%
	SF270-CS	1.72	0.29	71%	1.72	0.46	63%
	P695FF	1.28	0.41	86%	1.77	0.60	59%
Retrofitted[2]	SF270-UHS	2.35	0.11	8%	2.35	0.40	35%
	SF270-CS	3.00	0.22	4%	3.00	0.41	17%
	P695FF	2.35	0.38	35%	3.49	0.60	18%

[1] Curves shown in Figure 4.10(a).
[2] Curves shown in Figure 4.10(b).
[3] Light curves in Figure 4.10.
[4] Dark curves in Figure 4.10.

Early in this Project, the PEER–CEA team initially chose to characterize the seismic hazard and ground motions based on a UHS target. However, after recognizing the large conservatism in this approach, and with the support of external reviewers, the PEER–CEA Team decided to change to a CS target, which is considered to produce a better estimate of the expected performance. The results shown in Figure 4.10 illustrate that the use of CS-targeted ground motions with consideration for modeling uncertainty provides results that are consistent with *FEMA P-695* assessments, but without the need to adjust the median intensity for spectral shape effects. While the two approaches (CS and *FEMA P-695*) give similar collapse intensities, the CS method has the advantage of consistently characterizing the ground-motion response, from the onset of damage up through collapse. Moreover, the CS approach for characterizing record-to-record variability in the ground-motion record set is based on a more systematic approach that is linked to current methods in earthquake hazard calculations.

4.3.2 Influence of Damping versus Spectral Shape

This section reproduces the types of analyses for the SF270-CS and SF270-UHS record sets (similar to the analyses described previously in Section 4.3.1) to examine the sensitivity of the results to the assumed damping ratio. Specifically, results are presented for assumed damping ratios of 0.5% and 2.5% of critical, where the latter value is used as the basis for all other models presented in the report; see Section 2.4.4. Twelve preliminary case study variants are analyzed, where all have gypsum wallboard interiors and 2-ft-tall cripple walls. The variants include one- and two-story houses with either stucco or horizontal wood siding exterior. Crawlspace details include existing (unretrofitted) and retrofitted cripple walls as well as a fixed-base variant (i.e., without crawlspace vulnerability).

The twelve variants are analyzed for both structural performance (e.g., collapse) and loss assessment. Note that the structural and loss assessment models used in this comparison are preliminary and do not necessarily agree with the values used in the final analyses (i.e., as reported in Chapter 7). The values are, however, close enough to final values that the influence of damping in these analyses should be equally indicative of the final analyses.

The probability of collapse (using collapse fragility adjustment criteria described previously in Figure 4.7) at the 2500-year return period are shown in Figure 4.11. The cases with the assumptions used for final variant analysis (e.g., CS ground motions and 2.5% damping) are shown as solid blue bars with a bold border. These are compared to UHS ground motions with 2.5% damping (solid orange bars) and the same two ground-motion sets with 0.5% damping shown with hatched bars. As expected, the smaller damping results in slightly higher collapse probabilities, however the difference in probabilities due to the five-times change in damping (from 2.5% to 0.5%) has a much smaller (almost negligible) affect as compared to differences between the assumed ground-motion sets (CS versus UHS).

Shown in Figure 4.12 are expected annual loss (EAL in figure) values for the 12 variants, calculated using the two record sets with 2.5% and 0.5% damping. Comparing the expected annual loss results in Figure 4.12 to the collapse results in Figure 4.11, the expected annual loss values are less sensitive to the ground-motion set assumed, largely due to expected annual loss being controlled by low- to moderate- (short return period) intensity levels, where the spectral shapes are similar between UHS and CS. This is in contrast with the collapse response, which is influenced by differences in the spectra at moderate to high intensities. The effect of damping ratio on expected annual loss is small, less than about 0.1% expected annual loss for all cases, except for the two-story existing (non-retrofitted) wood siding case. In this case, the weak existing cripple wall is very susceptible to collapse at low ground-motion intensities, making it more sensitive than other cases to changes in assumed inherent viscous damping.

The expected repair costs at the 250-year return period (RC250) are compared in Figure 4.13. This intensity-based metric has *Sa*(0.25 sec) = 0.98*g* for the San Francisco site. The figure shows similar trends as the previous performance metrics discussed. In particular, the relative effect of the ground-motion sets and the assumed damping are similar to those in the collapse behavior (Figure 4.11), probably because of the relatively high intensity of the 250-year return period as compared to the collapse resistance of the existing (unretrofitted) houses. To summarize, the main conclusions drawn from the comparisons in this section are the following:

- The choice of ground-motion hazard characterization (UHS versus CS) has a significant effect on the collapse risk for the retrofit and rigid base conditions, which are controlled by high-intensity (long return period) ground motions. The difference in results between the record sets are less significant for collapse of the existing (unretrofitted) cases and on the repair costs (EAL and RC250), which are more influenced by low to moderate seismic intensities.
- Variation in the assumed equivalent viscous damping between 2.5% and 0.5% has a small, practically negligible, effect on the results, especially as compared to other sources of uncertainty in the structural analyses and loss calculations.

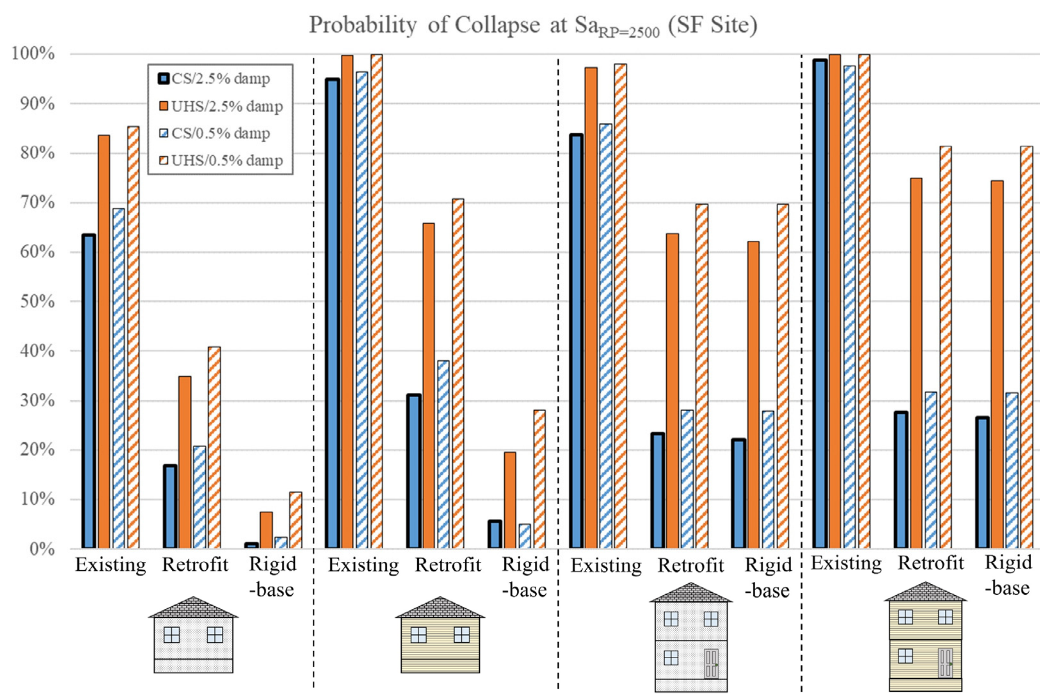

Figure 4.11 **Influence of ground motion spectral shape and damping ratio on the adjusted collapse probabilities at the 2500-year return period for the SF270 site (preliminary). Solid bar with bold border represents CS records with 2.5% damping (hatched bars assume 0.5%).**

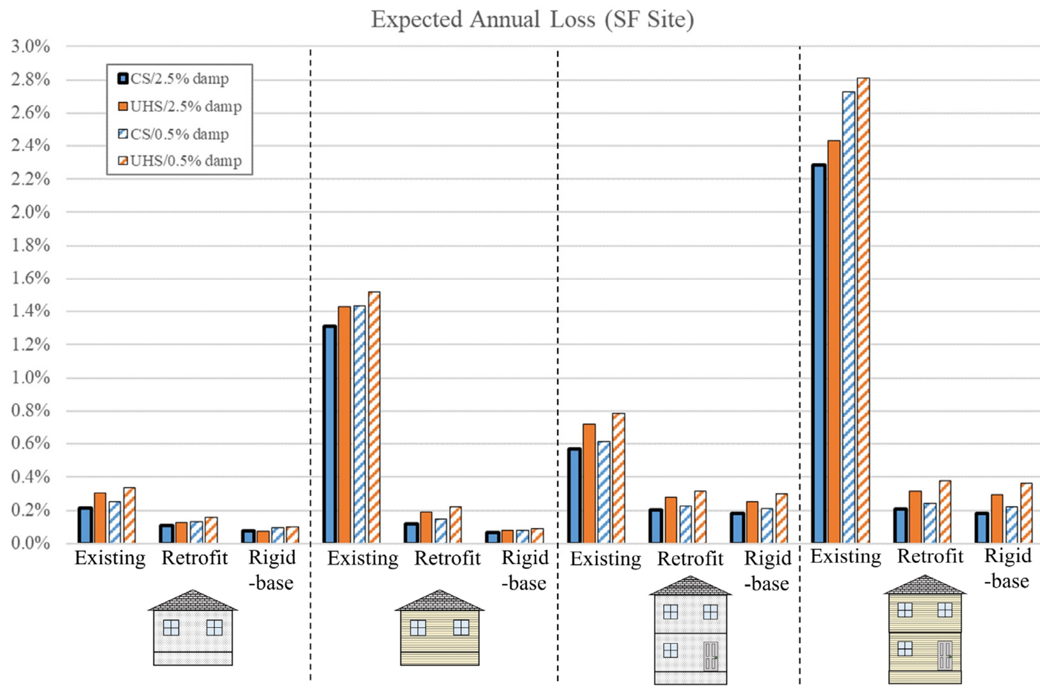

Figure 4.12 Influence of ground motion spectral shape and damping ratio on the expected annual loss for the SF270 site (preliminary). Solid bar with bold border represents CS records with 2.5% damping (hatched bars assume 0.5%).

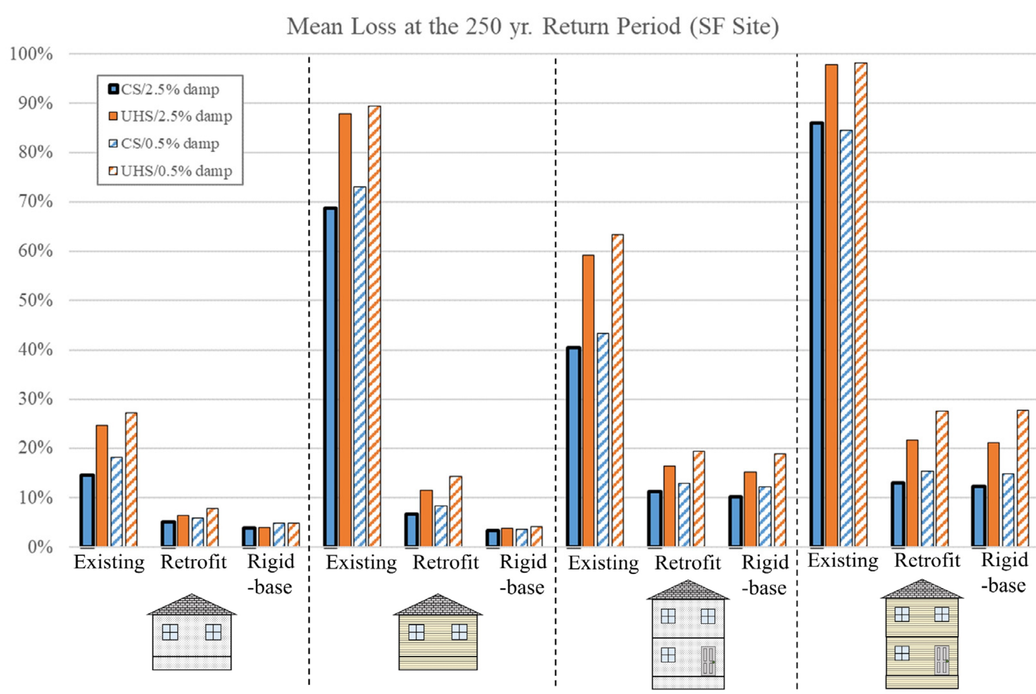

Figure 4.13 Influence of ground motion spectral shape and damping ratio on the mean loss at the 250-year return period for the SF270 site (preliminary). Solid bar with bold border represents CS records with 2.5% damping (hatched bars assume 0.5%).

4.4 INVESTIGATING THE USE OF A SINGLE CONDITIONING PERIOD FOR THE ASSESSMENT OF CRAWLSPACE DWELLINGS

4.4.1 Sensitivity Study on Conditioning Period

A sensitivity study was conducted to investigate the effect of the conditioning period on the collapse and loss assessment of building variants. For this study, WG3 produced two additional sets of CS ground motions for the SF270 site with conditioning periods (T^*) of 0.15 sec and 0.40 sec to compared with 0.25 sec assumed for the project. The comparison also includes a comparison to the UHS ground-motion sets. The CMS of the three ground-motion sets, and the UHS spectrum, are compared in Figure 4.14 for the 2500-year return period.

The three CS ground-motion sets are used to analyze three pairs of existing (unretrofitted) and retrofitted example variant pairs. All example variants are one-story with gypsum wallboard interior. These variant pairs are shown in Figure 4.14 with the elastic fundamental periods (T_1) annotated. The first variant pair has stucco exterior with 2-ft-tall cripple walls. This pair of variants have T_1 values of 0.14 sec and 0.15 sec that are among the shortest of the variant sets, where the focus is on comparing results for the T^* = 0.15 sec, T^* = 0.25 sec, and UHS ground-motion sets. The second variant pair has horizontal wood siding exterior with 2-ft cripple walls, with periods of T_1 equal to 0.29 sec (unretrofitted) and 0.21 sec (retrofitted), which straddle the default T^* = 0.25 sec. This variant pair is analyzed for the same T^* = 0.15 sec, T^* = 0.25 sec, and UHS ground-motion sets as the one-story stucco variant pair. The final variant pair has exterior horizontal wood siding with 4-ft-tall cripple walls, with T_1 equal to 0.39 sec (unretrofitted) and 0.21 sec (retrofitted). Note that for the wood siding variants, the WSP retrofit significantly increases the stiffness of the cripple wall, and thereby reduces the first-mode period. The 4-ft horizontal wood siding pair is analyzed with the T^* = 0.25 sec, T^* = 0.40 sec, and UHS ground-motion sets.

Analysis results for the three variant pairs are compared in terms of four metrics: (1) the adjusted probability of collapse at the 2500-year return period (see Figure 4.7 for adjustment assumptions); (2) the probability of collapse in 30 years; (3) the expected repair cost at the 250-year return period (RC250); and (4) the expected annual loss. Collapse fragility fitting for UHS records use Sa(0.25 sec) as an IM, whereas the CS cases are fit using spectral acceleration at their respective periods. Since the conditioning periods are varied in the sensitivity study, results are shown in terms of the hazard return period instead of IM for illustrating collapse probabilities and loss (damage) curves. Similar to the other sensitivity studies, these comparisons were made based on preliminary structural analysis and loss assessment models, results of which may not compare directly with the final results in Chapter 7, but are reasonably close to assess the relative performance between ground-motion sets for the pairs of existing (unretrofitted) and retrofitted houses.

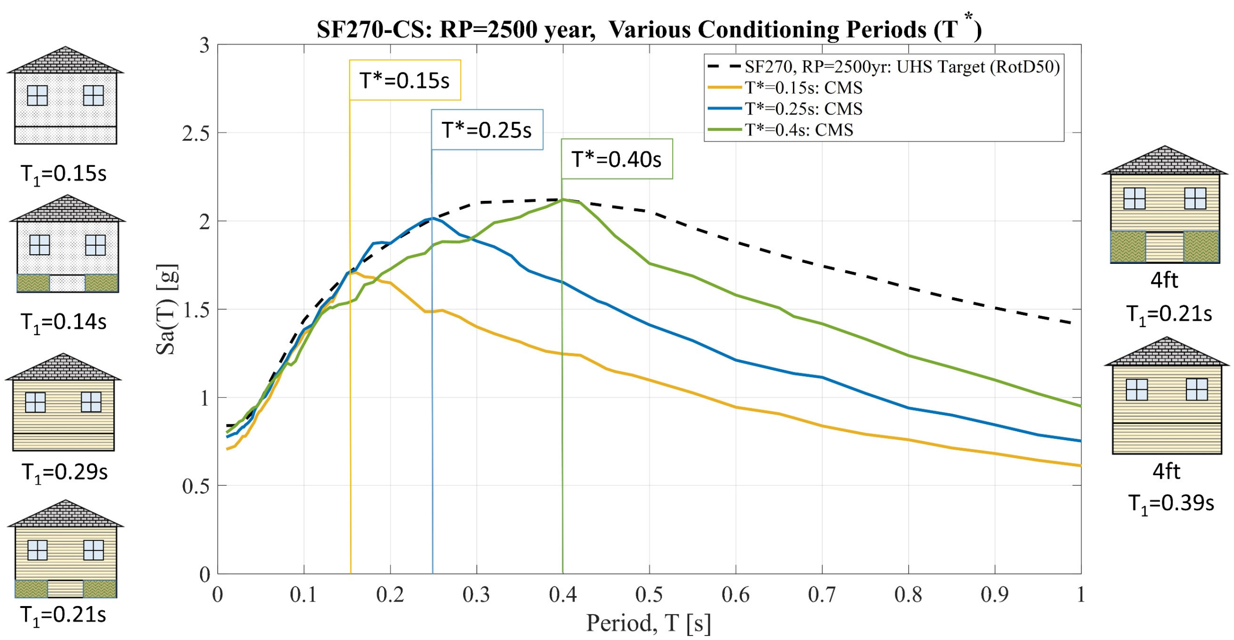

Figure 4.14 **Different conditional mean spectra for conditioning period of 0.15 sec, 0.25 sec, and 0.4 sec for the SF270 site compared with the UHS for the 2500-year return period. Pairs of building variants shown indicate those used in sensitivity study on conditioning period.**

Shown in Figure 4.15 is an illustration of the results for the 2-ft-tall stucco cripple wall variant pair, where the probability of collapse (left plot) and expected loss (right) are plotted versus the ground-motion return period. For both collapse and losses, the relationship between the response and return period is different, depending on the chosen ground-motion set. This is not unexpected, given the difference in spectral accelerations (Figure 4.14) for periods beyond 0.15 sec, which is the region that is especially important for collapse analyses. But, for the purposes of the PEER–CEA Project, of more importance is how the choice of ground motions affects the calculated relative difference in performance between the existing (unretrofitted) and retrofit case. To examine this question, the four scalar performance metrics are compared, in Table 4.4. In this table, the values shown in bold font are the difference in the respective metrics, between the existing (unretrofitted) and retrofitted condition. Comparing the difference statistics (bold results) across the three columns, one can see that the values are similar between the T^* = 0.15 sec and T^* = 0.25 sec record sets, as compared to the UHS record set. Moreover, the individual values (i.e., the probability of collapse in 30 years and the expected annual loss) are very close between the two conditioning periods.

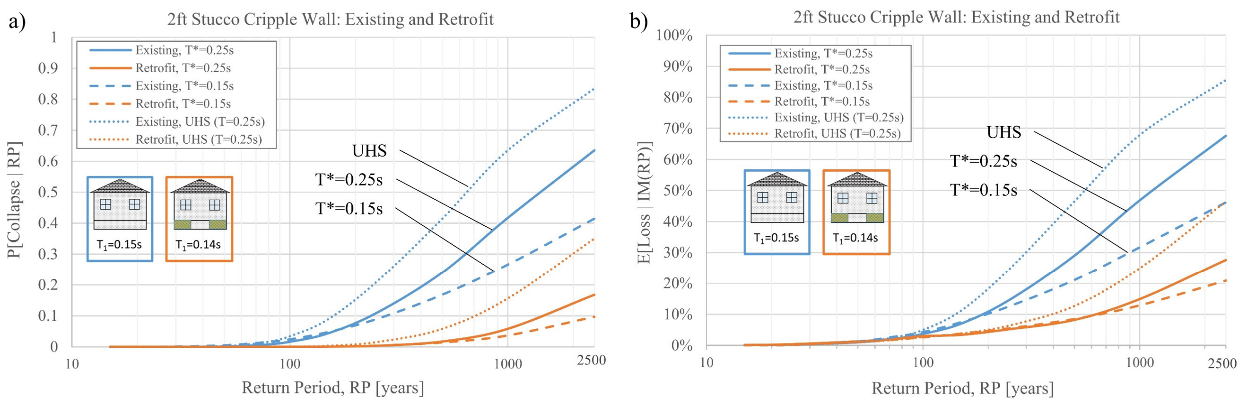

Figure 4.15 **Influence of varying ground motion target spectra for SF270 site and 2-ft-tall stucco cripple walls: (a) probability of collapse; and (b) mean loss as a function of return period.**

Table 4.4 **Seismic performance metrics and difference due to retrofit for varying ground motion targets for the SF270 site: 2-ft-tall stucco cripple walls.**

Metric	**Variant**	**Ground-motion set**		
		T* **= 0.25 sec** [3]	***T**** **= 0.15 sec** [3]	**UHS** [4]
P[C|RP=2500yr]	Existing	63.5%	41.5%	83.5%
	Retrofit	16.8%	9.7%	35.1%
	Difference[2]	**46.7%**	**31.8%**	**48.4%**
P[C|t=30yr]	Existing	4.5%	3.7%	7.2%
	Retrofit	0.5%	0.3%	1.3%
	Difference	**4.0%**	**3.4%**	**6.0%**
E[Loss | RP=250yr] (RC250)[1]	Existing	14.6%	12.6%	24.6%
	Retrofit	5.2%	5.5%	6.4%
	Difference	**9.4%**	**7.1%**	**18.2%**
Expected Annual Loss[1]	Existing	0.21%	0.19%	0.31%
	Retrofit	0.11%	0.10%	0.13%
	Difference	**0.10%**	**0.09%**	**0.18%**

[1] Loss metrics expressed in % replacement cost.
[2] Difference is the existing (unretrofitted) minus the retrofit metric.
[3] Conditional spectra with specified conditioning period.
[4] Uniform Hazard Spectrum

Results for the 2-ft-tall horizontal wood siding variant pair are presented and compared, in the same format as for the stucco pair, in Figure 4.16 and Table 4.5. In contrast to previous case with 2-ft-tall stucco cripple walls, the 2-ft horizontal wood siding variant pair has a significant change in T_1 due to the addition of retrofit material. Further, this pair has T_1 values that are just below (0.21 sec) and just above (0.29 sec) the primary conditioning period of $T^* = 0.25$ sec. The collapse fragilities and mean loss curves presented in Figure 4.16 illustrate that the $T^* = 0.25$ sec results are somewhat balanced between the $T^* = 0.15$ sec and the most conservative UHS results.

The T^* = 0.15 sec results are only used as an illustration since the T_1 values are already beyond 0.15 sec, where the capping of spectral demands (see Figure 4.14) at high intensities is reflected in the reduced collapse probabilities and mean losses when compared to the T^* = 0.25 sec results. Similar to the results for the 2-ft-tall stucco case, the time integrated metrics are fairly consistent across all three record sets, and the differences between the existing (unretrofitted) and retrofitted cases are very close between the T^* = 0.15 sec and T^* =0.25 sec record sets.

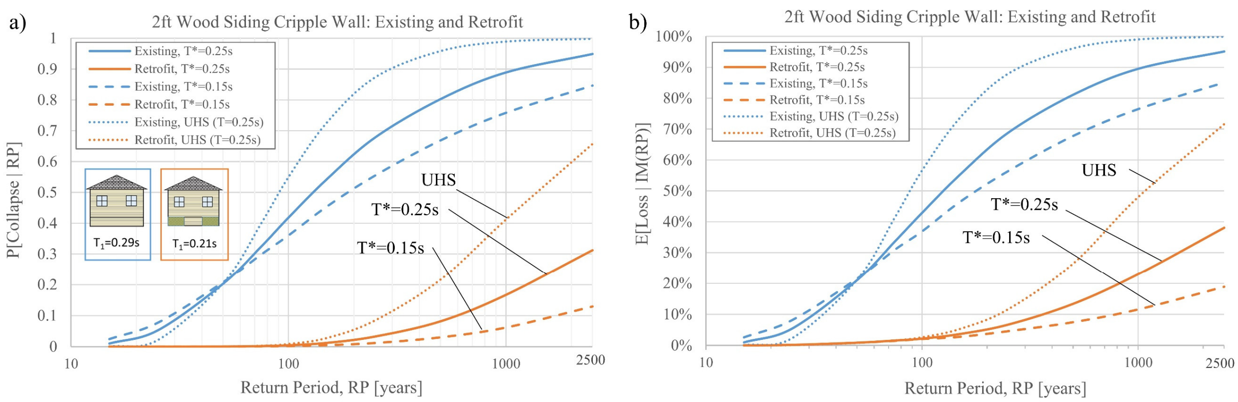

Figure 4.16 **Influence of varying ground motion target spectra for SF270 site and 2-ft-tall horizontal wood siding cripple walls: (a) probability of collapse; and (b) mean loss as a function of return period.**

Table 4.5 **Seismic performance metrics and difference due to retrofit for varying ground-motion targets for the SF270 site: 2-ft-tall wood horizontal wood siding cripple walls.**

Metric	Variant	Ground-motion set		
		T^* = 0.25 sec [3]	T^* = 0.15 sec [3]	UHS [4]
P[C|RP=2500yr]	Existing	94.9%	84.7%	99.8%
	Retrofit	31.2%	13.0%	65.8%
	Difference[2]	**63.6%**	**71.7%**	**34.1%**
P[C|t=30yr]	Existing	32.0%	31.6%	34.4%
	Retrofit	1.6%	0.6%	3.8%
	Difference	**30.4%**	**31.0%**	**30.6%**
E[Loss | RP=250yr] (RC250)[1]	Existing	68.8%	56.4%	87.9%
	Retrofit	6.7%	4.6%	11.6%
	Difference	**62.1%**	**51.8%**	**76.3%**
Expected Annual Loss[1]	Existing	1.31%	1.30%	1.43%
	Retrofit	0.12%	0.08%	0.19%
	Difference	**1.19%**	**1.22%**	**1.24%**

[1] Loss metrics expressed in % replacement cost.
[2] Difference is the existing (unretrofitted) minus the retrofit metric.
[3] Conditional spectra with specified conditioning period.
[4] Uniform Hazard Spectrum.

Results for the 4-ft-tall horizontal wood siding variant pair are presented and compared, in the same format as for the previous pairs, in Figure 4.17 and Table 4.6. This variant pair was purposefully developed to have an existing (unretrofitted) house with a long fundamental period (T_1 = 0.39 sec) that reflects the upper bound of most variants analyzed in the project. The corresponding retrofitted house has a T_1 of 0.21 sec, which is almost half of the period of the existing case. These two variants are analyzed with the T^* = 0.25 sec, T^* = 0.40 sec, and UHS ground-motion sets. The results shown in Figure 4.17 illustrate that the T^* = 0.40 sec results for the existing (unretrofitted) variant have larger collapse probabilities and mean losses than the T^* = 0.25 sec set, which is logical due to difference in mean spectral demands at the longer initial period (see Figure 4.14). Conversely, the retrofit variant shows much less difference between the two CS ground-motion sets, except at the largest 2500-year return period intensity. Similar to other conditioning period comparisons, the UHS ground-motion set results in the most conservative results. These results may suggest that the T^* = 0.25 sec conditioning period may be unconservative for the longer period variants, although it should be highlighted that the only variants with longer periods are those with extremely weak and flexible (taller) unretrofitted cripple walls. However, as noted for the other variant pairs, the apparent differences in the individual fragilities do not carry through to the time integrated metrics of probability of collapse in 30 years and expected annual loss (see Table 4.6). Moreover, the relative difference in metrics between the existing (unretrofitted) and retrofitted cases are fairly close for the T^* = 0.25 sec and T^* = 0.40 sec results.

As demonstrated by the sensitivity study of the three pairs of house variants, while there are differences between the individual loss curves, the time integrated scalar metrics are not very sensitive to CS conditioning periods between T^* = 0.15 sec and T^* = 0.40 sec. Moreover, the differences in loss metrics between the existing (unretrofitted) and retrofitted houses are similar between conditioning periods. On the other hand, comparison to results with the UHS ground motions show much larger differences. Use of a single conditioning period allows for all building variants to be subjected to the same ground motion input, which is important for comparing existing (unretrofitted) and retrofitted variant pairs on a consistent basis. In summary, these comparisons support the use of a single conditioning period of T^* = 0.25 sec for all of the house variants, which is consistent with methods employed by catastrophe loss modelers.

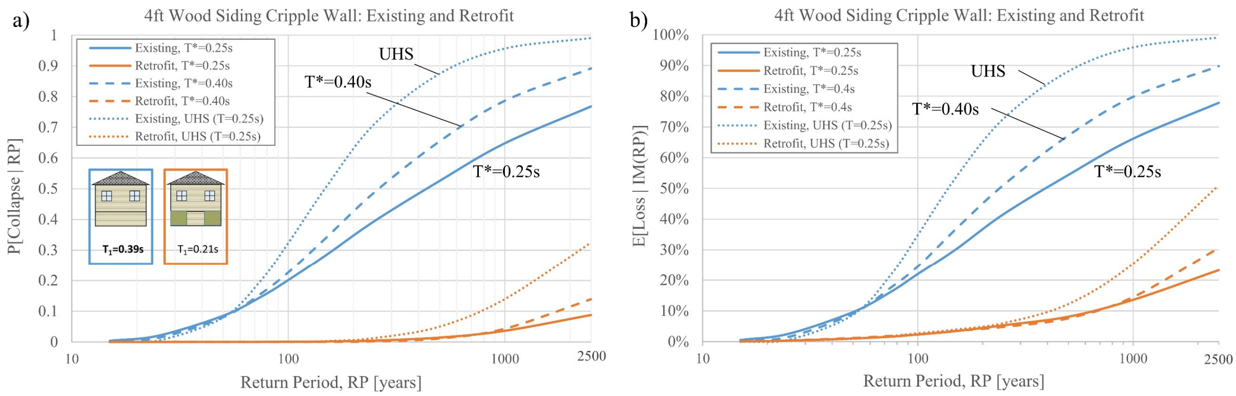

Figure 4.17 **Influence of varying ground motion target spectra for SF270 site and 4-ft-tall horizontal wood siding cripple walls: (a) probability of collapse; and (b) mean loss as a function of return period.**

Table 4.6 **Seismic performance metrics and difference due to retrofit for varying ground motion targets for the SF270 site: 4-ft-tall wood horizontal wood siding cripple walls.**

Metric	Variant	Ground-motion set		
		*T** = 0.25 sec [3]	*T** = 0.40 sec [3]	UHS [4]
P[C|RP=2500yr]	Existing	76.8%	89.2%	99.0%
	Retrofit	8.8%	13.9%	32.4%
	Difference[2]	**68.0%**	**75.3%**	**66.6%**
P[C|t=30yr]	Existing	18.0%	19.5%	23.7%
	Retrofit	0.3%	0.4%	1.2%
	Difference	**17.6%**	**19.1%**	**22.5%**
E[Loss | RP=250yr] (RC250)[1]	Existing	41.6%	51.1%	72.7%
	Retrofit	5.3%	4.8%	6.0%
	Difference	**36.3%**	**46.3%**	**66.7%**
Expected Annual Loss[1]	Existing	0.71%	0.77%	0.94%
	Retrofit	0.09%	0.11%	0.13%
	Difference	**0.62%**	**0.67%**	**0.82%**

[1] Loss metrics expressed in % replacement cost.
[2] Difference is the existing (unretrofitted) minus the retrofit metric.
[3] Conditional spectra with specified conditioning period.
[4] Uniform Hazard Spectrum.

4.4.2 Fundamental Period Comparison with Literature

A final discussion point on the topic of selecting an appropriate conditioning period compares the fundamental periods of all finalized best estimate building variants with limited values reported in the literature.

Figure 4.18 illustrates the fundamental periods obtained for the best estimate building variants used for final loss assessment; see Chapter 7. To calculate a statistically consistent average, only distinct building models are included, meaning that variants that are analyzed at different sites are not counted more than once. Further, retrofitted cripple walls only include the $S_{DS} = 1.2g$ designs (middle value), and existing (unretrofitted) stem wall houses are not double-counted with fixed-base variants since these have the same fundamental period. These include a total of 50 distinct variants with respect to: number of stories (1 or 2), cripple wall height (2 ft or 6 ft), exterior finish (wood siding, stucco, T1-11), and interior material (gypsum or plaster on wood lath). Figure 4.18 shows all data points at the left most column, with an average fundamental period of 0.26 sec. The same data is separated into a few subgroups, details of which are provided in Chapter 7. The key observation is that, on average, the different subgroups tend to have fundamental periods that fluctuate between 0.2-sec to 0.3-sec periods. However, there are a few cases with periods greater than 0.35 sec, where the longest period is about 0.57 sec. All these longer periods are for 6-ft-tall cripple walls with horizontal wood siding, with the highest value being for the two-story, pre-1945 era (lath and plaster interior), unretrofitted 6-ft-tall cripple wall with horizontal wood siding. It should be noted that the horizontal wood siding material assumes the presence of incidental bracing, which as discussed in Section 3.6.3.1, provides additional stiffness and strength beyond the wood siding alone.

A sub-set of period measurements on actual wood-frame structures is presented in Table 4.7. The measurements include laboratory testing and field measurements, the basis of which has already been discussed for damping measurements in Section 2.4.4.1. The table illustrates that the period ranges from the presented structures are in the range of 0.15 sec to 0.35 sec, noting that data on one-story structures is not presented in the table. The largest value of 0.46 sec in Table 4.7 was not included in the typical range since this structure is a two-story garage that has no interior finish material and has horizontal wood siding and diagonal cut-in braces (noting that the second translational period was 0.39 sec).

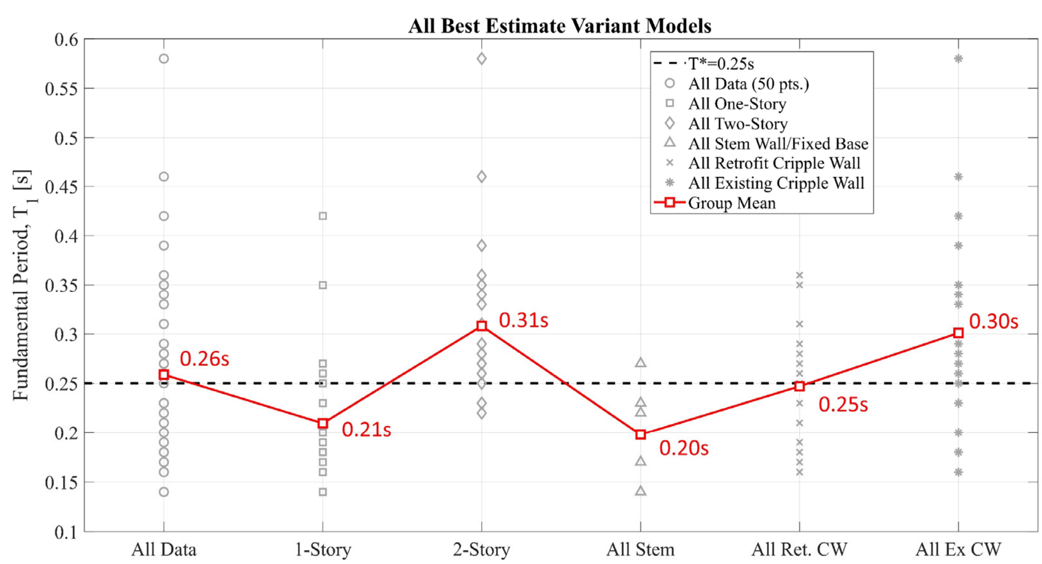

Figure 4.18 **Elastic fundamental periods of the 50 distinct best estimate variant models used for final analysis. Solid line indicates the average of each different group.**

Compared to the periods listed in Table 4.7, the calculated periods of the variant building analysis models tend to be on the high side. In particular, the longest analysis model period on the order of 0.57 sec (Figure 4.18) lies well outside the measured periods. However, consider the actual case of a two-story horizontal wood siding dwelling on tall (4- to 6-ft-tall) cripple walls with heavy plaster on wood lath as an interior finish, such as the dwelling shown in Figure 4.19. Without the influence of porches and chimneys to stiffen the structure (two aspects not considered in the current scope), then estimated periods could increase significantly compared to the measured garage case (period of 0.46 sec in Table 4.7) on the basis of increased weight alone.

Table 4.7 Fundamental period measurements of actual wood-frame structures.

Structure	Reference	Description	T_1 (sec)
Three-story laboratory test	Camelo [2003]; Mosalam et al. [2002]	Pre Phase I: No finish materials, only framing and plywood, large garage opening on one lower story side	0.35
		Pre Phase III: Stucco and gypsum finish materials added	0.26
Two-story laboratory test	Fischer et al. [2001]	Pre Phase 8: Conventional construction (no tie-downs), framing and plywood sheathing only	0.24
		Pre Phase 10: Stucco and gypsum finish added	0.15
Two-story house[1]	Camelo [2003]	Built around 1940, 2000 ft^2, on short (1ft) cripple walls, two chimneys, exterior is wood shingle, interior is plaster	0.20
Two-story house	Camelo [2003]	Built around 1920, 2000 ft^2, has crawlspace, one chimney, exterior is horizontal wood siding, interior is plaster	0.21
Two-story garage	Camelo [2003]	Wood sheathing and cut-in bracing only, 900 ft^2, no interior finish, second floor empty during measurement	0.46

[1] See Figure 2.11(a).
[2] See Figure 2.11(b)

Figure 4.19 Example of a two-story horizontal wood siding dwelling on taller cripple walls (photograph courtesy of Kelly Cobeen).

5 Development of Component Damage Fragility Functions for the Assessment of Older Single-Family Wood-Frame Dwellings

Structural engineering demand parameters (EDP) are translated into damage states (DS) of structural and nonstructural components using component-level damage fragility functions as specified in the *FEMA P-58* methodology. This chapter discusses the basis for the selected component damage fragilities. With a focus on older wood-frame dwellings, the chapter reviews currently available fragility functions (primarily those in the *FEMA P-58* database) along with proposed modifications based on review of existing data, extension to different material types and details, and information gained through experimental testing conducted as part of the project. The chapter begins with an overview of typical fragility functions for wood-frame houses, followed by a review of the available fragility functions within the *FEMA P-58* database. The remainder of the chapter reviews proposed modifications to existing fragility functions and development of new functions to conduct the building-specific loss assessment of the one- and two-story building variants.

5.1 BACKGROUND ON DAMAGE FRAGILITY FUNCTIONS FOR WOOD-FRAME DWELLINGS

Fragility functions are used in order to relate an EDP, such as story drift ratio, to the probability of individual components (or entire structures) being in a particular damage state (DS) (e.g., slight, moderate, etc.). This work focuses on fragility functions that are applied to individual components or sub-assemblies, as pertinent to the building-specific or assembly-based loss assessment framework adopted (i.e., *FEMA P-58* [2012]).

Fragility functions are commonly described as lognormal cumulative distributions [FEMA 2012; Beck et al. 2002; Porter and Kiremidjian 2001; and Kennedy and Ravindra 1984]. As pointed out by Porter [2019], there are many reasons for the lognormal distribution being widely adopted, not the least of which is the simplicity and ease of implementation (e.g., since the lognormal distribution constrains the demand parameters to positive values). Moreover, the lognormal distribution is widely used and has been shown to reliably fit observed damage trends.

For fragility development, the guidelines in *FEMA P-58*, Vol. 1, Appendix H, *Fragility Development*, are considered to maintain consistency with *FEMA P-58* and adhere to good practice. According to the guidelines, component damage fragilities are estimated using the method of moments to determine the median (θ; lognormal mean) and dispersion (β_r) of the available test data. The total fragility dispersion (β) is comprised of the random variability of the test data (β_r) and additional uncertainty to actual conditions (β_u). These two uncertainty factors are combined using the SRSS method as shown in Equation (5.1).

$$\beta = \sqrt{\beta_r^2 + \beta_u^2} \tag{5.1}$$

The fit of the lognormal distribution should pass the Lilliefors test [Lilliefors 1967] at a significance level of 5% (i.e., α = 0.05) prior to adjustment for additional uncertainty. The recommended values of β_u are 0.25 and 0.1. A value of 0.25 is recommended if any of the following conditions apply, 0.1 otherwise:

- Test data are available for five or fewer specimens;
- Situations where the configurations used for laboratory tests do not represent the complete range of configurations in realistic buildings;
- Limited range of loading protocols used in laboratory tests; and
- Actual behavior of the component is expected to be dependent on more demand parameters than those considered in the laboratory tests (e.g., simultaneous drift in two orthogonal directions versus uniaxial laboratory tests).

All proposed modifications to component damage fragilities assume cumulative lognormal distributions. Given the widely varying amount of information available for different materials considered in the current project, the *FEMA P-58*, Appendix H guidelines are followed when possible, yet more simplistic judgment-based assumptions are made, where necessary, in certain cases. The default total dispersion for judgment-based fragilities is 0.4 according to *FEMA P-58*, Appendix H. All assumptions and justification of proposed fragilities are documented.

5.2 COMPONENT FRAGILITIES FOR WOOD-FRAME STRUCTURES IN THE *FEMA P-58* DATABASE

The *FEMA P-58* fragility database [2012] consists of 980 fragilities and consequence functions (discussed in Chapter 6) for a wide range of structural and nonstructural systems. However, many of these categories are directed toward large commercial buildings. The available components for residential wood-frame construction are much more limited. Notable previous studies that developed fragility functions for wood-frame construction include the work of Porter et al. [2002] for the CUREE-Caltech Woodframe Project and also Porter [2009] for the CAPSS Project [ATC 2009].

The available damage fragilities within *FEMA P-58* for exterior structural materials of wood-frame houses is summarized in Table 5.1. These include fragility functions that are provided within the *FEMA P-58* Performance Assessment Calculation Tool (*PACT*) Fragility Specification Manager [2012b] or the Seismic Performance Prediction Program (*SP3*) offered by the Haselton Baker Risk Group (*www.hbrisk.com*). Damage states are listed exactly as they appear within the database. Each component and damage state DS_i lists the median ($\theta_{DS,i}$) and dispersion ($\beta_{DS,i}$) of the lognormal fragility function. The table illustrates that the first four structural components consist of structural panel sheathed walls (e.g., OSB or plywood), with or without hold-down devices. These are further distinguished by the presence or absence of stucco exterior. The last row of the table includes exterior walls with diagonal let-in bracing.

The available interior material fragilities are provided in Table 5.2. These include two different sets of fragilities for wood-stud framed gypsum walls. Assembly type C1011.011a is an interior gypsum partition wall that incorporates two sequential damage states in terms of story drift demand with the second having consequences (e.g., repair costs) split into a mutually exclusive damage state group (with a weighting of 80% for "a" and 20% for "b"). Assembly B1071.014 is nominally a gypsum exterior wall that includes three sequential damage states. These assembly types have similar costing associated with them (in PACT/SP3) with the main difference being that DS 2b for C1011.011a is consistent with DS3 for B1071.014. Interior wall finish includes wallpaper, ceramic tile, and high end or marble finish.

Table 5.1 Damage fragilities for exterior structural materials for wood-frame structures within the *FEMA P-58* database.

Index*	Material/ assembly	EDP	Damage state (DS_i)	Median $\theta_{DS,i}$	Dispersion $\beta_{DS,i}$
B1071.001	Light framed wood walls with **structural panel sheathing**, gypsum wallboard, **no hold-downs**	SDR (rad)	1: Slight separation of sheathing or nails which come loose	0.01	0.4
			2: Permanent rotation of sheathing, tear out of nails or sheathing	0.0175	0.4
			3: Fracture of studs, major sill plate cracking	0.025	0.4
B1071.002	Light framed wood walls with **structural panel sheathing**, gypsum wallboard, and **hold-downs**	SDR (rad)	1: Slight separation of sheathing or nails which come loose	0.015	0.4
			2: Permanent rotation of sheathing, tear out of nails or sheathing	0.0262	0.19
			3: Fracture of studs, major sill plate cracking	0.0369	0.2
B1071.011	Light framed wood walls with **structural panel sheathing**, **stucco**, **no hold-downs**	SDR (rad)	1: Cracking of stucco	0.0017	0.5
			2: Spalling of stucco, separation of sheathing from studs	0.0035	0.4
			3: Fracture of studs, major sill plate splitting	0.017	0.4
B1071.012	Light framed wood walls with **structural panel sheathing**, **stucco**, **hold-downs**	SDR (rad)	1: Cracking of stucco	0.0025	0.44
			2: Spalling of stucco, separation of sheathing from studs	0.0052	0.3
			3: Fracture of studs, major sill plate splitting	0.0252	0.16
B1071.031	Wood walls with diagonal let-in bracing	SDR (rad)	1: Failure of diagonal bracing	0.01	0.4

*Indices correspond to those used in *FEMA P-58* (PACT).

Table 5.2 Damage fragilities for interior partition and finish materials applicable to wood-frame structures within the *FEMA P-58* database.

Index*	Material/ assembly	EDP	Damage state (DS*i*)	Median $\theta_{DS,i}$	Dispersion $\beta_{DS,i}$
C1011.011a [2]	**Wall Partition**, Type: **Gypsum with wood studs**, Full Height, Fixed Below, Fixed Above	SDR (rad)	1: Cracking of paint over fasteners or joints	0.0021	0.6
			2a: Local and global buckling out-of-plane and crushing or gyspum wallboard. Studs are typically not damaged by failure of gypsum wallboard (25% damage)	0.0071	0.45
			2b: Local and global buckling out-of-plane and crushing or gyspum wallboard. Studs are typically not damaged by failure of gypsum wallboard (100% damage)	0.0071	0.45
B1071.041	**Exterior Wall** - Type: **Gypsum with wood studs**, Full Height, Fixed Below, Fixed Above	SDR (rad)	1: Cracking of paint over fasteners or joints	0.0021	0.6
			2: Moderate cracking or crushing of gypsum wallboards (typically in corners and in corners of openings)	0.0071	0.45
			3: Significant cracking and/or crushing of gypsum wall boards- **buckling of studs and tearing of tracks**.	0.012	0.45
C3011.001a	**Wallpaper** (Finish)	SDR (rad)	1: Wallpaper warped and torn	0.0021	0.6
C3011.002a	**Ceramic Tile** (Finish)	SDR (rad)	1: Minor cracked joints and tile	0.0021	0.6
			2: Cracked joints and tile	0.0071	0.45
C3011.003a	**High End Marble or Wood Paneling** (Finish)	SDR (rad)	1: Minor cracked joints and minor cracks in marble/wood paneling	0.0021	0.6
			2: Significant cracks in marble / wood paneling	0.0071	0.45

[1] Indices correspond to those used in *FEMA P-58* (PACT).
[2] C1011.011a has a mutually exclusive damage state group associated with the same damage fragility, 2a corresponds to 25% of area requiring replacement, and 2b requires 100% replacement. The net cost of damage state 2 is based on a weighting of 80% contribution from (2a) and 20% from (2b).

5.3 DAMAGE FRAGILITIES FOR OLDER WOOD-FRAME STRUCTURES: SUPERSTRUCTURE MATERIALS

5.3.1 Gypsum Wallboard

The damage state definitions for gypsum wallboard outlined in the *FEMA P-58* database are compared with definitions for different levels of repair within the CUREE EDA Repair Guidelines [CUREE EDA-02 2010] in Table 5.3. Notably, the EDA repair efforts do not distinguish between defined damage states and only describe types of damage that do and do not require a technical consultant. Interpretations are those used to prepare damage description packages for the PEER–CEA Earthquake Damage Workshop [Vail et al. 2020]. Although an exact comparison cannot be made, the *FEMA P-58* damage states do represent minor, significant and replacement level repair efforts, which are roughly aligned with the considerations outlined by the EDA guidelines. A main difference is that the EDA guidelines do not describe a replacement threshold.

Table 5.3 **Damage and repair descriptions for gypsum wallboard from *FEMA P-58* database and CUREE EDA Repair Guidelines.**

Damage state	*FEMA P-58* Damage description	*FEMA P-58* repairs[1]	EDA damage	EDA repairs
1	Cracking of paint over fasteners or joints, minor cracking of wall board, warping or cracking of tape.	Retape joints, paste and repaint both sides; Localized repair, patch and paint (Cut out gypsum board, 5%; Retape, 10%; Repaint, 25%)	(a) Short cracks (<6 in.) less than 1/64 in. wide (b) Cracks following taped joints and corner beads (c) Fastener pops	(a) Patch and refinish (b) Remove existing tape and joint compound, retape and refinish (c) Remove/reset existing fastener. Add drywall screw 1 in. from original fastener, patch, refinish
2	Moderate cracking or crushing of gypsum wall boards (typically in corners and in corners of openings). Local buckling out-of-plane and crushing of gypsum wallboards. Studs are typically not damaged by failure of the gypsum wallboard.	Retape joints, paste and repaint both sides (Cut out gypsum board, 10%; Retape, 25%; Repaint, 50%)	(a) through (c) (d) Longer cracks (>6 in.) extending through drywall	(a) through (c) (d) Remove and replace drywall to nearest studs beyond crack (min. 32 in. × 48 in.), refinish
3	Significant cracking and/or crushing of gypsum wall boards. Studs are typically not damaged by failure of the gypsum wallboard.	Remove existing gypsum board, replace gypsum board, finish and repaint	(a) through (d) (e) Fractured gypsum panels (f) Significant loosening of framing connection	(a) through (d) (e) Replaced in kind (f) Install new fasteners to eliminate relative movement

[1] Repairs only include description of gypsum wall repair line items, costing includes other factors, these descriptions for gypsum repair are taken directly from repair cost line items within *FEMA P-58* background documentation.

The gypsum wallboard fragilities for residential framing with wood studs in the PACT/SP3 databases are based on the same median drift demands and dispersion values proposed by Miranda and Mosqueda [2011] for commercial office partitions with cold-formed steel framing (This is reflected in the DS 3 description of B1071.014 in Table 5.1 including the tearing of metal tracks). There is no documentation to substantiate this decision. Moreover, the values for gypsum on cold-formed steel framing are not consistent with the reported gypsum fragilities using test data with wood framing reported by Ekiert and Filiatrault [2008]. As such, a review of the available gypsum testing on wood framing was conducted.

Damage state information collected by Ekiert and Filiatrault [2008] included information documented by McMullin and Merrick [2002]. The information documented by McMullin and Merrick [2002] included numerous types of gypsum damage that would overlap when defining when a specimen is in a single damage state corresponding to a threshold level of repair. These repeated values were all collected and placed into damage states, with multiple measurements per specimen, and included in the fragility development conducted by Ekiert and Filiatrault [2008]. As a comparison to the implemented *FEMA P-58* thresholds, the DS 1 and 2 fragilities were recalculated in the current study by taking the smallest drift value qualifying for the specific damage state for a given specimen for this set of tests.

Additional damage information is provided by the CUREE *Earthquake Damage Assessment* (EDA) *and Repair Project* [Arnold et al. 2003(a), (b)] and PEER–CEA large-component specimen C-2 [Cobeen et al. 2020] for the first two damage states. To verify DS 3 (replacement threshold), backbone data from tests were used in lieu of the inadequate documentation in the literature to estimate this damage state. A total of 16 tests from five different test programs [COLA 2001; McMullin and Merrick 2002; Gatto and Uang 2002; Pardoen et al. 2003; and Bahmani and van de Lindt 2016] were used to determine the drift at peak strength and the drift corresponding to 20% post-peak strength loss, which were considered as indicators of replacement thresholds for gypsum wallboard, with the latter assumed representative for DS 3. The data used for verification of all three damage states is provided in Appendix B. The reviewed data for three damage states are shown in Figure 5.1. The individual data points are shown using the Hazen plotting position. Fragility curves consider only test variability (β_r) and are estimated using the method of moments approach outlined in *FEMA P-58*, Appendix H [2012]. When including an adjustment dispersion (β_u) of 0.25 for comparison to the *FEMA P-58* functions for B1071.014, the results were very similar; see Figure 5.2. Due to this similarity, the provided B1071.041 fragilities (which as noted above are based on gypsum wallboard on cold-formed steel framing) were adopted in the current project to represent gypsum wallboard damage. Proposed fragility parameters for gypsum wallboard are defined in Table 5.4.

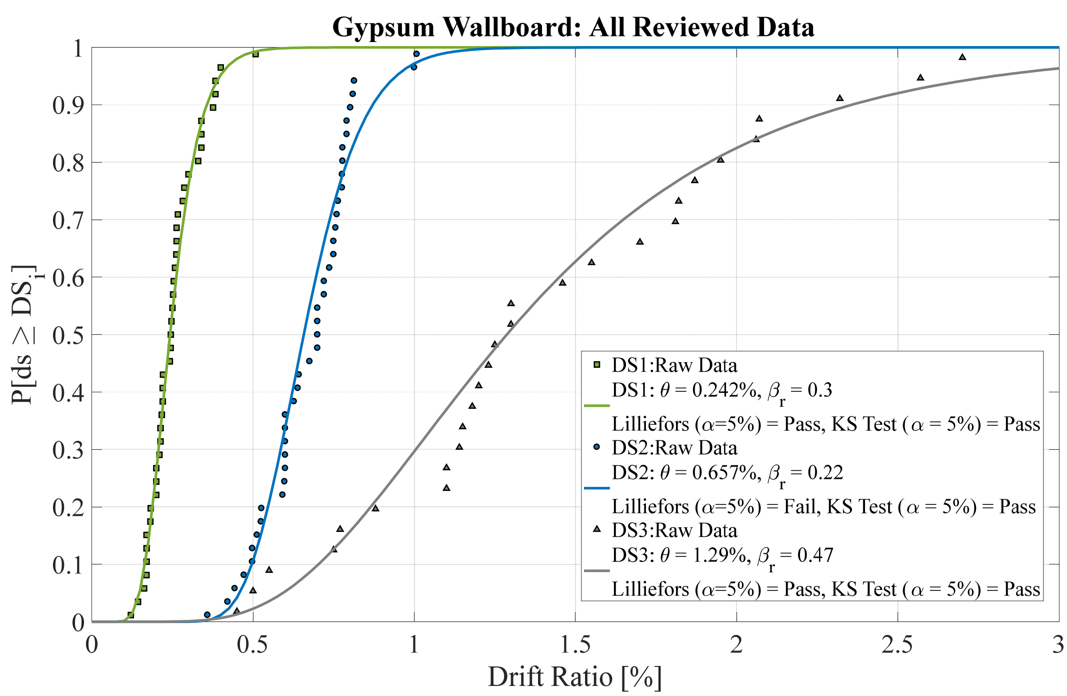

Figure 5.1 Reviewed gypsum wallboard with wood stud fragility data.

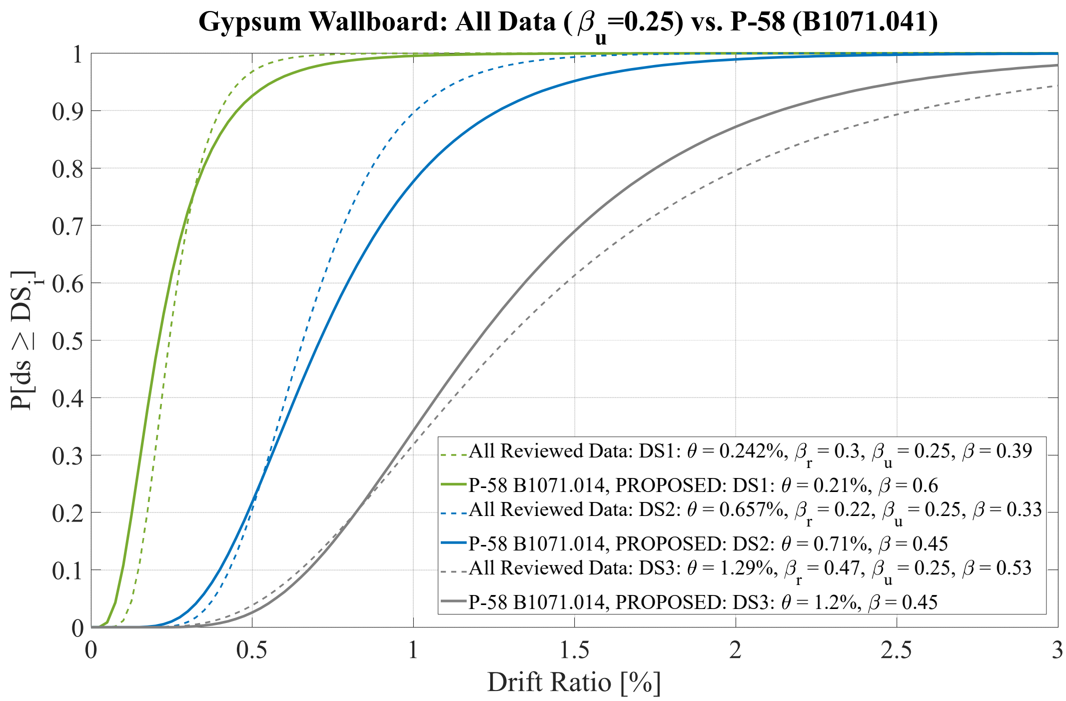

Figure 5.2 **Comparison of adjusted gypsum wallboard with wood stud fragility data (dashed lines) with the *FEMA P-58* B1071.014 exterior gypsum wallboard fragilities (solid lines). No further modification of B1071.014 values is proposed following review.**

Table 5.4 **Implemented gypsum wallboard damage fragility functions.**

Damage state	Damage description	EDP	Median (θ)	Dispersion (β)
1	Cracking of paint over fasteners or joints, minor cracking of wall board (< 6 in.), warping or cracking of tape	SDR (rad)	0.0021	0.60
2	Moderate cracking (> 6 in. in length, through thickness) or crushing of gypsum wall boards (typically in corners and in corners of openings). Local buckling out-of-plane and crushing of gypsum wallboards. Studs are typically not damaged by failure of the gypsum wallboard.		0.0071	0.45
3	Significant cracking and/or crushing of gypsum wall boards. Buckling and fracture of gypsum panels. Studs are typically not damaged by failure of the gypsum wallboard. Loosening of framing connections possible.		0.012	0.45

* Fragility parameters are based on assembly B1071.041 within *FEMA P-58* database.

5.3.2 Exterior Stucco

The damage state definitions for exterior stucco outlined in the *FEMA P-58* database are compared with definitions for different level of repair within the CUREE EDA Repair Guidelines [CUREE *EDA-02* 2010] in Table 5.5. Similar to the fragilities for interior walls, the EDA repair efforts do not distinguish between defined damage states and only describe types of damage that do and do not require a technical consultant. Although an exact comparison cannot be made, the *FEMA P-*

58 damage states do represent minor, significant, and replacement level repair efforts, which generally correspond to the considerations outlined by the EDA guidelines. A main difference is that the EDA guidelines do not describe a replacement threshold, but they do provide guidance on the lower bound threshold for requiring repairs (i.e., minimum stucco crack widths).

Table 5.5 Damage and repair descriptions for exterior stucco from *FEMA P-58* database and CUREE EDA repair guidelines.

Damage state	*FEMA P-58* damage description [1]	*FEMA P-58* repairs	EDA damage	EDA repairs
1	Cracking of stucco.	Clean stucco cracks. Fill cracks with cement compound. Repaint wall to hide cracks.	(a) Cracks < 1/64 in. wide (b) Cracks up to 1/8 in. wide, no delamination, no spalling	(a) No crack repair (b) Rout, patch, and refinish
2	Spalling of stucco, separation of stucco from sheathing and studs	Remove loose stucco and patch spalled areas with stucco. Repaint to hide repairs.	(c) Extensive minor cracking (d-) Severe cracking and minor delamination	(c) Remove color coat, rout, patch, recoat, refinish (d-) Stucco cut back to secure areas, lath and waterproofing repaired, replace stucco, refinish
3	Fracture of studs, major sill plate cracking	Remove and replace studs, plates, sheathing, and stucco. Shore as required.	(d+) Stucco has buckled, delaminated, detached from framing or has severe cracking	(d+) Stucco cut back, lath and waterproofing repaired, replace stucco, refinish to give uniform appearance

[1] All current *FEMA P-58* exterior stucco assemblies include structural panel sheathing beneath the stucco.

The FEMA P-58 background documentation for the fragility of wood light-frame walls [Ekiert and Filiatrault 2008] considered two different conditions for a stucco exterior: stucco over OSB with hold-downs, and stucco over OSB without hold-downs. The latter case is referred to as "basic strength design" by Ekiert and Filiatrault to distinguish between "engineered construction" with modern seismic detailing such as hold-downs.

An important underlying assumption in some of the fragility functions developed by Ekiert and Filiatrault [2008] is to increase of damageability of exterior wall components (stucco over OSB or OSB alone) by a factor of 1.5 when comparing assemblies without hold-downs to those with hold-downs. This is related to damage fragilities by multiplying the median damage fragilities obtained from specimens "with hold-downs" by 0.67 at all DSs. This assumption comes from the witnessed increase in displacements from shake table testing conducted by Fischer et al. [2001] as part of the CUREE Woodframe Project. A comparison of the roof displacement histories of the two-story structure with different construction details is shown in Figure 5.3. The figure shows the conventional-to-engineered displacement ratio is 2.49/1.66 = 1.5. Note that the data shown in Figure 5.3 are for walls without exterior stucco, i.e., with only OSB sheathing on the exterior, but Ekiert and Filiatrault imply that the trend between the two also applies to walls with stucco finish.

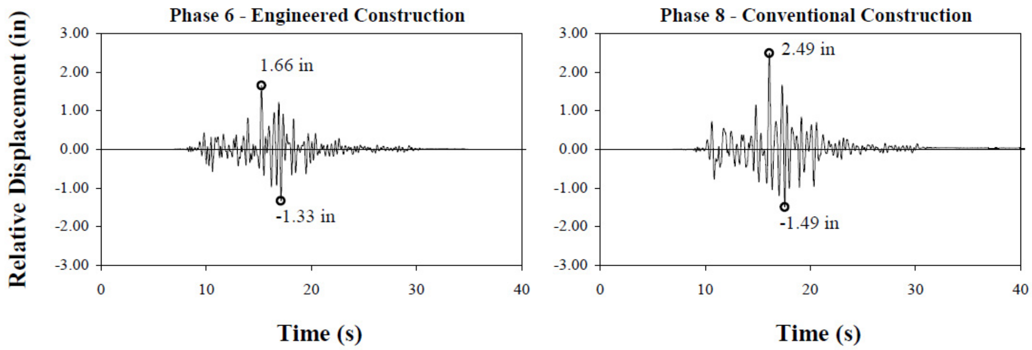

Figure 5.3 Roof displacements of a two-story wood-frame house with OSB exterior from shake table testing by Fischer et al. [2001]: engineered construction with hold-downs (left) and conventional construction (right).

The available stucco test data with damage documentation was reviewed for DS1 and DS2. This includes the cyclic data from the CUREE EDA study [Arnold et al. 2003(a), (b)] and shake table tests conducted by Mosalam et al. [2002] within the CUREE-Caltech Woodframe Project. DS1 data from Mosalam et al. [2002] included only Phase II (first phase with exterior and interior finish) at seismic test level (STL) 3. This phase and test level correspond to the point where reported stucco cracking occurred at all stories in the three-story building. Further, only reported drift values for the east, west, and back sides of the structure at the first story were included in this review, since the open garage front of the first story is not representative of the house variants in this study. Drift ratios for DS1 were taken as the average peak drift at each story and wall line in the positive and negative directions reported by Mosalam et al. [2002]. The values were averaged together to reflect the uncertainty with using drift envelopes from shake table testing combined with general damage descriptions and photographic documentation. Drift values for the CUREE EDA tests [Arnold et al. 2003(a), (b)] were estimated directly from provided photo documentation. Similar information was collected from the CUREE EDA tests for DS2. Notably, two data points were used from Mosalam et al. [2002] from Phase III testing based on descriptions and photo documentation of stucco spalling and more severely distributed stucco cracking for DS2. A summary of the collected data points collected from these tests is included in Appendix B.

Since DS3 represents the replacement threshold for the stucco finish, this damage state cannot be easily estimated from available photographic documentation. The DS3 fragility (replacement) was developed by Ekiert and Filiatrault [2008] for stucco walls with underlying structural sheathing and hold-down devices. This damage state was defined as the drift corresponding to stud fracture and major splitting of the underlying sill plate. This definition of damage is well defined and can be identified and documented from testing observations. The consistency of this damage state is also reflected in the low dispersion (β_r = 0.14) reported by Ekiert and Filiatrault [2008]. The available information for stucco without structural panel sheathing (e.g., no plywood or OSB) in DS3 is based on force-displacement behavior observed from testing of stucco without structural sheathing. Two main assumptions are made to inform decisions on the drift values corresponding to the replacement threshold of the exterior stucco. The first is that the drifts corresponding to peak strength of a specimen represent the lower bound of the replacement threshold. The second is that the drift corresponding to 80% post-peak strength (i.e., 20% strength loss) represents an upper bound of the replacement threshold. These assumptions must be interpreted through what inspection of the stucco is likely to reveal in terms of required repairs. Stucco that has not reached its peak strength is unlikely to have experienced distributed delamination, while stucco significantly beyond its peak strength will likely have numerous cracking and connection issues that would require full replacement, i.e., where local patching infeasible or impractical. Given the wide range of stucco properties that could exist, these measurements were taken from numerous cyclic testing campaigns in terms of specimen layout and boundary conditions from the CUREE Caltech Woodframe Project [Arnold et al. 2003(a), 2003(b); Pardoen et al. 2003] and other studies [COLA 2001; Bahmani and van de Lindt 2016]. The values collected from the various tests are provided in Appendix B.

The collected data for the different damage states of exterior stucco are summarized in Appendix B and assembled into the damage fragility functions in Figure 5.4. Individual tests are shown by points, and the fitted lognormal functions reflect the test-to-test variability (β_r).

The median and dispersion values from the reported data in Figure 5.4 are used as basis for damage fragility functions, taking into account additional factors and judgments. First, the drift values for DS1 and DS2 obtained from the fitted curves in Figure 5.4 were rounded down to the nearest 0.1% values, giving values of 0.2% and 0.5%, respectively. The dispersion values for DS1 and DS2 are then modified to consider additional model uncertainty of $\beta_u = 0.25$, and the resulting values were rounded up to the nearest 0.05. This resulted in assumed total dispersions of 0.45 and 0.40 for DS1 and DS2, respectively. The median drift corresponding to DS3 was taken as the average value between the lower (1.1%) and upper bound (1.9%) definitions from Figure 5.4, resulting in a median value of 1.5% drift. The dispersion for DS3 is assumed to be 0.40, which is the default for judgment-based fragilities within *FEMA P-58*. Based on these modifications, the final fragility functions for exterior stucco are shown in Figure 5.5 with values provided in Table 5.6. The figure illustrates how the assumptions used for DS3 match the upper bound data (drift at 20% strength loss) in the lower tail and the lower bound (drift at peak strength) in the upper tail.

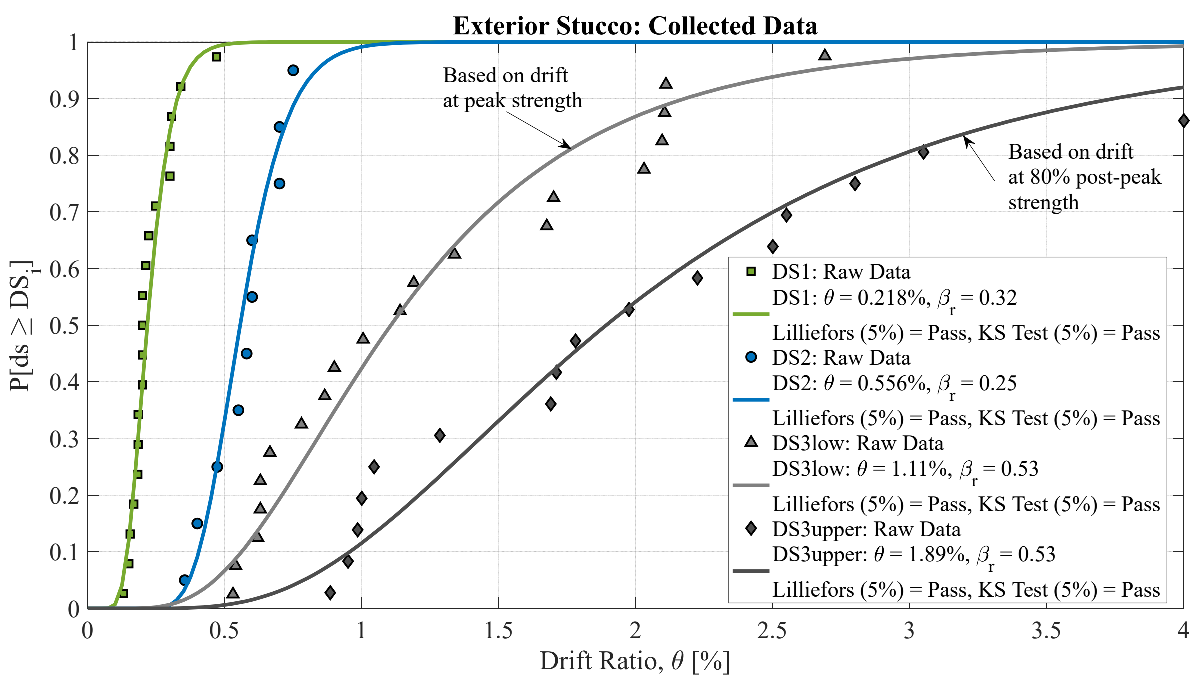

Figure 5.4 Reviewed data for exterior stucco without panelized structural sheathing fragility.

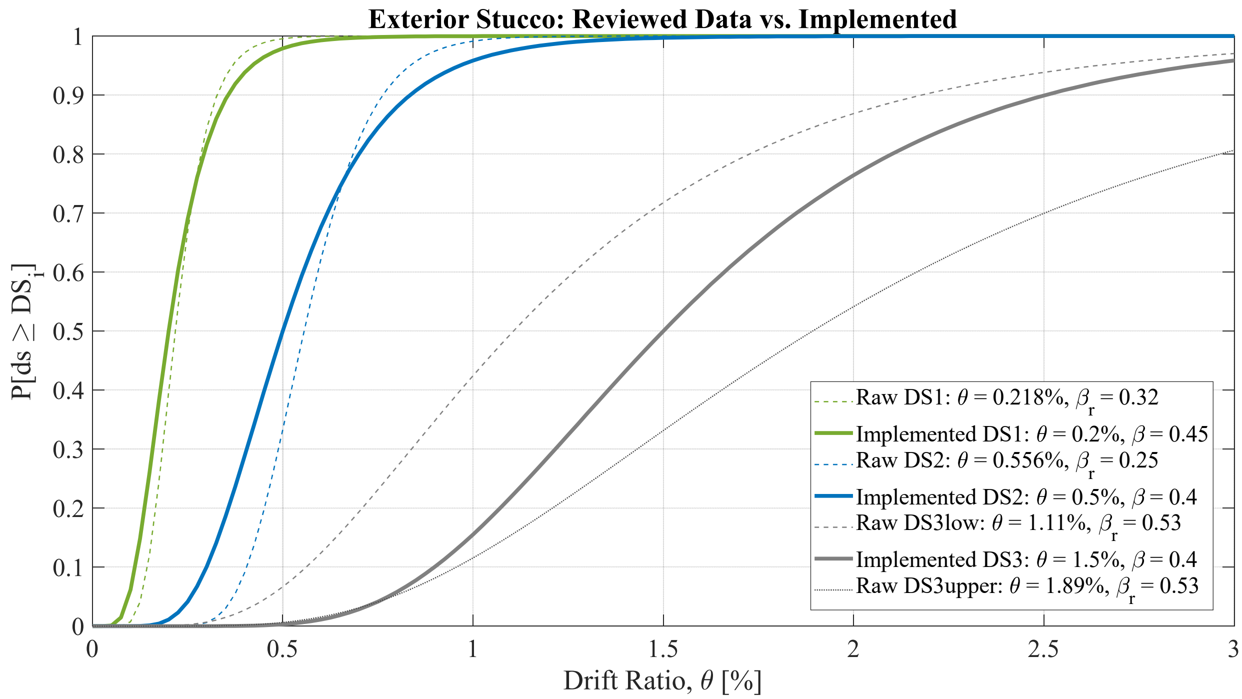

Figure 5.5 Implemented fragility functions for exterior stucco walls (solid lines) compared with reviewed test data (dashed lines).

Table 5.6 Implemented exterior stucco damage fragility functions.

Damage state	Damage description	EDP	Median (θ)	Dispersion (β)
1	Cracking of stucco with cracks between 1/64 in. and 1/8 in. wide. No delamination.	SDR (rad)	0.002	0.45
2	Moderate cracking with minor delamination or spalling. Extensive minor cracking possible. Local delamination can damage waterproofing and lath in damaged area.		0.005	0.40
3	Significant spalling and delamination of stucco. Loosening of framing connections possible.		0.015	0.40

5.3.3 Exterior Horizontal Wood Siding Walls

5.3.3.1 Horizontal Wood Siding and Sheathing with Unknown Bracing

There is very limited information on the seismic fragility of exterior wood walls with horizontal wood siding and wood board sheathing (i.e., straight sheathing). This section develops damage fragility curves for walls with unknown bracing conditions (e.g., no braced framing, cut-in block bracing, let-in bracing, etc.) and without diagonal sheathing behind the horizontal wood siding.

A good discussion and interpretation of the damageability of wood sided walls with straight sheathing is provided within the CAPSS project [ATC 2009; Porter 2009]. The lack of reported damage descriptions for straight-sheathed walls is acknowledged, noting that the only indication of damage is based on the drift corresponding to peak load of tested specimens. Porter [2009] interpreted older FPL testing [Trayer, 1956] and more recent testing conducted by Elkhoraibi and Mosalam [2003a, b] to estimate a median drift of 2.9% corresponding to peak strength.

For exterior walls with horizontal wood siding over horizontal wood sheathing, a simple single DS is assumed representing the likelihood that the wall needs to be completely replaced. The median drift value is assumed to be 3.0% based on Porter [2009]. The fragility dispersion is assumed to be 0.5. This increase from the *FEMA P-58* default of 0.4 was selected to reflect the large uncertainty with actual conditions for this wall material including interaction with doors or windows and the large residual strength behavior of unbraced horizontal sheathing witnessed from recent testing. The assumed fragility is presented in Figure 5.6 with defining parameters provided in Table 5.7.

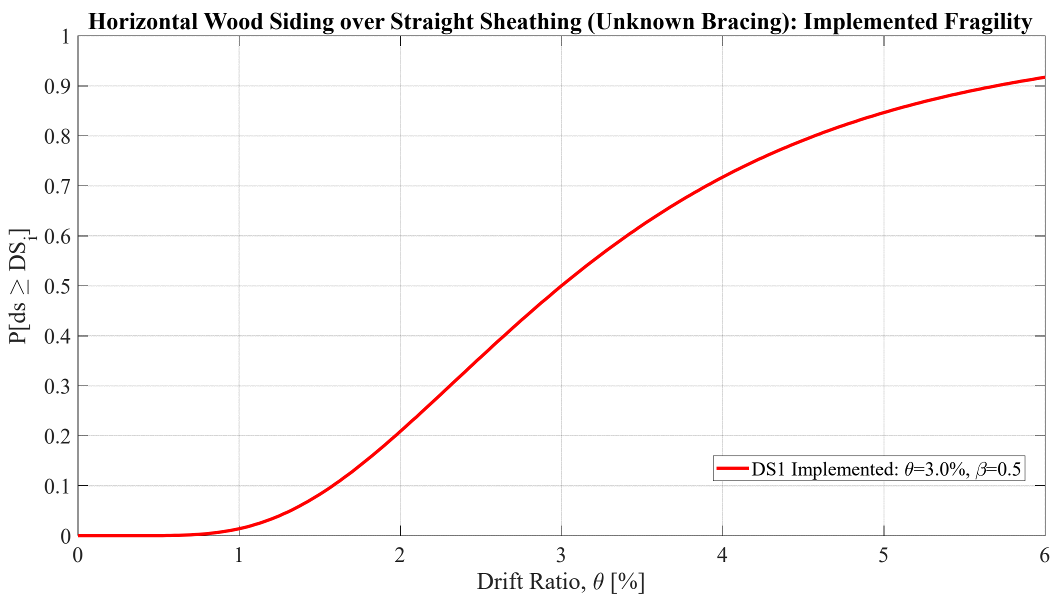

Figure 5.6 **Implemented fragility function representing horizontal wood siding over straight sheathing with unknown bracing.**

Table 5.7 **Implemented fragility function for damage to exterior walls with horizontal wood siding over straight sheathing with unknown bracing.**

Damage state	Damage description	EDP	Median (θ)	Dispersion (β)
1	Damage state reflects the likelihood that the entire exterior of wall will require replacement	Story Drift Ratio (SDR) [rad]	0.030	0.50

5.3.3.2 Horizontal Wood Siding with Braced Framing or Diagonal Sheathing

Tests have been conducted on various types of bracing used within wood framing. Early FPL testing [Trayer, 1956; Erickson, 1958; Tuomi and Gromala, 1977] looked at a range of bracing conditions including cut-in (block), herringbone, and let-in bracing (LIB). However, only a single test by Tuomi and Gromala [1977] provided a backbone curve to understand force-displacement behavior of a let-in brace tested in compression. Currently, the largest source of information on let-in braces comes from testing by the National Home Builders Association [NAHB 2008]. These tests consist of 25 monotonic tests of diagonal let-in bracing of several configurations, including compression only bracing, tension only bracing, coupled tension and compression braces, and specimens with gypsum wallboard. Typical brace angles were 45°.

The available let-in brace tests were used to document the drift ratio corresponding to peak load, which was usually governed by the braces loaded in compression for specimens with coupled tension and compression braces. In general, the peak load was reached at approximately 1% drift for braces in compression. A limited number of tension-only braces were tested (3 tests) that resulted in drift ratios at peak load ranging from 2.9% to 3.7% with an average value of 3.3%. The individual data points and brief test description are provided in Appendix B, and the fitted lognormal statistics for different subsets of bracing tests are summarized in Table 5.8.

Testing on diagonal sheathing was conducted during early monotonic testing by the FPL [Erickson, 1940; Trayer, 1956]. Notably, these tests do not provide explicit force-displacement behavior, yet the *FEMA P-807* document interpreted these tests to propose material backbones for diagonal sheathing and assumed an average peak strength (per linear foot of wall) of 913 lb/ft at a drift ratio of 1.5% [FEMA 2012d]. More recent tests by Ni and Karabeyli [2007] provide a good source of high-resolution diagonal sheathing testing, including monotonic and cyclic testing of various diagonal sheathing configurations. Additionally, Bahmani and van de Lindt [2016] conducted two tests combining horizontal wood siding, diagonal sheathing, and gypsum wallboard as a part of an investigation on combination of material properties. Tests conducted by Ni and Karacabeyli [2007] and another test HDG-02 by Bahmani and van de Lindt [2016] indicated that the average drift at peak load was approximately 2.0%, including data from all specimens and drift measurements from both positive and negative loading directions. The data were separated between cases with the sheathing boards loaded in tension with (e.g., gaps between boards closing at increased displacements) and compression (e.g., gaps between boards opening with increasing displacement). The data from these tests are summarized in Appendix B. Loading in the tension direction provides larger peak strength with average drift values of approximately 2.2%. Panels loaded in the compression direction are weaker, where the peak strength is reached at slightly smaller drifts of about 1.8%, on average. Lognormal fragility functions parameters fit to these diagonal sheathing tests are provided in Table 5.9. Interestingly, the test dispersion values (β_r) for the panels loaded in compression are significantly higher than those loaded in tension. This highlights that as the panels separate, there is more uncertainty in how the sub-assembly specimen will respond since the sheathing boards cannot bear on one another as displacements increase.

After reviewing the limited information on let-in bracing and diagonal sheathing behavior, a single damage state fragility function is proposed, representing the likelihood the wall will need to be replaced. The proposed fragility has a median drift ratio of 1.5% and a dispersion of 0.5 as shown in Figure 5.7.

Table 5.8 **Summary of different sub-sets of let-in bracing fragilities from testing by Tuomi and Gromala [1977] and NAHB [2008]. Values correspond to drifts (%) at peak load.**

	All data	No gypsum wallboard	No tension only	No tension-only or gypsum wallboard	Tension only[1]	Compression only[1]	Tension or compression only[1]	Tension + compression only (coupled)[2]
Npts	26	12	23	5	3	5	8	18
θ (%)	1.20	1.31	1.06	1.04	3.26	1.04	1.60	1.06
β_r	0.45	0.60	0.28	0.35	0.13	0.35	0.65	0.27
β_u	0.25	0.25	0.25	0.25	0.25	0.25	0.25	0.25
β	0.52	0.65	0.38	0.43	0.28	0.43	0.70	0.37

[1] Tests are for single diagonal braces.
[2] Tests have dual braces within the specimen with opposite brace orientations.

Table 5.9 **Summary of different sub-sets of diagonal sheathing fragility fits from testing by Ni and Karacabeyli [2007] and Bahmani and van de Lindt [2016]. Values correspond to drifts (%) at peak load.**

	All data	Boards in tension (*T*)[1]	Boards in compression (C)[2]	Average of *T* and *C*
Npts	22	11	11	11
θ [%]	1.95	2.15	1.77	1.98
β_r	0.31	0.21	0.37	0.24
β_u	0.25	0.25	0.25	0.25
β	0.40	0.33	0.45	0.35

[1] Sheathing boards are loaded in the direction causing tension based on strut action with gaps between boards closing.
Sheathing boards are loaded in the direction causing compression based on strut action with gaps between boards opening.

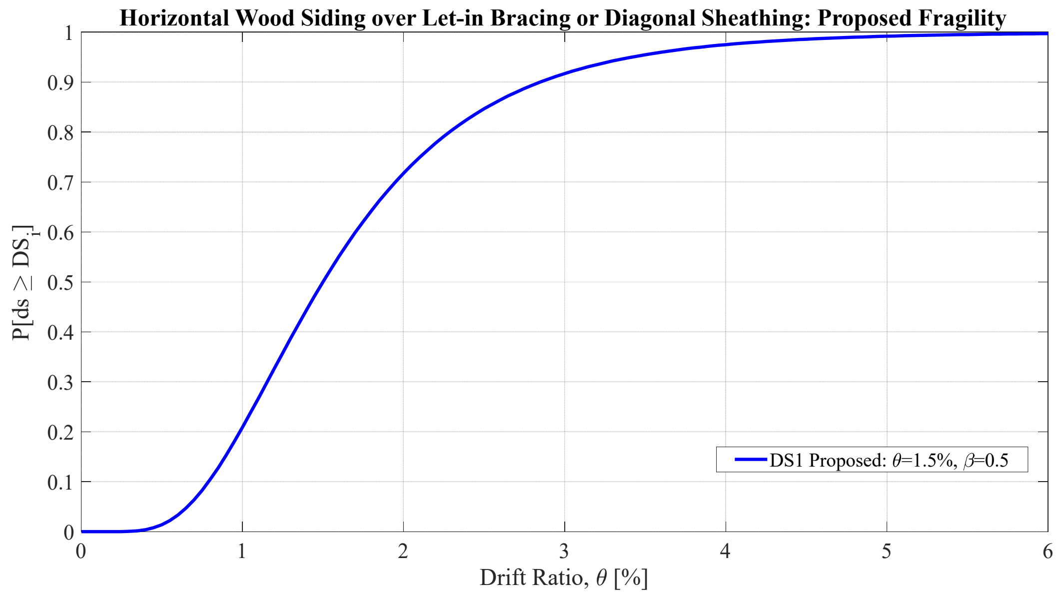

Figure 5.7 **Proposed fragility function representing the likelihood of exterior wall replacement for horizontal wood siding over diagonal let-in bracing or diagonal sheathing.**

It should be emphasized that the fragility function for exterior walls with let-in or diagonal bracing, shown in Figure 5.7, is largely based on judgment, similar to the fragility for horizontal siding over straight sheathing with unknown bracing that was discussed previously. For let-in bracing, the force-displacement behavior is governed by the capacity of the brace loaded in compression. The reviewed data for let-in bracing shows that the peak capacity of these braces is reached at approximately 1% drift. The proposed median of 1.5% drift is chosen considering that the compression brace should fail before 50% (e.g., median) of the wall unit is expected to need replacement. Further, the proposed fragility considers that when the capacity of braces loaded in tension is reached (at approximately 3% drift) there is a significant probability (e.g., >90%) that the wall line will require replacement.

Similar justification is provided for walls with diagonal sheathing. The condition of a diagonally sheathed wall will be controlled by the compression loading direction (e.g., with boards separating with increasing displacement) at the lower bound, where the median drift of 1.5% is chosen to be less than the measured mean drift at peak load of 1.8% to reflect uncertainty of the damage behavior for real conditions. The large dispersion of 0.5 also reflects this uncertainty, where interactions of diagonal sheathing boards with window and door openings in either loading direction is not well understood in terms of damage accumulation.

5.3.4 Panelized Wood Siding (T1-11)

Building variants for the 1956-1970 construction era include panelized plywood siding, commonly referred to as T1-11 siding. T1-11 siding is typically installed with 8d (or 6d in some cases) galvanized nails at a spacing of 6 or 12 in. for edge and field nailing, respectively. Although T1-11 siding can be used for shear wall design if properly nailed and installed [APA 1999], for the era considered, it is commonly installed with only one vertical edge nailed (e.g., on underlying tab at vertical joints). The T1-11 assumed for building variants within the project assumes this type of detailing to be representative for the construction era considered (i.e., 1956–1970). More discussion of T1-11 details is provided by Cobeen et al. [2020].

Given the lack of information available on the damageability of T1-11 plywood siding, the fragility functions proposed by Ekiert and Filiatrault [2008] for OSB sheathed walls without hold-down devices is assumed. This set of fragilities correspond to assembly B1071.001 that was introduced in Table 5.1 when discussing the existing functions within the *FEMA P-58* database. The fragility functions consist of three damage states: DS1 corresponds to light damage from loosening of nails induced by panel rotation; D2 includes nail tear through and the onset of separation of sheathing panels from framing; and DS3 represents the replacement threshold and includes distributed separation of sheathing and framing connections, panel damage at locations of fasteners and damage to the sill plate and wall framing. The assumed fragility functions for T1-11 siding are shown in Figure 5.8 with defining parameters provided in Table 5.10.

The fragilities developed by Ekiert and Filiatrault [2008] for OSB walls without hold-down devices were based on experimental sub-assembly data incorporating hold-downs, where the median values from the tests were scaled down by a factor of 0.67 (i.e., reducing median at all damage states). The 0.67 reduction factor is based on the observed difference in roof displacements between engineered construction (i.e., with hold-downs) and conventional construction (i.e., no hold-downs) from shake table tests conducted by Fischer et al. [2001] (see Figure 5.3). A constant dispersion value of 0.4 is applied to all damage states to include the larger uncertainty associated with conventional construction details that are not directly supported by experimental sub-assembly testing.

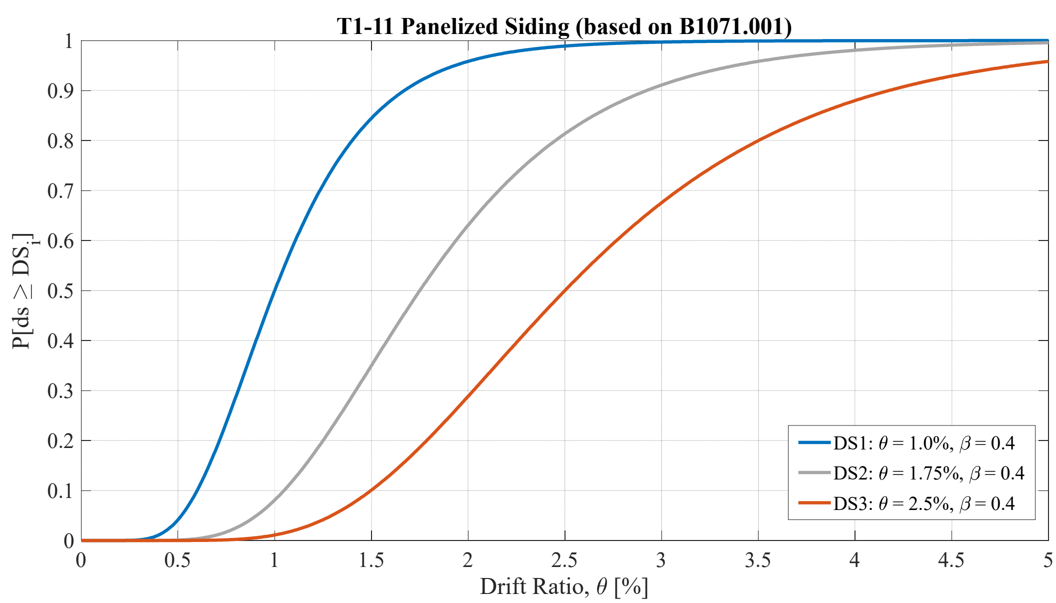

Figure 5.8 **Implemented fragility function for T1-11 panelized wood siding (based on B1071.001 fragility within *FEMA P-58* for OSB sheathed walls without hold-down devices).**

Table 5.10 Implemented panelized T1-11 siding fragility functions.

Damage state	Damage description	EDP	Median (θ)	Dispersion (β)
1	Loosening of nails due to panel rotation	SDR (rad)	0.010	0.40
2	Nail tear-through. Onset of panel separation from framing and uplift of studs and sill plates		0.0175	0.40
3	Delamination of panel from framing. Panel damage near openings and at fastener locations. Damage to framing connections, sill plates and studs.		0.025	0.40

* Note: this set of fragilities is take directly from assembly type B1071.001 from *FEMA P-58*. Damage state descriptions are modified slightly based on recent testing by Cobeen et al. [2020]

5.3.5 Plaster on Wood Lath Interior

Plaster on wood lath interior is a common interior material for older wood-frame homes. Despite its relevance to older construction eras of wood-frame structures, available information on the damage progression of plaster on wood lath is extremely limited within the literature. The work of Porter [2009] within the CAPSS Project [ATC 2009] provides valuable interpretation of older FPL testing [Trayer, 1956] and *in situ* testing by Schmid [1984]. Three damage states were proposed that are similar to those for gypsum wallboard fragilities: DS1 represents minor cracking around window and door openings; DS2 assumes large cracks at openings and the extension of cracks across solid panel areas; and DS3, which is based on the ultimate strength observed from previous testing, corresponds to an abrupt loss of strength where demolition and replacement is the expected level of repair. The median drift values proposed by Porter [2009] are 0.073%, 0.36%, and 1.5% drift, respectively. Since the work of the CAPSS project involved a HAZUS-type assessment, these damage states were combined to describe global damage states with other materials and a large lognormal dispersion of 1.0 was applied to each.

The current PEER–CEA study has included applicable data from tests that have been conducted since the development of the CAPSS fragilities. These tests include the cyclic testing conducted by Carroll [2006], specifically tests conducted on Specimens 1, 3, and 17. The testing by Carroll [2006] is used only to estimate DS1 and DS3. Damage State 1 was estimated by taking the average drift corresponding to the first loss of stiffness in the reported envelope curves (Figure 4.9 in Carroll [2006]) and the assumed equivalent yield displacement using an equal energy elastic perfectly plastic approximation. This was done to estimate when the onset of damage to plaster keys and cracking is likely to have occurred in lieu of explicit damage descriptions. Damage State 3 was approximated as the average drift at peak strength of each specimen in the positive and negative loading directions.

Additionally, the recent PEER–CEA large-component test C-1 [Cobeen et al. 2020] has allowed for photographic documentation of the damage progression of plaster on wood lath. The initial exceedance of DS1 for test C-1 is assumed to occur at a drift level of 0.15%. This is based on the witnessed (first author present for test) distributed cracking and spalling from the first excursions to 0.2% drift. The images in Figure 5.9 illustrate the cracking damage that occurred at the first loading excursion to 0.2% drift at window 1. This highlights the brittleness of plaster on wood lath and supports previous efforts to estimate the onset of cracking damage. Similarly in

Figure 5.10, the window on the opposite side of the specimen (window 2), showed a significant crack upon the first excursion to 0.2% drift [Figure 5.10(a)] and exhibited plaster bulging and new crack formation when the load direction was reversed; see Figure 5.10(b).

a) b)

Figure 5.9 **Cracking and minor spalling of lath and plaster near the corners of window 1 at first excursion to 0.2% drift: (a) lower left corner of window 1; and (b) lower right of window 1 (PEER–CEA Test C-1; Cobeen et al. [2020]).**

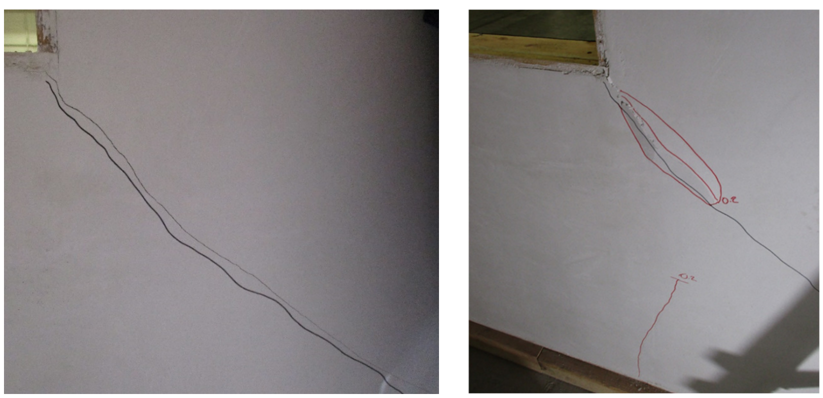

a) b)

Figure 5.10 **Lath and plaster damage of the bottom corner of window 2 at 0.2% drift: (a) first excursion to 0.2% drift; and (b) reversal of load direction to 0.2% drift (PEER–CEA Test C-1; Cobeen et al. [2020]).**

The drift corresponding to DS2 for test C-1 is estimated to be approximately 0.45%. This is supported by the photographic documentation at 0.4% drift and 0.6% drift. Figure 5.11 illustrates some of the observed damage at 0.4% drift, where concentrated cracks and plaster spalling near window corners is observed. An illustration of observed lath and plaster damage at 0.6% drift is shown in Figure 5.12. When interpreting the results of the test, it is assumed that the onset of DS2 repairs would require cutting back sections of plaster for local replacement near 0.4% drift. The damage at 0.6% drift is estimated to be well beyond the DS2 threshold. Accordingly, the drift of 0.45% drift is judged to be representative of the threshold for DS2.

Test C-1: 0.4% drift
Plaster spalling on floor

Test C-1: 0.4% drift
Widespread cracking and corner spalling around window 1

Test C-1: 0.4% drift
Damage around Window 2

Figure 5.11 Different locations of lath and plaster damage at a drift ratio of 0.4% for PEER–CEA large-component test C-1 [Cobeen et al. 2020].

Test C-1: 0.6% drift
Lath exposed above door

Test C-1: 0.6% drift
Extension of full depth crack and new bulging toward floor

Test C-1: 0.6% drift
Widespread cracking around corner

Figure 5.12 Different locations of lath and plaster damage at a drift ratio of 0.6% for PEER–CEA large-component test C-1 [Cobeen et al. 2020].

The drift ratio corresponding to DS3 representing the replacement threshold is estimated to be 1.1%. This is based on the drift corresponding to peak load in both directions during the cyclic testing, along with photographs of the test. The observed damage for Specimen C-1 at 0.8% drift incudes the onset of out-of-plane bulging and localized delamination of the plaster; see Figure 5.13. The next cyclic excursions were out to 1.4% drift, which was accompanied by widespread delamination of the plaster and spalling of plaster sections between the positive and negative excursions, as shown in Figure 5.14.

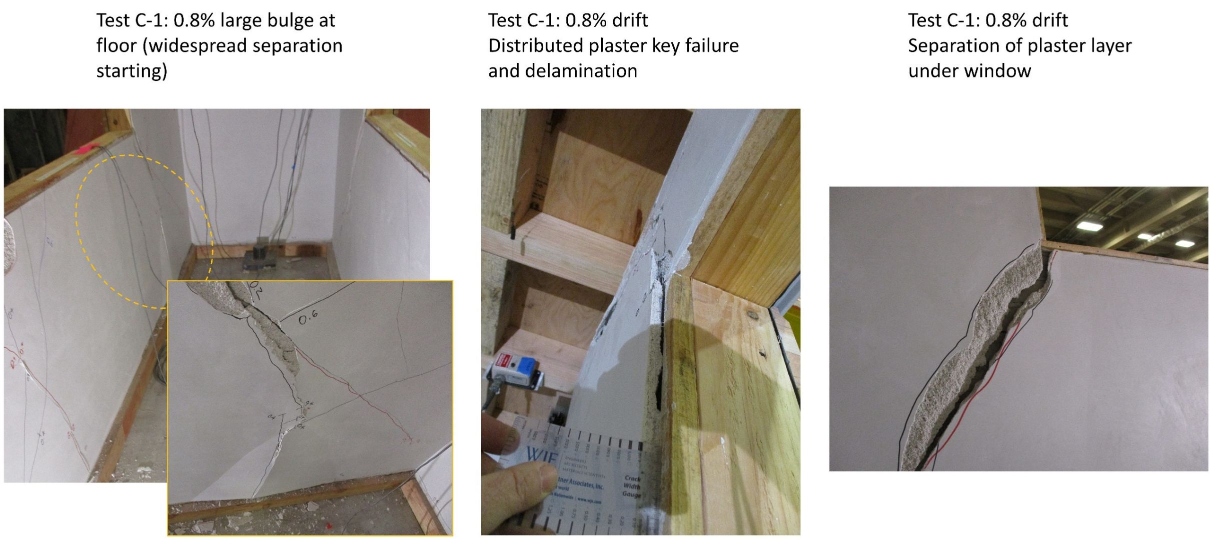

Figure 5.13 **Different locations of lath and plaster damage at a drift ratio of 0.8% for PEER–CEA large-component test C-1 [Cobeen et al. 2020].**

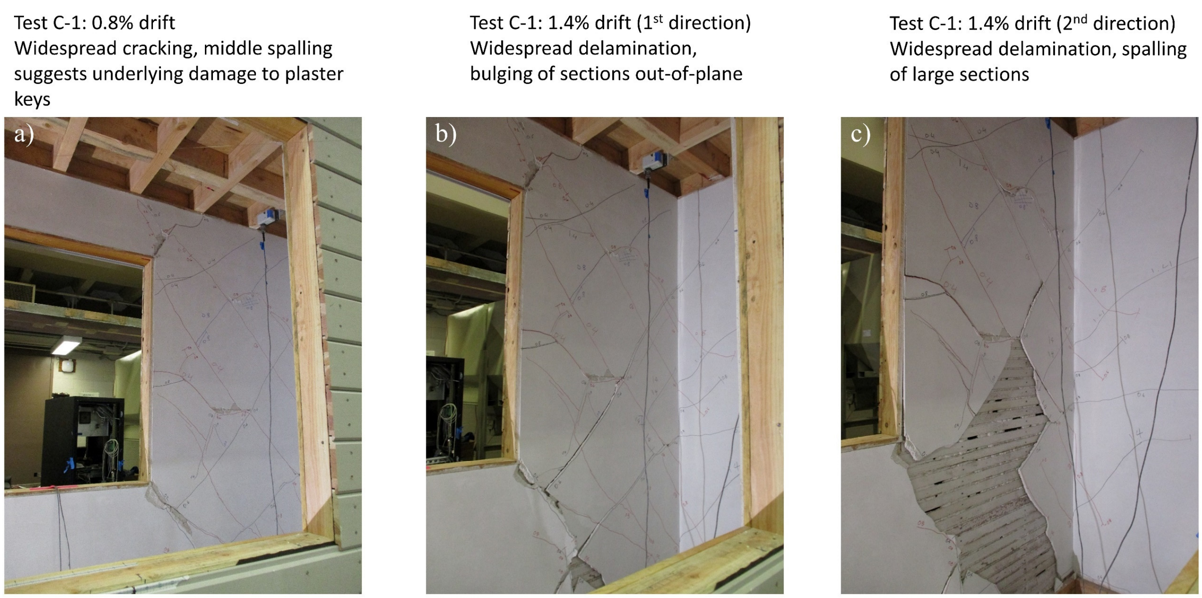

Figure 5.14 **Photos of significant lath and plaster damage at a drift ratios of 0.8% (a) and 1.4% (b, c) for PEER–CEA large-component test C-1 [Cobeen et al. 2020].**

The collection of all considered fragility data for plaster on wood lath is summarized in Table 5.11. The fitted lognormal fragility functions for each damage state are shown in Figure 5.15, reflecting only the test-to-test variability (β_r). The final median fragility values were estimated to be 0.13%, 0.45%, and 1.1% for the three sequential damage states, respectively. The final dispersion value for DS1 was assumed to be 0.55 based on the reviewed data considering additional uncertainty (β_u) of 0.1. This value reflects the already large test-to-test variability observed (i.e., $\beta_r = 0.53$) for DS1. The dispersion for DS2 and DS3 assumes the *FEMA P-58* default value of 0.4 for judgment-based fragilities. This value considers the few data points available for estimating DS2 as well as the difficulty in defining this damage state. The default dispersion of 0.4 is deemed appropriate for DS3 since global force-displacement behavior was used to estimate this damage state. The fragility functions implemented for wood lath and plaster are compared with those assumed for gypsum wallboard in Figure 5.16. This comparison between the two sets of fragilities illustrates that lath and plaster (solid lines) is more brittle than gypsum wallboard (dashed lines). Fragility parameters for the plaster on wood lath fragilities are summarized in Table 5.12.

Table 5.11 Collected damage fragility information for wood lath and plaster. Data is expressed as drift ratio related to damage state.

Study/Test	Description	DS1 (%)	DS2 (%)	DS3 (%)
Trayer [1956] - 12 [1]	Window and door openings	0.057	N/A	0.69
Trayer [1956] - 15	Window and door openings	0.093	N/A	1.39
Trayer [1956] - 11	Solid wall without openings	N/A	0.37	N/A
Trayer [1956] - 13&24	Solid wall without openings	N/A	0.56	N/A
Schmid [1984] - $W1_{pos}$ [1]	*In situ* lath and plaster w/o openings	N/A	0.46	1.62
Schmid [1984] - $W1_{neg}$	*In situ* lath and plaster w/o openings	N/A	0.42	N/A
Schmid [1984] - $W2_{pos}$	*In situ* lath and plaster w/o openings; existing crack	0.26	N/A	1.35
Schmid [1984] - $W2_{neg}$	*In situ* lath and plastic w/o openings; existing crack	0.20	N/A	N/A
PEER–CEA Test C-1[2]	Lath and plaster with openings	0.15	0.45	1.10
Carroll [2006] - 1	7'-5"x4' LP wall (CUREE protocol)	0.079	N/A	1.24
Carroll [2006] - 3	7'x4' LP wall (CUREE protocol)	0.099	N/A	0.67
Carroll [2006] - 17	6'x4' LP wall (CUREE protocol)	0.196	N/A	1.32

[1] Quantification of drift limits based on limited force-displacement data and reported damage.
[2] See Cobeen et al. [2020] for details.

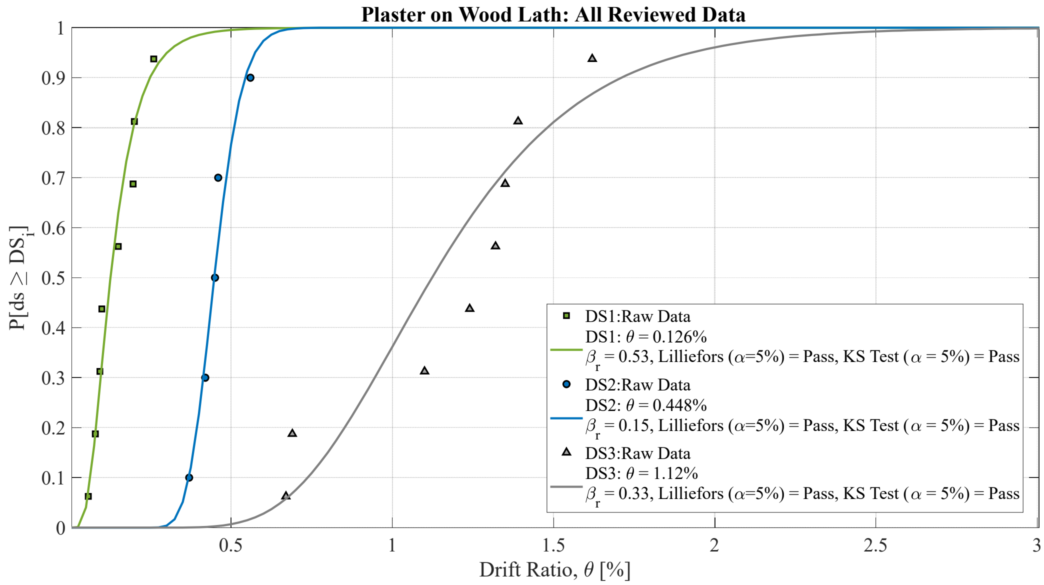

Figure 5.15 Reviewed interior plaster on wood lath fragility data.

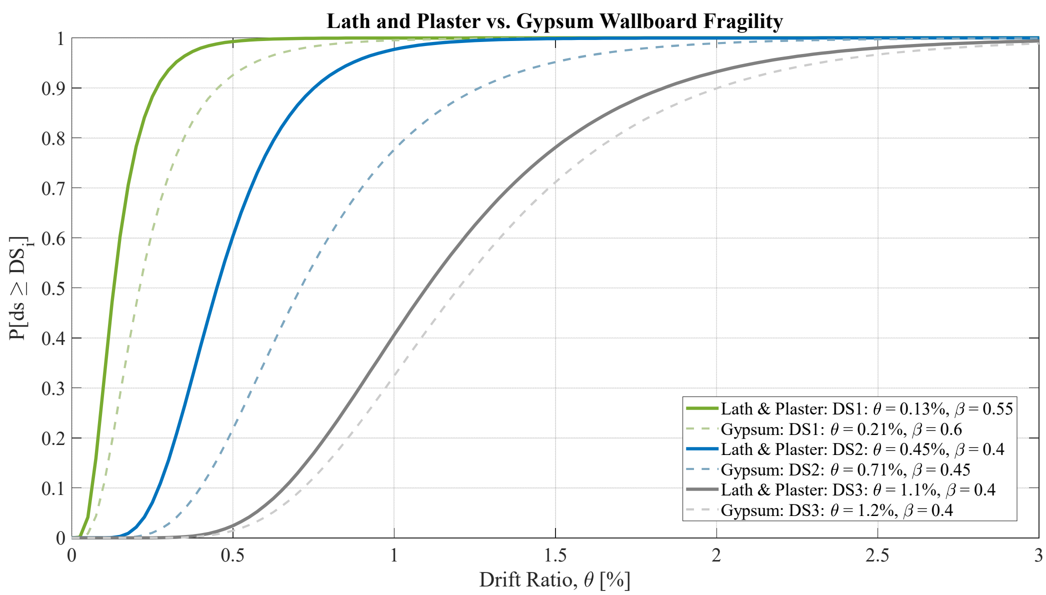

Figure 5.16 Comparison of implemented damage fragilities for plaster on wood lath (solid lines) and gypsum wallboard (dashed lines).

Table 5.12 Implemented plaster on wood lath damage fragility functions.

Damage state	Damage description	EDP	Median (θ)	Dispersion (β)
1	Cracking of plaster at corners of openings and wall intersections	SDR (rad)	0.0013	0.55
2	Significant cracking and spalling of plaster at corners of openings. Widespread minor cracking in continous sections of plaster. Local removal and repairs are still economical.		0.0045	0.40
3	Widespread damage of plaster finish including bulging out of plane and delamination. Repairs require removal of plaster and lath, furring of framing and repalcement with modern drywall.		0.0110	0.40

5.4 DAMAGE FRAGILITIES FOR OLDER WOOD-FRAME STRUCTURES: CRAWLSPACE MATERIALS

5.4.1 Fragility Adjustments for Cripple Walls

The damageability of exterior and interior finishes in wood-frame structures is commonly associated with SDR to relate building response to damage. An important difference between the damageability of shorter cripple walls compared to full-height walls is the difference in displacement demands associated with SDR of a full-height story in a house (8 to 9 ft) and a short cripple wall (typically 2 to 4 ft tall). Based on the structural behavior of different types of wall materials, the damage to horizontal siding materials is assumed to scale uniformly with height, while a height dependent relationship is used for other materials. This is shown in Figure 5.17, where comparing full-height (e.g., 8-ft-tall) versus short (e.g., 2-ft-tall) stucco walls at a given unit displacement at the top of the wall, the corresponding drift behavior varies significantly (i.e., $\theta_{8\text{ft}} \neq \theta_{2\text{ft}}$). Stucco is a good example of this since the peak force is typically controlled by the connection of the stucco to the sill plate [see Figure 5.17(a)] where, assuming similar fastener displacement capacity, the shorter cripple wall would have a significantly larger SDR (i.e., top displacement divided by height) than the full-height 8-ft wall for a given wall displacement. On the other hand, for wood siding, the local deformations scale with drift ratio for different height walls (i.e., $\theta_{8\text{ft}} = \theta_{2\text{ft}}$).

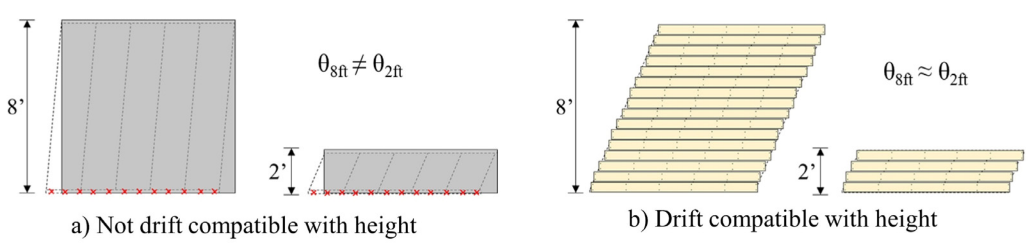

Figure 5.17 Illustration of different materials having different drift compatibilities with varying height: (a) material without drift compatibility (stucco); and (b) material with drift compatibility (horizontal wood siding or sheathing).

The *FEMA P-807* guidelines [2012(d)] use an adjustment factor for accommodating different height walls in the first story. The relationship between the drift at ultimate strength between a full height (i.e., 8-ft-tall) wall and a shorter wall is assumed to be related by the height ratio raised to an exponent of 0.7. This relationship is based on existing full height test data and cripple walls tested by Chai et al. [2002] within the CUREE-Caltech wood-frame project. The tests considered were 2-ft- and 4-ft-level cripple walls with OSB only or a combination of stucco and OSB. For cripple wall materials, other than horizontal wood siding, with a height less than eight feet, the superstructure fragility curves are assumed to have a median SDR value scaled by the height dependent relationship shown in Equation (5.2):

$$F_{CW} \approx (8/\mathrm{h_{CW}})^{0.7} \tag{5.2}$$

where F_{CW} is the cripple wall fragility factor and h_{CW} is the height of the cripple wall expressed in feet. This factor is applied to determine median values for cripple wall damage fragilities from the median drift values of the exterior superstructure material fragilities for exterior stucco and T1-11 siding presented in Section 5.3. The use of this adjustment factor is discussed for different materials in the following sub-sections.

5.4.2 Stucco Cripple Walls

The experimental testing conducted by WG4 as part of the PEER–CEA Project [Cobeen et al. 2020; Schiller and Hutchinson 2020] included a large number of 2-ft-tall cripple wall specimens. Data from a sub-set of ten of these specimens representing existing conditions (i.e., unretrofitted) were reviewed for fragility analysis. These specimens were reviewed for the three damage states previously defined for superstructure walls in Section 5.3.2. The first two damage states were estimated using photographic documentation. The third damage state, targeting the replacement threshold of the stucco, considered observations from photographic documentation as well as monitoring the force-displacement response of the test data. The median value for DS3, was based on drift values corresponding to the 80% post-peak strength, averaged between the two loading directions.

An example of photographic documentation to estimate drift levels at each stucco damage state are shown for PEER–CEA large-component Specimen AL-1 [Cobeen et al. 2020] in Figure 5.18. The figure illustrates how different photographs are provided to estimate the drift corresponding to each damage state.

Using photo documentation, drift ratios of 0.7%, 1.7% and 3.5% are defined for the three sequential damage states in this specimen. Additionally, the average drift ratio corresponding to 80% post-peak strength was determined to be 3.2%. This process was conducted for the ten specimens presented in Table 5.13, where the drift values for DS3 estimated from observed damage from photo documentation and force-displacement behavior are labeled $\mathrm{DS3_{Obs}}$ and $\mathrm{DS3_{80\%}}$, respectively. Each of the test specimens are described and discussed in detail within the PEER–CEA WG4 reports [Cobeen et al. 2020; Schiller and Hutchinson 2020]. The drift ratios (percentages) in Table 5.13 are based on the relative displacement between the top of the cripple wall and bottom sill plate. This measurement excludes the slip between the sill plate and foundation that was observed in many of the specimens. The observed damage was first documented from experimental photo collections based on the reported target global drift, and then the associated cripple wall drift ratios were verified using displacements at the top and bottom of the wall to remove any slip of the sill plate. The largest observed slip values were on the order of 0.25 in. which translates into 1% apparent drift for a short 2-ft-tall cripple wall. The drift values corresponding to 80% post-peak strength (e.g., $DS3_{80\%}$ in Table 5.13) are also based on the relative cripple wall drift displacements, excluding sill plate slip.

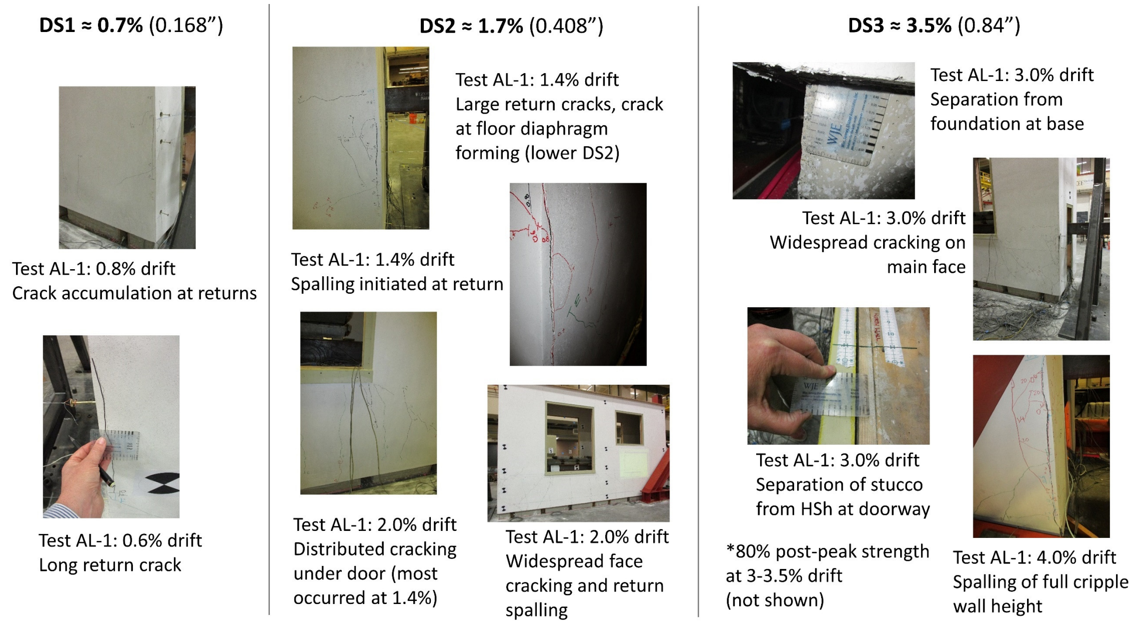

Figure 5.18 **Example of using photographic documentation and experimental results from testing to estimate damage states for the 2-ft-tall unretrofitted stucco cripple wall Specimen AL-1 (photographs courtesy of Kelly Cobeen).**

Table 5.13 Collected damage fragility information for 2-ft-tall stucco cripple walls. Data is expressed as drift ratio related to damage state.

Test [1]	Description [2]	DS1 (%)	DS2 (%)	$DS3_{Obs}$[3] (%)	$DS3_{80\%}$[3] (%)
A-1	Stucco+HSh; free edge boundary conditions	N/A	N/A	6.0	5.2
A-2	Stucco+HSh; small returns, stucco outboard of foundation; HSh bearing on foundation	0.7	2.4	6.0	4.4
A-3	Stucco+HSh; 2ft returns; HSh bearing on foundation	0.7	3.3	5.5	3.0
A-4	Stucco+HSh; small returns; Stucco/HSh bearing	0.9	3.0	6.5	6.5
A-6	Stucco+HSh; wet-set sill; stucco bearing on foundation; small returns	0.7	3.5	6.5	6.5
AL-1	Stucco+HSh; large component, stucco extension to footing with good bond; full returns	0.7	1.7	3.5	3.2
A-17	Stucco Only; stucco extension (poor bond); small returns	0.4	1.7	3.8	2.3
A-22	Stucco Only; no extension; small returns	0.4	0.7	2.7	4.2
A-20	Stucco+HSh; Stucco extension (poor bond); sheathing outboard	0.5	2.0	4.5	4.0
A-21	Stucco+HSh; wet-set sill; stucco extension (poor bond); sheathing bearing; stucco outboard	0.8	3.0	6.0	2.0

[1] All tests are from cyclic loading conducted by WG4 as part of the PEER–CEA Project.
[2] Stucco + HSh = stucco over horizontal wood sheathing (HSh), All specimens are 2 ft tall × 12 ft long except large-component Specimen AL-1, which is double sided with two 2-ft-tall × 20-ft-long walls.
[3] $DS3_{Obs}$ represents drifts estimated using photo documentation, $DS3_{80\%}$ is the average drift (of two directions) corresponding to 80% of post-peak strength using experimental force-displacement data.

The collected fragility data for 2-ft-tall stucco cripple walls (Table 5.13) was used to create the fitted fragility functions shown in Figure 5.19 including only test variability (β_r). Two important observations can be made from Figure 5.19. Firstly, the data for DS2 has much larger test-to-test variability than other damage states. This reflects the difficulty in estimating this damage state, which is associated with stucco spalling and significant cracking, since only the end corners of the specimen created stress concentrations in the stucco with visible spalling (noting that the test specimens did not include vents or access openings). Identification of this damage state in the cripple wall is more difficult than for full-height walls with openings, where the corners of each opening typically provide a location for cracks to develop into spalled areas. Similarly, the two definitions of DS3, representing the replacement threshold, result in significantly different results, where drift values from observed damage ($DS3_{Obs}$; dashed gray line in Figure 5.19) are much larger than those estimated using the 80% post-peak drift ratio ($DS3_{80\%}$; solid gray line in Figure 5.19). This highlights that photographs alone do not capture the actual conditions of the stucco and fastener connections along the main face of the cripple wall specimens, where the measured loss in peak strength undoubtedly indicates that the connection conditions have been degraded.

Figure 5.20 compares damage fragilities fit to the collected 2-ft-tall stucco cripple wall data (dashed lines, corresponding to plots from Figure 5.19) with solid line curves obtained by modifying the full-height stucco fragility curves (previously defined in Table 5.6) using Equation (5.2). The figure shows that the DS1 fragilities are in good agreement. The comparison for DS2 shows a much larger deviation, with the full-height adjustment values having median difference of nearly 1% drift (e.g., 0.25 in. of displacement for a 2-ft-tall cripple wall). This is attributed to the difficulty in estimating this damage state. The lower value of the solid line is assumed reasonable given that this damage state is likely to be observed sooner than observed in the cripple wall tests in real houses at locations of vent and access openings, where cracks and local spalling would likely develop. The height-adjusted fragility for DS3 matches very well with the data collected for 80% post-peak strength, which is considered more reliable than the photographic observations. Thus, it is proposed to use the height adjusted fragility curves (solid lines in Figure 5.20) for the cripple walls.

The available test information for 6-ft-tall stucco cripple walls is much more limited; however, it is possible to make a comparison between the height-adjustment relationship and observed damage. PEER–CEA small-component Specimen A-25 is a 6-ft-tall × 12-ft-long unretrofitted stucco cripple wall without horizontal sheathing [Schiller and Hutchinson 2020(c)]. The observed damage for Specimen A-25 is shown in Figure 5.21 with both the global and relative drift values attributed to each damage photo annotated. Notably, the 80% post-peak drift was estimated from force-displacement response to be approximately 1.4% drift for Specimen A-25.

The proposed cripple wall damage fragility functions obtained from the height adjustment to the full-height wall fragilities is further substantiated by comparisons to data obtained from the 6-ft-tall cripple wall test. A simple comparison of the proposed height-adjusted relationship for 6-ft-tall stucco cripple walls and the discrete observations from Specimen A-25 is shown in Figure 5.22. In this figure, the discrete observation points from Specimen A-25 are plotted along the continuous fragility functions for comparison purposes only. The comparison shows that the fragility curve median values for DS1 and DS2 are slightly less, but reasonable, relative to the Specimen A-25 observations. On the other hand, the fragility curve median for DS3 is slightly higher but close to the Specimen A-25 observation. Overall, considering the sparsity of data, the observations for the 6-ft-tall stucco cripple walls are considered to agree well with the proposed fragility functions. Fragility parameters defining the fragility functions for stucco cripple walls using the height-adjustment relationship are shown in comparison with full-height walls in Table 5.14.

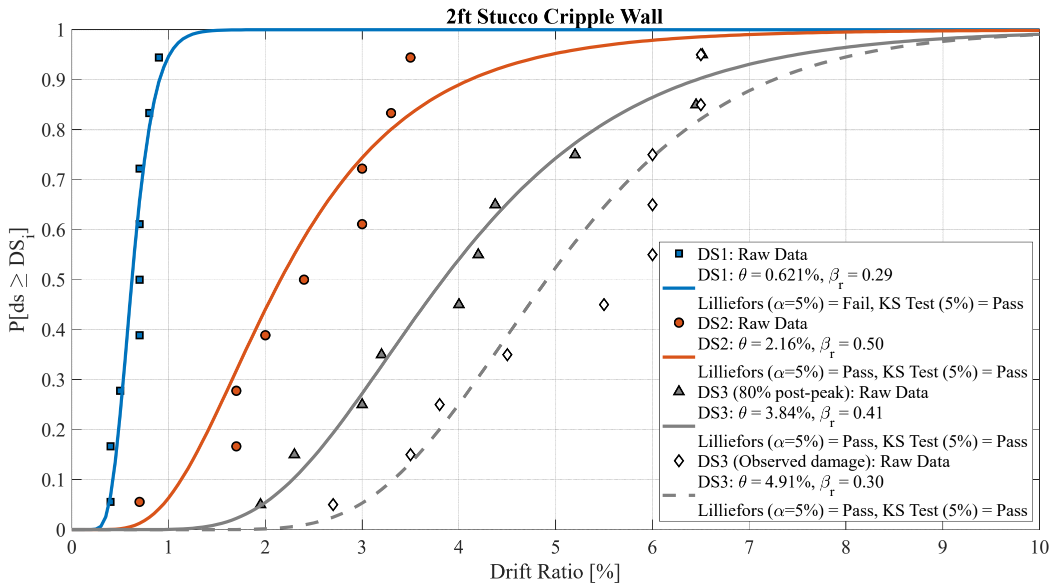

Figure 5.19 Collected fragility data for 2-ft-tall stucco cripple walls.

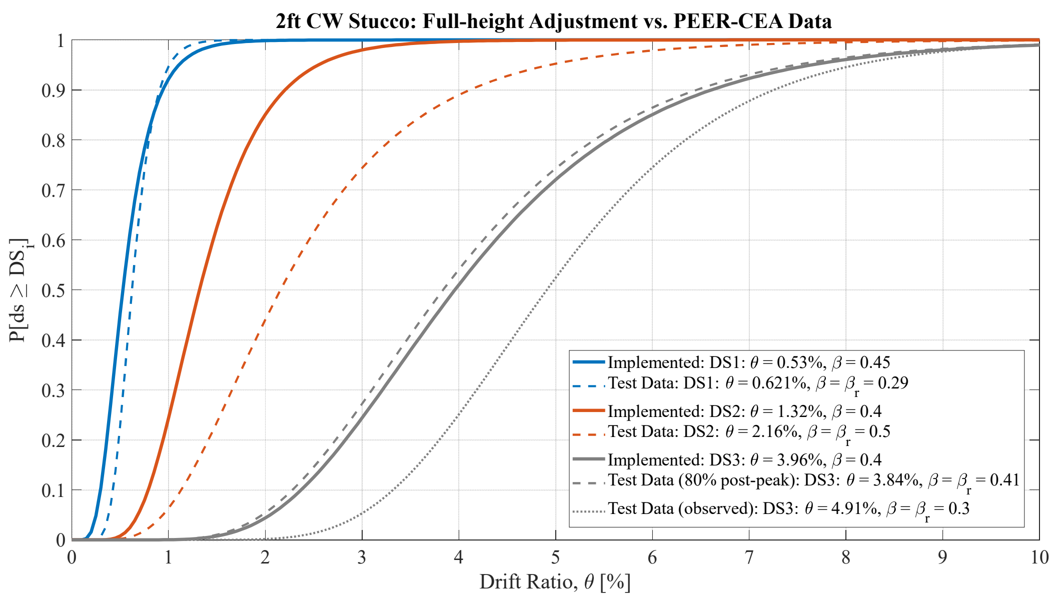

Figure 5.20 Comparison of the 2-ft-tall stucco cripple wall fragilities using implemented height adjustment factor (solid lines) with data collected from PEER–CEA testing (dashed lines).

DS1 ≈ 0.4% (0.29”)

Test A-25: 0.4% drift
(0.3% relative)
First return and face cracking

Test A-25: 0.6% drift
(0.4% relative)
Extended face crack

DS2 ≈ 0.7% (0.50”)

Test A-25: 0.8% drift
(0.5% relative)
Distributed corner cracking
(upper DS1, lower DS2)

Test A-25: 1.4% drift
(1.0% relative)
Spalling and deterioration of Corner. Significant strength loss after first cycle

DS3 ≈ 1.7% (1.22”)

Test A-25: 2.0% drift
(1.8% relative)
Stud damage. Onset of stucco separation from sill

Test A-25: 2.0% drift
(1.6% relative)
Corner destroyed. Out-of-plane movement of main stucco face visible

Figure 5.21 Example of using photographic documentation and experimental results from testing to estimate damage states for the 6-ft-tall unretrofitted stucco cripple wall Specimen A-25 (photographs courtesy of Brandon Schiller).

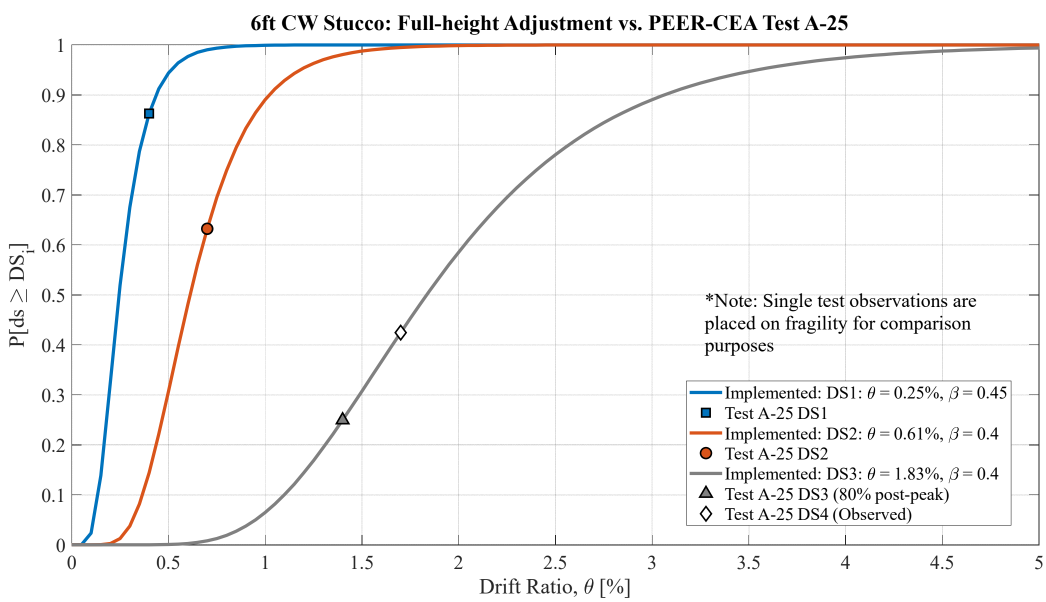

Figure 5.22 Comparing the implemented height-adjusted fragilities for 6-ft-tall stucco cripple walls (lines) with damage observed for PEER–CEA Specimen A-25 (points).

Table 5.14 Implemented stucco damage fragility functions for cripple walls using a height-dependent scaling relationship from full-height stucco fragilities.

Damage state	Damage description	EDP	Median full-height (θ_{Full})[1]	Median 6 ft (θ_{6ft})[2]	Median 2 ft (θ_{2ft})[2]	Dispersion (β)
1	Cracking of stucco with cracks between 1/64” and 1/8” wide. No delamination.	Story drift ratio (SDR) [rad]	0.0020	0.0025	0.0053	0.45
2	Moderate cracking with minor delamination or spalling. Extensive minor cracking possible. Local delamination can damage waterproofing and lath in damaged area.		0.0050	0.0061	0.0132	0.40
3	Significant spalling and delamination of stucco. Loosening of framing connections possible.		0.0150	0.0184	0.0396	0.40

[1] Full-height exterior stucco fragilities are presented in Section 5.3.2.
[2] Median fragilities are scaled from the full-height values by $(8/h_{CW})^{0.7}$ where h_{CW} is the cripple wall height in feet.

5.4.3 Panelized Wood Siding (T1-11) Cripple Walls

Experimental test data from WG4 for T1-11 cripple walls included two non-retrofitted cases with heights of 2 and 6 ft, labeled as Specimens A-11 (2 ft tall) and A-23 (6 ft tall) within WG4 small-component testing documentation [Schiller and Hutchinson 2020(b)]. The observed damage and drift ratios attributed to each of the three damage states for T1-11 panelized siding (see Section 5.3.4) were estimated from photo documentation and force-displacement response. Similar to the review of stucco cripple walls (Section 5.4.2), the third damage state, corresponding to the replacement threshold, is determined from the drift corresponding to 80% post-peak strength. The estimated damage state drift ratios are provided with supporting photo documentation in Figure 5.23 and Figure 5.24 for Specimens A-11 (2 ft) and A-23 (6 ft), respectively.

A comparison of the proposed height-adjusted relationship (i.e., using Equation (5.2) with Table 5.10) for 2-ft-tall T1-11 cripple walls and the discrete observations from Specimen A-11 is shown in Figure 5.25. The discrete points from Specimen A-11 are plotted along the continuous fragility functions, as was done previously for 6-ft-tall stucco walls. The figure shows that the observations from Specimen A-11 are in reasonable agreement with the proposed height-adjustment relationship. A similar comparison is provided for the 6-ft-tall T1-11 cripple walls compared with Specimen A-23 in Figure 5.26, where again the agreement is considered reasonable. Fragility parameters defining the fragility functions for T1-11 cripple walls using the height-adjustment relationship are shown in comparison with those assumed for full-height T1-11 walls in Table 5.15.

DS1 ≈ 2.5% (0.6”)

Test A-11: 4.0% drift
(3% relative)
First fastener tear through
(upper DS1)

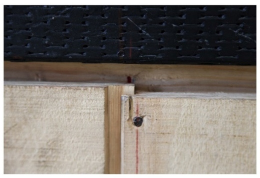

Test A-11: 3% drift
(2% relative)
Loosening of fasteners

DS2 ≈ 5.0% (1.2”)

Test A-11: 6.0% drift
(5% relative)
Fastener tear through

Test A-11: 4.0% drift
(3% relative)
First fastener tear through
(lower DS2)

DS3 ≈ 6.0% (1.44”)

Test A-11: 7.0% drift
(6% relative)
Onset of distributed
delamination

<u>Global Backbone Properties</u>

-Peak force at 4.8% (+ve) and 4.6% (-ve) relative drift

- 20% strength loss at 5.9% (+ve) and 5.7% (-ve) relative drift

Figure 5.23 Photographic documentation and experimental results from testing to estimate damage states for the 2-ft-tall unretrofitted T1-11 cripple wall Specimen A-11 (photographs courtesy of Brandon Schiller).

DS1 ≈ 1.1% (0.72”)

Test A-23: 0.8% drift
No significant slipping of nails. Start of relative panel movement. Global stiffness loss prior to 0.8%

Test A-23: 1.4% drift
First nail pull through
(upper bound DS1)

DS2 ≈ 2.5% (1.80”)

Test A-23: 2.0% drift
Fastener tear through at panel corner (near peak strength of this direction)

Test A-23: 3.0% drift
Pulling through of fastener at sill plate (near peak strength of this direction)

DS3 ≈ 4.0% (2.88”)

Test A-23: 4.0% drift
Tearing of top plate connections

Test A-23: 4.0% drift
Damage to top plate and sill connections from panel rotation (nearing 80% post-peak strength)

Figure 5.24 Photographic documentation and experimental results from testing to estimate damage states for the 6-ft-tall unretrofitted T1-11 cripple wall Specimen A-23 (photographs courtesy of Brandon Schiller).

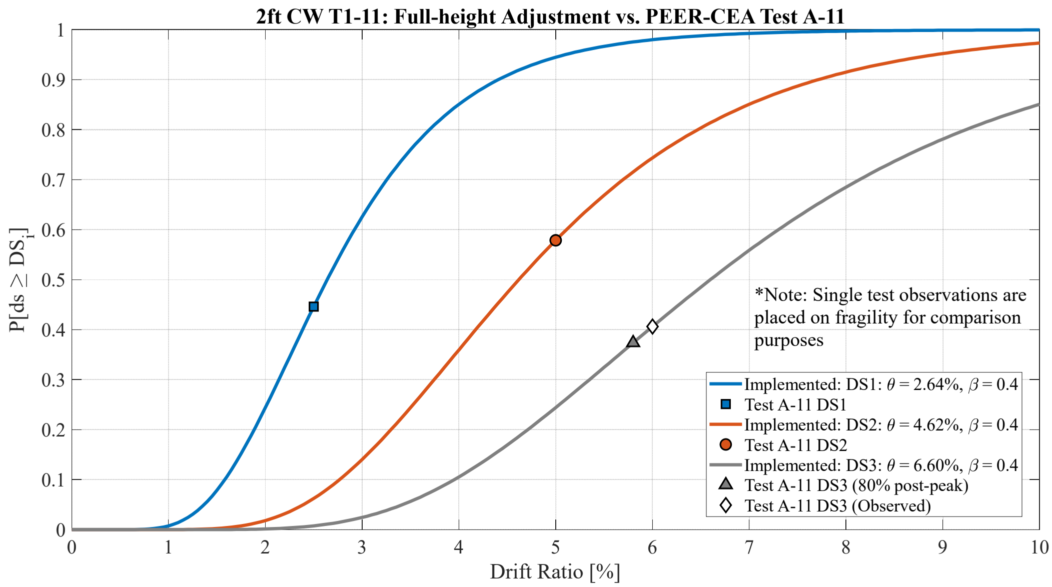

Figure 5.25 **Comparing the implemented height-adjusted fragilities for 2-ft-tall T1-11 cripple walls (lines) with damage observed for PEER–CEA Specimen A-11 (points).**

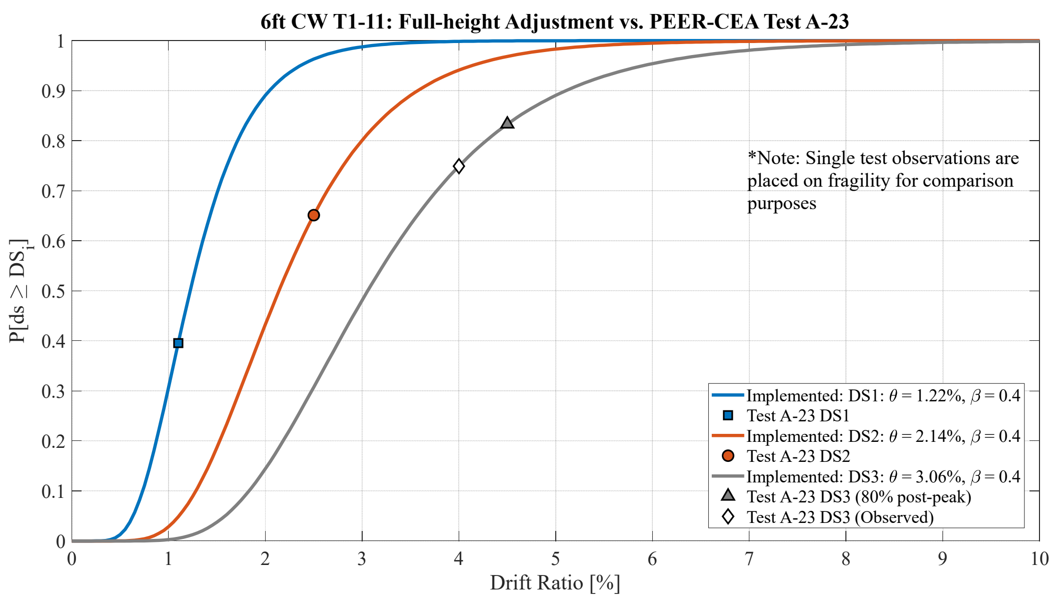

Figure 5.26 **Comparing the implemented height-adjusted fragilities for 6-ft-tall T1-11 cripple walls (lines) with damage observed for PEER–CEA Specimen A-23 (points).**

Table 5.15 Implemented T1-11 damage fragility functions for cripple walls using a height-dependent scaling relationship from full-height T1-11 fragilities.

Damage state	Damage description	EDP	Median full-height (θ_{Full})[1]	Median 6 ft (θ_{6ft})[2]	Median 2 ft (θ_{2ft})[2]	Dispersion (β)
1	Loosening of nails due to panel rotation	SDR (rad)	0.0100	0.0122	0.0264	0.40
2	Nail tear-through. Onset of panel separation from framing and uplift of studs and sill plates		0.0175	0.0214	0.0462	0.40
3	Delamination of panel from framing. Panel damage near openings and at fastener locations. Damage to framing connections, sill plates and studs.		0.0250	0.0306	0.0660	0.40

[1] Full-height exterior T1-11 fragilities are presented in Section 5.3.4.
[2] Median fragilities are scaled from the full-height values by $(8/h_{CW})^{0.7}$ where h_{CW} is the cripple wall height in feet.

5.4.4 Horizontal Wood Siding Cripple Walls

Damage fragilities for cripple walls with horizontal wood siding are based on the proposed fragilities for full-height walls discussed in Section 5.3.3. Similar to full-height exterior walls with horizontal wood siding, cripple walls with this material assume a single damage state fragility corresponding to the likelihood of replacement. Cripple walls with horizontal wood siding alone or in combination with horizontal sheathing (and without any other framing bracing) are defined by a median drift of 3.0% and a lognormal dispersion of 0.5. For wood siding cripple walls with braces within the framing (e.g., using material properties that reflect the possibility of effective bracing; see Chapter 3) the assumed fragility has a median drift ratio of 1.5% and a dispersion of 0.5. These fragilities are not adjusted for a reduction in height, based on the behavior described in Figure 5.17(b). For cripple walls with braces within the framing, this lack of height adjustment may be conservative; however, this is considered reasonable given that the basis for considering the effect of cripple wall bracing for horizontal wood sheathing walls is largely based on judgment and previous testing of different brace types for full height wall sub-assemblies.

5.4.5 Diagonal Sheathing Cripple Walls

The PEER–CEA testing by WG4 considered two variations of 2-ft-tall × 12-ft-long unretrofitted cripple wall specimens with horizontal wood siding over diagonal sheathing. Specimen A-9 had a gravity loading of 450 lb/ft applied, while Specimen A-28 had a lighter gravity loading of 250 lb/ft applied. These specimens were reviewed using the force-displacement behavior from cyclic testing to monitor the drifts corresponding to peak load in each direction; a similar measurement was used to inform the proposed fragility for full-height diagonal sheathing walls described in Section 5.3.3. Using relative cripple wall displacements (i.e., global measured displacement minus the sill plate slip displacement) the drift ratios corresponding to peak load for Specimen A-9 were 5.0% and 5.2% for the positive (sheathing board gaps opening) and negative (sheathing board gaps closing) loading directions. Corresponding values for Specimen A-28 were 3.2% and 4.2% for the positive and negative loading directions. The average of these four values is 4.4%. When applying the height-dependent adjustment in Equation (5.2), the full-height median value of 1.5% becomes 4.0%. This suggests that the height-dependent relationship is applicable to diagonal sheathing cripple walls. However, it should be noted that the available information on diagonal sheathing is significantly limited, and these fragility functions are based on a combination of judgment and limited data. Further, the cripple wall test specimens with diagonal sheathing do not consider the effect of continuous diagonal sheathing boards across the cripple wall and above the first-floor diaphragm. Thus, the actual behavior of this detail could vary significantly from the details considered here.

5.4.6 Damage Fragilities for Stem Wall Anchorage Connections

The treatment of existing (unretrofitted) stem wall dwellings in the PEER–CEA Project assumes that the most common and controlling failure mode occurs at the floor joist-to-sill plate connection on top of the stem wall. The damage fragilities for modeling existing (unretrofitted) stem wall conditions for the joist-to-sill plate connection were developed based on expert judgment and damage observed from previous seismic events; see Section 3.7 for further discussion.

The treatment of damage for stem wall connections assumes that the entire perimeter stem wall can be treated as a single damageable assembly. This differs significantly from the treatment of cripple wall collapse, where the consequences are represented by a fraction of replacement cost; see Section 6.5. The single damageable assembly assumption is based on previous observations of stem wall failures from seismic events showing that damage to the exterior finishes of a dwelling is likely to occur around the entire perimeter for even small to moderate displacements, and large displacements (i.e., floor framing moved considerably relative to sill plate and foundation) that require straightening and possibly jacking of the dwelling also involve the entire perimeter of the dwelling. An illustration of varying degrees of damage to stem wall dwellings with stucco exterior from previous seismic events is shown in Figure 5.27.

The damage states for the perimeter stem wall were assumed based on a team discussion between internal PEER Team Members and external experts. Three distinct damage states were defined that represent: (1) perimeter stem wall damage that requires repair without straightening; (2) displacements significant enough to require straightening (repositioning) of the house on the foundation; and (3) displacements causing loss of floor joist bearing on at least one side of the perimeter that will require jacking up of and more significant repairs to the house. A summary of the assumed damage and repair efforts for each damage state of perimeter stem walls are shown in Figure 5.28.

Figure 5.27 Examples of varying degrees of perimeter stucco damage to stem wall dwellings [CUREE 2010], bottom left photo (USGS).

The assumed EDP for stem wall buildings is the peak transient displacement of the floor joists relative to the sill plates occurring anywhere along the perimeter (i.e., the peak displacement demand at the slip interface). The bounding displacement thresholds for fragility development considered the onset of damage of the exterior of the perimeter occurring at displacements on the order of 0.25 in. and the loss of floor joist bearing occurring at a displacement of 4 in., assuming a 2 × 6 sill plate (5.5 in. wide) with an end joist (1.5 in. thick) capping the joists running perpendicular to the stem wall with ends bearing on the sill plate. Another key displacement threshold is the peak capacity assumed for the existing toe-nail joist-to-sill connections of 0.6 in.; see Section 3.7.

An illustration of these damage displacement thresholds is shown in comparison with the assumed fragility functions for joist-to-sill connections in Figure 5.29. For DS1, a median displacement of 0.4 in. and a dispersion of 0.3 was selected to include the onset of damage requiring repair at 0.25 in. of displacement (i.e., 6% probability of exceeding DS1) and include a confident probability of being in DS1 when the toe-nail capacity is reached (i.e., 91% probability of exceeding DS1). Similarly, for DS2, a median displacement of 0.85 in. and a dispersion of 0.4 targets the displacement capacity of the toe-nail connections (i.e., 0.6 in.) to represent the median minus one standard deviation value for requiring straightening of the first floor of the dwelling and a displacement demand of 2.0 in. has a high probability of requiring straightening (i.e., 98% probability of exceeding DS2). The fragility function for DS3 representing loss of bearing of floor joists on the sill has a median displacement of 3.5 in. and a low dispersion of 0.05. This reflects the assumption that unseating of joists occurs at 4.0 in. of displacement but allows for lesser values to account for uncertainties in the damage. The stem wall fragility parameters for existing (unretrofitted) stem wall dwellings with joist-to-sill connection vulnerability are in Table 5.16.

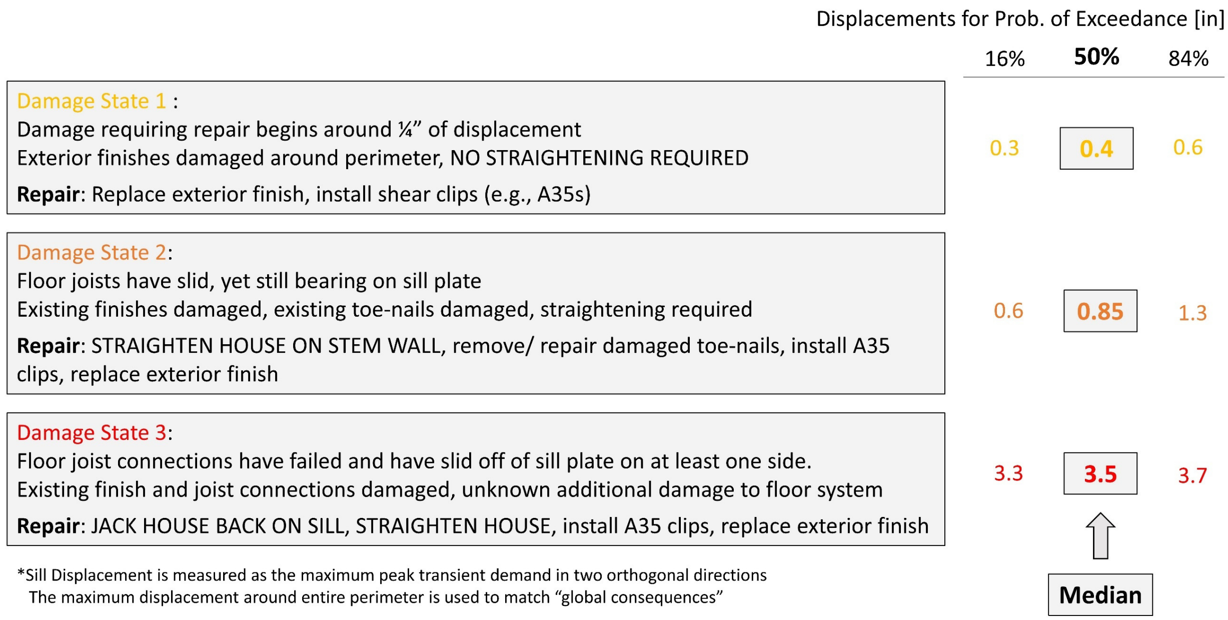

Figure 5.28 **Damage state definitions for perimeter stem walls compared with assumed peak relative joist-to-sill displacements defining the median values for fragility development.**

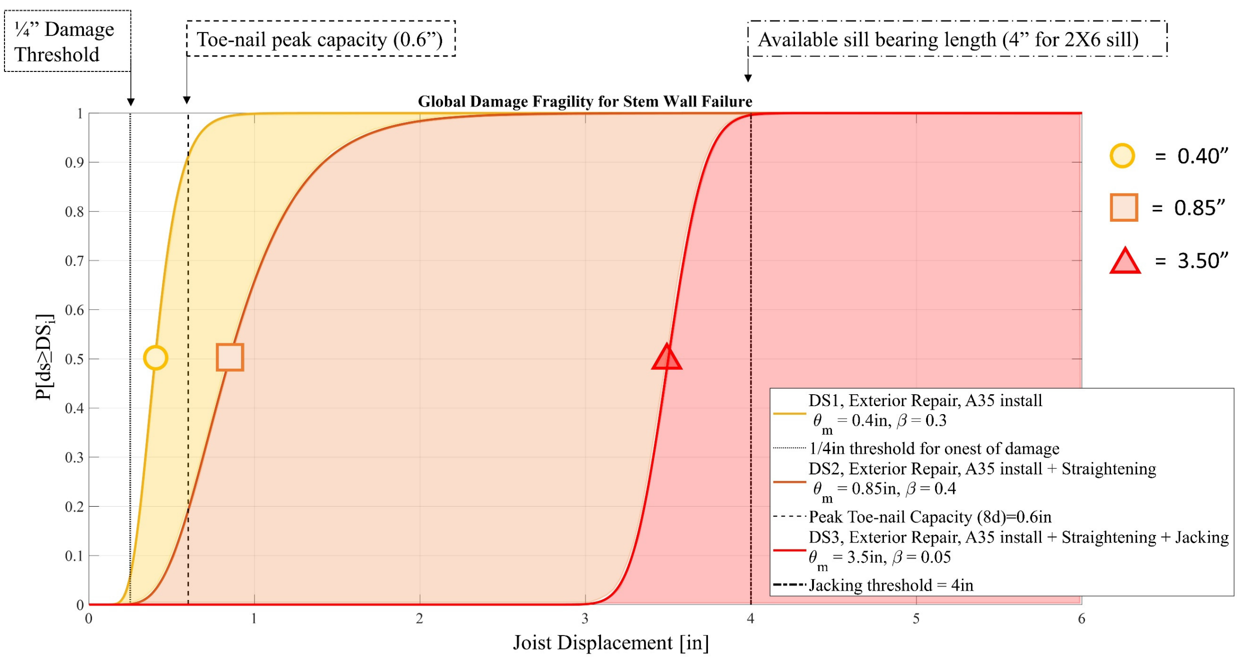

Figure 5.29 **Illustration of assumed damage fragility for perimeter stem walls in comparison with key displacement thresholds used to define fragility parameters.**

Table 5.16 Implemented damage fragility functions for existing (unretrofitted) joist-to-sill connections for stem wall dwellings.

Damage state	Damage description	EDP	Median (θ)	Dispersion (β)
1	Damage to exterior finish around perimeter and joist-to-sill connection.	Relative joist-to-sill displacement (in.)*	0.40	0.30
2	Damage to exterior finish around perimeter and joist-to-sill connection. Displacement is significant enough to require straightening.		0.85	0.40
3	Damage to exterior finish around perimeter and joist-to-sill connection. Displacement is significant enough to require jacking of the dwelling prior to straightening and repairs.		3.50	0.05

* Peak transient displacement of floor joists relative to mudsill at any location or orthogonal direction around perimeter.

6 Repair Cost and Economic Considerations

The final stage of the *FEMA P-58* process used for performance assessment of building variants within the PEER–CEA Project is the loss analysis or decision variable stage. This stage utilizes the structural analysis results (e.g., EDPs such as story drift ratio) combined with the damage analysis stage (e.g., probability of damage; estimation of collapse fragility) to attribute appropriate repair costs and economic consequences of damage and structural collapse. This chapter provides an overview of the treatment of repair costs and economic considerations for the analysis of building variants, including the main underlying assumptions behind the development of loss models (i.e., number and type of damageable assemblies, component cost functions, collapse consequences, etc.). The treatment of repair costs is outlined in light of a critical review of current *FEMA P-58* cost functions, with additional considerations based on information gained from the PEER–CEA Earthquake Damage Workshop [Vail et al 2020]. Discussion is provided on the treatment of collapse consequences for cripple walls and repair cost considerations for stem wall foundations that have deficient anchorage connections. Finally, details of the computational framework and software for performing the loss assessment calculations are provided.

6.1 ASSUMPTIONS FOR LOSS MODELING OF BUILDING VARIANTS

6.1.1 Damageable Assemblies Considered

The damageable assemblies considered for representing earthquake damage and repair costs include primarily drift-sensitive structural and nonstructural walls and finishes. As described later in this chapter, the associated repair costs for the walls account for damageable utilities within the walls. Damage and losses associated with acceleration-sensitive components are not included explicitly since, as described in this section, the two most relevant items are not considered to have a significant influence on differentiating between the loss risks associated with cripple wall and sill anchorage retrofits. Two relevant acceleration-sensitive components of single-family residential dwellings are masonry chimneys and water heaters. Masonry chimneys can be significant source of earthquake damage [Osteraas and Krawinkler 2010; FEMA 2015], yet this type of damage was not considered since it did not clearly represent a source of damage dependent on the retrofitting of crawlspace vulnerabilities [Reis 2020(a)].

Damage to water heaters following earthquakes can lead to significant consequences, including water damage and fire from ruptured gas lines. In terms of economic repair costs, limited reconnaissance reports, such as Levenson's [1992] investigation of water heater damage following the 1989 Loma Prieta, California, and 1992 Big Bear, California, earthquakes, suggest that the economic consequences of damaged water heaters are quite variable. Moreover, the majority of water heater damage observed following the 1989 Loma Prieta event was, on average, not a significant source of repair cost with respect to the value of the home. Further, the issue of fire ignition from damaged water heaters is a very complex issue with limited empirical data to incorporate it into loss modeling. Levenson [1992] reports an "overwhelming majority" of gas leaks observed following 1989 Loma Prieta did not result in fire ignition. On the other hand, he also reports that 13 out of 15 fire ignitions in the Big Bear Lake area were attributed to water heater damage, which illustrates that fire ignitions triggered by gas line failures can have serious consequences. However, given the large uncertainty associated with gas line breaks and fire ignitions, these are considered as outside the scope of this more limited study to quantify the reduction in direct damage and losses associated with retrofit of cripple wall and sill plate anchorage failures.

6.1.2 Inclusion of Additional Modeling Uncertainty

The primary demand parameter for the loss functions are story drift ratios, which are determined from the structural analyses. While the nonlinear dynamic analyses directly account for record-to-record variability at each intensity level, they do not include modeling uncertainties, associated with variations in structural modeling and response parameters. To account for modeling uncertainties in the loss calculations, additional modeling uncertainty is applied to the story drift demands prior to calculating damage and repair costs. An additional dispersion (similar to a coefficient of variation) of 0.35 is assumed based on guidance provided by *FEMA P-58* [2012], which takes into account the combined effects of uncertainty in building definition, quality assurance, and structural modeling. A constant value of 0.35 was also included for collapse fragilities, as discussed in Section 2.5.1.

Note that one could arguably apply different values of dispersion for the existing (unretrofitted) versus retrofitted building analyses, since presumably there would be less variability in estimating the response of the engineered cripple wall retrofit. Different uncertainty parameters were, in fact, applied in the ATC 110 project to development of the *FEMA P-1100* Prestandard [2018; 2019(b)] to evaluate collapse safety using the *FEMA P-695* [2009] approach. However, for the current project, where the goal is to estimate the relative seismic performance between unretrofitted and retrofitted crawlspace houses, it was assumed that applying the same modeling uncertainty in analyses of the unretrofitted and retrofitted cases would be more consistent.

6.2 REPAIR COST FUNCTIONS FOR WOOD-FRAME STRUCTURE SUB-ASSEMBLIES

Cost functions in the *FEMA P-58* loss assessment methodology relate the estimated damage probabilities obtained from component fragility functions (Chapter 5) into estimated repair costs. For a given sub-assembly, each damage state has a mean repair cost based on a costing unit expressed in either 100 ft^2 (100SF) or 100 linear feet (100LF) of that sub-assembly. The difference in mean repair costs, associated with economy and efficiency of construction, are defined by a lower quantity (LQ) of units and an upper quantity (UQ) of units. As illustrated in Figure 6.1, for a given damage state *i*, mean repair costs for quantities at or below LQ have a value $RC_{LQ,i}$ then transition to the upper quantity value of $RC_{UQ,i}$ for quantities greater than UQ. Uncertainty in repair costs (β_{Cost}) is applied as either a coefficient of variation (COV) or a lognormal standard deviation depending on whether repair costs for a given assembly and damage state are assumed to be normally or lognormally distributed.

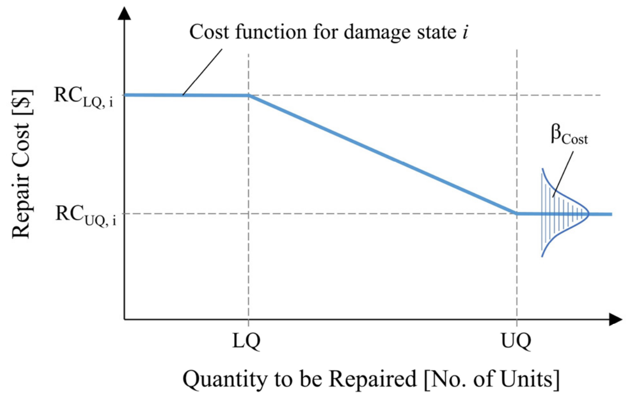

Figure 6.1 **Example of a repair cost function for a component or sub-assembly within *FEMA P-58*.**

The repair cost functions for wood-frame dwellings within the *FEMA P-58* database are used as a starting point for review and modification for the current project. These are summarized in Table 6.1 and Table 6.2 for exterior and interior wall assemblies, respectively. The corresponding damage fragility information for these assemblies is described in Section 5.2. These cost functions apply the exact index, assembly name, and repair measure description from the *FEMA P-58* database. Notably, all repair cost functions are 2011 U.S. dollars (2011USD).

Table 6.1 **Repair cost functions for exterior wall assemblies within the FEMA P-58 database considered for review and modification for the PEER–CEA Project.**

Index: name[1]	Unit (EDP)[2]	Repair measures for damage state *i*	$RC_{LQ,i}$ [3] [2011$]	LQ	$RC_{UQ,i}$ [2011$]	UQ	β_{Cost}[4]
B1071.001: Light framed wood walls with **structural panel sheathing**, **gypsum wallboard**, no hold-downs	100SF (SDR)	1: Remove exterior pliable siding, replace loose nails, reinstall siding	2134	3	1313	8	0.19
		2: Remove exterior pliable siding, remove wood sheathing, install new sheathing, reinstall siding	2570	3	1820	8	0.22
		3: Remove and replace siding, sheathing, studs and plates. Provide shoring as required	6450	3	4569	8	0.08
B1071.011: Light framed wood walls with structural panel sheathing, **stucco**, no hold-downs	100SF (SDR)	1: Clean stucco cracks. Fill cracks with cement compound. Repaint wall to hide cracks.	2990	2	1840	6	0.26
		2: Remove loose stucco and patch spalled areas with stucco. Repaint to hide repairs.	3300	2	2338	6	0.37
		3: Remove and replace studs, sheathing, and stucco. Shore as required.	5400	2	3825	6	0.11*
B1071.031: Wood walls with diagonal let-in bracing	100SF (SDR)	1: Remove and replace sheathing studs, plates and bracing and replace with new stud wall construction of plywood, hold-downs, etc. Provide shoring as required.	6165	4	3793	11	0.11*

[1] Indices correspond to *FEMA P-58* classification, see Table 5.1 for damage fragility information.
[2] All costing units are based of 100 ft^2 (SF) and correspond to damage fragilities using SDR.
[3] RC represents repair cost, LQ and UQ are lower- and upper-unit quantities, respectively.
[4] Costing dispersion with an asterisk is assumed for a normal distribution (COV), lognormal otherwise.

Table 6.2 Repair cost functions for interior wall assemblies and finishes within the *FEMA P-58* database considered for review and modification for the PEER–CEA Project.

Index: name[1]	Unit (EDP)[2]	Repair measures for damage state *i*	$RC_{LQ,i}$[3] [2011$]	LQ	$RC_{UQ,i}$ [2011$]	UQ	β_{Cost}[4]
B1071.041: Exterior Wall – Type: **Gypsum** with wood studs, full-height, fixed below, fixed above	100LF (SDR)	1: Retape joints, paste and repaint both sides of full 100 ft length of wall board.	5320	1	1596	10	0.42*
		2: Remove full 100 ft length of wall board (both sides), install new wall board (both sides), tape, paste and repaint.	11100	1	3330	10	0.49*
		3: Remove and replace full 100 ft length of metal stud wall, both sides of the gypsum wall board and any embedded utilities, and tape, paste, repaint	37600	1	11280	10	0.10
C3011.002a: Wall Partition [finish] – Type: Gypsum + **Ceramic Tile**, full-height, fixed below, fixed above	100LF (SDR)	1: Carefully remove cracked tile and grout at cracked joints, install new ceramic tile and re-grout joints for 10% of full 100 ft length of wall. Existing wall board will remain in place	8640	1	5760	3	0.22*
		2: Install ceramic tile and gorut all joints for full 100 ft length of wall. Note: gypsum wallboard will also be removed and replaced wich means the removal of ceramic tile will be part of the gypsum wall board removal.	34992	1	23328	3	0.10
C3011.001a: Wall Partition [finish] – Type: Gypsum + **Wallpaper**, full-height, fixed below, fixed above	100SF (SDR)	1: Remove existing wall paper (or wall) and install new wall paper for full 100ft length of wall.	3240	1	2160	3	0.15

[1] Indices correspond to *FEMA P-58* classification, see Table 5.2 for damage fragility information.
[2] All costing units are based of 100 linear feet (LF) and correspond to damage fragilities using SDR.
[3] RC represents repair cost, LQ and UQ are lower- and upper-unit quantities, respectively.
[4] Costing dispersion with an asterisk is assumed for a normal distribution (COV), lognormal otherwise.

6.2.1 Adjustments to *FEMA P-58* Functions

For this project, the sub-assembly cost functions of the *FEMA P-58* database were carefully reviewed, based on the detailed costing information provided in the electronic background documentation for *FEMA P-58* [FEMA 2012c], specifically, the information in *Section 3.2 - Provided Fragility Data* using the spreadsheet labeled *Consequence Estimation Summary* (.xlsx). This review confirmed how the line-by-line costing items were translated into the sub-assembly cost functions, such as those presented in Table 6.1 and Table 6.2. The reviewed cost information was verified with the *FEMA P-58* fragility database contained within *SP3 v2.6* (www.hbrisk.com), noting that additional steps are needed to translate the component cost information into the final cost units and quantity adjustments used for the *FEMA P-58* loss analysis. Note that this review did not identify any other information on the basis or assumptions for costing beyond the inputs provided in the consequence estimation summary.

Based on this review, several modifications were made to the existing *FEMA P-58* cost functions for use in this project. These are briefly summarized in this chapter and are described in further detail within the WG5 electronic documentation available at the PEER website [PEER 2020].

6.2.1.1 Reduced Height Basis for Gypsum Wallboard

One of the important findings of the cost function review clarified that the functions for walls with gypsum wallboard were based on original costing items for tall commercial partition walls with a height of 13 ft. Since the final units are in linear feet, the cost function required adjustment for houses with lower wall heights. To address this, all line items that were based on square footage of wall prior to summing up for damage state totals were adjusted to be based on 9-ft-tall walls. The adjustment was only applied to cost items related to the assumed wall height, where other considerations that are not based on wall height were maintained at their original values. The final modification factors for *FEMA P-58* assembly B1071.041 are estimated to be 0.74, 0.78, and 0.80 for Damage States 1 through 3, respectively. Figure 6.2 shows a comparison of the cost functions for interior gypsum walls adjusted for a 9-ft-wall height with the existing *FEMA P-58* assembly based on a 13-ft wall height (B1071.014). Input values defining the height-adjusted gypsum wall assembly cost functions are provided in Section 6.7. These cost functions are developed for interior partitions with gypsum wallboard on both sides of the framing.

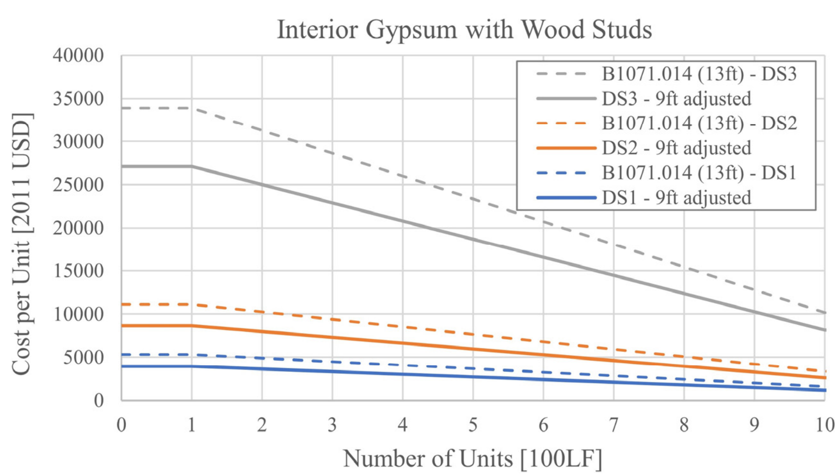

Figure 6.2 Comparing interior gypsum wall repairs adjusted for a height of 9 ft (solid lines) with existing FEMA P-58 function based on 13 ft (dashed lines).

6.2.1.2 Separation of Interior and Exterior Repairs

The most significant changes to the existing *FEMA P-58* cost functions involve the separation of exterior wall repair costs from the interior repair costs that are combined in the existing *FEMA P-58* exterior wall assemblies. As originally pointed out by Ekiert and Filiatrault [2008], this is important since the exterior and interior wall materials will be sensitive to different levels of drift demand for different damage states. Further, the inclusion of interior repairs for exterior wall assemblies in *FEMA P-58* was found to be somewhat arbitrary and inconsistent with the repair costs for interior walls, at least when considering the difference in damage fragilities assumed for exterior and interior materials. No documentation is provided in FEMA P-58 to understand whether these considerations were taken into account in the cost function development.

Specific to the current project needs, separation of interior and exterior repairs is required for two main reasons. Firstly, repair costs for exterior walls without interior finishes are required for modeling cripple wall assemblies. Secondly, the loss assessments in this study need to differentiate between different types of interior wall material (i.e., gypsum wallboard versus plaster on wood lath) which have different damage fragility and repair cost consequences.

Cost functions for exterior stucco walls are based on *FEMA P-58* assembly B1071.011, which represents an exterior wall with stucco over OSB without hold-downs. This function does not identify gypsum wallboard in the required repair measures, yet the description of the assembly includes 1/2-in.-thick gypsum wallboard on one side, which is included in the detailed repair line items. To separate exterior versus interior repairs, line items involving interior preparations (i.e., gypsum demolition, dust curtains, floor protection, etc.) were removed in addition to any line items involving gypsum wallboard repairs. Some judgment had to be used when lumped, single value, costs were attributed to things like mechanical and electrical items, considering the assumed damage state and how these items are treated for interior partition assemblies that would now be applied to the interior surface of exterior walls. The resulting adjustments to remove interior repairs resulted in adjustment factors of 0.56, 0.66, and 0.81, applied to exterior wall Damage States 1 through 3, respectively. A comparison of the adjusted exterior-only stucco wall functions with P-58 assembly B1071.011 is provided in Figure 6.3. Input values to define the cost functions are provided in Section 6.7.

Similar adjustments were made for the exterior wood siding wall assembly B1071.031, noting that this assembly only has one damage state representing replacement of the wall. To remove interior wall repairs, the scale factor applied to assembly B1071.031 was estimated at 0.49 for the replacement Damage State 1. A comparison of the adjusted exterior-only wood siding wall function with *FEMA P-58* assembly B1071.031 is provided in Figure 6.4, where the corresponding cost function values are provided in Section 6.7. The cost functions used as the basis for T1-11 panelized siding are from the *FEMA P-58* assembly B1071.001. Using a consistent procedure for removing interior repair costs, the relative scale factors for assembly B1071.001 are 0.22, 0.35, and 0.49 for Damage States 1 through 3, respectively. The low factors applied for Damage States 1 and 2 take into account that these damage states are associated with repairing loosened nails and replacing localized panel and fastener damage, which are much lower than initial damage states required for stucco repair. A comparison of the adjusted exterior-only cost functions for T1-11 panelized siding with the *FEMA P-58* assembly B1071.001 that includes interior repairs is shown in Figure 6.5 with input values provided in Section 6.7.

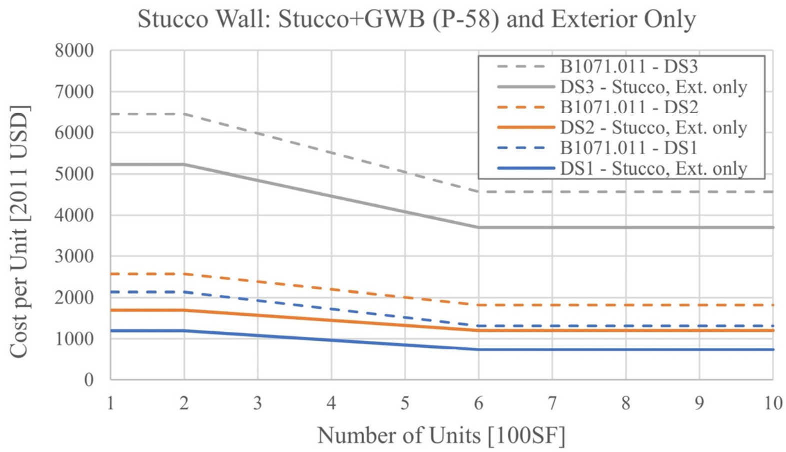

Figure 6.3 **Comparing exterior-only stucco wall repairs (solid) with existing *FEMA P-58* function including gypsum wallboard and interior repairs (dashed).**

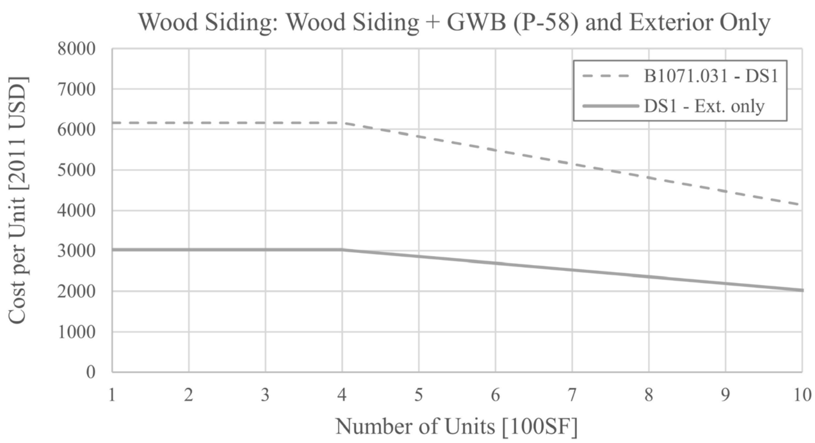

Figure 6.4 **Comparing exterior-only wood siding wall repairs (solid) with existing *FEMA P-58* function including gypsum wallboard and interior repairs (dashed).**

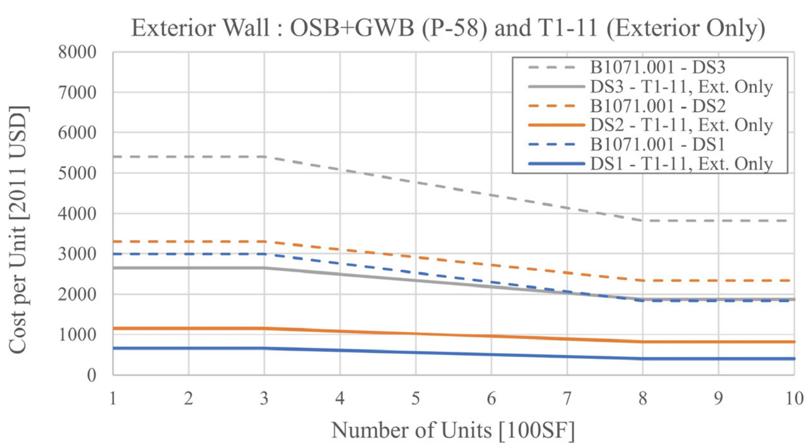

Figure 6.5 **Comparing exterior-only OSB/T1-11 wall repairs (solid) with existing *FEMA P-58* function including gypsum wallboard and interior repairs (dashed).**

6.2.2 Adjustments Based on Damage Workshop

The Earthquake Damage Workshop [Vail et al. 2020], organized by WG6, provides independent repair cost estimates from insurance claims adjustors that can be used to help validate the *FEMA P-58* cost estimates. As described by Vail et al. [2020], a set of three different case study buildings were created, each with its own damage description package. These were purposefully selected to compare to existing materials available in *FEMA P-58* (e.g., stucco exterior, gypsum wallboard) while details of others were developed to fill knowledge gaps in existing cost functions. Further, interaction with claims adjustors during the course of the workshop effort allowed for specific aspects of cost estimation to be clarified with respect to common practices.

6.2.2.1 Cost Modification for Plaster on Wood Lath Interior

The lack of information on repair costs for older plaster on wood lath walls, which is the assumed interior wall finish in the pre-1945 era houses, is one of the knowledge gaps that was addressed through the Earthquake Damage Workshop. A series of adjustment factors (one for each damage state) were estimated based on knowledge gained from the Earthquake Damage Workshop [Vail et al. 2020]. Notably, multipliers between interior wall repair cost estimates for lath and plaster versus gypsum wallboard finishes from individual adjustors varied from a 115% increase to a 14% decrease, highlighting the difficulty in obtaining this information. When considering all of the comparative cases from the workshop, adjustment factors of 1.30, 1.15, and 1.25 were determined for Damage States 1 through 3, respectively, to estimate repair costs for wood lath and plaster from existing functions for gypsum wallboard. These adjustments were made to the gypsum wallboard repair cost functions for *FEMA P-58* assembly B1071.041, in addition to the adjustments for 9-ft wall heights; see Figure 6.2. The gypsum-to-plaster adjustment factors were only applied to line items involving wall repairs (i.e., directly adjusting gypsum repairs for plaster on wood lath). The resulting relative scale factors applied to assembly B1071.041 to obtain cost functions for 9-ft-tall plaster walls are 0.92, 0.88 and 1.01 for Damage States 1 through 3, respectively. The comparison of the functions is illustrated in Figure 6.6, and the associated parameters for 9-ft-tall interior walls with plaster on wood lath are provided in Section 6.7.

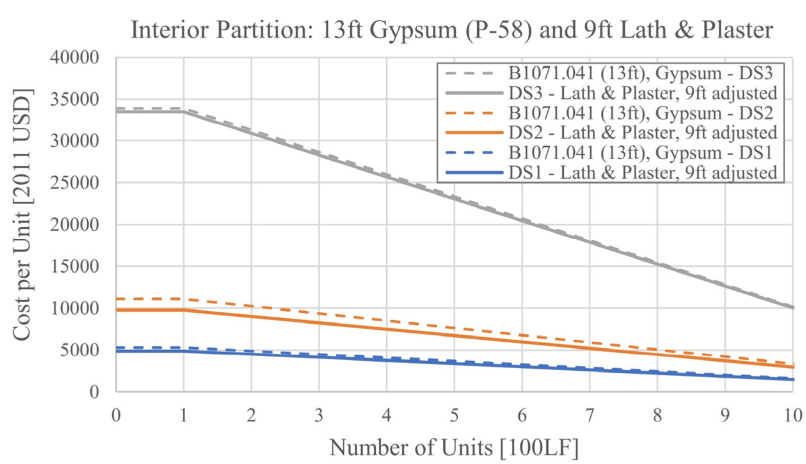

Figure 6.6 **Comparing interior plaster on wood lath wall repairs adjusted for a height of 9 feet (solid lines) with existing *FEMA P-58* function based on gypsum wallboard and a 13-ft height (dashed lines).**

6.2.2.2 Ceramic Tile and Wallpaper Repair

Another significant finding from the Earthquake Damage Workshop [Vail et al. 2020] is related to the repairs to cracked ceramic tile, where the practice is to typically replace tiled wall finish entirely (rather than partial repairs) due to issues with matching existing tiles and grout for appearance. The finish assembly of *FEMA P-58* for ceramic tile (C3011.002a) assumes two damage states corresponding to localized cracking of the tile requiring replacement of 10% of the tile area (DS1) and distributed cracking and damage requiring the full tile replacement (DS2). Based on the information from the Damage Workshop, the tile cost function was revised to include a single damage state DS1 for assembly C3011.002a, where the unit cost is assumed as full replacement cost. This first damage state fragility corresponds exactly to the DS1 associated with interior gypsum wallboard with a median story drift ratio of 0.21% and a lognormal standard deviation of 0.6. The corresponding cost function is already defined in Table 6.2 corresponding to DS2 for assembly C3011.002a. In contrast to the adjustments made for ceramic tile, the wallpaper finish using assembly C3011.001a was not modified from the original *FEMA P-58* function. The *FEMA P-58* cost basis for both ceramic tile and wallpaper assumes a 9-ft-wall height, so no adjustment was necessary for wall height.

6.3 BUILDING REPLACEMENT COST

A single building replacement value was sought to normalize repair costs for all building variants by the same value. The proposed value considers previous work of Porter et al. [2002], from the CUREE-Caltech Woodframe Project, default values used in the Seismic Performance Prediction (*SP3*) program (*www.hbrisk.com*), and information from the PEER–CEA Damage Workshop [Vail et al. 2020]. The intent is for the building replacement cost to generally represent Northern California (e.g., San Francisco Bay Area) so as to be consistent with component cost functions developed within *FEMA P-58* [2012].

Porter et al. [2002] provides a cost breakdown for the replacement value (i.e., reconstruction cost) of the CUREE Small House that is used as the basis for the 1200 ft^2 one-story (or lower story of two-story) configurations in this project (see Section 1.3.2; Appendix A). Porter et al. [2002] estimated the 1200 ft^2 small house to have a reconstruction cost of \$136,641, expressed in 2001 USD (United States Dollars) and assumed to be located in Santa Monica, California. Using typical ranges of regional factors discussed by Porter et al. [2002], this value was scaled by 10% (factor of 1.10) to translate from the Los Angeles area to the San Francisco Bay Area. Further, a 3% annual inflation was assumed, and the cost was adjusted from 2001 to 2017 (when initial analyses were conducted on the PEER–CEA Project). Considering these two factors, the resulting replacement cost is estimated to be \$241,196 expressed in 2017 USD and assumed to be located in the San Francisco Bay area. Normalizing by the floor area of 1200 ft^2, the replacement cost is estimated to be \$201/ft^2. A summary of these calculations and assumptions is provided in Figure 6.7.

The building replacement costs within the *SP3* program consider a wide variety of occupancy types and determine the building replacement cost in dollars per square foot based on the national average (this cost is adjusted for regional factors if a site location is specified). Single-family wood-frame dwellings are not included as one of the occupancy types in *SP3*, so the 'multi-unit residential' value is assumed as the most representative value. In late 2017, this value was reported as \$166/ft^2. Assuming this as a national average, an adjustment factor of 1.24 was applied to convert to the San Francisco Bay area based on information provided by Porter et al. [2002]. This returned a value of \$206/ft^2. Given the general consistency between values inferred from Porter et al. and *SP3*, a building replacement value of \$200/ft^2 is assumed for the PEER–CEA variant analysis, as shown in Figure 6.7. This value was further supported by the findings of the Earthquake Damage Workshop [Vail et al. 2020]. A comparison with insurance claims adjustors' estimates of building replacement cost is provided with other cost considerations in Section 6.4.

- The replacement cost of the small house considers adjusted values from Porter *et al.* [2002] (CUREE Woodframe) due to very similar 1200 ft^2 footprint and configuration
- Original replacement cost is \$136,641 in 2001 USD for a site in Santa Monica

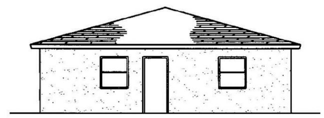

Porter et al. [2002]

- <u>Main Assumptions:</u>
  - Inflation is accounted for at 3% from 2001 to 2017 $P_n = P(1+i)^n$ i=0.03, n=16
  - Price is adjusted for the San Francisco area assuming a 10% increase from Los Angeles area (Porter *et al.* [2002])

$$Replacement\ Cost = \$136{,}641(1+0.03)^{16}(1.10) = \$241{,}196 \qquad \frac{Cost}{Area} = \frac{\$241{,}196}{1200ft^2} = \$201/ft^2$$

- The SP3 default value for multi-unit residential housing is \$166/ft^2 for the national average
- Porter *et al.* [2002] assume that the San Francisco area is 24% higher than the national average

Without more specific information, the current building replacement cost is assumed to be **\$200/ft²**

$$\frac{Cost}{Area} = \frac{\$166}{ft^2}(1.24) = \$206/ft^2$$

Figure 6.7 Summary of building replacement cost calculations used to inform the assumption used for the PEER–CEA Project (shown in red box with bold).

6.4 COMPARATIVE SUMMARY OF REVISED COMPONENT COST FUNCTIONS COMPARED WITH INSURANCE CLAIMS ADJUSTORS

This section compares the repair cost estimates provided by claims adjustors during the PEER–CEA Earthquake Damage Workshop [Vail et al. 2020] with the cost functions from the *FEMA P-58* database with proposed modifications. Except for the second case study building, which has an assumed lath and plaster interior for which no prior data existed, the cost function modifications discussed earlier in this chapter were derived prior to developing and exchanging cost estimates for the workshop. The cost estimates obtained using the adjusted *FEMA P-58* cost functions are based on the same damage descriptions as the case study buildings studied in the Earthquake Damage Workshop. In essence, the assembly-based cost functions were used as a cost estimation tool, in a parallel sense to the cost assessment software used by the claims adjustors. Four global (entire structure) damage states were considered in the workshop, generalized as light cosmetic damage (DS1), significant damage requiring a larger repair effort (DS2), severe damage requiring complete finish replacement and structural repair (DS3), and complete loss (DS4) requiring reconstruction.

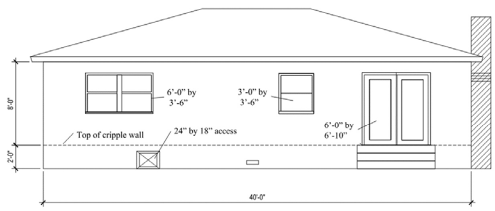

a) Rear façade of Case Study 1

b) Front façade of Case Study 2

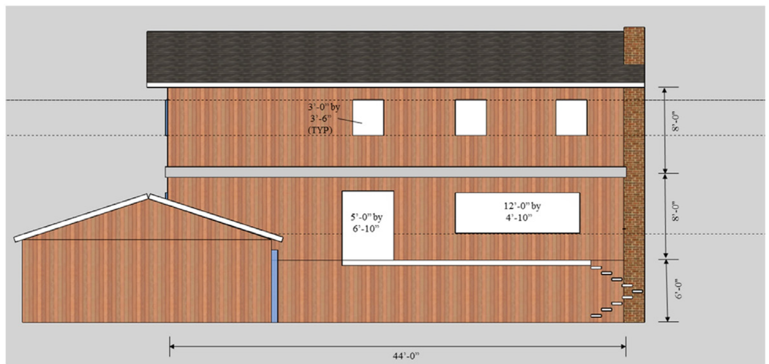

c) Front façade of Case Study 3

Figure 6.8 Elevation views of the three case study buildings used in the Earthquake Damage Workshop: (a) Case Study 1; (b) Case Study 2; and (c) Case Study 3 (images adapted from Vail et al. [2020]).

The three case study buildings are briefly introduced, where more detailed information can be found in the workshop report [Vail et al. 2020]. Each case study is defined as being in a global damage state, which is described by explicit levels of damage for each sub-assembly and material within the damage description package that was provided to the claims adjustors. Sample elevation views of the three case study buildings are shown in Figure 6.8.

The first case study building (CS1) is a 1200 ft^2 one-story house on a 2-ft-tall cripple wall. The exterior material is stucco, and the interior material is gypsum wallboard. The second case study building (CS2) is the same as CS1, with the only difference being the wall materials. The exterior material is horizontal wood siding, and the interior material is plaster on wood lath. The third case study building (CS3) is a 2464 ft^2 two-story house on a 6-ft-tall cripple wall, noting that the square footage does not include the attached garage. The exterior material is T1-11 panelized wood siding, and the interior material is gypsum wallboard. Interior finishes include ceramic tile for all case study buildings. Each case study includes a masonry chimney, damage descriptions for which were provided to the claims adjustors. However, the *FEMA P-58* assessments compared in this study did not include repair costs for masonry chimneys, and as described later, adjustments are made to account for this.

The first comparison between the claims adjustor estimates and those obtained using the assembly-based *FEMA P-58* functions considers the relative estimates for each case study building and assumed damage state expressed in present U.S. dollars (late 2018 to early 2019). The initial comparison is made using bar charts, such as those shown in Figure 6.9 for Case Study 1 (CS1) for each of the four assumed damage states. Each individual adjustor's estimate is shown in the blue bars and labeled with a number. The mean values from adjustors are shown with green bars with black borders. Note that the adjustor estimates herein correspond to the post-processed information that is described in Section 2.8 of the workshop report [Vail et al. 2020]. The "*FEMA P-58*" estimates are shown as mean (bar with black border) and one standard deviation bounds based on the cost dispersion assumed for each assembly cost function. *FEMA P-58* estimates for DS4 do not include dispersion, but rather are based on the assumed $200/ft^2 replacement cost. Dollar values are labeled as RCV, which represents 'replacement cost value' which does not include depreciation. The bar charts are provided for each case study building in Figure 6.9 through Figure 6.11. The main observations from these results are summarized as follows:

- In general, the mean estimates using *FEMA P-58* cost functions are in reasonable agreement with mean estimates from adjustors. Most discrepancies between the mean estimates do not exceed the range of values obtained by individual adjustors which is significant for most case studies and damage states;
- The assumption of $200/ft^2 for the building replacement cost for DS4 is in very good agreement with the values reported by claims adjustors;
- The plus and minus standard deviation bounds of cost estimates using *FEMA P-58* functions are reasonable in comparison to the ranges of estimates made by claims adjustors, acknowledging that this criterion is difficult to compare with such a small dataset;
- The largest discrepancy considering mean estimates and general trends of values between the adjustors and *FEMA P-58* estimates is for Case Study 3 at DS2.

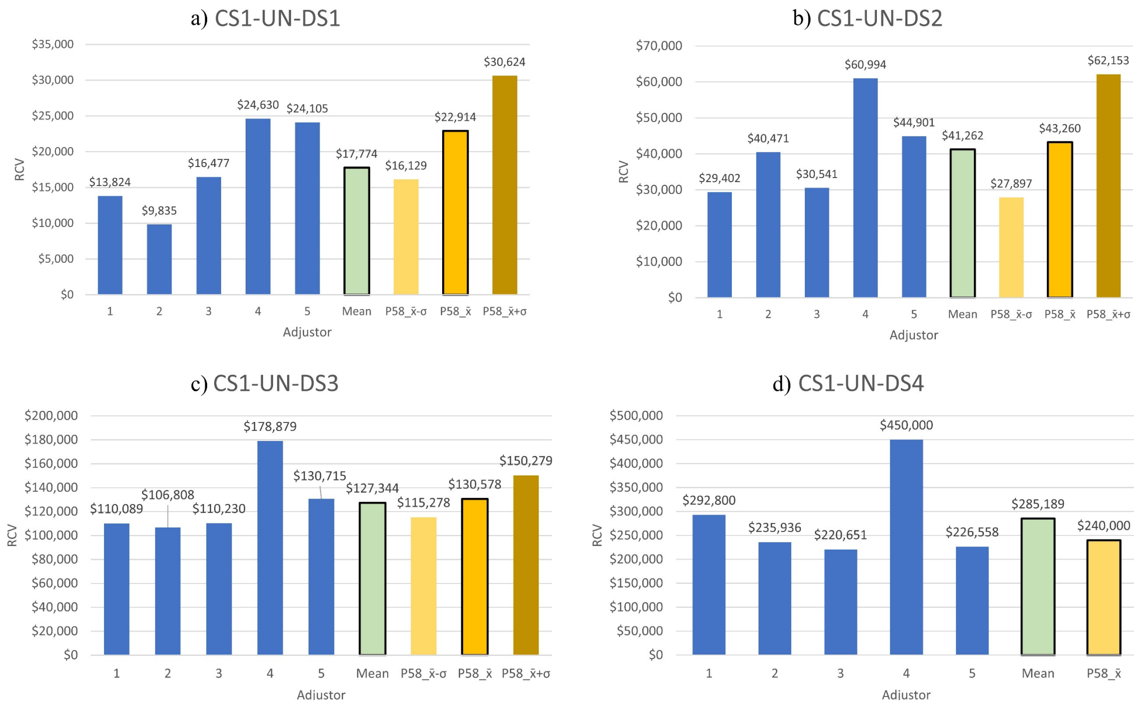

Figure 6.9 Comparison of claims adjustor estimates from the damage workshop with *FEMA P-58* assembly-based cost functions - Case Study 1 [Vail et al. 2020]: (a) DS1, (b) DS2, (c) DS3, and (d) DS4 (replacement cost of the dwelling).

Figure 6.10 Comparison of claims adjustor estimates from the damage workshop with *FEMA P-58* assembly-based cost functions - Case Study 2 [Vail et al. 2020]: (a) DS1, (b) DS2, (c) DS3, and (d) DS4 (replacement cost of the dwelling). Note: Adjustor 2 did not provide an estimate for DS3.

Figure 6.11 **Comparison of claims adjustor estimates from the damage workshop with *FEMA P-58* assembly-based cost functions - Case Study 3 [Vail et al. 2020]: (a) DS1, (b) DS2, (c) DS3, and (d) DS4 (replacement cost of the dwelling). Notes: Adjustors 1 and 5 did not provide replacement cost estimates (DS4), Adjustor 6 provided replacement cost (DS4) yet did not provide other damage state assessments.**

An alternate way to compare the Earthquake Damage Workshop results is in terms of percent replacement cost, where the repair cost estimates are normalized by the house replacement value as estimated by claims adjustors (i.e., normalizing by DS4 estimates). For this comparison, results can only be compared from adjustors that provided estimates of replacement cost. Each adjustor's estimate of total replacement cost is obtained as the DS4 estimate in Figure 6.9 to Figure 6.11. An additional consideration is the removal of estimated chimney damage from the adjustor estimates, which provides a more consistent comparison to the *FEMA P-58* estimates that do not include chimney damage.

The normalized replacement values for each of the three pre-replacement damage states (i.e., DS1, DS2, and DS3) for Case Study 1 are compared with the mean values obtained from the adjusted *FEMA P-58* functions in Figure 6.12. Figure 6.12(a) and Figure 6.12(b) show the estimates including and excluding chimney damage, respectively. Notably, all case studies assumed that DS1 did not include chimney damage. Similarly, the results for Case Study 2 and Case Study 3 are provided in Figure 6.13 and Figure 6.14, respectively. Note that the Case Study 3 results (Figure 6.14) use the mean adjustor replacement cost to normalize estimates for adjustors 1 and 5, since they did not provide estimates for DS4.

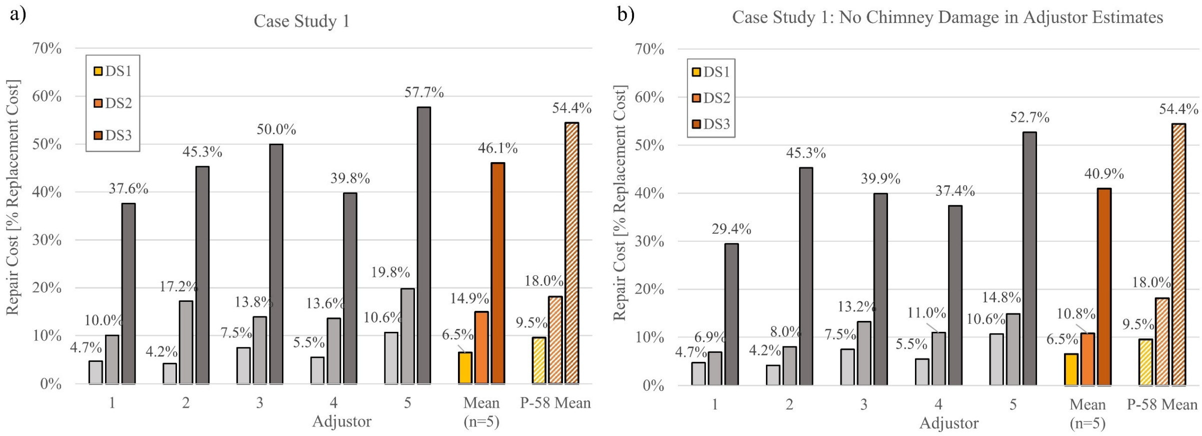

Figure 6.12 Case Study 1 repair estimates in terms of percent replacement cost: (a) including and (b) neglecting chimney damage in adjustors' estimates.

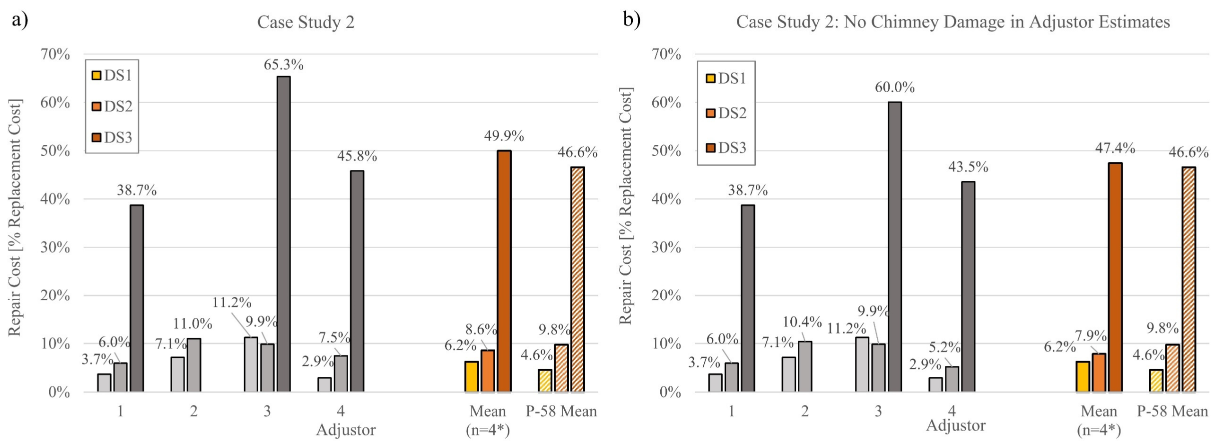

Figure 6.13 Case Study 2 repair estimates in terms of percent replacement cost: a) including and b) neglecting chimney damage in adjustors' estimates.

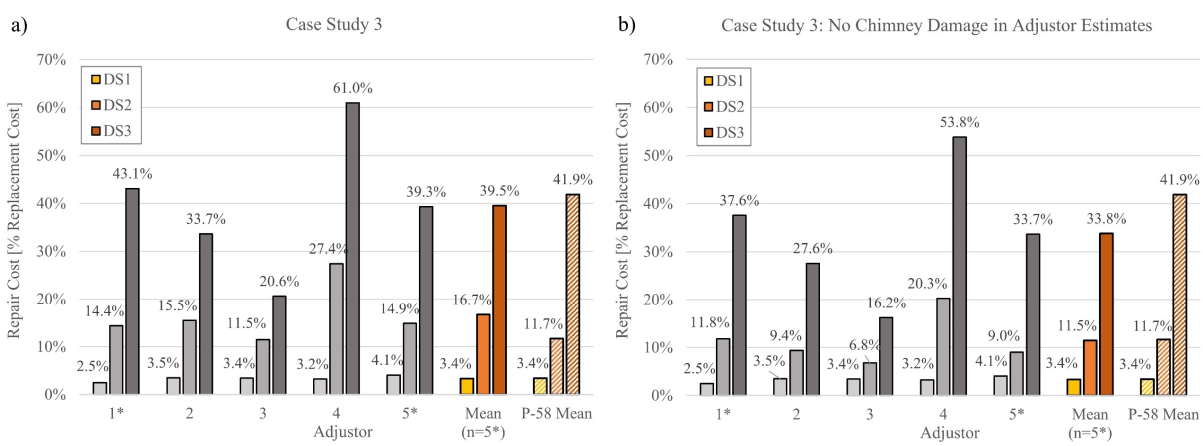

Figure 6.14 Case Study 3 repair estimates in terms of percent replacement cost: (a) including and (b) neglecting chimney damage in adjustors' estimates.

The normalized cost estimates provided in Figure 6.12 to Figure 6.14 allow for several observations to better understand earthquake damage cost estimation. A few of these observations are as follows:

- The claims adjustor estimates are shown to have widely varying contributions of chimney damage for different case studies and damage states. A clear example is shown for Case Study 2 (CS2; Figure 6.13), where adjustor 4 included chimney damage for DS2 and DS3 (as described in the case study package), adjustor 3 included chimney damage for DS3 and not for DS2, and adjustor 1 did not provide any estimates for chimney damage. Notably, adjustor 3 for CS2 estimated larger total costs for DS1 than DS2.
- Normalizing by replacement cost is shown to change mean comparison trends between adjustors and *FEMA P-58* estimates, as compared to comparisons based on total dollar amounts presented previously. Comparing Case Study 1 results, mean comparisons for DS2 and DS3 were shown to be relatively close in dollars (Figure 6.9), whereas with the normalized values (Figure 6.12), the *FEMA P-58* estimates of DS2 and DS3 seem to be considerably higher than adjustor means, even before removing chimney damage. Conversely, Case Study 3 in DS2 was shown to have the largest comparative discrepancies between adjustors and *FEMA P-58* estimates in dollars, with DS3 being in very good agreement (Figure 6.11). But, when normalizing by replacement cost and removing chimney damage, the *FEMA P-58* estimates appear to be in close agreement with DS2, yet seemingly overestimating DS3 when compared to adjustor means; see Figure 6.14.

These observations only scrape the surface of the numerous uncertainties in comparisons of earthquake damage cost estimates. In spite of the detailed damage descriptions, repair measures, cost considerations, and other constraints used in developing the case studies for the adjustor workshop, large variations in the adjustors' cost estimates arose due to different interpretations of the damage description packages, along with differences in the methods and assumptions applied by individual adjustors. On the *FEMA P-58* assessment side, review and modification of existing *FEMA P-58* cost functions also led to a better understanding of the cost considerations behind different assemblies and damage states. This information informed development of the damage description packages to define and describe damage in the most consistent way possible. Nevertheless, large differences persisted between the approaches used in *FEMA P-58* and by the claims adjustors.

The comparison of cost estimates presented in this section illustrate that there are numerous considerations that need to be acknowledged when assessing validity of one method over another. The comparison between the proposed *FEMA P-58* formatted cost functions, and the claims adjustor estimates was conducted as a semi-blind study. The resulting agreement between the two approaches was surprisingly good. Given the equally large variation in results between adjusters as there was between adjusters and *FEMA P-58*, it was decided that any further modification of the proposed assembly-based cost functions was not warranted.

6.5 ECONOMIC CONSEQUENCES OF CRIPPLE WALL COLLAPSE

When a cripple wall fails, there can be large variations in the resulting damage to both the crawlspace and the superstructure above. While there are anecdotal observations of possible damage, there is limited information within published literature to quantify the economic consequences of failed cripple walls. To take stock of the issue and decide on appropriate loss values associated with cripple wall collapse, this sub-section first provides discussion of the possible sources of damage due to cripple wall collapse. Following a brief overview of existing information, a proposal is developed for quantifying economic consequences of cripple wall collapse.

6.5.1 Different Damage Consequences for Cripple Wall Collapse

The California Seismic Safety Commission's *Homeowner's Guide to Earthquake Safety* [CSSC 2005] provides some exemplary photos that describe the large variation in consequences for houses with failed crawlspace walls and connections. Figure 6.15 illustrates two homes that have slid off of their foundations. The caption of the home in Figure 6.15(a) mentions that *sometimes* resulting damage can incur complete demolition and replacement of the home, while Figure 6.15(b) shows such a case for a failed cripple wall that, reportedly, resulted in a total loss following the 1989 Loma Prieta event. The guide [CSSC 2005] reflects this large uncertainty by giving likely ranges of damage for unretrofitted crawlspace dwellings between tens of thousands of dollars to the entire value of the structure.

"This house wasn't bolted and slid off its foundation. *Sometimes* the damage can be so bad that houses have to be demolished."

"[This] house moved off its foundation and was considered a *total loss*."

Figure 6.15 Examples of varying consequences for homes sliding off of foundations from the CSSC Homeowner's Guide to Earthquake Safety [CSSC 2005].

The large range of economic consequences due to cripple wall failure occurs due to different interactions between the superstructure and the supporting cripple walls and foundation. The FEMA-232 *Homebuilders' Guide to Earthquake Resistant Design and Construction* [FEMA 2006] provides two photographs, shown in Figure 6.16, that clearly illustrate the varying consequences of cripple wall failure. The house in Figure 6.16(a) seemingly came off of its cripple wall in a uniform fashion with the first-floor diaphragm resting on the foundation and the exterior of the home largely intact. The *minimum* repair effort for this home would be to jack up the home, reconstruct the cripple wall, and reconnect the utilities that were damaged during the cripple wall collapse. The home shown in Figure 6.16(b) shows significant damage to the exterior of the home caused by the separation between the roof supported by porch columns and main structure as the house displaced downward with the collapsed cripple wall. These two homes can clearly be identified as having drastically different levels of exterior damage, although the conditions of the interiors of the houses are unknown.

As pointed out by Osteraas [2019], even when a cripple wall collapses in a rather uniform manner, the first-floor framing is now "draped" over the perimeter foundation, interior supports, and any mechanical equipment that may have been located in the crawlspace. In the gentlest of collapses, the exterior siding, windows, doors, and roofing may have only minor repairable damage. However, the interior of the home could experience significant distortion, causing significant damage to floors, wall and ceiling finishes, cabinetry, and utility systems within the home.

Reconnaissance documentation of interior damage due to cripple wall failures is limited, yet a few cases are described in the following figures. Figure 6.17 shows the effect of a cripple wall collapsing downward on the connection to a split-level home following the 1971 San Fernando event. The interior damage shown was reportedly due to the collapse of the cripple wall following an aftershock. The main shock caused damage to the multi-story portion at the garage and split-level connection [ATC-HUD 1976]. Figure 6.18 shows an extreme case of vertical impact causing widespread interior damage. The figure shows an older home on a tall (~5 ft) unbraced cripple wall that suffered a cripple wall failure in the 1992 Cape Mendocino event, where the exterior superstructure remained largely intact; see Figure 6.18(a). The severe interior damage to lath and plaster was likely caused by the vertical impact when the superstructure was pulled downward, causing widespread shearing of plaster keys as shown in Figure 6.18(b).

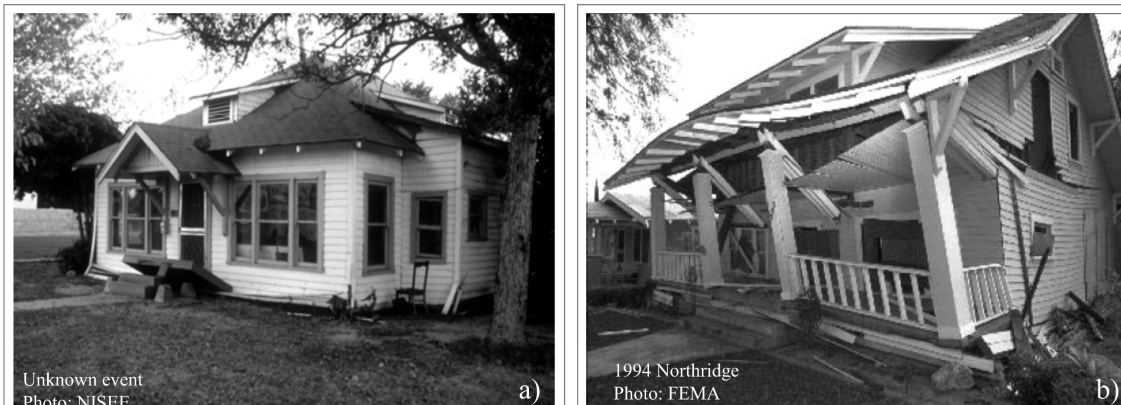

"As a *minimum*, this house will have to be jacked up to be repositioned on the foundation and have utilities reconnected."

"[This] house … suffered more severe damage due to cripple wall collapse."

Figure 6.16 Illustration of varying consequences due to cripple wall failure from *FEMA 232* [2006].

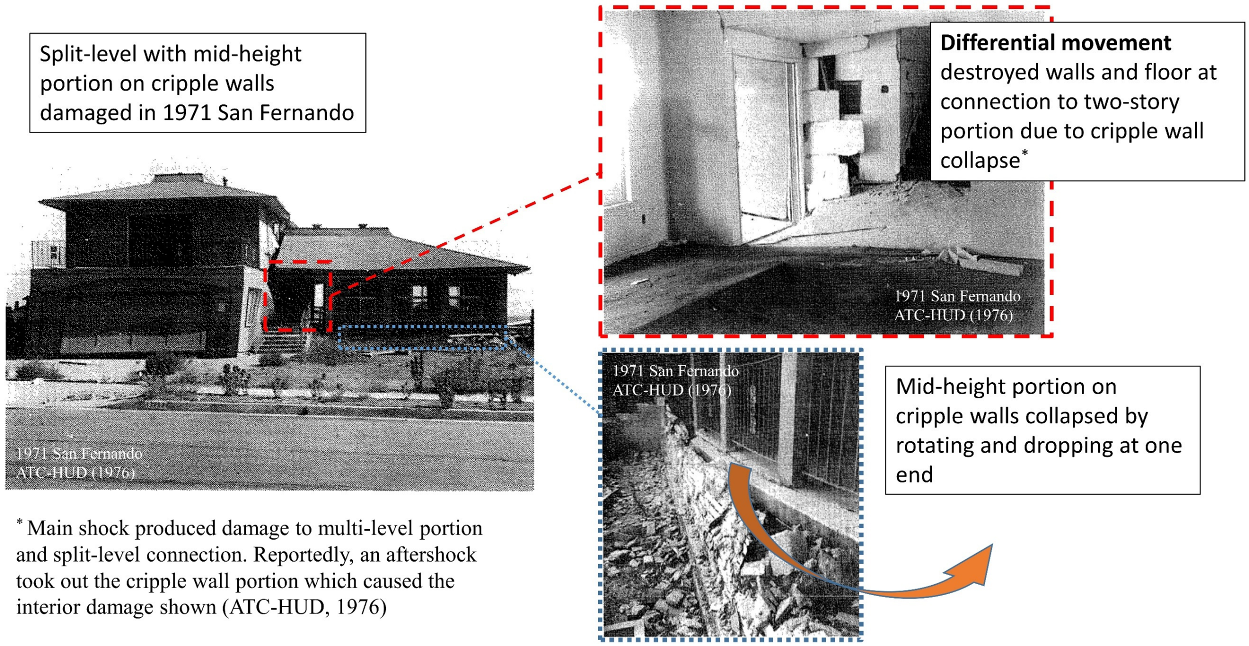

Figure 6.17 Illustration of how differential vertical displacements can affect the interior of a home. Note: this structure suffered from numerous seismic vulnerabilities, including unbraced cripple walls on the one-story portion of the home.

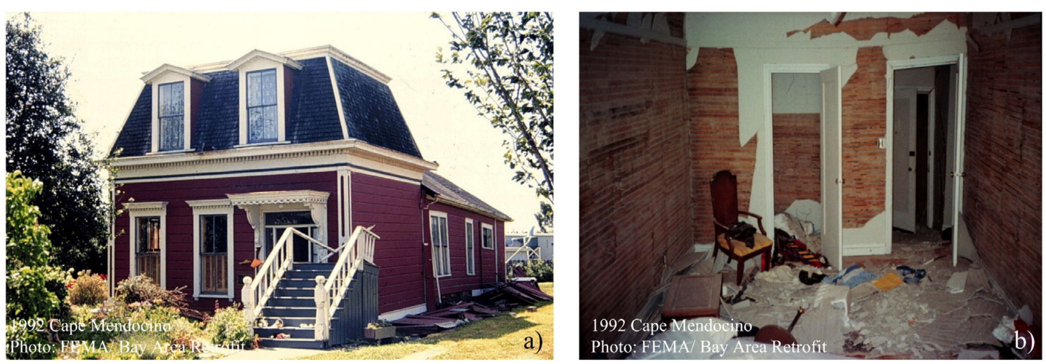

Figure 6.18 Influence of cripple wall collapse causing interior damage in superstructure due to impact: (a) older home with tall collapsed cripple wall (note height of front steps); and (b) extensive interior damage to same home despite superstructure appearing intact from exterior.

The two aforementioned cases (Figure 6.17 and Figure 6.18) could be viewed as extreme scenarios for damage induced by cripple wall failure. However, the large variation in damage due to cripple wall failure can be shown when comparing to other cases as well. Figure 6.19 illustrates two adjacent cripple wall failures from the 1987 Whittier Narrows earthquake. The one-story home on the left of the figure collapsed uniformly. However, the two-story home on the right of Figure 6.19 suffered an “uneven” collapse with the cripple wall forcing only half of the superstructure downward which plausibly caused interior damage similar to the split-level home shown in Figure 6.17.

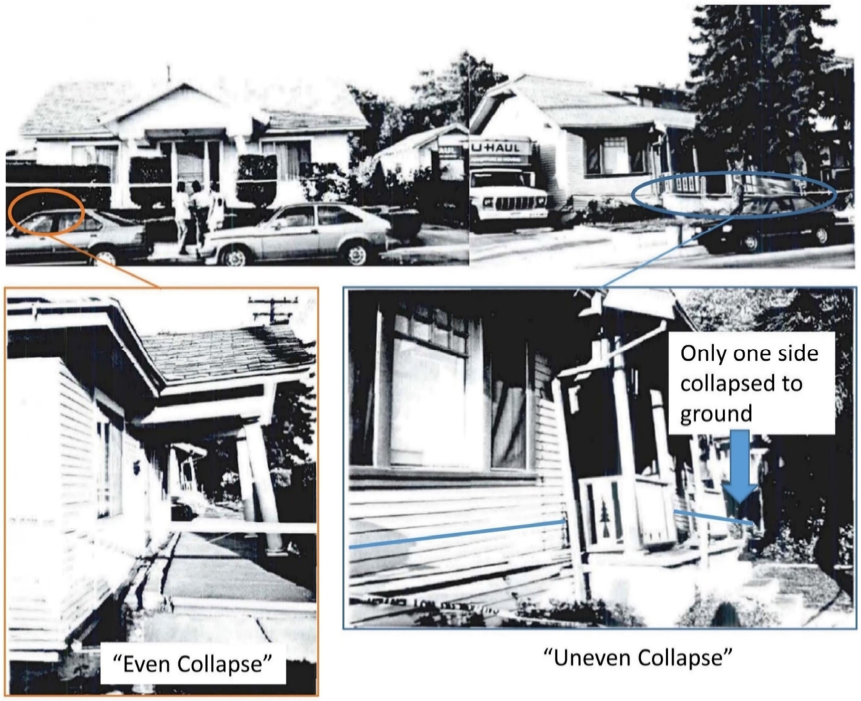

Figure 6.19 **Two adjacent cripple wall failures following the 1987 Whittier Narrows event: (a) one-story home with the entire cripple wall collapsing; and (b) two-story home with a partial cripple wall collapse on one side of the structure (photographs adapted from Lew [1987]).**

Following the 1994 Northridge earthquake, Hall et al. [1996] report a case where a retrofit cripple wall dwelling performed quite well with only minor finish damage (left of Figure 6.20). Importantly, there were five unbraced cripple wall failures on the same block as the retrofitted house that received red tags (right of Figure 6.20). Hall et al. [1996] reported that two of the five homes were demolished. No further information is known about the resulting losses of the homes, yet the possibility of cripple wall failure rendering homes uneconomical to repair is evident.

Figure 6.21 shows a two-story cripple wall failure from the 2014 South Napa earthquake [PEER 2014]. Google Streetview was used to capture the timeline of the dwelling for pre-event, post-event, rehabilitation, and a more recent view of the repaired and rehabilitated dwelling (left-to-right in Figure 6.21). Reportedly, this structure had repair costs on the order of hundreds of thousands of dollars [Lin 2018]. The third photo in Figure 6.21 shows that a drywall contractor was hired at some point during rehabilitation. This illustrates that the repair costs for this structure were partially due to interior damage to the occupied stories following cripple wall failure.

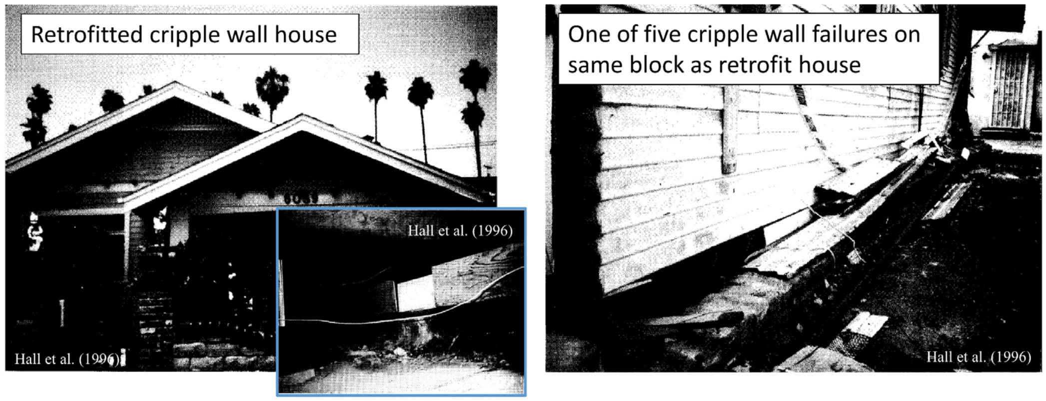

Figure 6.20 Cripple wall performance following the 1994 Northridge earthquake. The retrofitted house on the left performed well with minor damage, the photo on the right represents one of five cripple wall failures on the same block as the retrofitted house that received red tags. Two of the five unretrofitted houses were reportedly demolished [Hall et al. 1996].

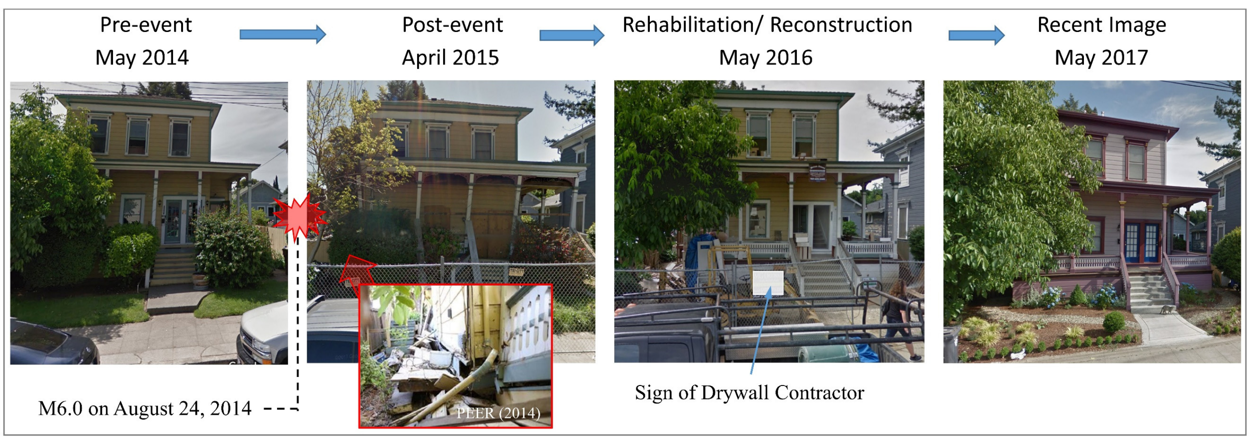

Figure 6.21 Google streetview timeline for a two-story cripple wall dwelling that collapsed during the 2014 South Napa earthquake. Sign of drywall contractor in rehabilitation photo indicates that collapsed cripple wall caused interior damage to the occupied stories (Timeline photos obtained from Google Maps 2019.).

6.5.2 Attempts to Quantify Repair Consequences for Cripple Wall Collapse within the Literature

There is very little information to statistically quantify the economic consequences of cripple wall failure. Two available sources described in this sub-section are from the work of Grossi [1998] and Porter et al. [2002].

The work by Grossi [1998] involved an in-depth survey of contractors and engineers to better understand the cost-benefit of seismic mitigation for older wood-frame dwellings. Most important to the current discussion is the survey results from practicing engineers that estimated the damage versus intensity relationship for an unbraced cripple wall dwelling. The survey included responses from 69 practicing engineers, who were asked to provide mean damage factor (MDF; fraction of replacement cost) values for increasing seismic intensity defined using the Modified Mercalli Intensity (MMI). The case structure under question was a two-story 2200 ft^2 pre-1940s home with an unbraced 2-ft-tall cripple wall. The structure was assumed to be located in Oakland, California, or Long Beach, California, depending on whether the engineer practiced in Northern or Southern California. The MMI values ranged from VI to XII. Grossi [1998] provides more in-depth discussion regarding responses of engineers with respect to the provided information and the use of MMI as an IM, among other considerations. The structure of the survey was purposefully intended to provide generic information and use MMI to be consistent with other studies, such as ATC-13 [1985], that were relevant at the time. A major assumption made for the interpretation of these results for the purposes of this study is that the engineer responses for the unbraced cripple wall at MMI XII reflects the economic consequences for cripple wall collapse. The survey results documented by Grossi [1998] are shown in Figure 6.22 for the unbraced cripple wall case (referred to as "before mitigation" in Grossi [1998]).

Figure 6.22 shows three different curves. The "upper" curve represents the group of engineers that attributed 100% loss (i.e., MDF = 1.0) at the highest intensity, representing an upper bound of responses. The "lower" curve represents the lower bound grouping of responses that had estimated curves at or below ATC-13 standard construction curves for low-rise wood-frame (ATC-13 also provides nonstandard construction curves for low-rise wood-frame that include pre-1940s construction with unbraced cripple walls). The "average" curve represents the mean of all 69 responses. The results clearly show a wide range of expected consequences, ranging from approximately 36% of replacement cost at the lower bound to 100% replacement cost at the upper bound. The average of all responses gave an estimate of approximately 70% of replacement cost for the highest seismic intensity considered in the survey.

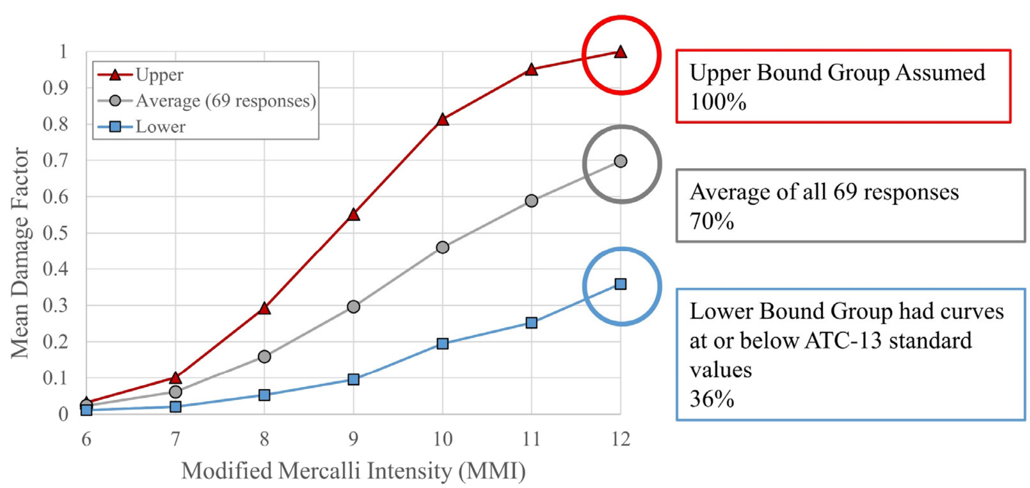

Figure 6.22 **Survey results from Grossi [1998] asking 69 engineers to estimate cost versus intensity curves for a two-story pre-1940s house with an unbraced 2-ft-tall cripple wall. Values at an MMI of XII are assumed to represent costs associated with cripple wall failure.**

Cost Data Sheet 9 [Porter et al. 2002]

This cost data sheet is very approximate, and is based on a rough picture of the potential damage resulting from cripple-wall collapse. Further study of this cost item is warranted.

Assembly Type

Collapsed small house.

Damage State

Cripple walls collapse, leaving first floor resting on the foundation. Electrical and plumbing hookups are fractured. Building above first floor is largely intact, with various damages to all the finishes.

Repairs Recommended

Raise the structure, rebuild the cripple wall with bracing, repair exterior stucco, patch interior drywall damage, repair broken ceramic tile, replace broken windows, reinstall carpet, and repaint.

Total Repair Cost and Duration

Raise structure:	$12,000
Rebuild and brace the cripple wall:	6,300
Stucco repairs:	3,500
Drywall repairs:	4,500
Ceramic tile:	2,300
Hookups, carpet, paint, glass, etc.:	9,400

Total cost, mean: $38,000 Upper bound: $43,000 Lower bound: $33,000

Comments, References

This cost is modeled as uniformly distributed between $33,000 and $43,000. Adding median contractor overhead and profit of 17.5% (being careful not to double-count O&P): $39,000 to $51,000.

- Mean cripple wall replacement cost is **$44,650** after considering contractor overhead and profit (2001 USD, Located in Santa Monica)
- Assuming 3% inflation (0.03) and regional factor (1.10) for Los Angeles area to San Francisco area:

$$\mathit{Cripple\ Wall\ Replacement\ Cost} = \$44{,}650(1+0.03)^{16}(1.10) = \$78{,}815$$

- Lower bound, mean, and upper bound expressed in % of total replacement cost ($240,000)

% Total Replacement Cost to Repair Failed Cripple Wall Based on CUREE Woodframe [Porter et al. 2002]		
Lower Bound	**Mean**	Upper Bound
28.7%	**32.8%**	37.5%

Figure 6.23 Recommended repair cost considerations for a cripple wall failure in a one-story dwelling by Porter et al. [2002] (left) and simple calculations and assumptions to translate this into a percentage of building replacement cost (right).

The work of Porter et al. [2002] within the CUREE-Caltech Woodframe Project included a cost breakdown for repairing a collapsed cripple wall for the 1200-ft^2 one-story house considered in their report. This breakdown is provided as *Cost Data Sheet 9* in the Appendices of the Porter et al. [2002] report, which is replicated in the left portion of Figure 6.23. The repair cost estimates include the following repair actions: raising the structure, rebuilding the cripple wall, exterior stucco repairs, interior drywall and tile repairs, mechanical hookups, painting, and window repair. Porter et al. [2002] assumed a median contractor overhead and profit of 17.5%. When including contractor overhead and profit and normalizing by the total replacement cost of the dwelling, the mean cost for restoring a failed cripple wall is estimated to be approximately 33% of the replacement cost. Interestingly, Porter et al. [2002] also provide lower and upper bound estimate values of 29% and 38%, respectively, which only has a range of 4 to 5% around the mean estimate. The normalized repair estimates are provided in the right portion of Figure 6.23.

Based on the limited information on the topic of repairs incurred by cripple wall collapse, a sensitivity study was conducted to quantify the influence of cripple wall collapse consequences on the economic loss. A sample of results of the sensitivity study are presented in Figure 6.24 for an existing (unretrofitted) and retrofitted pair of one-story horizontal wood siding variants with 2-ft-tall cripple walls, assumed to be located in Northridge, California. Similar trends are observed for other variants. Figure 6.24 provides the mean loss curves as a function of return period for the existing (solid lines) and retrofitted (dashed lines) models that are treated exactly the same with respect to structural analysis and loss modeling, except the consequence associated with cripple wall collapse varies in magnitude from 33% to 66% and 100% of replacement cost. The figure clearly shows the large influence on the collapse consequence assumption for the existing (unretrofitted) cripple wall case, with the general trend resembling the range of judgment-based curves from Grossi [1998] shown in Figure 6.22.

Conversely, the retrofit case is much less affected since retrofitting of the cripple wall drastically reduces collapse probability, which is the primary objective for the vulnerability-based retrofit according to *FEMA P-1100* [2018]. The significance of this modeling assumption is best reflected when looking at the relative difference (Δ) in values between existing (unretrofitted) and retrofitted cases, which represents the benefits due to retrofitting. The top of Figure 6.24 includes a summary table showing the influence of cripple wall failure consequences on the two primary loss metrics: expected annual loss and mean repair cost at the 250-year return period (RC250). The relative difference between existing (unretrofitted) and retrofitted structure is shown in bold (i.e., Δ_{EAL} and Δ_{RC250}) in the summary provided in Figure 6.24. These results show the relative benefits using these two loss metrics, which can vary by a factor of 3 to 3.5 times when considering 33% versus 100% replacement cost attributed to cripple wall failure. The sensitivity study shows that this assumption can have significant impact on the calculated economic benefits due to seismic retrofitting of cripple walls.

*All values in % replacement cost

CW Fail Cost	$EAL_{Existing}$	$RC250_{Existing}$	$EAL_{Retrofit}$	$RC250_{Retrofit}$	$\boldsymbol{\Delta_{EAL}}$	$\boldsymbol{\Delta_{RC250}}$
100%	1.48%	66.6%	0.11%	5.8%	**1.37%**	**60.8%**
66%	0.99%	45.0%	0.10%	5.3%	**0.89%**	**39.7%**
33%	0.51%	23.0%	0.09%	5.0%	**0.42%**	**18.0%**

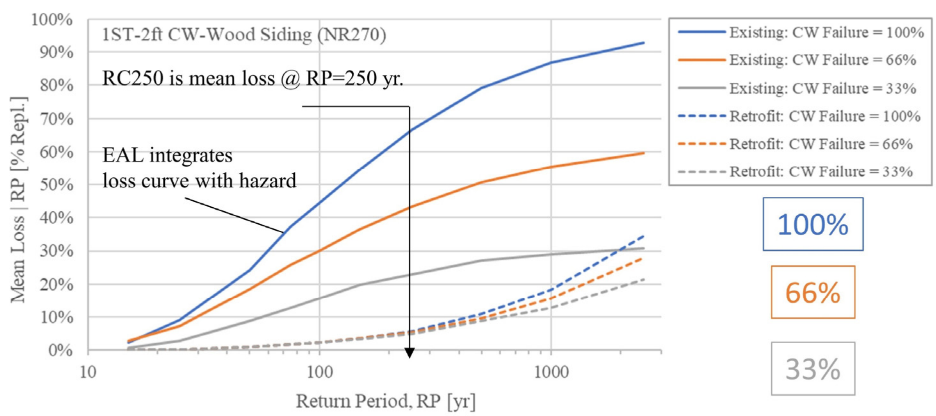

Figure 6.24 Sample results from preliminary sensitivity study on collapse consequence assumptions for cripple wall failure. Results shown are for a one-story cripple wall dwelling with horizontal wood siding assumed to be located in Northridge, California.

6.5.3 Assumption for Treatment of Cripple Wall Collapse

The preceding information in Section 6.5 was collected and presented for discussion among the PEER–CEA Project Team as well as internal and external reviewers. The information clearly demonstrates that numerous factors are involved with estimating the consequences of a failed cripple wall, as well as large implications on loss reduction benefits due to retrofitting. Since no better information could be obtained, for this Project it was decided to assume that cripple wall failure incurs 67% (i.e., two-thirds) of dwelling replacement cost as a baseline to be carried through the analysis. Accordingly, results presented in this report will be based on the 67% replacement cost as a baseline assumption for cripple wall failure. Importantly, data was preserved throughout the loss analysis calculations to modify this assumption in the future.

6.6 ECONOMIC CONSEQUENCES OF STEM WALL ANCHORAGE FAILURE

The economic consequences of stem wall failure are based on the assumption that the critical failure mode is at the floor joist-to-mudsill connection, consistent with the fragilities developed and discussed in Section 5.4.6. The repairs considered three distinct sequential damage states (see Figure 5.28). Damage State 1 assumes that the stem wall connections have been damaged enough to allow some relative displacement, but not enough to require straightening of the house, and includes damage to the toe-nail connections and damage to the perimeter finish of the home. Damage State 2 includes damage associated with DS1 but also includes costs of straightening the house. Damage State 3 includes DS1 and DS2, but the stem wall floor joists are assumed to have become unseated from the sill plates on at least one side of the dwelling, which requires that the dwelling must be jacked up in order to realign on the stem wall before making other repairs.

Repair costs estimates for stem wall damage states were determined considering input from the PEER–CEA Project team members as well as external and internal reviewers. The repair costs for DS1 distinguish between stucco and wood siding exterior for the repairs involving the finish of the dwelling. Exterior wall repairs include the bottom 2 ft of the exterior (i.e., 2 ft above the bottom of the exterior finish) and vary depending on the damage state. The repairs to the joist-to-sill connections of the stem wall assume that framing clips (e.g., A35s) will be installed. For the index house layout, a total of 122 clips are assumed to be required which correspond to two clips for each joist running perpendicular to the stem wall with ends bearing on the sill plate and one clip every 12 in. for rim joists running parallel to the stem wall. Costs associated with mechanical, electrical, and plumbing (MEP) are included for DS2 and DS3, but not for DS1.

Considerations for straightening the dwelling are included in the DS2 costs. For DS3, additional costs of jacking the dwelling prior to straightening are included. A factor of 1.5 (i.e., 50% increase) was applied to the straightening and jacking costs for two-story dwellings with respect to one-story dwellings. The contributions of different repair costs are illustrated in Table 6.3. The table also provides the total repair costs attributed to each of the three damage states for each type of stem wall dwelling. The variations include stucco or wood siding exterior with one or two stories. The values in Table 6.3 are expressed in terms of 2011 USD to be consistent with other *FEMA P-58* cost functions used for loss analysis. The total stem wall repair costs are expressed in terms of the percentage of dwelling replacement cost for each of the three damage states in Figure 6.25. Note that the normalized costs are generally less for the two-story configuration, even though the total costs are more since the normalizing replacement value of the two-story house is twice that of the one-story house.

Table 6.3 **Summary of estimated repair costs for stem wall dwellings.**

	DS1 [2011 USD][1]	DS2 [2011 USD]	DS3 [2011 USD]
	0.25 in. ≤ Δ_{SW} < 0.85 in. [2]	0.85 in. ≤ Δ_{SW} < 4.0 in.	Δ_{SW} ≥ 4.0 in.
	Exterior/ connection repair only	Straightening required before repairs	Jacking and straightening required before repairs
Clips and fasteners	3241	3241	3241
Wall repairs - stucco exterior	9724	29173	48622
Wall repairs - wood siding exterior	8104	24311	40519
MEP	N/A	8104	8104
Straightening/ Jacking - one story	N/A	24311	42545
Straightening/ Jacking - two story	N/A	36467	63817
Total: One-story, stucco exterior [3]	12966	64380	102512
Total: One-story, wood siding exterior [3]	11345	59968	94408
Total: Two-story, stucco exterior [3]	12966	76985	123784
Total:Two-story, wood siding exterior [3]	11345	72123	115681

[1] Values are expressed in 2011 USD to be consistent with other *FEMA P-58* cost functions, a factor of 1.234 is assumed to convert from 2011 to current project timeline USD.
[2] The displacement ranges of relative joist-to-sill displacement (Δ_{SW}) associated with the damage state (these values are generalized ranges, see Section 5.4.6 and Table 6.6 for fragility information).
[3] The total costs reflect the required repairs of the entire perimeter of the dwelling.

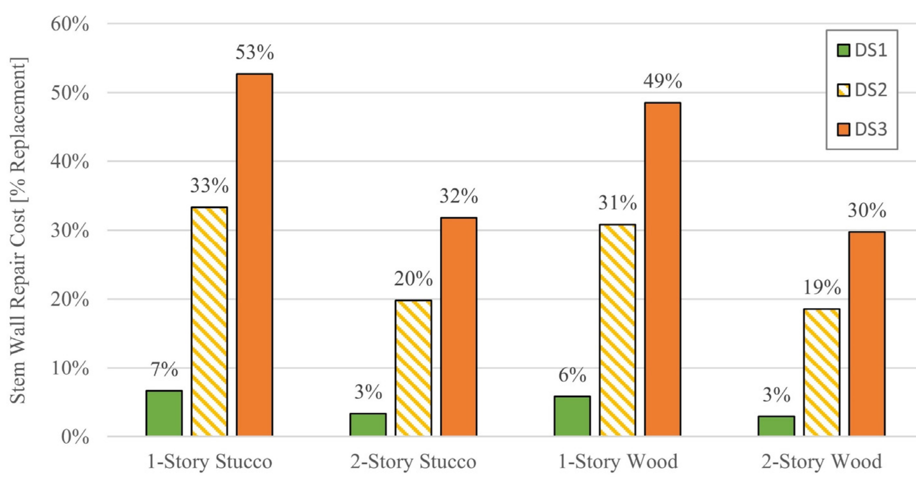

Figure 6.25 Stem wall repair costs normalized to the assumed replacement cost of each dwelling type.

6.7 SUMMARY OF COMPONENT DAMAGE FRAGILITIES AND COST FUNCTIONS USED FOR ASSESSMENT OF BUILDING VARIANTS

This section provides a summary of all component damage fragility and cost (consequence) functions used for the performance assessment of building variants in the PEER–CEA Project. All costing values are presented in 2011 U.S. dollars to be consistent with cost functions using the *FEMA P-58* database. The current project assumption is to use an inflation factor of 1.234 to translate into 2019 U.S. dollars. The assemblies considered for the superstructure (i.e., occupied stories) of building variants are provided in Table 6.4. This table includes exterior wall sub-assemblies as well as interior wall materials and additional finishes (i.e., ceramic tile). The damage fragilities and cost functions used for cripple wall sub-assemblies are summarized in Table 6.5. The cost functions presented in Table 6.4 and Table 6.5 maintain the same lower quantity (LQ), upper quantity (UQ), and cost dispersion (β_{cost}) as the original *FEMA P-58* functions that were the basis for the revised damage and cost information. Descriptions of damage states and repair efforts have already been defined in Chapter 5 and appropriate sections of Chapter 6.

The summarized damage fragilities and cost functions implemented for existing (unretrofitted) stem wall dwellings with anchorage deficiency in the floor joist-to-sill connections are presented in Table 6.6. These cost functions do not account for lower and upper quantities since the entire perimeter of the dwelling is considered as the damageable assembly. A small dispersion in repair costs of 0.1 was applied to each damage state. The indices provided for each sub-assembly in Table 6.4 to Table 6.6. are those used to flag the particular assembly within WG5 electronic documentation [PEER 2020].

Table 6.4 Summary of damage fragility and repair cost functions used for assessment of building variants: exterior and interior superstructure materials.

Assembly (index)	Unit	Damage fragility[1]			Repair cost function (2011 USD)[2,3]				
		DS_i	θ_{DSi} (rad)	β_{DSi}	$RC_{LQ,i}$ ($)	LQ	$RC_{UQ,i}$ ($)	UQ	β_{Cost}
Exterior stucco (EXT_STUCCO)	100SF	1	0.0020	0.45	1195	2	736	6	0.26
		2	0.0050	0.40	1696	2	1202	6	0.37
		3	0.0150	0.40	5225	2	3701	6	0.11*
Exterior T1-11 siding (EXT_T111)	100SF	1	0.0100	0.40	658	3	405	8	0.19
		2	0.0175	0.40	1155	3	818	8	0.22
		3	0.0250	0.40	2646	3	1874	8	0.12
Exterior horizontal wood siding/sheathing (Ext_HS_HSh)	100SF	1	0.0300	0.50	3020	4	1874	8	0.11*
Interior gypsum wallboard (INT_GWB)	100LF[4]	1	0.0021	0.60	3937	1	1181	10	0.42*
		2	0.0071	0.45	8658	1	2597	10	0.49*
		3	0.0120	0.45	27824	1	8347	10	0.10
Interior plaster on wood lath (INT_LP)	100LF[4]	1	0.0013	0.55	4894	1	1468	10	0.42*
		2	0.0045	0.40	9768	1	2930	10	0.49
		3	0.0110	0.40	33464	1	10039	10	0.10
Ceramic tile (FIN_TILE)	100LF[4]	1	0.0021	0.60	34992	1	23328	3	0.10*
Wallpaper finish (FIN_WP)	100LF[4]	1	0.0021	0.60	3240	1	2160	10	0.15

[1] All damage fragilities are expressed in terms of story drift ratio as the median engineering demand parameter.
[2] RC represents repair cost, LQ and UQ are lower and upper unit quantities, respectively.
[3] Costing dispersion with an asterisk is assumed as a normal distribution, lognormal otherwise.
[4] Interior materials are based units of 100 linear feet of wall with costing based on a 9-ft wall height.

Table 6.5 Summary of damage fragility and repair cost functions used for assessment of building variants: cripple wall materials.

Cripple wall assembly (Index)	Unit	Damage fragility[1]			Repair cost function (2011 USD)[2,3]				
		DS_i	θ_{DSi} (rad)	β_{DSi}	$RC_{LQ,i}$ ($)	LQ	$RC_{UQ,i}$ ($)	UQ	β_{Cost}
2 ft-tall stucco (2CW_ST) [4]	100SF	1	0.0053	0.45	1195	2	736	6	0.26
		2	0.0132	0.40	1696	2	1202	6	0.37
		3	0.0396	0.40	5225	2	3701	6	0.11*
6 ft-tall stucco (6CW_ST)	100SF	1	0.0025	0.45	1195	2	736	6	0.26
		2	0.0061	0.40	1696	2	1202	6	0.37
		3	0.0184	0.40	5225	2	3701	6	0.11*
Exterior horizontal wood siding (unknown bracing) (EXT_HS_HSh)	100SF	1	0.0300	0.50	3020	4	1874	8	0.11*
Exterior horizontal wood siding (bracing in framing considered) (EXT_HS_LIB)	100SF	1	0.0150	0.50	3020	4	1874	8	0.11*
2-ft-tall T1-11 siding (2CW_T111)	100SF	1	0.0264	0.40	658	3	405	8	0.19
		2	0.0462	0.40	1155	3	818	8	0.22
		3	0.0660	0.40	2646	3	1874	8	0.12
6-ft-tall T1-11 siding (6CW_T111)	100SF	1	0.0122	0.40	658	3	405	8	0.19
		2	0.0214	0.40	1155	3	818	8	0.22
		3	0.0306	0.40	2646	3	1874	8	0.12

[1] All damage fragilities are expressed in terms of story drift ratio as the median engineering demand parameter.
[2] RC represents repair cost, LQ and UQ are lower and upper unit quantities, respectively.
[3] Costing dispersion with an asterisk is assumed as a normal distribution, lognormal otherwise.
[4] All assemblies with a height distinction have damage fragilities based on an assumed height relationship to full-height wall damage discussed in Chapter 5

Table 6.6 Summary of damage fragility and repair cost functions used for assessment of building variants: perimeter stem wall assemblies.

Stem wall assembly (Index)	Unit	Damage fragility[1]			Repair cost function (2011 USD)[2,3]				
		DS_i	θ_{DSi} (rad)	β_{DSi}	$RC_{LQ,i}$ ($)	LQ	$RC_{UQ,i}$ ($)	UQ	β_{Cost}
One-story, wood siding exterior (TN_1HS_2)	140LF[4]	1	0.40	0.30	11345	1	11345	1	0.10*
		2	0.85	0.40	59968	1	59968	1	0.10
		3	3.50	0.05	94408	1	94408	1	0.10
One-story, stucco exterior (TN_1ST_2)	140LF[4]	1	0.40	0.30	12966	1	12966	1	0.10*
		2	0.85	0.40	64830	1	64830	1	0.10
		3	3.50	0.05	102512	1	102512	1	0.10
Two-story, wood siding exterior (TN_2HS_2)	140LF[4]	1	0.40	0.30	11345	1	11345	1	0.10*
		2	0.85	0.40	72123	1	72123	1	0.10
		3	3.50	0.05	115681	1	115681	1	0.10
Two-story, stucco exterior (TN_2ST_2)	140LF[4]	1	0.40	0.30	12966	1	12966	1	0.10*
		2	0.85	0.40	76985	1	76985	1	0.10
		3	3.50	0.05	123784	1	123784	1	0.10

[1] All damage fragilities are expressed in terms of the peak transient displacement (expressed in inches) between the floor joists and mudsill for any location and orthogonal direction.
[2] RC represents repair cost, LQ and UQ are lower and upper unit quantities, respectively.
[3] Costing dispersion with an asterisk is assumed as a normal distribution, lognormal otherwise.
[4] The unit is based on the entire perimeter of a 40-ft × 30-ft rectangular plan.

6.8 PROCESS AND MODELING FOR LOSS ASSESSMENT

6.8.1 Software to Carry Out Performance Assessment

The preliminary performance assessments were carried out using the Seismic Performance Prediction Program (*SP3*) developed by HBRisk (*www.hbrisk.com*). To facilitate calculation of the large number of multiple assessments within the numerical workflow, the final performance assessments were carried out using the Python library *pelicun*, which is part of the NHERI SimCenter's PBE workflow [Zsarnoczay 2019; Zsarnoczay and Deierlein 2020]. Both software programs are capable of producing damage and loss simulations, following the procedures of *FEMA P-58* [FEMA 2012]. This includes the treatment of EDP (story drift demand) fitting and the random generation and sampling of EDPs, damage probabilities and repair costs. More information on these procedures can be found in *FEMA P-58* (Chapter 7 and Appendix G).

An in-depth comparative study was conducted between the two programs (i.e., *SP3* and *pelicun*) to verify that, given the same input information, the same loss values and performance metrics could be obtained. A total of twelve preliminary variant models were analyzed for the San Francisco site (see Chapter 4). The buildings consisted of one- and two-story variants with either stucco or wood siding exterior and gypsum wallboard interior. The variants had 2-ft-tall cripple walls in existing (unretrofitted) and retrofit condition and a rigid base variation without a crawlspace vulnerability for total of twelve variant models. The structural analysis results (e.g., EDPs and collapse fragility) were identical for input into the respective loss assessment models. The loss modeling assumed the same number of damageable assemblies (e.g., square footage of stucco, total partition length) and the damage fragilities and cost functions were defined exactly the same. Each of the ten return periods that define the San Francisco site were analyzed assuming 2000 simulations of damage probability and cost estimation (i.e., 20,000 simulations total) for each building variant.

Initially, small (but non-negligible) differences were observed in the results. Through interaction with *SP3* and *pelicun* developers, the sources of these differences were found and *pelicun* settings were adjusted to best reflect *SP3* procedures. These differences were due to the treatment of collapse probabilities for simulations and how uncorrelated damage fragilities were treated in the simulation process between the programs. After incorporating the necessary adjustments, the comparison between the two programs gave essentially the same results for all twelve variants.

The loss metrics used for the comparative study included expected annual loss (EAL), mean repair cost at the 250-year return period (RC250), and a “250-year loss” estimated from a loss exceedance curve using all realizations. expected annual loss and RC250 represent the primary loss metrics that are summarized in Chapter 7 of this report and were used for interaction with catastrophe loss modelers by WG6 [Reis 2020(b)]: RC250 is a single value on the mean loss versus intensity curve corresponding to the 250-year return period; and expected annual loss is calculated by integrating the mean (expected) loss versus intensity curve ($E[Loss|IM]$) with the appropriate hazard curve for the site, which represents the annual probability of exceedance of a given IM ($\lambda[IM]$). This calculation is shown in Equation (6.1):

$$\text{EAL} = \int_x E[\text{Loss}|\text{IM}] \left| \frac{d\lambda(\text{IM}>x)}{dx} \right| dx \tag{6.1}$$

where the term $|d\lambda(IM > x)/dx|$ represents the absolute value of the slope of the hazard curve. Notably, the expected annual loss and other time-based metrics assume that the first and last intensities considered represent the lower and upper bounds for integration. This assumption is used in *SP3* and was carried through in the processing of results from *pelicun*.

Loss exceedance curves were not reported as a primary metric within the PEER–CEA Project, yet they provide a good test of the response (EDP), damage, and repair cost simulations, providing similar treatment of uncertainty propagation. The loss exceedance curves are constructed using all simulations performed across the intensities of interest (e.g., 20,000 total), relating each simulation to the appropriate probability of exceedance and occurrence probability using the hazard curve at each intensity. The values are then integrated to obtain the annual probability of exceeding a given value of loss ($\lambda[Loss > l]$). This relationship is shown in Equation (6.2).

$$\lambda[\text{Loss}>l]=\int_x P[\text{Loss}>l|\text{IM}=x]\left|\frac{d\lambda(\text{IM}>x)}{dx}\right|dx \tag{6.2}$$

An example illustration of a loss exceedance curve is shown in Figure 6.26 with the annual exceedance probability corresponding to 250 years (e.g., 1/250 = 0.004). Note that the "250-year loss," which is a time-based metric, is distinct from the RC250 loss, which is an intensity-based metric. Early interactions with catastrophe loss modelers during the project clarified that RC250 was the metric that was of interest for their comparisons. Further, note that single values on the loss exceedance curve are extracted to provide simple scalar comparison metrics, while the entire loss exceedance curve is important to verify the simulation process between the two software programs.

The comparison results between *SP3* and *pelicun* are found to give essentially identical results based on the mean loss versus intensity curves, loss exceedance curves and the three scalar metrics (EAL, RC250, and 250-year loss). Similar agreement is observed for all twelve building variant models considered for the comparison study. In the interest of brevity, complete information will only be shown for one of the building variants, while the scalar loss metrics are summarized for all variants. A slide deck illustrating the complete software comparison study results is provided within the WG5 electronic documentation available at the PEER website [PEER 2020].

Figure 6.27 provides a sample of comparison results for a two-story variant with retrofitted 2-ft-tall cripple walls. The exterior material is horizontal wood siding, and the interior material is gypsum wallboard. This variant model was selected since it has significant displacement response in various story levels and significant contributions of collapse at higher intensity levels. The loss exceedance curves in Figure 6.27(a) show very good agreement between the two software programs, especially noting that the "bump" in the curves near loss ratios of 10% of replacement cost are similar for *SP3* and *pelicun*. The *SP3* loss exceedance curve is not shown for loss ratios below 1% since *SP3* outputs these curves as 100 interpolated points ranging from 0% to 100% of the building replacement cost. This first zero point could be misleading when plotting in log scale. Recall that these loss exceedance curves incorporate 20,000 randomly sampled simulations, so slight differences in the curves can be expected. The values corresponding to mean loss estimates at the ten different return periods; EAL estimates are summarized in Figure 6.27(b). The EAL, RC250, and "250-year loss" (from loss exceedance curves) are provided for all 12 variants in Figure 6.28, Figure 6.29, and Figure 6.30, respectively.

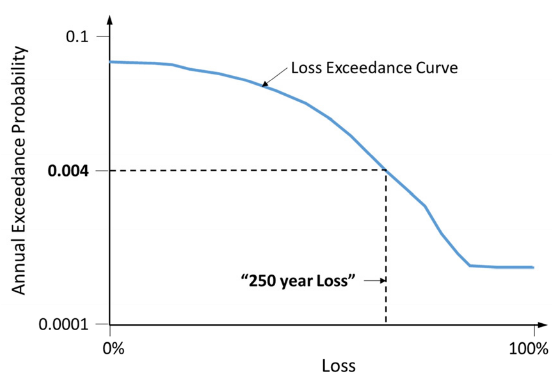

Figure 6.26 Example of a loss exceedance curve with the point representing a 250-year loss annotated.

a)

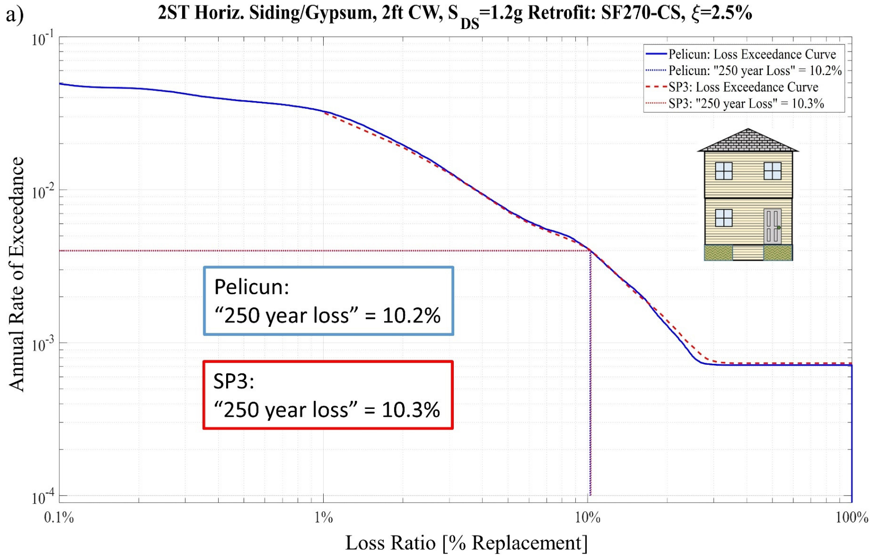

b)

Return Period	Intensity Measure	Loss | IM [% Repl.]	
RP [yr]	Sa(0.25s) [g]	Pelicun	SP3
15	0.178	0.19%	0.18%
25	0.274	0.67%	0.63%
50	0.444	2.00%	1.99%
75	0.560	3.56%	3.48%
100	0.652	4.85%	4.93%
150	0.790	8.22%	8.25%
250	0.982	13.47%	13.42%
500	1.246	19.95%	20.36%
1000	1.564	29.57%	29.68%
2500	2.014	41.18%	41.71%
EAL [% Repl.]		0.212%	0.211%

Figure 6.27 **Sample results from comparative study between the *SP3* and *pelicun* programs to perform loss assessment. Results shown are for a two-story retrofitted cripple wall dwelling with horizontal wood siding assumed to be located in San Francisco: (a) loss exceedance curves; and (b) mean loss estimates at each return period and expected annual loss estimates.**

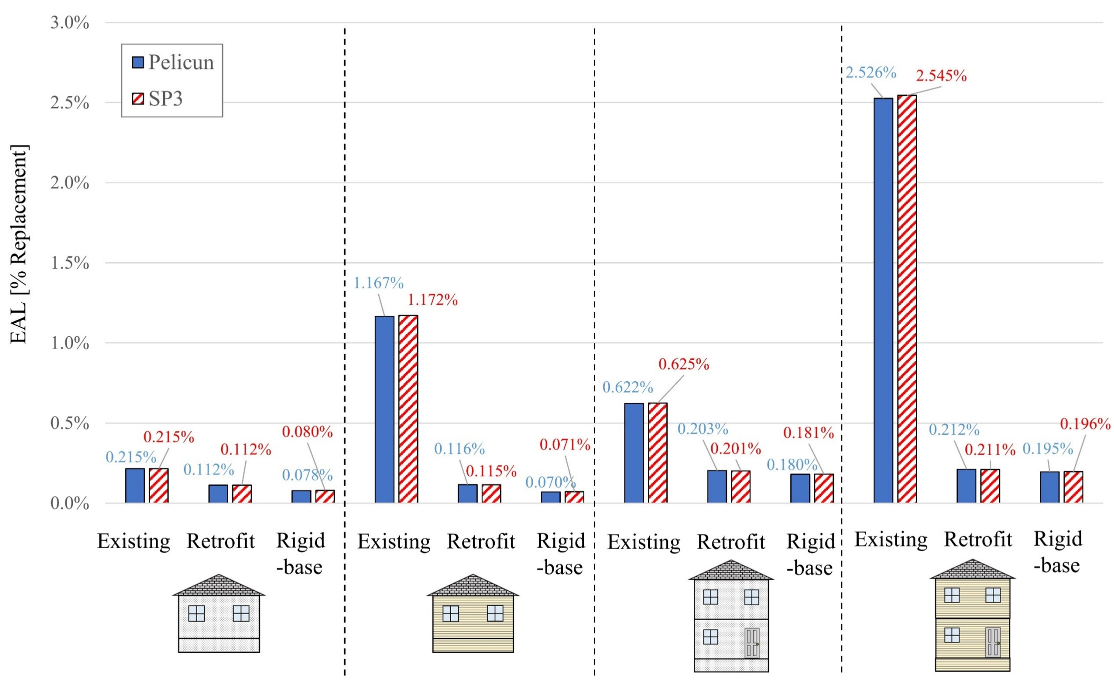

Figure 6.28 **Summary of expected annual loss estimates for all twelve variants comparing *pelicun* (solid) and *SP3* (hatched) results. Note: results presented are preliminary and do not reflect final analysis results.**

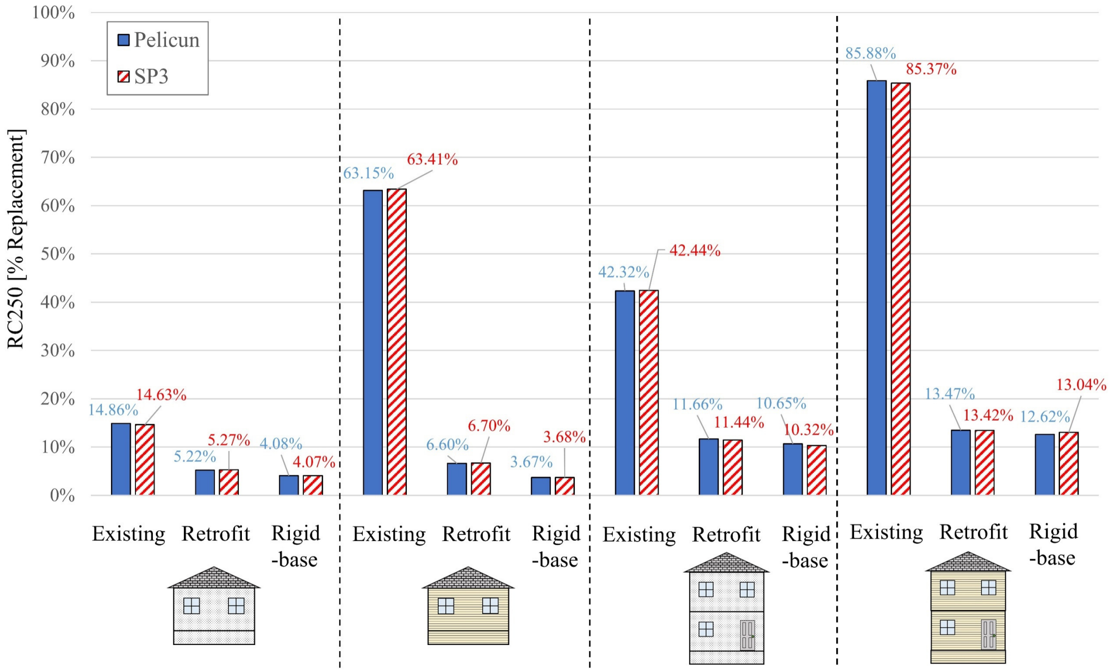

Figure 6.29 **Summary of mean loss conditioned on the 250-year return period (intensity-based) for all twelve variants comparing *pelicun* (solid) and *SP3* (hatched) results. Note: results presented are preliminary.**

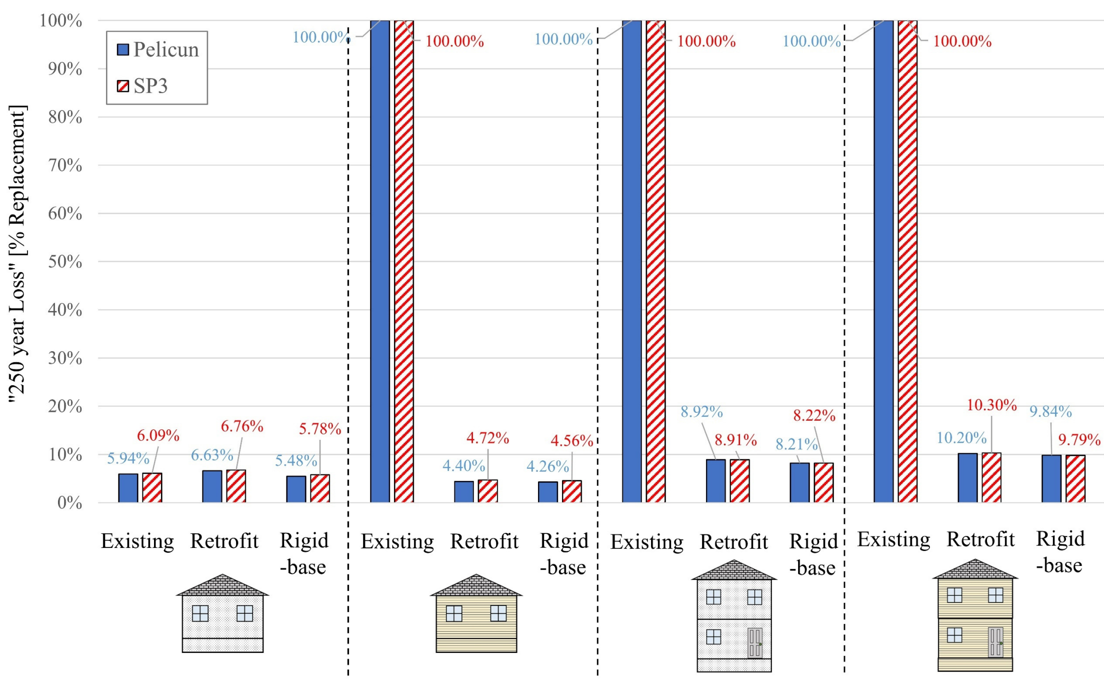

Figure 6.30 **Summary of 250-year loss (time-based) estimates for all twelve variants comparing *pelicun* (solid) and *SP3* (hatched) results. Note: results presented are preliminary.**

6.8.2 Damageable Quantities and Performance Groups

The damageable quantities assumed for the loss modeling of building variants define the quantity of various sub-assemblies considered for repair costs, the total of which defines the building-specific damageable inventory. Performance groups are sub-sets of the damageable inventory that have the same damage fragilities, are sensitive to the same EDP (e.g., second-story drift in the *X*-direction, first-floor acceleration in the *Y*-direction, etc.) and can be attributed the same repair cost functions. A summary of the performance groups assumed for building variants is provided in Table 6.7. The columns labeled QX-1 and QY-1 represent the quantities of assembly units applied to the performance groups of the first story in the *X*- and *Y*-directions; QX-2 and QY-2 are similar for the second superstructure story of two-story variants.

Table 6.7 Summary of damageable quantities and performance groups assumed for building variants to estimate repair costs.

Assembly type	Unit	First-story or cripple wall		Second story	
		QX-1 [1]	QY-1	QX-2	QY-2
Exterior Walls	100SF	7.20	5.40	7.20	5.40
Interior Partitions/ Interior Wall Material	100LF	0.94	0.735	0.80	0.875
Ceramic Tile	100LF	0.13	0.12	0.13	0.12
Wallpaper Finish	100LF	0.25	0.25	0.25	0.25
2-ft-tall cripple walls	100SF	1.60	1.20	N/A	N/A
6-ft-tall cripple walls	100SF	4.80	3.60	N/A	N/A

[1] QX-1 is the number of assembly units assumed in the *x*-direction for the first story. QY-2 is the number of assembly units assumed in the y-direction for the second story (2 story variants only).

Exterior wall quantities are expressed in units of 100 ft^2 (100SF) for all materials considered, including cripple walls. For superstructure materials, a constant story height of 9 ft is used within the project. A total of 140 linear feet is considered for the perimeter of each variant which results in a total of 12.6 units (1260SF) for each full height story. Note that the cost functions within *FEMA P-58* do not account for door and window openings in exterior walls of wood-frame houses, where cost functions presumably account for lower damage states requiring repairs in concentrated areas around openings (e.g., stucco and gypsum repairs). Every variant is 40 ft × 30 feet in plan with the longer dimension taken as the *X*-direction. This results in two separate exterior wall performance groups with 7.2 (720SF) and 5.4 (540SF) units in the *X*- and *Y*-directions, respectively for each full-height story. For cripple walls, the same calculations are used since units are 100SF, yet the number of units varies depending on the cripple wall height (h_{CW}). For 2-ft-tall cripple walls, 1.6 (160SF) and 1.2 (120SF) units are assumed in the *X*- and *Y*-directions, respectively. For 6-ft-tall cripple walls, these units increase to 4.8 (480SF) and 3.6 (360SF) for the *X*- and *Y*-directions, respectively. Existing (unretrofitted) stem walls with anchorage vulnerability assume a single performance group with a unit equal to the entire perimeter of the dwelling (140LF for the archetype configuration). This has already been defined in Table 6.6 for stem wall dwellings.

Interior wall materials and finishes have units of 100 linear feet (100LF), yet all have costs adjusted to 9-ft wall heights (see Section 6.2). Since interior wall assemblies are based on double-sided partition walls (i.e., gypsum wallboard or plaster on wood lath), the total interior quantities reflect the assumed length of interior walls plus one half of the perimeter walls of the house. The total interior wall assembly units are 1.675 (167.5LF) for each superstructure story, although the individual performance groups vary slightly due to the different orientations assumed for first- and second-story interior walls; see Section 2.2.1. For the first superstructure story, the total quantity of interior wall units is 0.94 (94LF) and 0.735 (73.5LF) for the *X*- and *Y*-directions, respectively.

The second superstructure stories (two-story variants only) have interior wall units of 0.80 (80LF) and 0.875 (87.5LF) for *X*- and *Y*- directions, respectively. The quantity of ceramic tile is assumed to be a total of 225 ft^2 of tile per superstructure story, reflecting the amount of tile assumed in the 1200SF case study buildings in the PEER–CEA Earthquake Damage Workhop [Vail et al. 2020]. Using a story height of 9 ft, this corresponds to a total length of 25LF per story. This was distributed as 0.13 (13LF) and 0.12 (12LF) units in the *X*- and *Y*-directions, respectively. The quantity of wallpaper finish is assumed as an equivalent of 450 ft^2 per story. This was split evenly between the two directions resulting in 100LF units of 0.25 (25LF) for each direction. Note that the ceramic tile has an order of magnitude larger unit cost than wallpaper (see Section 6.7), such that the tile repairs will dominate the repair costs associated with finishes.

6.8.3 Damage and Cost Simulations

A total of 3000 damage and cost simulations are performed for each of the ten intensities (i.e., return periods) used for loss assessment of building variants. This results in a total of 30,000 simulations for each building variant and site location. This is 50% greater than the minimum of 2000 specified by *SP3* for obtaining a USRC rating. Limited sensitivity studies were conducted, and 3000 simulations are shown to given more stable results (e.g., giving the same output values for repetitions of the simulations). No appreciable benefit (stability) was achieved when using more than 5000.

The damage fragilities for all damageable components are assumed to be uncorrelated within performance groups, which is the default *FEMA P-58* setting for the assembly types considered. Being uncorrelated implies that the damage state realization of a given unit within a performance group is not constrained to be the same as another unit in that performance group, even if the demand parameters are the same. The *pelicun* software allows users to adjust the granularity of damageable component fragilities based on whole component units or a fraction of unit. The treatment of uncorrelated damage fragilities splits each performance group into two separate values. Taking the exterior wall assemblies at the first story in the *X*-direction as an example, this roughly corresponds to separate sampling of the damage state of either side of the dwelling. This distinction was made for all interior and exterior wall assemblies. For interior partitions, this permits resampling of damage for partitions walls oriented in the *X*-direction, thus allowing for different damage states to be realized at different locations (i.e., rooms) of the house.

7 Performance Assessment Results for Building Variant Models

This chapter provides a summary of the results of the building variant evaluations. The chapter begins with an overview of the evaluation process that was implemented in a computational workflow. The nomenclature used to define building variants is discussed to assist in navigation of this chapter and the electronic documentation of results that is provided at the PEER website [PEER 2020]. An overview of the information collected and documented for the building variant analyses is reviewed in Section 7.3, noting that the entirety of information that is included in the electronic documentation is not presented within this report. The presentation in this chapter focuses on results of the baseline archetypes considered for comparison with catastrophe loss modelers (see Reis [2020(b)] for more details) along with sensitivity studies of some of the building variants.

7.1 GENERAL WORKFLOW FOR OBTAINING PERFORMANCE RESULTS

A computational workflow written in Matlab was used for data management and analyses control, including pre- and post-processing of structural analyses and performance (loss) analyses of the building variants. Structural analyses were run using *OpenSees* [McKenna et al. 2001] and the *FEMA P-58* damage and loss analyses were run using the *pelicun* software [Zsarnoczay 2019]. All analyses were run on the Sherlock High Performance Computing cluster [Sherlock 2020] at Stanford University. The general workflow is described to illustrate the process for each building variant. Notably, this workflow describes all steps following the development of input parameters that were discussed in previous chapters.

The general workflow is presented in Figure 7.1, showing the nominal start and end of the process within the shaded boxes. The first step is to define the general parameters of each building variant (e.g., number of stories, construction era, and site location), from which the engineering details are established, including the retrofit design according to the *FEMA P-1100* plan sets. Next, the *OpenSees* models are defined (e.g., material properties, seismic mass, etc.) and the appropriate loss model and damageable inventory of the building are assigned. Nonlinear static analyses and modal analyses are performed using *OpenSees* to determine basic response properties for each building variant (e.g., period of vibration, static strength ratios, etc.). Nonlinear dynamic analyses are performed using the sets of ground motions for the increasing earthquake intensity levels to calculate collapse fragilities and distributions of EDPs (primarily story drifts) for each intensity level. The *OpenSees* analysis data provides the input for the *FEMA P-58* loss assessment using the *pelicun* software. Results of the structural analyses and loss analyses, along with the input files for the *OpenSees* and *pelicun* analyses, are archived in the electronic documentation available at the PEER project archive [PEER 2020].

The building variants are evaluated at four sites that cover a range of seismicity and the applicable retrofit plan sets for prescriptive retrofit design according to *FEMA P-1100* [2018]. The sites considered are Bakersfield, San Francisco, Northridge, and San Bernardino; see Chapter 4. The ground-motion hazard is defined based on the 5% damped spectral acceleration at a period of 0.25 sec [Sa(0.25 sec)]. The IMs for each site are summarized in Table 7.1 for each of the ten return periods considered for loss assessment (i.e., Sa_{RP} for 15-year to 2500-year return periods). The table also provides two values of short-period design spectral acceleration (S_{DS}). The first is the nominal $S_{DS,\mathrm{Site}}$ obtained for the site location (see Table 4.1) based on the USGS design maps for default soil D. The second is the short-period design acceleration $S_{DS,\mathrm{P\text{-}1100}}$ controlling the prescriptive retrofit design for the site according to *FEMA P-1100*, where design schedules are provided for 1.0g, 1.2g, and 1.5g. Referring to the last two rows of the table, the prescriptive retrofit designs are: (1) slightly conservative compared to the site hazard, for the Bakersfield and Northridge sites: (2) optimal for the San Francisco site; and (3) slightly unconservative for the San Bernardino site.

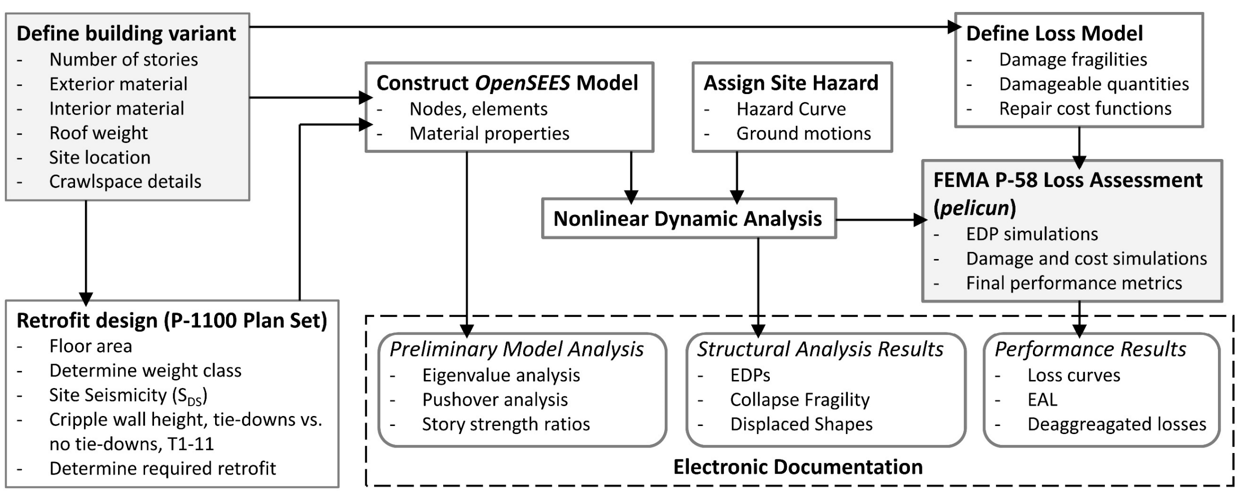

Figure 7.1 Overview of WG5 workflow to analyze building variants.

Table 7.1 Summary of site definition and IMs for the four baseline sites.

Site	Bakersfield	San Francisco	Northridge	San Bernardino
V_{S30} (m/sec)	270	270	270	270
Abbreviation	BF270	SF270	NR270	SB270
$Sa_{RP=15}(g)$[1]	0.119	0.178	0.217	0.252
$Sa_{RP=25}$ (g)	0.172	0.274	0.335	0.375
$Sa_{RP=50}$ (g)	0.271	0.444	0.540	0.590
$Sa_{RP=75}$ (g)	0.344	0.560	0.681	0.744
$Sa_{RP=100}$ (g)	0.405	0.652	0.785	0.861
$Sa_{RP=150}$ (g)	0.497	0.790	0.948	1.036
$Sa_{RP=250}$ (g)	0.626	0.982	1.152	1.265
$Sa_{RP=500}$ (g)	0.834	1.246	1.484	1.627
$Sa_{RP=1000}$ (g)	1.071	1.564	1.829	2.021
$Sa_{RP=2500}$ (g)	1.440	2.014	2.328	2.559
$S_{DS,\mathrm{site}}$ (g)[2]	0.741	1.200	1.398	1.778
$S_{DS,\mathrm{P\text{-}1100}}$ (g)	1.000	1.200	1.500	1.500

[1] Mean 5% damped spectral acceleration at a period of 0.25 sec for the site and return period of RP = x years.
[2] Short-period design spectral acceleration for the site assuming soil class D (https://earthquake.usgs.gov/designmaps/beta/us/).
[3] Short-period design acceleration that controls the prescriptive retrofit design according to *FEMA P-1100*.

7.2 NOMENCLATURE FOR BUILDING VARIANTS

Damage (loss) functions were developed and documented for a total of 255 building variants [PEER 2020]. The variants investigated were based on a larger building variant list, documented in the WG2 report [Reis 2020(a)], which was distilled down to a manageable list, considering information gained through testing and observed impact of variables on intermediate numerical results, as well as practical limitations and time constraints. The resulting variant list included combinations of one- and two-story houses, three exterior wall materials (stucco, wood siding, and T1-11 siding), two interior wall materials (lath and plaster or gypsum wallboard), four base conditions (2-ft-tall and 6-ft-tall cripple walls, stem walls, and rigid base), seismic retrofit (with and without retrofit), roof weight (light and heavy), and four building sites. Note that rigid base variants represent the condition where crawlspace vulnerability is removed, which serves as the retrofit condition for stem-wall dwellings and a point of comparison with cripple wall dwelling performance with and without retrofit.

An individual building variant (i.e., a single structural model that would be assembled for structural analysis and eventual performance assessment) is defined by a two-tiered taxonomy, i.e., class and index. The class of the variant defines the type of superstructure materials, assumed roof weight and general material that a cripple wall would be made of for that class (if applicable). The index of a building variant within a class completely defines the material and geometric assumptions. The classes and indices are described in this section.

7.2.1 Classes of Variants

The class of a variant is composed of four sub-units. These are defined as follows:

Class = RW - EXT - INT - cw

- *Roof Weight* (RW): The roof weight takes a value of "L" or "H" for light or heavy roof material, respectively. Light roof material (asphalt shingle) is the common assumption. Heavy roof assumes a concrete tile roof material. Note that heavy roofing is only considered as part of additional sensitivity studies and is not included as a target variant for comparison with catastrophe modelers.
- *Exterior Material* (EXT): The exterior material defines the properties of the exterior walls in the superstructure including the exterior façade and the interior finish material. The best estimate exterior materials used for catastrophe modeler comparison are:
  - *S2* – Stucco exterior with gypsum wallboard interior (1956–1970 era);
  - *W2* – Horizontal wood siding exterior with gypsum wallboard interior (1956–1970 era);
  - *SLP2* – Stucco exterior with plaster on wood lath interior (pre-1945 era);
  - *C1* – Horizontal wood siding exterior with plaster on wood lath interior (pre-1945 era).

  Additional exterior materials including other combinations that were not provided for the comparison with catastrophe modelers are:
  - *T1* – Panelized plywood (T1-11) siding exterior with gypsum wallboard interior assuming best estimate properties (1956–1970 era);
  - *S3* – Stucco exterior with gypsum wallboard interior. These materials reflect a stronger and stiffer material assumption with respect to best estimate S2 properties. Note this variation in exterior stucco wall strength is not included as a variant for comparison with catastrophe modelers.
- *Interior Material* (INT): The interior material defines the properties of the interior partition walls in the superstructure. Best estimate interior material properties are used to define the interior finish, based on assumed construction era:
  - *G2* – Gypsum wallboard interior (1956–1970 era);
  - *LP* – Plaster on wood lath interior (pre-1945 era).
- *Cripple Wall Material* (cw): The class nomenclature defines the type of cripple wall material included for the group of variants (if applicable). This class tag does not indicate the strength or explicit material property assumed, only the material type:

- *S* – Exterior stucco;
- *HS* – Horizontal wood siding;
- *T1* – Panelized plywood (T1-11) siding.

A summary of all the analyzed building variant classes is presented in Table 7.2.

Table 7.2 Summary of all building variant classes within WG5 documentation.

Variant class	Description	Applicable construction eras[1]	Included in catastrophe modeler set?[2]
L-S2-G2-S	Light roof, best estimate stucco exterior and gypsum wallboard interior, cripple walls are stucco if present	1945–1955, 1956–1970	Yes
L-W2-G2-HS	Light roof, best estimate horizontal wood siding exterior and gypsum wallboard interior, cripple walls are horizontal wood siding if present	1945–1955, 1956–1970	Yes
L-SLP2-LP-S	Light roof, best estimate stucco exterior and plaster on wood lath interior, cripple walls are stucco if present	pre-1945, 1945–1955	Yes
L-C1-LP-HS	Light roof, best estimate horizontal wood siding and plaster on wood lath interior, cripple walls are horizontal wood siding if present	pre-1945, 1945–1955	Yes
L-T1-G2-T1	Light roof, best estimate T1-11 panelized siding exterior and gypsum wallboard interior, cripple walls are stucco if present	1956–1970	No
H-S2-G2-S	Heavy roof, best estimate stucco exterior and gypsum wallboard interior, cripple walls are stucco if present	1945–1955, 1956–1970	No
L-S3-G2-S	Light roof, exterior stucco and gypsum walls have increased strength and stiffness compared to best estimate, best estimate gypsum wallboard partitions, cripple walls are stucco if present	1945–1955, 1956–1970	No
H-S3-G2-S	Heavy roof, exterior stucco and gypsum walls have increased strength and stiffness compared to best estimate, best estimate gypsum wallboard partitions, cripple walls are stucco if present	1945–1955, 1956–1970	No

[1] Applicable construction eras are based on interior finish type. Pre-1945 is exclusively lath and plaster, 1956–1970 is gypsum wallboard. The 1945–1955 era is the transition period where both finish types are considered. T1-11 siding is only applicable to the later 1956–1970 era.
[2] The catastrophe modeler comparison set are models that were presented to the groups during comparison studies.

7.2.2 Index of a Specific Variant

The variant indices within a given class have more detailed sub-units in the naming convention. The sub-units shown in parentheses are only applicable to cripple wall dwellings. The variant indexing sub-units are defined as follows:

Index = nRW - EXT - INT – CS – (CW)(R) – (EXRET)

- Number of Stories (n): The number of stories of the occupiable space (superstructure) of the building variant. Cripple walls, if present, are not considered a story. Values of "1" and "2" represent one- and two-story dwellings, respectively.

- *Roof Weight* (RW): As defined previously in Section 7.2.1.
- *Exterior Material* (EXT): As defined previously in Section 7.2.1.
- *Interior Material* (INT): As defined previously in Section 7.2.1.
- *Crawlspace* (CS): The crawlspace sub-unit identifies the assumed geometry of the variant below the first occupied story:
  - *2C* – two-ft-tall constant height cripple wall;
  - *6C* – 6-ft-tall constant height cripple wall;
  - *SW1* – existing (unretrofitted) stem wall;
  - *RB* – rigid-base crawlspace condition that is used to model retrofit stem wall dwellings with the vulnerability of failure at the stem wall removed.
- *Cripple Wall Material* (CW): This sub-unit is for cripple wall dwellings only. This flags the assumed material properties for the existing (unretrofitted) cripple wall material:
  - *S1* – exterior stucco with lower strength and stiffness than best estimate;
  - *S2* – best estimate stucco assuming no horizontal sheathing beneath stucco or horizontal sheathing beneath stucco is not bearing on foundation;
  - *S3* – exterior stucco with higher strength and stiffness than best estimate, representing stucco over horizontal wood sheathing with sheathing bearing on foundation;
  - *HS* – horizontal wood siding without contribution of braced framing to strength;
  - *HS2* – best estimate horizontal wood siding considering influence of braced framing and other details; and
  - *T1* – best estimate panelized plywood (T1-11) siding.
- *Retrofit Detail* (R): This sub-unit is for cripple wall dwellings only. This flags the assumed material properties for the retrofit material (combination of retrofit and existing) used in the retrofitted areas of the crawlspace;
  - *R2* – this signifies the best estimate material based on available testing and is largely based on tests with a wood structural panel (e.g., plywood) nailing of 8d nails spaced at 3 in. on center;
  - *R1* – this represents efforts to investigate the effect of increased nail spacing (8d nails at 4 in. on center) and lower retrofit material strength for horizontal wood siding and stucco cripple walls, and the only retrofit designation used for T1-11 siding cripple walls.
- *Cripple Wall Design* (EXRET): This sub-unit is for cripple wall dwellings only. This flags whether the case is an existing (unretrofitted) or retrofit case and, more importantly, the assumed seismic intensity used to design the retrofit according to *FEMA P-1100* [2018], which is site-specific;

- *EX* – existing (unretrofitted) case, not specific to any site;
- *SDS10* – the retrofit design is controlled by the "Seismic" plan set sheets with $S_{DS} = 1.0g$. Retrofitting is also a function of number of stories, building weight class and cripple wall height. These designs are applicable to the Bakersfield site.
- *SDS12* – the retrofit design is controlled by the "High Seismic" plan set sheets with $S_{DS} = 1.2g$. Retrofitting is also a function of number of stories, building weight class and cripple wall height. These designs are applicable to the San Francisco site.
- *SDS15* – the retrofit design is controlled by the "Very High Seismic" plan set sheets with $S_{DS} = 1.5g$. Retrofitting is also a function of number of stories, building weight class and cripple wall height. These designs are applicable to the Northridge and San Bernardino sites.

To help sort and organize the numerous individual variants that were analyzed, specific sets of variants are summarized in Table 7.3 to Table 7.6. Two baseline sets of archetypes for one- and two-story variants are listed in Table 7.3 and Table 7.4. These include retrofitted and unretrofitted variants, with either cripple walls (raised) or stem wall base conditions. These variants are all analyzed using best estimate material properties at all four building sites (i.e., Bakersfield, San Francisco, Northridge, and San Bernardino). This sub-set of building variants shown in Table 7.3 and Table 7.4 include the naming scheme used to describe these variants with catastrophe modelers. The index names for the cripple wall (raised) cases in Table 7.3 and Table 7.4 correspond to 2-ft-tall cripple walls. Another set of variants with 6-ft-tall cripple walls was also analyzed. The 6-ft-tall cases are not listed in Table 7.3 and Table 7.4; however, the index names would be identical to the corresponding variants in the tables, except with replacement of the qualifier "2C" with "6C" to distinguish between cripple wall heights. As summarized in Table 7.5, one- and two-story houses with T1-11 panelized siding and 2-ft-tall and 6-ft-tall cripple wall variants were also analyzed for all four building sites.

Summarized in Table 7.6 is another set of variants, analyzed only for the San Francisco site, to investigate sensitivity of the house response and losses to the assumed material properties in the structural analyses. The table includes a brief description of the change in assumed properties with respect to best estimate cases, and the variant index sub-units that reflect these changes are highlighted in **bold** in the index column of Table 7.6.

Table 7.3 Illustration of variant class and indices for baseline best estimate variant set used for catastrophe modeler comparison: one-story variants.

Height, age, siding, foundation, condition [1]	Class	Index [2]
One-story, pre-1945, Wood, Raised, Retrofitted	L-C1-LP-HS	1L-C1-LP-2C-HSR2-SDSx
One-story, pre-1945, Wood, Raised, Unretrofitted	L-C1-LP-HS	1L-C1-LP-2C-HS2-EX
One-story, pre-1945, Wood, Stem Wall, Retrofitted	L-C1-LP-HS	1L-C1-LP-RB
One-story, pre-1945, Wood, Stem Wall, Unretrofitted	L-C1-LP-HS	1L-C1-LP-SW1
One-story, pre-1945, Stucco, Raised, Retrofitted	L-SLP2-LP-S	1L-SLP2-LP-2C-S2R2-SDSx
One-story, pre-1945, Stucco, Raised, Unretrofitted	L-SLP2-LP-S	1L-SLP2-LP-2C-S2-EX
One-story, pre-1945, Stucco, Stem Wall, Retrofitted	L-SLP2-LP-S	1L-SLP2-LP-RB
One-story, pre-1945, Stucco, Stem Wall, Unretrofitted	L-SLP2-LP-S	1L-SLP2-LP-SW1
One-story 1956–1970, Wood, Raised, Retrofitted	L-W2-G2-HS	1L-W2-G2-2C-HSR2-SDSx
One-story, 1956–1970, Wood, Raised, Unretrofitted	L-W2-G2-HS	1L-W2-G2-2C-HS2-EX
One-story, 1956–1970, Wood, Stem Wall, Retrofitted	L-W2-G2-HS	1L-W2-G2-RB
One-story, 1956–1970, Wood, Stem Wall, Unretrofitted	L-W2-G2-HS	1L-W2-G2-SW1
One-story, 1956–1970, Stucco, Raised, Retrofitted	L-S2-G2-S	1L-S2-G2-2C-S2R2-SDSx
One-story, 1956–1970, Stucco, Raised, Unretrofitted	L-S2-G2-S	1L-S2-G2-2C-S2-EX
One-story, 1956–1970, Stucco, Stem Wall, Retrofitted	L-S2-G2-S	1L-S2-G2-RB
One-story, 1956–1970, Stucco, Stem Wall, Unretrofitted	L-S2-G2-S	1L-S2-G2-SW1

[1] All quality conditions are best estimate. Middle era (1945–1955) variants are not explicitly modeled. This era is taken as the average result from the two other eras, assuming equal contribution from gypsum wallboard and plaster on wood lath interior. [2] Cripple wall retrofit cases are denoted 'SDSx' to reflect that different sites are controlled by different levels of seismicity for retrofit design.

Table 7.4 Illustration of variant class and indices for baseline best estimate variant set used for catastrophe modeler comparison: two-story variants.

Height, age, siding, foundation, condition [1]	Class	Index [2]
Two-story, pre-1945, Wood, Raised, Retrofitted	L-C1-LP-HS	2L-C1-LP-2C-HSR2-SDSx
Two-story, pre-1945, Wood, Raised, Unretrofitted	L-C1-LP-HS	2L-C1-LP-2C-HS2-EX
Two-story, pre-1945, Wood, Stem Wall, Retrofitted	L-C1-LP-HS	2L-C1-LP-RB
Two-story, pre-1945, Wood, Stem Wall, Unretrofitted	L-C1-LP-HS	2L-C1-LP-SW1
Two-story, pre-1945, Stucco, Raised, Retrofitted	L-SLP2-LP-S	2L-SLP2-LP-2C-S2R2-SDSx
Two-story, pre-1945, Stucco, Raised, Unretrofitted	L-SLP2-LP-S	2L-SLP2-LP-2C-S2-EX
Two-story, pre-1945, Stucco, Stem Wall, Retrofitted	L-SLP2-LP-S	2L-SLP2-LP-RB
Two-story, pre-1945, Stucco, Stem Wall, Unretrofitted	L-SLP2-LP-S	2L-SLP2-LP-SW1
Two-story, 1956–1970, Wood, Raised, Retrofitted	L-W2-G2-HS	2L-W2-G2-2C-HSR2-SDSx
Two-story, 1956–1970, Wood, Raised, Unretrofitted	L-W2-G2-HS	2L-W2-G2-2C-HS2-EX
Two-story, 1956–1970, Wood, Stem Wall, Retrofitted	L-W2-G2-HS	2L-W2-G2-RB
Two-story, 1956–1970, Wood, Stem Wall, Unretrofitted	L-W2-G2-HS	2L-W2-G2-SW1
Two-story, 1956–1970, Stucco, Raised, Retrofitted	L-S2-G2-S	2L-S2-G2-2C-S2R2-SDSx
Two-story, 1956–1970, Stucco, Raised, Unretrofitted	L-S2-G2-S	2L-S2-G2-2C-S2-EX
Two-story, 1956–1970, Stucco, Stem Wall, Retrofitted	L-S2-G2-S	2L-S2-G2-RB
Two-story, 1956–1970, Stucco, Stem Wall, Unretrofitted	L-S2-G2-S	2L-S2-G2-SW1

[1] All quality conditions are best estimate. Middle era (1945-1955) variants are not explicitly modeled. This era is taken as the average result from the two other eras, assuming equal contribution from gypsum wallboard and plaster on wood lath interior. [2] Cripple wall retrofit cases are denoted "SDSx" to reflect that designs are controlled by different levels of seismicity for retrofit design.

Table 7.5 Definition of T1-11 siding variants analyzed.

Height, siding, foundation, CW height, retrofit? [1]	Class	Index [2]
One-story, T1-11, Raised, 2ft, Retrofitted	L-T1-G2-T1	1L-T1-G2-2C-T1-R1
One-story, T1-11, Raised, 2ft, Unretrofitted	L-T1-G2-T1	1L-T1-G2-2C-T1-EX
One-story, T1-11, Raised, 6ft, Retrofitted	L-T1-G2-T1	1L-T1-G2-6C-T1-R1
One-story, T1-11, Raised, 6ft, Unretrofitted	L-T1-G2-T1	1L-T1-G2-6C-T1-EX
One-story, T1-11, Rigid-base	L-T1-G2-T1	1L-T1-G2-RB
Two-story, T1-11, Raised, 2ft, Retrofitted	L-T1-G2-T1	2L-T1-G2-2C-T1-R1
Two-story, T1-11, Raised, 2ft, Unretrofitted	L-T1-G2-T1	2L-T1-G2-2C-T1-EX
Two-story, T1-11, Raised, 6ft, Retrofitted	L-T1-G2-T1	2L-T1-G2-6C-T1-R1
Two-story, T1-11, Raised, 6ft, Unretrofitted	L-T1-G2-T1	2L-T1-G2-6C-T1-EX
Two-story, T1-11, Rigid-base	L-T1-G2-T1	2L-T1-G2-RB

[1] All quality conditions are best estimate. T1-11 cases are assumed to be applicable to the 1956–1970 construction era.
[2] Cripple wall retrofit cases are denoted 'R1' to reflect that T1-11 retrofits include upgraded nailing around the entire perimeter according to FEMA P-1100 and are not site-specific.

Table 7.6 Additional variants analyzed as part of sensitivity studies for the San Francisco site only.

Modifications from best estimate properties [1]	Class	Index [2,3]
Reduced existing (unretrofitted) cripple wall stucco strength	L-S2-G2-S	1L-S2-G2-2C-**S1**-EX
Reduced existing cripple wall stucco strength, reduced retrofit material strength		1L-S2-G2-2C-**S1R1**-SDS12
Reduced retrofit material strength		1L-S2-G2-2C-S2**R1**-SDS12
Increased superstructure stucco+gypsum strength	L-S3-G2-S	1L-**S3**-G2-RB
Increased superstructure stucco+gypsum strength		2L-**S3**-G2-RB
Increased superstructure stucco+gypsum strength, increased existing cripple wall stucco strength		1L-**S3**-G2-2C-**S3**-EX
Increased superstructure stucco+gypsum strength, increased existing cripple wall stucco strength		1L-**S3**-G2-2C-**S3**R2-SDS12
Increased superstructure stucco+gypsum strength, increased existing cripple wall stucco strength, reduced retrofit material strength		1L-**S3**-G2-2C-**S3**R1-SDS12
Increased weight, concrete tile roof	H-S2-G2-S	1**H**-S2-G2-RB
Increased weight, concrete tile roof		2**H**-S2-G2-RB
Increased weight, concrete tile roof		1**H**-S2-G2-2C-S2-EX
Increased weight, concrete tile roof		1**H**-S2-G2-2C-S2R2-SDS12
Increased weight, concrete tile roof, increased superstructure stucco+gypsum strength	H-S3-G2-S	1**H**-**S3**-G2-RB
Increased weight, concrete tile roof, increased superstructure stucco+gypsum strength		2**H**-**S3**-G2-RB
Increased weight, concrete tile roof, increased superstructure stucco+gypsum strength, increased existing cripple wall stucco strength		1**H**-**S3**-G2-2C-**S3**-EX
Increased weight, concrete tile roof, increased superstructure stucco+gypsum strength, increased existing cripple wall stucco strength		1**H**-**S3**-G2-2C-**S3**R2-SDS12
Reduced existing cripple wall horizontal siding strength	L-W2-G2-HS	1L-W2-G2-2C-**HS**-EX
Reduced existing cripple wall horizontal siding strength		2L-W2-G2-2C-**HS**-EX
Reduced retrofit material strength		1L-W2-G2-2C-HS**R1**-SDS12
Reduced retrofit material strength		2L-W2-G2-2C-HS**R1**-SDS12
Increased existing stem wall anchorage strength		1L-W2-G2-**SW2**

[1] Material property descriptions are with respect to best estimate properties defined for project analysis.
[2] Cripple wall retrofit cases are denoted "SDS12" to reflect that all of these models are analyzed for the San Francisco site which is controlled by $S_{DS} = 1.2g$ for retrofit design according to *FEMA P-1100*.
[3] Index sub-units shown in **bold** highlight parameters that have changed in comparison with best estimate variants.

7.3 OVERVIEW OF INFORMATION COLLECTED FOR BUILDING VARIANTS

Detailed information and results are documented for each building variant in the electronic documentation for the PEER–CEA Project [PEER 2020]. These include input files, summary data files of results, and figures. This report summarizes and discusses a subset of the available information to (1) illustrate different types of information that is available in the documentation, and (2) summarize significant findings and trends from the structural and loss analyses.

7.3.1 Modal and Pushover Criteria

Modal and nonlinear static (pushover) analyses were performed for all variants to help validate the models and identify important summary variables that describe the structure, such as strength to weight ratios and relative story strength ratios. The modal periods, mode shapes and pushover curves are summarized in the electronic documentation [PEER 2020] for all building variants.

Eigenvalue analyses were conducted to obtain the first three elastic modal periods and mode shapes. Figure 7.2 provides an example of periods and modes shapes for a two-story building variant with wood siding, gypsum wallboard, and 2-ft-tall unretrofitted cripple walls (2L-W2-G2-2C-HS2-EX).

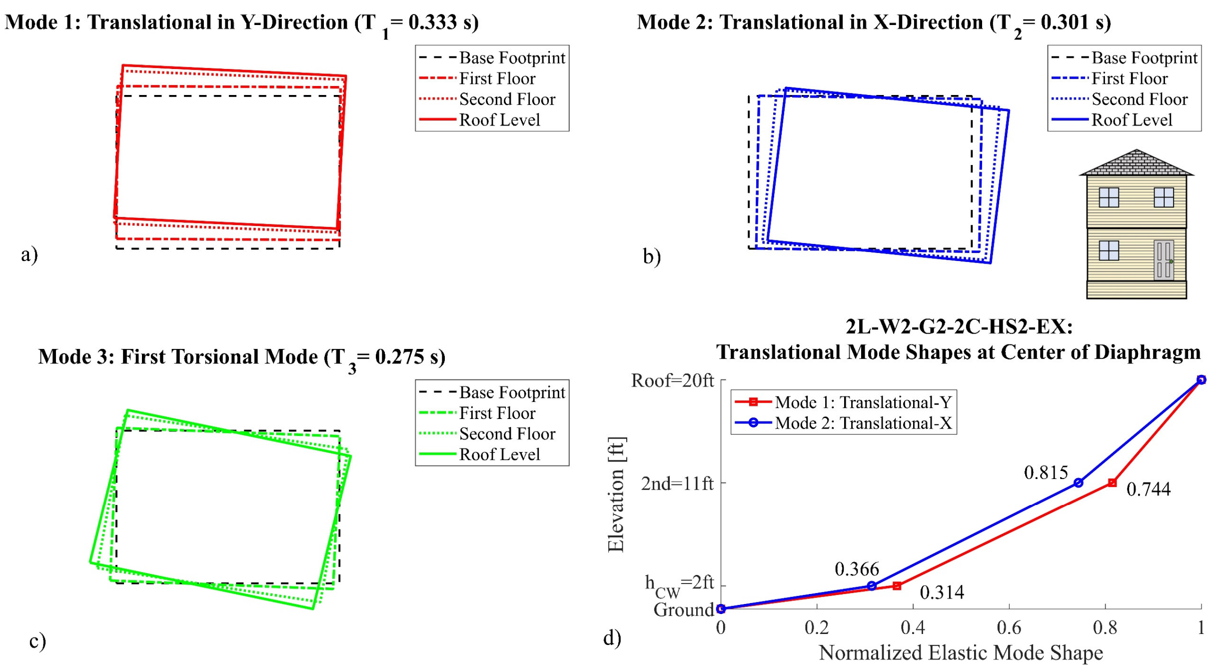

Figure 7.2 **Sample of modal analysis results for building variants: (a) first elastic period and mode shape in plan; (b) second elastic period and mode shape in plan; (c) third elastic period and mode shape in plan; and (d) elastic mode shapes for first two translational modes in elevation.**

Figure 7.2(a) through Figure 7.2(c) show plan views of the first three mode shapes, consisting of a translational mode in each orthogonal direction and a torsional mode, which are similar for all building variants. The periods of all three modes are closely spaced, which is typical of all building variants considered. The Figure 7.2(d) illustrates an elevation plot of the fundamental elastic mode shapes for each orthogonal direction (normalized to roof displacement). The force distribution associated with these mode shapes were used for the static pushover analyses to obtain global strength criteria.

Pushover analyses are used to define the global strength of building variants and to quantify the relative values of lateral strengths between the crawlspace and occupied stories of the superstructure. The standard pushover analysis is termed "modal pushover" in this report, which was conducted using a constant loading pattern according to the elastic translational mode shape in each orthogonal direction (i.e., X and Y). Figure 7.3(a) illustrates two modal pushover curves for a one-story existing (unretrofitted) cripple wall variant (1L-S2-G2-2C-S2-EX). To further define and differentiate between story strengths, two additional pushover analyses were conducted for each variant. First, a crawlspace-only pushover was conducted by loading only the first-floor diaphragm level to obtain the global strength of the crawlspace with all sources of gravity loading applied in the model. Additionally, pushover analyses were performed for each building variant with a rigid base version (i.e., without crawlspace vulnerability) to estimate the strength of the first occupied story. These additional pushover considerations are illustrated in Figure 7.3(b) for comparison with the modal pushover curves in Figure 7.3(a). The figure illustrates that the example variant has global force displacement behavior controlled by cripple wall strength.

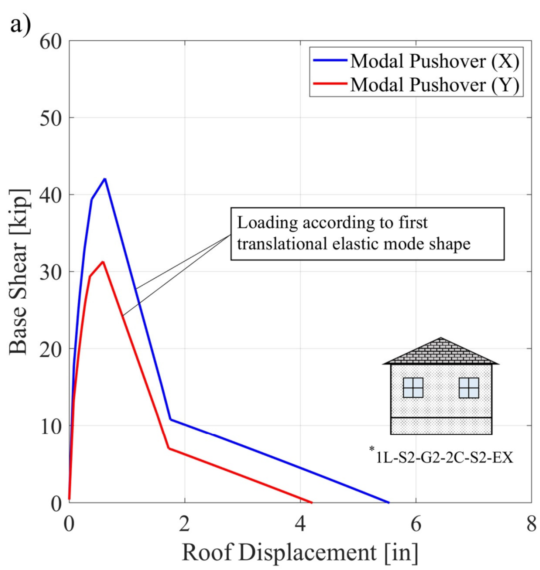

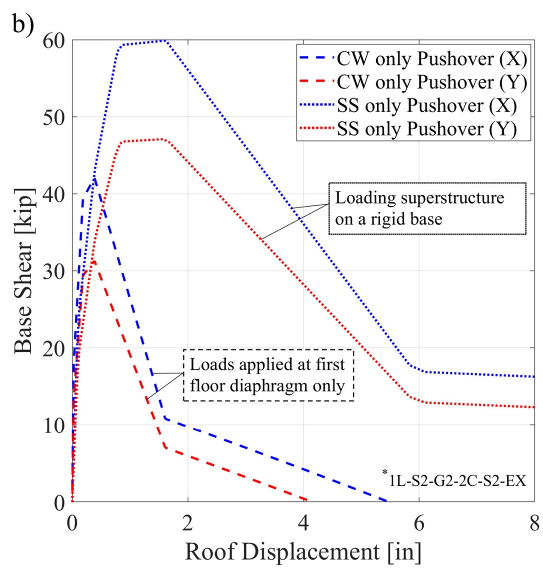

Figure 7.3 **Illustration of performing multiple pushover loadings to understand relative story strengths: (a) pushover loading defined by the elastic translational mode shape (loading at every floor location); and (b) cripple wall only and superstructure only pushover, indicating that modal pushover curve is controlled by cripple wall strength.**

The different types of pushover analysis are used to define important strength ratios of the building variants. The primary strength ratios are defined as follows:

- *Average strength to seismic weight ratio* $(V/W_S)_{\text{Avg}}$ - The average strength of the two orthogonal directions (X and Y) divided by the seismic weight of the model. Strengths were determined by pushover analysis loaded in proportion to the first translational mode shape in each orthogonal direction. Seismic weight is the weight associated with the lateral seismic mass of the model. For houses with cripple walls and stem walls, the seismic weight includes the entire weight at and above the first-floor diaphragm and, for cripple wall cases, half the weight of the cripple wall. For the rigid base analyses, the seismic weight excludes the weight of the first-floor diaphragm and the half the wall weight of the first occupied story (which is assumed to be directly resisted by the rigid base).
- *Average strength to baseline weight ratio* $(V/W_{BL})_{\text{Avg}}$ - The average strength of the two orthogonal directions (X and Y) divided by the baseline seismic weight of the model. Strengths were determined by pushover analysis loaded in proportion to the first elastic mode shape in each orthogonal direction. Baseline seismic weight is the lateral weight acting above the crawlspace including the first-floor diaphragm. Cripple wall weights were not included for comparison across variants of the same class and number of stories.
- *Average crawlspace to superstructure strength ratio* $(V_{CW}/V_{SS})_{\text{Avg}}$ - The ratio of the crawlspace (cripple wall or stem wall) strength to the strength of the first occupied story. Crawlspace strengths (V_{CW}) were estimated via pushover analysis loading at the first-floor diaphragm only. Superstructure strengths were derived from rigid-base cases of the same class and number of stories loaded according to first translational mode shape.

Additional pushover-based information is provided for each building variant in the electronic documentation [PEER 2020]. One example is the identification of key points along a modal pushover curve with corresponding displaced shapes as shown in Figure 7.4, which compares an existing (unretrofitted) and retrofitted one-story, 1956–1970 era, cripple wall variant with exterior wood siding. The left of the figure shows the modal pushover curves (i.e., loading proportional to translational mode shape) with points annotated corresponding to the 40% pre-peak point, the peak capacity point, and the 80% post-peak point. Plots on the right side of the figure illustrate the displaced shape at the center of the diaphragm at each of the annotated points. Figure 7.4(a) and (b) illustrate the low displacement capacity of the unretrofitted cripple wall and that modal pushover displacements are controlled by the cripple wall strength. Conversely, Figure 7.4(c) and (d) show that the retrofitted cripple wall was strong enough to shift inelastic displacements into the superstructure, for the static load distribution based on the elastic translational mode shapes.

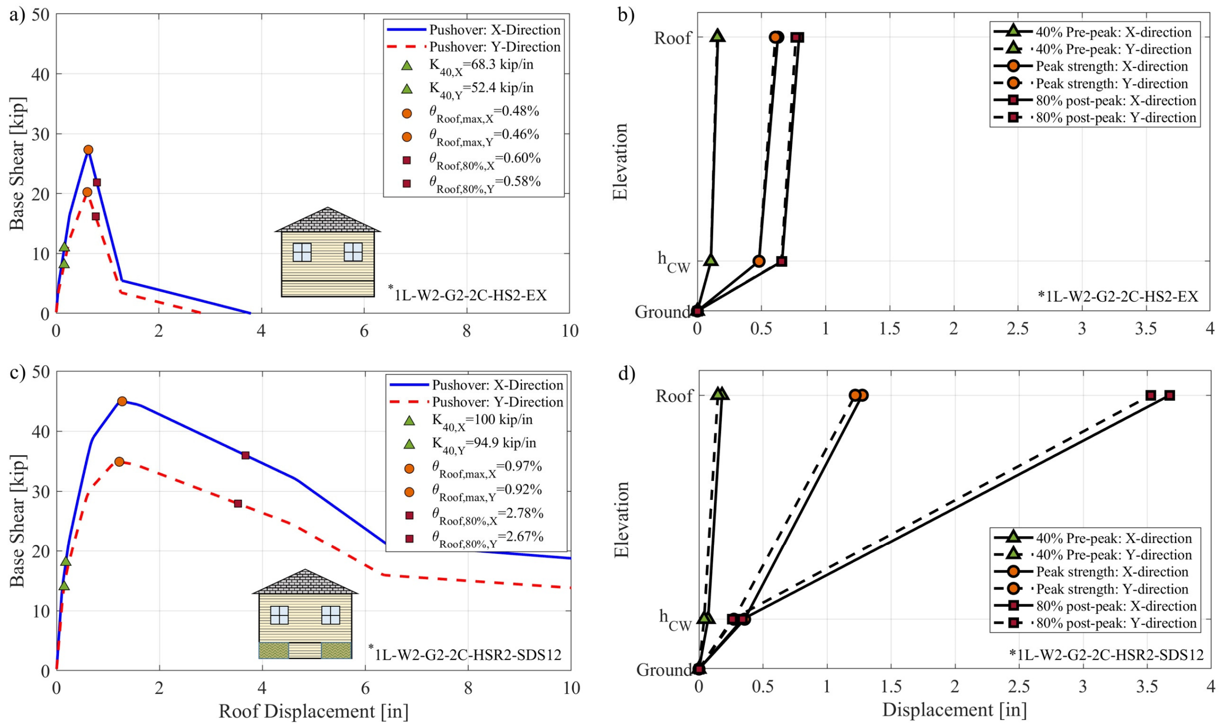

Figure 7.4 **Comparing an unretrofitted (a, b) and retrofitted (c, d) one-story cripple wall dwelling in terms of key points of a modal pushover response (left) and corresponding displaced shape (right).**

7.3.2 Collapse and EDP Response from Multiple Stripe Analyses

The primary outputs from structural analysis are the collapse fragility curve and the diaphragm drift displacements. Collapse is assumed to occur when the drift ratio in the cripple wall or any story exceeds 20%. At ground-motion intensities where drifts exceed this collapse criterion for some of the 45 ground motion pairs, the diaphragm drift displacements are recorded for the no-collapse cases (i.e., for a subset of the total number of ground motions). The collapse fragility is assumed to follow a lognormal distribution, defined by the median collapse intensity ($Sa_{\mathrm{Med,C}}$), the record-to-record dispersion (β_{RTR}), the applied modeling uncertainty ($\beta_{\mathrm{mod}} = 0.35$ for all variants), and the total dispersion (β_{c}), calculated as the SRSS of β_{RTR} and β_{mod}. The median ($Sa_{\mathrm{Med,C}}$) and record-to-record dispersion (β_{RTR}) are determined by maximum-likelihood fitting of a lognormal distribution to the collapse data [Baker 2015]. Additional information is recorded to define whether the collapse occurs due to excessive drifts in cripple wall or superstructure (first story).

Examples of the collapse data, including location of the collapses, are shown in Figure 7.5 for an existing (unretrofitted) and retrofitted two-story, 1956–1970 era, house with 2-ft-tall cripple walls with a stucco exterior, located at the San Francisco site. The figure shows the number of collapse occurrences for each of the ten return periods (e.g., 15-year to 2500-year) considered for loss assessment, where 45 ground-motion pairs are applied at each return period. Figure 7.5(a) shows that the existing (unretrofitted) cripple wall dwelling experiences collapse in the cripple wall that initiate at the 50-year return period. Beyond the 500-year return period, nearly all the ground-motion pairs cause cripple wall collapse. Conversely, the corresponding retrofit case in Figure 7.5(b) shows that collapses do not initiate until the 250-year return period, where they occur in the first story of the house. Aside from initiating at a higher earthquake intensity (longer return period), the rate of collapses in the retrofitted house is much lower than the existing (unretrofitted) house.

Figure 7.6 shows the SDR response, conditioned on the no-collapse cases, for the same two-story retrofitted cripple wall variant shown previously in Figure 7.5(b). The response is shown in terms of the lognormal mean and standard deviation bounds. The figure shows that the largest SDR demands are concentrated in the first story (middle subplots of Figure 7.6) with very little SDR demand occurring in the second story (upper subplots of Figure 7.6). The lower subplots of Figure 7.6 show the cripple wall SDR demands. While the SDR demands in the cripple wall are similar to those in the first story, the actual drift displacements are much smaller in the cripple wall owing to the difference in height between the cripple wall and the first story. To better illustrate drift demands, the displaced shapes (conditioned on no-collapse cases) for drifts in the *y*-direction are shown in Figure 7.7 for the existing (unretrofitted) and retrofit variant pair previously shown in Figure 7.5. The drift profiles in Figure 7.7 parallel the prevalence of collapse drifts in the cripple wall of the existing (unretrofitted) case and the first story of the retrofitted case.

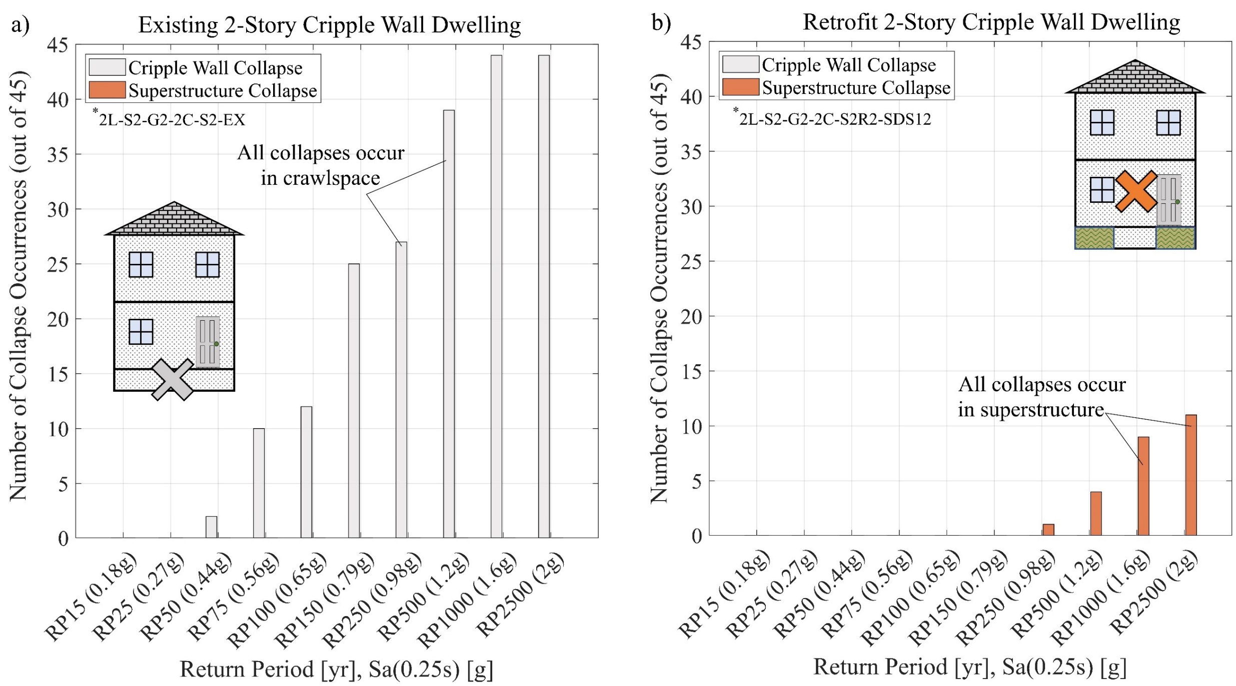

Figure 7.5 **Illustration of monitoring the number and locations of collapse occurrences for a two-story cripple wall dwelling for the San Francisco site: (a) without retrofit; and (b) with retrofit.**

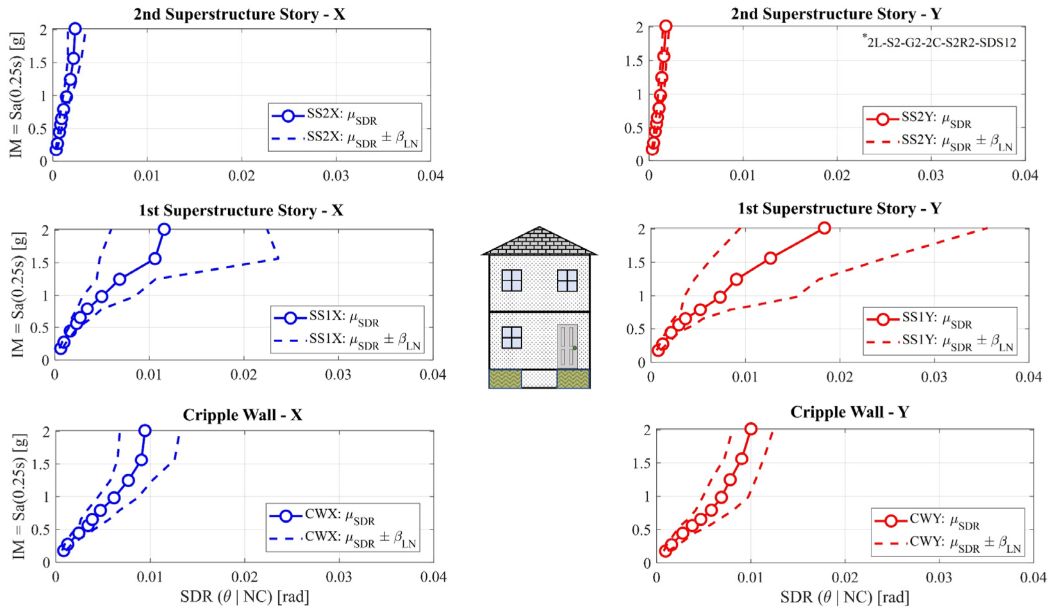

Figure 7.6 Example of story drift ratio (mean and dispersion) conditioned on no-collapse for each story and direction of a two-story cripple wall dwelling with retrofit for the San Francisco site.

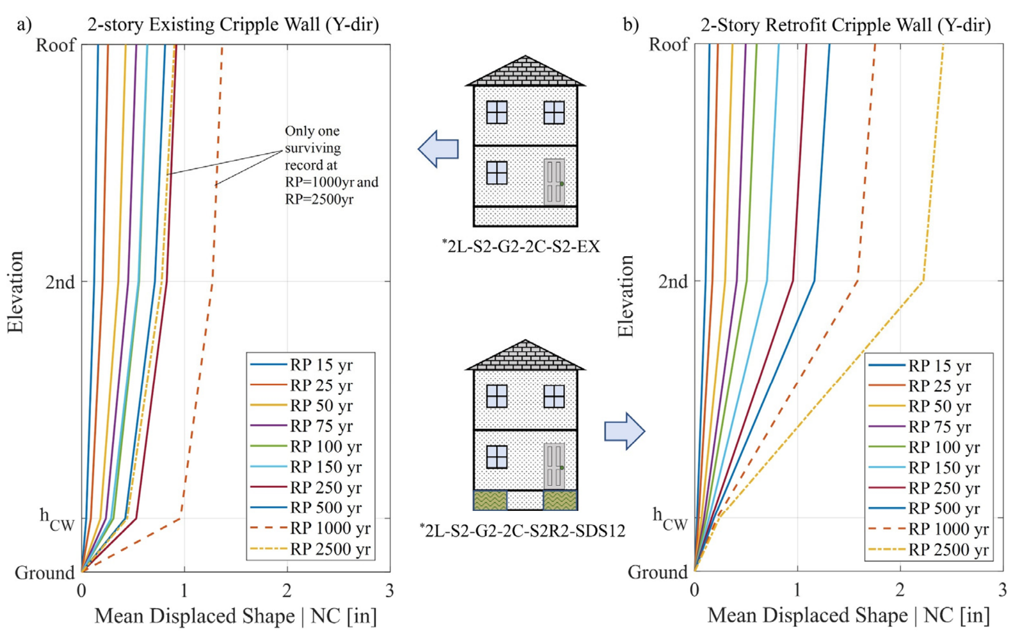

Figure 7.7 Mean displaced shapes conditioned on no collapse for (a) existing (unretrofitted) and (b) retrofitted two-story cripple wall dwellings for the San Francisco site.

Similar information is collected for the PFA and residual SDR demands of each building variant, although these two demand parameters were not used in the subsequent *FEMA P-58* loss analyses. These were documented for possible future analyses or research.

7.3.3 Performance Assessment Metrics

As shown in Figure 7.1, the collapse fragility curve and SDR demand data are input to the *FEMA P-58* loss analyses, performed using the *pelicun* software. Following the *FEMA P-58* procedures, 3000 loss realizations were calculated for each ground-motion intensity to calculate reliable loss ratio statistics. The primary loss outputs for each building variant are defined as follows:

- *Mean Loss* (Damage) *Curves* – The average (mean) loss, expressed in percent of house replacement cost, as a function of ground-motion shaking intensity, described in terms of spectral acceleration at 0.25 sec. This relationship is often referred to as a "damage function" by catastrophe risk modelers.
- *Expected Annual Loss* (EAL) – The expected (mean) loss, due to the risk of earthquake damage, calculated on an annualized basis. This value is obtained through integration of the mean loss versus intensity curve with the site hazard curve that relates ground-motion shaking intensity to an annual probability of exceedance.
- *Expected RC250 Loss* – The mean repair cost for earthquake shaking with a return period of 250 years (RC250). This is an intensity-based metric that represents the average loss for earthquake ground shaking with a specified return period. The 250-year return period was selected as a representative point of comparison based on discussion with catastrophe risk modelers.

The electronic documentation [PEER 2020] included these three datasets for each building variant, along with additional loss information, such as the deaggragation of mean (expected) loss between components of repair costs, and losses associated with collapse of the cripple wall or superstructure. Figure 7.8 compares the deaggregated losses for an existing (a) and retrofitted (b) two-story, 1956–1970 era, house with 2-ft-tall cripple walls with exterior stucco, located at the San Francisco site. The figure shows that losses in the existing (unretrofitted) case [Figure 7.8(a)] are dominated by the collapse of the cripple wall, which is also reflected in the relative contributions to the EAL. Conversely, losses in the retrofitted variant (Figure 7.8(b)] are due to a mix of global collapse and repair costs of different assemblies. The majority (about three-quarters) of the EAL for the retrofitted case is due to damage repair costs, since the retrofit prevents global collapse from occurring at low to moderate intensities compared to the existing (unretrofitted) case.

Other performance data include quantile statistics of the loss versus intensity curves and loss exceedance curves. An example of loss (damage) curve quantiles is shown along with mean loss curves for an existing (unretrofitted) and retrofitted variant pair in Figure 7.9. The quantiles for the existing (unretrofitted) house are dominated by collapse losses, which introduce tremendous variability into the loss data at an intensity of *Sa*(0.25 sec) equal to 1.0*g* (with losses varying from 5% to 100% replacement value). On the other hand, the variability for the retrofitted case is better controlled, where the damage and losses accumulate more gradually under increasing ground-motion intensity. However, even in this case the variability is significant, where for example, the losses at Sa(0.25 sec) equal to 1.0g varies from about 2% to 14% replacement value. A corresponding pair of loss exceedance curves are shown in Figure 7.10, where the annualized loss ratio is reported (i.e., annual rate of exceeding a specific loss ratio). The "250-year loss" ratios are annotated as an example, corresponding to the loss with an annual exceedance probability of 1/250 = 0.004. The 250-year loss ratios are 15.9% and 8.4%, respectively, for the existing (unretrofitted) and retrofitted house. Note that these annualized loss ratios are different than the RC250 loss, which is an intensity-based metric obtained directly from the mean loss curve for each variant. For the same two cases as shown in Figure 7.10, the RC250 losses are equal to about 28% and 8%, respectively (as read off of the loss curves in Figure 7.9 for the 250-year return period ground-motion intensity of Sa(0.25 sec) equal to 1.0g).

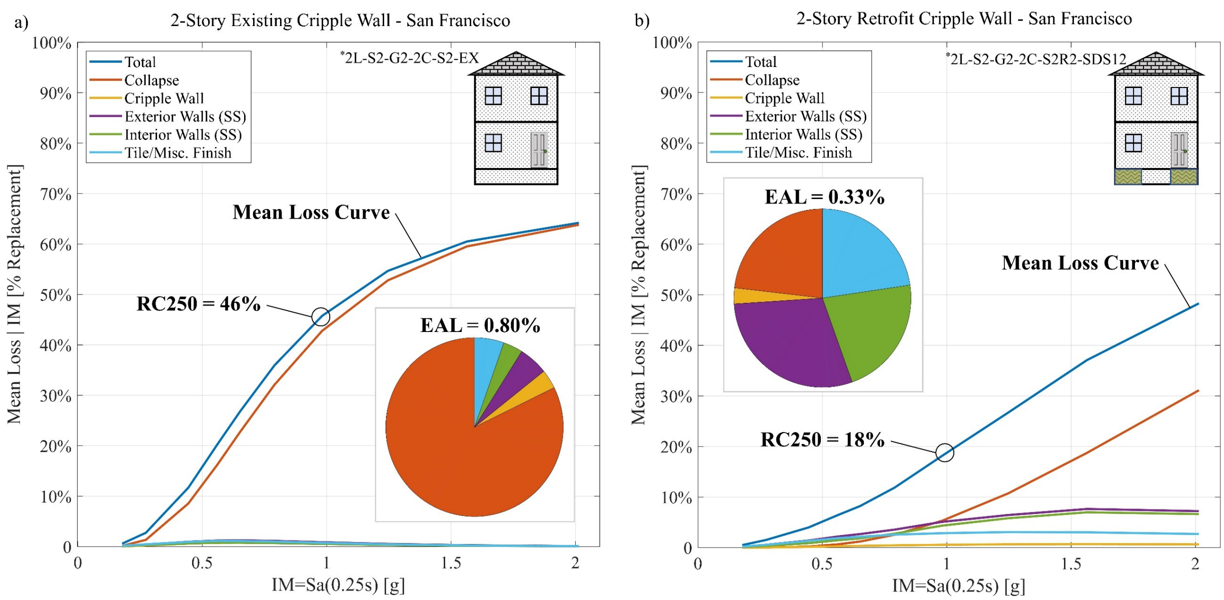

Figure 7.8 Illustration of deaggregating mean loss curves and expected annual loss for an (a) existing (unretrofitted) and (b) retrofitted 2-story cripple wall dwelling.

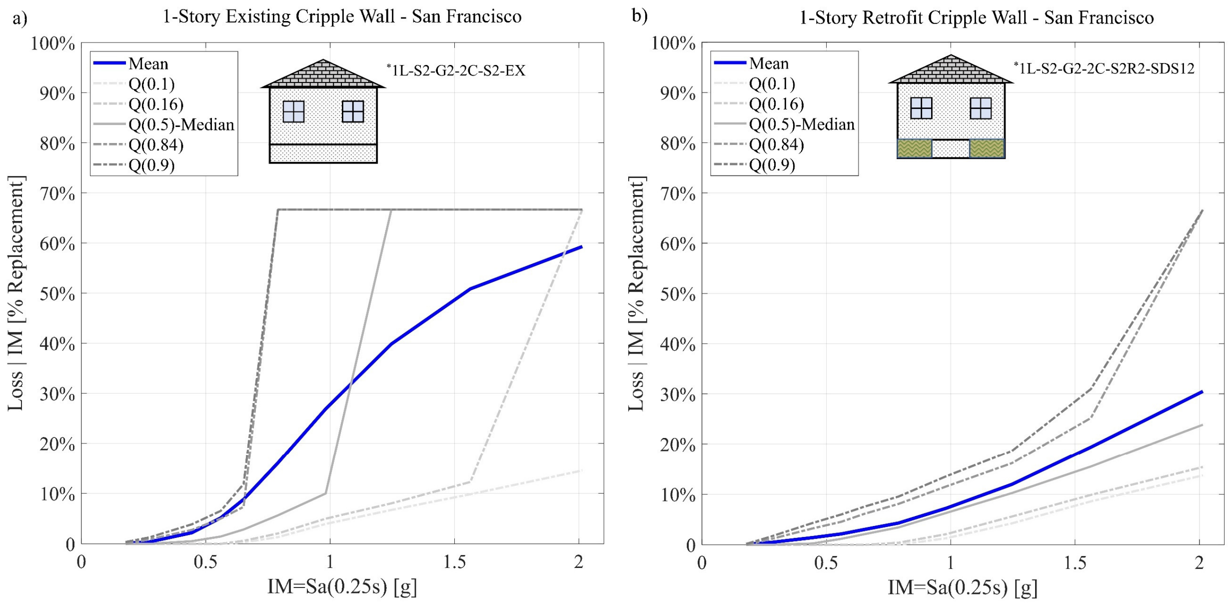

Figure 7.9 Illustration of comparing mean and quantile loss curves for an (a) existing (unretrofitted) and (b) retrofitted one-story cripple wall dwelling.

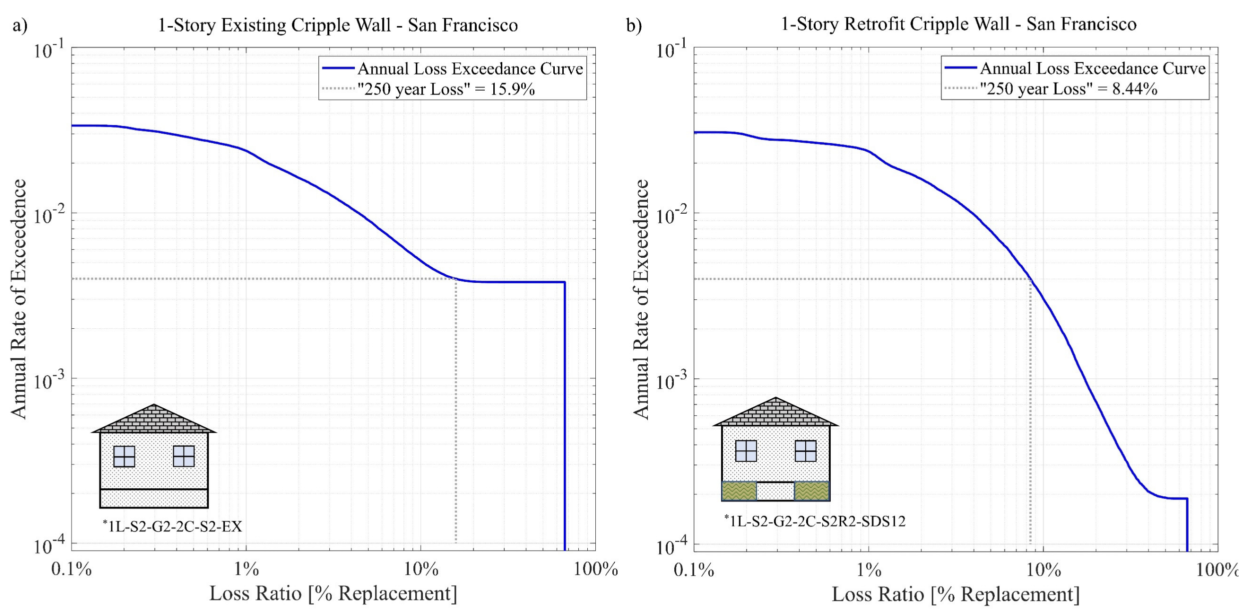

Figure 7.10 Illustration of comparing loss exceedance curves for an (a) existing (unretrofitted) and (b) retrofitted one-story cripple wall dwelling.

7.4 BASELINE CRIPPLE WALL VARIANT SET

The baseline cripple wall variant set is the group of variant models (see Table 7.3 and Table 7.4) used for comparison with data provided by the catastrophe loss modelers; see [Reis 2020(b)]. The variants consist of one- and two-story houses with 2-ft-tall cripple walls and either stucco or horizontal wood siding exteriors. The interior wall material distinguishes the variants for the assumed era of construction, with plaster on wood lath representing the pre-1945 era and gypsum wallboard representing the 1956–1970 era. All material properties represent best estimate values based on review of existing information and new information obtained through experimental testing conducted by WG4; see Chapter 3. Wood siding material for cripple walls uses material CW-HS2 (see Table 3.26), which was developed to acknowledge the possibility of effective framing braces within wood-sided cripple walls. Each variant is analyzed for the four baseline sites of Bakersfield, San Francisco, Northridge, and San Bernardino.

7.4.1 Modal and Pushover Criteria

A summary of elastic fundamental periods and key pushover-based criteria for the one- and two-story variants are summarized in Table 7.7 and Table 7.8, respectively, including the elastic fundamental period (T_1), the average strength to seismic weight ratio, $(V/W_S)_{\mathrm{Avg}}$, the average strength to baseline weight ratio, $(V/W_{BL})_{\mathrm{Avg}}$, and the average crawlspace to superstructure strength ratio, $(V_{CW}/V_{SS})_{\mathrm{Avg}}$. Additionally, the tables include the length of wood structural panel (L_{WSP}) applied in each corner and side of the crawlspace according to prescriptive retrofit designs according to *FEMA P-1100*. Each type of cripple wall variant (i.e., construction era, exterior material) is placed in sub-groups showing the existing (unretrofitted) variant with the three retrofitted variants corresponding to each level of design seismicity according to *FEMA P-1100*. The tables also include equivalent variants on a rigid base (i.e., without crawlspace vulnerability) for comparison.

The fundamental periods of the houses range from 0.2 sec to 0.3 sec for the existing (unretrofitted) one-story houses and 0.3 sec to 0.4 sec for the two-story houses; these reduce to less than 0.2 sec for the one-story and 0.3 sec for the two-story retrofitted houses. The base shear strength ratio $(V/W_S)_{\mathrm{Avg}}$ of the existing (unretrofitted) houses ranges from about 0.3 to 0.5 for the one-story houses and 0.2 to 0.3 for the two-story houses. The seismic retrofit roughly doubles the strength ratios to 0.8 to 1.0 for the one-story houses and 0.4 to 0.6 for the two-story houses.

Table 7.7 **Summary of modal and pushover criteria for the baseline cripple wall set and rigid base variants: one-story cases.**

Index [1]	T_1 (sec) [2]	$(V/W_S)_{Avg}$ [3]	$(V/W_{BL})_{Avg}$ [4]	$(V_{CW}/V_{SS})_{Avg}$ [5]	L_{WSP} (ft) [6]
1L-C1-LP-2C-HS2-EX	0.27	0.29	0.30	0.36	N/A
1L-C1-LP-2C-HSR2-SDS10	0.19	0.78	0.78	0.96	8.00
1L-C1-LP-2C-HSR2-SDS12	0.19	0.78	0.78	0.96	8.00
1L-C1-LP-2C-HSR2-SDS15	0.19	0.96	0.97	1.25	10.67
1L-C1-LP-RB	0.17	1.39	0.82	N/A	N/A
1L-SLP2-LP-2C-S2-EX	0.18	0.40	0.41	0.41	N/A
1L-SLP2-LP-2C-S2R2-SDS10	0.17	0.81	0.83	0.83	8.00
1L-SLP2-LP-2C-S2R2-SDS12	0.17	0.88	0.90	0.90	9.33
1L-SLP2-LP-2C-S2R2-SDS15	0.17	1.04	1.07	1.07	12.00
1L-SLP2-LP-RB	0.14	1.72	1.01	N/A	N/A
1L-W2-G2-2C-HS2-EX	0.23	0.47	0.48	0.72	N/A
1L-W2-G2-2C-HSR2-SDS10	0.19	0.81	0.82	1.65	6.67
1L-W2-G2-2C-HSR2-SDS12	0.18	0.79	0.80	1.93	8.00
1L-W2-G2-2C-HSR2-SDS15	0.18	0.76	0.77	2.49	10.67
1L-W2-G2-RB	0.17	1.18	0.66	N/A	N/A
1L-S2-G2-2C-S2-EX	0.16	0.57	0.59	0.68	N/A
1L-S2-G2-2C-S2R2-SDS10	0.16	1.02	1.05	1.27	6.67
1L-S2-G2-2C-S2R2-SDS12	0.16	1.03	1.06	1.38	8.00
1L-S2-G2-2C-S2R2-SDS15	0.16	1.02	1.05	1.65	10.67
1L-S2-G2-RB	0.14	1.56	0.86	N/A	N/A

[1] Cripple wall retrofit cases are denoted "SDSx" to reflect retrofits for S_{DS} = 1.0*g*, 1.2*g*, and 1.5*g* according to *FEMA P-1100*.
[2] Elastic fundamental period in seconds.
[3] Average strength to seismic weight ratio from pushover loading proportional to elastic translational mode shape in each direction, seismic weight is the total lateral weight acting in the model.
[4] Average strength to baseline weight ratio from pushover loading proportional to elastic mode shape in each direction, baseline weight is the weight of the dwelling including the first-floor diaphragm and above.
[5] Average crawlspace to first occupied story (superstructure) strength ratio, obtained from story-based pushover curves.
[6] Length of wood structural panel (WSP) required in each corner (two lengths per side) for retrofitting according to *FEMA P-1100*.

Table 7.8 Summary of modal and pushover criteria for the baseline cripple wall set and rigid base variants: two-story cases.

Index [1]	T_1 (sec) [2]	$(V/W_S)_{Avg}$ [3]	$(V/W_{BL})_{Avg}$ [4]	$(V_{CW}/V_{SS})_{Avg}$ [5]	L_{WSP} (ft) [6]
2L-C1-LP-2C-HS2-EX	0.39	0.16	0.16	0.34	N/A
2L-C1-LP-2C-HSR2-SDS10	0.30	0.52	0.52	1.20	10.67
2L-C1-LP-2C-HSR2-SDS12	0.29	0.52	0.52	1.35	12.00
2L-C1-LP-2C-HSR2-SDS15	0.29	0.51	0.51	1.64	14.67
2L-C1-LP-RB	0.27	0.63	0.48	N/A	N/A
2L-SLP2-LP-2C-S2-EX	0.28	0.23	0.23	0.40	N/A
2L-SLP2-LP-2C-S2R2-SDS10	0.26	0.58	0.59	1.05	12.00
2L-SLP2-LP-2C-S2R2-SDS12	0.26	0.61	0.61	1.14	13.33
2L-SLP2-LP-2C-S2R2-SDS15	0.26	0.63	0.63	1.29	16.00
2L-SLP2-LP-RB	0.23	0.75	0.57	N/A	N/A
2L-W2-G2-2C-HS2-EX	0.33	0.29	0.29	0.70	N/A
2L-W2-G2-2C-HSR2-SDS10	0.28	0.44	0.44	2.45	10.67
2L-W2-G2-2C-HSR2-SDS12	0.28	0.44	0.44	2.74	12.00
2L-W2-G2-2C-HSR2-SDS15	0.28	0.43	0.43	3.43	16.00
2L-W2-G2-RB	0.27	0.57	0.41	N/A	N/A
2L-S2-G2-2C-S2-EX	0.26	0.34	0.35	0.68	N/A
2L-S2-G2-2C-S2R2-SDS10	0.25	0.54	0.55	1.64	10.67
2L-S2-G2-2C-S2R2-SDS12	0.25	0.54	0.55	1.79	12.00
2L-S2-G2-2C-S2R2-SDS15	0.24	0.54	0.55	2.19	16.00
2L-S2-G2-RB	0.23	0.69	0.51	N/A	N/A

[1] Cripple wall retrofit cases are denoted "SDSx" to reflect retrofits for S_{DS}=1.0*g*, 1.2*g*, and 1.5*g* according to *FEMA P-1100*.
[2] Elastic fundamental period in seconds.
[3] Average strength to seismic weight ratio from pushover loading proportional to elastic translational mode shape in each direction, seismic weight is the total lateral weight acting in the model.
[4] Average strength to baseline weight ratio from pushover loading proportional to elastic mode shape in each direction, baseline weight is the weight of the dwelling including the first-floor diaphragm and above.
[5] Average crawlspace to first occupied story (superstructure) strength ratio, obtained from story-based pushover curves.
[6] Length of wood structural panel (WSP) required in each corner (two lengths per side) for retrofitting according to *FEMA P-1100*, if required length exceeds plan dimension then the plan dimension minus 16 in. is assumed for fully sheathed condition.

7.4.2 Collapse Performance

The collapse performance of the baseline cripple wall variant set is illustrated using two collapse metrics. The first is the probability of collapse at the 250-year return period ground motion intensity(P[C|RP250]), which represents a moderate earthquake intensity that is commonly used to report and compare seismic loss assessment. The second is the probability of collapse at the maximum considered earthquake intensity (P[C|MCE]), where the MCE intensity is defined by scaling the nominal design spectra $S_{DS,\text{Site}}$ for each site (see Table 7.1) by a factor of 1.5. The P[C|RP_{250}] values for existing (unretrofitted) and retrofit variant pairs are summarized in Figure 7.11, where the existing (unretrofitted) variants are shown with solid bars and corresponding retrofit variants are shown with overlaid hatched bars. Similarly, the P[C|MCE] results are summarized in Figure 7.12.

Collapse summaries are tabulated for the baseline cripple wall set for pre-1945 era variants with horizontal wood siding (Table 7.9) pre-1945 era variants with exterior stucco (Table 7.10) and corresponding 1956–1970 era variants in Table 7.11 and Table 7.12 for wood siding and stucco, respectively. Each variant is compared with the corresponding rigid base model (RB), i.e., a house without the cripple wall vulnerability. The collapse fragility information for each of the baseline cripple wall variants are tabulated in addition to probabilities of collapse at the 250-year return period and MCE level ground motion intensities. Each table provides the median collapse intensity ($Sa_{\text{Med,C}}$), record-to-record variability (β_{RTR}), and total collapse fragility dispersion ($\beta_{C,\text{Tot}}$). The final column of each table identifies the fraction of replacement cost assumed for the controlling collapse mode ($Cost_{\text{Col}}$), with 67% replacement cost for cases where cripple wall collapse is the controlling mechanism and 100% replacement cost for variants with collapse in the first occupied story.

General observations for collapse performance of the baseline set of cripple wall variants are summarized in the following:

- Houses with existing (unretrofitted) cripple walls pose very high collapse risks as compared to expectations for buildings constructed in accordance with current building code requirements. For existing houses in regions of high seismicity, the estimated collapse probabilities range from 30% to 95% under 250-year return period ground motions and 80% to 100% under MCE ground motions. The collapse risks are generally higher in the two-story houses, which impose larger seismic force demands on the cripple wall. The existing (unretrofitted) houses experience collapse exclusively in the cripple wall level. This is due to the weak existing cripple walls, whose strengths are generally much weaker than the stories above, where the interior walls and wall finishes add considerable strength.
- The cripple wall retrofits designed in accordance with *FEMA P-1100* significantly reduce the collapse risks. In the regions of high seismicity, the houses with retrofitted cripple walls have estimated collapse probabilities of 1% to 25% under 250-year return period ground motions and 5% to 60% under MCE ground motions. The collapse risks are generally higher in the two-story houses, where the benefit of the cripple wall retrofit is often limited by the strength of the occupied first story above the cripple wall. The collapse risks of the retrofitted houses are also generally higher in the older (pre-1945) houses, due to their larger seismic weight.
- One-story houses with retrofitted cripple walls generally have collapse occurring in the cripple wall. The only exception is that the one-story, 1956–1970 era, house with wood siding cripple walls retrofit for the highest seismic intensity (i.e., 1L-W2-G2-2C-HSR2-SDS15) have collapses occurring the superstructure. This case has the weakest combination of superstructure

materials and the strongest retrofit among the one-story houses (or alternatively, the highest $(Vcw/Vss)_{Avg}$ value among retrofit cases in Table 7.7).

- Two-story houses with retrofitted cripple walls generally have collapse occurring in the first occupied story of the superstructure. This is due to a combination of stronger retrofit designs for two-story versus one-story houses, according to *FEMA P-1100*, and the same existing superstructure materials resisting approximately 45% more lateral mass when compared to one-story houses. The only exception is the two-story, pre-1945 era, stucco cripple wall variant retrofit for the lowest seismic intensity according to *FEMA P-1100* (i.e., 2L-SLP2-LP-2C-S2R2-SDS10), where collapses are still controlled by the cripple wall strength. Despite this variant having the heaviest materials, the superstructure strength is substantially stronger than the weakest two-story retrofit (i.e., S_{DS} = 1.0g) for this weight class, which cannot overcome the strength of the first occupied story (this variant has the lowest $(V_{CW}/V_{SS})_{Avg}$ value among retrofit cases in Table 7.8).

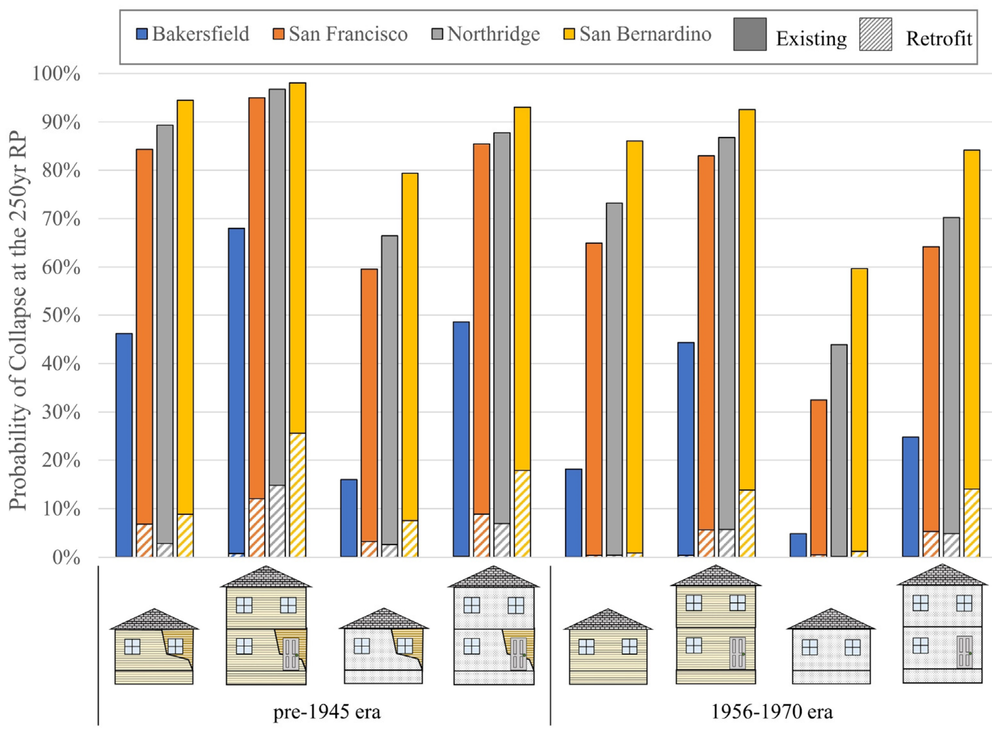

Figure 7.11 **Probability of collapse at the 250-year return period for baseline cripple wall set $Sa(0.25\ \text{sec})_{250}$: 0.63$g$ (BF), 0.98g (SF), 1.15g (NR), and 1.27g (SB).**

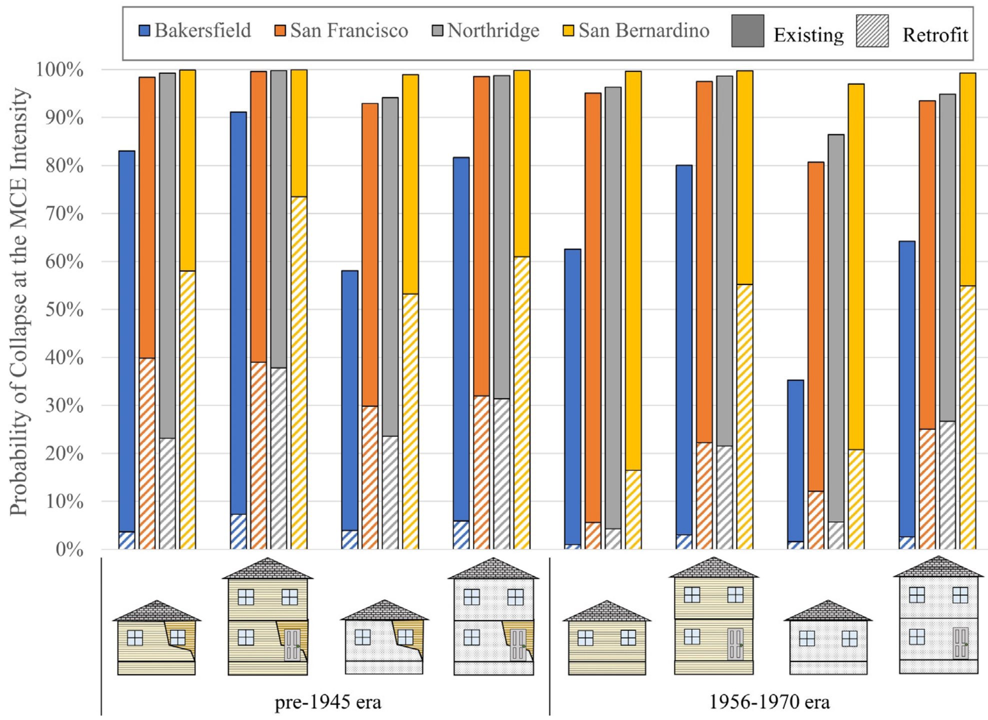

Figure 7.12 **Probability of collapse at MCE intensity results for baseline cripple wall set. *Sa*(0.25 sec)$_{MCE}$: 1.11g (BF), 1.80g (SF), 2.10g (NR), and 2.67g (SB).**

Table 7.9 Collapse performance summary for baseline cripple wall set and rigid base variants: pre-1945 era with horizontal wood siding.

Index [1]	Site [2] (Sa_{250}) (Sa_{MCE})	$Sa_{Med,C}$ (g) [3]	β_{RTR} [4]	$\beta_{C,Tot}$ [5]	P[C|RP250] [6]	P[C|MCE] [7]	$Cost_{Col}$ [8]
1L-C1-LP-2C-HS2-EX	BF270 (0.63g) (1.11g)	0.66	0.42	0.55	46.2%	83.0%	67%
1L-C1-LP-2C-HSR2-SDS10		2.42	0.26	0.44	0.1%	3.7%	67%
1L-C1-LP-RB		6.17	0.55	0.66	0.02%	0.4%	100%
1L-C1-LP-2C-HS2-EX	SF270 (0.98g) (1.80g)	0.57	0.41	0.54	84.3%	98.3%	67%
1L-C1-LP-2C-HSR2-SDS12		2.04	0.34	0.49	6.8%	39.8%	67%
1L-C1-LP-RB		4.49	0.41	0.54	0.2%	4.5%	100%
1L-C1-LP-2C-HS2-EX	NR270 (1.15g) (2.10g)	0.61	0.37	0.51	89.4%	99.2%	67%
1L-C1-LP-2C-HSR2-SDS15		3.05	0.37	0.51	2.8%	23.1%	67%
1L-C1-LP-2C-RB		5.04	0.42	0.54	0.32%	5.3%	100%
1L-C1-LP-2C-HS2-EX	SB270 (1.27g) (2.67g)	0.57	0.36	0.50	94.5%	99.9%	67%
1L-C1-LP-2C-HSR2-SDS15		2.42	0.33	0.48	8.8%	58.0%	67%
1L-C1-LP-RB		4.14	0.42	0.54	1.4%	20.9%	100%
2L-C1-LP-2C-HS2-EX	BF270 (0.63g) (1.11g)	0.46	0.56	0.66	68.0%	91.1%	67%
2L-C1-LP-2C-HSR2-SDS10		2.67	0.49	0.60	0.8%	7.3%	100%
2L-C1-LP-RB		2.52	0.41	0.54	0.5%	6.6%	100%
2L-C1-LP-2C-HS2-EX	SF270 (0.98g) (1.80g)	0.36	0.50	0.61	95.0%	99.6%	67%
2L-C1-LP-2C-HSR2-SDS12		2.18	0.59	0.68	12.0%	39.0%	100%
2L-C1-LP-RB		2.16	0.55	0.65	11.3%	39.0%	100%
2L-C1-LP-2C-HS2-EX	NR270 (1.15g) (2.10g)	0.38	0.49	0.60	96.8%	99.8%	67%
2L-C1-LP-2C-HSR2-SDS15		2.60	0.60	0.69	14.8%	37.8%	100%
2L-C1-LP-RB		2.47	0.55	0.65	12.0%	40.0%	100%
2L-C1-LP-2C-HS2-EX	SB270 (1.27g) (2.67g)	0.38	0.46	0.58	98.1%	99.9%	67%
2L-C1-LP-2C-HSR2-SDS15		1.85	0.46	0.58	25.6%	73.5%	100%
2L-C1-LP-RB		1.84	0.44	0.56	25.2%	74.5%	100%

[1] Cripple wall retrofit cases are denoted 'SDSx' to reflect retrofits for S_{DS} = 1.0g, 1.2g, and 1.5g according to *FEMA P-1100* plan sets.
[2] BF = Bakersfield, SF = San Francisco, NR = Northridge, and SB = San Bernardino, all sites assume V_{S30} = 270 m/sec, 250-year return period, and MCE Sa(0.25 sec) for site annotated.
[3] Median collapse intensity defined as Sa(0.25 sec).
[4] Record-to-record variability from collapse fragility fitting.
[5] Total collapse dispersion including β_{Mod} = 0.35 combined with β_{RTR} using SRSS.
[6] Probability of collapse at 250-year return period (RP_{250}).
[7] Probability of collapse at the MCE with intensity determined by nominal S_{DS} for site scaled by a factor of 1.5.
[8] Percentage of replacement cost attributed to collapse, 67% indicates that governing collapse mode occurs in crawlspace, and 100% indicates that governing collapse mode occurs in first occupied story.

Table 7.10 Collapse performance summary for baseline cripple wall set and rigid base variants: pre-1945 era with exterior stucco.

Index [1]	Site [2] (Sa_{250}) (Sa_{MCE})	$Sa_{Med,C}$ (g) [3]	β_{RTR} [4]	$\beta_{C,Tot}$ [5]	P[C|RP$_{250}$] [6]	P[C|MCE] [7]	$Cost_{Col}$ [8]
1L-SLP2-LP-2C-S2-EX	BF270 (0.63g) (1.11g)	1.01	0.34	0.49	16.0%	58.1%	67%
1L-SLP2-LP-2C-S2R2-SDS10		2.45	0.28	0.45	0.12%	3.9%	67%
1L-SLP2-LP-RB		6.40	0.45	0.57	0.002%	0.10%	100%
1L-SLP2-LP-2C-S2-EX	SF270 (0.98g) (1.80g)	0.87	0.35	0.50	59.6%	92.9%	67%
1L-SLP2-LP-2C-S2R2-SDS12		2.30	0.30	0.46	3.2%	29.8%	67%
1L-SLP2-LP-RB		5.67	0.43	0.56	0.09%	2.0%	100%
1L-SLP2-LP-2C-S2-EX	NR270 (1.15g) (2.10g)	0.92	0.40	0.53	66.4%	94.1%	67%
1L-SLP2-LP-2C-S2R2-SDS15		2.98	0.34	0.49	2.62%	23.6%	67%
1L-SLP2-LP-RB		6.10	0.38	0.52	0.07%	1.9%	100%
1L-SLP2-LP-2C-S2-EX	SB270 (1.27g) (2.67g)	0.84	0.36	0.50	79.4%	98.9%	67%
1L-SLP2-LP-2C-S2R2-SDS15		2.56	0.35	0.49	7.5%	53.2%	67%
1L-SLP2-LP-RB		4.89	0.31	0.46	0.16%	9.6%	100%
2L-SLP2-LP-2C-S2-EX	BF270 (0.63g) (1.11g)	0.64	0.49	0.61	48.6%	81.6%	67%
2L-SLP2-LP-2C-S2R2-SDS10		2.24	0.28	0.45	0.23%	5.9%	67%
2L-SLP2-LP-RB		2.99	0.41	0.54	0.19%	3.35%	100%
2L-SLP2-LP-2C-S2-EX	SF270 (0.98g) (1.80g)	0.55	0.42	0.55	85.4%	98.5%	67%
2L-SLP2-LP-2C-S2R2-SDS12		2.49	0.59	0.69	8.9%	31.9%	100%
2L-SLP2-LP-RB		2.72	0.53	0.63	5.3%	25.8%	100%
2L-SLP2-LP-2C-S2-EX	NR270 (1.15g) (2.10g)	0.60	0.44	0.56	87.8%	98.7%	67%
2L-SLP2-LP-2C-S2R2-SDS15		2.80	0.49	0.60	6.9%	31.4%	100%
2L-SLP2-LP-RB		2.67	0.44	0.56	6.7%	33.5%	100%
2L-SLP2-LP-2C-S2-EX	SB270 (1.27g) (2.67g)	0.56	0.42	0.55	93.1%	99.8%	67%
2L-SLP2-LP-2C-S2R2-SDS15		2.25	0.51	0.62	17.8%	61.0%	100%
2L-SLP2-LP-RB		2.23	0.49	0.60	17.2%	61.7%	100%

[1] Cripple wall retrofit cases are denoted 'SDSx' to reflect retrofits for S_{DS} = 1.0g, 1.2g, and 1.5g according to *FEMA P-1100* plan sets.
[2] BF = Bakersfield, SF = San Francisco, NR = Northridge, and SB = San Bernardino, all sites assume V_{S30} = 270 m/sec, 250-year return period, and MCE Sa(0.25 sec) for site annotated.
[3] Median collapse intensity defined as Sa(0.25 sec).
[4] Record-to-record variability from collapse fragility fitting.
[5] Total collapse dispersion including β_{Mod} = 0.35 combined with β_{RTR} using SRSS.
[6] Probability of collapse at the 250-year return period (RP$_{250}$).
[7] Probability of collapse at the MCE with intensity determined by nominal S_{DS} for site scaled by a factor of 1.5.
[8] Percentage of replacement cost attributed to collapse, 67% indicates that governing collapse mode occurs in crawlspace, and 100% indicates that governing collapse mode occurs in first occupied story.

Table 7.11 Collapse performance summary for baseline cripple wall set and rigid base variants: 1956–1970 era with horizontal wood siding.

Index [1]	Site [2] (Sa_{250}) (Sa_{MCE})	$Sa_{Med,C}$ (g) [3]	β_{RTR} [4]	$\beta_{C,Tot}$ [5]	P[C|RP$_{250}$] [6]	P[C|MCE] [7]	$Cost_{Col}$ [8]
1L-W2-G2-2C-HS2-EX	BF270 (0.63g) (1.11g)	0.96	0.32	0.47	18.2%	62.6%	67%
1L-W2-G2-2C-HSR2-SDS10		3.39	0.32	0.48	0.02%	1.0%	67%
1L-W2-G2-RB		8.04	0.66	0.75	0.03%	0.4%	100%
1L-W2-G2-2C-HS2-EX	SF270 (0.98g) (1.80g)	0.82	0.32	0.47	64.9%	95.1%	67%
1L-W2-G2-2C-HSR2-SDS12		4.45	0.45	0.57	0.40%	5.6%	67%
1L-W2-G2-RB		5.72	0.49	0.60	0.17%	2.8%	100%
1L-W2-G2-2C-HS2-EX	NR270 (1.15g) (2.10g)	0.84	0.37	0.51	73.2%	96.3%	67%
1L-W2-G2-2C-HSR2-SDS15		6.68	0.58	0.67	0.44%	4.3%	100%
1L-W2-G2-RB		6.85	0.51	0.62	0.20%	2.7%	100%
1L-W2-G2-2C-HS2-EX	SB270 (1.27g) (2.67g)	0.76	0.31	0.47	86.1%	99.6%	67%
1L-W2-G2-2C-HSR2-SDS15		4.53	0.42	0.54	0.91%	16.5%	100%
1L-W2-G2-RB		4.77	0.43	0.55	0.79%	14.5%	100%
2L-W2-G2-2C-HS2-EX	BF270 (0.63g) (1.11g)	0.68	0.46	0.58	44.4%	80.0%	67%
2L-W2-G2-2C-HSR2-SDS10		4.57	0.67	0.75	0.40%	3.0%	100%
2L-W2-G2-RB		4.27	0.64	0.73	0.43%	3.3%	100%
2L-W2-G2-2C-HS2-EX	SF270 (0.98g) (1.80g)	0.57	0.48	0.59	82.9%	97.5%	67%
2L-W2-G2-2C-HSR2-SDS12		3.17	0.65	0.74	5.7%	22.2%	100%
2L-W2-G2-RB		3.09	0.59	0.69	4.8%	21.6%	100%
2L-W2-G2-2C-HS2-EX	NR270 (1.15g) (2.10g)	0.63	0.42	0.54	86.8%	98.6%	67%
2L-W2-G2-2C-HSR2-SDS15		3.82	0.67	0.76	5.7%	21.5%	100%
2L-W2-G2-RB		3.91	0.66	0.74	4.9%	20.1%	100%
2L-W2-G2-2C-HS2-EX	SB270 (1.27g) (2.67g)	0.58	0.42	0.54	92.6%	99.7%	67%
2L-W2-G2-2C-HSR2-SDS15		2.46	0.50	0.61	13.8%	55.2%	100%
2L-W2-G2-RB		2.52	0.51	0.62	13.3%	53.8%	100%

[1] Cripple wall retrofit cases are denoted 'SDSx' to reflect retrofits for S_{DS} = 1.0g, 1.2g, and 1.5g according to *FEMA P-1100* plan sets.
[2] BF = Bakersfield, SF = San Francisco, NR = Northridge, and SB = San Bernardino, all sites assume V_{S30} = 270 m/sec, 250-year return period, and MCE Sa(0.25 sec) for site annotated.
[3] Median collapse intensity defined as Sa(0.25 sec).
[4] Record-to-record variability from collapse fragility fitting.
[5] Total collapse dispersion including β_{Mod} = 0.35 combined with β_{RTR} using SRSS.
[6] Probability of collapse at 250-year return period (RP$_{250}$).
[7] Probability of collapse at the MCE with intensity determined by nominal S_{DS} for site scaled by a factor of 1.5.
[8] Percentage of replacement cost attributed to collapse, 67% indicates that governing collapse mode occurs in crawlspace, and 100% indicates that governing collapse mode occurs in first occupied story.

Table 7.12 Collapse performance summary for baseline cripple wall set and rigid base variants: 1956–1970 era with exterior stucco.

Index [1]	Site [2] (Sa_{250}) (Sa_{MCE})	$Sa_{Med,C}$ (g) [3]	β_{RTR} [4]	$\beta_{C,Tot}$ [5]	P[C|RP250] [6]	P[C|MCE] [7]	$Cost_{Col}$ [8]
1L-S2-G2-2C-S2-EX	BF270 (0.63g) (1.11g)	1.32	0.28	0.45	4.9%	35.2%	67%
1L-S2-G2-2C-S2R2-SDS10		2.88	0.27	0.44	0.03%	1.6%	67%
1L-S2-G2-RB		8.28	0.57	0.66	0.005%	0.12%	100%
1L-S2-G2-2C-S2-EX	SF270 (0.98g) (1.80g)	1.21	0.29	0.46	32.5%	80.7%	67%
1L-S2-G2-2C-S2R2-SDS12		3.03	0.27	0.44	0.5%	12.1%	67%
1L-S2-G2-RB		5.54	0.39	0.52	0.044%	1.6%	100%
1L-S2-G2-2C-S2-EX	NR270 (1.15g) (2.10g)	1.24	0.33	0.48	43.9%	86.4%	67%
1L-S2-G2-2C-S2R2-SDS15		4.34	0.30	0.46	0.20%	5.7%	67%
1L-S2-G2-RB		6.19	0.36	0.50	0.039%	1.6%	100%
1L-S2-G2-2C-S2-EX	SB270 (1.27g) (2.67g)	1.13	0.29	0.46	59.7%	97.0%	67%
1L-S2-G2-2C-S2R2-SDS15		4.07	0.38	0.52	1.2%	20.7%	67%
1L-S2-G2-RB		5.04	0.29	0.46	0.13%	8.1%	100%
2L-S2-G2-2C-S2-EX	BF270 (0.63g) (1.11g)	0.91	0.42	0.55	24.8%	64.2%	67%
2L-S2-G2-2C-S2R2-SDS10		3.36	0.45	0.57	0.16%	2.6%	100%
2L-S2-G2-RB		3.53	0.48	0.59	0.17%	2.59%	100%
2L-S2-G2-2C-S2-EX	SF270 (0.98g) (1.80g)	0.81	0.40	0.53	64.2%	93.5%	67%
2L-S2-G2-2C-S2R2-SDS12		2.76	0.53	0.64	5.3%	25.0%	100%
2L-S2-G2-RB		2.83	0.50	0.61	4.1%	23.1%	100%
2L-S2-G2-2C-S2-EX	NR270 (1.15g) (2.10g)	0.86	0.42	0.55	70.2%	94.8%	67%
2L-S2-G2-2C-S2R2-SDS15		3.01	0.46	0.58	4.9%	26.7%	100%
2L-S2-G2-RB		3.13	0.50	0.61	6.9%	25.6%	100%
2L-S2-G2-2C-S2-EX	SB270 (1.27g) (2.67g)	0.76	0.38	0.51	84.1%	99.3%	67%
2L-S2-G2-2C-S2R2-SDS15		2.47	0.52	0.62	14.0%	54.9%	100%
2L-S2-G2-RB		2.54	0.52	0.63	13.4%	53.2%	100%

[1] Cripple wall retrofit cases are denoted 'SDSx' to reflect retrofits for S_{DS} = 1.0g, 1.2g, and 1.5g according to *FEMA P-1100* plan sets.
[2] BF = Bakersfield, SF = San Francisco, NR = Northridge, and SB = San Bernardino, all sites assume V_{S30} = 270 m/sec, 250-year return period, and MCE *Sa*(0.25 sec) for site annotated.
[3] Median collapse intensity defined as *Sa*(0.25 sec).
[4] Record-to-record variability from collapse fragility fitting.
[5] Total collapse dispersion including β_{Mod} = 0.35 combined with β_{RTR} using SRSS.
[6] Probability of collapse at 250-year return period (RP_{250}).
[7] Probability of collapse at the MCE with intensity determined by nominal S_{DS} for site scaled by a factor of 1.5.
[8] Percentage of replacement cost attributed to collapse, 67% indicates that governing collapse mode occurs in crawlspace, and 100% indicates that governing collapse mode occurs in first occupied story

7.4.3 Loss Assessment Summary

Shown in Figure 7.13 and Figure 7.14 are loss (damage) functions for one-story and two-story house variants, which are generally representative of the other variants. Loss functions are shown for the existing (unretrofitted) and retrofit cripple walls, along with ones for equivalent rigid base variants without crawlspace vulnerability. The variants shown in these figures are 1956–1970 era (i.e., gypsum wallboard interior) houses, where the seismic retrofit design of the cripple walls and the input ground motions are for the San Francisco site. Values of the RC250 losses (corresponding to the $Sa_{RP=250}$ intensity of 0.98g) and the expected annual loss (EAL, calculated for the hazard curve in San Francisco) are shown below the house icons on the right side of the figures. In all cases, the cripple wall retrofit dramatically improves the loss performance of the houses, where the relative improvement is larger for the houses with wood siding as compared to stucco exteriors. Notice that the loss curves for the retrofitted one-story houses (Figure 7.13) are slightly above those for the rigid base cases since collapses at higher intensities still occur in the cripple wall. On the other hand, the loss curves for the retrofitted two-story houses (Figure 7.14) are very close to the rigid base cases since collapses at higher intensities for both cases occur in the occupied first story. The loss functions shown in Figure 7.15 and Figure 7.16 illustrate the relative difference in performance based on construction era (pre-1945 versus 1956–1970), which are assumed to have different interior wall materials. In general, the new houses with gypsum board interiors perform better, primarily due to their lower seismic mass as compared to the older houses with lath and plaster interiors.

The EAL and RC250 loss metrics are compared for the entire set of baseline variants at all building sites in Figure 7.17 and Figure 7.18, respectively. The figures show losses for the retrofit cases (hatched bars) overlaid with the existing cases (solid bars), to help visualize the reduction in loss achieved by the seismic retrofit. The associated tabulated data for these cases are summarized in Table 7.13 and Table 7.14, where the "benefit" of the retrofit is calculated as the difference in loss metrics between existing (unretrofitted) and retrofit cases. A summary of loss curve data and EAL values are provided for the entire baseline cripple wall set and rigid base cases in Table 7.15 through Table 7.18, distinguishing between construction era and exterior material.

The general findings and observations for baseline set of houses with cripple walls and the effectiveness of the seismic retrofit are as follows:

- *Overall Reduction in Losses* – The analyses demonstrate that the cripple wall retrofit is very effective in reducing damage and losses. For sites with higher seismic hazard, the retrofit reduced the mean losses for the 250-year ground motion intensity by up to 50% of the house replacement value, i.e., from a loss of 60% replacement value in the existing (unretrofitted) house to about 11% in the retrofitted house. Across the range of building variants, the reduction in loss for high seismic regions ranged from 19% to 49% replacement value in the one-story variants and from 26% to 40% in the two-story variants. In absolute dollar terms, the reduction in losses is about double for the two-story variants, since they have a larger replacement value. The reduction in EALs for the high seismic sites ranged from 0.2% to 1.6% replacement value for the one-story variants and 0.5% to 2.3% for the two-story variants.

- *Influence of Exterior Material* –Wood siding cripple wall dwellings without retrofit are generally more susceptible to damage and losses than equivalent stucco exterior cases due to the lower strength of the wood siding cripple walls. Accordingly, houses with wood siding generally benefit the most from retrofitting the cripple walls. For houses with retrofitted cripple walls, the damage and losses are comparable for wood siding and stucco houses, since their superstructure strengths do not differ as much between wood and stucco exteriors, due the presence of common interior wall types. In fact, in some cases the retrofitted stucco houses experience slightly higher losses due to the lower drift damage threshold and higher repair costs for stucco, as compared to wood siding. However, these slight differences are much less than the overall reduction in losses achieved by retrofitting the vulnerable cripple walls.
- *One-Story versus Two-Story Houses* – As expected, the two-story houses perform worse than one-story houses, primarily because the weight (mass) of the second story effectively doubles the imposed earthquake forces on the cripple walls and first-story walls. For the existing (unretrofitted) cases, the two-story houses begin to experience cripple wall damage and losses at much lower seismic intensities (i.e., accelerations) as compared to equivalent one-story houses. The two-story houses with retrofitted cripple walls also experience higher losses as compared to one-story cases, although the differences between the two were more dependent on the exterior and interior wall materials and level of seismicity. Since the retrofitted cripple wall design accounts for the differences in building weight, the retrofitted cripple walls are much stronger for the two-story house as compared to one-story configurations. This stronger retrofit allowed higher forces to be developed in the first occupied story of the superstructure, with the net effect being that displacements and damage in the retrofit cases shifted from the cripple wall into the first story of the superstructure. However, it is important to note that the damage in the first story of the retrofitted houses initiated at much higher seismic intensity as compared to damage and collapse in the cripple walls of non-retrofitted houses.
- *Influence of Interior Wall Material* – Older pre-1945 variants with plaster on wood lath interior walls generally experienced more damage and losses than the 1956–1970 era houses with gypsum drywall interiors. While plaster on wood lath interior is generally stronger and stiffer than gypsum drywall, it is significantly heavier, more easily damaged, and more expensive to repair than gypsum drywall. The increased mass of houses with plaster and wood lath, leads to larger seismic forces in the cripple walls. Similar to the situation with two-story houses, the larger seismic inertial forces led to cripple wall damage and collapse at lower ground motion intensities for non-retrofitted cripple walls. The differences were less for retrofitted houses since the retrofit design of the cripple walls accounted for the seismic forces associated with the heavier plaster interior walls. Thus, the increase in

damage and losses for wood lath and plaster compared to gypsum wallboard was more significant for existing (unretrofitted) cripple wall cases as compared to the retrofitted cases.

- *Site Seismicity* – As expected, the overall risk of losses and the benefits of cripple wall retrofit were larger for sites with higher seismicity, i.e., for the San Francisco, Northridge, and San Bernardino sites, as compared to the Bakersfield site. Even in Bakersfield, however, the benefits of the cripple wall retrofit were significant. The smallest benefit occurred in the one-story 1956–1970 stucco house, where the overall losses were low and the reduction in the expected RC250 loss from the seismic retrofit was about 3% of the house replacement value (about $7500).

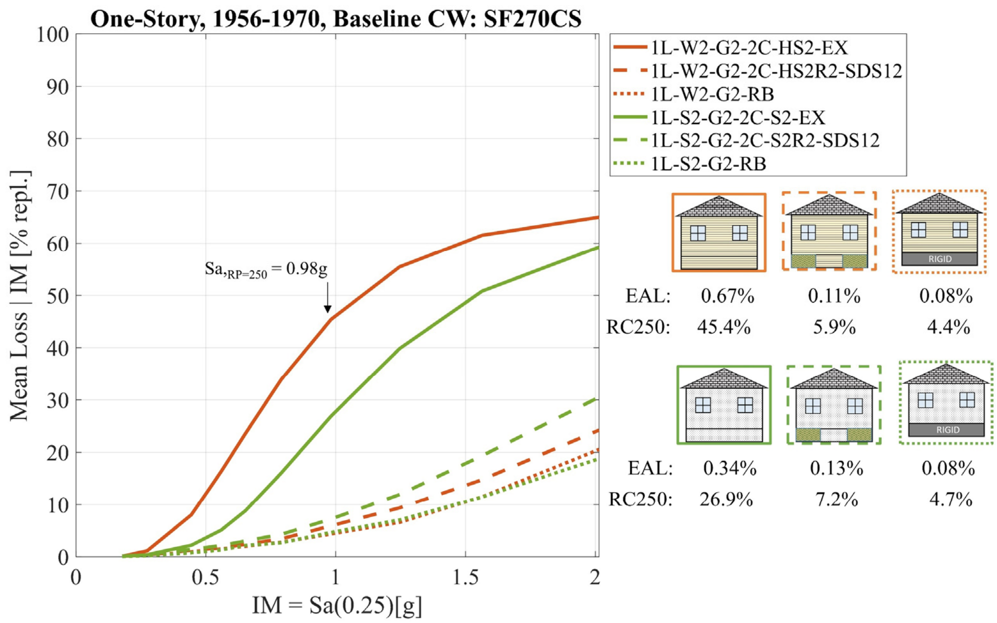

Figure 7.13 Example loss curves for baseline one-story, 1956–1970 era cripple wall variants comparing existing (solid), retrofit (dashed), and rigid base cases (dotted) for the San Francisco site.

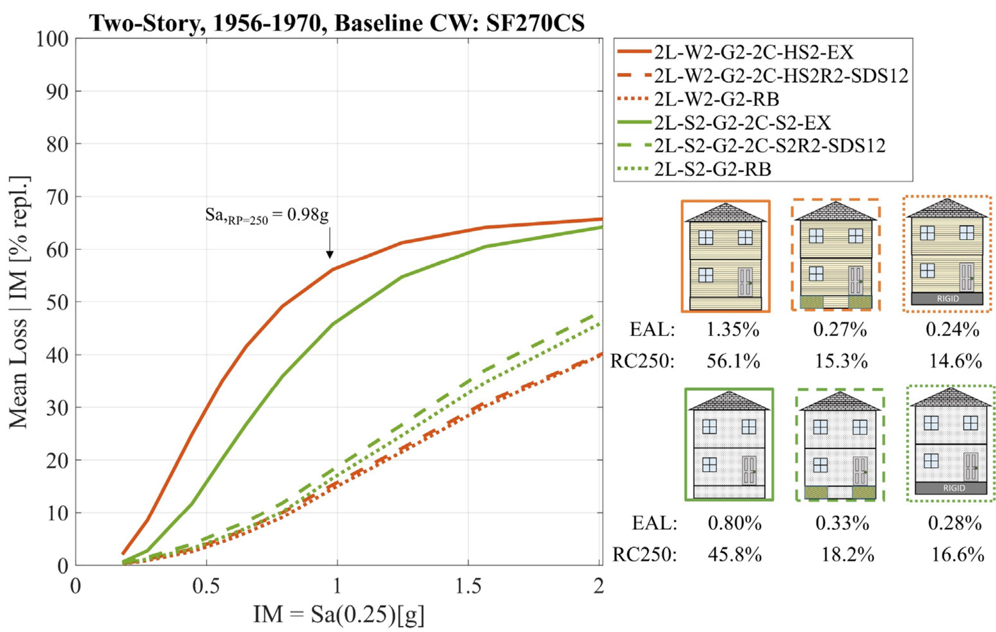

Figure 7.14 Example loss curves for baseline two-story, 1956–1970 era cripple wall variants comparing existing (solid), retrofit (dashed), and rigid base cases (dotted) for the San Francisco site.

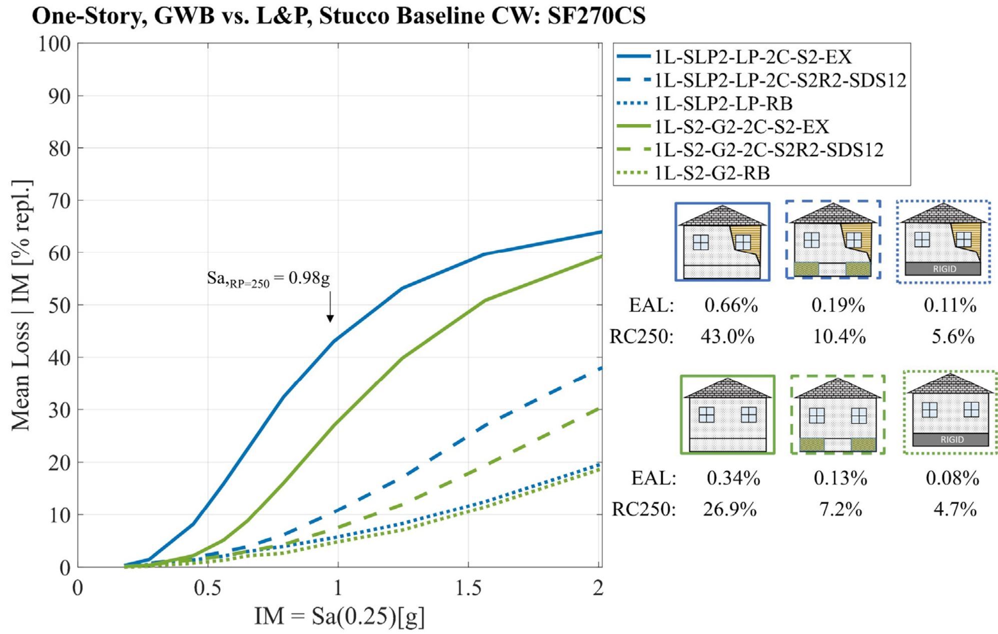

Figure 7.15 **Loss curves for baseline one-story stucco cripple wall variants for both construction eras comparing existing (solid), retrofit (dashed), and rigid base cases (dotted) for the San Francisco site.**

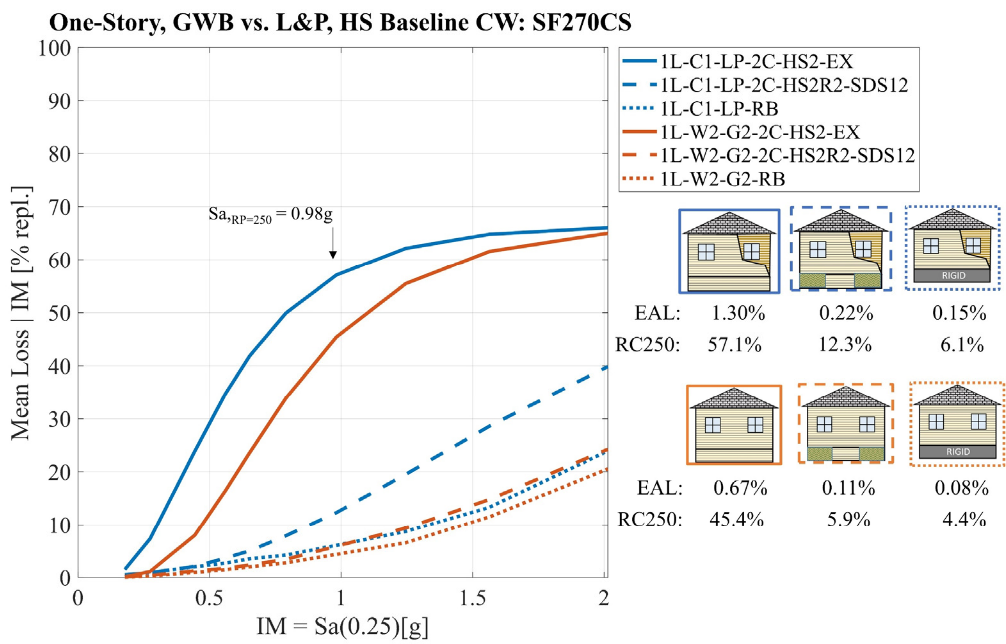

Figure 7.16 **Loss curves for baseline one-story horizontal wood siding cripple wall variants for both construction eras comparing existing (solid), retrofit (dashed), and rigid base cases (dotted) for the San Francisco site.**

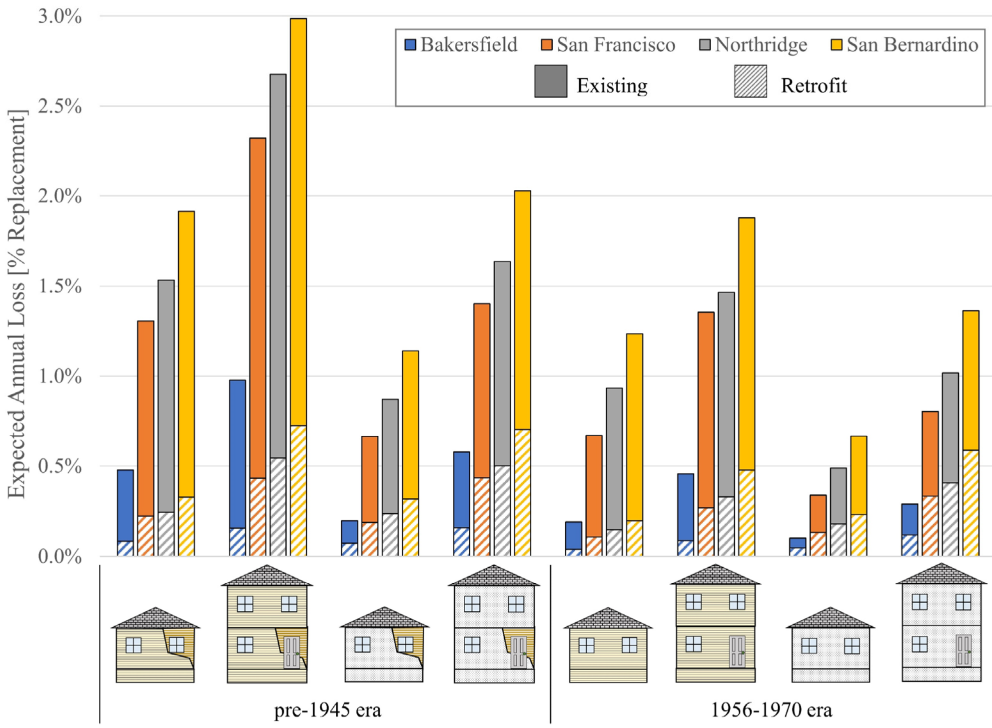

Figure 7.17 Expected annual loss results for baseline cripple wall set and all sites.

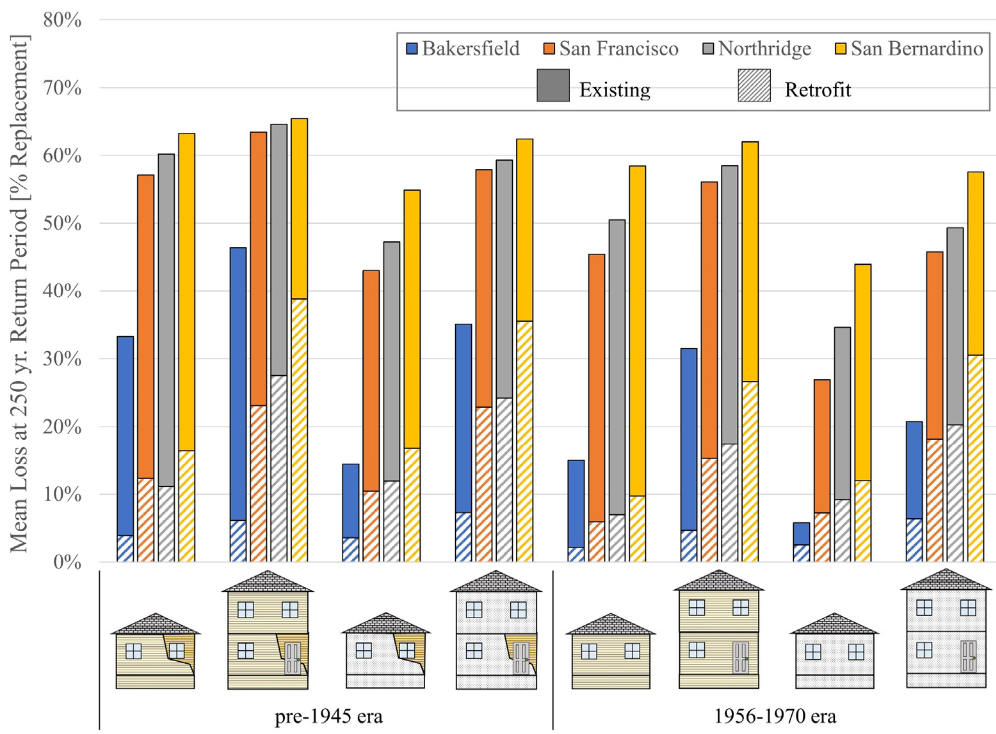

Figure 7.18 Expected loss at the 250-year return period (RC250) results for baseline cripple wall set and all sites.

Table 7.13 Summary of primary loss metrics and benefits due to retrofitting for baseline cripple wall set: one-story cases.

Description/index	Site	Condition	EAL (% repl.)	Benefit$_{EAL}$[1] (% repl.)	RC250 (% repl.)	Benefit$_{RC250}$[1] (% repl.)
One story, pre-1945, wood siding, 2-ft-tall cripple wall. (EX) 1L-C1-LP-2C-HS2-EX (R) 1L-C1-LP-2C-HSR2-SDSx	BF 270	Existing	0.478	0.39	33.23	29.3
		Retrofitted	0.083		3.89	
	SF 270	Existing	1.305	1.08	57.09	44.8
		Retrofitted	0.223		12.32	
	NR 270	Existing	1.534	1.29	60.20	49.1
		Retrofitted	0.244		11.14	
	SB 270	Existing	1.914	1.59	63.30	46.9
		Retrofitted	0.327		16.40	
One story, pre-1945, stucco, 2-ft-tall cripple wall. (EX) 1L-SLP2-LP-2C-S2-EX (R) 1L-SLP2-LP-2C-S2R2-SDSx	BF 270	Existing	0.197	0.13	14.43	10.9
		Retrofitted	0.072		3.56	
	SF 270	Existing	0.664	0.48	42.99	32.6
		Retrofitted	0.188		10.43	
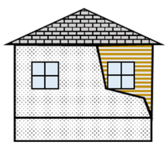	NR 270	Existing	0.872	0.64	47.21	35.3
		Retrofitted	0.236		11.93	
	SB 270	Existing	1.140	0.82	54.87	38.1
		Retrofitted	0.317		16.75	
One-story, 1956–1970, wood siding, 2-ft-t ll cripple wall. (EX) 1L-W2-G2-2C-HS2-EX (R) 1L-W2-G2-2C-HSR2-SDSx	BF 270	Existing	0.190	0.15	14.98	12.9
		Retrofitted	0.039		2.11	
	SF 270	Existing	0.670	0.56	45.42	39.5
		Retrofitted	0.107		5.92	
	NR 270	Existing	0.933	0.79	50.49	43.5
		Retrofitted	0.148		6.98	
	SB 270	Existing	1.235	1.04	58.40	48.7
		Retrofitted	0.197		9.73	
One story, 1956–1970, stucco, 2-ft-tall cripple wall. (EX) 1L-S2-G2-2C-HS2-EX (R) 1L-S2-G2-2C-HSR2-SDSx	BF 270	Existing	0.100	0.05	5.75	3.2
		Retrofitted	0.047		2.52	
	SF 270	Existing	0.338	0.21	26.88	19.7
		Retrofitted	0.132		7.23	
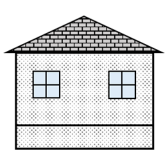	NR 270	Existing	0.488	0.31	34.59	25.4
		Retrofitted	0.180		9.20	
	SB 270	Existing	0.666	0.43	43.95	32.0
		Retrofitted	0.232		12.00	

[1] Benefits are the difference of the retrofit variant (R) subtracted from the existing (unretrofitted) variant (EX).

Table 7.14 Summary of primary loss metrics and benefits due to retrofitting for baseline cripple wall set: two-story cases.

Description/index	Site	Condition	EAL (% repl.)	Benefit$_{EAL}$[1] (% repl.)	RC250 (% repl.)	Benefit$_{RC250}$[1] (% repl.)
Two story, pre-1945, wood siding, 2-ft-tall cripple wall. (EX) 2L-C1-LP-2C-HS2-EX (R) 2L-C1-LP-2C-HSR2-SDSx	BF 270	Existing	0.978	0.82	46.39	40.3
		Retrofitted	0.157		6.11	
	SF 270	Existing	2.322	1.89	63.51	40.4
		Retrofitted	0.433		23.10	
	NR 270	Existing	2.676	2.13	64.63	37.1
		Retrofitted	0.544		27.51	
	SB 270	Existing	2.986	2.26	65.46	26.7
		Retrofitted	0.726		38.77	
Two story, pre-1945, stucco, 2-ft-tall cripple wall. (EX) 2L-SLP2-LP-2C-S2-EX (R) 2L-SLP2-LP-2C-S2R2-SDSx	BF 270	Existing	0.577	0.42	35.06	27.8
		Retrofitted	0.159		7.28	
	SF 270	Existing	1.400	0.97	57.87	35.0
		Retrofitted	0.435		22.89	
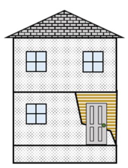	NR 270	Existing	1.637	1.14	59.27	35.0
		Retrofitted	0.501		24.23	
	SB 270	Existing	2.028	1.324	62.49	27.0
		Retrofitted	0.704		35.52	
Two story, 1956–1970, wood siding, 2-ft-tall cripple wall. (EX) 2L-W2-G2-2C-HS2-EX (R) 2L-W2-G2-2C-HSR2-SDSx	BF 270	Existing	0.456	0.37	31.50	26.9
		Retrofitted	0.087		4.63	
	SF 270	Existing	1.353	1.09	56.07	40.8
		Retrofitted	0.268		15.30	
	NR 270	Existing	1.464	1.13	58.47	41.0
		Retrofitted	0.329		17.46	
	SB 270	Existing	1.878	1.40	62.06	35.5
		Retrofitted	0.478		26.60	
Two-story, 1956–1970, stucco, 2-ft-tall cripple wall. (EX) 2L-S2-G2-2C-HS2-EX (R) 2L-S2-G2-2C-HSR2-SDSx	BF 270	Existing	0.290	0.17	20.74	14.4
		Retrofitted	0.118		6.34	
	SF 270	Existing	0.804	0.47	45.77	27.6
		Retrofitted	0.333		18.17	
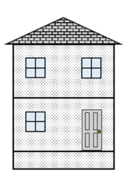	NR 270	Existing	1.017	0.61	49.30	29.1
		Retrofitted	0.407		20.25	
	SB 270	Existing	1.361	0.78	57.55	27.0
		Retrofitted	0.586		30.53	

[1] Benefits are the difference of the retrofit variant (R) subtracted from the existing (unretrofitted) variant (EX).

Table 7.15 Loss assessment summary for baseline cripple wall set and rigid base variants: pre-1945 era with horizontal wood siding.

Index [1]	Site[2]	Mean loss at return period (% of replacement cost)										EAL[4] (%)
		15	25	50	75	100	150	250 [3]	500	1000	2500	
1L-C1-LP-2C-HS2-EX	BF 270	0.22	0.85	4.70	9.91	14.8	22.8	33.2	46.1	55.1	61.9	0.48
" "-HSR2-SDS10		0.20	0.51	0.89	1.23	1.56	2.30	3.89	6.49	10.3	17.6	0.08
" "-RB		0.20	0.44	0.80	1.38	1.64	2.15	3.04	4.61	6.35	9.90	0.07
1L-C1-LP-2C-HS2-EX	SF 270	1.52	7.36	23.9	34.7	41.8	49.9	57.1	62.2	64.8	66.1	1.30
" "-HSR2-SDS12		0.51	0.91	2.10	3.66	5.06	7.92	12.3	19.6	28.6	39.9	0.22
" "-RB		0.46	0.95	2.03	2.72	3.54	4.24	6.11	8.74	13.3	23.9	0.15
1L-C1-LP-2C-HS2-EX	NR 270	2.22	9.89	29.5	41.1	47.5	54.9	60.2	64.2	65.7	66.4	1.53
" "-HSR2-SDS15		0.82	1.41	2.78	4.28	5.58	7.74	11.1	17.3	24.0	34.2	0.24
" "-RB		0.66	1.32	2.64	3.64	4.28	5.59	7.32	11.0	17.3	29.0	0.19
1L-C1-LP-2C-HS2-EX	SB 270	4.44	15.6	37.3	48.4	54.1	59.6	63.3	65.6	66.3	66.6	1.91
" "-HSR2-SDS15		1.00	1.67	3.34	5.66	7.61	11.4	16.4	25.9	35.6	46.3	0.33
" "-RB		0.80	1.55	3.01	4.35	5.29	6.67	9.95	17.7	27.4	41.8	0.25
2L-C1-LP-2C-HS2-EX	BF 270	1.75	5.39	15.4	23.5	29.6	37.7	46.4	55.0	60.3	64.0	0.98
" "-HSR2-SDS10		0.57	1.00	1.92	2.61	3.17	4.40	6.11	10.1	16.2	27.2	0.16
" "-RB		0.54	0.90	1.94	2.72	3.19	4.45	6.29	9.95	16.7	28.3	0.16
2L-C1-LP-2C-HS2-EX	SF 270	9.19	23.1	43.4	51.8	56.2	60.4	63.5	65.4	66.2	66.5	2.32
" "-HSR2-SDS12		1.17	2.14	4.91	7.70	10.4	15.4	23.1	33.0	44.0	56.7	0.43
" "-RB		1.04	2.05	4.67	7.36	9.91	14.6	22.6	32.7	44.7	57.3	0.42
2L-C1-LP-2C-HS2-EX	NR 270	12.7	29.2	48.9	56.2	59.5	62.6	64.6	65.9	66.4	66.6	2.68
" "-HSR2-SDS15		1.54	2.94	6.50	10.7	13.4	19.3	27.5	38.2	48.5	60.8	0.54
" "-RB		1.43	2.72	5.77	9.59	12.0	17.4	25.5	35.7	46.1	58.6	0.50
2L-C1-LP-2C-HS2-EX	SB 270	17.3	34.1	52.5	58.9	61.7	64.0	65.5	66.3	66.5	66.6	2.99
" "-HSR2-SDS15		1.96	3.52	8.32	14.0	19.0	28.1	38.8	53.3	66.3	78.5	0.73
" "-RB		1.79	3.40	7.86	13.1	18.3	27.5	37.9	53.1	66.5	79.0	0.70

[1] Cripple wall retrofit cases are denoted 'SDSx' to reflect retrofits for S_{DS} = 1.0*g*, 1.2*g*, and 1.5*g* according to *FEMA P-1100* plan sets.
[2] BF = Bakersfield, SF = San Francisco, NR = Northridge, and SB = San Bernardino; all sites assume V_{S30} = 270 m/sec.
[3] Mean loss at the 250-year return period is a primary loss metric and is also referred to as 'RC250'.
[4] Expected annual loss expressed in percentage of building replacement cost.

Table 7.16 Loss assessment summary for baseline cripple wall set and rigid base variants: pre-1945 era with exterior stucco.

Index [1]	Site[2]	Mean loss for return period (% of replacement cost)										EAL[4] (%)
		15	25	50	75	100	150	250[3]	500	1000	2500	
1L-SLP2-LP-2C-S2-EX	BF 270	0.11	0.23	0.81	1.96	3.60	7.24	14.4	27.5	40.5	53.5	0.20
" "-S2R2-SDS10		0.12	0.29	0.67	1.01	1.36	2.06	3.56	6.48	11.4	19.9	0.07
" "-RB		0.08	0.16	0.43	0.76	1.09	1.53	2.43	3.99	6.11	9.50	0.04
1L-SLP2-LP-2C-S2-EX	SF 270	0.32	1.47	8.20	15.9	22.5	32.4	43.0	53.2	59.7	64.0	0.66
" "-S2R2-SDS12		0.36	0.74	1.79	2.92	3.91	6.15	10.4	17.1	27.0	38.1	0.19
" "-RB		0.17	0.51	1.41	2.11	2.98	3.96	5.58	8.27	12.5	19.7	0.11
1L-SLP2-LP-2C-S2-EX	NR 270	0.67	3.02	13.5	22.9	29.6	38.6	47.2	56.2	61.1	64.4	0.87
" "-S2R2-SDS15		0.52	1.17	2.55	4.17	5.79	8.34	11.9	18.9	26.6	37.4	0.24
" "-RB		0.33	0.81	2.05	3.03	4.07	5.35	7.35	10.4	15.1	23.5	0.16
1L-SLP2-LP-2C-S2-EX	SB 270	1.20	5.11	19.6	30.8	38.3	47.2	54.9	61.3	64.4	65.9	1.14
" "-S2R2-SDS15		0.73	1.50	3.22	5.66	7.84	11.0	16.8	26.5	36.7	46.8	0.32
" "-RB		0.43	1.02	2.53	3.73	4.69	6.25	8.50	14.0	20.6	34.0	0.20
2L-SLP2-LP-2C-S2-EX	BF 270	0.56	1.84	7.09	12.8	17.7	25.4	35.1	46.5	54.6	61.2	0.58
" "-S2R2-SDS10		0.39	0.85	1.97	2.97	3.74	5.15	7.28	10.8	16.4	26.1	0.16
" "-RB		0.28	0.67	1.75	2.69	3.51	4.64	6.72	10.6	16.3	26.7	0.14
2L-SLP2-LP-2C-S2-EX	SF 270	2.18	8.60	25.9	36.7	43.5	51.2	57.9	62.6	64.9	66.1	1.40
" "-S2R2-SDS12		0.95	2.27	5.30	8.40	10.6	15.1	23.0	32.5	42.2	54.4	0.43
" "-RB		0.76	1.90	4.21	6.56	8.56	12.3	19.4	28.4	39.0	50.6	0.36
2L-SLP2-LP-2C-S2-EX	NR 270	3.51	12.2	31.0	41.5	47.4	54.1	59.3	63.5	65.3	66.2	1.64
" "-S2R2-SDS15		1.38	2.97	6.36	10.0	12.0	16.6	24.2	33.5	43.9	56.3	0.50
" "-RB		1.17	2.64	5.76	8.41	10.8	15.4	23.3	34.0	44.5	57.8	0.46
2L-SLP2-LP-2C-S2-EX	SB 270	6.27	18.2	38.3	48.3	53.5	58.7	62.5	65.1	66.1	66.5	2.03
" "-S2R2-SDS15		1.83	3.85	8.86	13.4	18.5	26.7	35.5	47.9	60.0	71.8	0.70
" "-RB		1.52	3.43	7.59	12.3	17.1	25.1	34.5	47.6	59.6	71.9	0.65

[1] Cripple wall retrofit cases are denoted "SDSx" to reflect retrofits for S_{DS} = 1.0g, 1.2g, and 1.5g according to *FEMA P-1100* plan sets.
[2] BF = Bakersfield, SF = San Francisco, NR = Northridge, and SB = San Bernardino; all sites assume V_{S30} = 270 m/sec.
[3] Mean loss at the 250-year return period is a primary loss metric and is also referred to as 'RC250'.
[4] Expected annual loss expressed in percentage of building replacement cost.

Table 7.17 **Loss assessment summary for baseline cripple wall set and rigid base variants: 1956–1970 era with horizontal wood siding.**

Index [1]	Site[2]	Mean loss for return period (% of replacement cost)										EAL[4] (%)
		15	25	50	75	100	150	250[3]	500	1000	2500	
1L-W2-G2-2C-HS2-EX	BF 270	0.01	0.05	0.60	1.75	3.23	7.29	15.0	28.6	42.0	55.0	0.19
" "-HSR2-SDS10		0.03	0.07	0.34	0.65	0.85	1.25	2.11	3.84	6.52	11.8	0.04
" "-RB		0.02	0.07	0.20	0.42	0.58	1.03	1.70	3.03	4.68	8.77	0.03
1L-W2-G2-2C-HS2-EX	SF 270	0.11	1.13	8.04	16.4	23.6	33.9	45.4	55.5	61.6	65.0	0.67
" "-HSR2-SDS12		0.10	0.38	1.27	1.71	2.37	3.43	5.92	9.38	14.8	24.3	0.11
" "-RB		0.06	0.25	0.96	1.49	2.01	2.78	4.38	6.60	11.5	20.6	0.08
1L-W2-G2-2C-HS2-EX	NR 270	0.43	3.10	15.0	25.4	32.5	41.8	50.5	58.7	62.8	65.3	0.93
" "-HSR2-SDS15		0.19	0.65	1.76	2.63	3.31	4.93	6.98	12.9	18.8	29.0	0.15
" "-RB		0.14	0.46	1.33	2.20	2.80	3.92	5.76	10.3	15.8	25.5	0.12
1L-W2-G2-2C-HS2-EX	SB 270	0.94	5.44	22.2	34.7	42.5	51.3	58.4	63.5	65.6	66.4	1.24
" "-HSR2-SDS15		0.29	0.85	2.07	3.25	4.35	6.10	9.73	18.3	28.1	40.4	0.20
" "-RB		0.21	0.56	1.59	2.77	3.53	4.75	7.85	14.8	23.4	36.2	0.16
2L-W2-G2-2C-HS2-EX	BF 270	0.16	0.83	4.63	9.40	14.0	21.6	31.5	44.0	53.2	60.6	0.46
" "-HSR2-SDS10		0.10	0.28	0.96	1.58	2.12	3.05	4.63	7.40	11.7	18.3	0.09
" "-RB		0.09	0.24	0.81	1.37	1.87	2.85	4.54	7.53	12.2	19.3	0.08
2L-W2-G2-2C-HS2-EX	SF 270	2.05	8.53	24.9	35.1	41.6	49.1	56.1	61.2	64.1	65.7	1.35
" "-HSR2-SDS12		0.34	1.13	3.06	4.99	6.92	10.0	15.3	22.2	30.9	40.2	0.27
" "-RB		0.28	0.91	2.61	4.45	6.15	9.11	14.6	21.5	30.2	40.1	0.24
2L-W2-G2-2C-HS2-EX	NR 270	2.09	9.39	27.8	38.8	45.2	52.7	58.5	63.2	65.2	66.2	1.46
" "-HSR2-SDS15		0.58	1.56	4.10	6.93	8.64	12.4	17.5	24.1	31.1	40.2	0.33
" "-RB		0.52	1.35	3.68	6.29	7.91	11.5	16.5	22.7	30.0	39.0	0.30
2L-W2-G2-2C-HS2-EX	SB 270	4.77	15.6	35.8	46.5	52.2	57.9	62.1	64.9	66.0	66.5	1.88
" "-HSR2-SDS15		0.87	2.11	5.54	8.80	12.4	18.8	26.6	37.9	49.7	62.6	0.48
" "-RB		0.74	1.84	5.17	8.49	12.0	18.3	25.8	37.2	48.5	61.2	0.45

[1] Cripple wall retrofit cases are denoted "SDSx" to reflect retrofits for $S_{DS} = 1.0g$, $1.2g$, and $1.5g$ according to *FEMA P-1100* plan sets.
[2] BF = Bakersfield, SF = San Francisco, NR = Northridge, and SB = San Bernardino; all sites assume $V_{S30} = 270$ m/sec.
[3] Mean loss at the 250-year return period is a primary loss metric and is also referred to as 'RC250'.
[4] Expected annual loss expressed in percentage of building replacement cost.

Table 7.18 Loss assessment summary for baseline cripple wall set and rigid base variants: 1956–1970 era with exterior stucco.

Index [1]	Site[2]	Mean loss for return period (% of replacement cost)										EAL[4] (%)
		15	25	50	75	100	150	250[3]	500	1000	2500	
1L-S2-G2-2C-HS2-EX	BF 270	0.03	0.11	0.33	0.68	1.07	2.34	5.75	14.6	27.0	43.2	0.10
“ “-S2R2-SDS10		0.03	0.09	0.37	0.75	1.09	1.53	2.52	4.55	8.04	15.4	0.05
“ “-RB		0.02	0.05	0.17	0.34	0.55	0.92	1.62	2.97	4.85	8.44	0.03
1L-S2-G2-2C-HS2-EX	SF 270	0.13	0.39	2.20	5.15	8.81	16.0	26.9	39.8	50.8	59.3	0.34
“ “-S2R2-SDS12		0.12	0.45	1.42	2.16	3.02	4.30	7.23	12.0	19.4	30.5	0.13
“ “-RB		0.05	0.21	0.78	1.32	2.17	2.67	4.67	7.06	11.5	18.8	0.08
1L-S2-G2-2C-HS2-EX	NR 270	0.23	0.82	4.51	10.2	15.6	24.5	34.6	47.2	55.3	61.5	0.49
“ “-S2R2-SDS15		0.24	0.79	2.21	3.32	4.37	6.31	9.20	14.3	21.5	31.6	0.18
“ “-RB		0.12	0.42	1.19	2.12	2.91	4.24	6.05	9.40	14.7	23.0	0.11
1L-S2-G2-2C-HS2-EX	SB 270	0.37	1.36	7.63	16.0	22.8	33.5	44.0	54.9	61.1	64.6	0.67
“ “-S2R2-SDS15		0.33	1.05	2.55	4.22	5.55	7.67	12.0	20.8	28.2	39.4	0.23
“ “-RB		0.18	0.53	1.53	2.75	3.56	5.14	7.56	13.3	20.1	31.6	0.15
2L-S2-G2-2C-HS2-EX	BF 270	0.16	0.45	2.22	4.58	7.13	12.4	20.7	33.3	44.4	55.1	0.29
“ “-S2R2-SDS10		0.15	0.44	1.35	2.26	2.93	4.27	6.34	9.61	14.5	23.4	0.12
“ “-RB		0.08	0.31	0.99	1.72	2.43	3.68	5.61	8.89	13.7	22.5	0.10
2L-S2-G2-2C-HS2-EX	SF 270	0.59	2.76	11.7	20.2	26.8	36.0	45.8	54.7	60.5	64.2	0.80
“ “-S2R2-SDS12		0.50	1.51	3.98	6.39	8.23	11.9	18.2	26.7	37.1	48.3	0.33
“ “-RB		0.33	1.17	3.16	5.27	6.99	10.2	16.6	24.6	34.8	46.1	0.28
2L-S2-G2-2C-HS2-EX	NR 270	1.11	4.73	17.1	26.5	32.8	41.4	49.3	57.4	61.8	64.7	1.02
“ “-S2R2-SDS15		0.88	2.16	5.32	8.10	10.1	13.6	20.3	29.1	38.7	50.7	0.41
“ “-RB		0.59	1.72	4.72	7.33	9.64	14.2	20.6	31.1	41.1	53.4	0.38
2L-S2-G2-2C-HS2-EX	SB 270	2.13	7.93	24.7	36.0	43.0	50.9	57.6	62.8	65.1	66.2	1.36
“ “-S2R2-SDS15		1.29	2.93	7.35	11.2	15.6	22.4	30.5	42.2	53.7	66.0	0.59
“ “-RB		0.87	2.33	6.49	10.3	14.4	21.5	28.8	40.9	52.0	64.2	0.53

[1] Cripple wall retrofit cases are denoted “SDSx” to reflect retrofits for S_{DS} = 1.0*g*, 1.2*g*, and 1.5*g* according to *FEMA P-1100* plan sets.
[2] BF = Bakersfield, SF = San Francisco, NR = Northridge, and SB = San Bernardino; all sites assume V_{S30} = 270 m/sec.
[3] Mean loss at the 250-year return period is a primary loss metric and is also referred to as ‘RC250’.
[4] Expected annual loss expressed in percentage of building replacement cost.

7.5 INFLUENCE OF CRIPPLE WALL HEIGHT

The baseline cripple wall variants discussed in Section 7.4 are all based on 2-ft-tall cripple walls. In this section, results are compared for 2-ft-tall versus 6-ft-tall cripple walls. The comparative analyses of the 2-ft-tall versus 6-ft-tall variants utilize experimental test data developed by WG4 of the PEER–CEA Project.

7.5.1 Modal and Pushover Criteria for 6-Ft-Tall Cripple Walls

As compared to the 2-ft-tall cripple wall variants, the 6-ft-tall cripple wall houses typically exhibit longer fundamental periods due to the increased height of the cripple wall. The increase is more pronounced for wood siding cripple walls than stucco cripple walls. In terms of force-displacement behavior, a key difference is that the taller 6-ft-tall cripple walls have a larger displacement capacity (inches) and are generally less susceptible to P-delta effects, since the reduction in effective stiffness of the cripple walls due to geometric effects is inversely proportional to their height (i.e., the translational geometric stiffness term is W/L, where W is the house weight and L is the cripple wall height). Distinguishing between materials, the 6-ft-tall stucco cripple walls are about 20% stronger and have nearly twice the displacement capacity of the 2-ft-tall stucco cripple walls, based on experimental testing; see Chapter 3. The 6-ft-tall wood siding cripple walls have about the same strength and about three times the drift capacity (increasing roughly in proportion to their height) as the 2-ft-tall wood siding cripple walls. These differences are compared in the static pushover analysis results (loading the cripple wall only) shown in Figure 7.19. A summary of the modal and pushover criteria for the 6-ft-tall cripple wall set is provided in Table 7.19 and Table 7.20 for one- and two-story variants, respectively.

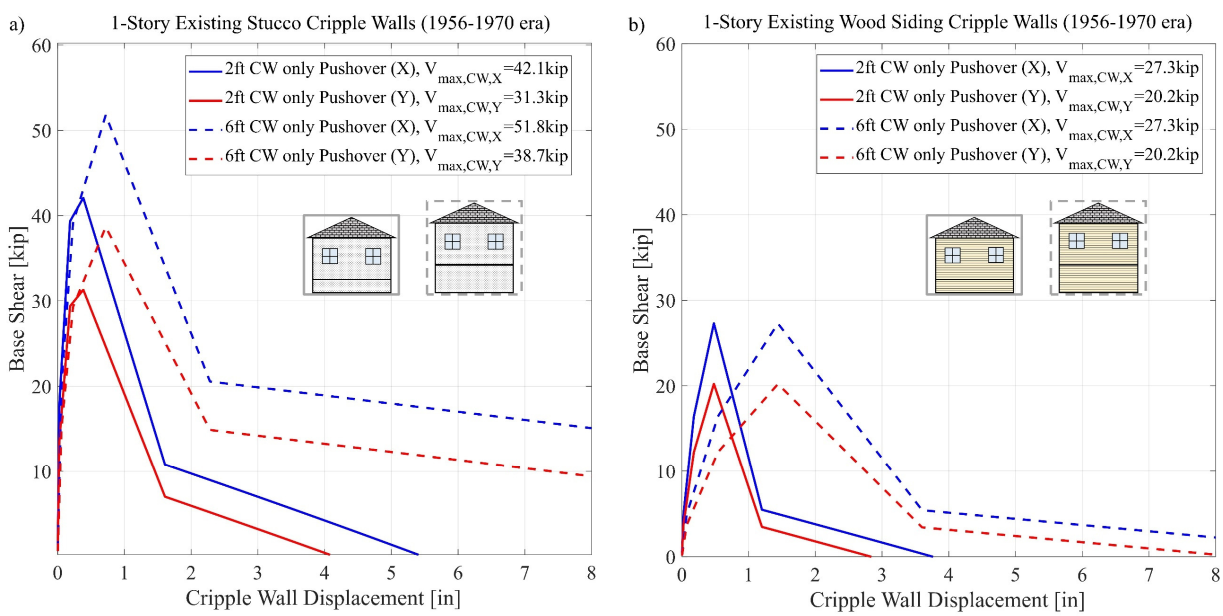

Figure 7.19 Existing (unretrofitted) cripple wall force-displacement behavior for 2-ft-tall (solid) and 6-ft-tall (dashed) cripple walls from cripple wall only pushovers for the one-story, 1956–1970 era variants: (a) exterior stucco; and (b) horizontal wood siding.

Table 7.19 Summary of modal and pushover criteria for the 6-ft-tall cripple wall set and rigid base variants: one-story cases.

Index [1]	T_1 (sec) [2]	$(V/W_S)_{Avg}$ [3]	$(V/W_{BL})_{Avg}$ [4]	$(V_{CW}/V_{SS})_{Avg}$ [5]	L_{WSP} (ft) [6]
1L-C1-LP-6C-HS2-EX	0.42	0.29	0.30	0.36	N/A
1L-C1-LP-6C-HSR2-SDS10	0.28	0.77	0.79	0.97	8.00
1L-C1-LP-6C-HSR2-SDS12	0.27	0.88	0.90	1.11	9.33
1L-C1-LP-6C-HSR2-SDS15	0.25	1.09	1.13	1.38	12.00
1L-C1-LP-RB	0.17	1.39	0.82	N/A	N/A
1L-SLP2-LP-6C-S2-EX	0.23	0.48	0.51	0.5	N/A
1L-SLP2-LP-6C-S2R2-SDS10	0.21	0.85	0.91	0.91	9.33
1L-SLP2-LP-6C-S2R2-SDS12	0.21	0.92	0.98	0.98	10.67
1L-SLP2-LP-6C-S2R2-SDS15	0.20	1.08	1.16	1.17	13.33
1L-SLP2-LP-RB	0.14	1.72	1.01	N/A	N/A
1L-W2-G2-6C-HS2-EX	0.35	0.46	0.48	0.71	N/A
1L-W2-G2-6C-HSR2-SDS10	0.24	1.01	1.04	1.92	8.00
1L-W2-G2-6C-HSR2-SDS12	0.23	0.98	1.02	2.19	9.33
1L-W2-G2-6C-HSR2-SDS15	0.22	0.96	1.00	2.46	10.67
1L-W2-G2-RB	0.17	1.18	0.66	N/A	N/A
1L-S2-G2-6C-S2-EX	0.20	0.66	0.72	0.84	N/A
1L-S2-G2-6C-S2R2-SDS10	0.18	1.09	1.19	1.4	8.00
1L-S2-G2-6C-S2R2-SDS12	0.18	1.12	1.23	1.52	9.33
1L-S2-G2-6C-S2R2-SDS15	0.18	1.12	1.22	1.65	10.67
1L-S2-G2-RB	0.14	1.56	0.86	N/A	N/A

[1] Cripple wall retrofit cases are denoted "SDSx" to reflect retrofits for S_{DS} = 1.0*g*, 1.2*g*, and 1.5*g* according to *FEMA P-1100*.
[2] Elastic fundamental period in seconds.
[3] Average strength to seismic weight ratio from pushover loading proportional to elastic translational mode shape in each direction, seismic weight is the total lateral weight acting in the model.
[4] Average strength to baseline weight ratio from pushover loading proportional to elastic mode shape in each direction, baseline weight is the weight of the dwelling including the first-floor diaphragm and above.
[5] Average crawlspace to first occupied story (superstructure) strength ratio, obtained from story-based pushover curves.
[6] Length of wood structural panel (WSP) required in each corner (two lengths per side) for retrofitting according to *FEMA P-1100*, 6-ft-tall cripple walls assume tie-downs.

Table 7.20 Summary of modal and pushover criteria for the 6-ft-tall cripple wall set and rigid base variants: two-story cases.

Index [1]	T_1 (sec) [2]	$(V/W_S)_{Avg}$ [3]	$(V/W_{BL})_{Avg}$ [4]	$(V_{CW}/V_{SS})_{Avg}$ [5]	L_{WSP} (ft) [6]
2L-C1-LP-6C-HS2-EX	0.58	0.16	0.16	0.34	N/A
2L-C1-LP-6C-HSR2-SDS10	0.37	0.58	0.59	1.37	12.00
2L-C1-LP-6C-HSR2-SDS12	0.36	0.58	0.59	1.51	13.33
2L-C1-LP-6C-HSR2-SDS15	0.35	0.57	0.58	1.71	16.00
2L-C1-LP-RB	0.27	0.63	0.48	N/A	N/A
2L-SLP2-LP-6C-S2-EX	0.34	0.28	0.29	0.50	N/A
2L-SLP2-LP-6C-S2R2-SDS10	0.31	0.56	0.58	1.15	13.33
2L-SLP2-LP-6C-S2R2-SDS12	0.31	0.56	0.58	1.25	14.67
2L-SLP2-LP-6C-S2R2-SDS15	0.31	0.56	0.58	1.37	18.67
2L-SLP2-LP-RB	0.23	0.75	0.57	N/A	N/A
2L-W2-G2-6C-HS2-EX	0.46	0.29	0.29	0.70	N/A
2L-W2-G2-6C-HSR2-SDS10	0.33	0.49	0.50	2.45	10.67
2L-W2-G2-6C-HSR2-SDS12	0.32	0.48	0.49	2.99	13.33
2L-W2-G2-6C-HSR2-SDS15	0.31	0.47	0.48	3.39	16.00
2L-W2-G2-RB	0.27	0.57	0.41	N/A	N/A
2L-S2-G2-6C-S2-EX	0.29	0.41	0.43	0.84	N/A
2L-S2-G2-6C-S2R2-SDS10	0.27	0.56	0.59	1.65	10.67
2L-S2-G2-6C-S2R2-SDS12	0.27	0.55	0.59	1.95	13.33
2L-S2-G2-6C-S2R2-SDS15	0.27	0.55	0.58	2.18	16.00
2L-S2-G2-RB	0.23	0.69	0.51	N/A	N/A

[1] Cripple wall retrofit cases are denoted "SDSx" to reflect retrofits for S_{DS} = 1.0*g*, 1.2*g*, and 1.5*g* according to *FEMA P-1100*.
[2] Elastic fundamental period in seconds.
[3] Average strength to seismic weight ratio from pushover loading proportional to elastic translational mode shape in each direction, seismic weight is the total lateral weight acting in the model.
[4] Average strength to baseline weight ratio from pushover loading proportional to elastic mode shape in each direction, baseline weight is the weight of the dwelling including the first-floor diaphragm and above.
[5] Average crawlspace to first occupied story (superstructure) strength ratio, obtained from story-based pushover curves.
[6] Length of wood structural panel (WSP) required in each corner (two lengths per side) for retrofitting according to *FEMA P-1100*, if required length exceeds plan dimension then the plan dimension minus 16 in. is assumed for fully sheathed condition, 6-ft-tall cripple walls assume tie-downs.

7.5.2 Collapse Performance of 6-Ft-Tall Cripple Walls

The collapse performance of the 6-ft-tall cripple wall variant set is illustrated using the P[C|RP_{250}] and P[C|MCE] metrics for pairs of existing (unretrofitted) and retrofit variants in Figure 7.20 and Figure 7.21. These comparisons are analogous to those for the 2-ft-tall cripple walls, shown previously in Figure 7.11 and Figure 7.12, where the existing (unretrofitted) variants are shown with solid bars and corresponding retrofit variants are shown with overlaid hatched bars for comparison. The existing (unretrofitted) houses with 6-ft-tall cripple walls have lower collapse risks than corresponding houses with 2-ft-tall cripple walls, due to the combined effects of reduced P-delta effects, higher deformation capacities, and higher strengths (for stucco walls). The collapse risks for the retrofitted 6-ft-tall cripple walls are similar to those of the 2-ft-tall walls since the retrofitted shear walls are designed with similar strength criteria.

Similar to the tabulations for 2-story tall cripple walls in Section 7.4.2, collapse fragility curve parameters and collapse risks for the 6-ft-tall cripple wall variants are tabulated in Table 7.21 for pre-1945 era variants with horizontal wood siding, Table 7.22, for pre-1945 era variants with exterior stucco, and in Table 7.23 and Table 7.24 for the corresponding 1956–1970 era variants with wood siding and stucco, respectively. Apart from the generally lower collapse risks for the existing (unretrofitted) houses with 6-ft-tall versus 2-ft-tall cripple walls, the trends between collapse risk for the 6-ft-tall cripple walls of various exterior materials, interior wall materials, and number of stories are similar to those discussed previously for the 2-ft-tall cripple wall variants.

The general observations for collapse mechanisms controlling the 6-ft-tall cripple wall set are summarized in the following:

- Existing (unretrofitted) 6-ft-tall cripple walls exhibit collapse exclusively in the cripple wall. This is due to the weak existing cripple wall having a strength much weaker than the occupied story above.
- One-story retrofitted 6-ft-tall cripple walls generally exhibit collapse in the cripple wall. The only exception is that the one-story, 1956–1970 era, wood siding cripple walls retrofit for all seismic intensities according to *FEMA P-1100* (i.e., 1L-W2-G2-2C-HSR2-SDSx) that exhibit collapse in the superstructure. This case has the weakest combination of superstructure materials, and the additional displacement capacity of the 6-ft retrofit material caused these failure trends for all sites considered. Notably, although the lowest seismic retrofit for the Bakersfield site exhibited mixed failure locations (e.g., cripple wall and superstructure), the majority of the cases were observed in the first occupied story.
- Two-story retrofitted 6-ft-tall cripple walls were observed to exclusively experience collapse occurring in the first occupied story of the superstructure. This is due to a combination of much stronger retrofit schedules for two-story dwellings versus one-story according to *FEMA P-1100* and the same superstructure materials resisting approximately 45% more lateral mass when compared to one-story variants.

The collapse performance of the 6-ft-tall cripple wall variant set is illustrated using the two different collapse metrics used for comparing the baseline 2-ft cripple wall performance in Section 7.4.2, namely, $P[C|RP_{250}]$ and $P[C|MCE]$. The $P[C|RP_{250}]$ values for existing (unretrofitted) and retrofit variant pairs are provided in Figure 7.20, where the existing variants are shown with solid bars and corresponding retrofitted variants are shown with overlaid hatched bars for comparison. Similarly, the $P[C|MCE]$ results are summarized in Figure 7.21. In general, the unretrofitted 6-ft-tall cripple wall dwellings performed better than corresponding 2-ft-tall cripple walls. The retrofitted cases performed similar between the two cripple wall heights.

Collapse summaries are tabulated for the 6-ft-tall cripple wall set for pre-1945 era variants with horizontal wood siding (Table 7.21), pre-1945 era variants with exterior stucco (Table 7.22), and corresponding 1956–1970 era variants in Table 7.23 and Table 7.24 for wood siding and stucco, respectively. Each variant is compared with the corresponding rigid base model representing a variant without crawlspace vulnerability. The collapse fragility information for each of the 6-ft-tall cripple wall variants are tabulated in addition to the selected intensities to output collapse probabilities. Each table provides the median collapse intensity ($Sa_{\mathrm{Med,C}}$), record-to-record variability (β_{RTR}), and total collapse fragility dispersion ($\beta_{C,\mathrm{Tot}}$) that includes modeling uncertainty. The final column of each table identifies the fraction of replacement cost assumed for the provided fragility ($Cost_{\mathrm{Col}}$), with 67% indicating that cripple wall collapse is the controlling collapse mechanism and 100% for variants with collapse being controlled by the first occupied story.

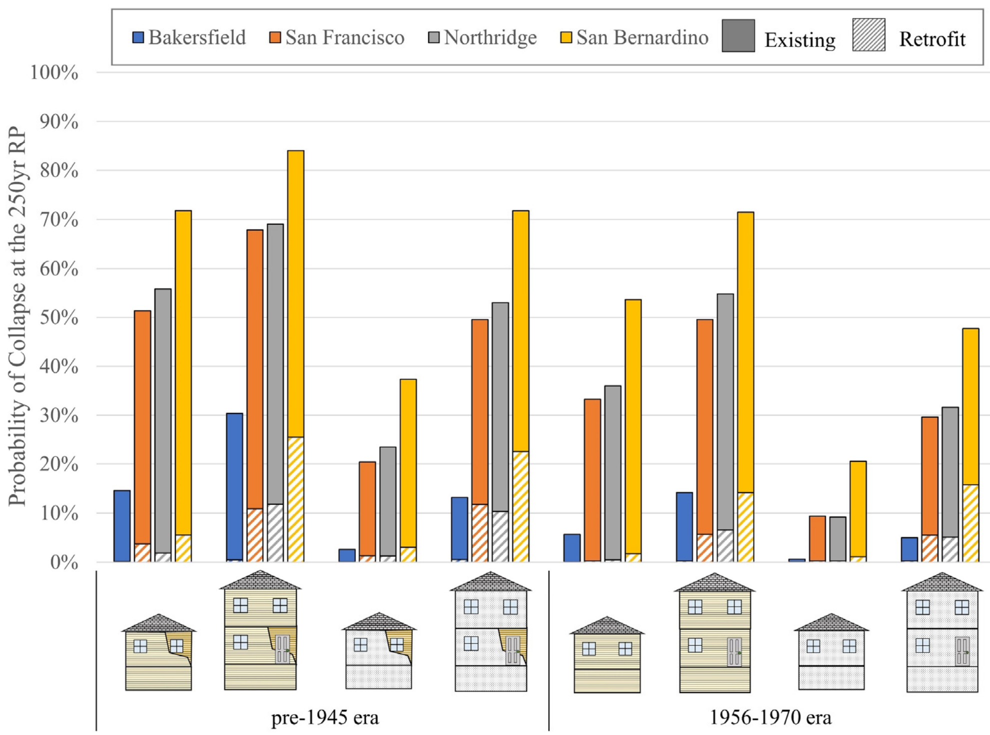

Figure 7.20 **Probability of collapse at the 250-year return period for 6-ft-tall cripple wall set, *Sa*(0.25 sec)$_{250}$: 0.63*g* (BF), 0.98*g* (SF), 1.15*g* (NR), and 1.27*g* (SB).**

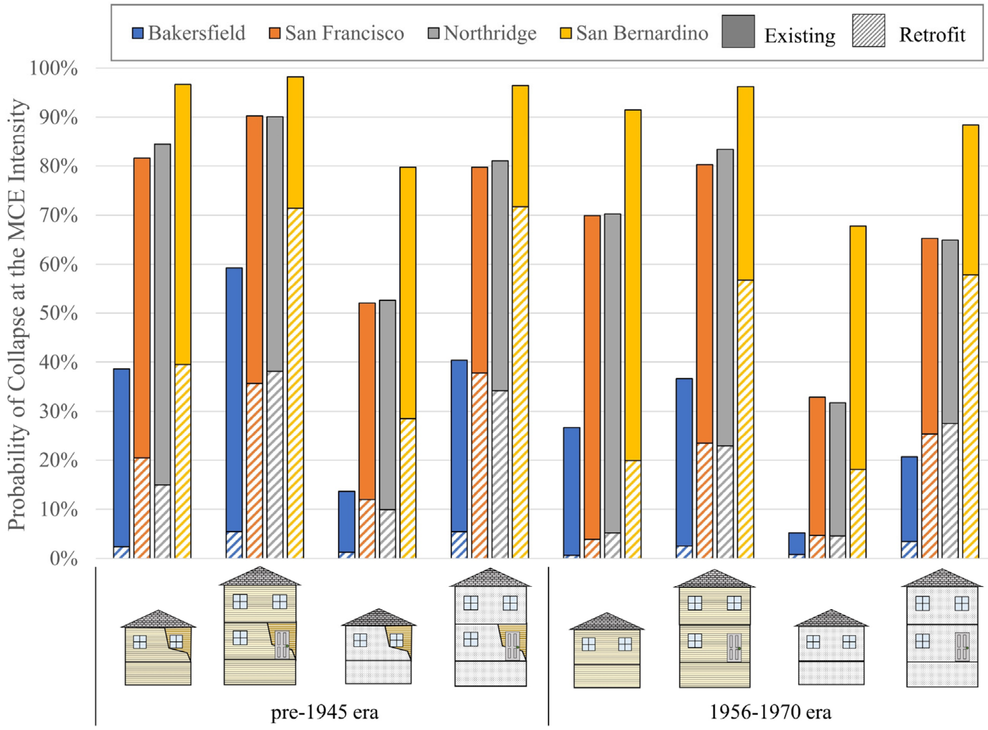

Figure 7.21 **Probability of collapse at MCE intensity results for 6-ft-tall cripple wall set, *Sa*(0.25 sec)$_{MCE}$: 1.11*g* (BF), 1.80*g* (SF), 2.10*g* (NR), and 2.67*g* (SB).**

Table 7.21 Collapse performance summary for 6-ft-tall cripple wall set and rigid base variants: pre-1945 era with horizontal wood siding.

Index [1]	Site [2] (Sa_{250}) (Sa_{MCE})	$Sa_{Med,C}$ (g) [3]	β_{RTR} [4]	$\beta_{C,Tot}$ [5]	P[C|RP$_{250}$] [6]	P[C|MCE] [7]	$Cost_{Col}$ [8]
1L-C1-LP-6C-HS2-EX	BF270 (0.63g) (1.11g)	1.38	0.66	0.75	14.6%	38.6%	67%
1L-C1-LP-6C-HSR2-SDS10		3.20	0.41	0.54	0.13%	2.4%	67%
1L-C1-LP-6C-RB		6.17	0.55	0.66	0.02%	0.4%	100%
1L-C1-LP-6C-HS2-EX	SF270 (0.98g) (1.80g)	0.96	0.60	0.69	51.3%	81.6%	67%
1L-C1-LP-6C-HSR2-SDS12		3.02	0.52	0.63	3.7%	20.5%	67%
1L-C1-LP-RB		4.49	0.41	0.54	0.24%	4.5%	100%
1L-C1-LP-6C-HS2-EX	NR270 (1.15g) (2.10g)	1.04	0.60	0.69	55.9%	84.5%	67%
1L-C1-LP-6C-HSR2-SDS15		3.85	0.47	0.58	1.90%	15.0%	67%
1L-C1-LP-6C-RB		5.04	0.42	0.54	0.32%	5.3%	100%
1L-C1-LP-6C-HS2-EX	SB270 (1.27g) (2.67g)	0.90	0.48	0.59	71.8%	96.7%	67%
1L-C1-LP-6C-HSR2-SDS15		3.09	0.44	0.56	5.5%	39.5%	67%
1L-C1-LP-6C-RB		4.14	0.42	0.54	1.4%	20.9%	100%
2L-C1-LP-6C-HS2-EX	BF270 (0.63g) (1.11g)	0.93	0.69	0.78	30.4%	59.3%	67%
2L-C1-LP-6C-HSR2-SDS10		2.79	0.46	0.58	0.50%	5.5%	100%
2L-C1-LP-6C-RB		2.52	0.41	0.54	0.50%	6.6%	100%
2L-C1-LP-6C-HS2-EX	SF270 (0.98g) (1.80g)	0.70	0.64	0.73	67.9%	90.3%	67%
2L-C1-LP-6C-HSR2-SDS12		2.33	0.61	0.70	10.9%	35.7%	100%
2L-C1-LP-6C-RB		2.16	0.55	0.65	11.3%	39.0%	100%
2L-C1-LP-6C-HS2-EX	NR270 (1.15g) (2.10g)	0.79	0.68	0.76	69.0%	90.1%	67%
2L-C1-LP-6C-HSR2-SDS15		2.58	0.59	0.68	11.8%	38.1%	100%
2L-C1-LP-6C-RB		2.47	0.55	0.65	12.0%	40.0%	100%
2L-C1-LP-6C-HS2-EX	SB270 (1.27g) (2.67g)	0.65	0.57	0.67	84.0%	98.2%	67%
2L-C1-LP-6C-HSR2-SDS15		1.89	0.50	0.61	25.5%	71.4%	100%
2L-C1-LP-6C-RB		1.84	0.44	0.56	25.2%	74.5%	100%

[1] Cripple wall retrofit cases are denoted 'SDSx' to reflect retrofits for S_{DS}=1.0g, 1.2g, and 1.5g according to *FEMA P-1100* plan sets.
[2] BF = Bakersfield, SF = San Francisco, NR = Northridge, and SB = San Bernardino, all sites assume V_{S30} = 270 m/sec, 250-year return period, and MCE Sa(0.25 sec) for site annotated.
[3] Median collapse intensity defined as Sa(0.25 sec).
[4] Record-to-record variability from collapse fragility fitting.
[5] Total collapse dispersion including β_{Mod} = 0.35 combined with β_{RTR} using SRSS.
[6] Probability of collapse at 250-year return period (RP$_{250}$).
[7] Probability of collapse at the MCE with intensity determined by nominal S_{DS} for site scaled by a factor of 1.5.
[8] Percentage of replacement cost attributed to collapse, 67% indicates that governing collapse mode occurs in crawlspace, 100% indicates that governing collapse mode occurs in first occupied story.

Table 7.22 Collapse performance summary for 6-ft-tall cripple wall set and rigid base variants: pre-1945 era with exterior stucco.

Index [1]	Site [2] (Sa_{250}) (Sa_{MCE})	$Sa_{Med,C}$ (g) [3]	β_{RTR} [4]	$\beta_{C,Tot}$ [5]	P[C|RP$_{250}$] [6]	P[C|MCE] [7]	$Cost_{Col}$ [8]
1L-SLP2-LP-6C-S2-EX	BF270 (0.63g) (1.11g)	2.35	0.59	0.68	2.6%	13.6%	67%
1L-SLP2-LP-6C-S2R2-SDS10		4.08	0.46	0.58	0.06%	1.2%	67%
1L-SLP2-LP-RB		6.40	0.45	0.57	0.002%	0.1%	100%
1L-SLP2-LP-6C-S2-EX	SF270 (0.98g) (1.80g)	1.74	0.59	0.69	20.4%	52.0%	67%
1L-SLP2-LP-6C-S2R2-SDS12		3.55	0.46	0.58	1.3%	12.0%	67%
1L-SLP2-LP-RB		5.67	0.43	0.56	0.09%	2.0%	100%
1L-SLP2-LP-6C-S2-EX	NR270 (1.15g) (2.10g)	2.00	0.67	0.76	23.4%	52.6%	67%
1L-SLP2-LP-6C-S2R2-SDS15		4.69	0.52	0.63	1.3%	9.9%	67%
1L-SLP2-LP-RB		6.10	0.38	0.52	0.07%	1.9%	100%
1L-SLP2-LP-6C-S2-EX	SB270 (1.27g) (2.67g)	1.56	0.54	0.65	37.4%	79.7%	67%
1L-SLP2-LP-6C-S2R2-SDS15		3.69	0.45	0.57	3.0%	28.6%	67%
1L-SLP2-LP-RB		4.89	0.31	0.46	0.16%	9.6%	100%
2L-SLP2-LP-6C-S2-EX	BF270 (0.63g) (1.11g)	1.31	0.56	0.66	13.2%	40.4%	67%
2L-SLP2-LP-6C-S2R2-SDS10		2.89	0.48	0.60	0.54%	5.4%	100%
2L-SLP2-LP-RB		2.99	0.41	0.54	0.19%	3.4%	100%
2L-SLP2-LP-6C-S2-EX	SF270 (0.98g) (1.80g)	1.00	0.62	0.71	49.6%	79.7%	67%
2L-SLP2-LP-6C-S2R2-SDS12		2.23	0.59	0.69	11.7%	37.8%	100%
2L-SLP2-LP-RB		2.72	0.53	0.63	5.3%	25.8%	100%
2L-SLP2-LP-6C-S2-EX	NR270 (1.15g) (2.10g)	1.09	0.65	0.74	53.0%	81.0%	67%
2L-SLP2-LP-6C-S2R2-SDS15		2.79	0.61	0.70	10.3%	34.2%	100%
2L-SLP2-LP-RB		2.67	0.44	0.56	6.7%	33.5%	100%
2L-SLP2-LP-6C-S2-EX	SB270 (1.27g) (2.67g)	0.89	0.50	0.61	71.8%	96.5%	67%
2L-SLP2-LP-6C-S2R2-SDS15		1.93	0.44	0.56	22.5%	71.7%	100%
2L-SLP2-LP-RB		2.23	0.49	0.60	17.2%	61.7%	100%

[1] Cripple wall retrofit cases are denoted "SDSx" to reflect retrofits for S_{DS}=1.0g, 1.2g, and 1.5g according to *FEMA P-1100* plan sets.
[2] BF = Bakersfield, SF = San Francisco, NR = Northridge, and SB = San Bernardino, all sites assume V_{S30} = 270 m/sec, 250-year return period, and MCE Sa(0.25 sec) for site annotated.
[3] Median collapse intensity defined as Sa(0.25 sec).
[4] Record-to-record variability from collapse fragility fitting.
[5] Total collapse dispersion including β_{Mod} = 0.35 combined with β_{RTR} using SRSS.
[6] Probability of collapse at 250-year return period (RP$_{250}$).
[7] Probability of collapse at the MCE with intensity determined by nominal S_{DS} for site scaled by a factor of 1.5.
[8] Percentage of replacement cost attributed to collapse, 67% indicates that governing collapse mode occurs in crawlspace, 100% indicates that governing collapse mode occurs in first occupied story.

Table 7.23 Collapse performance summary for 6-ft-tall cripple wall set and rigid base variants: 1956–1970 era with horizontal wood siding.

Index [1]	Site [2] (Sa_{250}) (Sa_{MCE})	$Sa_{Med,C}$ (g) [3]	β_{RTR} [4]	$\beta_{C,Tot}$ [5]	P[C|RP250] [6]	P[C|MCE] [7]	$Cost_{Col}$ [8]
1L-W2-G2-6C-HS2-EX	BF270 (0.63g) (1.11g)	1.62	0.49	0.60	5.7%	26.7%	67%
1L-W2-G2-6C-HSR2-SDS10		5.73	0.56	0.66	0.04%	0.6%	100%
1L-W2-G2-RB		8.04	0.66	0.75	0.03%	0.4%	100%
1L-W2-G2-6C-HS2-EX	SF270 (0.98g) (1.80g)	1.29	0.53	0.63	33.3%	69.9%	67%
1L-W2-G2-6C-HSR2-SDS12		4.96	0.46	0.58	0.26%	3.9%	100%
1L-W2-G2-RB		5.72	0.49	0.60	0.17%	2.8%	100%
1L-W2-G2-6C-HS2-EX	NR270 (1.15g) (2.10g)	1.47	0.58	0.68	36.0%	70.2%	67%
1L-W2-G2-6C-HSR2-SDS15		5.95	0.54	0.64	0.52%	5.2%	100%
1L-W2-G2-RB		6.85	0.51	0.62	0.20%	2.7%	100%
1L-W2-G2-6C-HS2-EX	SB270 (1.27g) (2.67g)	1.20	0.47	0.59	53.6%	91.5%	67%
1L-W2-G2-6C-HSR2-SDS15		4.40	0.48	0.59	1.7%	19.9%	100%
1L-W2-G2-RB		4.77	0.43	0.55	0.79%	14.5%	100%
2L-W2-G2-6C-HS2-EX	BF270 (0.63g) (1.11g)	1.46	0.71	0.79	14.2%	36.6%	67%
2L-W2-G2-6C-HSR2-SDS10		4.11	0.57	0.67	0.25%	2.5%	100%
2L-W2-G2-RB		4.27	0.64	0.73	0.43%	3.3%	100%
2L-W2-G2-6C-HS2-EX	SF270 (0.98g) (1.80g)	0.99	0.61	0.70	49.5%	80.3%	67%
2L-W2-G2-6C-HSR2-SDS12		3.02	0.62	0.72	5.7%	23.4%	100%
2L-W2-G2-RB		3.09	0.59	0.69	4.8%	21.6%	100%
2L-W2-G2-6C-HS2-EX	NR270 (1.15g) (2.10g)	1.06	0.61	0.70	54.7%	83.4%	67%
2L-W2-G2-6C-HSR2-SDS15		3.75	0.70	0.78	6.6%	22.9%	100%
2L-W2-G2-RB		3.91	0.66	0.74	4.9%	20.1%	100%
2L-W2-G2-6C-HS2-EX	SB270 (1.27g) (2.67g)	0.89	0.51	0.62	71.5%	96.2%	67%
2L-W2-G2-6C-HSR2-SDS15		2.41	0.49	0.60	14.1%	56.8%	100%
2L-W2-G2-RB		2.52	0.51	0.62	13.3%	53.8%	100%

[1] Cripple wall retrofit cases are denoted "SDSx" to reflect retrofits for S_{DS}=1.0g, 1.2g, and 1.5g according to *FEMA P-1100* plan sets.
[2] BF = Bakersfield, SF = San Francisco, NR = Northridge, and SB = San Bernardino, all sites assume V_{S30} = 270 m/sec, 250-year return period, and MCE Sa(0.25 sec) for site annotated.
[3] Median collapse intensity defined as Sa(0.25 sec).
[4] Record-to-record variability from collapse fragility fitting.
[5] Total collapse dispersion including β_{Mod} = 0.35 combined with β_{RTR} using SRSS.
[6] Probability of collapse at 250-year return period (RP_{250}).
[7] Probability of collapse at the MCE with intensity determined by nominal S_{DS} for site scaled by a factor of 1.5.
[8] Percentage of replacement cost attributed to collapse, 67% indicates that governing collapse mode occurs in crawlspace, 100% indicates that governing collapse mode occurs in first occupied story.

Table 7.24 Collapse performance summary for 6-ft-tall cripple wall set and rigid base variants: 1956–1970 era with exterior stucco.

Index [1]	Site [2] (Sa_{250}) (Sa_{MCE})	$Sa_{Med,C}$ (g) [3]	β_{RTR} [4]	$\beta_{C,Tot}$[5]	P[C|RP250] [6]	P[C|MCE] [7]	$Cost_{Col}$[8]
1L-S2-G2-6C-S2-EX	BF270 (0.63g) (1.11g)	3.32	0.58	0.67	0.64%	5.2%	67%
1L-S2-G2-6C-S2R2-SDS10		6.01	0.61	0.70	0.06%	0.8%	67%
1L-S2-G2-RB		8.28	0.57	0.66	0.005%	0.1%	100%
1L-S2-G2-6C-S2-EX	SF270 (0.98g) (1.80g)	2.44	0.59	0.69	9.4%	32.9%	67%
1L-S2-G2-6C-S2R2-SDS12		4.58	0.43	0.56	0.30%	4.7%	67%
1L-S2-G2-RB		5.54	0.39	0.52	0.04%	1.6%	100%
1L-S2-G2-6C-S2-EX	NR270 (1.15g) (2.10g)	2.92	0.61	0.70	9.2%	31.8%	67%
1L-S2-G2-6C-S2R2-SDS15		5.40	0.44	0.56	0.29%	4.6%	67%
1L-S2-G2-RB		6.19	0.36	0.50	0.04%	1.6%	100%
1L-S2-G2-6C-S2-EX	SB270 (1.27g) (2.67g)	2.04	0.47	0.58	20.5%	67.8%	67%
1L-S2-G2-6C-S2R2-SDS15		4.37	0.41	0.54	1.1%	18.1%	67%
1L-S2-G2-RB		5.04	0.29	0.46	0.13%	8.1%	100%
2L-S2-G2-6C-S2-EX	BF270 (0.63g) (1.11g)	1.98	0.61	0.71	5.0%	20.7%	67%
2L-S2-G2-6C-S2R2-SDS10		3.52	0.53	0.63	0.31%	3.4%	100%
2L-S2-G2-RB		3.53	0.48	0.59	0.17%	2.6%	100%
2L-S2-G2-6C-S2-EX	SF270 (0.98g) (1.80g)	1.40	0.55	0.65	29.7%	65.3%	67%
2L-S2-G2-6C-S2R2-SDS12		2.77	0.55	0.65	5.5%	25.4%	100%
2L-S2-G2-RB		2.83	0.50	0.61	4.1%	23.1%	100%
2L-S2-G2-6C-S2-EX	NR270 (1.15g) (2.10g)	1.61	0.60	0.70	31.6%	64.9%	67%
2L-S2-G2-6C-S2R2-SDS15		2.97	0.47	0.59	5.1%	27.6%	100%
2L-S2-G2-RB		3.13	0.50	0.61	6.9%	25.6%	100%
2L-S2-G2-6C-S2-EX	SB270 (1.27g) (2.67g)	1.31	0.48	0.60	47.7%	88.4%	67%
2L-S2-G2-6C-S2R2-SDS15		2.36	0.51	0.62	15.7%	57.8%	100%
2L-S2-G2-RB		2.54	0.52	0.63	13.4%	53.2%	100%

[1] Cripple wall retrofit cases are denoted "SDSx" to reflect retrofits for S_{DS}=1.0g, 1.2g, and 1.5g according to *FEMA P-1100* plan sets.
[2] BF = Bakersfield, SF = San Francisco, NR = Northridge, and SB = San Bernardino, all sites assume V_{S30} = 270 m/sec, 250-year return period, and MCE Sa(0.25 sec) for site annotated.
[3] Median collapse intensity defined as Sa(0.25 sec).
[4] Record-to-record variability from collapse fragility fitting.
[5] Total collapse dispersion including β_{Mod} = 0.35 combined with β_{RTR} using SRSS.
[6] Probability of collapse at 250-year return period (RP_{250}).
[7] Probability of collapse at the MCE with intensity determined by nominal S_{DS} for site scaled by a factor of 1.5.
[8] Percentage of replacement cost attributed to collapse, 67% indicates that governing collapse mode occurs in crawlspace, 100% indicates that governing collapse mode occurs in first occupied story.

7.5.3 Loss Assessment Summary for 6-Ft-Tall Cripple Walls

The loss (damage) curves for houses with 6-ft-tall versus 2-ft-tall cripple walls are compared in Figure 7.22 and Figure 7.23, for the wood siding houses, and Figure 7.24 and Figure 7.25, for the stucco siding houses. These comparisons are all based on the 1956–1970 era (i.e., gypsum wallboard interior) house variants for the San Francisco site. In all cases, the loss curves reveal smaller losses for houses with 6-ft-tall versus 2-ft-tall existing (unretrofitted) cripple walls, which reflects the trend observed in collapse risk. Similarly, the loss curves are comparable between the houses with retrofitted 6-ft-tall and 2-ft-tall cripple walls, except that the losses are slightly higher for the 6-ft-tall stucco cripple wall cases, due to the increased cripple wall area, which is susceptible to damage that warrants repair.

The EAL and RC250 loss metrics are shown for the 6-ft-tall cripple wall variants for all building sites in Figure 7.26 and Figure 7.27, similar to the comparisons for comparable 2-ft-tall cripple wall variants presented in Section 7.4.3. The EAL estimates are compared between the 6-ft-tall and 2-ft-tall cripple wall variants for horizontal wood siding and exterior stucco in Figure 7.28 and Figure 7.29, respectively. The RC250 estimates are compared between the 6-ft-tall and 2-ft-tall cripple wall variants for horizontal wood siding and exterior stucco in Figure 7.30 and Figure 7.31, respectively. Overall, the trends between the 2-ft- and 6-ft-tall cripple walls reflect the points made previously, i.e., that (1) the losses are a bit less for the 6-ft-tall versus 2-ft-tall existing (unretrofitted) cases, (2) the losses are comparable for the 6-ft and 2-ft retrofit wood siding cases, and (3) the losses are slightly higher for the 6-ft-tall versus 2-ft retrofitted stucco cases.

Detailed tabular summaries of the loss statistics and loss functions are provided for the 6-ft-tall cripple wall variants in Table 7.25, Table 7.26, Table 7.27, Table 7.28, Table 7.29, and Table 7.30, similar to the tables presented previously for 2-ft-tall cripple wall variants.

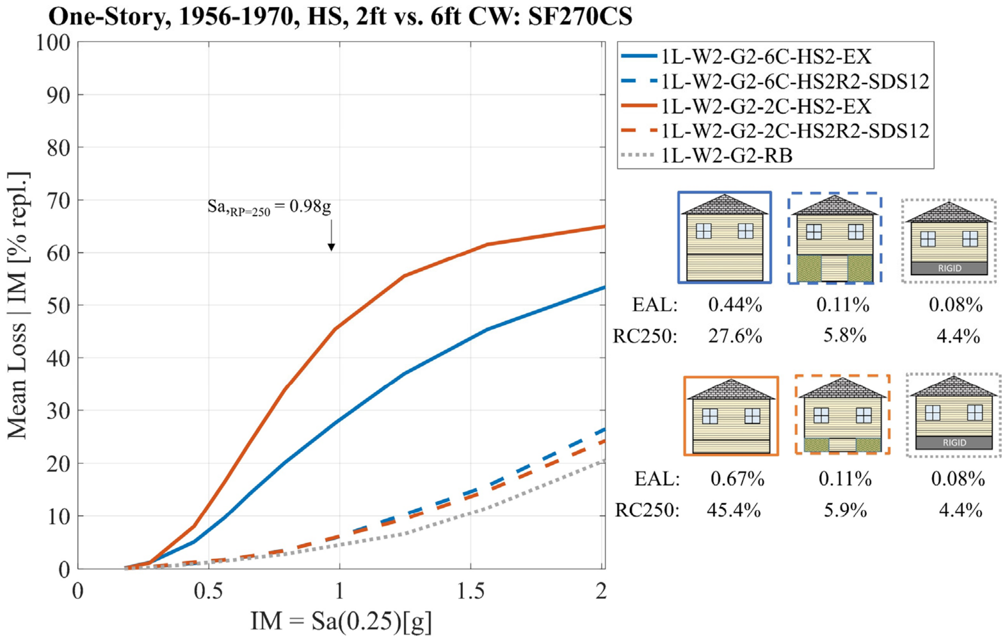

Figure 7.22 Loss curves comparing the 6-ft-tall and 2-ft-tall cripple wall heights for the one-story 1956–1970-era variants with horizontal wood siding: existing (solid), retrofit (dashed), and rigid base cases (dotted) for the San Francisco site.

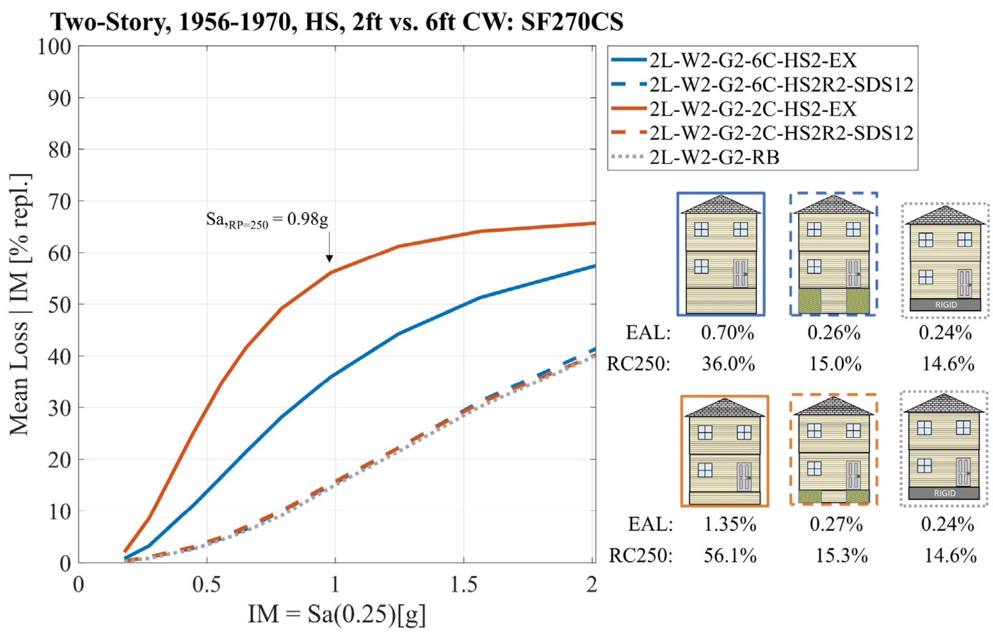

Figure 7.23 Loss curves comparing the 6-ft-tall and 2-ft-tall cripple wall heights for the two-story 1956–1970-era variants with horizontal wood siding: existing (solid), retrofit (dashed), and rigid base cases (dotted) for the San Francisco site.

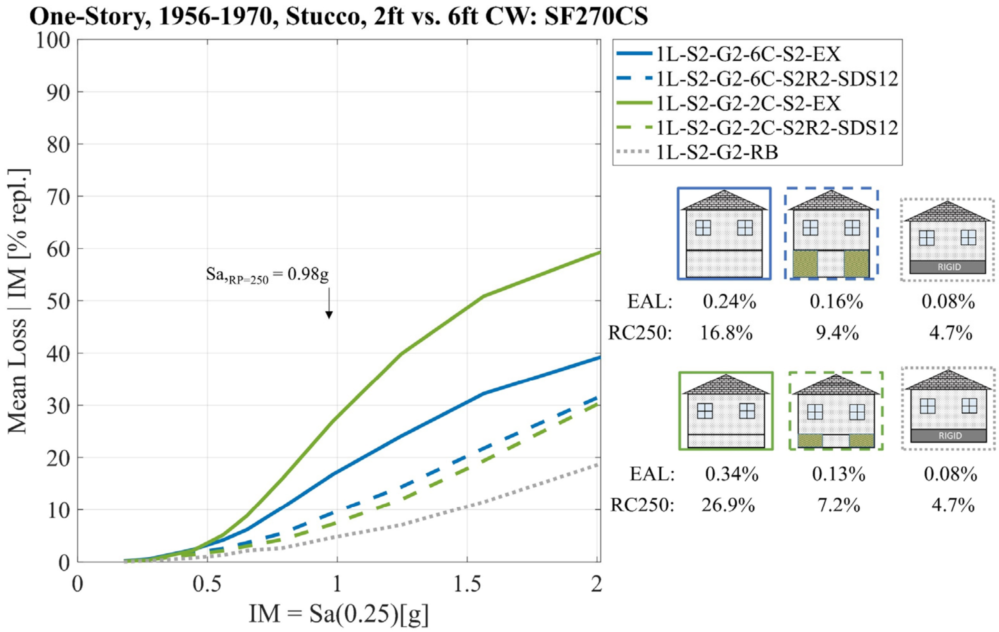

Figure 7.24 Loss curves comparing the 6-ft-tall and 2-ft cripple wall heights for the one-story 1956–1970-era variants with exterior stucco: existing (solid), retrofit (dashed), and rigid base cases (dotted) for the San Francisco site.

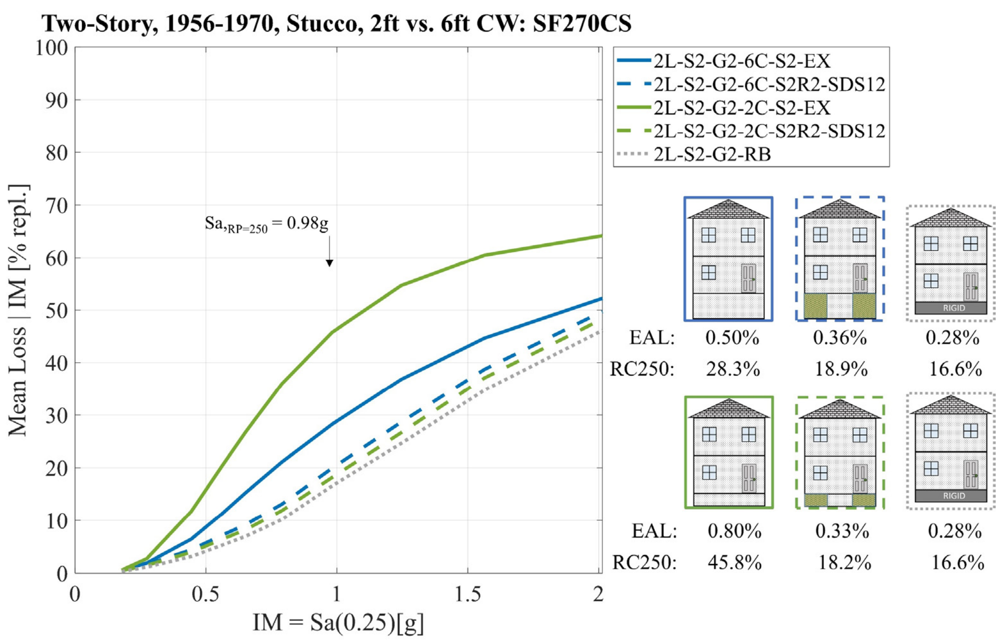

Figure 7.25 Loss curves comparing the 6-ft-tall and 2-ft-tall cripple wall heights for the two-story 1956–1970-era variants with exterior stucco: existing (solid), retrofit (dashed), and rigid base cases (dotted) for the San Francisco site.

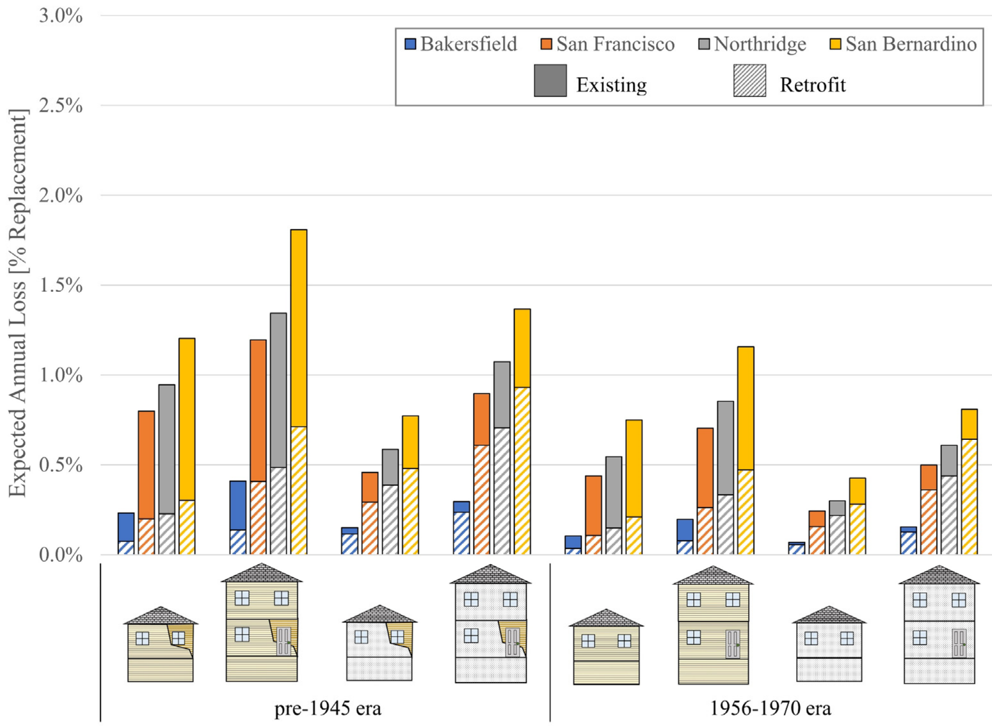

Figure 7.26 Expected annual loss results for the 6-ft-tall cripple wall set and all sites.

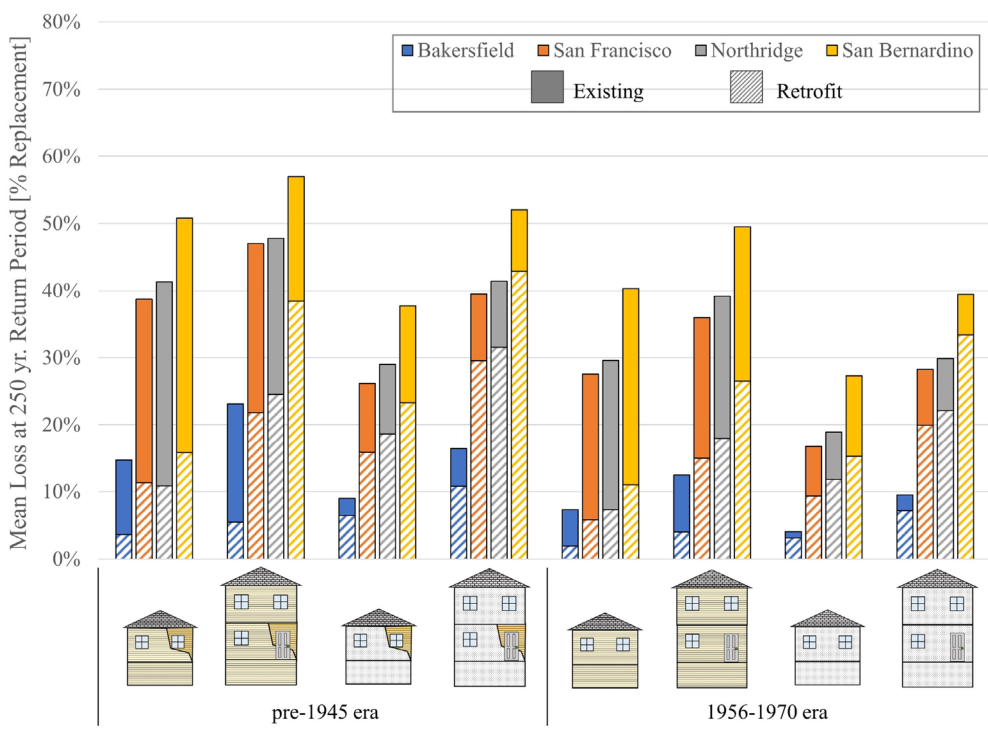

Figure 7.27 Expected loss at the 250-year return period (RC250) results for 6-ft-tall cripple wall set and all sites.

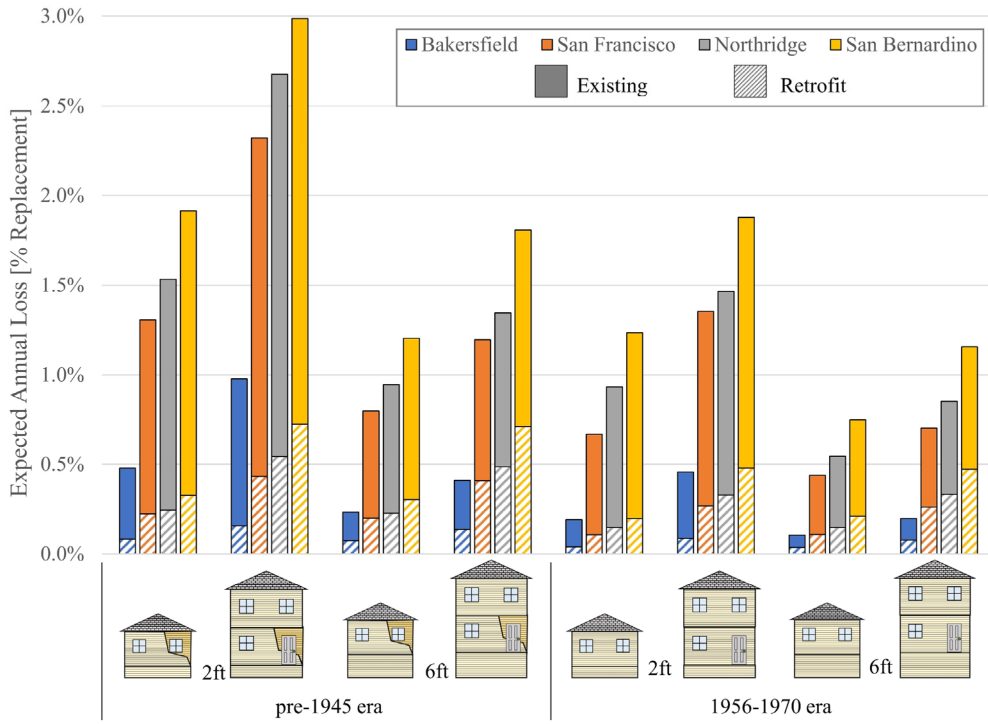

Figure 7.28 **Expected annual loss results comparing the 2-ft-tall and 6-ft-tall cripple wall sets with horizontal wood siding and all sites.**

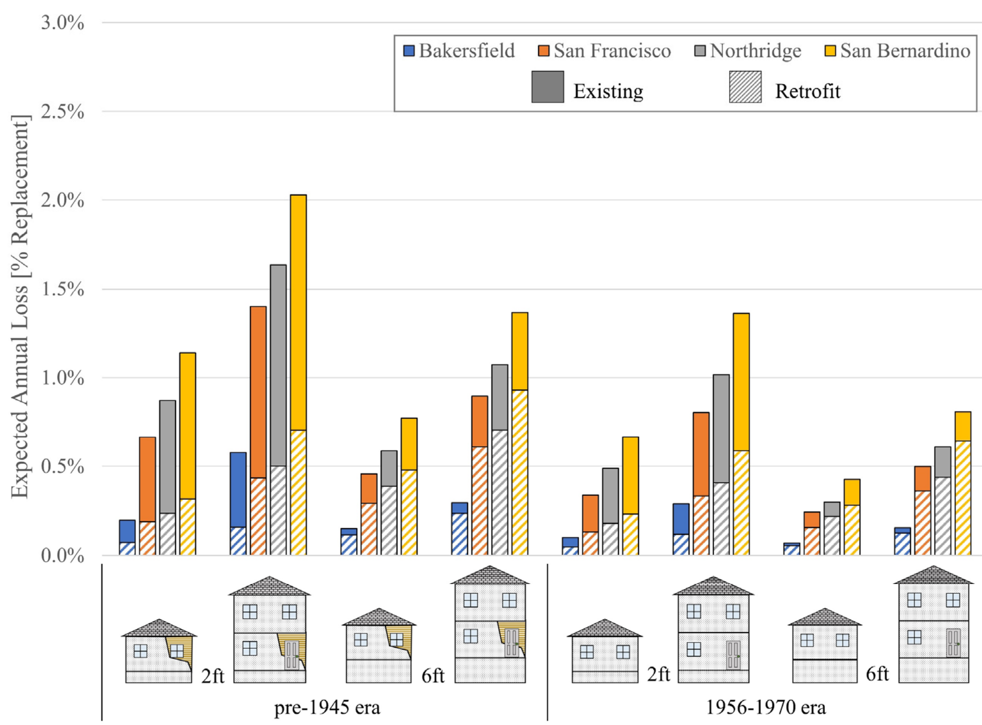

Figure 7.29 **Expected annual loss results comparing the 2-ft-tall and 6-ft-tall cripple wall sets with exterior stucco and all sites.**

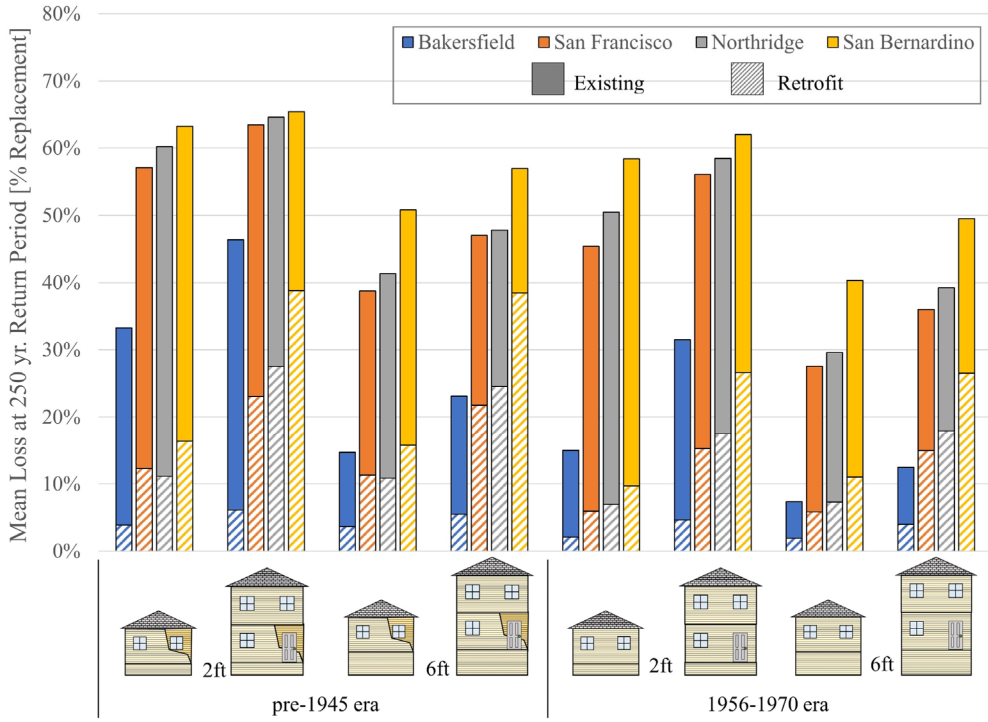

Figure 7.30 **Expected loss at the 250-year return period (RC250) results comparing the 2-ft-tall and 6-ft-tall cripple wall sets with horizontal wood siding and all sites.**

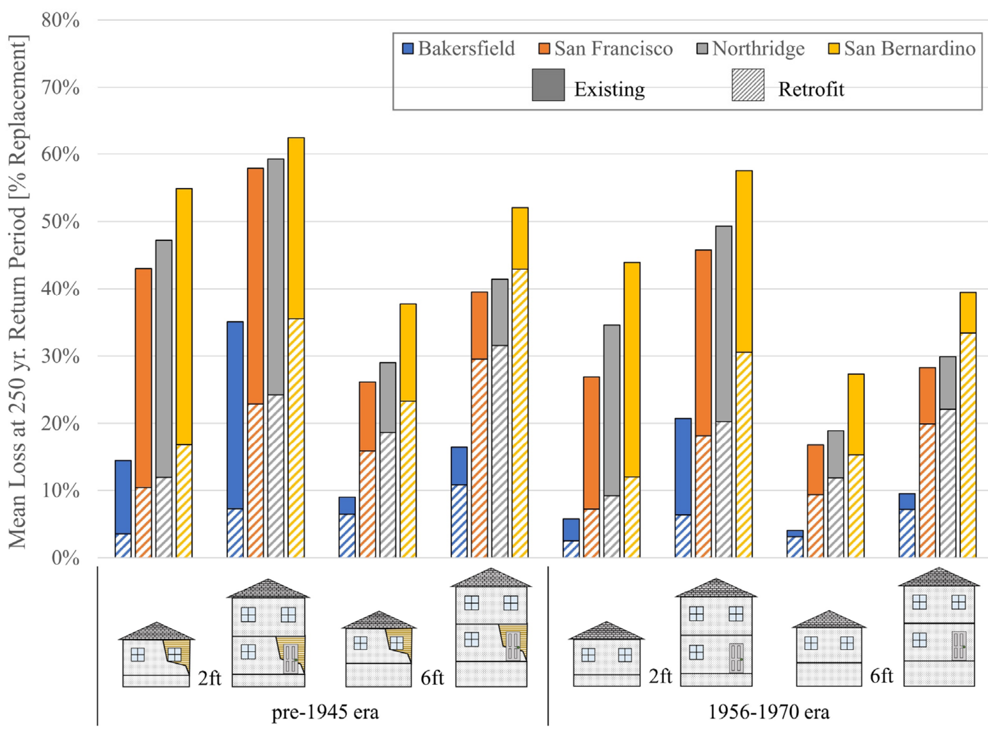

Figure 7.31 **Expected loss at the 250-year return period (RC250) results comparing the 2-ft-tall and 6-ft-tall cripple wall sets with exterior stucco and all sites.**

Table 7.25 Summary of primary loss metrics and benefits due to retrofitting for 6-ft-tall cripple wall set: one-story cases.

Description/Index	Site	Condition	EAL (% repl.)	Benefit_{EAL}[1] (% repl.)	RC250 (% repl.)	Benefit_{RC250}[1] (% repl.)
One-story, pre-1945, wood siding, 6-ft-tall cripple wall. (EX) 1L-C1-LP-6C-HS2-EX (R) 1L-C1-LP-6C-HSR2-SDSx 	BF 270	Existing	0.233	0.16	14.70	11.1
		Retrofitted	0.074		3.64	
	SF 270	Existing	0.798	0.60	38.71	27.4
		Retrofitted	0.199		11.32	
	NR 270	Existing	0.946	0.72	41.34	30.5
		Retrofitted	0.227		10.86	
	SB 270	Existing	1.203	0.90	50.80	35.0
		Retrofitted	0.303		15.80	
One-story, pre-1945, stucco, 6-ft-tall cripple wall. (EX) 1L-SLP2-LP-6C-S2-EX (R) 1L-SLP2-LP-6C-S2R2-SDSx 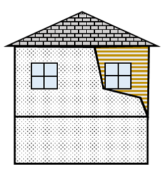	BF 270	Existing	0.151	0.04	9.00	2.5
		Retrofitted	0.116		6.46	
	SF 270	Existing	0.458	0.17	26.16	10.3
		Retrofitted	0.293		15.86	
	NR 270	Existing	0.587	0.20	29.01	10.4
		Retrofitted	0.388		18.64	
	SB 270	Existing	0.772	0.29	37.71	14.4
		Retrofitted	0.480		23.28	
One-story, 1956–1970, wood siding, 6-ft-tall cripple wall. (EX) 1L-W2-G2-6C-HS2-EX (R) 1L-W2-G2-6C-HSR2-SDSx 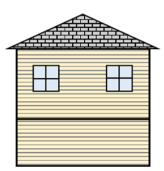	BF 270	Existing	0.105	0.07	7.34	5.4
		Retrofitted	0.035		1.93	
	SF 270	Existing	0.439	0.33	27.56	21.7
		Retrofitted	0.108		5.84	
	NR 270	Existing	0.545	0.40	29.60	22.3
		Retrofitted	0.148		7.32	
	SB 270	Existing	0.749	0.54	40.35	29.3
		Retrofitted	0.210		11.01	
One-story, 1956–1970, stucco, 6-ft-tall cripple wall. (EX) 1L-S2-G2-6C-HS2-EX (R) 1L-S2-G2-6C-HSR2-SDSx 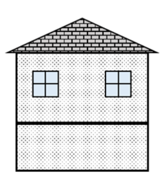	BF 270	Existing	0.069	0.01	4.08	0.9
		Retrofitted	0.055		3.14	
	SF 270	Existing	0.243	0.09	16.75	7.4
		Retrofitted	0.156		9.35	
	NR 270	Existing	0.299	0.08	18.92	7.1
		Retrofitted	0.218		11.83	
	SB 270	Existing	0.427	0.15	27.32	12.1
		Retrofitted	0.282		15.26	

[1] Benefits are the difference of the retrofit variant (R) subtracted from the existing (unretrofitted) variant (EX).

Table 7.26 Summary of primary loss metrics and benefits due to retrofitting for 6-ft-tall cripple wall set: two-story cases.

Description/Index	Site	Condition	EAL (% repl.)	Benefit$_{EAL}$[1] (% repl.)	RC250 (% repl.)	Benefit$_{RC250}$[1] (% repl.)
Two-story, pre-1945, wood siding, 6-ft-tall cripple wall. (EX) 2L-C1-LP-6C-HS2-EX (R) 2L-C1-LP-6C-HSR2-SDSx 	BF 270	Existing	0.410	0.27	23.13	17.6
		Retrofitted	0.136		5.50	
	SF 270	Existing	1.195	0.79	47.04	25.3
		Retrofitted	0.408		21.79	
	NR 270	Existing	1.344	0.86	47.80	23.3
		Retrofitted	0.486		24.55	
	SB 270	Existing	1.808	1.10	56.96	18.5
		Retrofitted	0.712		38.42	
Two-story, pre-1945, stucco, 6-ft-tall cripple wall. (EX) 2L-SLP2-LP-6C-S2-EX (R) 2L-SLP2-LP-6C-S2R2-SDSx 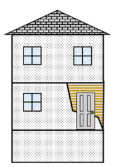	BF 270	Existing	0.296	0.06	16.42	5.6
		Retrofitted	0.236		10.80	
	SF 270	Existing	0.897	0.29	39.53	10.0
		Retrofitted	0.608		29.53	
	NR 270	Existing	1.074	0.37	41.44	9.9
		Retrofitted	0.705		31.54	
	SB 270	Existing	1.366	0.44	52.05	9.1
		Retrofitted	0.931		42.91	
Two-story, 1956–1970, wood siding, 6-ft-tall cripple wall. (EX) 2L-W2-G2-6C-HS2-EX (R) 2L-W2-G2-6C-HSR2-SDSx 	BF 270	Existing	0.197	0.12	12.48	8.5
		Retrofitted	0.078		3.98	
	SF 270	Existing	0.704	0.44	35.97	21.0
		Retrofitted	0.261		14.96	
	NR 270	Existing	0.853	0.52	39.17	21.2
		Retrofitted	0.333		17.94	
	SB 270	Existing	1.156	0.69	49.53	23.0
		Retrofitted	0.471		26.49	
Two-story, 1956–1970, stucco, 6-ft-tall cripple wall. (EX) 2L-S2-G2-6C-HS2-EX (R) 2L-S2-G2-6C-HSR2-SDSx 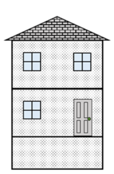	BF 270	Existing	0.155	0.03	9.52	2.3
		Retrofitted	0.126		7.18	
	SF 270	Existing	0.499	0.14	28.26	8.3
		Retrofitted	0.361		19.93	
	NR 270	Existing	0.608	0.17	29.89	7.8
		Retrofitted	0.439		22.09	
	SB 270	Existing	0.809	0.17	39.50	6.1
		Retrofitted	0.641		33.41	

[1] Benefits are the difference of the retrofit variant (R) subtracted from the existing (unretrofitted) variant (EX)

Table 7.27 Loss assessment summary for 6-ft-tall cripple wall set and rigid base variants: pre-1945 era with horizontal wood siding.

Index [1]	Site[2]	Mean loss at return period (% of replacement cost)										EAL[4] (%)
		15	25	50	75	100	150	250 [3]	500	1000	2500	
1L-C1-LP-6C-HS2-EX	BF 270	0.17	0.55	2.27	4.97	5.94	9.67	14.7	22.0	29.9	39.5	0.23
" "-HSR2-SDS10		0.21	0.36	0.77	1.15	1.48	2.30	3.64	5.99	9.23	15.5	0.07
" "-RB		0.20	0.44	0.80	1.38	1.64	2.15	3.04	4.61	6.35	9.90	0.07
1L-C1-LP-6C-HS2-EX	SF 270	1.08	4.11	12.9	19.2	24.3	30.8	38.7	46.7	53.2	58.8	0.80
" "-HSR2-SDS12		0.41	0.88	2.16	3.40	4.61	6.96	11.3	16.8	23.1	30.7	0.20
" "-RB		0.46	0.95	2.03	2.72	3.54	4.24	6.11	8.74	13.3	23.9	0.15
1L-C1-LP-6C-HS2-EX	NR 270	1.51	5.65	16.2	23.2	27.8	34.6	41.3	49.6	55.1	59.9	0.95
" "-HSR2-SDS15		0.60	1.26	2.71	4.12	5.40	7.62	10.9	16.8	22.5	31.4	0.23
" "-RB		0.66	1.32	2.64	3.64	4.28	5.59	7.32	11.0	17.3	29.0	0.19
1L-C1-LP-6C-HS2-EX	SB 270	2.24	7.45	21.1	30.1	36.1	43.5	50.8	57.8	61.9	64.5	1.20
" "-HSR2-SDS15		0.75	1.51	3.34	5.31	7.36	10.9	15.8	23.7	32.4	41.8	0.30
" "-RB		0.80	1.55	3.01	4.35	5.29	6.67	9.95	17.7	27.4	41.8	0.25
2L-C1-LP-6C-HS2-EX	BF 270	0.53	1.58	5.03	8.63	11.7	16.8	23.1	32.2	40.5	49.3	0.41
" "-HSR2-SDS10		0.46	0.83	1.63	2.25	2.78	3.82	5.50	9.32	14.6	25.1	0.14
" "-RB		0.54	0.90	1.94	2.72	3.19	4.45	6.29	9.95	16.7	28.3	0.16
2L-C1-LP-6C-HS2-EX	SF 270	2.87	8.67	20.7	28.1	33.3	40.0	47.0	53.6	58.5	62.2	1.20
" "-HSR2-SDS12		1.03	2.02	4.57	7.26	10.0	14.4	21.8	31.3	42.6	54.6	0.41
" "-RB		1.04	2.05	4.67	7.36	9.91	14.6	22.6	32.7	44.7	57.3	0.42
2L-C1-LP-6C-HS2-EX	NR 270	4.05	10.8	23.5	30.9	35.6	41.9	47.8	54.3	58.6	62.0	1.34
" "-HSR2-SDS15		1.32	2.55	5.72	9.61	12.2	17.6	24.6	34.7	44.5	57.2	0.49
" "-RB		1.43	2.72	5.77	9.59	12.0	17.4	25.5	35.7	46.1	58.6	0.50
2L-C1-LP-6C-HS2-EX	SB 270	6.61	16.3	32.1	40.9	46.0	51.9	57.0	61.5	63.9	65.4	1.81
" "-HSR2-SDS15		1.58	3.36	8.38	14.1	19.7	28.4	38.4	52.3	65.3	77.1	0.71
" "-RB		1.79	3.40	7.86	13.1	18.3	27.5	37.9	53.1	66.5	79.0	0.70

[1] Cripple wall retrofit cases are denoted "SDSx" to reflect retrofits for S_{DS} = 1.0g, 1.2g, and 1.5g according to *FEMA P-1100* plan sets.
[2] BF = Bakersfield, SF = San Francisco, NR = Northridge, and SB = San Bernardino; all sites assume V_{S30} = 270 m/sec.
[3] Mean loss at the 250-year return period is a primary loss metric and is referred to as "RC250".
[4] Expected annual loss expressed in percentage of building replacement cost.

Table 7.28 Loss assessment summary for 6-ft-tall cripple wall set and rigid base variants: pre-1945 era with exterior stucco.

Index [1]	Site[2]	Mean loss at return period (% of replacement cost)										EAL[4] (%)
		15	25	50	75	100	150	250[3]	500	1000	2500	
1L-SLP2-LP-6C-S2-EX	BF 270	0.24	0.48	1.28	2.32	3.26	5.34	9.00	15.7	22.5	31.0	0.15
" "-S2R2-SDS10		0.21	0.43	1.13	1.77	2.46	3.92	6.46	10.9	16.3	23.9	0.12
" "-RB		0.08	0.16	0.43	0.76	1.09	1.53	2.43	3.99	6.11	9.50	0.04
1L-SLP2-LP-6C-S2-EX	SF 270	0.58	1.78	5.63	10.4	13.6	19.6	26.2	34.2	41.3	48.2	0.46
" "-S2R2-SDS12		0.54	1.29	3.43	5.56	7.55	11.0	15.9	23.1	30.8	40.7	0.29
" "-RB		0.17	0.51	1.41	2.11	2.98	3.96	5.58	8.27	12.5	19.7	0.11
1L-SLP2-LP-6C-S2-EX	NR 270	0.92	2.77	8.68	14.0	18.2	23.7	29.0	36.4	42.3	48.4	0.59
" "-S2R2-SDS15		0.90	1.87	5.05	8.00	10.2	13.8	18.6	29.0	34.5	45.7	0.39
" "-RB		0.33	0.81	2.05	3.03	4.07	5.35	7.35	10.4	15.1	23.5	0.16
1L-SLP2-LP-6C-S2-EX	SB 270	1.34	3.75	11.8	18.9	24.0	30.7	37.7	45.5	51.6	57.1	0.77
" "-S2R2-SDS15		1.13	2.47	6.01	9.80	12.9	17.5	23.3	34.9	43.7	52.2	0.48
" "-RB		0.43	1.02	2.53	3.73	4.69	6.25	8.50	14.0	20.6	34.0	0.20
2L-SLP2-LP-6C-S2-EX	BF 270	0.56	1.21	3.34	5.54	7.37	10.7	16.4	24.8	33.3	43.4	0.30
" "-S2R2-SDS10		0.64	1.33	3.00	4.43	5.48	7.88	10.8	15.9	22.7	33.3	0.24
" "-RB		0.28	0.67	1.75	2.69	3.51	4.64	6.72	10.6	16.3	26.7	0.14
2L-SLP2-LP-6C-S2-EX	SF 270	1.91	5.39	14.8	21.2	25.8	32.2	39.5	47.0	53.2	58.5	0.90
" "-S2R2-SDS12		1.55	3.32	8.16	12.2	16.3	21.7	29.5	39.8	50.8	62.1	0.61
" "-RB		0.76	1.90	4.21	6.56	8.56	12.3	19.4	28.4	39.0	50.6	0.36
2L-SLP2-LP-6C-S2-EX	NR 270	2.86	7.56	18.6	25.0	29.4	35.5	41.4	49.1	54.3	58.8	1.07
" "-S2R2-SDS15		2.20	4.58	9.80	14.9	18.3	23.3	31.5	40.5	49.1	59.6	0.70
" "-RB		1.17	2.64	5.76	8.41	10.8	15.4	23.3	34.0	44.5	57.8	0.46
2L-SLP2-LP-6C-S2-EX	SB 270	3.68	9.88	23.9	32.8	38.4	45.3	52.1	58.4	62.1	64.5	1.37
" "-S2R2-SDS15		2.81	5.88	12.4	18.6	24.3	33.1	42.9	56.4	68.8	80.3	0.93
" "-RB		1.52	3.43	7.59	12.3	17.1	25.1	34.5	47.6	59.6	71.9	0.65

[1] Cripple wall retrofit cases are denoted "SDSx" to reflect retrofits for S_{DS} = 1.0g, 1.2g, and 1.5g according to *FEMA P-1100* plan sets.
[2] BF = Bakersfield, SF = San Francisco, NR = Northridge, and SB = San Bernardino; all sites assume V_{S30} = 270 m/sec.
[3] Mean loss at the 250-year return period is a primary loss metric and is referred to as "RC250".
[4] Expected annual loss expressed in percentage of building replacement cost.

Table 7.29 Loss assessment summary for 6-ft-tall cripple wall set and rigid base variants: 1956–1970 era with horizontal wood siding.

Index [1]	Site[2]	Mean loss at return period (% of replacement cost)										EAL[4] (%)
		15	25	50	75	100	150	250[3]	500	1000	2500	
1L-W2-G2-6C-HS2-EX	BF 270	0.01	0.07	0.51	1.22	1.87	3.62	7.34	14.0	22.2	33.7	0.10
" "-HSR2-SDS10		0.02	0.08	0.26	0.54	0.72	1.14	1.93	3.55	6.27	12.1	0.04
" "-RB		0.02	0.07	0.20	0.42	0.58	1.03	1.70	3.03	4.68	8.77	0.03
1L-W2-G2-6C-HS2-EX	SF 270	0.16	1.21	5.10	9.65	14.0	20.1	27.6	37.0	45.4	53.4	0.44
" "-HSR2-SDS12		0.09	0.38	1.09	1.75	2.34	3.50	5.84	10.3	15.7	26.5	0.11
" "-RB		0.06	0.25	0.96	1.49	2.01	2.78	4.38	6.60	11.5	20.6	0.08
1L-W2-G2-6C-HS2-EX	NR 270	0.38	1.91	8.00	13.3	17.4	23.0	29.6	38.7	45.9	52.9	0.55
" "-HSR2-SDS15		0.22	0.62	1.64	2.49	3.23	4.87	7.32	13.5	19.4	30.0	0.15
" "-RB		0.14	0.46	1.33	2.20	2.80	3.92	5.76	10.3	15.8	25.5	0.12
1L-W2-G2-6C-HS2-EX	SB 270	0.55	2.69	11.6	18.8	24.4	32.0	40.4	49.9	56.5	61.5	0.75
" "-HSR2-SDS15		0.34	0.78	2.01	3.26	4.50	7.08	11.0	20.5	30.8	43.8	0.21
" "-RB		0.21	0.56	1.59	2.77	3.53	4.75	7.85	14.8	23.4	36.2	0.16
2L-W2-G2-6C-HS2-EX	BF 270	0.12	0.43	1.95	3.75	5.05	8.05	12.5	19.3	26.7	36.1	0.20
" "-HSR2-SDS10		0.12	0.31	0.83	1.31	1.69	2.59	3.98	6.58	10.5	17.5	0.08
" "-RB		0.09	0.24	0.81	1.37	1.87	2.85	4.54	7.53	12.2	19.3	0.08
2L-W2-G2-6C-HS2-EX	SF 270	0.82	3.26	11.0	16.8	21.5	28.1	36.0	44.3	51.3	57.4	0.70
" "-HSR2-SDS12		0.37	1.06	2.83	4.72	6.48	9.99	15.0	22.2	31.2	41.4	0.26
" "-RB		0.28	0.91	2.61	4.45	6.15	9.11	14.6	21.5	30.2	40.1	0.24
2L-W2-G2-6C-HS2-EX	NR 270	1.18	4.76	14.2	20.8	25.4	32.2	39.2	47.8	53.7	58.9	0.85
" "-HSR2-SDS15		0.58	1.54	4.08	6.99	8.79	12.5	17.9	24.7	32.0	41.3	0.33
" "-RB		0.52	1.35	3.68	6.29	7.91	11.5	16.5	22.7	30.0	39.0	0.30
2L-W2-G2-6C-HS2-EX	SB 270	2.03	7.17	20.0	28.9	34.8	42.2	49.5	56.8	61.1	64.0	1.16
" "-HSR2-SDS15		0.86	2.01	5.23	8.68	12.3	18.7	26.5	38.3	50.5	63.9	0.47
" "-RB		0.74	1.84	5.17	8.49	12.0	18.3	25.8	37.2	48.5	61.2	0.45

[1] Cripple wall retrofit cases are denoted "SDSx" to reflect retrofits for S_{DS}=1.0g, 1.2g, and 1.5g according to *FEMA P-1100* plan sets.
[2] BF = Bakersfield, SF = San Francisco, NR = Northridge, and SB = San Bernardino; all sites assume V_{S30} = 270 m/sec.
[3] Mean loss at the 250-year return period is a primary loss metric and is referred to as "RC250".
[4] Expected annual loss expressed in percentage of building replacement cost.

Table 7.30 Loss assessment summary for 6-ft-tall cripple wall set and rigid base variants: 1956–1970 era with exterior stucco.

Index [1]	Site[2]	Mean loss at return period (% of replacement cost)										EAL[4] (%)
		15	25	50	75	100	150	250[3]	500	1000	2500	
1L-S2-G2-6C-S2-EX	BF 270	0.07	0.15	0.44	0.77	1.22	2.17	4.08	8.09	13.9	21.9	0.07
" "-S2R2-SDS10		0.04	0.11	0.41	0.75	1.09	1.81	3.14	5.89	10.1	17.4	0.05
" "-RB		0.02	0.05	0.17	0.34	0.55	0.92	1.62	2.97	4.85	8.44	0.03
1L-S2-G2-6C-S2-EX	SF 270	0.20	0.57	2.35	4.19	6.16	10.4	16.8	24.1	32.2	39.2	0.24
" "-S2R2-SDS12		0.14	0.48	1.68	2.57	3.67	5.51	9.35	14.4	21.8	31.7	0.16
" "-RB		0.05	0.21	0.78	1.32	2.17	2.67	4.67	7.06	11.5	18.8	0.08
1L-S2-G2-6C-S2-EX	NR 270	0.29	0.87	3.21	6.29	8.50	13.1	18.9	26.5	32.4	39.3	0.30
" "-S2R2-SDS15		0.31	0.86	2.43	4.10	5.54	8.14	11.8	18.4	25.9	36.6	0.22
" "-RB		0.12	0.42	1.19	2.12	2.91	4.24	6.05	9.40	14.7	23.0	0.11
1L-S2-G2-6C-S2-EX	SB 270	0.41	1.16	4.58	9.00	12.8	20.0	27.3	36.5	44.3	51.7	0.43
" "-S2R2-SDS15		0.40	1.15	3.06	5.23	6.89	10.3	15.3	25.6	33.9	45.3	0.28
" "-RB		0.18	0.53	1.53	2.75	3.56	5.14	7.56	13.3	20.1	31.6	0.15
2L-S2-G2-6C-S2-EX	BF 270	0.16	0.40	1.45	2.48	3.65	5.93	9.52	15.8	22.1	31.3	0.15
" "-S2R2-SDS10		0.13	0.37	1.39	2.29	3.13	4.61	7.18	11.0	16.5	25.6	0.13
" "-RB		0.08	0.31	0.99	1.72	2.43	3.68	5.61	8.89	13.7	22.5	0.10
2L-S2-G2-6C-S2-EX	SF 270	0.54	1.93	6.46	11.2	15.3	21.1	28.3	36.8	44.7	52.2	0.50
" "-S2R2-SDS12		0.49	1.63	4.44	7.14	9.20	13.1	19.9	28.7	38.7	49.7	0.36
" "-RB		0.33	1.17	3.16	5.27	6.99	10.2	16.6	24.6	34.8	46.1	0.28
2L-S2-G2-6C-S2-EX	NR 270	0.89	2.90	9.16	14.4	18.5	23.8	30.0	38.5	45.0	51.6	0.61
" "-S2R2-SDS15		0.87	2.22	5.88	9.30	11.2	15.2	22.1	30.7	40.5	52.3	0.44
" "-RB		0.59	1.72	4.72	7.33	9.64	14.2	20.6	31.1	41.1	53.4	0.38
2L-S2-G2-6C-S2-EX	SB 270	1.30	4.04	12.5	19.5	24.7	31.7	39.5	48.3	54.8	60.1	0.81
" "-S2R2-SDS15		1.26	3.23	8.36	12.8	17.2	24.7	33.4	45.2	56.7	68.9	0.64
" "-RB		0.87	2.33	6.49	10.3	14.4	21.5	28.8	40.9	52.0	64.2	0.53

[1] Cripple wall retrofit cases are denoted "SDSx" to reflect retrofits for S_{DS}=1.0*g*, 1.2*g*, and 1.5*g* according to *FEMA P-1100* plan sets.
[2] BF = Bakersfield, SF = San Francisco, NR = Northridge, and SB = San Bernardino; all sites assume V_{S30} = 270 m/sec.
[3] Mean loss at the 250-year return period is a primary loss metric and is referred to as "RC250".
[4] Expected annual loss expressed in percentage of building replacement cost.

7.6 PERFORMANCE OF CRIPPLE WALLS WITH PANELIZED T1-11 SIDING

Structural analysis and loss results for house variants with panelized T1-11 siding include one- and two-story superstructures with cripple wall heights of 2 ft and 6 ft. All T1-11 variants are assumed to belong to the 1956–1970 era of construction, where the interior walls are sheathed in gypsum wallboard.

7.6.1 Modal and Pushover Criteria for T1-11 Cripple Walls

The elastic fundamental vibration periods and key pushover analysis results are summarized in Table 7.31, similar to the data summarized previously for the houses with stucco and wood siding exteriors. Each retrofitted T1-11 variant has the suffix “R1” regardless of assumed building site, since *FEMA P-1100* specifies only one retrofit for houses with T-11 siding, consisting of upgraded nailing around the entire perimeter of the T-11 panels. Accordingly, the wood-structural panel length (L_{WSP}) column of Table 7.31 supplies “N/A” for T1-11 variants since the retrofit does not involve the addition of wood-structural panels. Table 7.31 also includes equivalent variants on a rigid base (RB), i.e., without crawlspace vulnerability, for comparison. In general, the existing (unretrofitted) cripple wall strengths, e.g., $(V/W_S)_{\mathrm{Avg}}$ for houses with T-11 panels are a bit larger than corresponding houses with stucco or wood siding.

Table 7.31 Summary of modal and pushover criteria for the T1-11 siding cripple wall set and rigid base variants.

Index [1]	T_1 (sec) [2]	$(V/W_S)_{\mathrm{Avg}}$ [3]	$(V/W_{BL})_{\mathrm{Avg}}$ [4]	$(V_{CW}/V_{SS})_{\mathrm{Avg}}$ [5]	L_{WSP} (ft) [6]
1L-T1-G2-2C-T1-EX	0.18	0.75	0.76	0.72	N/A
1L-T1-G2-2C-T1-R1	0.16	1.25	1.27	1.50	N/A
1L-T1-G2-6C-T1-EX	0.25	0.49	0.50	0.48	N/A
1L-T1-G2-6C-T1-R1	0.26	1.12	1.15	1.11	N/A
1L-T1-G2-RB	0.14	1.85	1.04	N/A	N/A
2L-T1-G2-2C-T1-EX	0.27	0.46	0.46	0.70	N/A
2L-T1-G2-2C-T1-R1	0.25	0.70	0.70	1.48	N/A
2L-T1-G2-6C-T1-EX	0.35	0.30	0.31	0.47	N/A
2L-T1-G2-6C-T1-R1	0.35	0.70	0.72	1.10	N/A
2L-T1-G2-RB	0.22	0.89	0.65	N/A	N/A

[1] Cripple wall retrofit of T1-11 siding requires upgraded nailing around perimeter and is not site-dependent according to *FEMA P-1100*.
[2] Elastic fundamental period in seconds.
[3] Average strength to seismic weight ratio from pushover loading proportional to elastic translational mode shape in each direction, seismic weight is the total lateral weight acting in the model.
[4] Average strength to baseline weight ratio from pushover loading proportional to elastic mode shape in each direction, the baseline weight is the weight of the dwelling including the first-floor diaphragm and above.
[5] Average crawlspace to first occupied story (superstructure) strength ratio, obtained from story-based pushover curves.
[6] Upgraded T1-11 nailing is assumed to be conducted around entire perimeter; no wood structural panel lengths are used in retrofit design.

7.6.2 Collapse Performance of T1-11 Cripple Walls

The $P[C|RP_{250}]$ and $P[C|MCE]$ collapse statistics for the T1-11 house variants are compared to corresponding values for the wood siding variants in Figure 7.32 and Figure 7.33, respectively. Both the T-11 and wood siding cases are based on 1956–1970 era construction, with gypsum wallboard interior walls. Overall, these data show that the existing (unretrofitted) houses with T1-11 siding have lower collapse risks than corresponding existing houses with wood siding, and as with wood siding, the risks are slightly less for 6-ft-tall versus 2-ft-tall cripple walls. The data further indicate that the collapse risks are roughly the same for the retrofitted T1-11 and wood siding houses, except that the retrofitted T1-11 cases with 6-ft-tall cripple walls have slightly higher collapse risks than the 2-ft-tall counterparts (which is contrary to the trends for the existing cases).

Similar to tabulations for the houses with stucco and wood siding, collapse fragility curve parameters and collapse risks for the T1-11 variants are summarized in Table 7.32 and Table 7.33, for the one-story and two-story houses, respectively.

The general observations for collapse mechanisms controlling T1-11 houses without (existing) and with retrofit are generally similar to those for houses with other finishes, i.e.,

- Existing (unretrofitted) 2-ft- and 6-ft tall T1-11 cripple walls have collapse occurring exclusively in the cripple wall. This is due to the existing cripple wall having a strength much weaker than the occupied story above.
- One-story retrofitted T1-11 cripple walls have collapse exclusively occurring within the crawlspace.
- Two-story retrofitted 2-ft-tall T1-11 cripple walls were observed to exclusively have collapse occurring in the first occupied story of the superstructure.
- Two-story retrofitted 6-ft-tall cripple walls were observed to exclusively have collapse occurring within the crawlspace, an opposite trend than that observed for 2-ft-tall T1-11 cripple walls. This is likely due to the upgraded nailing for T1-11 cripple walls only achieving a normalized strength of 844 plf. Since no tie-downs or other improved detailing is included, the 6-ft-tall T1-11 cripple walls cannot achieve enough strength to push inelastic displacements into the superstructure.

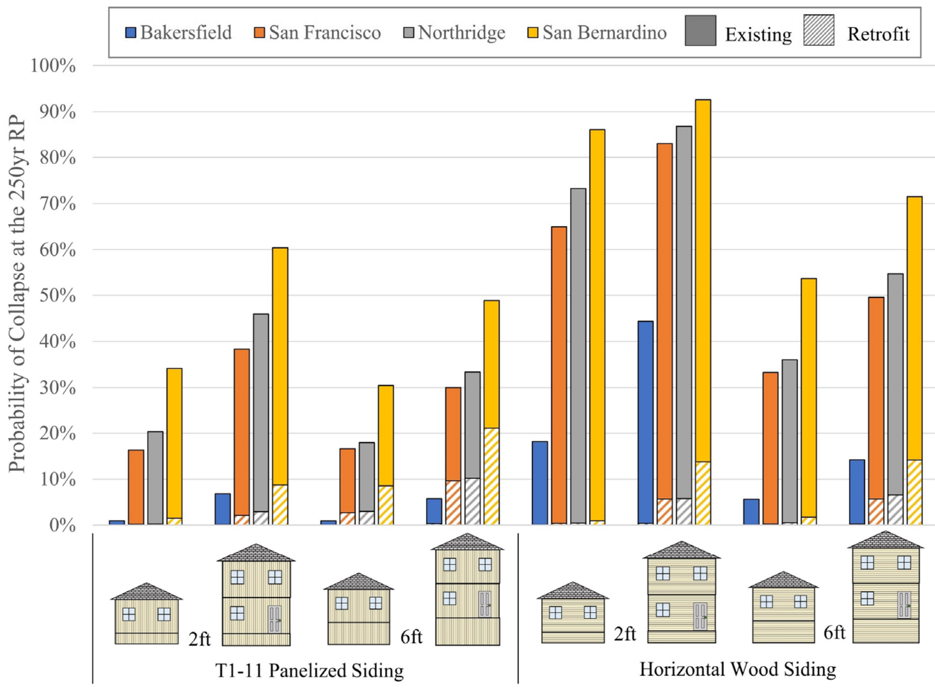

Figure 7.32 **Probability of collapse at the 250-year return period for cripple walls with T1-11 and horizontal siding, *Sa*(0.25 sec)$_{250}$: 0.63*g* (BF), 0.98*g* (SF), 1.15*g* (NR), and 1.27*g* (SB).**

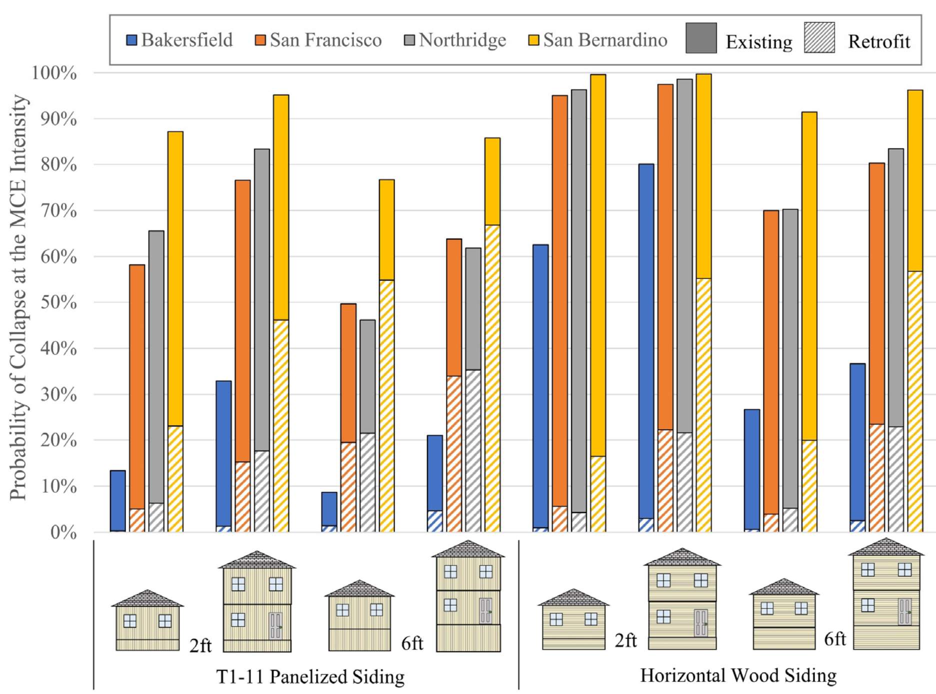

Figure 7.33 **Probability of collapse at the MCE for cripple walls with T1-11 and horizontal siding, *Sa*(0.25 sec)$_{MCE}$: 1.11*g* (BF), 1.80*g* (SF), 2.10*g* (NR), and 2.67g (SB).**

Table 7.32 Collapse performance summary for 2-ft-tall and 6-ft-tall T1-11 cripple wall set and rigid base variants: one-story cases.

Index [1]	Site [2] (Sa_{250}) (Sa_{MCE})	$Sa_{Med,C}$ (g) [3]	β_{RTR} [4]	$\beta_{C,Tot}$ [5]	P[C|RP$_{250}$] [6]	P[C|MCE] [7]	$Cost_{Col}$ [8]
1L-T1-G2-2C-T1-EX	BF270 (0.63g) (1.11g)	1.84	0.29	0.46	0.96%	13.3%	67%
1L-T1-G2-2C-T1-R1		5.16	0.43	0.56	0.01%	0.3%	67%
1L-T1-G2-RB		8.58	0.52	0.63	0.002%	0.1%	100%
1L-T1-G2-2C-T1-EX	SF270 (0.98g) (1.80g)	1.62	0.37	0.51	16.3%	58.2%	67%
1L-T1-G2-2C-T1-R1		3.98	0.33	0.48	0.18%	5.0%	67%
1L-T1-G2-RB		5.43	0.32	0.47	0.01%	1.0%	100%
1L-T1-G2-2C-T1-EX	NR270 (1.15g) (2.10g)	1.73	0.34	0.49	20.3%	65.5%	67%
1L-T1-G2-2C-T1-R1		4.33	0.32	0.47	0.24%	6.3%	67%
1L-T1-G2-RB		5.88	0.28	0.45	0.01%	1.1%	100%
1L-T1-G2-2C-T1-EX	SB270 (1.27g) (2.67g)	1.54	0.33	0.48	34.1%	87.2%	67%
1L-T1-G2-2C-T1-R1		3.92	0.39	0.52	1.5%	23.0%	67%
1L-T1-G2-RB		5.01	0.21	0.41	0.04%	6.1%	100%
1L-T1-G2-6C-T1-EX	BF270 (0.63g) (1.11g)	2.46	0.47	0.58	0.92%	8.6%	67%
1L-T1-G2-6C-T1-R1		3.40	0.37	0.51	0.05%	1.4%	67%
1L-T1-G2-RB		8.58	0.52	0.63	0.002%	0.1%	100%
1L-T1-G2-6C-T1-EX	SF270 (0.98g) (1.80g)	1.81	0.52	0.63	16.6%	49.6%	67%
1L-T1-G2-6C-T1-R1		2.94	0.45	0.57	2.7%	19.5%	67%
1L-T1-G2-RB		5.43	0.32	0.47	0.01%	1.0%	100%
1L-T1-G2-6C-T1-EX	NR270 (1.15g) (2.10g)	2.25	0.64	0.73	18.0%	46.1%	67%
1L-T1-G2-6C-T1-R1		3.24	0.42	0.55	3.0%	21.5%	67%
1L-T1-G2-RB		5.88	0.28	0.45	0.01%	1.1%	100%
1L-T1-G2-6C-T1-EX	SB270 (1.27g) (2.67g)	1.72	0.49	0.61	30.4%	76.7%	67%
1L-T1-G2-6C-T1-R1		2.51	0.36	0.51	8.5%	54.8%	67%
1L-T1-G2-RB		5.01	0.21	0.41	0.04%	6.1%	100%

[1] Cripple wall retrofit of T1-11 siding requires upgraded nailing around perimeter and is not site-dependent according to *FEMA P-1100*.
[2] BF = Bakersfield, SF = San Francisco, NR = Northridge, and SB = San Bernardino; all sites assume V_{S30} = 270 m/sec, 250-year return period, and MCE Sa(0.25 sec) for site annotated.
[3] Median collapse intensity defined as Sa(0.25 sec).
[4] Record-to-record variability from collapse fragility fitting.
[5] Total collapse dispersion including β_{Mod} = 0.35 combined with β_{RTR} using SRSS.
[6] Probability of collapse at 250-year return period (RP$_{250}$).
[7] Probability of collapse at the MCE with intensity determined by nominal S_{DS} for site scaled by a factor of 1.5.
[8] Percentage of replacement cost attributed to collapse, 67% indicates that governing collapse mode occurs in crawlspace, 100% indicates that governing collapse mode occurs in first occupied story.

Table 7.33 Collapse performance summary for 2-ft-tall and 6-ft-tall T1-11 cripple wall set and rigid base variants: two-story cases.

Index [1]	Site [2] (Sa_{250}) (Sa_{MCE})	$Sa_{Med,C}$ (g) [3]	β_{RTR} [4]	$\beta_{C,Tot}$ [5]	P[C|RP250] [6]	P[C|MCE] [7]	$Cost_{Col}$ [8]
2L-T1-G2-2C-T1-EX	BF270 (0.63g) (1.11g)	1.42	0.42	0.55	6.83%	32.9%	67%
2L-T1-G2-2C-T1-R1		4.07	0.47	0.58	0.06%	1.3%	100%
2L-T1-G2-RB		3.91	0.44	0.56	0.05%	1.2%	100%
2L-T1-G2-2C-T1-EX	SF270 (0.98g) (1.80g)	1.17	0.48	0.59	38.3%	76.5%	67%
2L-T1-G2-2C-T1-R1		3.32	0.48	0.60	2.1%	15.2%	100%
2L-T1-G2-RB		3.53	0.53	0.63	2.1%	14.3%	100%
2L-T1-G2-2C-T1-EX	NR270 (1.15g) (2.10g)	1.22	0.44	0.56	45.9%	83.3%	67%
2L-T1-G2-2C-T1-R1		3.74	0.52	0.62	2.9%	17.7%	100%
2L-T1-G2-RB		3.76	0.51	0.62	2.8%	17.3%	100%
2L-T1-G2-2C-T1-EX	SB270 (1.27g) (2.67g)	1.10	0.40	0.53	60.4%	95.2%	67%
2L-T1-G2-2C-T1-R1		2.82	0.47	0.59	8.7%	46.1%	100%
2L-T1-G2-RB		3.01	0.47	0.58	6.8%	41.8%	100%
2L-T1-G2-6C-T1-EX	BF270 (0.63g) (1.11g)	2.04	0.67	0.75	5.8%	21.0%	67%
2L-T1-G2-6C-T1-R1		2.80	0.42	0.55	0.32%	4.6%	67%
2L-T1-G2-RB		3.91	0.44	0.56	0.05%	1.2%	100%
2L-T1-G2-6C-T1-EX	SF270 (0.98g) (1.80g)	1.41	0.59	0.69	30.0%	63.8%	67%
2L-T1-G2-6C-T1-R1		2.38	0.58	0.68	9.7%	33.9%	67%
2L-T1-G2-RB		3.53	0.53	0.63	2.1%	14.3%	100%
2L-T1-G2-6C-T1-EX	NR270 (1.15g) (2.10g)	1.64	0.74	0.82	33.3%	61.8%	67%
2L-T1-G2-6C-T1-R1		2.70	0.58	0.68	10.2%	35.3%	67%
2L-T1-G2-RB		3.76	0.51	0.62	2.8%	17.3%	100%
2L-T1-G2-6C-T1-EX	SB270 (1.27g) (2.67g)	1.29	0.58	0.68	48.9%	85.8%	67%
2L-T1-G2-6C-T1-R1		2.05	0.49	0.60	21.1%	66.8%	67%
2L-T1-G2-RB		3.01	0.47	0.58	6.8%	41.8%	100%

[1] Cripple wall retrofit of T1-11 siding requires upgraded nailing around perimeter and is not site-dependent according to *FEMA P-1100*.
[2] BF = Bakersfield, SF = San Francisco, NR = Northridge, and SB = San Bernardino; all sites assume V_{S30} = 270 m/sec, 250-year return period, and MCE Sa(0.25 sec) for site annotated.
[3] Median collapse intensity defined as Sa(0.25 sec).
[4] Record-to-record variability from collapse fragility fitting.
[5] Total collapse dispersion including β_{Mod} = 0.35 combined with β_{RTR} using SRSS.
[6] Probability of collapse at 250-year return period (RP_{250}).
[7] Probability of collapse at the MCE with intensity determined by nominal S_{DS} for site scaled by a factor of 1.5.
[8] Percentage of replacement cost attributed to collapse, 67% indicates that governing collapse mode occurs in crawlspace, 100% indicates that governing collapse mode occurs in first occupied story.

7.6.3 Loss Assessment Summary for T1-11 Siding Cripple Walls

The loss (damage) curves for houses with T-11 siding and 6-ft-tall and 2-ft-tall cripple walls are compared in Figure 7.34 and Figure 7.35 for the one-story and two-story variants, respectively. The comparisons are all for 1956–1970 era (i.e., gypsum wallboard interior) house variants, for the San Francisco site. In general, the trends between the loss functions for existing (unretrofitted) versus retrofitted cripple walls cases, and 2-ft-tall versus 6-ft-tall walls are similar to those observed in house variants with stucco and wood siding exteriors.

The EAL and RC250 loss metrics for the T1-11 variants are compared to those of wood siding variants for all building sites in Figure 7.36 and Figure 7.37. Overall, the data show that the losses for the existing (unretrofitted) T1-11 variants are about one-half to two-thirds of those for variants with wood siding, and that the losses for the retrofit T1-11 variants are slightly less than the comparable retrofitted wood siding variants.

Detailed tabular summaries of the loss statistics and loss functions for the T1-11 variants are provided in Table 7.34, Table 7.35 and Table 7.36, similar to tables presented previously for the stucco and wood siding variants.

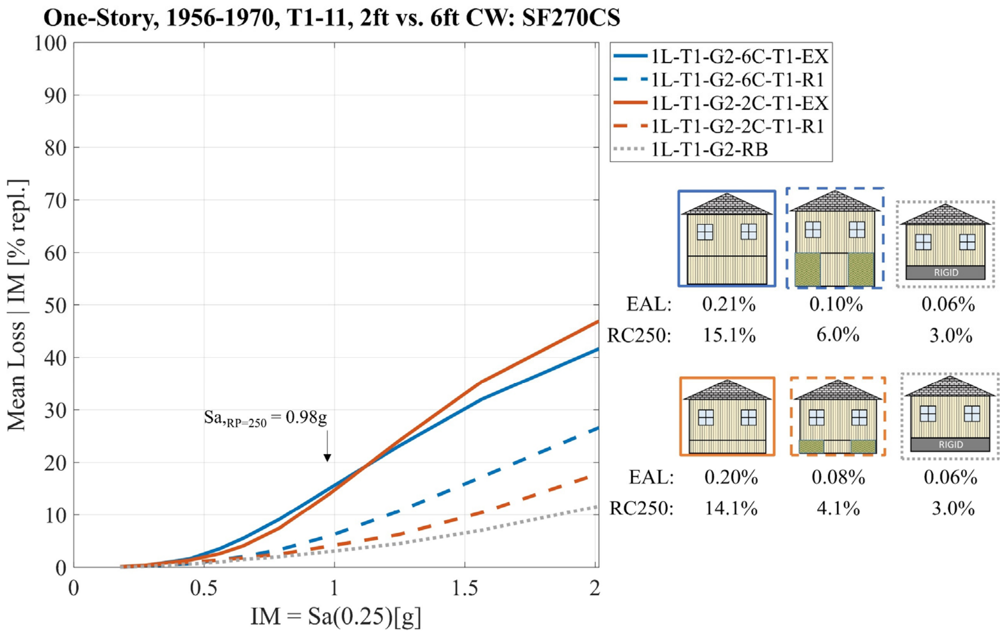

Figure 7.34 Loss curves comparing 6-ft-tall and 2-ft-tall cripple wall heights for the one-story, 1956–1970 era variants with T1-11 siding: existing (solid), retrofit (dashed), and rigid base cases (dotted) for the San Francisco site.

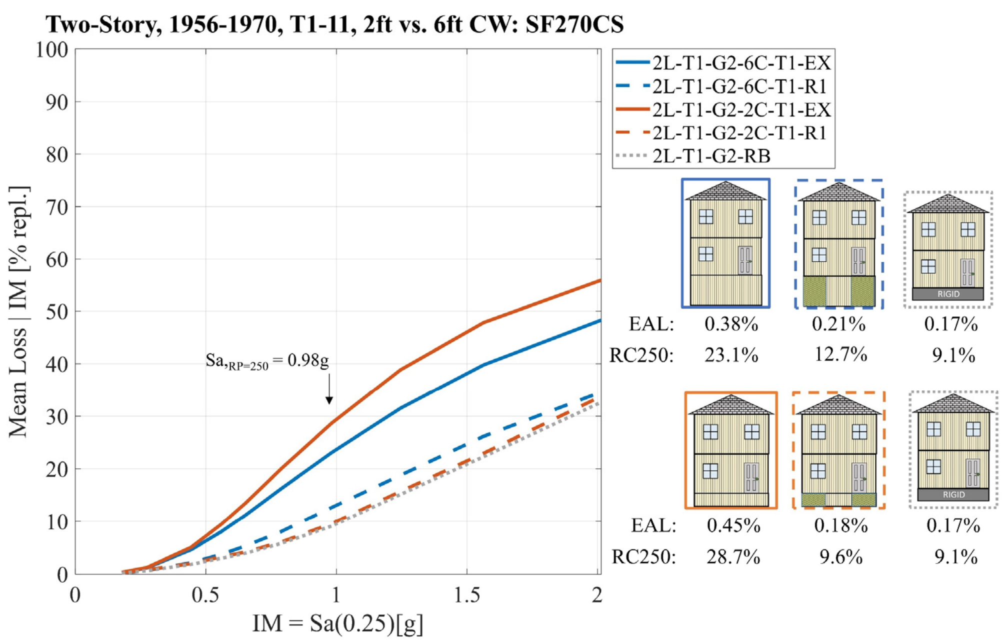

Figure 7.35 Loss curves comparing 6-ft-tall and 2-ft-tall cripple wall heights for the two-story, 1956–1970 era variants with T1-11 siding: existing (solid), retrofit (dashed), and rigid base cases (dotted) for the San Francisco site.

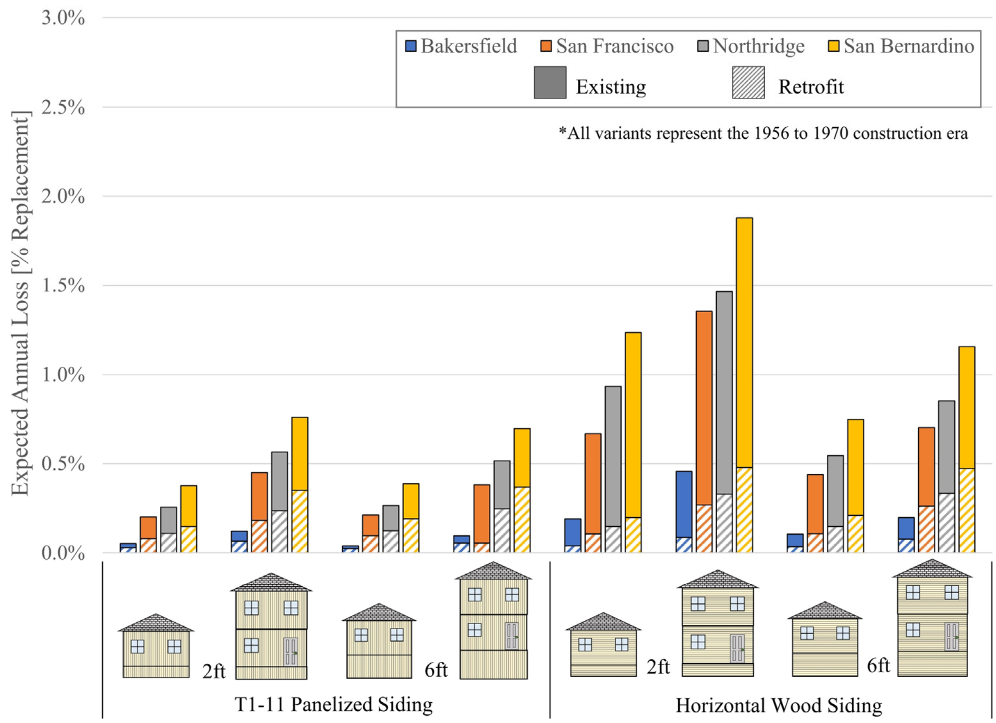

Figure 7.36 **Expected annual loss results comparing T1-11 panelized siding and horizontal wood siding cripple walls.**

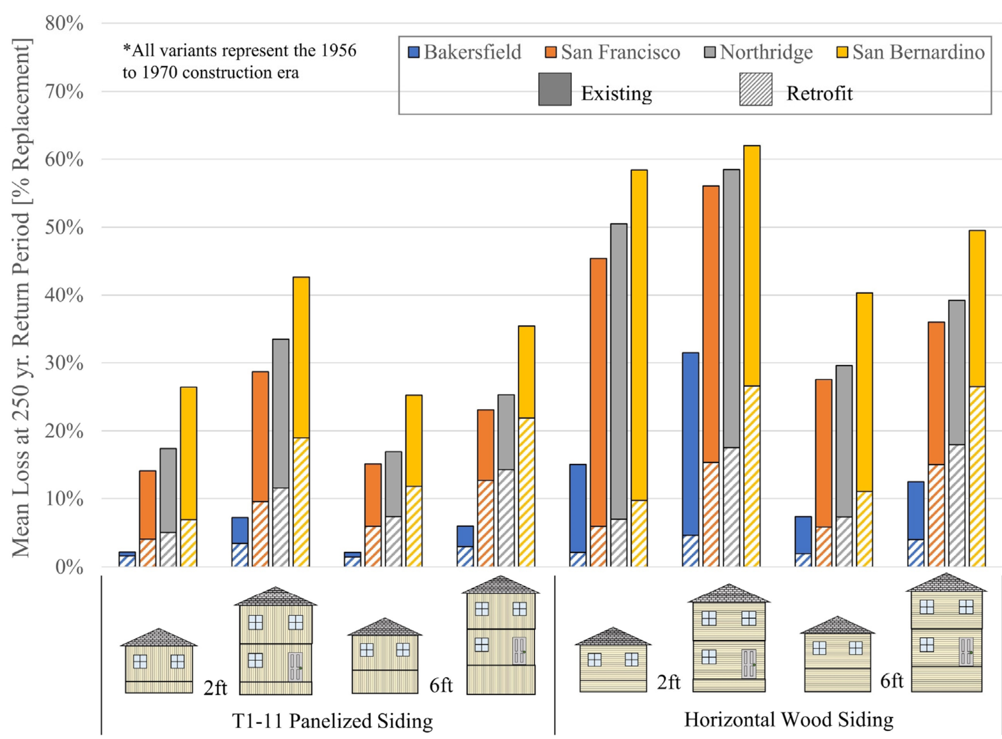

Figure 7.37 **Expected loss at the 250-year return period (RC250) results comparing T1-11 panelized siding and horizontal wood siding cripple walls.**

Table 7.34 Summary of primary loss metrics and benefits due to retrofitting for T1-11 siding cripple walls.

Description/Index	Site	Condition	EAL (% repl.)	Benefit$_{EAL}$[1] (% repl.)	RC250 (% repl.)	Benefit$_{RC250}$[1] (% repl.)
One-story, 1956–1970, T1-11 siding, 2-ft-tall cripple wall.	BF 270	Existing	0.052	0.02	2.17	0.6
(EX) 1L-T1-G2-2C-T1-EX		Retrofitted	0.029		1.60	
(R) 1L-T1-G2-2C-T1-R1	SF 270	Existing	0.201	0.12	14.06	10.0
		Retrofitted	0.080		4.05	
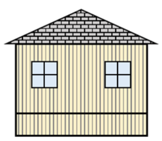	NR 270	Existing	0.257	0.15	17.32	12.3
		Retrofitted	0.109		5.03	
	SB 270	Existing	0.377	0.23	26.43	19.5
		Retrofitted	0.147		6.90	
One-story, 1956–1970, T1-11 siding, 6-ft-tall cripple wall.	BF 270	Existing	0.039	0.01	2.14	0.7
(EX) 1L-T1-G2-6C-T1-EX		Retrofitted	0.025		1.45	
(R) 1L-T1-G2-6C-T1-R1	SF 270	Existing	0.212	0.12	15.09	9.1
		Retrofitted	0.096		5.96	
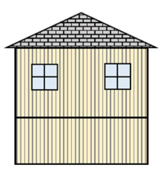	NR 270	Existing	0.266	0.14	16.87	9.5
		Retrofitted	0.124		7.34	
	SB 270	Existing	0.387	0.20	25.23	13.4
		Retrofitted	0.191		11.79	
Two-story, 1956–1970, T1-11 siding, 2-ft-tall cripple wall.	BF 270	Existing	0.122	0.06	7.21	3.8
(EX) 2L-T1-G2-2C-T1-EX		Retrofitted	0.065		3.42	
(R) 2L-T1-G2-2C-T1-R1	SF 270	Existing	0.450	0.27	28.67	19.1
		Retrofitted	0.183		9.57	
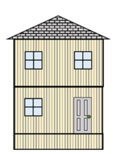	NR 270	Existing	0.564	0.33	33.48	21.9
		Retrofitted	0.236		11.56	
	SB 270	Existing	0.761	0.41	42.68	23.7
		Retrofitted	0.351		18.96	
Two-story, 1956–1970, T1-11 siding, 6-ft-tall cripple wall.	BF 270	Existing	0.095	0.04	5.99	3.0
(EX) 2L-T1-G2-6C-T1-EX		Retrofitted	0.055		2.98	
(R) 2L-T1-G2-6C-T1-R1	SF 270	Existing	0.381	0.17	23.09	10.4
		Retrofitted	0.208		12.66	
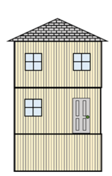	NR 270	Existing	0.516	0.27	25.30	11.1
		Retrofitted	0.247		14.23	
	SB 270	Existing	0.699	0.33	35.42	13.5
		Retrofitted	0.369		21.89	

[1] Benefits are the difference of the retrofit variant (R) subtracted from the existing (unretrofitted) variant (EX)

Table 7.35 Loss assessment summary for T1-11 siding cripple walls and rigid base variants: one-story cases.

Index [1]	Site[2]	Mean loss at return period (% of replacement cost)										EAL[4] (%)
		15	25	50	75	100	150	250 [3]	500	1000	2500	
1L-T1-G2-2C-T1-EX	BF 270	0.04	0.11	0.36	0.63	0.78	1.26	2.17	5.15	11.4	23.9	0.05
" "-R1		0.02	0.08	0.26	0.53	0.68	1.09	1.60	2.69	4.25	7.56	0.03
" "-RB		0.01	0.03	0.14	0.30	0.41	0.68	1.20	2.01	3.22	5.50	0.02
1L-T1-G2-2C-T1-EX	SF 270	0.13	0.40	1.36	2.59	4.11	7.48	14.1	24.0	35.3	46.9	0.20
" "-R1		0.09	0.32	1.00	1.38	1.83	2.49	4.05	6.21	10.4	17.9	0.08
" "-RB		0.04	0.18	0.64	1.01	1.51	2.01	2.99	4.49	7.04	11.6	0.06
1L-T1-G2-2C-T1-EX	NR 270	0.27	0.64	1.85	3.67	5.78	10.3	17.3	29.1	40.0	50.8	0.26
" "-R1		0.19	0.53	1.33	1.94	2.49	3.63	5.03	8.29	13.1	21.2	0.11
" "-RB		0.09	0.30	0.89	1.59	2.04	2.81	3.94	5.86	8.65	15.0	0.08
1L-T1-G2-2C-T1-EX	SB 270	0.34	0.92	2.95	6.39	10.0	17.1	26.4	39.6	49.9	58.3	0.38
" "-R1		0.27	0.70	1.61	2.45	3.12	4.40	6.90	12.6	19.7	29.8	0.15
" "-RB		0.16	0.40	1.17	1.90	2.49	3.40	4.77	7.92	12.3	20.9	0.10
1L-T1-G2-6C-T1-EX	BF 270	0.02	0.06	0.22	0.35	0.51	1.01	2.14	4.58	9.16	16.9	0.04
" "-R1		0.01	0.03	0.16	0.32	0.44	0.81	1.45	2.79	4.92	9.85	0.03
" "-RB		0.01	0.03	0.14	0.30	0.41	0.68	1.20	2.01	3.22	5.50	0.02
1L-T1-G2-6C-T1-EX	SF 270	0.08	0.35	1.60	3.55	5.56	9.17	15.1	23.1	32.0	41.7	0.21
" "-R1		0.05	0.20	0.69	1.43	2.05	3.36	5.96	10.7	17.2	26.6	0.10
" "-RB		0.04	0.18	0.64	1.01	1.51	2.01	2.99	4.49	7.04	11.6	0.06
1L-T1-G2-6C-T1-EX	NR 270	0.17	0.64	2.77	5.61	7.75	11.9	16.9	24.1	30.9	39.0	0.27
" "-R1		0.09	0.31	1.13	2.00	2.70	4.37	7.34	13.0	19.5	29.1	0.12
" "-RB		0.09	0.30	0.89	1.59	2.04	2.81	3.94	5.86	8.65	15.0	0.08
1L-T1-G2-6C-T1-EX	SB 270	0.25	0.82	4.11	8.10	11.8	17.8	25.2	35.3	44.2	52.3	0.39
" "-R1		0.13	0.46	1.53	2.78	4.34	7.53	11.8	21.2	31.4	42.7	0.19
" "-RB		0.16	0.40	1.17	1.90	2.49	3.40	4.77	7.92	12.3	20.9	0.10

[1] Cripple wall retrofit of T1-11 siding requires upgraded nailing around perimeter and is not site-dependent according to *FEMA P-1100*.
[2] BF = Bakersfield, SF = San Francisco, NR = Northridge, and SB = San Bernardino; all sites assume V_{S30} = 270 m/sec.
[3] Mean loss at the 250-year return period is a primary loss metric and is referred to as "RC250."
[4] Expected annual loss expressed in percentage of building replacement cost.

Table 7.36 Loss assessment summary for T1-11 siding cripple walls and rigid base variants: two-story cases.

Index [1]	Site[2]	Mean loss at return period (% of replacement cost)										EAL[4] (%)
		15	25	50	75	100	150	250 [3]	500	1000	2500	
2L-T1-G2-2C-T1-EX	BF 270	0.09	0.26	0.82	1.43	2.16	3.84	7.21	14.6	23.8	37.0	0.12
“ “-R1		0.07	0.22	0.77	1.20	1.62	2.32	3.42	5.31	8.21	14.0	0.07
“ “-RB		0.05	0.16	0.58	0.99	1.42	2.19	3.22	5.21	7.94	14.3	0.06
2L-T1-G2-2C-T1-EX	SF 270	0.34	1.24	5.10	9.49	13.5	20.1	28.7	38.9	47.9	55.9	0.45
“ “-R1		0.26	0.82	2.00	3.29	4.19	6.11	9.57	15.7	23.0	33.8	0.18
“ “-RB		0.19	0.65	1.85	3.01	3.96	5.84	9.11	15.2	22.3	32.6	0.17
2L-T1-G2-2C-T1-EX	NR 270	0.52	1.78	7.08	12.9	17.6	25.0	33.5	44.7	52.6	59.2	0.56
“ “-R1		0.44	1.13	2.88	4.45	5.69	8.01	11.6	18.5	26.0	36.3	0.24
“ “-RB		0.36	0.98	2.63	4.10	5.26	7.45	11.3	18.3	25.9	36.1	0.22
2L-T1-G2-2C-T1-EX	SB 270	0.83	2.83	10.6	18.4	24.6	33.3	42.7	52.8	59.2	63.4	0.76
“ “-R1		0.67	1.55	3.81	6.06	8.28	12.9	19.0	29.7	41.3	55.0	0.35
“ “-RB		0.50	1.32	3.33	5.30	7.32	11.5	17.3	26.8	38.2	51.3	0.31
2L-T1-G2-6C-T1-EX	BF 270	0.10	0.21	0.69	1.37	1.95	3.28	5.99	10.6	16.3	24.8	0.10
“ “-R1		0.05	0.15	0.54	0.87	1.17	1.89	2.98	5.13	8.34	15.1	0.05
“ “-RB		0.05	0.16	0.58	0.99	1.42	2.19	3.22	5.21	7.94	14.3	0.06
2L-T1-G2-6C-T1-EX	SF 270	0.30	1.17	4.64	8.07	11.2	16.3	23.1	31.5	39.8	48.3	0.38
“ “-R1		0.22	0.70	2.15	3.76	5.35	8.09	12.7	18.8	26.2	34.6	0.21
“ “-RB		0.19	0.65	1.85	3.01	3.96	5.84	9.11	15.2	22.3	32.6	0.17
2L-T1-G2-6C-T1-EX	NR 270	0.74	2.54	7.82	12.0	15.1	19.9	25.3	33.0	39.4	46.4	0.52
“ “-R1		0.33	0.91	2.75	5.05	6.50	9.62	14.2	20.7	27.5	36.0	0.25
“ “-RB		0.36	0.98	2.63	4.10	5.26	7.45	11.3	18.3	25.9	36.1	0.22
2L-T1-G2-6C-T1-EX	SB 270	0.93	3.20	10.6	16.9	21.5	27.9	35.4	44.4	51.3	57.2	0.70
“ “-R1		0.43	1.36	4.18	7.29	10.3	15.3	21.9	30.7	39.7	48.6	0.37
“ “-RB		0.50	1.32	3.33	5.30	7.32	11.5	17.3	26.8	38.2	51.3	0.31

[1] Cripple wall retrofit of T1-11 siding requires upgraded nailing around perimeter and is not site-dependent according to *FEMA P-1100*.
[2] BF = Bakersfield, SF = San Francisco, NR = Northridge, and SB = San Bernardino; all sites assume V_{S30} = 270 m/sec.
[3] Mean loss at the 250-year return period is a primary loss metric and is referred to as “RC250.”
[4] Expected annual loss expressed in percentage of building replacement cost.

7.7 BASELINE STEM WALL VARIANT SET

The stem wall variant set consists of the same superstructures (i.e., number of stories, exterior and interior materials) as the baseline cripple wall set presented in Section 7.4. The key difference is that the existing (unretrofitted) condition considers the crawlspace vulnerability to be the anchorage of the first-floor framing (e.g., floor joists) to the sill plate on top of the perimeter stem wall. As previously discussed in Chapter 3, the strength of the existing sill plate connection is calculated as a combination of friction and the capacity of existing toe-nail connections. The performance of the stem walls retrofitted in accordance with *FEMA P-1100* retrofit, i.e., with improved sill anchorage, is assumed to be represented by analysis models that assume a rigid base condition, i.e., precluding any failure at the sill plate anchorage.

7.7.1 Modal and Pushover Criteria

The elastic fundamental periods and key pushover analysis metric criteria of the stem wall variants are summarized in Table 7.37. In contrast to the houses with cripple walls, for the stem wall cases the fundamental periods of existing (unretrofitted) and retrofit pairs are identical, which reflects the initially stiff stem wall connection for the existing condition. Notably, the crawlspace to superstructure strength ratios, $(V_{SW}/V_{SS})_{\mathrm{Avg}}$, of the existing (unretrofitted) cases are generally close to or below 1.0 (e.g., occupied story stronger than the existing stem wall connection). The two-story, 1956–1970 era variant with horizontal wood siding (e.g., 2L-W2-G2-SW1) is a notable exception to this, having approximately 37% more strength (on average) in the sill plate connection than the first occupied story.

Table 7.37 Summary of modal and pushover criteria for the baseline stem wall set.

Index [1]	T_1 (sec) [2]	$(V/W_S)_{Avg}$ [3]	$(V/W_{BL})_{Avg}$ [4]	$(V_{SW}/V_{SS})_{Avg}$ [5]
1L-C1-LP-SW1	0.17	0.57	0.57	0.69
1L-C1-LP-RB	0.17	1.39	0.82	N/A
1L-SLP2-LP-SW1	0.14	0.54	0.54	0.55
1L-SLP2-LP-RB	0.14	1.72	1.01	N/A
1L-W2-G2-SW1	0.17	0.66	0.66	1.16
1L-W2-G2-RB	0.17	1.18	0.66	N/A
1L-S2-G2-SW1	0.14	0.67	0.67	0.80
1L-S2-G2-RB	0.14	1.56	0.86	N/A
2L-C1-LP-SW1	0.27	0.41	0.41	0.89
2L-C1-LP-RB	0.27	0.63	0.48	N/A
2L-SLP2-LP-SW1	0.23	0.42	0.42	0.74
2L-SLP2-LP-RB	0.23	0.75	0.57	N/A
2L-W2-G2-SW1	0.27	0.41	0.41	1.37
2L-W2-G2-RB	0.27	0.57	0.41	N/A
2L-S2-G2-SW1	0.23	0.46	0.46	1.02
2L-S2-G2-RB	0.23	0.69	0.51	N/A

[1] Retrofit stem wall cases are represented by variant models on a rigid base with no crawlspace vulnerability.
[2] Elastic fundamental period in seconds.
[3] Average strength to seismic weight ratio from pushover loading proportional to elastic translational mode shape in each direction, seismic weight is the total lateral weight acting in the model.
[4] Average strength to baseline weight ratio from pushover loading proportional to elastic mode shape in each direction, baseline weight is the weight of the dwelling including the first-floor diaphragm and above.
[5] Average crawlspace to first occupied story (superstructure) strength ratio, obtained from story-based pushover curves.

7.7.2 Collapse Performance of Stem Wall Variants

The collapse assessment of houses with stem wall failures are different from ones with cripple wall collapse, in that the stem wall connection failure is not treated as collapse. Instead, the sliding displacements at the stem wall connection are translated into damage measures with increasing repair costs, based on the magnitude of peak displacement between the floor joists and sill plate. In general, all except for one of the existing (unretrofitted) stem wall cases experienced significant slip, which tended to shield (isolate) the superstructure from damage leading to collapse. One exception is the two-story, 1956–1970 era, horizontal wood siding variant (e.g., 2L-W2-G2-SW1), where significant failures occurred in the first story as well as those occurring at the stem wall connection. Response of this case is discussed later. Data and collapse behavior of the rigid base variants, which are considered representative of the retrofitted stem wall condition, were presented previously in the discussion related to data in Table 7.9 through Table 7.12.

The response of the 2L-W2-G2-SW1 variant is shown in Figure 7.38, which illustrates the story drift and stem wall displacement response, conditioned on the non-collapse analyses, for the ground motions at the San Francisco site. The different sub-plots represent the *X*- (left) and *Y*- (right) directions of the house, where the top two plots show SDRs in the first and second story, and the bottom plot shows sliding displacement at the joist-to-sill connection. The figure clearly shows that the controlling failure mechanisms are different in each orthogonal direction. In the *X*-direction, Figure 7.38(e) shows large stem wall displacements developing with increasing ground motion intensity, while the story drift demands of the upper stories remain relatively small. On the other hand, the *Y*-direction demands show that the first-story experiences large drift demands at higher earthquake intensities; see Figure 7.38(d). Due to the assumed configuration of the superstructure, the *Y*-direction has the weaker strength of the two orthogonal directions. This, combined with the lower strength of the wood siding and gypsum wallboard, produced the only existing (unretrofitted) variant with significant collapses.

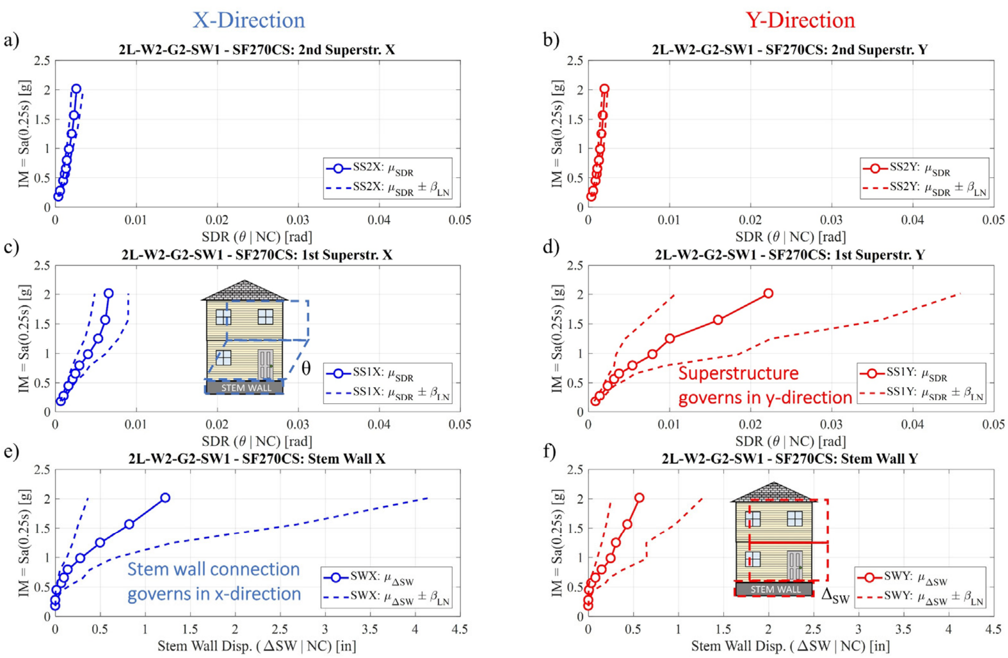

Figure 7.38 **Illustration of story drift and stem wall displacement demand for variant 2L-W2-G2-SW1 that was the only stem wall variant to have mixed failure modes between the stem wall connection and superstructure.**

7.7.3 Loss Assessment Summary for Stem Wall Variants

The general loss assessment observations for existing and retrofitted stem wall variants are discussed by comparing deaggregated losses and trends for key examples. Figure 7.39 compares the deaggregated loss curves and EAL between existing (unretrofitted) and retrofit stem wall variants for one-story, 1956–1970 era, horizontal wood siding variants located in San Francisco. The deaggregation of the loss curve for the existing variant in Figure 7.39(a) reveals that the dominant contributor is damage and repairs to the stem wall connection. The dashed line in Figure

7.39(a) represents the total mean loss curve for the corresponding retrofit (rigid base) case, which is deaggregated into its component parts in Figure 7.39(b). As illustrated in Figure 7.39(a), the existing (unretrofitted) and retrofit loss curves are similar at low intensities before the anchorage capacity of the joist-to-sill connection is reached. As intensity increases, the existing (unretrofitted) loss curve rises above the retrofitted (rigid base) curve, largely due to repair costs associated with the stem wall connection sliding. This general trend is observed for all of the one-story stem wall variants.

In contrast to the one-story cases, the analyses of the two-story stem wall houses indicate that under increasing ground motion intensities, the retrofitted (fixed-base) cases experience larger losses than the existing (unretrofitted) cases. Figure 7.40 compares the deaggregated loss curves and EAL values between existing and retrofitted stem wall conditions for a two-story, pre-1945 era, exterior stucco variant located in San Francisco. As shown in Figure 7.40(a), the existing (unretrofitted) variant has a mean loss curve that is lower than the corresponding retrofit loss curve (dashed line). This occurs because the stem wall repair costs for the existing case, combined with repair costs to other components, are less than repairs of the retrofit (rigid base) condition. Losses to the existing (unretrofitted) stem wall case are limited by sliding of the existing stem wall connection, which shields the first and second stories from damage. In contrast, the retrofitted case shown in Figure 7.40(b) begins to accumulate large losses due to the risk of collapse, beyond spectral accelerations of about 1.0*g*. By 1.5*g*, the risk of collapse accounts for more than 50% of the mean losses. Of course, as with all of the analyses presented here, the calculated response and losses depend on many assumptions, which in this case hinge largely on the assumed consequences and repair costs associated with the sill plate sliding failure of the existing (unretrofitted) condition and the collapse failure of the retrofit condition.

The two-story, 1956–1970 era, horizontal wood siding variant (e.g., 2L-W2-G2-SW1) was the only stem wall variant to have mixed failure modes between global superstructure collapse and stem wall anchorage failure. The deaggregated loss curves for this variant are shown in Figure 7.41 for the San Francisco site. As shown in Figure 7.41(a), the loss curve for the existing (unretrofitted) condition exhibits contributions from both stem wall repairs and collapse costs. In this case, the loss curves for the existing and retrofitted conditions are similar until intensities approaching the 250-year return period (1.0*g*). At higher intensities, the mean loss curves for this variant also drops below the corresponding retrofit case yet to a lesser extent than the other two-story variants.

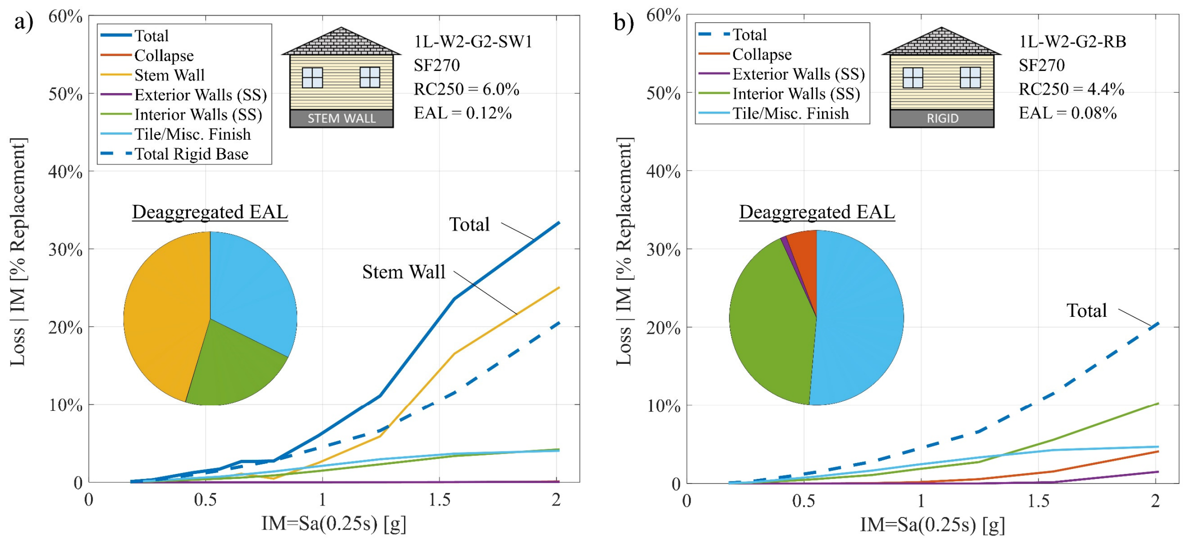

Figure 7.39 Comparing deaggregated mean losses for the one-story, 1956–1970 era stem wall variant with horizontal wood siding for the San Francisco site: (a) existing; and (b) retrofit.

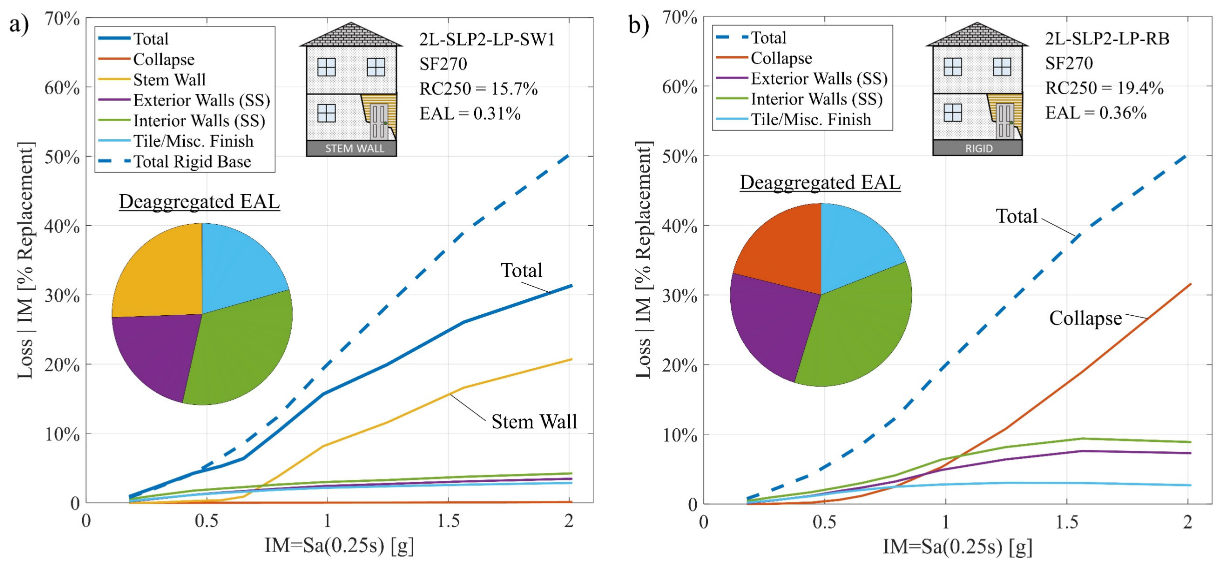

Figure 7.40 Comparing deaggregated mean losses for the two-story, pre-1945 era, stem wall variant with exterior stucco for the San Francisco site: (a) existing; and (b) retrofit.

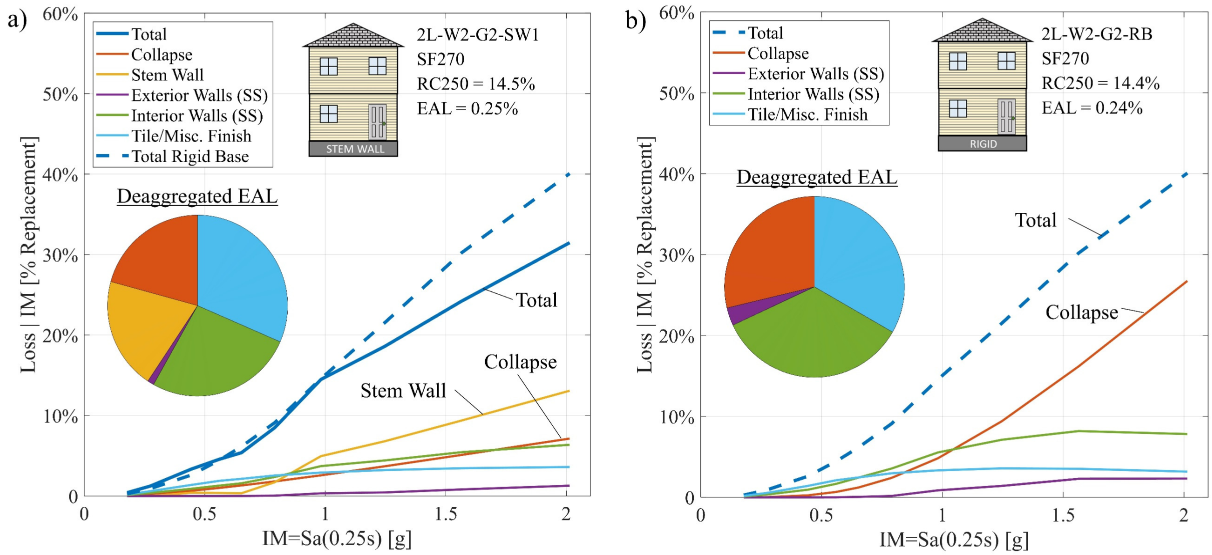

Figure 7.41 Comparing deaggregated mean losses for the two-story, 1956–1970 era, stem-wall variant with horizontal wood siding for the San Francisco site: (a) existing; and (b) retrofit.

The EAL and RC250 loss metrics are summarized for the stem wall variants for all sites in Figure 7.42 and Figure 7.43. Similar to previously described plots for the cripple wall variants, the figures show the retrofit variant (hatched bars) overlaid with the existing (unretrofitted) variant (solid bars). However, for the two-story stem wall variants where the calculated losses for the retrofit condition are larger than the existing (unretrofitted) case, the retrofit case is shown as an empty (white shaded) bar. Following from the trends observed in the loss functions, discussed previously, the EAL and RC250 data indicate that the stem wall retrofit would reduce the loss risk for the one-story variants, but that the retrofit would have little if any benefit (possibly even an adverse effect) for the two-story variants.

Detailed tabulated data for the stem wall variants are summarized for the existing (unretrofitted) and retrofit cases for one- and two-story houses in Table 7.38 and Table 7.39, respectively. The reduced losses, or “benefit,” between existing and retrofit cases is expressed as a positive value to indicate the reduction in loss due to retrofitting. Negative values indicate that the retrofit (rigid-base) condition is calculated to cause an increase in the estimated loss. A summary of mean loss curves and EAL values are provided for the entire stem wall variant set in Table 7.40 and Table 7.41 for pre-1945 and 1956–1970 era variants, respectively.

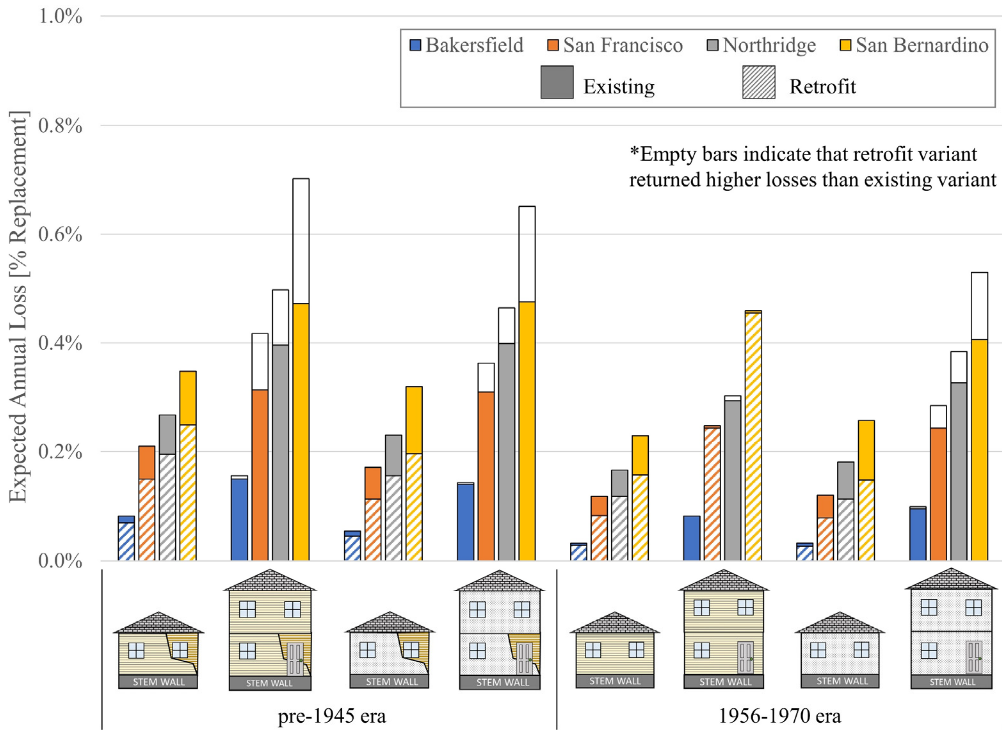

Figure 7.42 Expected annual loss results for baseline stem wall set and all sites.

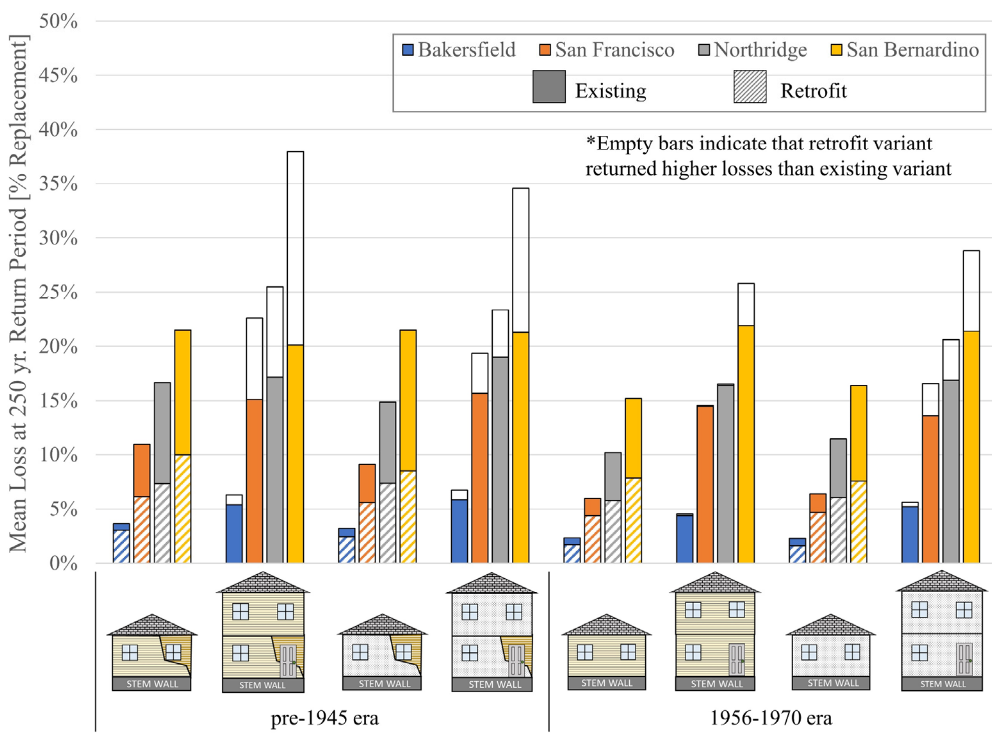

Figure 7.43 Expected loss at the 250-year return period (RC250) results for baseline stem wall set and all sites.

Table 7.38 Summary of primary loss metrics and benefits due to retrofitting for baseline stem wall set: one-story cases.

Description/Index	Site	Condition	EAL (% repl.)	Benefit$_{EAL}$[1] (% repl.)	RC250 (% repl.)	Benefit$_{RC250}$[1] (% repl.)
One-story, pre-1945, wood siding, stem wall. (EX) 1L-C1-LP-SW1 (R) 1L-C1-LP-RB 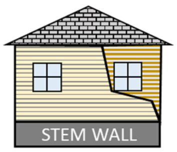	BF 270	Existing	0.082	0.013	3.64	0.6
		Retrofit	0.069		3.04	
	SF 270	Existing	0.210	0.060	10.98	4.9
		Retrofit	0.149		6.11	
	NR 270	Existing	0.268	0.073	16.65	9.3
		Retrofit	0.195		7.32	
	SB 270	Existing	0.348	0.098	21.50	11.6
		Retrofit	0.250		9.95	
One-story, pre-1945, stucco, stem wall. (EX) 1L-SLP2-SW1 (R) 1L-SLP2-LP-RB 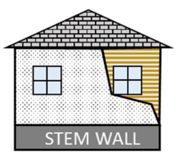	BF 270	Existing	0.054	0.009	3.20	0.8
		Retrofit	0.045		2.43	
	SF 270	Existing	0.171	0.058	9.10	3.5
		Retrofit	0.113		5.58	
	NR 270	Existing	0.231	0.075	14.89	7.5
		Retrofit	0.156		7.35	
	SB 270	Existing	0.320	0.124	21.49	13.0
		Retrofit	0.196		8.50	
One-story, 1956–1970, wood siding, stem wall. (EX) 1L-W2-G2-SW1 (R) 1L-W2-G2-RB 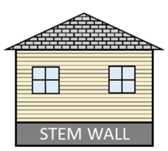	BF 270	Existing	0.033	0.005	2.33	0.6
		Retrofit	0.028		1.70	
	SF 270	Existing	0.118	0.035	5.96	1.6
		Retrofit	0.082		4.38	
	NR 270	Existing	0.166	0.048	10.24	4.5
		Retrofit	0.119		5.76	
	SB 270	Existing	0.230	0.073	15.21	7.4
		Retrofit	0.157		7.85	
One-story, 1956–1970, stucco, stem wall. (EX) 1L-S2-G2-SW1 (R) 1L-S2-G2-RB 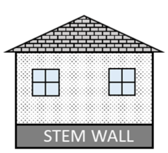	BF 270	Existing	0.032	0.006	2.28	0.7
		Retrofit	0.027		1.62	
	SF 270	Existing	0.120	0.042	6.39	1.7
		Retrofit	0.078		4.67	
	NR 270	Existing	0.181	0.068	11.49	5.4
		Retrofit	0.113		6.05	
	SB 270	Existing	0.258	0.110	16.40	8.8
		Retrofit	0.148		7.56	

[1] Benefits are the difference of the retrofit (R) and existing (unretrofitted) variant (EX), negative indicates lack of benefit

Table 7.39 Summary of primary loss metrics and benefits due to retrofitting for baseline stem wall set: two-story cases.

Description/Index	Site	Condition	EAL (% repl.)	Benefit$_{EAL}$[1] (% repl.)	RC250 (% repl.)	Benefit$_{RC250}$[1] (% repl.)
Two-story, pre-1945, wood siding, stem wall. (EX) 2L-C1-LP-SW1 (R) 2L-C1-LP-RB	BF 270	Existing	0.150	-0.006	5.38	-0.9
		Retrofit	0.156		6.29	
	SF 270	Existing	0.314	-0.104	15.12	-7.5
		Retrofit	0.417		22.59	
	NR 270	Existing	0.396	-0.102	17.17	-8.3
		Retrofit	0.498		25.51	
	SB 270	Existing	0.472	-0.230	20.10	-17.8
		Retrofit	0.702		37.92	
Two-story, pre-1945, stucco, stem wall. (EX) 2L-SLP2-LP-SW1 (R) 2L-SLP2-LP-RB	BF 270	Existing	0.140	-0.003	5.85	-0.9
		Retrofit	0.143		6.72	
	SF 270	Existing	0.310	-0.054	15.68	-3.7
		Retrofit	0.363		19.37	
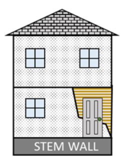	NR 270	Existing	0.399	-0.065	19.01	-4.3
		Retrofit	0.464		23.34	
	SB 270	Existing	0.475	-0.176	21.27	-13.3
		Retrofit	0.651		34.54	
Two-story, 1956–1970, wood siding, stem wall. (EX) 2L-W2-G2-SW1 (R) 2L-W2-G2-RB	BF 270	Existing	0.082	0.000	4.39	-0.2
		Retrofit	0.082		4.54	
	SF 270	Existing	0.248	0.004	14.49	-0.1
		Retrofit	0.244		14.59	
	NR 270	Existing	0.294	-0.008	16.45	-0.1
		Retrofit	0.303		16.53	
	SB 270	Existing	0.459	0.004	21.92	-3.9
		Retrofit	0.455		25.80	
Two-story, 1956–1970, stucco, stem wall. (EX) 2L-S2-G2-SW1 (R) 2L-S2-G2-RB	BF 270	Existing	0.095	-0.004	5.19	-0.4
		Retrofit	0.099		5.61	
	SF 270	Existing	0.244	-0.041	13.62	-3.0
		Retrofit	0.285		16.57	
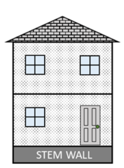	NR 270	Existing	0.327	-0.057	16.88	-3.7
		Retrofit	0.384		20.60	
	SB 270	Existing	0.406	-0.124	21.36	-7.5
		Retrofit	0.530		28.82	

[1] Benefits are the difference of the retrofit (R) and existing (unretrofitted) variant (EX), negative indicates lack of benefit.

Table 7.40 Loss assessment summary for baseline stem wall set: pre-1945 era.

Index	Site [2]	Mean loss at return period (% of replacement cost)										EAL[3] (%)
		15	25	50	75	100	150	250 [2]	500	1000	2500	
1L-C1-LP-SW1	BF 270	0.22	0.48	0.98	1.49	1.71	2.30	3.64	4.44	8.75	18.9	0.08
1L-C1-LP -RB		0.20	0.44	0.80	1.38	1.64	2.15	3.04	4.61	6.35	9.9	0.07
1L-C1-LP-SW1	SF 270	0.55	1.10	2.56	2.87	3.62	4.81	11.0	17.7	29.1	37.5	0.21
1L-C1-LP -RB		0.46	0.95	2.03	2.72	3.54	4.24	6.11	8.74	13.3	23.9	0.15
1L-C1-LP-SW1	NR 270	0.75	1.37	2.71	4.16	5.01	8.55	16.7	22.2	31.3	39.1	0.27
1L-C1-LP -RB		0.66	1.32	2.64	3.64	4.28	5.59	7.30	11.0	17.3	29.0	0.19
1L-C1-LP-SW1	SB 270	0.93	1.59	3.40	4.58	8.01	14.3	21.5	31.9	37.1	42.1	0.35
1L-C1-LP -RB		0.80	1.55	3.01	4.35	5.29	6.67	9.95	17.7	27.4	41.8	0.25
1L-SLP2-LP-SW1	BF 270	0.11	0.18	0.47	0.80	1.27	1.78	3.20	3.75	7.09	17.2	0.05
1L-SLP2-LP -RB		0.08	0.16	0.43	0.76	1.09	1.53	2.43	3.99	6.11	9.5	0.04
1L-SLP2-LP-SW1	SF 270	0.23	0.55	1.67	2.75	3.69	4.70	9.10	16.8	29.7	39.0	0.17
1L-SLP2-LP -RB		0.17	0.51	1.41	2.11	2.98	3.96	5.58	8.27	12.5	19.7	0.11
1L-SLP2-LP-SW1	NR 270	0.34	0.79	2.44	4.43	4.18	6.99	14.9	22.5	31.4	41.0	0.23
1L-SLP2-LP -RB		0.33	0.81	2.05	3.03	4.07	5.35	7.40	10.4	15.1	23.5	0.16
1L-SLP2-LP-SW1	SB 270	0.49	1.07	3.36	4.26	6.79	13.8	21.5	31.9	39.1	46.0	0.32
1L-SLP2-LP -RB		0.43	1.02	2.53	3.73	4.69	6.25	8.5	14.0	20.6	34.0	0.20
2L-C1-LP-SW1	BF 270	0.63	1.01	2.06	2.82	3.37	4.34	5.38	7.61	13.3	17.6	0.15
2L-C1-LP-RB		0.54	0.90	1.94	2.72	3.19	4.45	6.29	9.95	16.7	28.3	0.16
2L-C1-LP-SW1	SF 270	1.17	2.14	4.37	5.10	6.17	9.69	15.1	19.6	24.0	30.5	0.31
2L-C1-LP-RB		1.04	2.05	4.67	7.36	9.91	14.6	22.6	32.7	44.7	57.3	0.42
2L-C1-LP-SW1	NR 270	1.54	2.77	5.54	7.64	9.87	12.3	17.2	21.6	25.6	30.3	0.40
2L-C1-LP-RB		1.43	2.72	5.77	9.59	12.0	17.4	25.5	35.7	46.1	58.6	0.50
2L-C1-LP-SW1	SB 270	1.95	3.48	5.76	9.08	12.1	16.9	20.1	26.0	28.6	33.3	0.47
2L-C1-LP-RB		1.79	3.40	7.86	13.1	18.3	27.5	37.9	53.1	66.5	79.0	0.70
2L-SLP2-LP-SW1	BF 270	0.37	0.80	1.96	2.89	3.5	4.53	5.85	8.13	13.5	18.6	0.14
2L-SLP2-LP-RB		0.28	0.67	1.75	2.69	3.51	4.64	6.72	10.6	16.3	26.7	0.14
2L-SLP2-LP-SW1	SF 270	0.89	2.07	4.25	5.28	6.38	10.2	15.7	19.9	26.1	31.4	0.31
2L-SLP2-LP-RB		0.76	1.90	4.21	6.56	8.56	12.3	19.4	28.4	39.0	50.6	0.36
2L-SLP2-LP-SW1	NR 270	1.30	2.88	5.41	7.55	9.43	12.6	19.0	22.8	28.4	32.9	0.40
2L-SLP2-LP-RB		1.17	2.64	5.76	8.41	10.8	15.4	23.3	34.0	44.5	57.8	0.46
2L-SLP2-LP-SW1	SB 270	1.7	3.44	5.83	8.66	12.8	16.8	21.3	27.6	33.3	35.6	0.48
2L-SLP2-LP-RB		1.52	3.43	7.59	12.3	17.1	25.1	34.5	47.6	59.6	71.9	0.65

[1] BF = Bakersfield, SF = San Francisco, NR = Northridge, and SB = San Bernardino.
[2] Mean loss at the 250-year return period is also referred to as "RC250."
[3] Expected annual loss expressed in percentage of building replacement cost.

Table 7.41 Loss assessment summary for baseline stem wall set: 1956–1970 era.

Index	Site[2]	Mean loss at return period (% of replacement cost)										EAL[3] (%)
		15	25	50	75	100	150	250[2]	500	1000	2500	
1L-W2-G2-SW1	BF 270	0.02	0.07	0.22	0.50	0.65	1.10	2.33	2.92	4.98	12.5	0.03
1L-W2-G2 RB		0.02	0.07	0.20	0.42	0.58	1.03	1.70	3.03	4.68	8.77	0.03
1L-W2-G2-SW1	SF 270	0.09	0.31	1.22	1.69	2.65	2.71	5.96	11.1	23.6	33.5	0.12
1L-W2-G2 RB		0.06	0.25	0.96	1.49	2.01	2.78	4.38	6.60	11.5	20.6	0.08
1L-W2-G2-SW1	NR 270	0.16	0.47	1.62	2.70	2.83	4.92	10.2	18.6	26.8	36.0	0.17
1L-W2-G2 RB		0.14	0.46	1.33	2.20	2.80	3.92	5.80	10.3	15.8	25.5	0.12
1L-W2-G2-SW1	SB 270	0.23	0.58	2.04	3.53	4.22	10.2	15.2	25.0	33.4	41.7	0.23
1L-W2-G2 RB		0.21	0.56	1.59	2.77	3.53	4.75	7.85	14.8	23.4	36.2	0.16
1L-S2-G2-SW1	BF 270	0.03	0.06	0.2	0.38	0.58	0.93	2.28	3.05	5.52	13.1	0.03
1L-S2-G2 -RB		0.02	0.05	0.17	0.34	0.55	0.92	1.62	2.97	4.85	8.44	0.03
1L-S2-G2-SW1	SF 270	0.07	0.22	0.87	1.97	2.97	2.91	6.39	12.0	26.7	37.1	0.12
1L-S2-G2 -RB		0.05	0.21	0.78	1.32	2.17	2.67	4.67	7.06	11.5	18.8	0.08
1L-S2-G2-SW1	NR 270	0.16	0.42	1.78	3.10	3.34	5.16	11.5	20.0	31.0	39.2	0.18
1L-S2-G2 -RB		0.12	0.42	1.19	2.12	2.91	4.24	6.1	9.4	14.7	23.0	0.11
1L-S2-G2-SW1	SB 270	0.20	0.54	2.66	4.12	5.97	11.7	16.4	26.4	36.7	44.4	0.26
1L-S2-G2 -RB		0.18	0.53	1.53	2.75	3.56	5.14	7.56	13.3	20.1	31.6	0.15
2L-W2-G2-SW1	BF 270	0.11	0.29	0.9	1.48	2.04	2.96	4.39	6.56	10.4	17.0	0.08
2L-W2-G2-RB		0.09	0.24	0.81	1.37	1.87	2.85	4.54	7.53	12.2	19.3	0.08
2L-W2-G2-SW1	SF 270	0.42	1.23	3.35	4.56	5.38	8.49	14.5	18.6	24.2	31.5	0.25
2L-W2-G2-RB		0.28	0.91	2.61	4.45	6.15	9.11	14.6	21.5	30.2	40.1	0.24
2L-W2-G2-SW1	NR 270	0.60	1.50	3.73	6.00	7.54	10.7	16.5	20.9	25.7	32.9	0.29
2L-W2-G2-RB		0.52	1.35	3.68	6.29	7.91	11.5	16.5	22.7	30.0	39.0	0.30
2L-W2-G2-SW1	SB 270	1.37	2.88	5.95	8.95	11.9	17.1	21.9	28.4	34.4	37.7	0.46
2L-W2-G2-RB		0.74	1.84	5.17	8.49	12.0	18.3	25.8	37.2	48.5	61.2	0.45
2L-S2-G2-SW1	BF 270	0.09	0.34	1.13	1.87	2.54	3.75	5.19	7.30	11.2	17.4	0.10
2L-S2-G2-RB		0.08	0.31	0.99	1.72	2.43	3.68	5.61	8.89	13.7	22.5	0.10
2L-S2-G2-SW1	SF 270	0.42	1.26	3.26	4.54	5.53	8.48	13.6	17.3	25.5	30.7	0.24
2L-S2-G2-RB		0.33	1.17	3.16	5.27	6.99	10.2	16.6	24.6	34.8	46.1	0.28
2L-S2-G2-SW1	NR 270	0.70	1.88	4.62	6.51	8.26	11.4	16.9	20.9	26.9	32.9	0.33
2L-S2-G2-RB		0.59	1.72	4.72	7.33	9.64	14.2	20.6	31.1	41.1	53.4	0.38
2L-S2-G2-SW1	SB 270	0.97	2.37	5.14	8.11	11.1	15.4	21.4	26.2	33.0	34.7	0.41
2L-S2-G2-RB		0.87	2.33	6.49	10.3	14.4	21.5	28.8	40.9	52.0	64.2	0.53

[1] BF = Bakersfield, SF = San Francisco, NR = Northridge, and SB = San Bernardino.
[2] Mean loss at the 250-year return period is also referred to as "RC250."
[3] Expected annual loss expressed in percentage of building replacement cost.

7.8 INFLUENCE OF MATERIAL ASSUMPTIONS ON PERFORMANCE RESULTS

This section presents the results of studies that were conducted to assess the sensitivity of the structural analysis and loss results to the material properties used in the nonlinear structural analyses. Each study is briefly described in terms of the variable considered and the effects it has on the loss assessment results in comparison with the baseline models presented earlier in the chapter. All models are analyzed for the San Francisco site only.

7.8.1 Influence of Roof Weight and Stucco Strength on Superstructure Response

The influence of increasing the roof weight and the strength and stiffness of the exterior stucco and interior gypsum wallboard are investigated for the rigid base variants for the 1956–1970 construction era. The increased roof weight corresponds to a change to concrete tile roofing from the asphalt composition shingle roofing used for baseline building variants. The roof weight including concrete tile is 20.5 psf, which is 57% higher than the 13.0 psf assumed for asphalt shingle roofing. The exterior wall material S3 has a 20% larger initial stiffness and peak strength, as compared to the best estimate material S2 that was used for baseline variants. A comparison of the normalized material backbone curves for S3 and S2 is provided in Figure 7.44. The influence of the increased material strength and roof weight were analyzed separately and in a combined case for both one- and two-story variants. The resulting mean loss curves and metrics are provided in Figure 7.45 and Figure 7.46 for one- and two-story variants, respectively. A summary of the modal, collapse, and loss criteria are provided for this sub-set of building variants in Table 7.42.

Referring to the green and blue curves in Figure 7.45 and Figure 7.46, the 20% increase in wall strength and stiffness leads to about a 20% to 30% decrease in the losses (measured by EAL and RC250). Comparing the corresponding pairs of solid and dashed lines, the 57% increase (7.5 psf) in roof weight leads to about a two-fold increase in losses for the one-story houses and 1.5 times increase for the two-story houses.

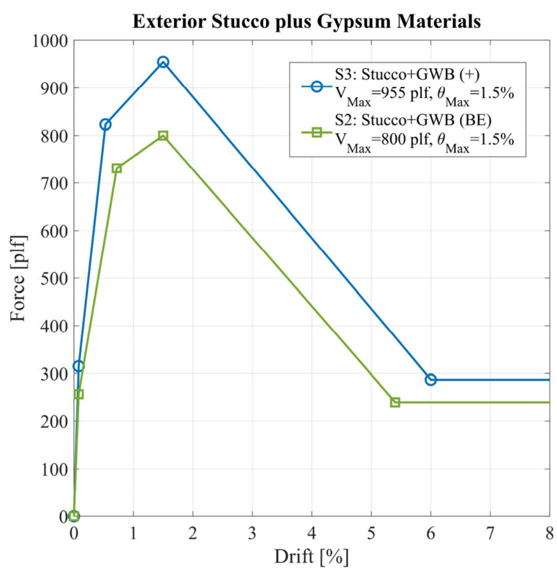

Figure 7.44 **Exterior stucco plus gypsum material backbones: S2 is best estimate (squares), and S3 has a 20% increase in initial stiffness and strength (circles).**

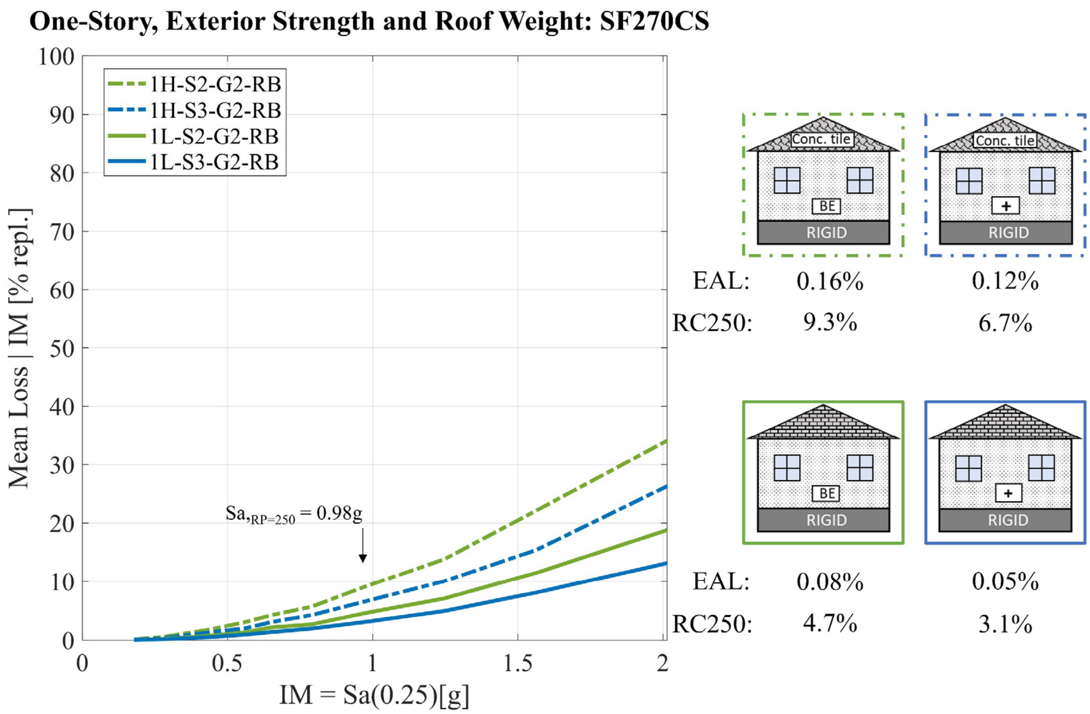

Figure 7.45 Influence of exterior stucco wall strength and roof weight on the one-story, 1956–1970 era, rigid-base variants for the San Francisco site.

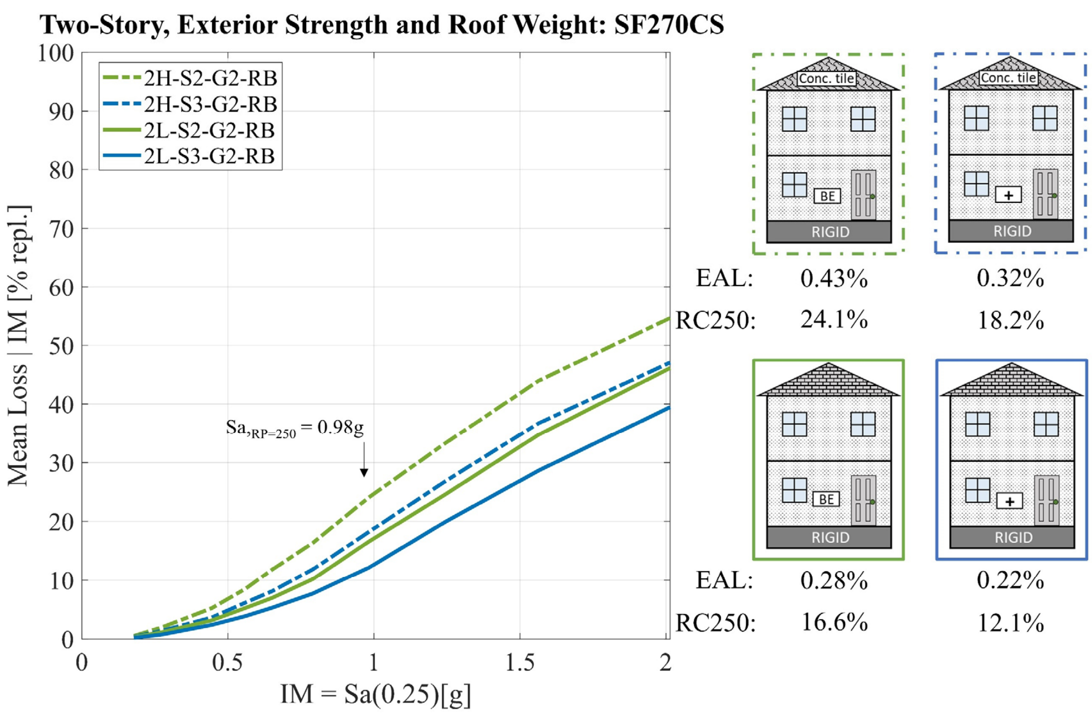

Figure 7.46 Influence of exterior stucco wall strength and roof weight on the two-story, 1956–1970 era, rigid-base variants for the San Francisco site.

Table 7.42 Summary for 1956–1970 era stucco rigid base variants with variations in exterior wall strength and roof weight for the San Francisco site.

Index [1]	T_1 (sec)[2]	$(V/W_S)_{Avg}$[3]	$(V_{CW}/V_{SS})_{Avg}$[4]	P[C|RP_{250}][5]	P[C|MCE][6]	RC250[7]	EAL[8]
1L-S2-G2-RB*	0.14	1.56	0.86	0.044%	1.6%	4.7%	0.08%
1L-**S3**-G2-RB	0.13	1.76	0.97	0.026%	1.0%	3.1%	0.05%
1**H**-S2-G2-RB	0.16	1.16	0.72	0.32%	5.0%	9.3%	0.16%
1**H**-**S3**-G2-RB	0.15	1.30	0.81	0.16%	3.0%	6.7%	0.12%
2L-S2-G2-RB*	0.23	0.69	0.51	4.1%	23.1%	16.6%	0.28%
2L-**S3**-G2-RB	0.21	0.78	0.57	2.7%	16.5%	12.1%	0.22%
2**H**-S2-G2-RB	0.25	0.57	0.44	9.4%	32.7%	24.1%	0.43%
2**H**-**S3**-G2-RB	0.24	0.64	0.49	5.4%	24.1%	18.2%	0.32%

[1] Indices with an asterisk indicate best estimate models, sub-indices in bold reflect changes from the best estimate assumptions
[2] Elastic fundamental period in seconds.
[3] Average strength to seismic weight ratio from pushover loading proportional to elastic translational mode shape in each direction, seismic weight is the total lateral weight acting in the model.
[4] Average crawlspace to first occupied story (superstructure) strength ratio, obtained from story-based pushover curves.
[5] Probability of collapse at 250-year return period (RP_{250}).
[6] Probability of collapse at the MCE with intensity determined by nominal S_{DS} for site scaled by a factor of 1.5.
[7] Mean loss at the 250-year return period in percentage of replacement cost.
[8] Expected annual loss expressed in percentage of building replacement cost.

7.8.2 Influence of Retrofit Strength for 2-ft-Tall Cripple Walls

The influence of the wood structural panel (WSP) material strength, used for the seismic retrofit, in combination with the existing (unretrofitted) wood siding or stucco cripple wall material is investigated for the one-story, 1956–1970 era, 2-ft-tall cripple wall houses. Specifically, the study is intended to quantify the effect of nail spacing for the retrofit WSP. The best estimate retrofit materials used in the baseline cases is based on cripple wall retrofit tests by WG4 with WSP nailing of 8d at 3 in. Since the "Light" weight classification of *FEMA P-1100* specifies 8d at 4-in. edge nailing for WSP, the sensitivity to nail spacing is relevant to loss results for variants with this weight classification. Moreover, the sensitivity to nailing can be considered as relevant to the variability in the retrofit properties.

Background on development of the material strengths is discussed in Chapter 3. A comparison of the best estimate retrofit materials (i.e., based on recent testing with 8d at 3 in. nailing) and reduced strength materials to roughly reflect 8d at 4-in. spacing is shown in Figure 7.47. The stucco plus WSP material has a strength reduction of approximately 22% between the best estimate (CW2-S-R2) and reduced strength (CW2-S-R1) materials. The horizontal wood siding plus WSP material has a strength reduction of approximately 30% between the best estimate (CW2-HS-R2) and reduced strength (CW2-HS-R1) materials. Note that in general these material strength reductions are considered to investigate the sensitivity of retrofit strength reduction, and do not necessarily reflect the actual strength of retrofits according to *FEMA P-1100* with 8d at 4 in. nailing, as supported by recent testing; see Chapter 3 for discussion.

The mean loss curves and loss metrics for the variants with the best estimate and reduced retrofit strengths are provided in Figure 7.48. Comparing the EAL and RC250 losses for the retrofit cases with different nail spacings, the 22% reduction in wall strength translates to about a 10% to 15% increase in the losses. A summary of the modal, collapse, and loss criteria are provided for this set of building variants in Table 7.43.

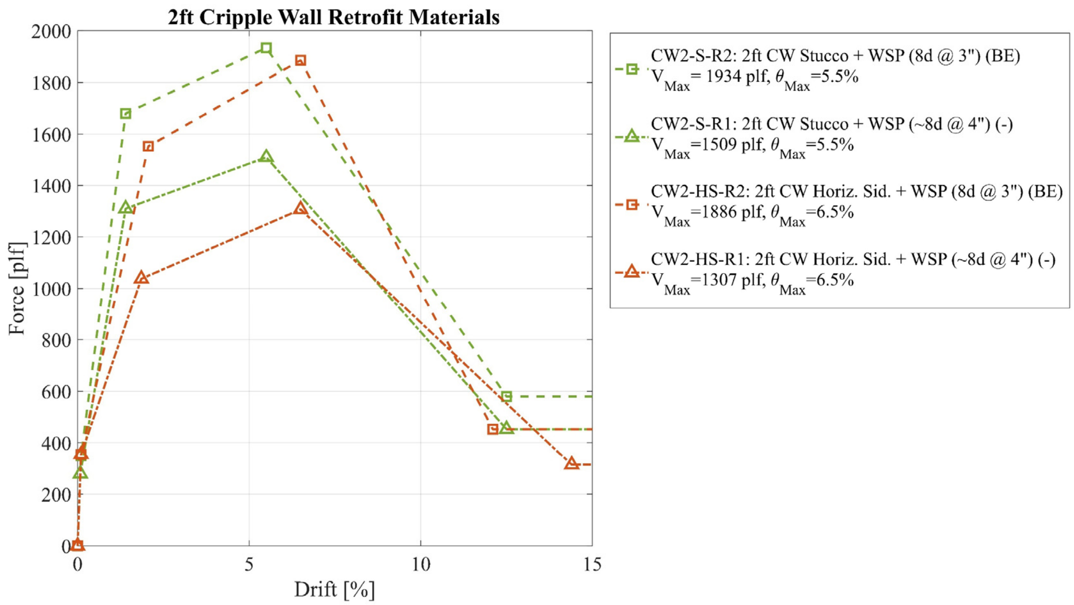

Figure 7.47 The 2-ft-tall cripple wall retrofit materials with stucco and horizontal wood siding: best estimate materials are based on testing with 8d @ 3 in. nailing (squares), reduced materials are approximated to reflect a reduction in strength based on 8d @ 4 n. nailing (triangles).

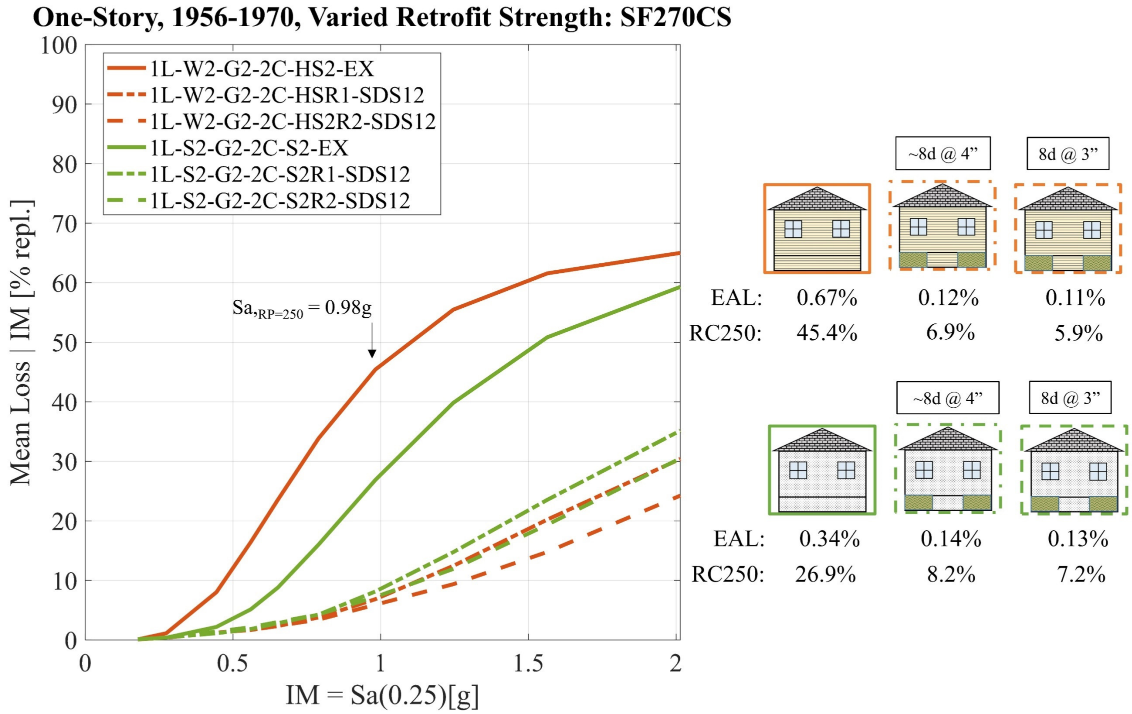

Figure 7.48 Influence of cripple wall retrofit material strength on the one-story, 1956–1970 era, 2-ft-tall cripple wall variants for the San Francisco site.

Table 7.43 Summary for the one-story, 1956–1970 era, 2-ft-tall cripple wall variants with variations in retrofit material strength for the San Francisco site.

Index [1]	T_1 (sec)[2]	$(V/W_S)_{Avg}$[3]	$(V_{CW}/V_{SS})_{Avg}$[4]	P[C|RP250][5]	P[C|MCE][6]	RC250[7]	EAL[8]
1L-W2-G2-2C-HS2-EX*	0.23	0.47	0.72	64.9%	95.1%	45.4%	0.67%
" "-2C-HS**R1**-SDS12	0.18	0.79	1.36	3.5%	25.9%	6.9%	0.12%
" "-2C-HSR2-SDS12*	0.18	0.79	1.93	0.4%	5.6%	5.9%	0.11%
1L-S2-G2-2C-S2-EX*	0.16	0.57	0.68	32.5%	80.7%	26.9%	0.34%
" "-2C-S2**R1**-SDS12	0.16	0.96	1.16	4.8%	32.3%	8.2%	0.14%
" "-2C-S2R2-SDS12*	0.16	1.03	1.38	0.5%	12.1%	7.2%	0.13%

[1] Indices with an asterisk indicate best estimate models, sub-indices in bold reflect changes from the best estimate assumptions
[2] Elastic fundamental period in seconds.
[3] Average strength to seismic weight ratio from pushover loading proportional to elastic translational mode shape in each direction, seismic weight is the total lateral weight acting in the model.
[4] Average crawlspace to first occupied story (superstructure) strength ratio, obtained from story-based pushover curves.
[5] Probability of collapse at 250-year return period (RP_{250}).
[6] Probability of collapse at the MCE with intensity determined by nominal S_{DS} for site scaled by a factor of 1.5.
[7] Mean loss at the 250-year return period in percentage of replacement cost.
[8] Expected annual loss expressed in percentage of building replacement cost.

7.8.3 Material Properties for Existing 2-Ft-Tall Stucco Cripple Walls

The influence of assumed 2-ft-tall cripple wall stucco properties is investigated to illustrate the sensitivity of loss estimates to the existing (unretrofitted) cripple wall material. The sensitivity is evaluated for one-story, 1956–1970 era building variants with stucco exterior, both with and without retrofit. Material properties were varied to reflect a range conditions that were simulated through interpretations of the available experimental data; see Chapter 3 for further discussion. The normalized material backbone curves for three alternative models of existing 2-ft-tall stucco cripple walls are presented in Figure 7.49. The materials are varied by a 36% increase (CW2-S3) and a 32% reduction (CW2-S1) in peak strength with respect to the best estimate properties (CW2-S2). The stucco material is applicable both to the existing (unretrofitted) and retrofit case, where for the retrofit case the modified material is applied over the length of the cripple wall outside of the retrofitted region. To give a range of performance values, the weaker stucco strength case (i.e., assuming material CW2-S1) is coupled with the reduced retrofit material strength (CW2-S-R1) that was described in Section 7.8.2. Further, the stronger cripple wall stucco strength case assumes the stronger stucco plus gypsum exterior wall material (S3) in the superstructure (see Section 7.8.1).

The mean loss curves and metrics for these variants are illustrated in Figure 7.50. In general, the trends are as expected, where the losses reduce with stronger, stiffer walls and increase with weaker, less stiff walls, however, the relative changes are much larger for the existing (unretrofitted) as compared to the retrofit cases. For the existing cases, the 32% reduction in strength increases the EAL and RC250 losses by 80% to 130%, and the 36% increase in strength reduces the losses by about 50%. This suggests that losses in existing (unretrofitted) houses with deteriorated walls can be much more vulnerable than reflected by the best estimate model, and correspondingly that the economic benefits of cripple wall retrofit would be even larger. For the retrofit cases, the increase and decrease in losses were roughly proportional to the change in wall strengths, where the 32% reduction in wall strength resulted in loss increases of 20% to 40%, and the 36% increase in wall strength reduced the losses by about 30%. A summary of the modal, collapse, and loss criteria are provided for this sub-set of building variants in Table 7.44.

An additional set of material variations for one-story 2-ft-tall cripple walls includes variation of cripple wall strength, superstructure strength and roof weight. This sub-set of variants compliments the one-story rigid base variants presented in Section 7.8.1 and Figure 7.45. Superstructure and cripple wall stucco strengths are increased from best estimate properties (e.g., changed to S3 and CW2-S3), and the addition of concrete tile roof weight is assumed. The retrofit cases consider the different weight class for assuming a concrete tile roof (e.g., moving from “Light” to “Medium”), although per the *FEMA P-1100* plan sets, the change in classification does not require a change in the WSP braced length for the San Francisco seismicity and geometry of the archetype buildings. An average loss comparison of best estimate and increased existing material strength variants, with and without additional weight due to concrete tile roofing is shown in Figure 7.51. In general, the change in losses as a function of these variables are of similar amounts to those described previously for the other sensitivity studies. A summary of the modal, collapse, and loss criteria are provided for this sub-set of building variants in Table 7.45.

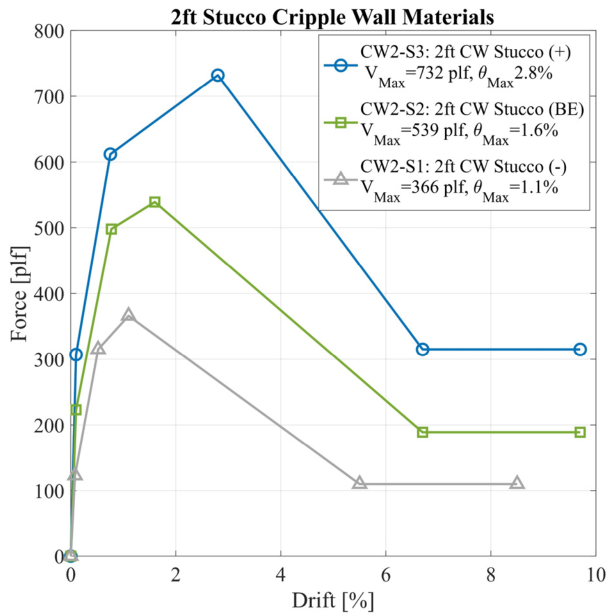

Figure 7.49 **Existing 2-ft-tall cripple wall stucco material backbones: CW2-S2 is best estimate (squares), CW2-S3 has a 36% increase in strength (circles), and CW2-S1 has a 32% reduction in strength (triangles).**

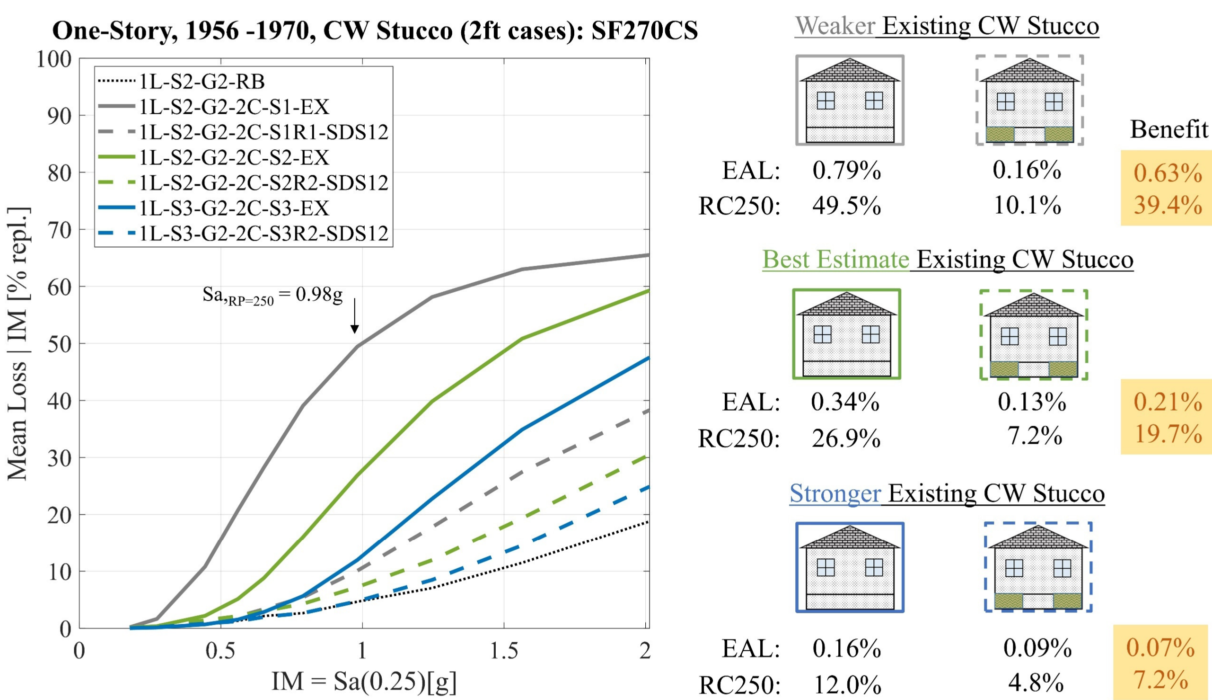

Figure 7.50 **Influence of different existing (unretrofitted) cripple wall strength properties on the loss assessment of the one-story, 1956–1970 era, 2-ft-tall cripple wall variants for the San Francisco site.**

Table 7.44 Summary for the one-story, 1956–1970 era, 2-ft-tall cripple wall variants with variations in cripple wall stucco strength for the San Francisco site.

Index [1]	T_1 (sec)[2]	$(V/W_S)_{Avg}$[3]	$(V_{CW}/V_{SS})_{Avg}$[4]	P[C|RP$_{250}$][5]	P[C|MCE][6]	RC250[7]	EAL[8]
1L-S2-G2-2C-**S1**-EX	0.18	0.39	0.46	71.3%	96.4%	49.5%	0.79%
" "-2C-**S1R1**-SDS12	0.16	0.84	1.02	4.8%	32.3%	10.1%	0.16%
1L-S2-G2-2C-S2-EX *	0.16	0.57	0.68	32.5%	80.7%	26.9%	0.34%
" "-2C-S2R2-SDS12*	0.16	1.03	1.38	0.5%	12.1%	7.2%	0.13%
1L-**S3**-G2-2C-**S3**-EX	0.15	0.77	0.82	11.6%	54.8%	12.0%	0.16%
" "-2C-**S3**R2-SDS12	0.15	1.16	1.37	0.3%	10.5%	4.8%	0.09%

[1] Indices with an asterisk indicate best estimate models, sub-indices in bold reflect changes from the best estimate assumptions
[2] Elastic fundamental period in seconds.
[3] Average strength to seismic weight ratio from pushover loading proportional to elastic translational mode shape in each direction, seismic weight is the total lateral weight acting in the model.
[4] Average crawlspace to first occupied story (superstructure) strength ratio, obtained from story-based pushover curves.
[5] Probability of collapse at 250-year return period (RP$_{250}$).
[6] Probability of collapse at the MCE with intensity determined by nominal S_{DS} for site scaled by a factor of 1.5.
[7] Mean loss at the 250-year return period in percentage of replacement cost.
[8] Expected annual loss expressed in percentage of building replacement cost.

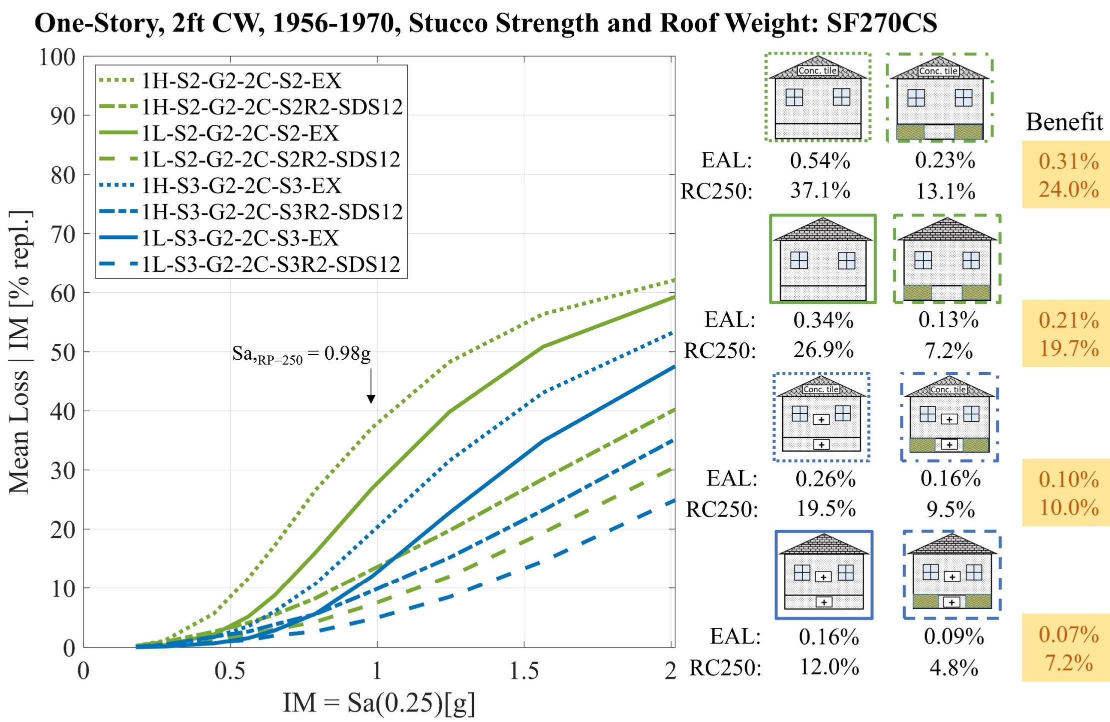

Figure 7.51 Influence of exterior stucco wall strength and roof weight on the loss assessment of the one-story, 1956–1970 era, 2-ft-tall cripple wall variants for the San Francisco site.

Table 7.45 Summary for the one-story, 1956–1970 era, 2-ft-tall cripple wall variants with variations in stucco strength and roof weight for the San Francisco site.

Index [1]	T_1 (sec)[2]	$(V/W_S)_{Avg}$[3]	$(V_{CW}/V_{SS})_{Avg}$[4]	P[C|RP$_{250}$][5]	P[C|MCE][6]	RC250[7]	EAL[8]
1L-S2-G2-2C-S2-EX*	0.16	0.57	0.68	32.5%	80.7%	26.9%	0.34%
" "-2C-S2R2-SDS12*	0.16	1.03	1.38	0.5%	12.1%	7.2%	0.13%
1**H**-S2-G2-2C-S2-EX	0.19	0.48	0.68	47.0%	87.0%	37.1%	0.54%
" "-2C-S2R2-SDS12	0.18	0.86	1.39	1.7%	16.1%	13.1%	0.23%
1L-**S3**-G2-2C-**S3**-EX	0.15	0.77	0.82	11.6%	54.8%	12.0%	0.16%
" "-2C-**S3**R2-SDS12	0.15	1.16	1.37	0.3%	10.5%	4.8%	0.09%
1**H**-**S3**-G2-2C-**S3**-EX	0.17	0.64	0.81	19.1%	66.2%	19.5%	0.26%
" "-2C-**S3**R2-SDS12	0.17	0.97	1.37	1.1%	16.3%	9.5%	0.16%

[1] Indices with an asterisk indicate best estimate models, sub-indices in bold reflect changes from the best estimate assumptions
[2] Elastic fundamental period in seconds.
[3] Average strength to seismic weight ratio from pushover loading proportional to elastic translational mode shape in each direction, seismic weight is the total lateral weight acting in the model.
[4] Average crawlspace to first occupied story (superstructure) strength ratio, obtained from story-based pushover curves.
[5] Probability of collapse at 250-year return period (RP$_{250}$).
[6] Probability of collapse at the MCE with intensity determined by nominal S_{DS} for site scaled by a factor of 1.5.
[7] Mean loss at the 250-year return period in percentage of replacement cost.
[8] Expected annual loss expressed in percentage of building replacement cost.

7.8.4 Influence of Braced and Unbraced Horizontal Wood Siding

The material assumed for wood siding cripple walls within the best estimate variants reflects some additional strength, beyond the bare siding, associated with some incidental diagonal bracing within the framing of the cripple wall; see Chapter 3. This material was based on review of full height walls tested with different bracing configurations and represents a judgment-based increase from pure unbraced horizontal wood siding that was tested by WG4. This assumption was influenced by review of photographic documentation, which showed examples of incidental bracing in existing (unretrofitted) houses, and discussion with PEER Team Members.

A comparison of the material properties for horizontal wood siding cripple walls without any bracing (CW-HS1) and including some bracing contribution (CW-HS2) is shown in Figure 7.52. The wood siding with bracing has about twice the strength as compared to the siding-only case yet with one half the displacement capacity and a steep post-peak failure slope. The influence of these two material properties is investigated with one-story, 1956–1970 era, cripple wall variants with 2-ft-tall cripple walls.

A comparison of the mean loss curves and loss metrics for variants with and without the cripple wall bracing is shown in Figure 7.53. Remarkably, the loss curves and metrics are fairly close for the two cases in spite of the large difference in strength and deformation capacity. Presumably, the benefit provided by the large increase in strength for the braced case is offset by the reduced deformation capacity, yet the low intensity losses for the braced case do reflect the additional strength when comparing to the unbraced case. These analyses provide some assurance that the calculated losses for cripple wall with wood siding are not overly sensitive to the assumption with regards to bracing. A summary of the modal, collapse and loss criteria are provided for this sub-set of building variants in Table 7.46.

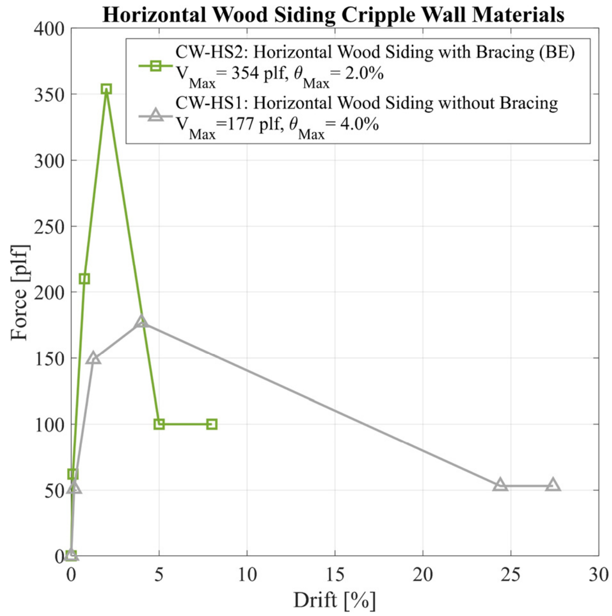

Figure 7.52 Material backbone curves comparing horizontal wood siding that includes possibility of effective braces (best estimate) and unbraced horizontal wood siding for cripple wall dwellings.

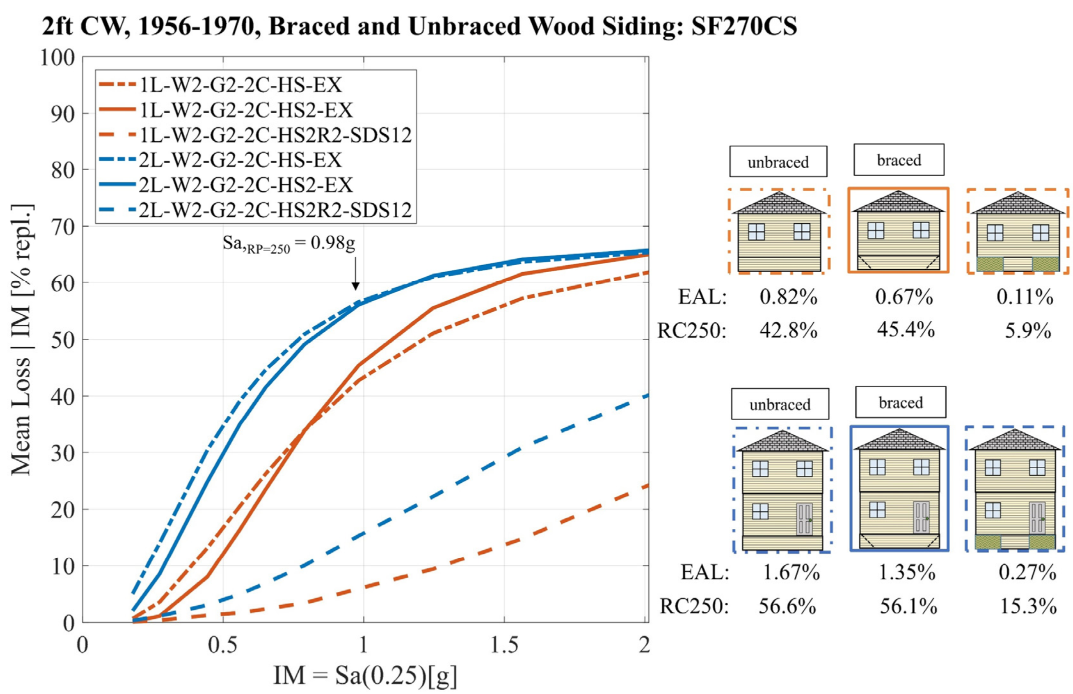

Figure 7.53 Influence of horizontal wood siding cripple wall strength properties on the loss assessment of different variants for the San Francisco site.

Table 7.46 Summary for one- and two-story, 1956–1970 era, 2-ft-tall cripple wall variants with variations in cripple wall wood siding properties for the San Francisco site.

Index [1]	T_1 (sec)[2]	$(V/W_S)_{Avg}$[3]	$(V_{CW}/V_{SS})_{Avg}$[4]	P[C|RP$_{250}$][5]	P[C|MCE][6]	RC250[7]	EAL[8]
1L-W2-G2-2C-**HS**-EX	0.29	0.21	0.31	61.8%	89.4%	42.8%	0.82%
1L-W2-G2-2C-HS2-EX*	0.23	0.47	0.72	64.9%	95.1%	45.4%	0.67%
" "-2C-HSR2-SDS12*	0.18	0.79	1.93	0.4%	5.6%	5.9%	0.11%
2L-W2-G2-2C-**HS**-EX	0.40	0.12	0.29	84.3%	97.0%	56.6%	1.67%
2L-W2-G2-2C-HS2-EX*	0.33	0.29	0.70	82.9%	97.5%	56.1%	1.35%
" "-2C-HSR2-SDS12*	0.28	0.44	2.74	5.7%	22.2%	15.3%	0.27%

[1] Indices with an asterisk indicate best estimate models, sub-indices in bold reflect changes from the best estimate assumptions
[2] Elastic fundamental period in seconds.
[3] Average strength to seismic weight ratio from pushover loading proportional to elastic translational mode shape in each direction, seismic weight is the total lateral weight acting in the model.
[4] Average crawlspace to first occupied story (superstructure) strength ratio, obtained from story-based pushover curves.
[5] Probability of collapse at 250-year return period (RP_{250}).
[6] Probability of collapse at the MCE with intensity determined by nominal S_{DS} for site scaled by a factor of 1.5.
[7] Mean loss at the 250-year return period in percentage of replacement cost.
[8] Expected annual loss expressed in percentage of building replacement cost.

8 Conclusions

8.1 SUMMARY

This report summarizes technical background and results of the PEER–CEA Project numerical studies to quantifying the performance improvements (loss reduction) achieved through seismic retrofit of wood-frame houses with crawlspace vulnerabilities. The performance (loss) assessment framework follows the *FEMA P-58* methodology [2012], which was implemented through a large collaborative effort of multiple working groups of the PEER–CEA Project. Chapter 2 describes the structural modeling assumptions of three-dimensional models of the one- and two-story houses, which were implemented and analyzed using the *OpenSees* software platform. The development of idealized structural material models, based on both previously published experimental testing and recent testing conducted by WG4 [Cobeen et al. 2020; Schiller et al. 2020], is presented in Chapter 3. Chapter 4 describes the background and sensitivity studies to inform the site selection, earthquake hazard characterization, and related considerations implemented by WG3 [Mazzoni et al. 2020] to develop seismic hazard models and suites of input ground motions for the nonlinear response history analyses of archetype house models. Chapter 5 summarizes the review of existing literature on component damage fragility functions and proposed modifications to evaluate wood-frame house damage according the *FEMA P-58* methodology. Chapter 6 provides a review and updates to repair cost functions of *FEMA P-58*, summary of proposed consequence models for cripple wall collapse, and a summary of comparisons to validate the *FEMA P-58* loss models with independent damage estimates from the Earthquake Damage Workshop [Vail et al. 2020], conducted by WG6. Chapter 7 summarizes the performance assessment workflow and development of loss (damage) curves for building variants identified by WG6 [Reis, 2020(a)]. These results include a subset of variants that were used for direct comparison and interaction with catastrophe loss modelers, coordinated by WG6 [Reis 2020(b)], along with parametric and sensitivity studies of other building variants.

8.2 HIGHLIGHTS OF BASELINE STUDY OF CRIPPLE WALL VARIANTS

The baseline cripple wall variant set is the group of house models (see Table 7.3 and Table 7.4) used for comparison with data provided by the catastrophe loss modelers; see Reis [2020(b)]. The variants consist of one- and two-story houses with 2-ft-tall cripple walls and either stucco or horizontal wood siding exteriors. The interior wall material distinguishes the variants for the assumed era of construction, with plaster on wood lath representing the pre-1945 era and gypsum wallboard representing the 1956–1970 era. This set of building variants represents the primary dataset for cripple wall dwellings considered in the project scope. The general findings and observations for the baseline cripple wall dwellings are summarized as follows:

- *Influence of Exterior Material* – Existing (unretrofitted) houses with wood siding cripple walls are significantly more susceptible to damage and losses than equivalent stucco exterior cases. This due to the lower strength of the wood siding cripple walls. Accordingly, houses with wood siding generally benefit the most from retrofitting the cripple walls. When the cripple walls are retrofit in accordance with the *FEMA P-1100* guidelines, the damage and losses are comparable for wood siding and stucco houses, since their superstructure strengths (based on strength-to-weight ratio) do not differ as much between wood and stucco exteriors, due the presence of common interior wall types. In some cases, the retrofitted stucco houses experience slightly higher losses due to the lower drift damage threshold and higher repair costs for stucco as compared to wood siding. However, these slight differences are much less than the overall reduction in losses achieved by retrofitting the vulnerable cripple walls;
- *One-Story versus Two-Story Houses* – As expected, the two-story houses perform worse than one-story houses, primarily because the weight (mass) of the second story effectively doubles the imposed earthquake forces on the cripple walls and first-story walls. This trend was also observed during *FEMA P-1100* numerical studies [2019(b)], and the physical basis of the trend is discussed in the work of Heresi and Miranda [2019]. For the existing (unretrofitted) cases, the two-story houses begin to experience cripple wall damage and losses at much lower seismic intensities as compared to equivalent one-story houses. The two-story houses with retrofitted cripple walls also experience higher losses as compared to one-story cases, although the differences between the two vary more depending on the exterior and interior wall materials and level of seismicity. Since the *FEMA P-1100* retrofit guidelines for cripple walls account for the differences in building weight, the retrofitted cripple walls are much stronger for two-story as compared to one-story configurations. This stronger retrofit transmits higher forces into the first occupied story of the superstructure, with the net effect being that displacements and damage in the retrofit cases shift from the cripple wall into the first story of the superstructure. However, it is important to note that the damage in the first story of the retrofitted houses initiates at much higher seismic intensity as compared to damage and collapse in the cripple walls of unretrofitted houses;
- *Influence of Interior Wall Material* – Older pre-1945 variants with plaster on wood lath interior walls generally experience more damage and losses than the 1956–1970 era houses with gypsum drywall interiors. While plaster on wood lath interior is generally stronger and stiffer than gypsum drywall, it is significantly heavier, more easily damaged, and more expensive to repair than gypsum drywall. The increase in mass of houses with plaster and wood lath leads to larger seismic forces in the cripple walls. Similar to the situation with two-story houses, the larger seismic inertial forces lead to cripple wall damage

and collapse at lower ground-motion intensities for unretrofitted cripple walls. The differences are less for retrofitted houses since the retrofit design of the cripple walls accounts for the seismic forces associated with the heavier plaster interior walls. Thus, the increase in damage and losses for wood lath and plaster compared to gypsum wallboard is more significant for unretrofitted cripple wall cases as compared to the retrofitted cases; and

- *Site Seismicity* – As expected, the overall risk of losses and the benefits of cripple wall retrofit are larger for sites with higher seismicity, i.e., for the San Francisco, Northridge, and San Bernardino sites, as compared to the Bakersfield site. But, even in Bakersfield, the benefits of the cripple wall retrofit are significant. The smallest benefit occurs in the one-story 1956–1970 stucco house, where the overall losses are low and the reduction in the expected RC250 loss from the seismic retrofit is about 3% of the house replacement value (about $7,500).

8.3 HIGHLIGHTS OF STEM WALL VARIANT STUDY

This study also investigated the benefits of anchorage retrofit to older houses with stem wall foundations. These houses have a crawlspace below the first-floor framing, which is created by a concrete or masonry "stem" wall, where there is a potential vulnerability at the connection between the first-floor framing (i.e., floor joists) to the wooden sill plate attached to the stem wall (i.e., foundation). Retrofitting of sill plate connections can eliminate this vulnerability by installing framing-to-sill clips and foundation anchor bolts (or other anchorage devices). The main observations for seismic damage and losses related to retrofit of stem wall connections are summarized as follows:

- *Stem Wall versus Cripple Wall* – Houses with deficient stem wall connections are generally observed to be less vulnerable to earthquake damage than equivalent unretrofitted cripple walls with the same superstructure. This reflects the fact that typical stem wall connections (i.e., toe-nails and friction between the floor joists and sill plate) are inherently more resistant to failure than unbraced cripple walls. Further, the consequence of damage to the stem wall connections is generally less than that associated with failure of cripple walls. In many of the cases that were studied, damage to the stem wall connection was limited to small to moderate sliding displacements, repairs of which are less extensive as compared to cripple wall damage and collapse. Even in the most extreme cases where the house slides off the stem walls, the damage and required repairs are assumed to cost less than the 67% replacement cost assumed for cripple wall collapses; and
- *One-Story versus Two-Story Stem Wall* – Owing to the lower vulnerability in unretrofitted stem walls as compared to cripple walls, the expected benefits for retrofitting of stem walls are significantly less than for retrofitting equivalent houses with cripple walls. The one-story houses with stem walls are observed to show benefits due to retrofitting that range from almost no benefit for the Bakersfield site with relatively low seismicity to slight benefits for the higher

seismicity sites. For example, at the San Francisco site, retrofitting of the stem wall connection reduced the mean repair cost for the 250-year return period hazard from about 8–14% (of house replacement value) for the unretrofitted case to 4–6% with the retrofit (savings on the order of $14,000 for a one-story house). Results for two-story houses with stem wall show mixed results, where in some cases the stem wall connection retrofit slightly increased the losses compared to unretrofitted stem wall cases. For example, at the San Francisco site, the losses for the two-story houses at the 250-year return period hazard change from about 15–16% for the unretrofitted cases to 15–23% for the retrofit cases. This is explained by the fact that the damage and losses calculated for the two-story stem wall houses typically occur in the first story. In some cases, the unretrofitted cases experienced connection failure and sliding that resulted in a base isolation effect for the superstructure, such that the repair costs for the stem wall connection failure are offset by reduced repairs in the superstructure. It should be noted, however, that the net differences in these cases is small and subject to assumptions made in the analysis models. Should the actual stem wall connections between weaker than assumed, leading to larger sliding displacements of the unretrofitted cases, or should the superstructure be stronger than assumed, then the retrofitted cases would likely have lower relative losses.

8.4 HIGHLIGHTS OF ADDITIONAL CRIPPLE WALL VARIANTS

In addition to the building variants considered for comparison with catastrophe loss modelers by WG6 [Reis 2020(b)], this study evaluated the influence of the following parameters on the performance of houses with vulnerable cripple walls: cripple wall height, T1-11 siding, roof weight, and uncertainty in the strength and stiffness of structural response (i.e., approximately including the inherent variability in materials due to configuration, quality of construction, aging/deterioration, etc.). Key observations from these additional variants are as follows:

- *Cripple Wall Height* – Comparisons between baseline cripple wall variants with 2-ft-tall versus 6-ft-tall cripple walls demonstrated that the existing (unretrofitted) 6-ft-tall cripple walls are less sensitive to damage and collapse than 2-ft-tall cripple walls of the same material. This is attributed mostly due to the increased displacement capacity and lower susceptibility to P-delta effects of the 6-ft walls, as compared to the 2-ft walls. To a lesser extent, the better performance of the 6-ft walls with horizontal wood siding may also be due to their longer fundamental periods as compared to the corresponding 2-ft variants. In general, all three of these sources of increased performance relate to the ability of the structure to elongate its period while maintaining lateral resistance. As noted by Kircher et al. [2016], the ability for (typical) short-period structures to elongate in period beyond the constant acceleration region of typical ground-motion spectra is an important collapse survival mechanism. This effect is observed for the 6-ft-tall versus 2-ft-tall cripple wall comparison. Retrofitted 6-ft-tall cripple walls were shown to give similar performance to corresponding 2-ft-tall walls, yet with slightly higher losses due to higher total repair costs associated with the cripple wall conditioned on no collapse, i.e., more material to repair and higher likelihood of significant drift demands prior to collapse;

- *T1-11 Siding* – Houses clad with T-11 siding, which is a characteristic of houses constructed in the 1956–1970 era, had performance between that of comparable houses with wood siding or stucco cladding. The existing (unretrofitted) T1-11 cripple walls have more strength when compared to horizontal wood siding, which translates into lower damage and losses. Retrofitted T1-11 cripple wall variants showed similar performance to corresponding horizontal wood siding variants, with differences in benefits due to retrofitting attributed mostly to the better performance of the existing (unretrofitted) T1-11 cripple wall cases. For the existing (unretrofitted) case, 6-ft-tall T1-11 cripple walls were shown to perform better than 2-ft-tall cripple walls of the same material for two-story houses, whereas performance between the two are similar for one-story houses; and
- *Roof Weight and Material Strength* – In general, the effect of variations in roof weight and wall strengths on structural response and damageability of the houses followed expected trends. For example, the presence of heavy tile roofs or lower wall strength/stiffness compared to the best estimate material values, led to increased damage and repair costs. An examination of strengths for 2-ft-tall cripple walls with stucco material, based on data from the PEER–CEA laboratory tests, shows that material uncertainty can be very significant. Structural analyses and loss studies made with the range of existing (unretrofitted) stucco wall strengths revealed losses that ranged as high as those for horizontal wood siding (at the lower strength bound) and as low as those for retrofit cases (at the upper strength bound). These analyses illustrate the potentially large range of expected losses (and associated retrofit benefits) that may be observed in large inventories of existing houses.

8.5 LIMITATIONS AND FUTURE WORK

As summarized in this report, seismic retrofitting of unbraced cripple walls can significantly reduce the risk of earthquake damage and repair costs to one- and two-story residential houses. Seismic retrofit of sill plate connections for stem-wall foundations can also reduce losses, though not to the same extent as the seismic retrofit of cripple walls. Overall, the results offer compelling evidence that cripple wall and stem-wall retrofits can be a cost-effective investment to significantly reduce the risk of earthquake damage and associated repair and replacement costs. An important additional benefit is the reduced risk of major damage and collapse that can displace residents from their houses.

While the structural and loss analyses employ the latest technologies, data, and methods for performance-based engineering, there are significant uncertainties in each step of the analysis—from characterization of the seismic hazard, through structural analysis and estimation of damage and repair costs. Most of the analyses are based on mean values of the expected damage or loss for typical conditions, which are primarily intended for estimates of overall losses over large inventories of houses. Owing to the inherent diversity of housing and uncertainties in response and damage estimates, the actual damage and losses for individual houses are likely to vary considerably, on the order of plus/minus 50% from the expected values. For example, whereas the expected loss for cripple wall failure is assumed to be 67%, data suggest that the actual loss could range from 30% to 100% of the house replacement value. Nevertheless, the comparative estimates of expected losses provide robust and compelling evidence of the cost-effectiveness of seismic retrofit of houses with unbraced cripple walls and/or vulnerable sill-plate connections.

Over the course of developing and conducting the structural and loss analyses, a few areas emerged where future work could further enhance the analyses to support the goals of the CEA's program to improve the resilience of California's housing stock through seismic retrofit and earthquake insurance. These suggested areas for future study include:

- *More Realistic Testing and Analysis* – The nonlinear structural analyses used in this study employed the best available models that were calibrated to data from available tests of wood-frame components. While efforts were made to model all significant behavioral effects, the analysis models and underlying test data were limited in several respects. For example, the nonlinear spring models were calibrated to data from wall tests that were loaded in the plane of the wall, neglecting the effect that out-of-plane deformations may have on the in-plane response. Data from the tests, and the associated analysis models, also reflected idealized boundary conditions, construction details, and materials that may not fully represent the conditions in actual houses. These limitations could be addressed by testing of larger specimens that capture the three-dimensional response characteristics and realistic boundary conditions. Data from these tests could inform the development and application of computational models that more realistically capture the nonlinear response of wood frame houses;
- *Field Validation* - This study has employed state-of-the-art methods and information for the structural analyses, damage evaluations, and loss assessment; and components of the models have been vetted by engineering professionals, catastrophe modelers, and insurance adjustors. This includes the incorporation of recent experimental data from WG4, which provided invaluable information for furthering the numerical analysis capabilities of the structures considered within the study. However, to the extent that questions persist as to the reliability of the results, further collection and interpretation of field data could provide ways to validate and increase confidence in the models. Efforts in this regard could include data collection from the following sources for comparison with the models and results of this Project: (1) Systematic review of records of damage from past earthquakes (using insurance data, building tagging records, building permits for repair/reconstruction); (2) Measurements from *in situ* testing of existing houses, including ambient vibration testing and destructive (pushover or mobile shaker tests) of houses slated for demolition and replacement; and (3) Preparation of protocols and plans to collect and synthesize detailed damage observations and loss data from future earthquakes;

- *Inventory of Building Stock* - The house variants and analysis models used in this study are based largely on: (1) current loss models employed by catastrophe modelers; (2) information from practicing structural engineers involved in evaluation and retrofit of houses; and (3) review of historic home builder catalogs (e.g., see Appendix A of this report). In the absence of specific inventory data on the prevalence of certain construction practices, the PEER–CEA Team made several assumptions regarding structural details, building finish materials, and other aspects about existing houses that can affect the analysis results. For example, as noted in Chapter 3, the presence of incidental diagonal bracing in cripple walls with exterior wood siding can significantly influence the strength and stiffness of the existing cripple walls. Improved information on the building stock would both inform the loss data for individual building variants and regional loss analyses. In this regard, it would be useful to develop an improved inventory of the existing building stock, including information on both observable and unobservable variants (as defined in the WG2 report [Reis 2020(a)]). Suggestions for sources to collect and interpret such data include: (1) reports collected as part of the CEA's Brace and Bolt program; (2) databases and other information from the real estate industry (e.g., house assessments collected by home mortgage lenders); and (3) interpretation of publicly accessible house photographs collected by satellite imagery, Google street view, or other sources;
- *Impact of Retrofit of Downtime and Recovery* - This study limited the evaluation of economic losses to the direct costs of house repair or replacement from earthquake damage. To the extent that earthquake damage to homes can displace large numbers of residents, leading to long downtime and slow recovery trajectories, it would be useful to evaluate and quantify these effects to inform and further incentivize homeowners and other stakeholders to invest in mitigation strategies; and
- *Regional Earthquake Simulations and Impacts* - Following up on the previous suggestion regarding downtime and recovery, the damage (loss) functions developed as part of this Project could be integrated into models to perform regional earthquake scenario studies to explore the broader impact of seismic retrofit and other mitigation measures. Such studies would benefit from improved inventory models of the current housing stock. The hundreds of individual building variant models, developed as part of this Project, could be used in the development of surrogate models to facilitate regional simulations. Many of these possibilities for future development and furthering of the analysis produced by WG5 are beyond the current project scope, with much of the areas for improvement requiring a larger community-based effort in order to enhance knowledge and information for the assessment of single-family wood-frame dwellings.

REFERENCES

Acevedo C. (2018). *Development and Assessment of Wood Light-Frame Unibody Structures for Enhanced Seismic Performance*, Ph.D. Dissertation, Department of Civil and Environmental Engineering, Stanford University, Stanford, CA.

Anderson L.O. (1965). Guides to Improved Framed Walls for Houses, *Report No. FPL-31*, U.S. Department of Agriculture, Forest Products Laboratory, Madison, WI.

APA (1993). Wood Structural Panel Shear Walls, *APA Report 154*, American Plywood Association, Tacoma, WA.

APA (1999). *Wood Design Concepts – Introduction to Lateral Design*, American Plywood Association, Tacoma, WA.

Arnold A.E., Uang C.-M., Filiatrault A. (2003a). Cyclic behavior and repair of stucco and gypsum woodframe walls: Phase I, *CUREE Publication No. EDA-03*, Consortium of Universities for Research in Earthquake Engineering, Richmond, CA.

Arnold A.E., Uang C.-M., Filiatrault A. (2003b). Cyclic behavior and repair of stucco and gypsum sheathed woodframe walls: Phase II, *CUREE Publication No. EDA-07*, Consortium of Universities for Research in Earthquake Engineering, Richmond, CA.

ASCE (2013). Seismic evaluation and retrofit of existing buildings, *ASCE 41-13*, American Society of Civil Engineers, Reston, VA.

ATC (1985). Earthquake damage evaluation data for California, *ATC-13*, Applied Technology Council, Redwood City, CA.

ATC (2009). Here Today – Here tomorrow: The road to earthquake resilience in San Francisco, earthquake safety for soft-story buildings: documentation appendices, *ATC-52-3A*, Prepared by the Applied Technology Council for the San Francisco Department of Building Inspection under the Community Action Plan for Seismic Safety (CAPSS) Project.

ATC (2018). Development of a prestandard for the assessment and retrofit of one and two family light frame residential buildings, *ATC-110*, 100% Draft, Applied Technology Council, Redwood City, CA.

ATC-HUD (1976). *A Methodology for Seismic Design and Construction of Single Family Dwellings*, Ralph W. Goers and Associates Structural Engineers, Applied Technology Council, Department of Housing and Urban Development, Washington, D.C.

AWC (2015). *Special Design Provisions for Wind and Seismic*. American Wood Council, Washington, D.C.

Ayoub A. (2007). Seismic analysis of wood building structures, *Engineering Structures*, 29: 213–223.

Bahmani P., van de Lindt J.W. (2016). Experimental and numerical assessment of woodframe sheathing layer combinations for use in strength-based and performance-based design, ASCE, *J. Struct. Eng.,* 142(4): E4014001, doi: 10.1061/(ASCE)ST.1943-541X.0001134.

Baker, J.W. (2011). Conditional mean spectrum: tool for ground-motion selection, ASCE, *J. Struct. Eng.,* 137(3): 322–331.

Baker J.W. (2015). Efficient analytical fragility function fitting using dynamic structural analysis, *Earthq. Spectra*, 31(1): 579–599.

Baker J.W., Cornell C.A. (2005). A vector-valued ground motion intensity measure consisting of spectral acceleration and epsilon, *Earthq. Eng. Struct. Dyn.*, 34: 1193–1217.

Baker J.W., Cornell C.A. (2006). Spectral shape, epsilon and record selection, *Earthq. Eng. Struct. Dyn.*, 35: 1077–1095.

Baker J.W., Jayaram N. (2008). Correlation of spectral acceleration values from NGA ground motion models, *Earthq. Spectra*, 24(1): 299–317.

Baker J.W., Lee C. (2018). An improved algorithm for selecting ground motions to match a conditional spectrum, *J. Earthq. Eng.*, 22(4): 708–723.

Beck J.L., Porter K.A., Shaikhutdinov R., Au S.K., Moroi T., Tsukada Y., Masuda M. (2002). Impact of seismic risk on lifetime property values, *Final Report for CUREE-Kajima Phase IV Project*, Consortium of Universities for Research in Earthquake Engineering, Richmond, CA.

Black G., Davidson R.A., Pei S., van de Lindt J. (2010). Empirical loss analysis to support definition of seismic performance objectives for woodframe buildings, *Struct. Safety*, 32: 209–219.

Boore D.M. (2010). Orientation-independent, nongeometric-mean measures of seismic intensity from two horizontal components of motion, *Bull. Seismol. Soc. Am.*, 100: 1830–1835.

Camelo V., Beck J., Hall J. (2002). Dynamic characteristics of woodframe structures, *CUREE Publication No. W-11*, Consortium of Universities for Research in Earthquake Engineering, Richmond, CA.

Camelo V. (2003). Dynamic characteristics of woodframe buildings, *Report No. EERL 2003-04*, California Institute of Technology, Pasadena, CA.

Carroll C.T. (2006). *Wood Materials and Shearwalls of Older Light-Frame Residential Structures*, M.Sc. Thesis, Department of Civil and Construction Engineering, Oregon State University, Corvallis, OR.

Chai Y.H., Hutchinson T.C., Vukazich S.M. (2002). Seismic behavior of level and stepped cripple walls, *CUREE Publication No. W-17*, Consortium of Universities for Research in Earthquake Engineering, Richmond, CA.

Chandramohan R., Lin T., Baker J.W., Deierlein G.G. (2013). Influence of ground motion spectral shape and duration on seismic collapse risk, *Proceedings of the 10th International Conference on Urban Earthquake Engineering*, Tokyo, Japan.

Charney F.A. (2008). Unintended consequences of modeling damping in structures, ASCE, *J. Struct. Eng.*, 134(4): 581–592.

Chopra A.K., McKenna F. (2016). Modeling viscous damping in nonlinear response history analysis of buildings for earthquake excitation, *Earthq. Eng. Struct. Dyn.*, 45: 193–211.

Christovasilis I.P., Filiatrault A., Constantinou M.C., Wanitkorkul A. (2009a). Incremental dynamic analysis of woodframe buildings, *Earthq. Eng. Struct. Dyn.*, 438:477–496.

Christovasilis I.P., Filiatrault A. (2009b). *SAWS – Version 2.1: A Computer Program for the Seismic Analysis of Woodframe Structures*, User Manual, Department of Civil, Structural and Environmental Engineering, State University of New York at Buffalo, Buffalo, NY.

Chui Y.H., Smith I. (1989). Quantifying damping in structural timber components, *Proceedings, 2nd Pacific Timber Engineering Conference*, Wellington, New Zealand, 1:S7–S60.

Cobeen K. (2018). Personal communication following in-person PEER team meeting on February 13, 2018, at UC Berkeley, PEER–CEA Wood-frame Project.

Cobeen K., Mahdavifar V., Hutchinson T., Schiller B., Welch D.P., Kang G.S., Bozorgnia Y. (2020). Large-component seismic testing for existing and retrofit single-family wood-frame dwellings, *PEER Report No. 2020/20*, Pacific Earthquake Engineering Research Center, University of California, Berkeley, CA.

COLA (2001). Report of a testing program of light-framed walls with wood sheathed shear panels, *Final Report to the City of Los Angeles Department of Building and Safety*, SEAOSC COLA-UCI Light Frame Test Committee, University of California, Irvine, CA.

CUREE (2010). General guidelines for the assessment and repair of earthquake damage in residential woodframe buildings, *CUREE Publication No. EDA-02*, J. Osteraas (ed.), Consortium of Universities for Research in Earthquake Engineering, Richmond, CA.

CSSC (2005). Homeowner's Guide to Earthquake Safety, *SSC No. 05-01*, California Seismic Safety Commission, 2005 Edition, Sacramento, CA.

Ekiert C., Filiatrault A. (2008). *FEMA P-58: Fragility Curves for Wood Light-Frame Structural Systems*, *Background Document FEMA P-58/BD-3.8.1*, prepared by the Applied Technology Council for the Federal Emergency Management Agency, Washington, DC.

Elkady A., Lignos D.G. (2015) Effect of gravity framing on the overstrength and collapse capacity of steel frame buildings with perimeter special moment frames, *Earthq. Eng. Struct. Dyn.*, 44: 1289–1307.

Elkhoraibi T., Mosalam K.M. (2007a). Towards error-free hybrid simulation using mixed variables, *Earthq. Eng. Struct. Dyn.*, 36: 1497–1522.

Elkhoraibi T., Mosalam K.M. (2007b). Generalized hybrid simulation framework for structural systems subjected to seismic loading, *Report PEER 2007-101*, Pacific Earthquake Engineering Research Center, University of California, Berkeley, CA.

Erickson E.C.O. (1958). The rigidity and strength of braced and unbraced walls covered with bevel siding, *Report No. FPL-1261*, U.S. Department of Agriculture, Forest Products Laboratory, Madison, WI.

Fragiacomo M., Amadio C., Rinaldin G., Sanci, L. (2012). Non-linear modelling of wooden light-frame and X-lam structures, *Proceedings, 2012 World Conference on Timber Engineering*, Auckland, New Zealand.

Fennell W.A., Line P., Mochizuki G.L., Moore K.S., VanDorpe T.D., Voss T.A. (2009). *Report on Laboratory Testing of Anchor Bolts Connecting Wood Sill Plates to Concrete with Minimum Edge Distance*, Structural Engineers Association of California (SEAOC), Seismology Committee, Sacramento, CA.

FEMA (2006). *FEMA 232: Homebuilders' Guide to Earthquake Resistant Design and Construction*, prepared by the Building Seismic Safety Council for the Federal Emergency Management Agency, Washington, DC.

FEMA (2006b). *FEMA G225-CD*: *Seismic Retrofit Training for Building Contractors and Inspectors*, Federal Emergency Management Agency, Washington, DC.

FEMA (2009). *FEMA P-695*: *Quantification of Building Seismic Performance Factors*, prepared by the Applied Technology Council for the Federal Emergency Management Agency, Washington, DC.

FEMA (2012). *FEMA P-58-1*: *Seismic Performance Assessment of Buildings*, Volume 1 – Methodology, prepared by the Applied Technology Council for the Federal Emergency Management Agency, Washington, DC.

FEMA (2012b). *FEMA P-58-2*: *Seismic Performance Assessment of Buildings*, Volume 2 – Implementation Guide, prepared by the Applied Technology Council for the Federal Emergency Management Agency, Washington, DC.

FEMA (2012c). *FEMA P-58-3*: *Seismic Performance Assessment of Buildings*, Volume 3 – Supporting Electronic Materials and Background Documentation, 3rd Ed., prepared by the Applied Technology Council for the Federal Emergency Management Agency, Washington, DC.

FEMA (2012d). *FEMA P-807*: *Seismic Evaluation and Retrofit of Multi-Unit Wood-Frame Buildings with Weak First Stories*, prepared by the Applied Technology Council for the Federal Emergency Management Agency, Washington, DC.

FEMA (2015). *FEMA P-1024*: *Performance of Buildings and Nonstructural Components in the 2014 South Napa Earthquake*, prepared by the Applied Technology Council for the Federal Emergency Management Agency, Washington, DC.

FEMA (2018). *FEMA P-1100*: *Vulnerability-Based Seismic Assessment and Retrofit of One- and Two-Family Dwellings*, Volume 1 – Prestandard, prepared by the Applied Technology Council for the California Earthquake Authority, Sacramento, CA, and the Federal Emergency Management Agency, Washington, DC.

FEMA (2019a). *FEMA P-1100-2A*: *Vulnerability-Based Seismic Assessment and Retrofit of One- and Two-Family Dwellings*, Volume 2A – Plan Set for Crawlspace Dwellings, prepared by the Applied Technology Council for the California Earthquake Authority, Sacramento, CA, and the Federal Emergency Management Agency Washington, DC.

FEMA (2019b). *FEMA P-1100-3*: *Vulnerability-Based Seismic Assessment and Retrofit of One- and Two-Family Dwellings*, Volume 3 – Background Documentation, prepared by the Applied Technology Council for the California Earthquake Authority, Sacramento, CA, and the Federal Emergency Management Agency, Washington, DC.

Ficcadenti S.J., Freund E.J., Pardoen G.C., Kazanjy R.P. (2004). Cyclic response of shear transfer connections between shearwalls and diaphragms in woodframe construction, *CUREE Publication No. W-28*, Consortium of Universities for Research in Earthquake Engineering, Richmond, CA.

Filiatrault A., Isoda H., Folz, B. (2003). Hysteretic damping of wood framed buildings, *Engineering Structures*, 25: 461-471.

Fischer D., Filiatrault A., Folz B., Uang C.-M., Seible F. (2001). Shake table tests of a two-story woodframe house, *CUREE Publication No. W-06*, Consortium of Universities for Research in Earthquake Engineering, Richmond, CA.

Foliente G.C. (1995). Hysteresis modeling of wood joints and structural systems, ASCE, *J. Struct. Eng.*, 121(6): 1013–1022.

Folz B., Filiatrault A. (2000). CASHEW – Version 1.0: A computer program for cyclic analysis of wood shear walls, *Report No. SSRP 2000/10*, Division of Structural Engineering, University of California, San Diego, La Jolla, CA.

Folz B., Filiatrault, A. (2001). Cyclic analysis of wood shear walls, ASCE, *J. Struct. Eng.*, 127(4): 433–441.

Folz, B., Filiatrault, A. (2004a). Seismic analysis of woodframe structures I: Model formulation, ASCE, *J. Struct. Eng.*, 130(9): 1353–1360.

Folz B., Filiatrault A. (2004b). Seismic analysis of woodframe structures II: Model Implementation and validation, ASCE, *J. Struct. Eng.*, 130(9): 1361–1370.

Folz B., Filiatrault A. (2004c). Blind predictions of the seismic response of a woodframe house: An international benchmark study, *Earthq. Spectra*, 20(3): 825–851.

Foschi R.O. (1974). Load-slip characteristics of nails, *Wood Science*, 7(1): 69–76.

Foschi R.O. (1977). Analysis of wood diaphragms and trusses, Part 1: Diaphragms, *Can. J. Civil Eng.*, 4(3): 345–362.

Gatto K., Uang C.-M. (2002). Cylic response of woodframe shearwalls: loading protocol and rate of loading effects, *CUREE Publication No. W-13*, Consortium of Universities for Research in Earthquake Engineering, Richmond, CA.

Grossi P. (1998). Assessing the benefits and costs of earthquake mitigation, *Working Paper 98-11-11*, Risk Management and Decisions Processes Center, The Wharton School, University of Pennsylvania, Philadelphia, PA.

Goda K., Atkinson, G.M. (2010). Seismic performance of wood-frame houses in south-western British Columbia, *Earthq. Eng. Struct. Dyn.*, 40(8): 903–924.

Hall J.F. (2006). Problems encountered from the use (or misuse) of Rayleigh damping, *Earthq. Eng. Struct. Dyn.*, 35(5): 525–545.

Hall J.F. (2016). Discussion of 'Modelling viscous damping in nonlinear response history analysis of buildings for earthquake excitation' by Anil K. Chopra and Frank McKenna, *Earthq. Eng. Struct. Dyn.*, 45(13): 2229–2233.

Hall J.F. (2017). Discussion on 'An investigation into the effects of damping and nonlinear geometry models in earthquake engineering analysis' by Andrew Hardyniec and Finley Charney, *Earthq. Eng. Struct. Dyn.*, 46(2): 341–342.

Hall J.F., Schmid B., Comerio M., Russell J., Delli Quadri N., Harder R., Powell B., Hamburger R., Steinburg R. (1996). Wood Buildings, Chapter 6 in 1994 Northridge Earthquake Reconnaissance Report (Volume 2), W.T. Holmes, P. Somers (eds.), *Earthq. Spectra*, 12(S1): 125–176.

Hardyniec A., Charney, F. (2015). An investigation into the effects of damping and nonlinear geometry models in earthquake engineering analysis, *Earthq. Eng. Struct. Dyn.*, 44(15): 2695–2715.

Haselton C.B., Baker J.W., Liel A.B., Deierlein G.G. (2011). Accounting for ground-motion spectral shape characteristics in structural collapse assessment through an adjustment for epsilon, ASCE, *J. Struct. Eng.,* 137(3): 332–344.

HBrisk (2020). *Seismic Performance Prediction Program*, Haselton Baker Risk Group, https://www.hbrisk.com/.

HAZUS (2013). H*AZUS-MH 2.1 Technical Manual*, Department of Homeland Security, Federal Emergency Management Agency, Washington, D.C., *https://www.fema.gov/media-library-data/20130726-1820-25045-6286/hzmh2_1_eq_tm.pdf*.

Heresi P., Miranda E. (2019). Evaluation of relative seismic performance between one- and two-story houses, *J. Earthq. Eng.,* doi: 10.1080/13632469.2019.1693447.

HUD (2001). *Review of Structural Materials and Methods for Home Building in the United States: 1900 to 2000. Partnership for Advanced Technology in Housing*, U.S. Department of Housing and Urban Development, Washington, D.C..

ICC (2018). International Residential Code for One- and Two-Family Dwellings, *IRC 2018*, International Code Council.

Isoda H., Folz B., Filiatrault A. (2002). Seismic modeling of index woodframe buildings, *CUREE Publication No. W-12*, Consortium of Universities for Research in Earthquake Engineering, Richmond, CA.

Jayamon J.R., Line P., Charney F.A. (2015). An assessment of uncertainty in the performance evaluation of wood shear wall structures, *Proceedings*, *ASCE Structures Congress 2015*, Portland, OR.

Jayamon J.R., Line P., Charney F.A. (2018). State-of-the-art review on damping in wood-frame shear wall structures, ASCE, *J. Struct. Eng.*, 144(12): 03118003, 1–13, doi: 10.1061/(ASCE)ST.1943-541X.0002212.

Jalayer F. (2003). *Direct Probabilistic Seismic Analysis: Implementing Non-Linear Dynamic Assessments*, Ph.D. Dissertation, Department of Civil and Environmental Engineering, Stanford University, Stanford, CA.

Jayaram N., Lin T., Baker J.W. (2011). A Computationally efficient ground-motion selection algorithm for matching a target response spectrum and variance, *Earthq. Spectra*, 27(3): 797–815.

Jayaram N., Baker J.W. (2008). Statistical tests of the joint distribution of spectral acceleration values, *Bull. Seismol. Soc. Am.*, 98(5): 2231–2243.

Johnson A.J. (1997). *Monotonic and Cyclic Performance of Long Shear Walls with Openings*, M.Sc. Thesis, Department of Civil and Environmental Engineering, Virginia Polytechnic Institute and State University, Blacksburg, VA.

Kennedy R.P., Ravindra M.K. (1984). Seismic fragilities for nuclear power plant risk studies, in *Nuclear Engineering and Design 79*, Philadelphia, PA: Elsevier Science Publishers.

Kircher C.A., Nassar A.A., Kustu O., Holmes W.T. (1997). Development of building damage functions for earthquake loss estimation, *Earthq. Spectra*, 13(4): 663–682.

Kircher C.A., Whitman R.V., Holmes W.T. (2006). HAZUS earthquake loss estimation methods, ASCE, *Nat. Hazards Rev.*, 7(2): 45–59.

Kircher C.A., Pang W., Ziaei E., Filiatrault A., Schiff S.D. (2016). Solutions to the short-period building performance paradox: A focus on light-frame wood buildings, *Proceedings, 2016 SEAOC Convention*, Structural Engineers Association of California, Maui, HI.

Krawinkler H., Parisi F., Ibarra L., Ayoub A., Medina R. (2000). Development of a testing protocol for wood frame structures, *CUREE Publication No. W-02*, Consortium of Universities for Research in Earthquake Engineering, Richmond, CA.

Koliou M., Filiatrault A. (2017). Development of wood and steel diaphragm connector database for performance-based earthquake engineering, *Bull. Earthq. Eng.*, 15(10): 4319–4347.

Koliou M., van de Lindt J.W., Hamburger R.O. (2018). Nonlinear modeling of wood-frame shear wall systems in performance-based earthquake engineering: Recommendations for the ASCE 41 Standard, ASCE, *J. Struct. Eng.,* 144(8): 04018095. doi: 10.1061/(ASCE)ST.1943-S41X.0002083.

LATF (1992). *Task Force on Evaluating Damage from the Northridge Earthquake: Wood Frame Subcommittee Construction Report and Recommendations,* City of Los Angeles Department of Building and Safety and the Structural Engineers Association of Southern California (SEAOSC), San Dimas, CA.

Levenson L.M. (1992). Residential water heater damage and fires following the Loma Prieta and Big Bear Lake earthquakes, *Earthq. Spectra*, 8(4): 595–603.

Lew H.S. (1987). *The Whittier Narrows Earthquake of October 1, 1987: A Reconnaissance Report*, National Bureau of Standards, U.S. Department of Commerce, Gaithersburg, MD.

Lilliefors H.W. (1967). On the Kolmogorov-Smirnov test for normality with mean and variance unknown, *J. Am. Stat. Assoc.*, 62(318): 399–402.

Lin R-G. (2018). *Must Reads: A simple earthquake flaw can invite financial catastrophe. Most Californian homeowners ignore it*, Los Angeles Times, Retrieved from *https://www.latimes.com/local/lanow/la-me-ln-earthquake-homeowner-fix-20181018-story.html.*

Lowes L.N., Mitra N., Altoontash A. (2004). A beam-column joint model for simulating the earthquake response of reinforced concrete frames, *Report PEER 2003/10*, Pacific Earthquake Engineering Research Center, University of California, Berkeley, CA.

Mahaney J.A., Kehoe B.E. (2002). Anchorage of woodframe buildings: laboratory testing report, *CUREE Publication No. W-14*, Consortium of Universities for Research in Earthquake Engineering, Richmond, CA.

Massey F.J. (1951). The Kolmogorov-Smirnov test for goodness of fit, *J. Am. Stat. Assoc.*, 46(253): 68–78.

Mazzoni S., Gregor N., Al Atik L., Bozorgnia Y., Welch D.P., Deierlein G.G. (2020). Probabilistic seismic hazard analysis and selecting and scaling ground-motion records, *PEER Report No. 2020/14*, Pacific Earthquake Engineering Research Center, University of California, Berkeley, CA.

McClure F.E. (1973). *Performance of Single Family Dwellings in the San Fernando Earthquake of February 9, 1971*, Report prepared for the National Oceanic and Atmospheric Administration, Washington, D.C.

McCormick D.L. (2018). *Personal communication regarding FEMA P-1100 plan set assumptions and influence of design assumption changes*, May 2018.

McKenna F., Fenves G., Filippou F.C., Mazzoni S. (2000). *Open System for Earthquake Engineering Simulation* (*OpenSees*), *http://OpenSees.berkeley.edu/wiki/index.php/Main_Page*.

McMullin K.M., Merrick D. (2002). Seismic performance of gypsum walls: experimental test program, *CUREE Publication No. W-15*, Consortium of Universities for Research in Earthquake Engineering, Richmond, CA.

Miranda E., Mosqueda, G. (2011). *FEMA P-58: Seismic Fragility of Building Interior Cold-Formed Steel Framed Gypsum Partition Walls*, *Background Document FEMA P-58/BD-3.9.2*, prepared by the Applied Technology Council for the Federal Emergency Management Agency, Washington, DC.

Mitrani-Reiser J. (2007). *An Ounce of Prevention: Probabilistic Loss Estimation for Performance-Based Earthquake Engineering*, Ph.D. Dissertation, Department of Mechanical and Civil Engineering, California Institute of Technology, Pasadena, CA.

Moehle J., Deierlein G.G. (2004). A framework methodology for performance-based earthquake engineering, *Proceedings, 13th World Conference on Earthquake Engineering*, Vancouver, BC, Canada.

Mosalam K., Machado C., Liniorz K.-U., Naito C., Kunkel E., Mahin S.A. (2002). Seismic evaluation of an asymmetric three-story woodframe building, *CUREE Publication No. W-19*, Consortium of Universities for Research in Earthquake Engineering, Richmond, CA.

NAHB (2008). Evaluation of the lateral performance of let-in bracing and mixed bracing systems, *Report EG5736_052908*, National Association of Home Builders (NAHB) Research Center, Washington, D.C.

NAHB-HUD. (1994). Assessment of damage to residential buildings caused by the Northridge earthquake, *Cooperative Agreement DU100K000005911*, *Report prepared by the NAHB Research Center for the U.S. Department of Housing and Urban Development*, Washington, D.C.

Nakata J.K., Meyer C.E., Wilshire H.G., Tinsley J.C., Updegrove W.S., Peterson D.M., Ellen S.D., Haugerud R.A., McLaughlin R.J., Fisher G.R., Diggles M.F. (1999). The October 17, 1989, Loma Prieta, California, earthquake – selected photographs, *Digital Data Series DDS-29*, Version 1.2, U.S. Geological Survey, Menlo Park, CA.

Newmark N.M., Hall W.J. (1969). Seismic design criteria for nuclear reactor facilities, *Proceedings, 4th World Conference on Earthquake Engineering*, Santiago, Chile.

Ni C., Karacabeyli E. (2007). Performance of shear walls with diagonal or transverse lumber sheathing, ASCE, *J. Struct. Eng.*, 133(12): 1832–1842.

NIBS (1997). *Earthquake Loss Estimation Methodology. HAZUS97: Technical Manual*, Prepared by the National Institute of Building Sciences for the Federal Emergency Management Agency, Washington, D.C.

NIST (2017). Guidelines for nonlinear structural analysis and design of buildings: Part 1 – General, *Report NIST GCR 17-917-46v1*, Prepared by the Applied Technology Council for the National Institute of Standards and Technology, Gaithersburg, MD.

Osteraas J. (2019). Thoughts regarding cripple wall "collapse", *Personal communication to PEER working groups*, PEER–CEA Wood-frame Project, August, 2019.

Osteraas J., Krawinkler H. (2010). *FEMA P-58/BD-3.9.7*: *Fragility of Masonry Chimneys*, Prepared by the Applied Technology Council for the Federal Emergency Management Agency, Washington, DC.

Pang W., Rosowsky D.V., Ellingwood B.R., Wang Y. (2009). Seismic fragility analysis and retrofit of conventional residential wood-frame structures in the Central United States, ASCE, *J. Struct. Eng.*, 135(3): 262–271.

Pang W., Ziaei E., Filiatrault A. (2012). A 3D model for collapse analysis of soft-story light-frame wood buildings, *Proceedings, World Conference on Timber Engineering* (WCTE 2012), Auckland, New Zealand.

Pang W., Shirazi S.M.H. (2012). Stochastic response of light-frame wood buildings under earthquake loading, *Proceedings, World Conference on Timber Engineering* (WCTE 2012), Auckland, New Zealand.

Pardoen G.C., Waltman A., Kazanjy R., Freund E., Hamilton C.H. (2003). Testing and analysis of one-story and two-story shear walls under cyclic loading, *CUREE Publication No. W-18*, Consortium of Universities for Research in Earthquake Engineering, Richmond, CA.

Park Y.J., Ang A.H.S. (1985). Mechanistic seismic damage model for reinforced concrete, ASCE, *J. Struct. Eng.*, 111(4): 722–739.

Patton-Mallory M., Wolfe R.W., Soltis L.A. (1985). Light-frame shear wall length and opening effects, ASCE, *J. Struct. Eng.*, 111(10): 2227–2239.

PEER (2014). PEER Preliminary notes and observations on the August 24, 2014, South Napa earthquake, G. Kang and S. Mahin (eds.), *PEER Report 2014/13*, Pacific Earthquake Engineering Research Center, University of California, Berkeley, CA.

PEER (2020). PEER–CEA Project Archive, *https://peer.berkeley.edu/cw-woodframe*.

Pei S., van de Lindt J.W. (2009). Methodology for earthquake-induced loss estimation: An application to woodframe buildings, *Struct. Safety*, 31: 31–42.

Pei S., van de Lindt J.W. (2010). Influence of structural properties and hazard level on seismic loss estimation for light-frame wood structures, *Eng. Struct.*, 32: 2183–2191.

Porter K.A. (2003). An overview of PEER's performance-based earthquake engineering methodology, *Proceedings, 9th International Conference on Applications of Statistics and Probability in Civil Engineering* (ICASP9), San Francisco, CA.

Porter K.A. (2006). Evaluating Premium Incentives for the California Earthquake Authority, California Institute of Technology, Pasadena, CA, 60 p. *http://www.sparisk.com/pubs/Porter-2006-CEA-premium-incentives.pdf*

Porter K.A. (2009). *Component Fragility Functions for Older Woodframe Construction*, Community Action Plan for Seismic Safety (CAPSS) Fragility Functions, Prepared for the Applied Technology Council, SPA Risk, Denver, CO.

Porter K.A. (2019). *A Beginner's Guide to Fragility, Vulnerability, and Risk*, University of Colorado Boulder, 119 pp., *http://spot.colorado.edu/~porterka/Porter-beginnersguide.pdf.*

Porter K.A., Beck J.L., Seligson H.A., Scawthorn C.R., Tobin L.T., Young R., Boyd T. (2002). Improving loss estimation for woodframe buildings, *CUREE Publication No. W-18*, Consortium of Universities for Research in Earthquake Engineering, Richmond, CA.

Porter K.A., Kiremidjian A.S. (2001). Assembly-based vulnerability of buildings and its uses in seismic performance evaluation and risk-management and decision-making, *Technical Report No. 139*, John A. Blume Earthquake Engineering Research Center, Stanford, CA.

Priestley M.J.N., Calvi G.M., Kowalsky M.J. (2007). *Direct Displacement-based Seismic Design*: Pavia, IUSS Press.

Reis E. (2020a). Development of index buildings, *PEER Report No. 2020/13*, Pacific Earthquake Engineering Research Center, University of California, Berkeley, CA.

Reis E. (2020b). Seismic performance of single-family wood-frame houses: comparing analytical and industry catastrophe models, *PEER Report No. 2020/24*, Pacific Earthquake Engineering Research Center, University of California, Berkeley, CA.

Reitherman R., Cobeen K. (2003). Design Documentation of Woodframe Project Index Buildings, *CUREE Publication No. W-29*, Consortium of Universities for Research in Earthquake Engineering, Richmond, CA.

Rosowsky D.V. (2002). Reliability-based seismic design of wood shearwalls, ASCE, *J. Struct. Eng.,* 128(11): 1439–1453.

Ryan T.J., Fridley K.J., Pollock D.G., Itani R.Y. (2003). Inter-story shear transfer in woodframe buildings, *CUREE Publication No. W-22*, Consortium of Universities for Research in Earthquake Engineering, Richmond, CA.

Schierle G.G. (2001). Woodframe project case studies, *CUREE Publication No. W-04*, Consortium of Universities for Research in Earthquake Engineering, Richmond, CA.

Schiller B., Hutchinson T.C., Cobeen, K. (2020a). Cripple wall small-component test program: Wet specimens I, *PEER Report No. 16*, Pacific Earthquake Engineering Research Center, University of California, Berkeley, CA.

Schiller B., Hutchinson T.C., Cobeen, K. (2020b). Cripple wall small-component test program: Dry specimens, *PEER Report No. 17*, Pacific Earthquake Engineering Research Center, University of California, Berkeley, CA.

Schiller B., Hutchinson T.C., Cobeen, K. (2020c). Cripple wall small-component test program: Wet specimens II, *PEER Report No. 18*, Pacific Earthquake Engineering Research Center, University of California, Berkeley, CA.

Schiller B., Hutchinson T.C., Cobeen K. (2020d). Cripple wall small-component test program: comparisons, *PEER Report No. 19*, Pacific Earthquake Engineering Research Center, University of California, Berkeley, CA.

Schmid B. (1984). *Shear test of existing wood lath and plaster walls relative to division 88*, Pasadena, CA, Ben L. Schmid Consulting Structural Engineer.

Sherlock (2020). *Sherlock High-Performance Computing Cluster*, Stanford University, https://www.sherlock.stanford.edu/.

Soroushian S., Zaghi A.E., Maragakis E., Echevarria A. (2015). Seismic fragility study of fire sprinkler piping systems with grooved fit joints, ASCE, *J. Struct. Eng.,* 141(6): 04014157.

Steinbrugge K.V., Fowkes E.J., Lagorio H.J., Algermissen S.T. (1990). Dwelling monetary losses, Chapter 20 in *The Coalinga, California Earthquake of May 2, 1983*, M.J. Rymer and W.L. Ellsworth (eds.), *U.S. Geological Survey Professional Paper 1487*, pp. 359–380, Washington, D.C.

Stewart W.G. (1987). *The Seismic Design of Plywood Sheathed Shearwalls*, PhD Dissertation, Department of Civil and Natural Resources Engineering, University of Canterbury, Christchurch, New Zealand.

Sugiyama H., Matsumoto T. (1994). *Empirical Equations for the Estimation of Racking Strength of a Plywood-Sheathed Shear Wall with Openings*, Architectural Institute of Japan (AIJ), Tokyo, Japan.

Tesfamariam S., Stiemer S.F., Dickof C., Bezabe, M.A. (2014). Seismic Vulnerability assessment of hybrid steel-timber structure: steel moment-resisting frames with CLT infill, *J. Earthq. Eng.*, 18(6): 929–944.

Trayer G.W. (1956). The rigidity and strength of frame walls, *Report No. FPL-896*, U.S. Department of Agriculture, Forest Products Laboratory, Madison, WI.

Tuomi R.L., Gromala D.S. (1977). Racking strength of walls: Let-in corner bracing, sheet materials, and effect of loading rate, *Report No. FPL-301*, U.S. Department of Agriculture, Forest Products Laboratory, Madison, WI.

Vail K., Lizundia B., Welch D.P., Reis E. (2020). Earthquake damage workshop, Project, *PEER Report No. 2020/23*, Pacific Earthquake Engineering Research Center, University of California, Berkeley, CA.

van de Lindt J.W., Pei S., Liu H., Filiatrault A. (2010) Three-dimensional seismic response of a full-scale light-frame wood building: numerical study, ASCE, *J. Struct. Eng.,* 136(1): 56–65.

Whitman R.V., Anagnos T., Kircher C.A., Lagorio H.J., Lawson R.S., Schneider P. (1997). Development of a national earthquake loss estimation methodology, *Earthq. Spectra*, 13(4): 643-–661.

Yasamura M., Sugiyama H. (1984). Shear properties of plywood-sheathed wall panels with opening, *Trans. Arch. Inst. Japan*, 338(4): 88–98.

Yeh, T.C., Hartz, B.J., Brown, C.B. (1971). Damping sources in wood structures, *Journal of Sound and Vibration*, 19(4): 411-419.

Yin Y.-J., Li Y. (2010). Seismic collapse risk of light-frame wood construction considering aleatoric and epistemic uncertainties, *Struct. Safety*, 32: 250–261.

Zareian F., Lanning J. (2020). Development of testing protocol for cripple wall components, *PEER Report No. 2020/15*, Pacific Earthquake Engineering Research Center, University of California, Berkeley, CA

Zsarnoczay A. (2019). *NHERI-SimCenter/pelicun: pelicun v2.0.0* (Version 2.0.0), Zenodo, *http://doi.org/10.5281/zenodo.34910*.

Zsarnoczay A., Deierlein G.G. (2020). peilcun – A Computational Framework for Estimating Damage, Loss and Community Resilience, *Proceedings, 17th World Conference on Earthquake Engineering*, Sendai, Japan.

APPENDIX A Study of Historic Floor Plan Information to Develop Baseline Superstructure Configurations

A1 SUMMARY

This appendix provides the background documentation for the development of baseline building configurations for analysis of building variants within the PEER–CEA Project. The main assumptions driving archetype development are provided with distinctions made with respect to previous studies involving the analysis of wood light-frame dwellings and the specific needs of the current project.

The specific needs of the current project are clearly discussed in terms of how an assumed building configuration can affect the seismic performance results. Previous assumptions made within the ATC-110 project [ATC 2018] for retrofit guideline development, including the details of the configuration database used are illustrated. Inherent limitations of the approach used within the ATC-110 project are illustrated with the recommended modifications for analysis within the PEER–CEA Project identified.

The proposed baseline archetype configurations consist of a one-story and two-story superstructure layout. Statistics gathered from a configuration database of 42 different houses from the 1900s to the 1960s are used to support assumptions made for archetype development. The key difference is the use of geometry-based wall density parameters to appropriately capture the likely mass, strength and stiffness for each combination of sheathing materials considered within the project. A review of the available configuration statistics found that the one-story small house configuration used in the CUREE-Caltech Woodframe Project [Isoda et al. 2002] was an appropriate baseline for one story archetype development. Slight modifications to this previously studied layout are clearly discussed and justified. The extension to a two-story archetype involved careful review of the configuration data and subsequent assumptions considering the needs of the current project.

The two proposed baseline configurations are assumed adequate to compile and adjust the various aspects of structural analysis and loss modeling techniques to achieve the goal of quantifying the performance of single-family dwellings with cripple wall and anchorage deficiencies.

A2 BUILDING CONFIGURATIONS FROM THE ATC-110 SUPERSTRUCTURE STUDY

This section provides background information on the development of archetype buildings within the ATC-110 project: *Development of a Prestandard for the Assessment and Retrofit of One and Two Family Light Frame Residential Buildings* [ATC 2018]. The section outlines the configuration data that was used to develop superstructure configurations within the cripple wall dwelling portion of the ATC-110 project. The manner in which the superstructure information was utilized within ATC-110 is briefly described.

A2.1 ATC-110 Configuration Data

Within the ATC-110 project, a number of older building configurations were obtained from older housing catalogs representing typical construction from the 1900s to the 1960s. Configurations were purposefully selected to represent "stand-alone" or detached dwellings without attached garage space. Further, selection criteria also aimed for minimizing the amount of plan eccentricity observed (i.e., without significant T- or L-shaped plans). Upon completion, the study consisted of both one- and two-story homes. The one-story configurations considered three configurations from each decade ranging from 1900s to 1960s (i.e., seven eras of construction for a total of 28 one-story configurations). The two-story configurations consisted of two configurations per era for a total of 14 different layouts for two story homes. The summary of the configurations considered in the study is shown in Figure A2.1. More information of the reviewed configurations can be found in Chapter 6 of F*EMA P-1100*, Vol. 3 [2019].

Each configuration was scaled and measured for a variety of parameters including: floor area (A), interior wall length (L_{Int}), and exterior wall length (L_{Ext}). The configuration 1910-1B is shown as an example in Figure A2.2.

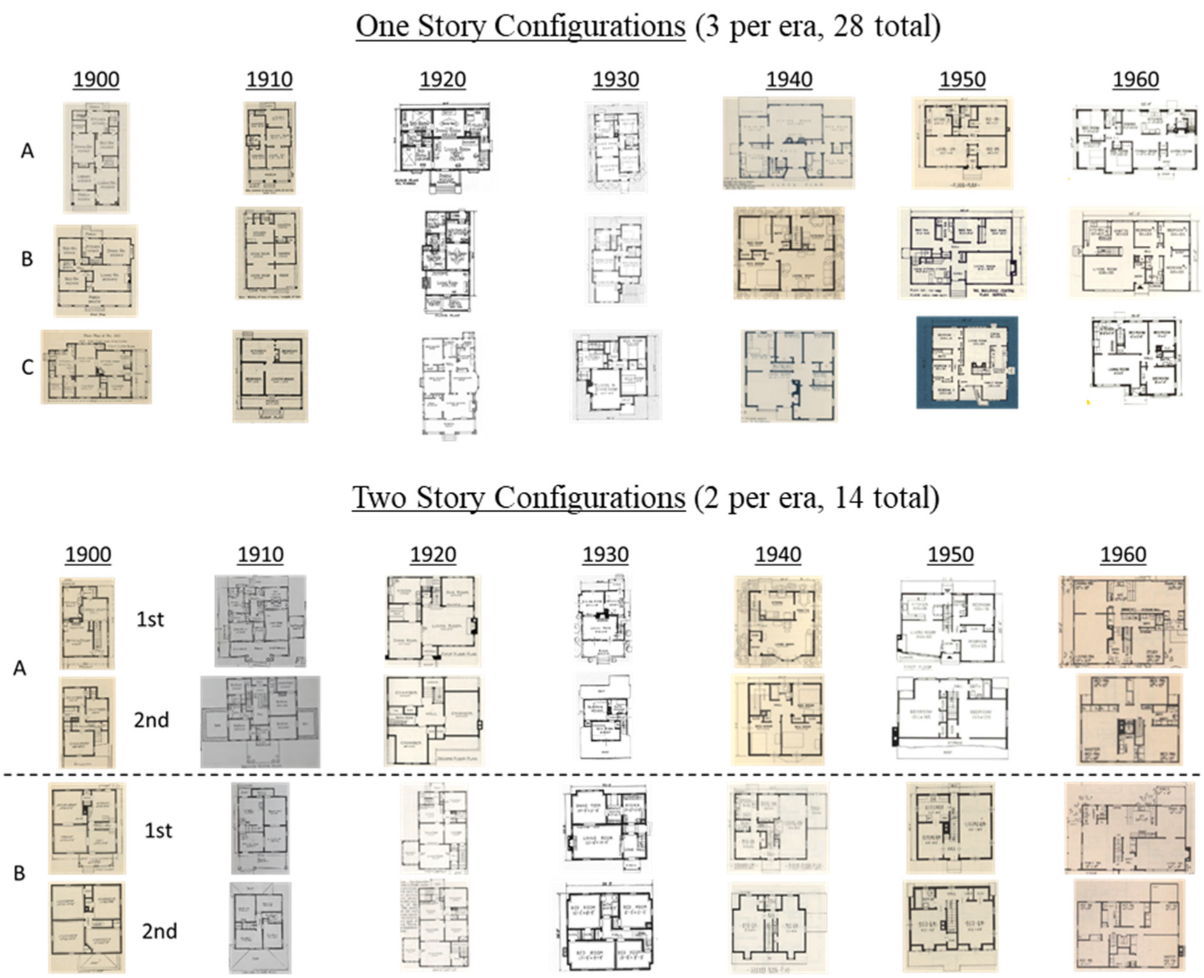

Figure A2.1 Considered plan configurations within the ATC-110 superstructure configuration set [FEMA 2019].

Figure A2.2(b) shows that configuration 1910-B has a total plan area of 1128 ft^2. When measuring for interior and exterior wall quantities, only full pier height sections were considered, and the horizontal dimension of each plan was taken as the "*X*-direction" for each case. Figure A2.2(c) illustrates that the example configuration has 42.5 ft of interior wall in the *X*-direction ($L_{\mathrm{Int},X}$) and 29.5 ft in in the *Y*-direction ($L_{\mathrm{Int},Y}$). Similarly, the exterior walls are measured as 63.0 ft and 62.0 ft in the *X*- and *Y*-directions, respectively. More complete information on individual configurations, including tabulated measurements, can be found in Chapter 6 of *FEMA P-1100*, Vol. 3 [2019].

a)

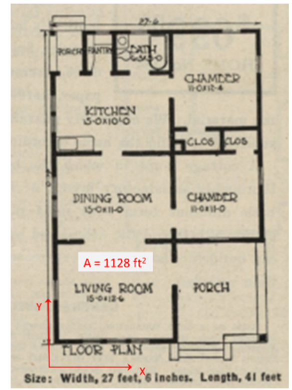

b)

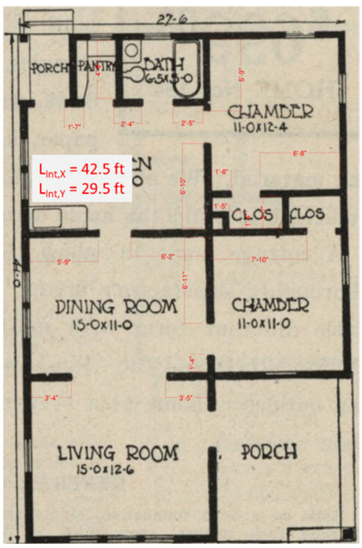

c)

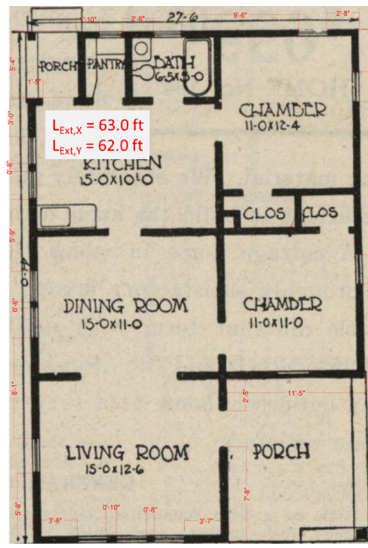

d)

Figure A2.2 **Example of configuration measurements within ATC-110 superstructure study for configuration 1910-1B: (a) exterior view of house; (b) plan configuration; (c) plan measured for interior walls; and (d) plan measured for exterior walls [FEMA 2019].**

A2.2 Superstructure Assumptions within the ATC-110 Project

The ATC-110 project [ATC 2018] used the configuration data described in Section A2.1 in order to estimate appropriate strength and weight (mass) properties for a generic archetype layout. This was performed by first selecting a range of material strength and weight properties assumed representative of different eras of construction. Within the ATC-110 project, material selection targeted the likely upper and lower bounds of material strength and stiffness properties. In terms of exterior materials, stucco and horizontal siding were considered. For interior materials, plaster on wood lath (i.e., lath and plaster) and gypsum wallboard were selected. It was also assumed that the use of gypsum wallboard would not be applicable until the 1930s era and lath and plaster would no longer be applicable after the 1940s. These "era specific" materials were considered in terms of appropriate wall weights and force-deformation backbone curves for application to the various configurations shown in Figure A2.1. Given these assumptions, the configurations representing the 1930s and 1940s eras of construction would consider all combinations of sheathing materials since this was assumed representative of the transition period for interior wall finish material; see Figure A2.3.

For each configuration, combined pushover curves and seismic weights were calculated and recorded. The criteria extracted from the configuration data set included:

- Seismic weight to floor area ratios (W_S/A);
- Average strength to area ratios $(V/A)_{\mathrm{Avg}}$;
- Average strength to seismic weight ratios $(V/W_S)_{\mathrm{Avg}}$; and
- Strong to weak direction ratios ($V_{\mathrm{strong}}/V_{\mathrm{weak}}$).

The term average strength refers to the average of the two horizontal directions (e.g., X and Y). A sample of the average strength to weight ratios for one-story configurations is shown in Figure A2.3. The different material combinations assumed for each era are also annotated.

To utilize the superstructure strength statistics in structural analysis, a configuration plan was assumed. The generic plan configuration used within the ATC-110 project was based on a simplified variation of the CUREE Small House [Isoda et al. 2002], as shown in Figure A2.4. The generic ATC-110 layout [Figure A2.4(a)] assumes a similar 40-ft × 30-ft plan (A = 1200 ft^2) yet has a much simpler interior wall layout and fewer openings around the perimeter when compared to the CUREE Small House; see Figure A2.4(b). This configuration was selected to minimize torsional effects; also, it assumed that representative wall lengths could be scaled to fit target strength criteria.

The ATC-110 project targeted two ranges of strength properties to provide a reasonable range of superstructure strength and stiffness to evaluate expected retrofit performance. On the upper end, the median strength statistics from the pre-1950 eras were targeted. This strength was controlled by exterior stucco and interior lath and plaster. On the lower end, the median minus one standard deviation strength for the post-1950 eras were selected. This era was controlled by exterior horizontal wood siding and interior gypsum wallboard. An example of the different strength targets selected for the ATC-110 project is illustrated in Figure A2.5.

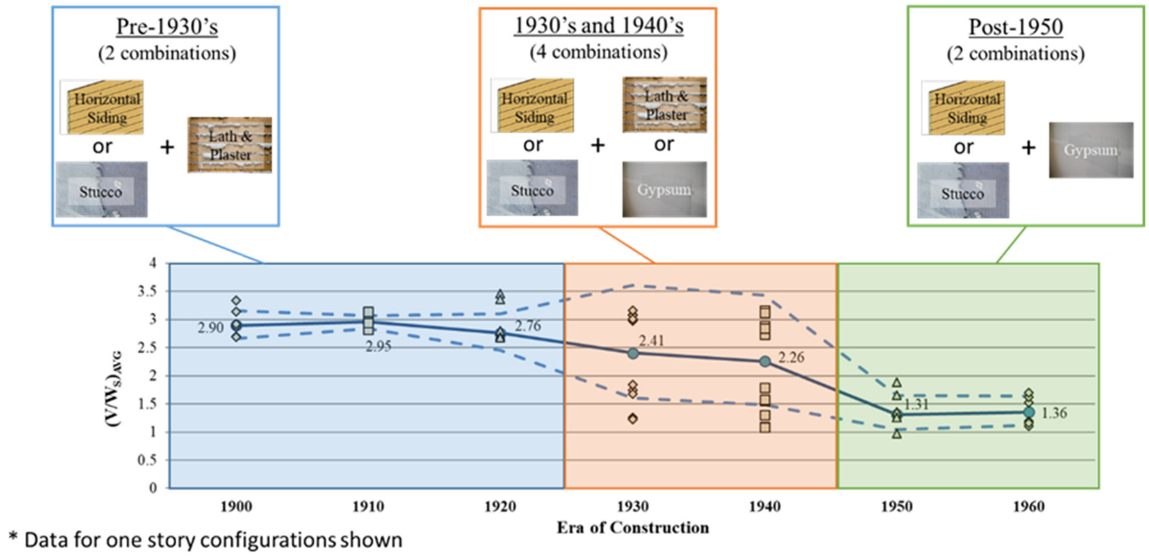

Figure A2.3 **Illustration of attributing material combinations based on era of construction for superstructure strength calculations used in the ATC-110 project. The current figure shows strength to weight ratios for one story configurations.**

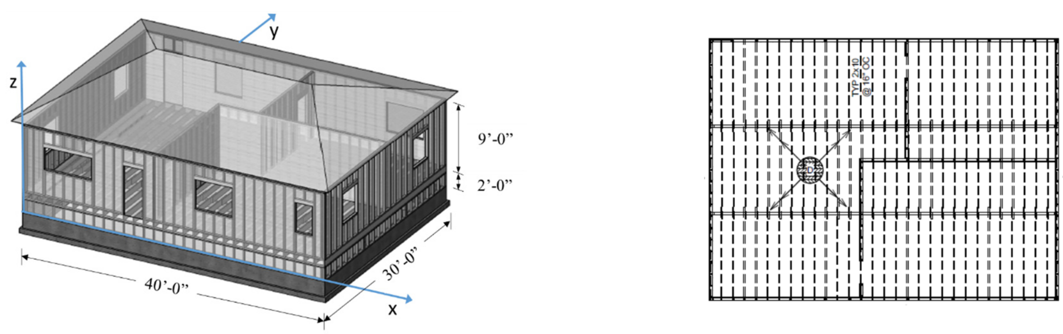

a) Generic ATC-110 Layout

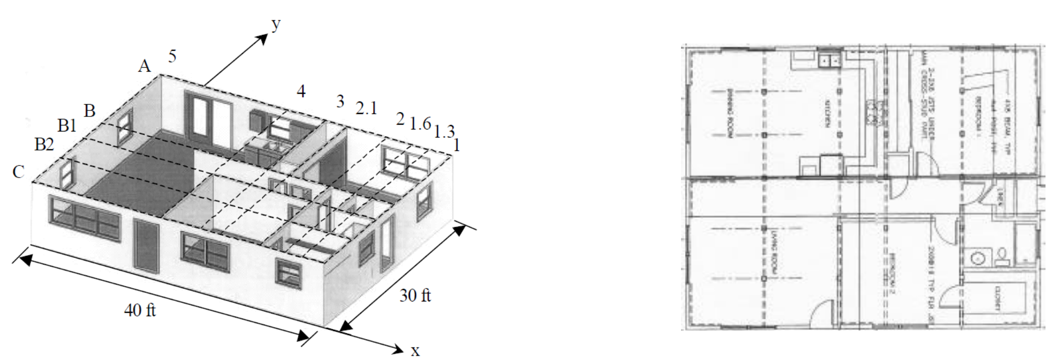

b) CUREE Small House

Figure A2.4 **(a) Basic one-story layout of the case study buildings considered for cripple wall dwellings within the ATC-110 project [2018]; and (b) layout of one story CUREE Small House [Isoda et al. 2002]**

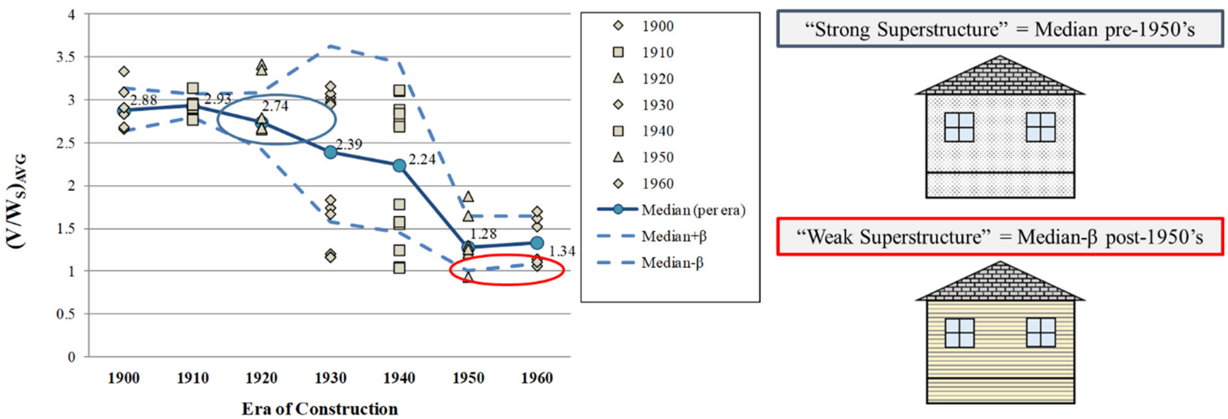

Figure A2.5 **Illustration of using upfront strength and weight statistics to scale the generic ATC-110 layout to provide two superstructure strengths for retrofit guideline development: stucco with lath and plaster (strong and stiff); horizontal siding with gypsum wallboard (weak and flexible).**

A3 DEVELOPMENT OF BASELINE CONFIGURATIONS FOR THE PEER–CEA PROJECT

The use of a single building layout is proposed for one-story and two-story configurations, respectively. The justification for the single geometrical configuration is supported by similar considerations that drive existing assumptions set in place for the PEER–CEA Project, including the adoption of superstructure strength criteria used in the ATC-110 project as well as using simplified geometrical layouts also implemented within ATC-110. Further, neglecting the effects of re-entrant corners and other geometrical details that will not necessarily be captured in structural analysis models of building variants supports the use of single building configurations based on the primary objective of quantifying the differential in seismic performance due to retrofitting.

Necessary deviations from the procedures used in ATC-110 for configuration development are clearly stated and justified in light of the distinct differences in objectives of ATC-110 and the current project. Available configuration data from the ATC-110 project is introduced with different criteria to support the needs of the current project. The proposed configuration is presented for one- and two-story cases based on the information collected within this section in Section A4.

A3.1 Geometry-Based versus Strength-Based Configuration Verification

The ATC-110 project used information from actual building configurations to determine likely distributions and quantities of interior and exterior walls. This was combined with estimated material properties for horizontal sheathing, exterior stucco, interior gypsum wallboard, and interior plaster on wood lath.

An illustration of the general approach used in ATC-110 to develop the baseline archetype configurations to guide the development of retrofit design procedures is shown in Figure A3.1. The figure shows that material properties (strength, stiffness, and weight) are estimated upfront and combined with plan configuration data. This then allowed for a range of strength and stiffness values to be attributed to a generic archetype layout upfront. The two resulting archetypes provided reasonable bounds of strength and stiffness for retrofit guideline development.

The key point to highlight from the ATC-110 configuration development is that the resulting superstructure models were scaled in terms of mass and effective wall length based on the generic layout in Figure A2.4(a). Assuming single scaling factors for mass and wall length (strength), the resulting configurations were targeting strength and weight criteria primarily, where the resulting stiffness of the two superstructures would implicitly consider upper and lower bounds.

In light of the needs for the current PEER–CEA Project, superstructure configurations will need to maintain a realistic balance of strength, mass and stiffness since all three of these properties will affect different aspects of the seismic performance assessment process as shown in Figure A3.2.

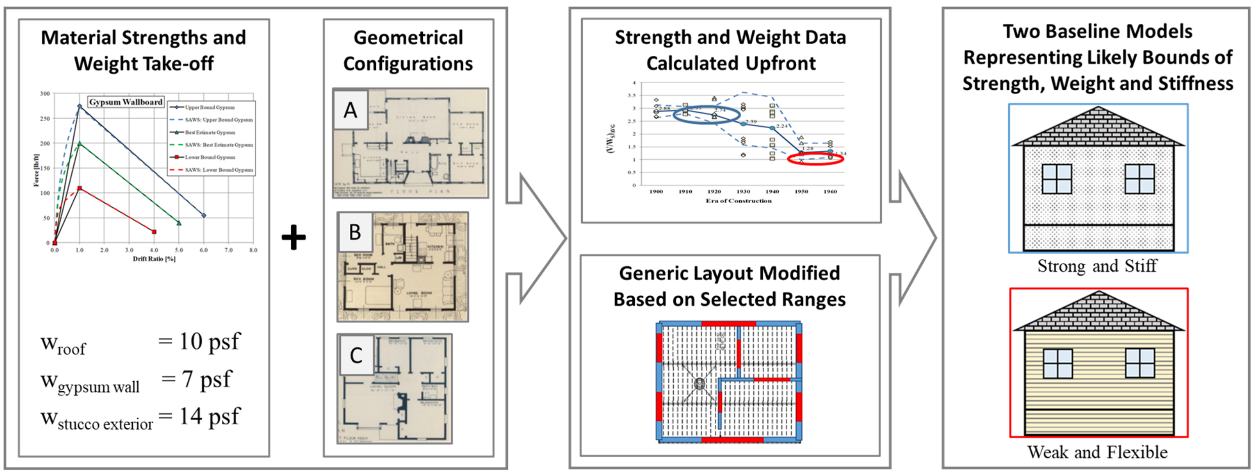

Figure A3.1 **Illustration of the strength-based configuration development used within the ATC-110 Project.**

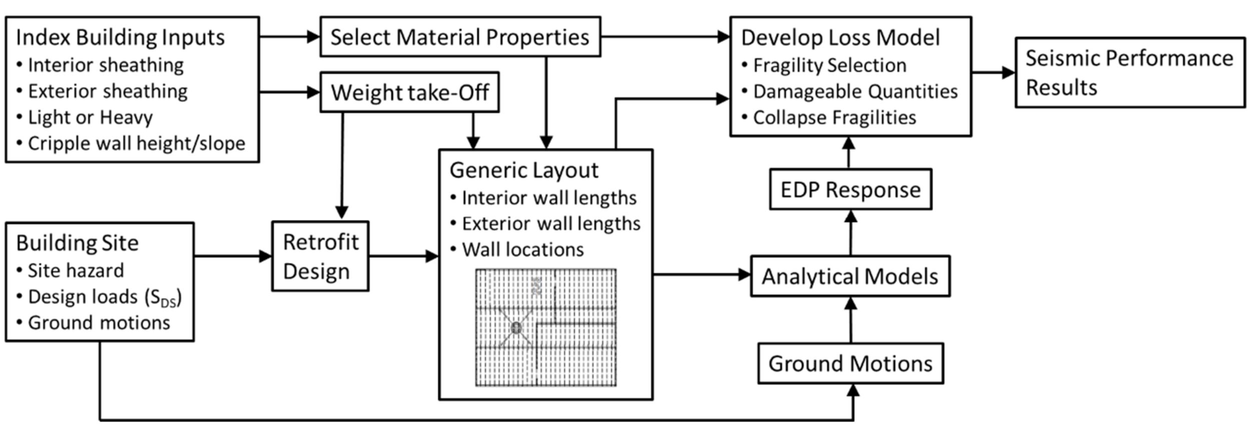

Figure A3.2 **Illustration of the role of building configuration in development of existing and retrofit building variants within the PEER–CEA Project.**

A single building variant from the WG2 matrix (e.g., single-story pre-1945 era, light construction, 2-ft-tall cripple walls, stucco exterior, lath and plaster interior) will determine the structural weights (i.e., seismic mass) and material properties required for interior and exterior sheathing (i.e., strength and stiffness). Further, when combined with an assumed site hazard, the total building weight and cripple wall geometry will be combined with seismic design loads to develop the appropriate retrofitting scheme. These properties can then be combined into the analytical models where the mass, strength, and stiffness will be in proportion to the variant properties assumed. This proportioning is critical since it will affect both structural response (i.e., EDP response) as well as loss model development. The types of interior and exterior sheathing materials will drive component fragility selection while the amount of interior and exterior walls (governed by the assumed configuration) will determine the damageable quantities to be combined with component consequence (i.e., repair cost) functions.

Given this, it is assumed that the PEER–CEA Project archetype configurations will target realistic wall geometry and density rather than pre-determined strength. This will allow for any number of material property combinations and strength assumptions to be combined using a realistic density of walls that will remain consistent throughout the performance assessment process.

A3.2 Geometry-Based Statistics from the ATC-110 Configuration Dataset

The same set of building configurations used in the ATC-110 project (see section A2.1) are also used as a guide for archetype development for the current project. The key difference is that configuration data is collected based on geometrical properties rather than strength. The configuration criteria for single story cases are summarized as follows:

- *Exterior wall density* (L_{EXT}/A): Total full-height exterior wall length divided by the floor area;
- *Maximum-to-minimum exterior wall length ratio* $(L_{\max}/L_{\min})_{\mathrm{EXT}}$: Ratio of larger exterior wall length of two perpendicular directions to the lesser of the two perpendicular directions;
- *Interior wall density* (L_{INT}/A): Total full-height interior wall length divided by the floor area, and;
- *Maximum-to-minimum interior wall length ratio* $(L_{\max}/L_{\min})_{\mathrm{INT}}$: Ratio of larger interior wall length of two perpendicular directions to the lesser of the two perpendicular directions.

The combination of the measured wall density with the maximum to minimum ratio allows for the total length of interior or exterior wall to be defined, as well as the amount of wall expected in the two perpendicular directions of the configuration. The one-story configuration data are shown as a function of construction era in Figure A3.3 and Figure A3.4 for exterior and interior walls, respectively. The figures clearly show that there are not strong enough trends across construction era to make distinctions. This is largely due to the rather small dataset under consideration, despite the significant effort involved in obtaining it. Given this, the current archetype buildings will target the mean values extracted from the ATC-110 configurations, irrespective of construction era. This assumption targets capturing typical floor layout characteristics with different structural responses resulting from the different material property combinations placed within the assumed layout.

Additionally, the figures show standard deviation bounds (dashed lines) under the assumption that the data is lognormal. The data was checked for both normal and lognormal distribution fitting using the Kolmogorov-Smirnov (K-S) and Lilliefors tests at 5% significance; returning the exact same trends for both distributions. The lognormal assumption was adopted after reviewing the histograms of the data. A comparison of normal and lognormal assumptions for the interior wall density (L_{INT}/A) for the one-story configurations is shown in Figure A3.5.

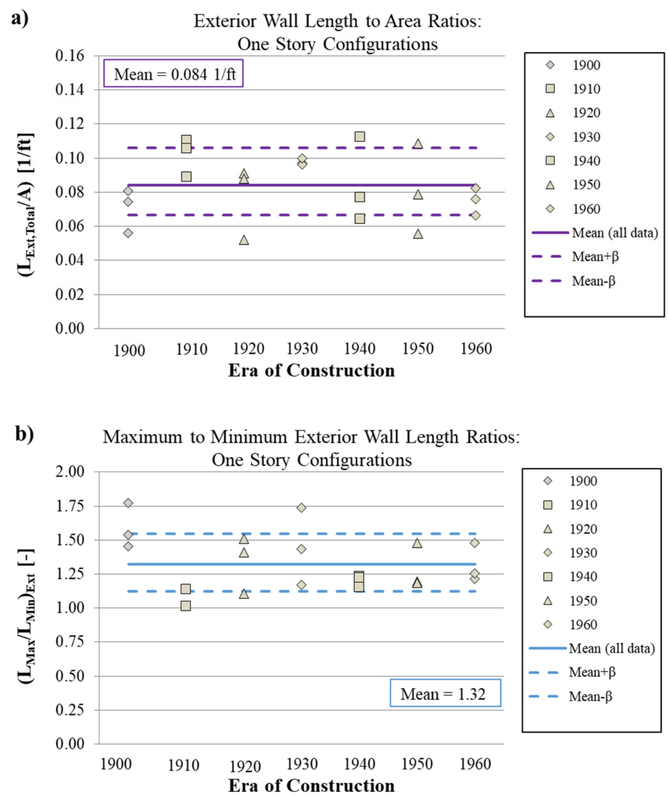

Figure A3.3 **Exterior wall criteria for one-story configurations: (a) exterior wall density; and (b) maximum to minimum exterior wall length ratio.**

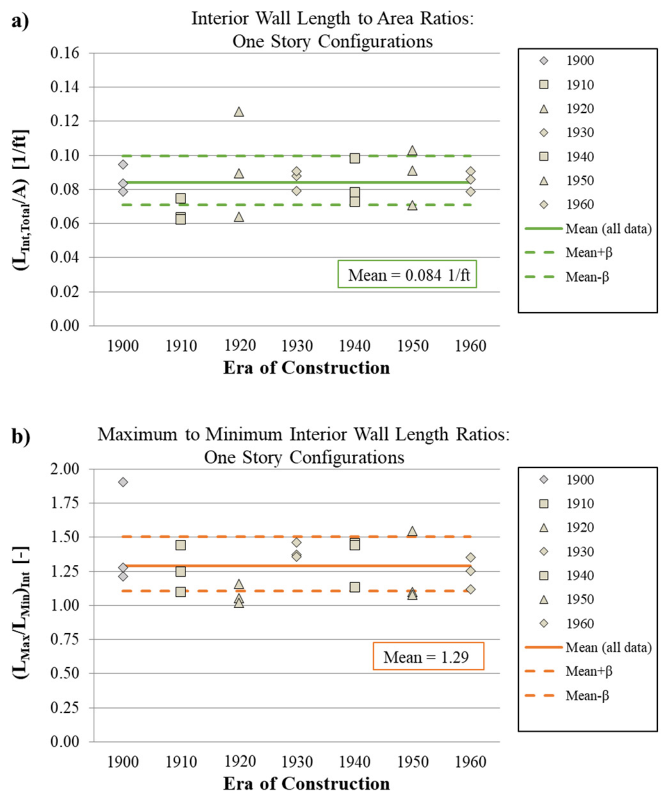

Figure A3.4 **Interior wall criteria for one-story configurations: (a) Interior wall density; and (b) maximum to minimum interior wall length ratio.**

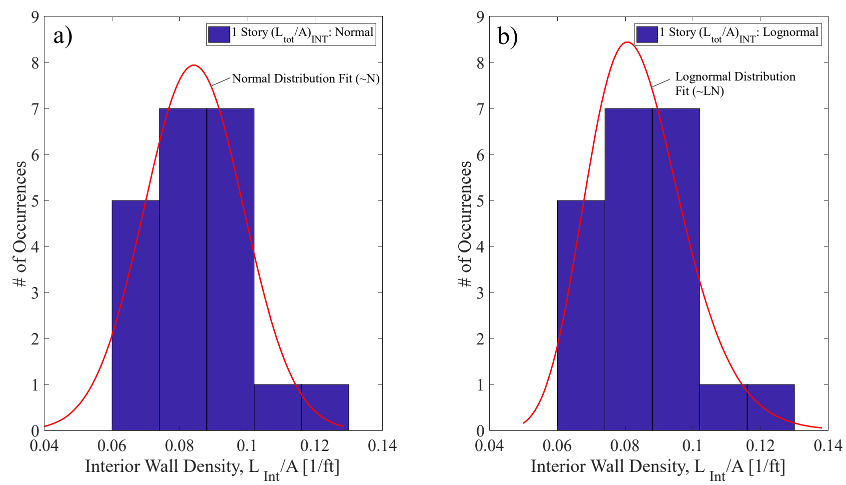

Figure A3.5 **Comparing normal (a) and lognormal (b) distribution fits to interior wall density data for one-story cases.**

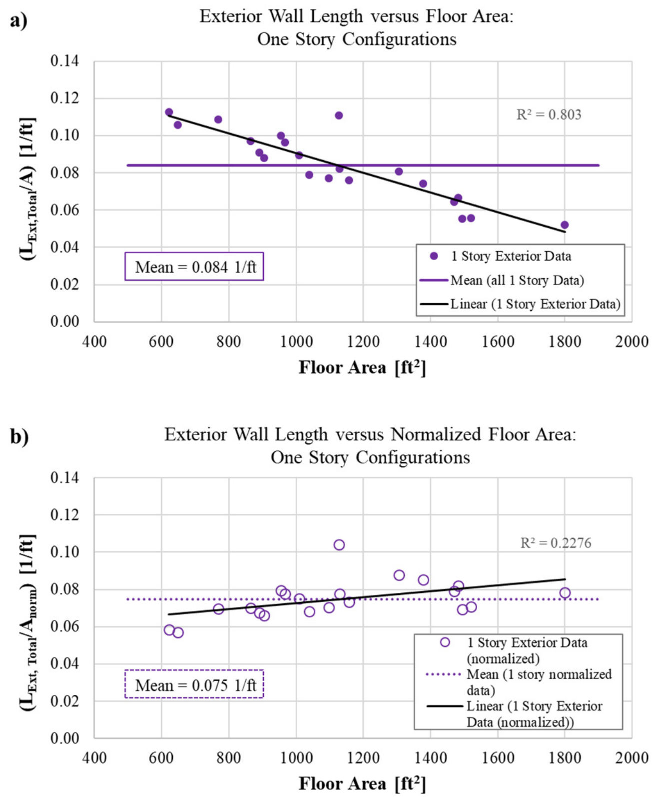

Figure A3.6 Comparing exterior wall densities versus plan area for one-story configurations: (a) original configuration data; and (b) data normalized by target plan area of 1200 ft^2.

Another important consideration for interpreting the configuration data is the treatment of target plan area for exterior wall densities. First, it is assumed that the baseline archetypes will have a 1200 ft^2 plan with 0.75 aspect ratio (i.e., 40 ft × 30 ft) in line with previous ATC-110 work and deemed adequate by the WG2 building variant report [Reis 2020(a)]. Based on this assumption, the exterior wall densities are normalized by the target area of 1200 ft^2. The results of the original exterior wall densities versus plan area are compared with normalized values for the one-story configurations in Figure A3.6.

The original data in Figure A3.6(a) shows that there is a clear trend between the exterior wall density and plan area. Although the difference in the mean values is on the order of 10% between original and normalized densities, the normalized values are deemed a more appropriate average for an archetype with a footprint of 1200 ft^2. Notably, the interior wall densities did not show a strong dependence on floor area. Based on this, the interior wall densities assume the original mean values.

The configuration data for the two-story cases considers the same four criteria to define interior and exterior wall densities yet are recorded separately for the first and second story. First floor information for the two-story cases is provided in Figure A3.7 and Figure A3.8 for exterior and interior walls, respectively. Similarly, the data is presented for the second floor of the two-story configurations in Figure A3.9 and Figure A3.10. The comparisons of nominal and normalized exterior wall density versus floor area data are presented for the two-story cases in

Figure A3.11 and Figure A3.12 for the first story and second story, respectively. Notably, the normalized exterior wall densities (using target area of 1200 ft^2) show a reduction of approximately 25-30% when compared to mean values using nominal data for the two-story configurations.

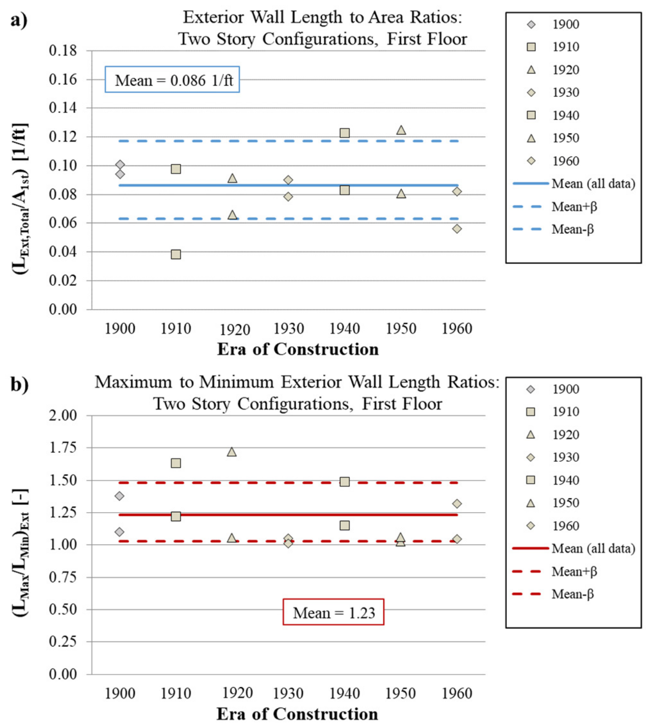

Figure A3.7 **Exterior wall criteria for the first floor of two-story configurations: (a) exterior wall density; and b) maximum to minimum exterior wall length ratio.**

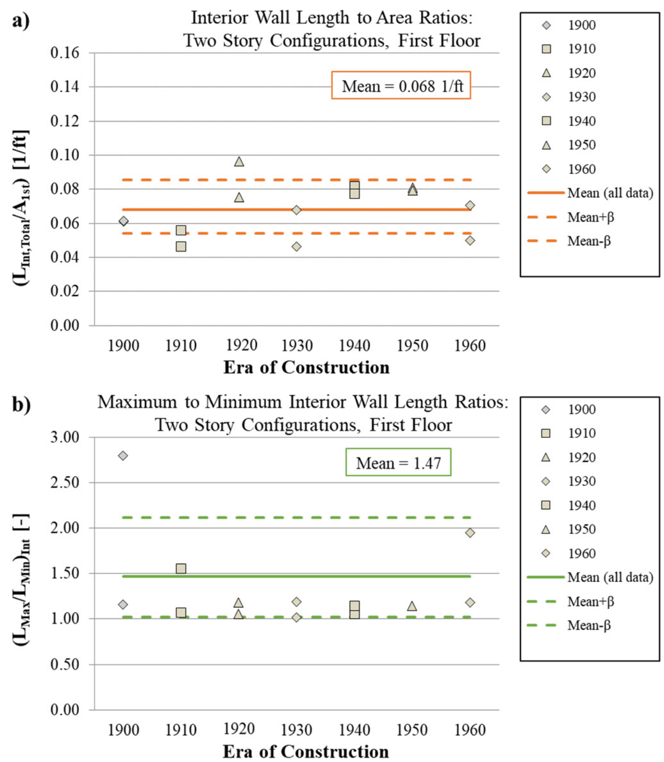

Figure A3.8 **Interior wall criteria for the first floor of two-story configurations: (a) interior wall density; and (b) maximum to minimum interior wall length ratio.**

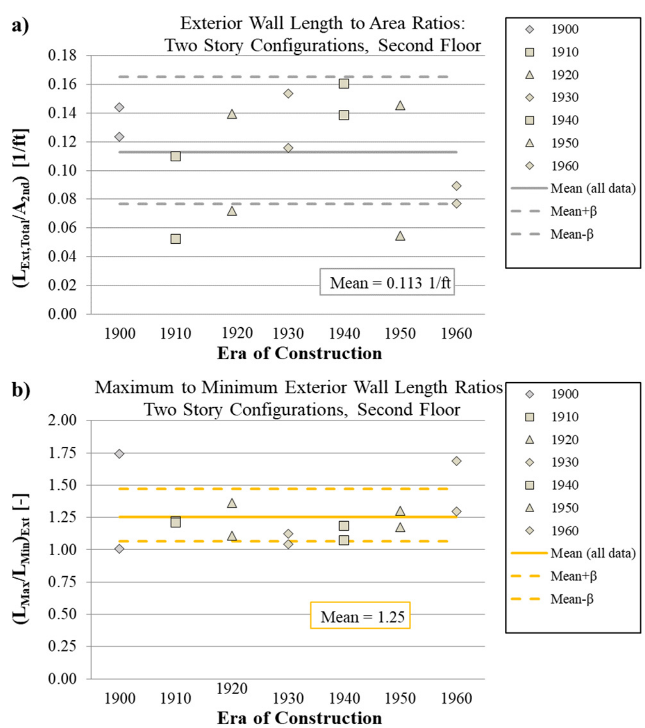

Figure A3.9 **Exterior wall criteria for the second floor of two-story configurations: (a) exterior wall density; and (b) maximum to minimum exterior wall length ratio.**

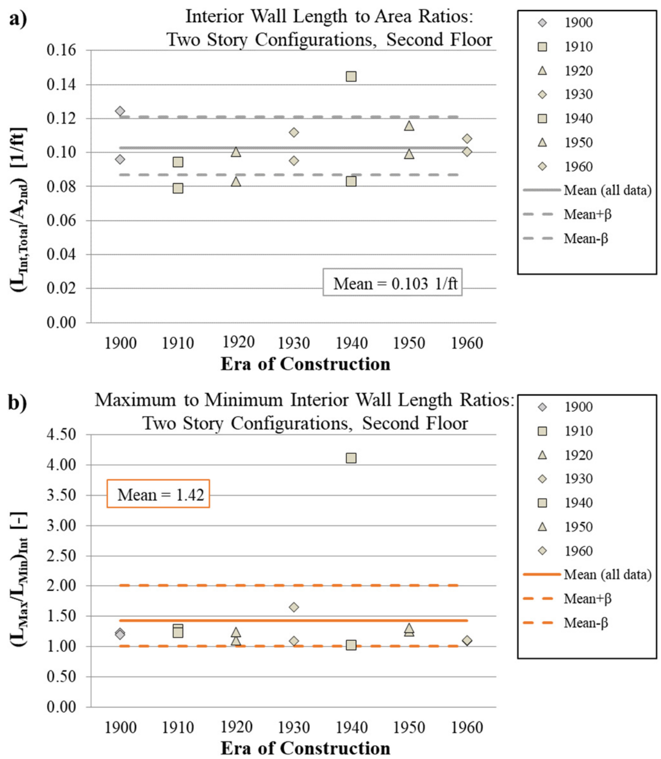

Figure A3.10 Interior wall criteria for the second floor of two-story configurations: (a) interior wall density; and (b) maximum to minimum interior wall length ratio.

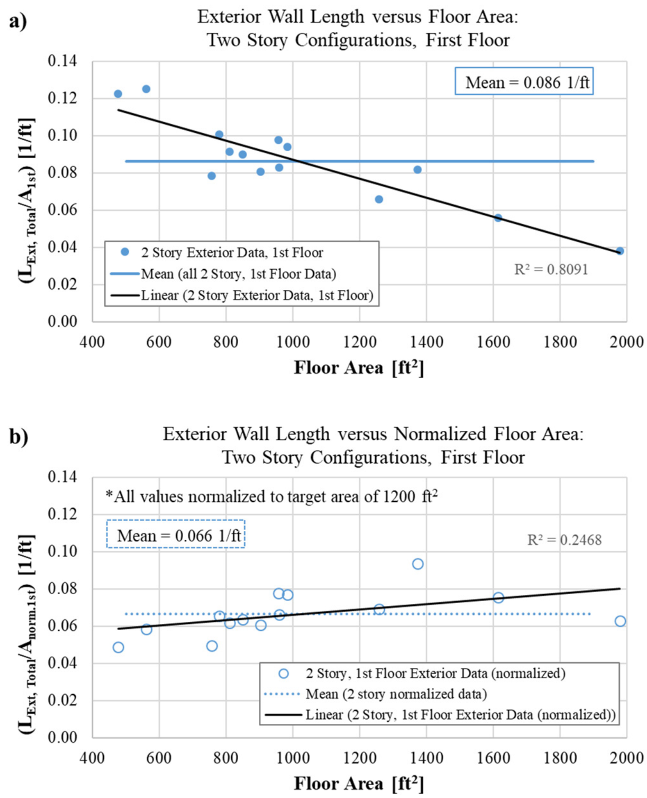

Figure A3.11 **Comparing exterior wall densities versus plan area for the first story of two-story configurations: (a) original configuration data; and (b) data normalized by target plan area of 1200 ft^2.**

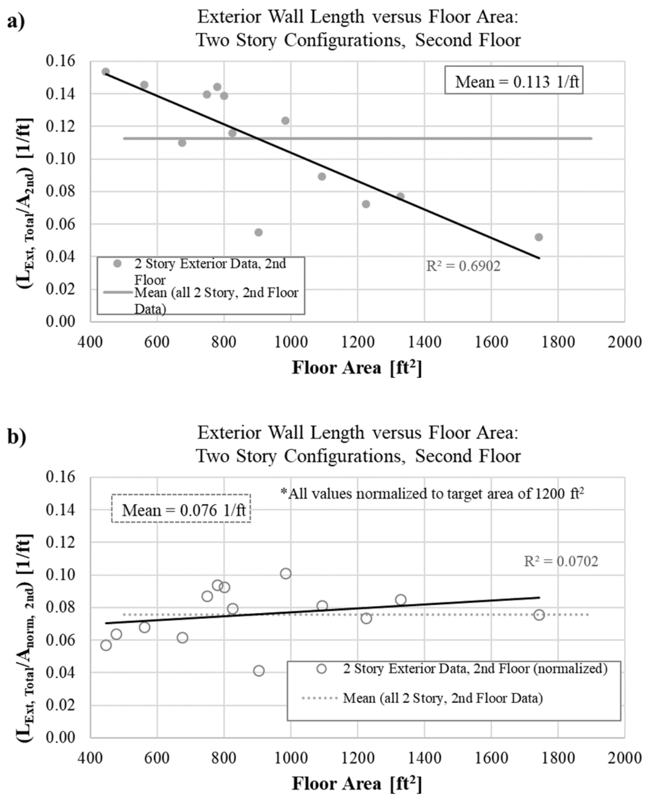

Figure A3.12 Comparing exterior wall densities versus plan area for the second story of two-story configurations: (a) original configuration data; and (b) data normalized by target plan area of 1200 ft^2.

In addition to recording the wall density information for each story of the two-story cases, two additional criteria are recorded:

- *Second-to-first floor interior wall density* $(L_{INT}/A)_2/(L_{INT}/A)_1$: The relative amount of second floor interior walls relative to the first floor, and;
- *Second-to-first floor exterior wall density* $(L_{EXT}/A)_2/(L_{EXT}/A)_1$: The relative amount of second floor exterior walls relative to the first floor.

These parameters are important for understanding the typical wall density trends from the first to second story. Another important consideration is difference in floor plan area between the second and first stories (i.e., A_2/A_1). Configurations with smaller plan areas in the second story may lead to skewed results in terms of wall length to area densities. As such, the second to first-floor wall densities are scaled by the area ratio A_2/A_1 in order to normalize the wall densities to a case where the plan area is consistent in lower and upper stories. The influence of the second story to first-story area ratios (A_2/A_1) on the equivalent ratio of interior and exterior wall density is shown in Figure A3.13. The figure shows both interior and exterior wall density is typically larger in the upper stories than lower stories. This is logical since the first story of many homes has larger open spaces for living rooms and kitchen/dining compared to an upper story that consists mostly of bedrooms. Similarly, the bottom story of a home would likely have larger and more numerous windows with respect to the upper story. Figure A3.13 shows that this increase in wall density in upper floors is reflected by the results even for configurations with equal first and second story areas (i.e., $A_2/A_1 = 1.0$). Using mean data, the second story would have roughly a 40% increase in interior walls and a 15% increase in exterior walls. This will be an important consideration for the development of a two-story baseline configuration in Section A4.

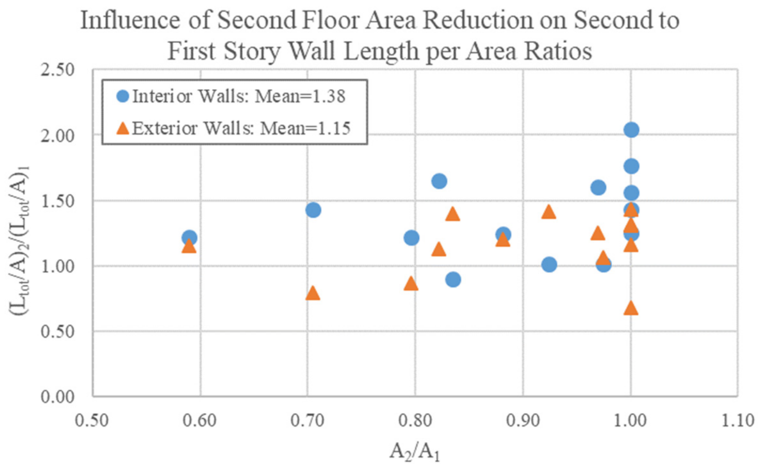

Figure A3.13 Influence of second story to first story area ratios on second to first story wall density ratios: interior walls (blue circles); exterior walls (orange triangles). Note: Nominal density ratios are scaled by A_2/A_1 to account for smaller upper floor areas in some cases.

A4 PROPOSED ONE- AND TWO-STORY BASELINE ARCHETYPE CONFIGURATIONS

This section provides the proposed configurations for use as baseline archetypes for analysis of building variants within the PEER–CEA Project. These buildings will be implemented to investigate the numerous sheathing material, cripple wall geometry and anchorage conditions proposed within the WG2 building variant list [Reis 2020(a)].

A4.1 One-Story Configuration

The collection and review of the one-story configuration data allowed for the central tendency trends to be quantified. In addition to quantifying the expected wall density for the baseline archetype, the spatial distribution of walls must also be realistic. The data was then compared to the equivalent values from two previously studied archetype configurations, namely; the ATC-110 layout, and the CUREE Small House; see Figure A2.4). A comparison of one-story configuration data (including the first story of two-story cases) is shown in Table A4.1.

Upon reviewing the mean data in comparison with previously studied configurations, it was found that the CUREE Small House fit the one-story criteria very well across all categories. Given this, the CUREE Small House configuration was assumed adequate for the basis of the baseline superstructure layout used within the PEER–CEA Project. This configuration was also selected since accurate drawings are available from previous work within the CUREE Caltech project as well as its development being based on an actual house layout [Cobeen 2018]. The mean configuration data for the first story is also plotted for wall length to area density and maximum-to-minimum wall length ratios in Figure A4.1 and Figure A4.2, respectively. The figures have the

CUREE Small House columns highlighted to indicate that this is the selected configuration for baseline development.

Table A4.1 Comparison of previously studied one-story configurations with data obtained from the ATC-110 configuration dataset.

Dataset		Total interior wall length to first-floor area ratio **$(L_{INT}/A)_{1st}$ (1/ft)**	Maximum to minimum interior wall length ratio **$(L_{max}/L_{min})_{INT}$**	Total exterior wall length to first-floor normalized area ratio* **$(L_{EXT}/A_{norm})_{1st}$ (1/ft) ***	Maximum to minimum exterior wall length ratio **$(L_{max}/L_{min})_{EXT}$**
All 1-story data (21 configurations)	**Mean**	**0.084**	**1.29**	**0.075**	**1.32**
	Mean + β	0.100	1.51	0.085	1.55
	Mean - β	0.071	1.10	0.065	1.13
	β	0.17	0.16	0.13	0.16
All 2-story data (14 configurations)	**Mean**	**0.068**	**1.47**	**0.066**	**1.23**
	Mean + β	0.085	2.11	0.079	1.48
	Mean - β	0.054	1.02	0.056	1.03
	β	0.23	0.36	0.17	0.18
All data (35 configurations)	**Mean**	**0.078**	**1.36**	**0.071**	**1.29**
	Mean + β	0.097	1.76	0.084	1.52
	Mean - β	0.062	1.05	0.061	1.08
	β	0.22	0.26	0.16	0.17
Generic layout used in ATC-110	ATC-110	0.036	1.13	0.078	1.19
CUREE Small House	CSH	0.081	1.24	0.074	1.28

* Exterior wall values normalized for target area of 1200 ft^2.

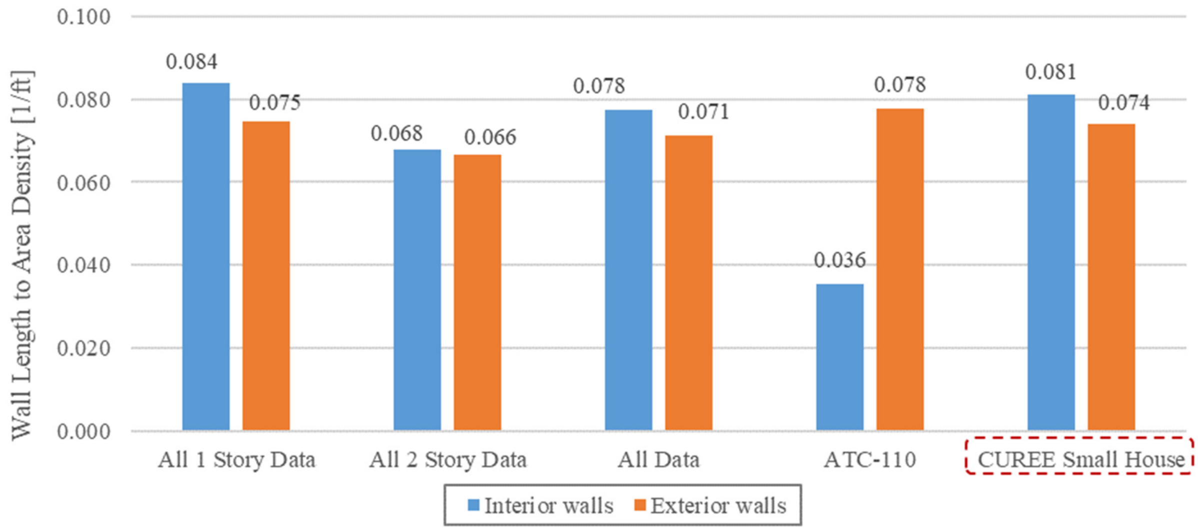

Figure A4.1 Comparing mean first-floor wall density data to previously studied archetype configurations. NOTE: the CUREE Small House is highlighted to illustrate that this is the proposed one-story baseline configuration based on observed fit to mean data.

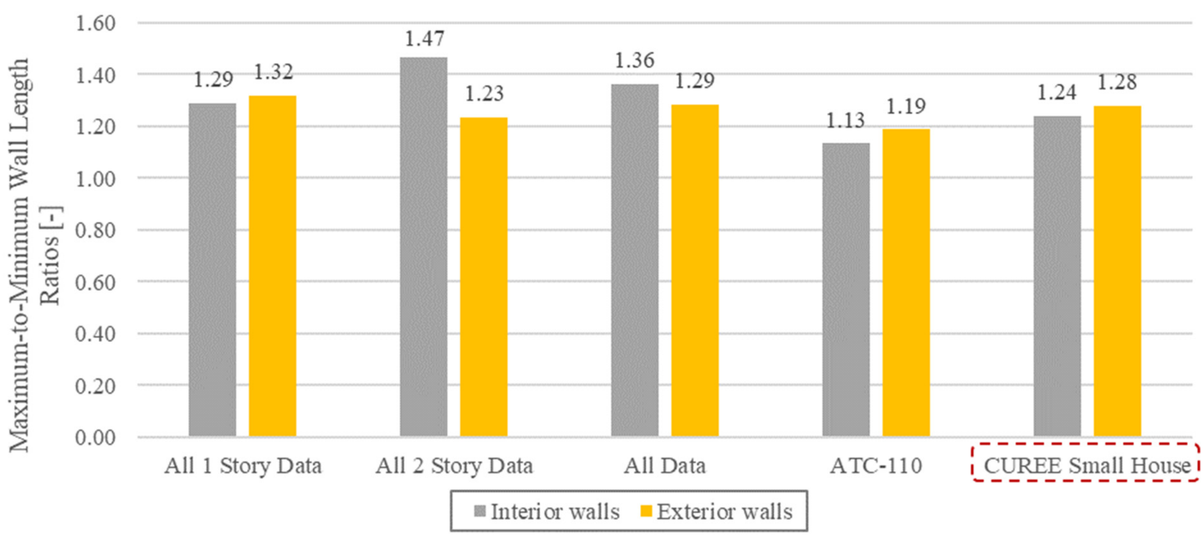

Figure A4.2 Comparing mean first-floor maximum to minimum wall length ratios to previously studied archetype configurations. NOTE: the CUREE Small House is highlighted to illustrate that this is the proposed one-story baseline configuration based on observed fit to mean data.

To efficiently represent the CUREE Small House configuration within structural analysis models, the interior wall lines are combined to eliminate small sections of wall (e.g., closets) from needing separate wall elements to be modeled. Similar assumptions were made within the CUREE Caltech Woodframe project [Isoda et al. 2002]. The proposed wall idealization for the one-story configuration is compared with the original CUREE Small House configuration in Figure A4.3. The figure shows that the exterior wall lines are straightforward with only full wall height sections combined. This results in symmetrical exterior walls in the *X*-direction of the house (i.e., 40-ft dimension) and different exterior wall lengths in *Y*-direction (i.e., 30-ft dimension) due to the difference in openings. The interior walls are combined into three different walls for each principal direction. The main modifications for combining walls lines involve taking small closet walls and combining them with nearby principal wall lines. For example, the closet walls in the bathroom area were added to the main interior walls surrounding bedroom 2 keeping the principal directions consistent in the *X*- and *Y*-directions. These combinations of interior wall lines will maintain the expected wall density (i.e., effective wall length) in each direction without drastically changing the stiffness and strength eccentricities associated with combining walls. For completeness, the actual locations and assumed effective wall lengths for all wall lines within the proposed one-story configuration are provided in Table A4.2.

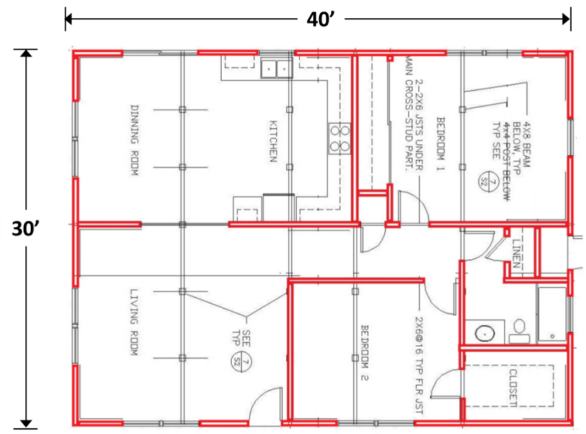

a) CUREE Small House

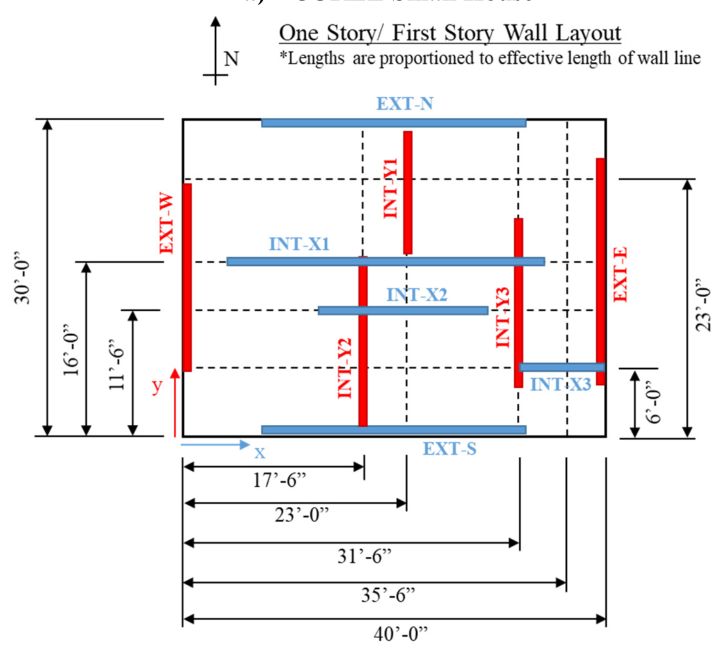

b) Idealized one story configuration based on CUREE Small House

Figure A4.3 Illustration of equivalent wall lines assumed for structural modeling of the CUREE Small House: (a) original configuration; and (b) idealized configuration with combined wall lines.

Table A4.2 **Effective wall lengths and locations of wall lines assumed for the baseline one story configuration (refer to Figure A4.3b for wall indices).**

Index[1]	Direction	L_W (ft)[2]	L_{eff} (ft)[3]	x_{coord} (ft)	y_{coord} (ft
EXT-S (south)	X	40.0	25.0	20.0	0
EXT-N (north)	X	40.0	25.0	20.0	30.0
EXT-W (west)	Y	30.0	17.67	0	15.0
EXT-E (east)	Y	30.0	21.33	40.0	15.0
INT-X1	X	30.0	60.0	23.0	16.0
INT-X2	X	16.0	32.0	23.0	11.5
INT-X3	X	8.0	16.0	35.5	6.0
INT-Y1	Y	11.5	23.0	23.0	23.0
INT-Y2	Y	16.0	32.0	17.5	6.0

[1] EXT = exterior wall, INT = interior wall.
[2] Total wall length used for weight take-off.
[3] Effective wall length used for strength and stiffness (interior walls reflect a single-sided material on each side of wall).

A4.2 Two-Story Configuration

The development of a two-story configuration requires a few underlying assumptions that will maintain consistency across all building variants to be investigated. The assumptions include:

- *Equivalent first story layout* – The two-story configuration will assume the same bottom story configuration as the one-story baseline (see Figure A4.3). This is assumed to maintain the most consistency when understanding differences in performance between one- and two-story variants; and
- *Equal second and first story areas* – The two-story configuration will assume the same plan area (i.e., 1200 ft^2) as the one-story configuration. This assumption will be the most in line with the underlying assumptions of the ATC-110 plan sets used for retrofit design; where stories were "doubled" when considering weight take-offs for two-story designs;
- *Symmetrical wall layout* – The second story wall configurations will assume a symmetrical layout for baseline analysis. This assumption is made in lieu of an actual wall layout to be coupled with the CUREE Small House configuration assumed at the bottom story. This is justified by typical wall damage concentrating at the bottom story of two-story configurations [CUREE 2010]. All sources of mass and stiffness will be preserved based on the configuration data set only without explicit consideration of eccentricities due to openings and interior wall placement;
- *Equal interior wall density* – The interior wall density of the second floor will assume the same as the lower story. This assumption targets consistency between stories in terms of the amount of damageable interior wall area applied

in each story. Further, although nominal data suggests that the wall density could be increased by 40% considering mean two story data (Figure A3.13), the average difference between one- and two-story interior wall densities at the first floor is already 20% higher for one story configurations; which forms the basis of the first story layout; and

- *Scaled exterior wall density* – The exterior wall density will be scaled by 15% with respect to the bottom story based on the observed ratios from two-story configuration data. This will accept a moderate increase in second story stiffness without changing the damageable quantities with respect to the first floor. This is due to exterior material fragilities and cost functions being defined in terms of total wall area without considering reduction for openings.

Based on these assumptions, the appropriate modifications to the wall densities of the one-story configuration must be made to produce a representative second story according to the mean data extracted from the ATC-110 configuration set. Since the same lower story will be assumed, only the relative wall densities from the second to first floor are considered in combination with the expected maximum to minimum wall length ratios. A summary of the information used to create the second story of the two-story baseline configuration is provided in Table A4.3. Notably, Table A4.3 does not include the interior wall density ratio since this will be assumed consistent with the lower story.

Table A4.3 Second-story configuration data used to modify the baseline first-story configuration. Baseline configuration targets mean properties.

		Maximum to minimum second-story interior wall length ratio	Second- to first-story exterior wall length to area ratio *	Maximum to minimum second-story exterior wall length ratio
Dataset		$(L_{max}/L_{min})_{2,INT}$	$(L_{EXT}/A)_2/(L_{EXT}/A)_1$ (1/ft) *	$(L_{max}/L_{min})_{2,EXT}$
All 2-Story Data (14 configurations)	**Mean**	**1.42**	**1.15**	**1.25**
	Mean + β	1.68	1.45	1.47
	Mean - β	1.21	0.92	1.06
	β	0.17	0.23	0.16

* Second to first-floor wall density ratios are scaled by $A2/A1$ to account for smaller upper stories. Note: the second-floor interior wall length to area ratio (density) assumes the same as the first floor.

The interior wall layout assumes that more wall length will be applied in the shorter 30-ft dimension of the house (Y-direction). Using the $(L_{max}/L_{min})_{2,INT}$ of 1.42 and a total interior wall length of 97.5 ft, this corresponds to 40 ft of wall in the X-direction and 57.5 ft of wall in the Y-direction. This is applied symmetrically to the configuration assuming one long wall of 40 ft in the X-direction and three distributed walls of 19.17 ft (19 ft-2 in.) in the Y-direction; see Figure A4.4. The exterior walls assume the same proportions in X and Y as the first story configuration and are scaled by 1.15 to represent the expected increase from the first to second story (e.g., smaller window openings). The resulting values are two exterior walls of 22.5 ft in the Y-direction and two walls of 28.75 ft in the X-direction. Notably, the maximum to minimum exterior wall length ratio is very close to the target from mean data of two-story configurations (i.e., 1.28 actual vs. 1.25 target). The second-story configuration is presented in Figure A4.4, recalling that the second story targets a symmetrical configuration in terms of strength and stiffness eccentricity. The locations and effective wall lengths for the two-story configuration are provided in Table A4.4.

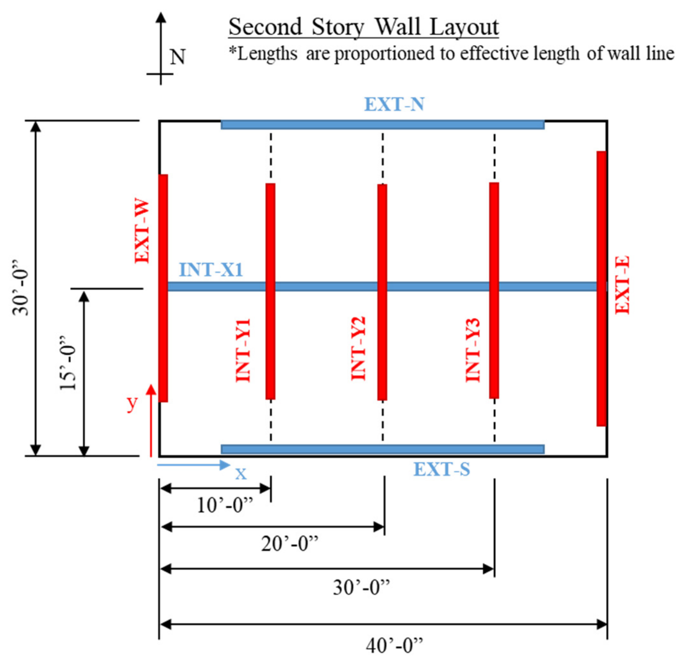

Figure A4.4 **Illustration of equivalent wall lines assumed for structural modeling of the second story of the two-story baseline configuration. NOTE: first story assumes the configuration presented in Figure A4.3(b).**

Table A4.4 Effective wall lengths and locations of wall lines assumed for the upper story of the two-story baseline configuration (refer to Figure A4.4).

Index[1]	Direction	L_W (ft)[2]	L_{eff} (ft)[3]	x_{coord} (ft)	y_{coord} (ft)
EXT-S (south)	X	40.0	28.75	20.0	0
EXT-N (north)	X	40.0	28.75	20.0	30.0
EXT-W (west)	Y	30.0	22.50	0	15.0
EXT-E (east)	Y	30.0	22.50	40.0	15.0
INT-X1	X	40.0	80.0	20.0	15.0
INT-Y1	Y	19.17	38.33	10.0	15.0
INT-Y2	Y	19.17	38.33	20.0	15.0
INT-Y3	Y	19.17	38.33	30.0	15.0

[1] EXT = exterior wall, INT = interior wall.
[2] Total wall length used for weight take-off.
[3] Effective wall length used for strength and stiffness (interior walls reflect a single-sided material on each side of wall).

A5 ADDITIONAL CONFIGURATIONS FOR CONSIDERATION OF CONFIGURATION VARIABILITY

This section illustrates a few key configurations taken from the ATC-110 configuration set that could allow for further investigation of configuration influence on seismic performance assessment. The proposed baseline configurations (Section A4) will allow for the numerous building variants to be compared and contrasted in terms of material combinations and cripple wall geometries. However, the baseline configurations will treat wall density, floor plan area, and wall locations as constants during the variant analysis. This section provides a sample of configurations that may be considered for investigating the effects of configuration and plan size on the seismic performance of cripple wall dwellings.

The ATC-110 configuration dataset was used in order to target simple upper and lower bounds in terms of wall density. This was done by calculating a combined error of interior and exterior wall density (wall length to area ratio) in comparison to mean plus and minus one standard deviation of the dataset. The error is defined as the absolute value of one minus the ratio of the current case to the target criterion and then taking the sum for interior and exterior walls. This was done for both one- and two-story configurations, yet the two-story configurations targeted the wall density at the bottom story.

The one-story configuration best fitting the mean minus one standard deviation wall density is 1910-1C, which is shown in Figure A5.1. This configuration shows a very simple interior wall layout. The plan area of 528 ft^2 is less than half of the target plan area of 1200 ft^2 for the baseline archetypes. In addition to having lower wall density, the smaller plan area would also put this structure in a different plan set class for retrofitting according to ATC-110 (e.g., current baseline is in the 1001 to 1200 ft^2 category), which could also be investigated.

a) b)

Figure A5.1 One-story configuration close to mean minus one standard deviation wall density from ATC-110 data (Configuration 1910-1C; $A_{plan.}$=.528 ft^2): (a) rendering of house; and (b) floor plan.

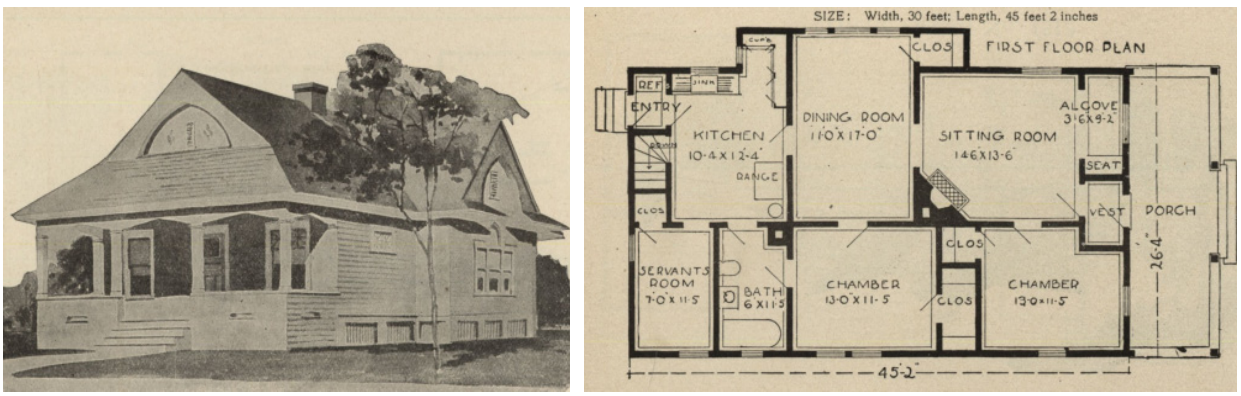

a) b)

Figure A5.2 One-story configuration close to mean plus one standard deviation wall density from ATC-110 data (Configuration 1900-1B; $A_{plan.}$=.1305 ft^2): (a) rendering of house; and (b) floor plan.

Towards the upper bound, the one-story configuration closest to mean plus one standard deviation wall density is 1900-1B; see Figure A5.2. This configuration has a larger plan area (1305 ft^2) compared to the baseline configuration. The layout of configuration 1900-1B could be presumably changed considering the age of the home due to remodeling, yet this configuration does give insight as to how an upper bound wall density may be represented.

For the two-story configurations, 1900-2A (Figure A5.3) and 1920-2B (Figure A5.4) were found to best match the mean minus one standard deviation and plus one standard deviation wall densities, respectively. Similar to the one-story configurations, the mean minus one standard deviation case is a smaller first floor plan area (780 ft^2) with respect to the baseline configuration. The mean plus one standard deviation case has an area similar to the baseline configuration (1258 ft^2) yet would still require a different plan set retrofit according to the ATC-110 guidelines.

These additional configurations are not intended to represent the actual standard deviation of the pre-1970s building stock yet do allow for some reference to investigate the effects of different floor plan configurations. Notably, all four of the additional configurations show steps leading up to the front entrance, suggesting that all four could have been constructed on cripple walls.

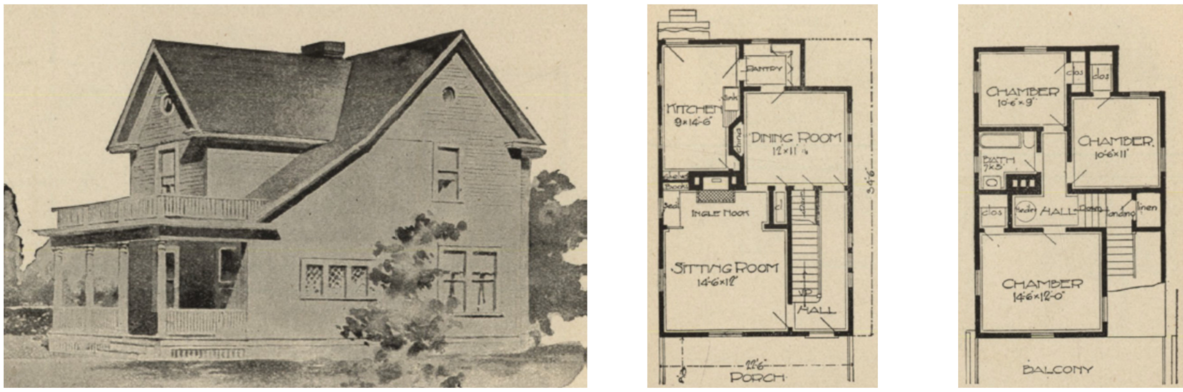

(a) (b) (c)

Figure A5.3 Two-story configuration close to mean minus one standard deviation wall density from ATC-110 data (Configuration 1900-2A; A_{plan}.=.780 ft^2): (a) rendering of house; (b) first-floor plan; and (c) second-floor plan.

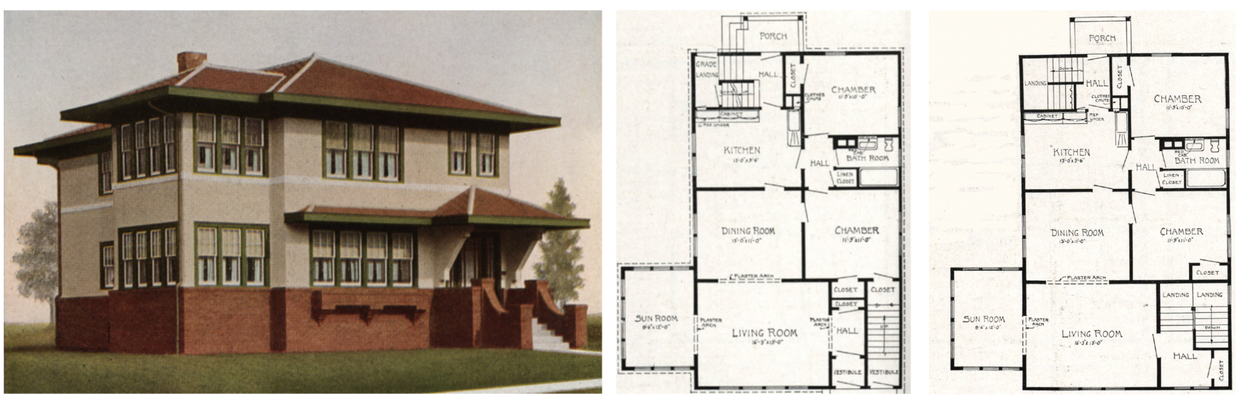

(a) (b) (c)

Figure A5.4 Two-story configuration close to mean plus one standard deviation wall density from ATC-110 data (Configuration 1920-2B; A_{plan} = 1258 ft^2): (a) rendering of house; (b) first-floor plan; and (c) second-floor plan.

APPENDIX B Supplemental Information on Component Damage Fragility Review and Development

This appendix provides additional information used during the component damage fragility function review and development process for the PEER–CEA Wood-Frame Project. This information supports the main document content within Chapter 5.

Supplemental information used for the review of gypsum wallboard fragilities is provided in Table B.1 for damage states 1 and 2. Damage State 3 information is provided in Table B.2. Information for exterior stucco in damage state 1 is provided in Table B.3. Stucco fragility information used for DS2 and DS3 are provided in Table B.4 and Table B.5, respectively. Information used to estimate damage fragility of diagonal let-in bracing is provided in Table B.6. Finally, information on diagonal wood sheathing used for fragility development is provided in Table B.7.

Table B.1 Reviewed fragility data for gypsum wallboard in damage states one and two. Values are drift ratio at observed damage state.

Test index	Reference	DS1 (%)	DS2 (%)		Test index	Reference	DS1 (%)	DS2 (%)
1M-F[1]	McMullin and Merrick [2002]	0.247	0.525		11C-F	McMullin and Merrick [2002]	0.121	0.592
1M-B	“ “	0.254	0.760		11C-B	“ “	0.258	0.472
2M-F	“ “	0.221	0.777		12C-F	“ “	0.144	0.756
2M-B	“ “	0.287	0.777		12C-B	“ “	0.376	0.676
3M-F	“ “	0.245	0.778		13C-F	“ “	0.217	0.810
3M-B	“ “	0.262	0.778		13C-B	“ “	0.283	0.764
4M-F	“ “	0.384	0.513		14C-F	“ “	0.162	0.814
4M-B	“ “	0.384	0.639		14C-B	“ “	0.242	0.737
5M-F	“ “	0.220	0.498		15C-F	“ “	0.170	0.791
5M-B	“ “	0.220	0.498		15C-B	“ “	0.182	0.791
5M-F	“ “	0.263	0.444		16C-F	“ “	0.183	0.422
5M-B	“ “	0.263	0.527		16C-B	“ “	0.252	0.802
8M-F	“ “	0.213	0.750		17C-F	“ “	0.330	0.721
8M-B	“ “	0.213	0.643		17C-B	McMullin and Merrick [2002]	0.170	0.721
9M-F	“ “	0.267	0.627		EDA5	Arnold et al. [2003(b)]	0.20	0.60
9M-B	“ “	0.508	1.008		EDA6	“ “	0.34	0.70
10M-F	“ “	0.245	0.750		EDA7	“ “	0.20	0.60
10M-B	“ “	0.210	1.000		EDA8	“ “	0.34	0.60
6C-F	“ “	0.170	0.598		EDA11	“ “	0.20	0.70
6C-B	“ “	0.170	0.359		EDA12	Arnold et al. [2003(b)]	0.34	0.70
7C-F	“ “	0.254	0.760		EDA1	Arnold et al. [2003(a)]	0.25	0.60
7C-B	McMullin and Merrick [2002]	0.221	0.777		EDA2	Arnold et al. [2003(a)]	0.30	0.70
					PEER C2	Cobeen et al. [2020]	0.40	0.60

[1] McMullin amd Merrick [2002] test indices denote monotonic (M) or cyclic (C) loading, and front (F) or back (B) of specimen.

Table B.2 Reviewed fragility data for gypsum wallboard in damage state three. Values are drift ratio at observed damage state.

Test index	Reference	DS3 (%) 1
8A (-ve) [2]	COLA [2001]	0.88
8A (+ve)	" "	0.77
8B (-ve)	" "	0.75
8B (+ve)	" "	0.50
8C (-ve)	" "	0.55
8C (+ve)	COLA [2001]	0.45
G-01 (-ve)	Bahmani and van de Lindt [2016]	2.32
G-01 (+ve)	" "	2.57
G-02 (-ve)	" "	2.07
G-02 (+ve)	Bahmani and van de Lindt [2016]	2.06
1 (M)	McMullin and Merrick [2002]	1.70
4 (M)	" "	1.55
5 (M)	" "	1.81
8 (M)	" "	1.30
7 (-ve)	" "	1.23
7 (+ve)	" "	1.95
11 (-ve)	" "	2.70
11 (+ve)	" "	1.87
6 (-ve)	" "	1.15
6 (+ve)	" "	1.82
17 (-ve)	" "	1.10
17 (+ve)	McMullin and Merrick [2002]	1.30
19A (-ve)	Pardoen et al. [2003]	1.20
19A (+ve)	" "	1.10
19B (-ve)	" "	1.25
19B (+ve)	Pardoen et al. [2003]	1.18
12E (M)	Gatto and Uang [2002]	1.14
12W (M)	Gatto and Uang [2002]	1.46

[1] Observed drifts corresponding to 80% post-peak load assumed to represent DS3.
[2] Positive (+ve) or negative (-ve) loading direction for cyclic tests, monotonic tests (M).

Table B.3 Reviewed fragility data for exterior stucco in damage state one. Values are drift ratio at observed damage state.

Test Index	Reference	DS1 (%)
Story 1 - Back	Mosalam et al. [2002] [1]	0.200
Story 1 - East	" "	0.247
Story 1- West	" "	0.184
Story 2 - Back	" "	0.184
Story 2 - Front	" "	0.155
Story 2 - East	" "	0.223
Story 2 - West	" "	0.306
Story 3 - Back	" "	0.168
Story 3 - Front	" "	0.131
Story 3 - East	" "	0.183
Story 3 - West	Mosalam et al. [2002]	0.212
EDA-01	Arnold et al. [2003(a)] (Phase 1)	0.20
EDA-02	Arnold et al. [2003(a)] (Phase 1)	0.20
EDA-05	Arnold et al. [2003(b)] (Phase 2)	0.30
EDA-07	" "	0.30
EDA-11	" "	0.20
EDA-06	" "	0.34
EDA-08	" "	0.47
EDA-12	Arnold et al. [2003(b)] (Phase 2)	0.15

[1] All values for DS1 from Mosalam et al. [2002] are from Phase II at seismic test level (STL) 3. Average of reported peak drift of positive and negative directions assumed for each story location and wall line.

Table B.4 **Reviewed fragility data for exterior stucco in damage state two. Values are drift ratio at observed damage state.**

Test index	Reference	DS2 (%)
Story 1 - STL3 - east	Mosalam et al. [2002] [1]	0.354
Story 1 - STL4 - back	Mosalam et al. [2002] [1]	0.473
EDA-01	Arnold et al. [2003(a)] (Phase 1)	0.55
EDA-02	Arnold et al. [2003(a)] (Phase 1)	0.70
EDA-05	Arnold et al. [2003(b)] (Phase 2)	0.40
EDA-07	“ “	0.60
EDA-11	“ “	0.75
EDA-06	“ “	0.58
EDA-08	“ “	0.55
EDA-12	Arnold et al. [2003(b)] (Phase 2)	0.70

[1] All values for DS2 from Mosalam et al. [2002] are from Phase III.

Table B.5 Reviewed fragility data for exterior stucco to inform DS3. Values are drift ratio at peak strength and 80% post-peak.

Test index	Reference	θ_{peak} (%)[1]	$\theta_{80\%}$ (%)[1]
EDA-01	Arnold et al. [2003(a)] (Phase 1)	1.01	1.69
EDA-02	Arnold et al. [2003(a)] (Phase 1)	1.14	1.98
EDA-05	Arnold et al. [2003(b)] (Phase 2)	1.19	2.55
EDA-07	“ “	1.34	2.23
EDA-11	“ “	1.70	2.50
EDA-06	“ “	2.03	3.05
EDA-08	“ “	0.87	1.78
EDA-12	Arnold et al. [2003(b)] (Phase 2)	1.68	2.80
20A	COLA [2001]	0.62	0.95
20B	“ “	0.63	1.05
20C	“ “	0.67	0.89
21A	“ “	0.63	0.99
21B	“ “	0.53	1.00
21C	COLA [2001]	0.54	N/A [2]
S-01	Bahmani and van de Lindt [2016]	0.90	1.71
S-02	Bahmani and van de Lindt [2016]	0.78	1.29
17A	Pardoen et al. [2003]	2.105	4.25
17B	“ “	2.11	N/A [2]
15A	“ “	2.69	4.00
15B	Pardoen et al. [2003]	2.10	4.15

[1] Drift values represent the average of two directions (positive and negative) from quasi-static cyclic testing.
[2] 20% strength loss was not observed within extent of displacements tested.

Table B.6 Reviewed data for diagonal let-in bracing to estimate damage fragility. Values are drift ratio at peak strength from experimental testing.

Test index	Reference	Description	θ_{peak} (%)
Type 1 – Test 2	Tuomi and Gromala [1977]	8-ft×8-ft panel with 45° 1-in.×4-in. LIB, Compression (frame failed before brace)	1.67
Conf. 1 - Test 1	NAHB [2008]	9.33-ft×8-ft LIB, 45°, compression, SG=0.35	1.08
Conf. 1 - Test 2	" "	9.33-ft×8-ft LIB, 45°, compression, machined structural stud	1.20
Conf. 1 - Test 3	" "	9.33-ft×8-ft LIB, 45°, compression, SG=0.44	0.65
Conf. 1 - Test 4	" "	9.33-ft×8-ft LIB, 45°, compression, SG=0.44	0.87
Conf. 2 - Test 1	" "	9.33-ft×8-ft LIB, 45°, tension, 2-8d nails at plate	3.72
Conf. 2 -Test 2	" "	9.33-ft×8-ft LIB, 45°, tension, 2-8d nails at plate	3.26
Conf. 2 - Test 3	" "	9.33-ft×8-ft LIB, 45°, tension, 3-8d nails at plate	2.85
Conf. 3 - Test 1	" "	20-ft×8-ft LIB, 45°, T+C, fully restrained, no open, 2-8d	1.00
Conf. 3 - Test 2	" "	20-ft×8-ft LIB, 45°, T+C, fully restrained, no open, 3-8d	0.89
Conf. 3 - Test 3	" "	20-ft×8-ft LIB, 45°, T+C, fully restrained, no open, 2-8d, shifted	0.95
Conf. 3 - Test 4	" "	20-ft×8-ft LIB, 45°, T+C, fully restrained, no open, 3-8d, shifted	0.70
Conf. 4 - Test 1	" "	20-ft×8-ft LIB, 45°, T+C, GWB on opp. Side, fully restrained	1.04
Conf. 4 - Test 2	" "	20-ft×8-ft LIB, 45°, T+C, GWB on opp. Side, fully restrained	0.89
Conf. 5 -Test 1	" "	20-ft×8-ft LIB, 60°., T+C, GWB on opp. Side, fully restrained	0.80
Conf. 6 - Test 1	" "	20-ft×8-ft LIB, 45°, T+C, float GWB on opp. Side, fully rest.	1.32
Conf. 6 - Test 2	" "	20-ft×8-ft LIB, 45°, T+C, floated GWB on opp. Side, fully rest.	1.07
Conf. 7 - Test 1	" "	20-ft×8-ft LIB, 45°, T+C, GWB on both sides, fully restrained	1.24
Conf. 8 - Test 1	" "	20-ft×8-ft LIB, 45°, T+C, GWB on opp. Side, low bound rest.	0.78
Conf. 8 - Test 2	" "	20-ft×8-ft LIB, 45°, T+C, GWB on opp. Side, lower bound rest.	0.94
Conf. 9 - Test 1	" "	20-ft×8-ft LIB, 45°, T+C, GWB on opp. side, 20% restraint	1.05
Conf. 10 - Test 1	" "	20-ft×8-ft LIB, 45°, T+C, GWB on opp. Side, 30% restraint	1.07
Conf. 10 - Test 2	" "	20-ft×8-ft LIB, 45°, T+C, GWB on opp. Side, 30% restraint	2.34
Conf. 11 - Test 1	" "	20-ft×8-ft LIB, 45°, T+C, GWB on opp. Side, 30% restraint	1.22
Conf. 12 - Test 1	" "	20-ft×8-ft LIB, 45°, T+C, GWB on opp. Side, 60% restraint	1.15
Conf. 12 - Test 2	NAHB [2008]	20-ft×8-ft LIB, 45°, T+C, GWB on opp. Side, 60% restraint	1.44

[1] All tests are from monotonic loading. All braces are let-in to framing, but not confined with sheathing or siding except Configuration 7 from NAHB [2008], which is confined by gypsum wallboard.

Table B.8 Reviewed data for diagonal wood sheathing to estimate damage fragility. Values are drift ratio (%) at peak strength from experimental testing.

Test index	Reference	Boards in tension [1]	Boards in compression [2]	Average of both directions
Test 4	Ni and Karacabeyli [2007]	1.99	1.48	1.74
Test 5	" "	1.97	2.53	2.25
Test 6	" "	2.40	1.81	2.11
Test 7	" "	2.42	2.71	2.57
Test 8	" "	1.59	1.79	1.69
Test 9	" "	1.47	1.07	1.27
Test 10 [3]	" "	1.95	0.81	1.38
Test 11	" "	2.50	2.00	2.25
Test 15	" "	2.87	1.93	2.40
Test 16	Ni and Karacabeyli [2007]	2.36	1.92	2.14
HDG-02 [3]	Bahmani and van de Lindt [2016]	2.58	2.51	2.55

[1] Sheathing boards are loaded in the direction causing tension based on strut action with gaps between boards closing.
[2] Sheathing boards are loaded in the direction causing compression based on strut action with gaps between boards opening.
[3] These tests include gypsum wallboard on the opposite side of the test specimen.

The Pacifi c Earthquake Engineering Research Center (PEER) is a multi-institutional research and education center with headquarters at the University of California, Berkeley. Investigators from over 20 universities, several consulting companies, and researchers at various state and federal government agencies contribute to research programs focused on performance-based earthquake engineering.

These research programs aim to identify and reduce the risks from major earthquakes to life safety and to the economy by including research in a wide variety of disciplines including structural and geotechnical engineering, geology/seismology, lifelines, transportation, architecture, economics, risk management, and public policy.

PEER is supported by federal, state, local, and regional agencies, together with industry partners.

PEER Core Institutions

University of California, Berkeley (Lead Institution)
California Institute of Technology
Oregon State University
Stanford University
University of California, Davis
University of California, Irvine
University of California, Los Angeles
University of California, San Diego
University of Nevada, Reno
University of Southern California
University of Washington

PEER reports can be ordered at https://peer.berkeley.edu/peer-reports or by contacting

Pacific Earthquake Engineering Research Center
University of California, Berkeley
325 Davis Hall, Mail Code 1792
Berkeley, CA 94720-1792
Tel: 510-642-3437
Email: peer_center@berkeley.edu

ISSN 2770-8314
https://doi.org/10.55461/YYQH3072